RELATIVISTIC DESCRIPTIONS OF POLARIZATION TRANSFER OBSERVABLES FOR QUASIELASTIC PROTON SCATTERING

G. C. Hillhouse

Dissertation submitted in partial fulfillment of the requirements

for the degree of Doctor of Philosophy

at the University of Stellenbosch

Supervisor: Prof. P. R. De Kock

March 1999

Declaration

I the undersigned hereby declare that the work contained in this dissertation is my own original work and has not previously in its entirety or in part been submitted at any university for a degree.

05/02/1999

Date

Abstract

This thesis is devoted to the development of relativistic Dirac–based models for describing complete sets of quasielastic $(\vec{p},\vec{p}')$ and $(\vec{p},\vec{n})$ polarization transfer observables at medium energies.

The original relativistic–plane–wave–impulse–approximation (RPWIA) model of Horowitz and Murdock is modified to include the phenomenological Horowitz–Love–Franey meson–exchange (HLF) model for the NN amplitudes, and new HLF parameter sets are generated between 80 and 200 MeV. Medium effects are incorporated by replacing free nucleon masses in the Dirac plane waves with more refined effective projectile and target nucleon masses.

For a ^{40}Ca target at a fixed momentum transfer of 1.97 fm^{-1}, and incident energies between 135 and 300 MeV, the sensitivity of complete sets of quasielastic $(\vec{p},\vec{p}')$ and $(\vec{p},\vec{n})$ polarization transfer observables is investigated with respect to nuclear medium effects, ambiguities in πNN coupling, exchange contributions to NN amplitudes, and spin–orbit distortions. It is seen that, (1) compared to $(\vec{p},\vec{p}')$ scattering, the $(\vec{p},\vec{n})$ polarization transfer observables are more sensitive to pseudoscalar versus pseudovector forms of the πNN coupling, (2) as the incident proton energy is lowered, nuclear medium effects and spin–orbit distortions become more important, (3) nuclear medium effects are extremely sensitive to the type of pion coupling, (4) contrary to the original RPWIA, exchange contributions cannot be neglected at energies as high as 500 MeV. For an optimal study of nuclear medium effects, this investigation stresses the urgent need for measurements of complete sets of quasielastic polarization transfer observables for *both* $(\vec{p},\vec{p}')$ and $(\vec{p},\vec{n})$ reactions at energies lower than 200 MeV. Comparison of RPWIA predictions with the small amount of available data yields an inconsistent picture: The $(\vec{p},\vec{p}')$ data favour a pseudoscalar coupling for the pion, whereas the limited $(\vec{p},\vec{n})$ data suggest a pseudovector form. Our poor treatment of distortions is considered to be the main source for this inconsistency.

The issue of distortion effects on polarization transfer observables is addressed by developing the theoretical framework for the relativistic distorted wave impulse approximation. As an additional improvement over the RPWIA, models of nuclear structure (relativistic Fermi–gas model, relativistic mean–field approximation, and local–density–approximation) are developed, whereby the nuclear structure information is contained in a large set of nuclear response functions, which are systematically evaluated using standard many–body techniques.

Samevatting

Hierdie proefskrif handel oor die ontwikkeling van relatiwistiese modelle, gebaseer op die Dirac–formalisme, vir volledige stelle parameters vir spinpolarisasie–oordrag in die geval van kwasi–elastiese $(\vec{p},\vec{p}\,')$ en $(\vec{p},\vec{n})$ verstrooiing by medium energieë.

Die oorspronklike Relatiwistiese Vlakgolf–Impulsbenadering (RVI) van Horowitz en Murdock is gewysig om ook die fenomenologiese meson–uitruilmodel van Horowitz, Love en Franey (HLF–model) vir die nuckleon–nukleon (NN) amplitudes in te sluit. Hiervoor is 'n nuwe stel HLF–parameters vir die energiegebied 80 – 100 MeV bereken. Om effekte van die omringende kernmedium in te sluit, is effektiewe nukleon massas tans vir beide die projektiel– en die teiken-nukleon op 'n nuwe, verfynde wyse bereken.

Vir die kwasi–elastiese reaksies $(\vec{p},\vec{p}\,')$ en $(\vec{p},\vec{n})$ met ^{40}Ca as teikenkern, invallende energieë tussen 135 en 500 MeV en 'n (vaste) momentum–oordrag van 1,97 fm^{-1}, is volledige stelle polarisasie–parameters bereken. Laasgenoemde se gevoeligheid is ondersoek ten opsigte van effekte van die kernmedium, dubbelsinnighede ten opstigte van die πNN–interaksie, die bydraes van uitruilterme tot die NN–interaksie en die golfvervorming as gevolg van spin–baan koppeling. Die volgende is bevind: (1) Die polarisasieveranderlikes van die $(\vec{p},\vec{n})$–reaksie is meer gevoelig ten opsigte van die keuse tussen 'n pseudoskalare of 'n pseudovektor term in die πNN–interaksie, as dié van die $(\vec{p},\vec{p}\,')$ reaksie; (2) Effekte van die kernmedium en spin–baan vervorming word belangrik by lae energieë; (3) Die effekte van die kernmedium is uiters gevoelig vir die tipe pion–koppeling; (4) In teenstelling met die oorspronklike RVI, kan uitruileffekte nie by hoër energieë, byvoorbeeld 500 MeV, verontagsaam word nie.

Hierdie ondersoek beklemtoon dat, vir 'n behoorlike studie van effekte van die kernmedium, veral vir energieë laer as 200 MeV, volledige stelle van polarisasie–veranderlikes van beide $(\vec{p},\vec{p}\,')$ en $(\vec{p},\vec{n})$ reaksies gemeet moet word. Vergelykings met die beperkte beskikbare data (hoofsaaklik vanaf onvolledige stelle veranderlikes) lewer 'n onsamehangende prentjie: Die $(\vec{p},\vec{n})$–polarisasieveranderlikes gee voorkeur aan 'n pseudovektor term in die πNN–interaksie, waar die $(\vec{p},\vec{p}\,')$ veranderlikes egter 'n pseudoskalare–term verkies. Die oorsaak van hierdie nie–konsistensie kan moontlik aan die weglating van vervorming van die invallende golf deur die kernmedium gewyt word.

Laagenoemde vervorming is aangespreek deur 'n rekenaarprogram te ontwikkel, waarmee vervormde Dirac–golwe beken kan word. Verder is die totale formalisme is ontwikkel, waaruit verder polarisasie–parameters met sulke vervormde golwe bereken kan word. Dit wend die sogenaamde "reponse"–funksie vir veeldeeltjiesisteme aan, waarmee die kernmedium se nie–homogeniteite, geassosieerd met die vervorming (byvoorbeeld die benadering vir plaaslike digtheid) en ander effekte elegant hanteer kan word.

Acknowledgments

I am greatly indebted to the following people who contributed towards the successful completion of my dissertation:

- My beautiful wife, Marianne, for her unconditional love, understanding, encouragement and support; and for giving me every possible opportunity for pursuing my physics passions.
- My adorable son, Ryan, for asking me more questions than all the postgraduate students and my supervisor combined, and for understanding why I wasn't at home for most of this year.
- My supervisor, friend and colleague, Prof. Runan de Kock, for his continual support, advice, constructive criticism, perfectionist approach, and guidance at all stages of my Ph.D; and also playing the organ so beautifully at our wedding.
- Both the Hillhouse and Smit families for their emotional support.
- Prof. Chuck Horowitz for his invaluable theoretical input, without which this dissertation would not have been possible.
- The Dean of Sciences, Prof. Hahne, for focusing my interest on the application of Dirac phenomenology to nuclear reactions.
- My co–supervisor, Prof. Cowley, for involving me in hands–on experimental work at the National Accelerator Centre at Faure in South Africa, and also for directing my project towards polarization transfer observables for quasielastic proton–nucleus scattering. I am also grateful to Prof. Cowley for partially funding a visit to Japan in 1997.
- My friends and colleagues, Brandon van der Ventel and Shaun Wyngaardt, for the many discussions on various aspects of theoretical physics, and for continually bombarding me with thought–provoking questions. In particular, I would like to thank Shaun for assisting with the generation of the Horowitz–Love–Franey parameters, and Brandon for checking most of the trace algebra and for working closely with me during most stages of my dissertation.

- My Japanese collaborators, Prof. Sakai, Drs Otsu and Wakasa, for the many fruitful discussions relating to their experimental $(\vec{p},\vec{p}')$ and $(\vec{p},\vec{n})$ programs at the Research Centre for Nuclear Physics at Osaka in Japan.

- Javed Iqbal and Tim Cooper for supplying me with some of the codes used for the generation of effective masses and relativistic Coulomb wave functions.

- My friend, Gillian Arendse, for helping me to maintain a healthy perspective on life, and for accompanying me on many of the much–needed social calls to some of the local restaurants and bars.

- The University of Stellenbosch physics department for giving me a lighter lecture load towards the end of the project.

- Mrs De Waal, Miss Visser and Miss Van den Berg, for producing some of the figures in the dissertation.

- The Universities of Stellenbosch and the Western Cape for financing two short visits to the Indiana University Nuclear Theory Centre as well as a number of national and international conferences.

Dedicated to Marianne and Ryan

Contents

List of Figures

List of Tables

Chapter 1

Scientific motivation

1.1 Introduction

Historically, work in medium energy nucleon–nucleus scattering physics started in the 1950's [Ra92] and has continued since. As we enter the new millennium, research in medium energy ($\sim$100 MeV to $\sim$1 GeV) proton–nucleus scattering continues to attract widespread theoretical interest, and accounts for a significant fraction of the experimental effort at medium energies.

Traditionally, nuclear structure and nuclear reactions have been studied using models based on the nonrelativistic Schrödinger equation. In recent years, however, considerable attention has been devoted to relativistic descriptions of nuclei and nuclear reactions based on the Dirac equation. In particular, this thesis is concerned with the development of relativistic Dirac–based models for the interpretation of complete sets of quasielastic $(\vec{p},\vec{p}')$ and $(\vec{p},\vec{n})$ polarization transfer observables (also called spin observables), for targets nuclei ranging from ^{12}C to ^{208}Pb, incident proton energies between 100 and 500 MeV, and for three–momentum transfers larger than $\sim$0.5 fm^{-1}. The next sections expand on the following:

- quasielastic scattering,
- both $(\vec{p},\vec{p}')$ and $(\vec{p},\vec{n})$ reactions,
- complete sets of polarization transfer observables, and
- relativistic models.

1.2 Why consider quasielastic proton scattering?

At moderate momentum transfers ($|\vec{q}| > 0.5$ fm^{-1}) quasielastic proton scattering is the dominant mechanism for nuclear excitation: the status of quasielastic scattering is reviewed in Chapter 2. Quasielastic proton scattering is considered to be a single–step process, whereby a projectile proton knocks out a single bound nucleon in the surface of the target nucleus, while the remainder of the nucleons act as "spectators". This quasielastic process is characterized by a broad peak in the nuclear excitation spectrum, the centroid of which nearly corresponds to free NN kinematics, and a width resulting from the initial momentum distribution of the struck nucleon. At the high momentum transfers of interest, nuclear shell effects are unimportant, and the quasielastic peak is well separated from the discrete states and low–lying resonances in the excitation spectrum. Hence, deviations of the scattering observables from the corresponding free NN values could be attributed to medium modifications of the free NN interaction. Consequently these reactions offer a direct means to study how the fundamental free NN interaction is modified by the surrounding medium of the nucleus in which it occurs.

One of the aims of this thesis is to investigate to what extent a single–step, surface–peaked, NN interaction can account for data at the quasielastic peak. In addition, by comparing quasielastic scattering from a nuclear target to free NN scattering from a hydrogen target at the same kinematic conditions, differences in the observables are used to understand how the nuclear environment affects the free NN interaction.

1.3 Why consider both (p, p') and (p, n) reactions?

Quasielastic (p, p') and (p, n) reactions probe different parts of the medium–modified NN interaction: (p, p') scattering probes both isovector and isoscalar parts of the NN interaction, whereas (p, n) charge–exchange reactions sample only the isovector components, particularly those directly related to pion exchange [Wa94, Ho94]. Furthermore, since the Lorentz character of the isovector amplitudes is totally different from that of the isoscalar amplitudes, one expects quasielastic (p, p') and (p, n) reactions to yield different, but complementary, information about the different components of the NN interaction.

1.4 Why consider complete sets of spin observables?

With the recent developments in polarized proton beams and high resolution spectrometers with focal plane polarimeters, it now becomes possible to measure complete sets of quasielastic polarization transfer observables (also called spin observables), in which incident proton beams polarized in an arbitrary orientation are utilized, to determine the components of the polarization of the scattered protons (see Appendix G).

Polarization transfer observables are sensitive to any changes in the spin dependence of the NN interaction in the medium. The primary role of distortions on the incoming and outgoing proton wave functions is to reduce the cross section. However, since polarization transfer observables are essentially ratios of cross sections, handwaving arguments suggest that these distortions largely cancel, and thus the polarization observables should be insensitive to distortions. Hence, simple plane wave models, which ignore distortions, should provide an adequate first–order description of the quasielastic polarization transfer observables. In addition, experimental data in the quasielastic region seem to be almost independent of the type of nucleus: at the high excitation energies of interest one nucleus looks like another. This suggests that one is extracting fundamental properties of nuclear matter, rather than the individual properties of a single state. Hence, by considering quasielastic scattering to the continuum, one minimizes the uncertainties in nuclear structure of discrete final states, and thus, relatively simple models of the target nucleus, such as a Fermi–gas description, should be adequate. Indeed, one of the aims of this thesis is to investigate to what extent nuclear matter at high excitation energies behaves as a collection of nearly free nucleons.

Comparison of theoretical predictions of polarization transfer observables to data, for both quasielastic $(\vec{p},\vec{p}')$ and $(\vec{p},\vec{n})$ reactions, provide extremely stringent tests for the various models for quasielastic proton scattering.

1.5 Why consider relativistic models?

The term "relativistic", as used in this thesis, is associated with the use of the Dirac equation, with its relativistic treatment of the dynamics and kinematics, as opposed to the nonrelativistic Schrödinger equation with either nonrelativistic or relativistic kinematics.

Conventional wisdom claims that relativistic effects are unimportant for nuclear structure problems. Indeed, considering that the maximum kinetic energy T_{max} of a nucleon (with free mass m) in the nucleus is determined by the groundstate Fermi momentum $k_F \approx 1.4$ fm^{-1} to be

$$T_{max} = \frac{\hbar^2 k_F^2}{2m} \approx 40 \text{ MeV} ,$$

which corresponds to a velocity of about one–third that of light ($v \approx 0.28\, c$), one expects only minor modifications due to relativistic kinematics and dynamics. Nevertheless, there are a number of compelling reasons for pursuing relativistic models of nuclear structure and nuclear scattering, a few of which are listed below [Se86, Ho91b, Ho94a]:

- It is important to have a manifestly Lorentz covariant formalism, especially for reliable extrapolation of nuclear systems to extreme conditions of density, temperature, or momentum transfer. These conditions may arise in astrophysics (early universe, supernovas, neutron stars), relativistic heavy ion collisions, and in experiments performed at large momentum transfers.

- Historically, the first great triumph of the Dirac equation was its explanation of the spin and magnetic moment of the electron. One can label spin as an intrinsically relativistic phenomenon. The relativistic 4–component Dirac equation provides a natural explanation of the nuclear spin–orbit force. Useful and successful relativistic formalisms have recently been developed for nuclei, for instance, the relativistic mean field theory [Se86].

- Nuclear saturation is a basic consequence of the nuclear force that causes all nuclei to have about the same density and binding energy per nucleon. A simple and intrinsically relativistic mechanism for nuclear saturation is found in a simple relativistic mean field approximation.

- Simple relativistic models provide an excellent description of spin observables for elastic proton scattering at medium energies. Only very sophisticated state–of–the–art nonrelativistic models [Al91] can describe elastic proton scattering with the same level of accuracy.

- Compared to nonrelativistic Schrödinger optical potentials, relativistic Dirac optical potentials exhibit a much more systematic and physical behaviour as functions of energy,

nuclear radius, and nuclear mass; for example, global Dirac optical potentials exist [Co92] which describe all elastic proton scattering observables in the 65 to 1040 MeV range, and for various nuclei from ^{12}C to ^{208}Pb.

Although there are a number of theoretical reasons for preferring relativistic Dirac–based models to nonrelativistic Schrödinger–based models, the justification for the use of the Dirac equation, in this project, lies largely in the outstanding success of this phenomenological approach to date. Currently an extremely useful phenomenological theory, referred to as Dirac phenomenology, exists which yields a comprehensive description of many aspects of nuclear dynamics: for review articles, see Refs. [Pi84, Ce86, Se86, Wa87, Re89, Ho91b, Ra92, Se97].

It is interesting to understand exactly how Dirac phenomenology achieves its remarkable success. This is briefly discussed in the next section.

1.5.1 How does Dirac phenomenology achieve its success?

Most relativistic approaches to nuclear physics, such as mean field theories [Se86], optical fits to elastic proton–nucleus scattering data [Cl83], and the relativistic impulse approximation [Sh83a], suggest that the optical potential, involves large attractive Lorentz scalar (typically ~ -400 MeV) and repulsive time–like vector (typically $\sim +350$ MeV) contributions. Relativistic mean field theory relates these potentials to large sigma (scalar) and omega (vector) meson fields [Se86]. This theory is phenomenological in the sense that, once the scalar and vector couplings are adjusted to reproduce the saturation density and binding energy of nuclear matter, relativistic mean field theory provides a good description of the ground state properties of many nuclei, and also accounts for spin–orbit coupling in nuclei.

The scalar potentials enter the Dirac equation on the same footing as the free nucleon mass m. Since these potentials are quite large (~ -400 MeV), they have the effect of introducing a major reduction of the nucleon mass when the nucleon is in nuclear matter. The combination of the attractive scalar potential and the free nucleon mass m is often referred to as an effective mass m^*, and is equal to $\sim 0.6\,m$ in infinite nuclear matter. This concept of an effective mass is an essential element in the success of Dirac phenomenology, and will be discussed in more detail in Chapter 3. On the other hand, the time–like vector potentials enter the Dirac equation in

the same way as the energy eigenvalues. The combination of the large repulsive vector potential ($\sim +350$ MeV) and the larger attractive scalar potential (~ -400 MeV), yields a dispersion relation, between the momentum and energy of a relativistic nucleon in nuclear matter, which is essentially the same as the corresponding relation for the nonrelativistic Schrödinger equation which, for decades, has provided a reasonably satisfactory description of nuclear structure [Ce82].

An alternative approach to relativistic nucleon dynamics, which also gives large scalar and time–like vector potentials, comes from the work of Bunny Clark and collaborators [Cl83] who studied the phenomenology of the Dirac equation for elastic proton–nucleus scattering. In this work, the Dirac equation with phenomenological scalar and time–like vector potentials replaces the standard central and spin–orbit potentials of traditional Schrödinger phenomenology. Using just as many fitting parameters as in nonrelativistic phenomenology, Clark and collaborators provided a superior description of elastic scattering spin observables. Again, the strengths of the scalar and time–like vector potentials are ~ -400 MeV and $\sim +350$ MeV in the nuclear interior, with geometries following the nuclear densities. The relativistic potentials show less energy dependence than equivalent nonrelativistic potentials. There exists a relation between the relativistic scalar and time–like vector potentials and the usual spin–independent and spin–orbit potentials of the Schrödinger equation: this is readily understood by reducing the Dirac equation to an equivalent Schrödinger–like second order differential equation [Cl83] as shown in Appendix A. The resulting effective spin–independent and spin–orbit potentials, which are an order of magnitude smaller than the relativistic potentials, are referred to as the "Schrödinger–equivalent potentials". The large scalar and time–like vector potentials nearly cancel to form the relatively small spin–independent potential, whereas they constructively add to reproduce the relatively strong spin–orbit potential: the strengths of these central and spin–orbit potentials are in close agreement with those obtained by a pure nonrelativistic Schrödinger–based analysis of elastic scattering data.

The successful description of elastic scattering spin observables, based on the Dirac phenomenology of Clark and collaborators, was initially viewed with skepticism because, as pointed out by Stephen Wallace [Pi84], "you can fit almost anything with enough free parameters". However, to the surprise of McNeil, Shepard and Wallace, their *parameter–free* development of the relativistic impulse approximation (RIA) [Cl83a, Mc83, Sh83a], gave essentially the same nuclear potentials as those found by Clark's phenomenological fits: in the RIA, free NN ampli-

tudes, from phase shift data in an invariant Dirac representation, are folded with nuclear target densities, determined from the relativistic Dirac–Hartree equations, to generate microscopic scalar and time–like vector optical potentials without any free parameters. Consequently, the RIA (and subsequent developments by Horowitz and Murdock [Mu87b], and Tjon and Wallace [Tj85, Tj85a, Tj85b, Tj87, Tj87a]) served to strengthen the idea of a Dirac phenomenology based on strong opposing scalar and time–like vector potentials. The RIA provides an excellent description of all elastic scattering spin observables over a wide range of energies and nuclei [Ho91b].

1.5.2 Dirac phenomenology and quasielastic scattering

The failure of *all* nonrelativistic Schrödinger–based models [Sm88] to describe the quasielastic $(\vec{p},\vec{p}')$ analyzing power at 500 MeV, together with the tremendous success of Dirac phenomenology discussed in the previous section, lead to the development of the Relativistic (Dirac) Plane Wave Impulse Approximation (RPWIA) by Horowitz and collaborators [Ho86, Mu87a, Ho88, Iq88], where the NN amplitudes are based on the Lorentz invariant parametrization of the standard five Fermi invariants, and the target nucleus is treated as a Fermi gas. Indeed, the accurate prediction of the above–mentioned quasielastic $(\vec{p},p')$ analyzing power, based on the RPWIA, has been regarded as a "clear relativistic signature" [Ho86, Mu87a, Ho88, Iq88, Ho91b].

The success of the simple relativistic plane wave model is attributed to the implicit treatment of medium modifications of the NN interaction. These medium effects (often referred to as relativistic effects), which predict an enhancement of lower Dirac components of the nucleon in the presence of strong scalar and time–like vector potentials at nuclear densities, are incorporated by replacing free nucleon masses in the Dirac plane waves with effective projectile and target nucleon masses in the context of relativistic mean field theory [Se86]. To date, and to my knowledge, no nonrelativistic Schrödinger–based model has quantitatively explained the above–mentioned $(\vec{p},p')$ analyzing power, although a possible nonrelativistic explanation has been suggested by Brieva and Love [Br90].

Despite the successful prediction of the $(\vec{p},p')$ analyzing power, however, the RPWIA model fails to predict some of the other polarization transfer observables [Ho88]. However, rather than abandon the original RPWIA in favour of more sophisticated relativistic models, and inspired

by the encouraging results of the original RPWIA, my approach in this project is to critically review the underlying assumptions and input parameters of the RPWIA, and to perform more refined calculations so as to reveal the limitations of the model.

1.6 Scientific goals of this project

The main goal of this project is to develop a *consistent* description of complete sets of polarization transfer observables for both quasielastic $(\vec{p},\vec{p}')$ and $(\vec{p},\vec{n})$ reactions. More specifically, the aims of this project are:

- to verify that nuclear matter at high excitation energies behaves as a collection of nearly free nucleons,
- to search for medium modifications of the NN interaction due to relativistic effects,
- to critically review, and improve, the approximations of the original relativistic plane wave impulse approximation of Horowitz and Murdock [Mu87a, Ho88, Ho91b],
- to perform a systematic comparison of my refined, and improved, RPWIA calculations with the available data on complete sets of quasielastic $(\vec{p},\vec{p}')$ and $(\vec{p},\vec{n})$ polarization transfer observables, so as to reveal any limitations of the model.

1.7 Organization of thesis

The structure of this thesis is organized as follows:

- In Chapter 2, the concept of "quasielastic scattering" is defined, and the current theoretical and experimental status of quasielastic polarized–proton scattering is reviewed.
- The aim of Chapter 3 is to critically review, and improve, the approximations of the original relativistic plane wave impulse approximation (RPWIA) of Horowitz and Murdock [Mu87a, Ho88, Ho91b], and to perform a systematic comparison of my more refined calculations to the available data on complete sets of quasielastic $(\vec{p},\vec{p}')$ and $(\vec{p},\vec{n})$ polarization

transfer observables, so as to reveal any limitations of the model. Some of the work in Chapter 3 is published in Refs. [Hi94, Hi95, Hi97, Hi98].

- Based on the conclusions of Chapter 3, a theoretical framework is developed in Chapter 4 for calculating complete sets of quasielastic proton–nucleus polarization transfer observables, based on the relativistic distorted wave impulse approximation.

Chapter 2

Quasielastic proton–nucleus scattering

2.1 Introduction

The phrase "quasielastic proton–nucleus scattering", as used in the title of this chapter, refers collectively to **both** quasielastic (p, p') and (p, n) scattering. The aim of this chapter is to define and illustrate what is meant by the concept of "quasielastic scattering", and also to briefly review the current theoretical and experimental status of quasielastic polarized–proton scattering.

2.2 What is quasielastic proton scattering?

The aim of this section is to define and illustrate what is meant by quasielastic proton–nucleus scattering. Consider the inclusive proton–nucleus spectra in Fig. 2.1: the upper and lower figures display the double differential cross sections for inclusive (p, p') and (p, n) scattering respectively, as a function of the energy transfer ω (also called excitation energy) to a ^{12}C nucleus, at a fixed laboratory scattering angle of 20°, and for incident proton energies $T_{\rm lab}$ of 400 and 392 MeV [Ot97a]. Although the spectra in Fig. 2.1 are related to a specific nucleus, scattering angle, and incident proton energy, they are nevertheless representative of typical inclusive (p, p') and (p, n) spectra, for incident proton energies between 100 MeV and 500 MeV, and exhibit a number of characteristic features. The peak close to zero energy transfer in the (p, p') spectrum is produced by elastic scattering, which is defined to be a collision whereby the colliding particles only change their direction of motion, and possibly spin orientation; none of the kinetic energy is used to excite the colliding systems internally. The sharp peaks for nonzero values of ω correspond to the excitation of discrete levels in the target nucleus. For small scattering angles, the excitation region just above the low–lying discrete states usually exhibits giant resonances associated with

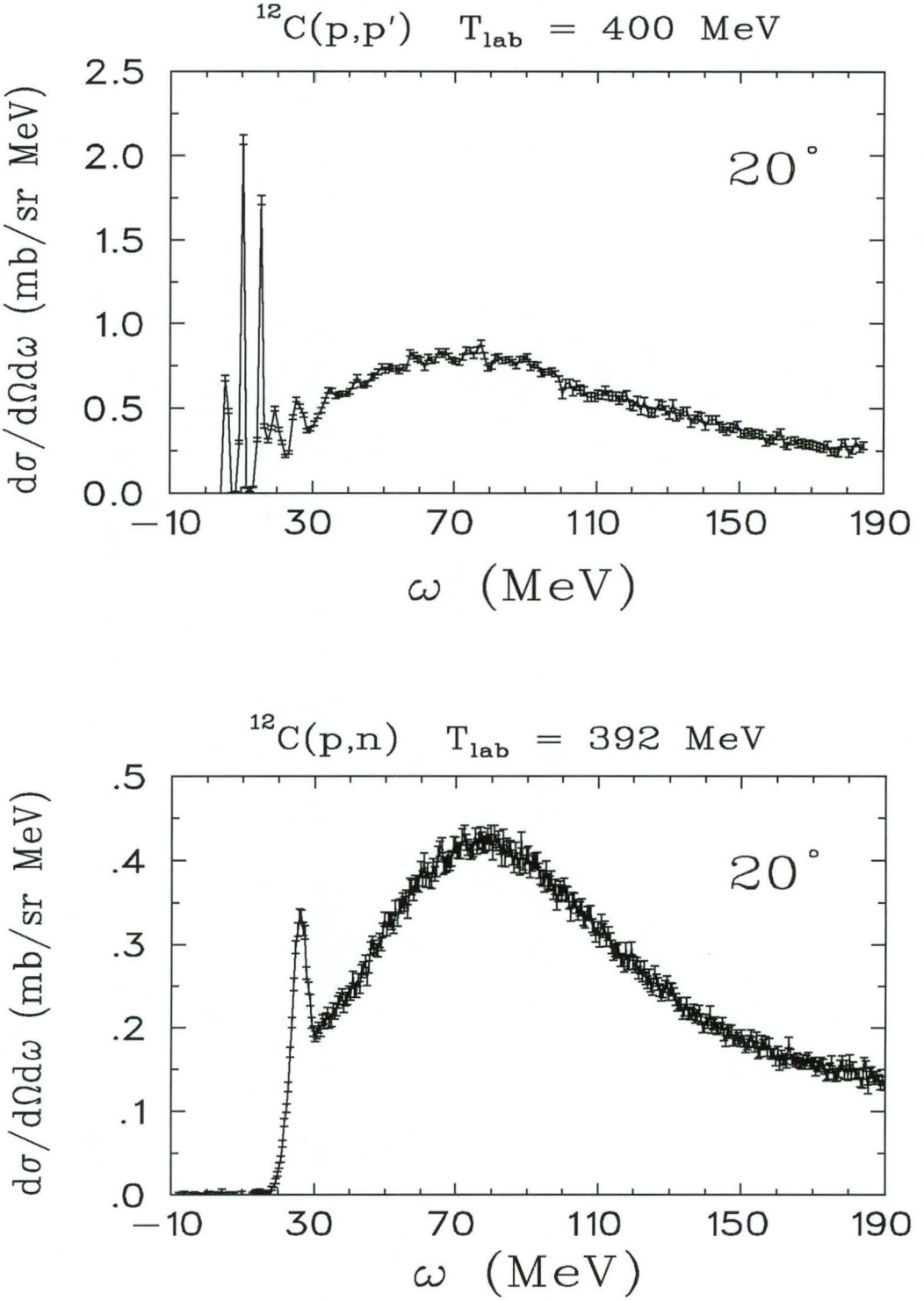

Figure 2.1: Double differential cross sections $\frac{d\sigma}{d\Omega d\omega}$ (in mb sr^{-1} MeV^{-1}) for inclusive ^{12}C(p,p') and ^{12}C(p,n) scattering as a function of the energy transferred to the nucleus (ω), for a laboratory scattering angle of 20°, and incident laboratory kinetic energies ($T_{\rm lab}$) of 400 MeV and 392 MeV respectively. The data are from Ref. [Ot97a].

the collective behaviour of the nucleus [Sw89]. At higher excitation energies, one observes a broad peak (or bump) centered near the expected energy–loss for free nucleon–nucleon (NN) scattering, and appropriately called the quasielastic peak (a term first coined by Wall and Roos [Wa66]). If the nucleons in the target nucleus were at rest and free, a very sharp spike (or peak) would be seen at an energy loss $\omega = \frac{|\vec{q}|^2}{2m}$ corresponding to free NN scattering (see Sec. I.9 in Appendix I), where $|\vec{q}|$ is the momentum transfer and m the free nucleon mass. However, instead of a sharp spike, a broad peak is observed, the width of which is attributed to the internal momentum distribution, or Fermi motion, of the target nucleons.

Note that for incident proton energies larger than 500 MeV, a second broad peak called the quasielastic–Δ peak is observed at energy transfers above the quasielastic peak [Ch80, Sm85, Fe88]. The quasielastic–Δ peak occurs at energy transfers which are sufficient to excite individual nucleons to their first excited state, the delta (Δ), roughly 300 MeV above the quasielastic peak. This project is mainly concerned with incident proton energies between 100 MeV and 500 MeV, where the quasielastic–Δ is not observed.

For the purpose of this project, the term *quasielastic scattering* (sometimes, also called quasifree scattering) refers to the process whereby a projectile nucleon knocks out a single bound nucleon in the target nucleus, while the remainder of the target nucleons act as "spectators"; the experimental signature for quasielastic scattering is a broad peak (in the inclusive spectrum), the centroid of which moves in accordance with momentum and energy conservation for free NN scattering.

2.3 Empirical features of quasielastic proton spectra

Unpolarized double differential cross section data for quasielastic proton scattering are now available for a wide range of target nuclei (^{2}H – ^{238}U) and incident beam energies (100 MeV–800 MeV): see Tables 2.1 and 2.2, and also Refs. [Wa66, Wa72, Co72, Wu79, Ch80, An81, Mo82, Ma84, Mc84, Se85, Fo88, Sw89]. The aim of this section is to identify general empirical features of inclusive (p, p') and (p, n) spectra for quasielastic scattering of unpolarized protons. These features are extremely useful, and need to be incorporated when developing models for quasielastic proton reactions: see, for example, Sec. 3.2.1 in Chapter 3.

After the first observation of so–called quasielastic peaks by Wall and Roos [Wa66] for (p,p') reactions at 160 MeV, on a variety of targets ranging from ^{9}Be to ^{209}Bi, and for scattering angles between 10° and 60°, there was a great deal of controversy regarding the interpretation thereof as arising from genuine quasielastic scattering. However, it is now well established that for incident energies between 100 MeV and 200 MeV, inclusive spectra only exhibit clear quasielastic peaks for targets with mass numbers less than about 60, and scattering angles less than about 25° (see for example Refs. [Ch81, Se86, We85]). There are, however, exceptions to the rule. For example, the continuum spectra for ^{4}He at 98.7 MeV and 149.3 MeV, show no pronounced quasielastic peaks [We85, Wh90].

Generally, it has been observed that the quasielastic peak becomes more pronounced with increasing bombarding energy. Furthermore, as the angle increases, the width of the quasielastic peak broadens, the magnitude of the peak drops, and the centroid moves with free NN kinematics. This kinematic behaviour is in contrast to that for the discrete states, which move with the kinematics of a nucleon striking a heavy target, that is, with nucleon–nucleus kinematics. The above–mentioned features are beautifully illustrated in Figs. 2.2 and 2.3, which display inclusive spectra for (p,p') and (p,n) scattering, at various laboratory scattering angles, and incident proton energies of 400 MeV and 392 MeV, respectively. Also, note the striking similarity between the quasielastic peak positions for the ^{2}H data (which essentially represents free NN scattering [Sa94]) and the ^{12}C data.

Note, from Figs. 2.2 and 2.3, that at low excitation energies the quasielastic region overlaps with giant resonances and some low–lying discrete–state transitions: At high excitation energies the inclusive (p,n) spectra exhibit sharp cut-offs due to experimental limitations. For a quantitative analysis of quasielastic scattering, it is necessary to obtain stand–alone quasielastic spectra that are free from mixing with the low–lying structures, and which may be extrapolated into the high excitation energy region. For these purposes, a useful semiphenomenological parametrization of the empirical quasielastic peak has been developed by Wang [Wa93, Wa94]: the latter encompasses a semiphenomenological Lorentzian function which consistently describes all inclusive (p,n) spectra at 186 MeV for all targets and scattering angles. In addition, a number of phenomenological approaches have also been developed for studying the systematics of quasielastic scattering, so as to provide reliable estimates of the continuum background under the giant resonances: see, for example, Refs. [Mc86, Ch89, Sw89].

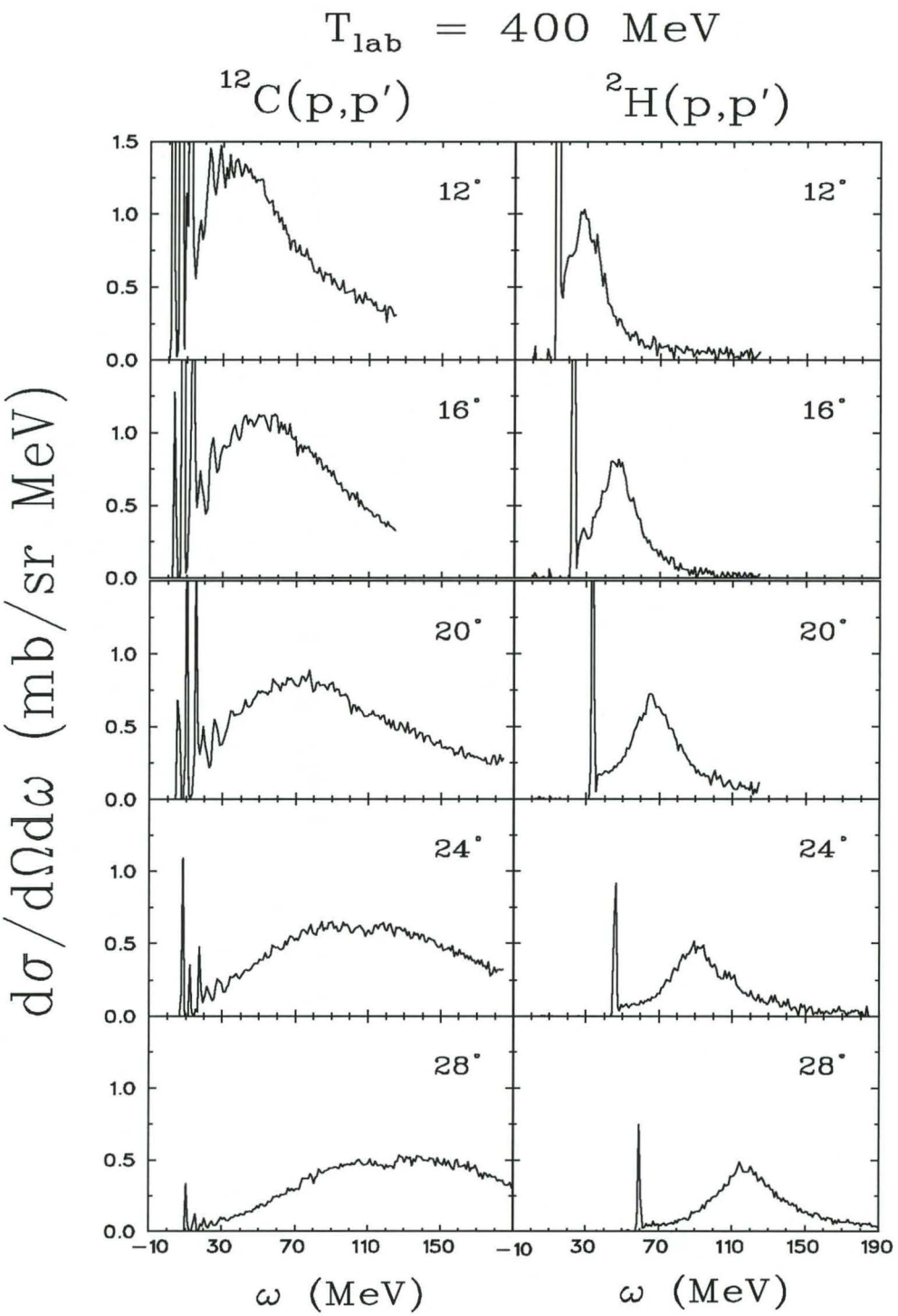

Figure 2.2: Double differential cross sections $\frac{d\sigma}{d\Omega d\omega}$ (in mb sr^{-1} MeV^{-1}) for inclusive (p,p') scattering from ^{12}C and ^{2}H at 400 MeV, as a function of the energy transferred to the nucleus (ω), for various laboratory scattering angles. The data are from Ref. [Ot97a].

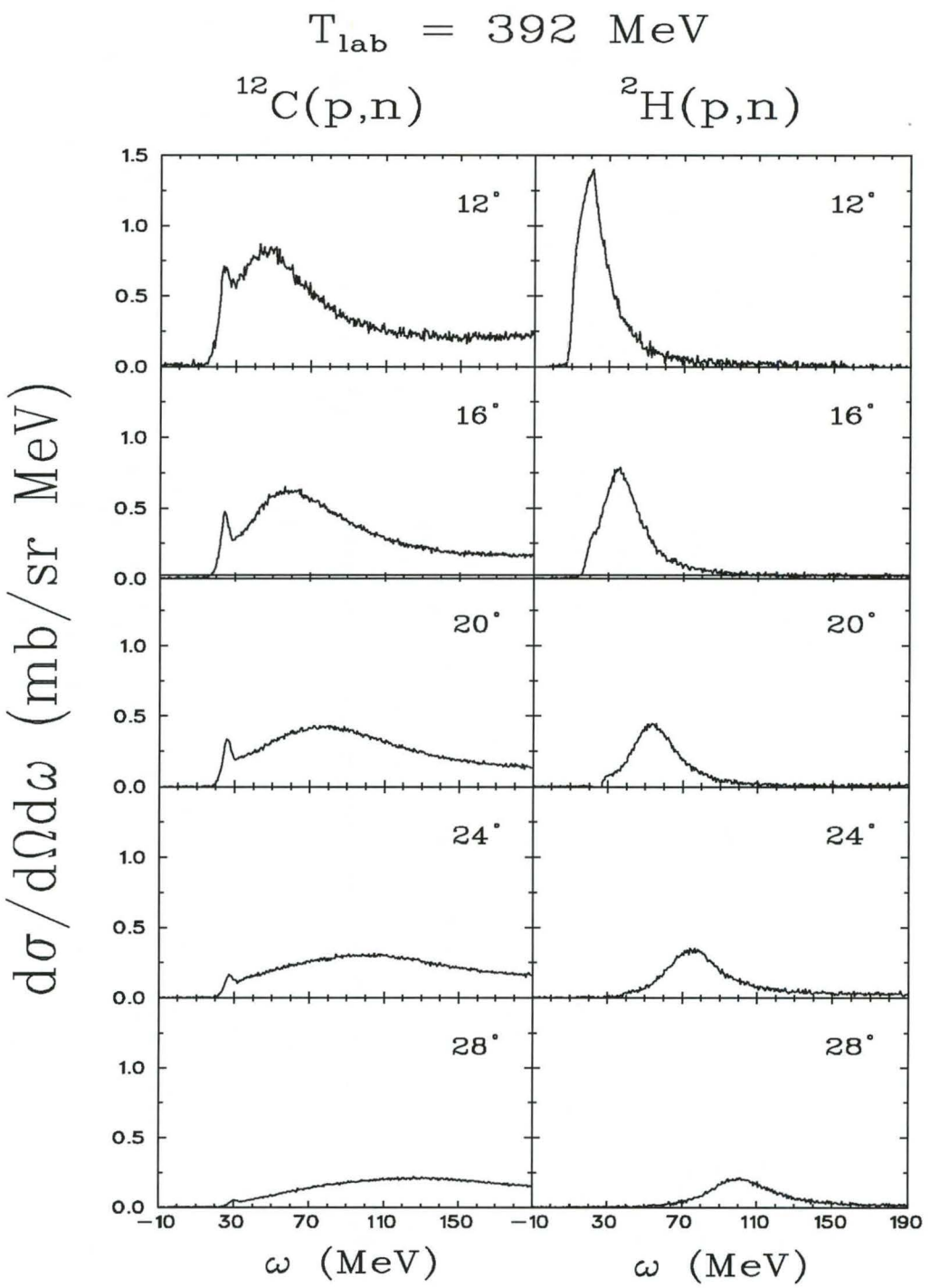

Figure 2.3: Double differential cross sections $\frac{d\sigma}{d\Omega d\omega}$ (in mb sr^{-1} MeV^{-1}) for inclusive (p,n) scattering from ^{12}C and ^{2}H at 392 MeV, as a function of the energy transferred to the nucleus (ω), for various laboratory scattering angles. The data are from Ref. [Ot97a].

Recently, Kalbach [Ka90] has studied and parametrized the systematics of quasifree (p,p') and (p,n) spectra for a range of scattering angles and target nuclei, at incident proton energies between 100 – 1000 MeV. The following phenomenological trends are observed:

- The position of the quasielastic peak closely tracks free NN kinematics. At incident energies above 400 MeV, the (p,p') quasielastic peak occurs at very nearly the energy calculated for free scattering, while the (p,n) quasielastic peak occurs 40 to 45 MeV below the free value. As the incident energy decreases, the peaks for the two reactions approach the same energy loss value.

- The shape of the quasielastic peak is typically asymmetric (or Lorentzian–shaped [Wa93, Wa94]), with the low energy–loss side usually somewhat wider than the high energy–loss side. The width of the peak generally increases with increasing emission angle up to at least 50° in the NN centre–of–mass. The general behaviour of the peak widths is parametrized in terms of the incident energy and $\sin\theta$ in the NN centre–of–mass.

- The quasielastic peak positions and peak widths do not vary significantly or systematically with target mass.

- The angle–integrated cross section is described in terms of a peripheral interaction with a single nucleon in the target nucleus, and has a threshold of 150 – 200 MeV. For (p,p') scattering, the cross section roughly varies as $A^{1/3}$, whereas for (p,n) scattering, for which the projectile must strike a neutron in the target, the cross section varies approximately as $(\frac{N}{Z})\,A^{1/3}$.

Besides the peaks exhibited by quasielastic proton spectra, inclusive studies carried out with other projectiles also show strong quasielastic peaks. For example, (e,e'), (π,π') and $(^3\mathrm{He},t)$ reactions exhibit very pronounced quasielastic peaks for a range of target nuclei. Fig. 2.4 shows the energy loss ω of the centroid of the quasielastic peak versus three–momentum transfer $|\vec{q}|$ for different probes on a ^{12}C nucleus [Ga90]. The quasielastic peak for (e,e') scattering behaves just like that obtained in the (p,n) reaction, that is, shifted about 30 MeV towards higher excitation energy, while that of the (p,p') reaction follows precisely the relation for free scattering (indicated by the solid line), namely $\omega = \frac{|\vec{q}|^2}{2m}$ (see Appendix I), where m is the rest mass of a nucleon. The difference in quasielastic peak positions for the (p,p') and (p,n) reactions

has been explained through sum rules Refs. [Wa82, Pa94]; Distortions could also explain the difference [De91, De93].

Until the early eighties, most studies of quasielastic scattering focused on the interpretation of *unpolarized* double differential cross sections. More recently, however, the emphasis has shifted towards studying complete sets of polarization transfer observables, namely P, A_y, D_{nn}, $D_{s's}$, $D_{\ell'\ell}$, $D_{\ell's}$ and $D_{s'\ell}$, for both quasielastic $(\vec{p},\vec{p}\,')$ and $(\vec{p},\vec{n})$ scattering: In each $D_{i'j}$ the primed and unprimed subscripts refer to outgoing and incoming spin directions, respectively (see Appendix G). Together with the unpolarized double differential cross sections, the polarization transfer observables provide extremely stringent tests of theoretical models for quasielastic proton scattering.

2.4 Polarization data for quasielastic proton scattering

With the recent developments in polarized proton beams and high resolution spectrometers with focal plane polarimeters, it is now possible to measure complete sets of quasielastic polarization observables (see Appendix G) in which incident proton beams polarized in an arbitrary orientation are utilized, to determine all the components of the polarization of the scattered protons.

The aim of this section is to give an overview of existing polarization transfer observable data for quasielastic $(\vec{p},\vec{p}\,')$ and $(\vec{p},\vec{n})$ reactions for incident proton energies between 100 MeV and 800 MeV. In addition to the usual polarization transfer observables $D_{i'j}$, more recently, attention has also shifted to other polarization observables, such as the spin–longitudinal and spin–transverse nuclear responses; this is briefly discussed in Sec. 2.4.3.

2.4.1 Polarization transfer observables

Tables 2.1 and 2.2 list the quasielastic $(\vec{p},\vec{p}\,')$ and $(\vec{p},\vec{n})$ polarization data, respectively, for incident laboratory kinetic energies $T_{\rm lab}$ between 100 MeV and 800 MeV, where σ refers to the unpolarized double differential cross section $\frac{d\sigma}{d\Omega dE}$, P is the induced polarization, A_y is the analyzing power, $D_{i'j}$ denotes complete sets of polarization transfer observables [$D_{0n} = A_y$,

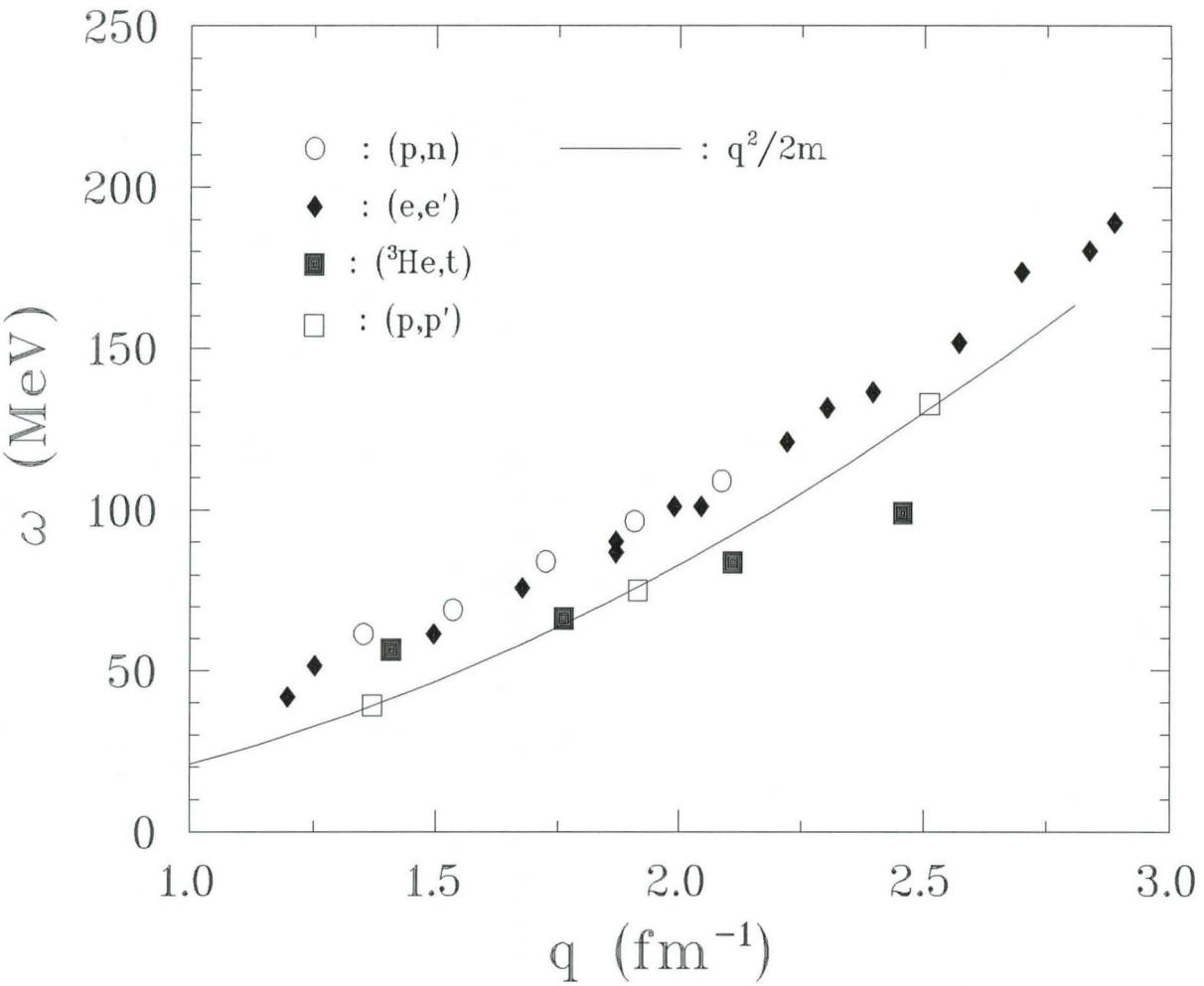

Figure 2.4: The centroid energy of the quasielastic peak for ^{12}C as observed in different reactions, plotted as a function of laboratory energy–loss ω versus three–momentum transfer $q = |\vec{q}|$. The data are from Ref. [Ga90].

D_{nn}, $D_{s's}$, $D_{\ell'\ell}$, $D_{s'\ell}$ and $D_{\ell's}$ – see also Appendix G], and $\theta_{\rm lab}$ denotes the laboratory scattering angle, unless otherwise specified.

The first measurements of complete sets of quasielastic polarization transfer observables $D_{i'j}$ for $(\vec{p},\vec{p}')$ and $(\vec{p},\vec{n})$scattering, for targets heavier than ^{2}H, were done as recently as 1984 [Ca84] and 1991 [Ta91], respectively. Currently a number of experimental programs are in progress at RCNP (Research Centre for Nuclear Physics, Osaka, Japan) and IUCF (Indiana University Cyclotron Facility, Bloomington, Indiana, USA) to measure complete sets of polarization transfer observables for both $(\vec{p},\vec{p}')$ and $(\vec{p},\vec{n})$ reactions [Sa96, Ra98].

2.4.2 Empirical features of polarization data

Unfortunately, Kalbach's [Ka90] phenomenological analysis has not yet been extended to polarization data. With the current availability of polarization data, it would be a useful exercise to study the systematics thereof. Some of the interesting features exhibited by inclusive $(\vec{p},\vec{p}')$ polarization data in Table 2.1, for energy losses spanning the quasielastic peak, are summarized below:

- Within the experimental uncertainty, the 200 MeV analyzing power data on ^{60}Ni and ^{208}Pb, for scattering angles between 6° and 20°, are identical [Li84]. The measured values fall somewhat below the free NN values, but the overall trend with angle follows the kinematics for free NN scattering.

- The analyzing power for ^{2}H, ^{4}He, ^{12}C and ^{40}Ca, at 200 MeV and 30°, is suppressed relative to the free NN values. Qualitatively, the latter suppression follows the trend of the nuclear density in that it appears to increase monotonically from ^{2}H to ^{40}Ca [Ca95, Ca95a].

- For scattering angles less that 10°, the analyzing power for ^{208}Pb at 290 MeV is identical to the corresponding values for free NN scattering [Ch88, Ch89a]. Above 10°, the analyzing power falls appreciably below the free NN values. At 26° the analyzing power is almost constant above excitation energies of 80 MeV. The slope of the A_y with excitation energy is relatively small for all scattering angles below 26°.

- For a scattering angle of 20° at 290 MeV, the analyzing power for ^{54}Fe, which is identical to the induced polarization P, is reduced relative to the corresponding free NN value. The

Table 2.1: List of quasielastic $(\vec{p},\vec{p}\,')$ polarization transfer observables measured at incident laboratory kinetic energies $T_{\rm lab}$ below 800 MeV, where σ is the unpolarized double differential cross section, P is the induced polarization, A_y is the analyzing power, $D_{i'j}$ denotes complete sets of polarization transfer observables [$D_{0n} = A_y$, D_{nn}, $D_{s's}$, $D_{\ell'\ell}$, $D_{s'\ell}$ and $D_{\ell's}$ – see also Appendix G], and $\theta_{\rm lab}$ denotes the laboratory scattering angle, unless otherwise specified.

$T_{\rm lab}$ [MeV]	Observables	Target	$\theta_{\rm lab}$ [degrees]	References
50	σ, A_y	^{58}Ni	$\geq 6°$	[Sa83a]
60	σ, A_y	^{58}Ni	15° – 40°	[Ko76]
65	σ, A_y	^{6,7}Li	6° – 85°	[To87]
65	σ, A_y	^{12}C, ^{28}Si, ^{45}Sc, ^{58}Nb	20° – 150°	[Sa80]
65	σ, A_y	^{156}Ho, ^{166}Er, ^{209}Bi	20° – 150°	[Sa80]
80	σ, A_y	^{58}Ni	$\geq 6°$	[Sa83a]
100	σ, A_y	^{2}H, ^{3,4}He, ^{12}C, ^{58}Ni	17.5°, 30°, 45°, 60°	[We85]
100	σ, A_y	^{3,4}He	0° – 34°	[Ed94]
150	σ, A_y	^{2}H, ^{3,4}He, ^{12}C, ^{58}Ni	17.5, 30°, 45°, 60°	[We85]
150	σ, A_y	^{24}Mg, ^{40}Ca, ^{51}V	5° – 140° in 5° steps	[St97]
165	σ, A_y	^{24}Mg, ^{40}Ca, ^{51}V	5° – 140° in 5° steps	[St97]
186	σ, A_y	^{24}Mg, ^{40}Ca, ^{51}V	5° – 140° in 5° steps	[St97]
200	σ, $D_{i'j}$	^{60}Ni, ^{90}Zr, ^{208}Pb	6° – 20° in 2° steps	[Li84]
200	σ, A_y, D_{nn}	^{40}Ca	30°	[Ma93a, Ca95]
200	σ, A_y	^{3,4}He	0° – 34°	[Ed94]
200	σ, P, A_y, D_{nn}	^{2}H, ^{3,4}He	30°	[Li94]
200	σ, A_y	^{2}H, ^{12}C	30°	[Ca95]
200	σ, A_y	^{2}H, ^{3,4}He	20°, 30°, 40°	[Gu95]
290	σ, $D_{i'j}$	^{12}C	29.5°	[Ch90]
290	σ, A_y	^{208}Pb	4° – 26°	[Ch88, Ch89a]
290	σ, $D_{i'j}$	^{54}Fe	20°	[Ha88, Ha91]
316	σ, A_y	^{12}C	119° – 157°	[Ka78]
400	σ, A_y	^{116}Sn, ^{208}Pb, ^{90}Zr	$< 6°$	[Mo82]
400	σ, A_y	^{2}H, ^{6,7}Li, ^{9}Bi	12° – 28° in 4° steps	[Ot97a, Ot97b]
400	σ, A_y	^{12,13}C, $^{\rm nat}$Ca, $^{\rm nat}$Cu	12° – 28° in 4° steps	[Ot97a, Ot97b]
400	σ, A_y	^{181}Ta, $^{\rm nat}$Pb	12° – 28° in 4° steps	[Ot97a, Ot97b]
420	P, D_{nn}, $D_{s's}$, $D_{\ell's}$	^{12}C, ^{16}O	23.5°	[Ch89]
420	σ, $D_{i'j}$	^{12}C	23.5°	[Ch90]
500	σ, A_y	^{12}C	119° – 157°	[Ka78]
500	σ, A_y	^{4}He, ^{58}Ni, ^{181}Ta	65°, 90°, 120°, 160°	[Ro81]
500	σ, A_y	^{116}Sn, ^{208}Pb, ^{90}Zr	$< 6°$	[Mo82]
500	σ, $D_{i'j}$	^{2}H, $^{\rm nat}$Ca, $^{\rm nat}$Pb	18.5°	[Ca84, Re86]
500	σ, A_y	^{208}Pb	4° – 26°	[Ch89a]
500	σ, $D_{i'j}$	^{2}H	22.4° – 55.4° †	[Ma86]
800	σ, A_y	^{116}Sn, ^{208}Pb, ^{90}Zr	$< 6°$	[Mo82]
800	σ, A_y	^{1}H, ^{12}C	5, 11°, 15°, 20°	[Mc84]
800	σ, $D_{i'j}$	^{1}H, ^{2}H, ^{12}C	5°, 11°, 20°	[Fe88]
647	σ, $D_{i'j}$	^{2}H	46.9° – 118.0° †	[Ba89]
800	σ, $D_{i'j}$	^{2}H	58.3° – 110.0° †	[Ba89]

† Scattering angle specified in NN centre–of–mass system

Table 2.2: List of quasielastic $(\vec{p},\vec{n})$polarization transfer observables measured at incident laboratory kinetic energies $T_{\rm lab}$ below 800 MeV, where σ is the unpolarized double differential cross section, P is the induced polarization, A_y is the analyzing power, $D_{i'j}$ denotes complete sets of polarization transfer observables [$D_{0n} = A_y$, D_{nn}, $D_{s's}$, $D_{\ell'\ell}$, $D_{s'\ell}$ and $D_{\ell's}$ – see also Appendix G], and $\theta_{\rm lab}$ denotes the laboratory scattering angle, unless otherwise specified.

$T_{\rm lab}$ [MeV]	Observables	Target	$\theta_{\rm lab}$ [degrees]	References
186	σ, P, A_y, $D_{n\,n}$	^{6,7}Li, ^{10,11}B	15.1°, 20.0°	[Wa93, Wa94]
186	σ, P, A_y, $D_{n\,n}$	^{12,13}C	15.1°, 20.0°	[Wa93, Wa94]
200	σ, $D_{i'\,j}$	^{2}H, ^{3,4}He, ^{12}C	13°, 37°	[Ra98]
200	σ, $D_{i'\,j}$	$^{\rm nat}$Ca, $^{\rm nat}$Pb	13°, 24°37°, 48°	[Ha98]
200	σ, $D_{i'\,j}$	^{2}H, ^{12}C	24°, 48°	[Ra98]
200	σ, A_y	^{3}He, ^{4}He	30°	[Pa98]
290	σ, A_y	^{12}C, ^{54}Fe	20.4°, 27.0° (for ^{12}C)	[Hi93]
295	σ, A_y	^{2}H, ^{12}C, ^{40}Ca	15° – 35° in 5° steps	[Ot97a]
346	σ, P, $D_{i'\,j}$	^{2}H, ^{10}Li, ^{12}C	22°	[Wa96]
346	σ, P, $D_{i'\,j}$	^{40}Ca, ^{208}Pb	22°	[Wa96]
392	σ, A_y	^{2}H, ^{6,7}Li, ^{9}Bi	12° – 28° in 4° steps	[Sa94, Ot97a, Ot97b]
392	σ, A_y	^{12,13}C, $^{\rm nat}$Ca	12° – 28° in 4° steps	[Sa94, Ot97a, Ot97b]
392	σ, A_y	$^{\rm nat}$Cu	12° – 28° in 4° steps	[Sa94, Ot97a, Ot97b]
392	σ, A_y	^{181}Ta, $^{\rm nat}$Pb	12° – 28° in 4° steps	[Sa94, Ot97a, Ot97b]
420	σ, A_y	^{12}C, ^{54}Fe	24.0°	[Hi93]
495	σ, $D_{i'\,j}$	^{2}H, ^{12}C, ^{40}Ca	18°	[Ta91]
495	σ, A_y	^{2}H, ^{12}C, $^{\rm nat}$Pb	9° – 22°	[Ta91a, Pr95]
495	σ, $D_{i'\,j}$	^{2}H, ^{12}C, ^{40}Ca	12.5°, 18°, 27°	[Mc92, Ch93, Ta94]
500	σ, $D_{i'\,j}$	^{2}H	22.4° – 55.4° †	[Ma86]
647	σ, $D_{i'\,j}$	^{2}H	46.9° – 118.0° †	[Ba89]
795	σ, A_y	^{2}H, ^{12}C, $^{\rm nat}$Pb	9° – 18°	[Ta91a, Pr95]
800	σ, $D_{i'\,j}$	^{2}H	58.3° – 110.0° †	[Ba89]

† Scattering angle specified in NN centre–of–mass system

most striking feature of the data is the variation (mainly a decrease) of the polarization transfer observables with increasing excitation energy [Ha88].

- For ^{12}C, and scattering angles of 29.5° at 290 MeV, and 23.5° at 420 MeV, the symmetry relations amongst the polarization transfer observables for time–reversal invariance, which are strictly applicable only to free NN elastic scattering, are valid over the full width of the quasielastic peak [Ch90]. The induced polarization P is identical to the analyzing power A_y, and both are quenched relative to the corresponding free values.

- The A_y data of Otsu et al. [Ot97a, Ot97b] at 295 and 392 MeV are reduced compared to the corresponding free values.

- For a scattering angle of 23.5° at 420 MeV, all polarization transfer observables for ^{12}C and ^{16}O are identical. The variation of the polarization transfer observables as a function of excitation energy is smooth and without structure [Ch89].

- The polarization transfer observables (excluding A_y) for ^{2}H and ^{208}Pb, at 500 MeV and 18.5°, are identical [Ca84].

- For scattering angles less than 15°, the analyzing powers for ^{116}Sn at 800 MeV, ^{90}Zr at 500 MeV, and ^{208}Pb at 400 MeV, are similar to the corresponding free NN values [Mo82].

- At 800 MeV, the polarization transfer observables for ^{1}H, ^{2}H and ^{208}Pb are similar for scattering angles 5°, 11° and 20° [Fe88]. The variation of the polarization transfer observables as a function of excitation energy is smooth and without structure.

Some of the interesting features exhibited by inclusive $(\vec{p},\vec{n})$ polarization data in Table 2.2, for energy losses spanning the quasielastic peak, are summarized below:

- At an incident energy of 186 MeV for a variety of p–shell nuclei (^{6,7}Li, ^{10,11}B, ^{12,13}C), the A_y data show a slight enhancement relative to the free NN values. The D_{nn} data at 15° are close to the free NN values, while at 20° the data in the quasielastic region (excitation energies greater than 30 MeV) are higher than the free values. In the lower excitation region (less than 30 MeV), interference between quasielastic scattering and the giant resonances makes the polarization observables change more drastically than in the

"pure" quasielastic region. Also, the induced polarization P is almost identical to the analyzing power A_y [Wa94].

- At 200 MeV, the A_y data for ^{3}He are similar to those for free NN scattering, whereas for ^{4}He the A_y data are generally larger than the free values [Pa98].

- The A_y data of Otsu et al. [Ot97a, Ot97b] at 295 and 392 MeV are slightly enhanced compared to the corresponding free values.

- Sakai et al. [Sa94] have measured double differential cross sections and analyzing powers for quasielastic $(\vec{p},\vec{n})$ scattering from a variety of targets ranging from ^{2}H to ^{nat}Pb (^{6,7}Li, ^{nat}Be, ^{nat}C, ^{nat}Ca, ^{nat}Cu, ^{nat}Ta, ^{nat}Pb), and for a wide range of scattering angles corresponding to momentum transfers ranging from 1.0 fm^{-1} to 2.4 fm^{-1}, at incident proton energies of 300 and 400 MeV. The excitation energy of the quasielastic peak for the ^{2}H reaction almost coincides with that expected for free NN scattering. Thus, the neutron in a deuteron behaves like a free neutron. Energy shifts of the quasielastic (p,n) peak from that of ^{2}H to higher excitation energy is observed for all the targets studied at 300 MeV and 400 MeV, with a gradual increase with target mass reaching almost a constant value of ~26 MeV beyond ^{12}C. The neutron–number dependence of the effective neutron number N_{eff} (see Sec. 3.2.7 in Chapter 3) for the (p,n) quasielastic scattering process is well represented by $N_{eff} = 0.85\,N^{0.5}$ over a wide mass range from ^{2}H to ^{nat}Pb, except for ^{6,7}Li and ^{9}Be which deviate significantly. The quasielastic analyzing powers for the ^{2}H$(\vec{p},\vec{n})$ reaction are almost identical to the free NN values. However, the analyzing powers for the ^{12}C$(\vec{p},\vec{n})$ and ^{40}Ca$(\vec{p},\vec{n})$ reactions behave very differently. In the range of small scattering angles ($|\vec{q}| \leq 1.5$ fm^{-1}) they agree with those of the ^{2}H$(\vec{p},\vec{n})$ reaction, while they are significantly reduced at large angles ($|\vec{q}| \geq 2$ fm^{-1}).

- At 346 MeV and 22°, the analyzing power A_y and induced polarization P are virtually identical for ^{2}H, ^{6}Li, ^{40}Ca and ^{208}Pb [Wa96]. The latter is not true for ^{12}C. All the polarization transfer observables (for ^{2}H, ^{6}Li, ^{12}C, ^{40}Ca and ^{208}Pb), except $D_{n\,n}$, show no target dependence, and essentially agree with the free values. This is beautifully illustrated by the data of Wakasa et al. [Wa96] in Fig. 2.5.

- The A_y data for ^{12}C at 420 MeV and 24.0° follow a different trend in excitation energy than for ^{54}Fe at the same angle and beam energy [Hi93]. At the quasielastic peak, the

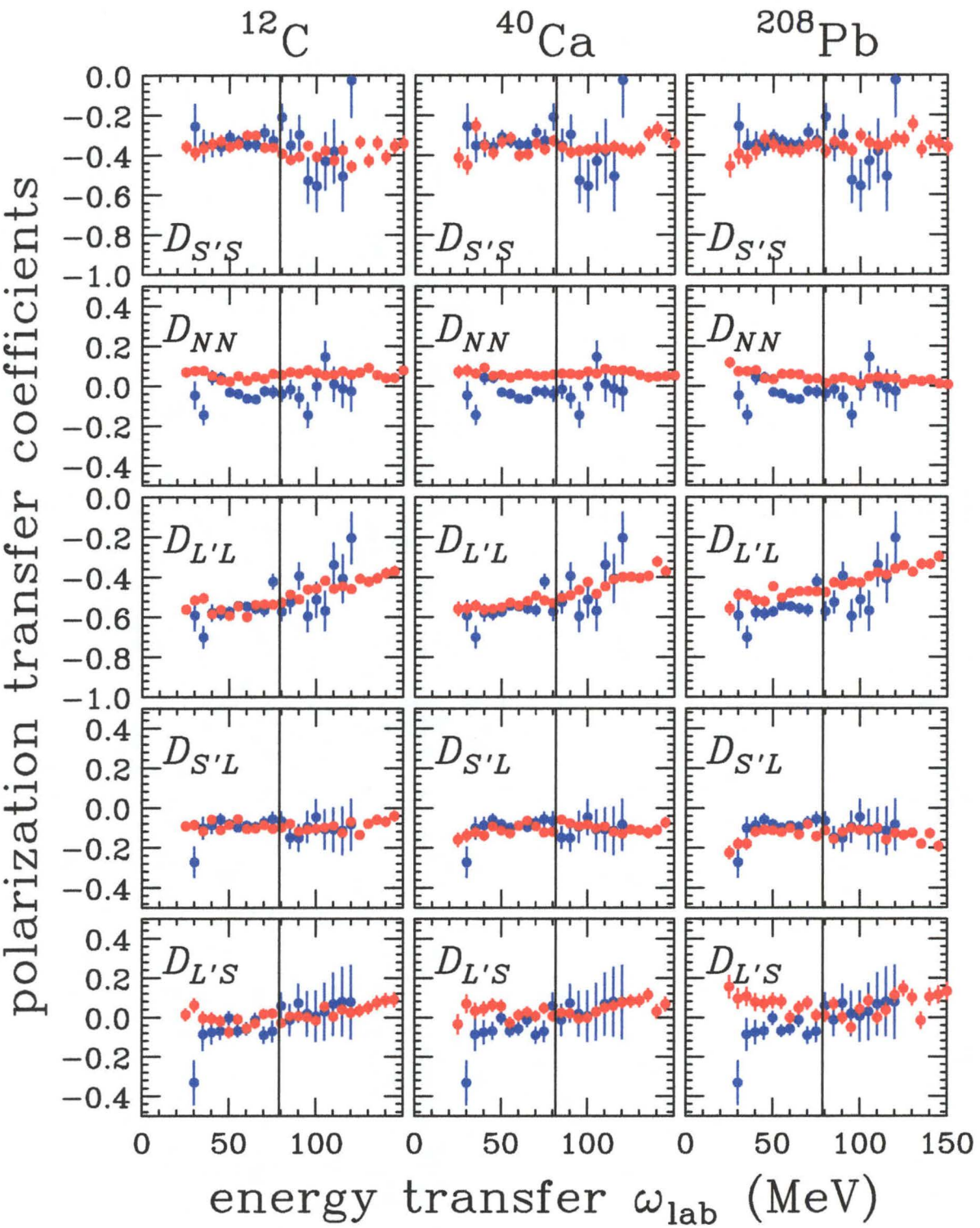

Figure 2.5: Polarization transfer observables (or coefficients) $D_{s's}$, $D_{n,n}$, $D_{\ell'\ell}$, $D_{s'\ell}$ and $D_{\ell's}$ for quasielastic ^{2}H$(\vec{p},\vec{n})$ (blue/black data points), ^{12}C$(\vec{p},\vec{n})$ (red/grey data points), ^{40}Ca$(\vec{p},\vec{n})$ (red/grey data points), and ^{208}Pb$(\vec{p},\vec{n})$ (red/grey data points) scattering at $T_{\rm lab}$ and 22°. The vertical solid lines mark the energy–loss of the centroid of the experimental quasielastic peak. The data are from Ref. [Wa96].

A_y data for ^{12}C and ^{54}Fe, at both incident energies of 290 and 420 MeV, are close to the free NN values. At both incident energies of 290 MeV and 420 MeV, the analyzing power data for ^{54}Fe are more steeply sloped as a function of excitation energy, than the corresponding ^{12}C data, suggesting the importance of structure effects. The A_y data for both ^{12}C and ^{54}Fe at 420 MeV exhibit trends that are closer to what is expected from quasielastic scattering than the 290 MeV data.

- Polarization transfer observables for ^{2}H, ^{12}C and ^{40}Ca, at 495 MeV and 18°, are virtually identical. Also, the induced polarization P is almost identical to the analyzing power A_y [Mc92, Ch93].

- The A_y data for ^{12}C and ^{208}Pb, at incident energies of 495 and 795 MeV, show a slight enhancement relative to corresponding free NN values [Ta91a]. The angular dependence of the centroid of the quasielastic peak tracks very well with free NN scattering.

- The analyzing power for ^{12}C at 495 MeV, for angles between 9° and 22°, is consistent with the free charge–exchange value [Pr95]. The analyzing power for ^{12}C at 795 MeV, however, is on average significantly below the free value. On the other hand, the analyzing power for ^{nat}Pb at 795 MeV is consistent with the free NN value.

In general, it is seen that for excitation energies spanning the quasielastic peak, and for scattering angles where the quasielastic peak is well above the low–lying resonances and well below the quasielastic–Δ peak, the variation of both $(\vec{p},\vec{p}')$ and $(\vec{p},\vec{n})$ polarization transfer is smooth without any structure. As the momentum transfer decreases, so the polarization transfer observables start to exhibit pronounced slopes as a function of excitation energy. Furthermore, for quasielastic $(\vec{p},\vec{n})$ scattering most polarization transfer observables are consistent with free NN scattering. For $(\vec{p},\vec{p}')$ scattering, however, the analyzing power is reduced relative to the values for free NN scattering.

2.4.3 Combinations of polarization transfer observables

Recently, several papers [Bl82, Mo82a, Ic92] have defined a new set of polarization observables (D_0, D_x, D_y, D_z) which are appropriate for investigating specific spin channels in inelastic scattering to discrete states, and also for studying inclusive quasielastic $(\vec{p},\vec{p}')$ and $(\vec{p},\vec{n})$ reactions

[Bl82, Ca84, Re86, Fe88, Ch90, Mc92, Mo82a, Ic92, Os92, Ch93, Ra94, Ta94, Wa96, Ha98]. These new polarization observables merely represent an alternative parametrization of experimental results, and are expressed as linear combinations of the conventional polarization transfer observables $D_{i'j}$ (excluding A_y) defined in Appendix G. The advantage of using this parametrization is that the experimental longitudinal and transverse spin–flip probabilities are now directly related (albeit in a model–dependent way) to the theoretical spin–longitudinal and spin–transverse nuclear response functions, whose interpretation is currently the focus of much theoretical activity (see the references cited above).

The disadvantage in studying the spin–longitudinal and spin-transverse nuclear response functions is that the "experimentally" extracted quantities are model–dependent, and hence do not represent true experimental data [Sh88]. Apart from experimental uncertainties, there are several potential sources of systematic errors in the absolute magnitude of the separated responses [Ch93], for example, the model dependence associated with the calculation of distortion factors [Ic97], uncertainties introduced by the choice of the phase–shift solution used to generate the NN amplitudes, and multiple scattering effects. *Although a lot of interesting physics can be extracted from studies of spin–longitudinal and spin-transverse nuclear response functions, this project rather focuses on understanding complete sets of polarization transfer observables, the latter being directly measured by experimentalists. Once these are properly understood, it would seem more appropriate to study spin–longitudinal and spin–transverse nuclear response functions.*

2.5 Why is it important to study quasielastic scattering?

The aim of this section is to briefly mention some of the interesting physics issues which are studied via quasielastic $(\vec{p},\vec{p}')$ and $(\vec{p},\vec{n})$ reactions. For more detailed information, the reader is encouraged to consult the references cited below.

- The cross sections leading to bound states of the residual nucleus comprise only a small portion of the total cross section, whereas the quasielastic region, on the other hand, constitutes a large fraction of the inclusive proton–nucleus spectrum. Hence, it is important that the mechanism for quasielastic scattering should be properly understood, and

included in the framework of theoretical models.

- Quasielastic $(\vec{p},\vec{p}')$ and $(\vec{p},\vec{n})$ reactions probe different parts of the NN interaction: $(\vec{p},\vec{p}')$ scattering probes both isovector and isoscalar parts of the NN interaction, whereas $(\vec{p},\vec{n})$ charge–exchange reactions sample only the isovector components, particularly those directly related to pion exchange [Wa94, Ho94]. Furthermore, since the Lorentz character of the isovector amplitudes is totally different from the isoscalar amplitudes, one expects quasielastic $(\vec{p},\vec{p}')$ and $(\vec{p},\vec{n})$ polarization transfer observables to yield different, but complementary, information about the spin–dependent components of the NN interaction (see Chapter 3). Hence, measurements of complete sets of polarization transfer observables for both quasielastic $(\vec{p},\vec{p}')$ and $(\vec{p},\vec{n})$ scattering provide stringent tests of current theoretical models.

- An important question in nuclear physics is how the nuclear environment modifies the scattering interaction between two nucleons. In free space, the NN interaction is well known. The recent interest in the role of relativity in nucleon–nucleus scattering [Ho86, Mu87a, Ho88, Iq88, Hi94, Hi95, Hi98] has suggested that the quasielastic polarization transfer observables may provide a clean signature of relativistic effects for the NN interaction in the nuclear medium. Hence, quasielastic reactions offer a means to study how the fundamental free NN interaction is modified by the surrounding medium of the nucleus in which it occurs. The latter topic is discussed in detail in Chapter 3.

- Quasielastic scattering can also be used to study the residual particle–hole interaction, which induces collective motion as the struck nucleon interacts with other target nucleons. Although signatures of shell structure, such as low–lying collective states and giant resonances, disappear at large excitation energies [Ch89, Wa96], the nucleus continues to respond collectively through the interaction of the residual particle–hole interaction. This collectivity does not manifest itself in sharp states or resonances, but in gross features of the spectrum, such as shifts in the position of the quasielastic peak and deviations of the polarization transfer observables from the free values [Sm88]. Quasielastic scattering, therefore, offers a means of studying the residual interaction in a region where it is currently not well known, namely at large energy– and momentum–transfers.

- One of the major aims of experiments performed in the quasielastic region is to separate

the spin–longitudinal from the spin–transverse nuclear response [Os92, Ra94]. Here an interesting question is whether the virtual pion field inside the nucleus is strong enough to cause a collective enhancement of the spin–longitudinal over the spin–transverse nuclear response. The existence of such a phenomenon would be very significant because of its direct relation to Migdal's original suggestion of the existence of a pion condensate at sufficiently high nuclear densities [Mi78]. The spin–longitudinal and spin–transverse nuclear response functions have simple connections to the exchange of ρ and π mesons between nucleons, and between nucleons and delta isobars, and hence are very relevant to current investigations into the effects of the isobar on nuclear properties. Beyond this, there are many issues connected with the spin–isospin resonances that carry over into the discussion of the role of quarks and gluons in the description of nuclear properties and interactions, such as the the so–called European Muon Colloboration (EMC) effect, for example [Ca84, Re86, Be93].

- Nuclear structure usually plays a minimal role in the quasielastic region [Ch89, Wa96] and, hence, from a theoretical point of view, quasielastic scattering is an attractive problem to study, that is, simple models of nuclear structure can be used.

- During the past few years, several studies [Sw89, Os92, Ra94] have demonstrated the usefulness of inelastic proton scattering at medium energies for the study of giant resonances. The continuum background under the giant resonances appears to be dominated by quasielastic scattering [Sw89]. The largest uncertainty in the determination of giant resonance strengths arises because of a lack of knowledge of the shape and magnitude of the underlying continuum [Be81] which needs to be subtracted. The empirical procedure often used in the past consists of representing the continuum shape with straight lines or smooth polynomial curves. Different choices of background can, however, lead to quite different resonance parameters. Hence, current progress in determining these parameters is closely coupled with the progress in modeling the quasielastic scattering to the nuclear continuum.

2.6 Models of quasielastic proton scattering

In order to extract detailed information on collectivity and medium–modified two–body interactions from experimental data, it is necessary to have a good theoretical handle on the important features of the reaction mechanism and the nuclear structure input. At small momentum– and energy–transfers, nuclear structure aspects can be incorporated into distorted–wave impulse approximation (DWIA) calculations either using a large–basis shell model or the random phase approximation. A large momentum– and energy–transfers, these calculations become more difficult and sometimes impossible to implement numerically [Sm88]. Approximate methods must be used. In this section, a brief overview is given of the successes and failures of various theoretical models which have been used for describing *both* the unpolarized double differential cross sections and polarization transfer observables for quasielastic $(\vec{p},\vec{p}')$ and $(\vec{p},\vec{n})$ reactions, for incident proton energies ranging between 100 MeV and 800 MeV, and for target nuclei greater or equal to ^{12}C. Additional, but less complete, reviews of the current status of quasielastic proton scattering can also be found in Refs. [Sm88, Os92, Ra94].

2.6.1 Simple Fermi–gas model

Perhaps the simplest, but yet most instructive, model is the simple Fermi–gas model of Bertsch and Scholten [Be82]. This model ignores nuclear structure (as suggested by the experimental data of Refs. [Ch89, Wa96]) and treats the nuclear ground state as a Fermi sea with all states below the maximum Fermi momentum k_F occupied. For quasielastic scattering, the struck nucleon is removed from the Fermi sea, and the recoiled ejectile is also left above the Fermi sea, that is, Pauli blocking is explicitly incorporated. Despite the simplicity of the Fermi–gas model, it does, however, provide a qualitative description of unpolarized double differential cross sections [Be82, Wa93, Wa94], as well as the most polarization transfer observables [Ch90]. For example, for quasielastic (p,n) scattering from p–shell nuclei at 186 MeV the simple Fermi–gas model qualitatively reproduces the centroid and width of the quasielastic double differential cross section [Wa93, Wa94]. For 420 MeV $(\vec{p},\vec{p}')$ scattering on ^{12}C, this simple model reproduces the general variation of the complete sets of polarization transfer observables with excitation energy, except for $D_{\ell' s}$ and $D_{s' \ell}$ [Ch90]. Generally, for light nuclei ($A \leq 7$), and small momentum transfers ($|\vec{q}| < \frac{k_F}{2}$), the simple Fermi–gas model breaks down and completely fails to describe

quasielastic scattering data [Be82, Wa93, Wa94].

2.6.2 Semi–infinite slab model (SISM)

Hadronic probes are strongly absorbed in the interior of a nucleus, and hence, quasielastic proton reactions are strongly surface peaked. A better description than the simple Fermi–gas model, which takes account of the surface nature of the reaction, is the semi–infinite slab model (SISM) of Bertsch, Esbenson, Scholten, and Smith [Be82, Es84, Es85, Es86, Sm88]: see Ref. [Sm88] for a review of the SISM plus subsequent modifications and extensions. In the original SISM model of Bertsch and Scholten [Be82], the nucleus is approximated as a semi–infinite slab of fermions. Absorption is treated via an approximate form of Glauber theory, and kinematic effects of Fermi motion and Pauli blocking are included. The SISM does not account for distortion effects other than eikonal attenuation of the initial and final nucleon waves. With the omission of distortions, the SISM reduces to the simple Fermi–gas model discussed in Sec. 2.6.1.

The SISM model has been applied successfully to a wide variety of intermediate energy reactions which proceed primarily via one–step NN collisions. The model has three notable features: it redistributes some of the effects of the single–scattering response into a long tail, it smoothes the response in the low–excitation Pauli–blocking region, and it includes the binding energy of the nucleus [Ta91a, Pr95]. A distinguishing feature of slab model calculations is that peak shapes are well reproduced. Compared to Fermi–gas calculations, the slab model puts a long tail on the high energy–loss side of the quasielastic peak and fills in the region of low energy loss where Fermi–gas calculations produce a sharp cutoff.

For large momentum transfers ($|\vec{q}| > k_F$) the predictions of the SISM and simple Fermi–gas model are similar, and qualitatively predict the essential features of inclusive unpolarized double differential cross sections [Be82]. Generally, it is seen that, at intermediate scattering angles, predictions of the SISM for quasielastic $(\vec{p},\vec{p}')$ scattering improve with increasing beam energy [Ch89a].

For quasielastic $(\vec{p},\vec{n})$ scattering from p–shell nuclei at 186 MeV [Wa93, Wa94], the SISM provides a good description of the shapes of the spectra, whereas the overall magnitudes are not correctly predicted and need a $|\vec{q}|$–dependent normalization. A similar result was obtained by

Swenson et al. [Sw89]: For (p,p') scattering on ^{208}Pb at 400 MeV, the SISM calculations had to be renormalized to fit inclusive data at high excitation energies above the giant resonances; It is not possible to fit the spectra at all the angles with the same renormalization factor.

Esbenson and Bertsch [Es84] extended the SISM to include one–particle–one–hole random phase approximation (RPA) correlations due to the nuclear medium. In particular, no account was taken of spin–orbit distortion. Esbenson, Toki and Bertsch [Es85a] adapted the latter model to study the ratio of spin–longitudinal to spin–transverse nuclear response functions for quasielastic $(\vec{p},\vec{p}')$ scattering. Compared to the 500 MeV $(\vec{p},\vec{p}')$ data of Refs. [Ca84, Re86] on ^{40}Ca and ^{208}Pb at $|\vec{q}| = 1.75$ fm^{-1}, which give a ratio of unity, the SISM model with RPA correlations overpredicts the data. With the omission of central distortions and RPA correlations, the SISM reduces to the simple Fermi–gas model.

Okuhara et al. [Ok87] pointed out that the assumption of a semi–infinite slab geometry is not altogether realistic, especially for lighter nuclei: there work indicates that finite geometry and absorption effects are crucial in bringing the ratio of spin–longitudinal to spin–transverse nuclear responses closer to the 500 MeV $(\vec{p},\vec{p}')$ data of Carey [Ca84].

Smith and collaborators modified the RPA SISM to include 2–particle–2–hole (2p2h) states as well as two–step processes [Sm88]. Häusser et al. [Ha88, Ha91] compared data for complete sets of polarization transfer observables, for quasielastic ^{56}Fe$(\vec{p},\vec{p}')$ scattering at 290 MeV and $|\vec{q}| = 1.75$ fm^{-1}, to the SISM results of Smith [Sm88]. The calculated observables $D_{s's}$, $D_{s'\ell}$, and $D_{\ell's}$ are predicted to be close to the free response values, showing little sensitivity to the residual interaction and to the inclusion of 2p2h damping or two–step processes. The SISM model of Smith et al. [Sm88] predicts D_{nn}, P, and A_y values which are substantially different from the free values. For the latter observables the slopes versus excitation energy are mainly caused by the residual interaction and are found to be in reasonable agreement with the data, although the absolute values for P and A_y are considerably larger than the data. Häusser et al. [Ha88] also find that the use of the Breit frame [Sm88], rather than the optimal frame, produces the wrong sign for the slopes of $D_{\ell'\ell}$ and $D_{s's}$.

Hicks et al. [Hi89] compared their quasielastic $(\vec{p},\vec{n})$ data (double differential cross sections and analyzing powers) measured for ^{12}C and ^{54}Fe targets at 290 MeV for a scattering angle of 20.4°, and at 420 MeV for a lab angle of 24.0°, to calculations using the nonrelativistic SISM

model of Smith [Sm88]. The shapes of the inclusive spectra as a function of excitation energy are in reasonable agreement with the model. It appears that the surface response model, which has been successful in predicting $(\vec{p},p')$ data [Ha88], is also adequate to describe the shape of the quasielastic charge exchange cross sections. The model does not, however, consistently reproduce the analyzing power data. Smith's RPA calculations are always very close to the free NN values of A_y, and cannot explain the enhancement (^{54}Fe data at 420 MeV) or suppression (^{54}Fe data at 290 MeV, and ^{12}C data at both 290 and 420 MeV) of the A_y data. For $^{12}C(\vec{p},\vec{p}')$ scattering at 800 MeV at scattering angles of 5°, 11° and 20° [Fe88], the SISM model of Smith [Sm88] yields qualitatively good agreement with all the polarization transfer data ($D_{n\,n}$, $D_{s'\,s}$, $D_{s'\,\ell}$, $D_{\ell'\,s}$), except for $D_{\ell'\,\ell}$ at 5°. The values of the polarization transfer observables at the quasielastic peak are often precisely predicted; far away from the calculated peak position, the agreement can become quite poor, as in $D_{\ell'\,s}$ at 5°, or $D_{\ell\,\ell}$ at 11°. With the accuracy of the data, typically about ±0.1, specific nuclear effects are essentially absent; the nucleus seems to behave approximately as a free Fermi–gas, and a single–step reaction mechanism seems sufficient [Fe88].

Smith and Wambach have developed a model for easily including the effects of 2p2h excitations in calculations of the nuclear response function at large momentum– and energy–transfers [Sm88a]. They analyzed $^{54}Fe(\vec{p},\vec{p}')$ data at 290 MeV [Ha88, Ha91], using the slab–model of Esbenson and Bertsch [Es84, Es86], and found improved agreement with spin–flip cross sections, although calculations underpredict the data above ~25 MeV excitation.

Prout et al. [Pr95] have performed calculations which are similar to the SISM of Ref. [Es85], and also include contributions from two–step scattering. Compared to cross section data for inclusive (p,n) scattering on ^{12}C and ^{nat}Pb at 495 MeV and 795 MeV [Pr95], the calculations are able to account very well for the shape, but not for the absolute magnitude, of the quasielastic peak at both energies and for both targets. The two–step contributions do not significantly alter the shapes of the calculations, but they do add substantial cross section at the largest momentum transfers.

2.6.3 Nonrelativistic eikonal approximation

Theoretical calculations by Tzeng and Tamura [Tz83], based on the eikonal approximation and utilizing spin–dependent amplitudes, provide a consistent description of quasielastic unpolarized

double differential cross sections and analyzing powers for $(\vec{p},p')$ data at 200 MeV [Li84], and 800 MeV [Mc84, Mc84a]. In general, the analyzing power predictions are enhanced relative to the data, particularly at large scattering angles.

Smith and Wallace [Sm85] have developed a formalism for calculating quasielastic $(\vec{p},\vec{p}')$ spin observables at incident energies larger than 800 MeV. They studied the spin dependence of quasielastic $(\vec{p},\vec{p}')$ scattering using Glauber's eikonal multiple scattering theory, which is extended to include multiple knockout collisions as well as the full spin dependence of the NN amplitudes. Calculations were done for both unpolarized double differential cross sections as well as complete sets of polarization transfer observables and compared to data (cross sections and analyzing powers) for $^{12}C(\vec{p},\vec{p}')$ scattering at 800 MeV [Ch80, Mc84, Mc84a]. The normalization of the quasielastic peak agrees well with the data, although the peak position is shifted towards larger energy loss. Such a shift had been seen before in PWIA and DWIA calculations [Kr70, Ch80]. Distortions have little effect on spin observables. The normalization of the analyzing power is a little off: $\sim$0.4 in the single knockout region compared to $\sim$0.3 in the data.

Brieva and Love have developed a nonrelativistic finite–nucleus model based on a local density approximation to the nuclear response, including nonlocal couplings and off–shell effects arising from the antisymmetrization of the NN interaction [Br90]. The model relies on the energy–dependent Franey–Love effective nucleon–nucleon interaction, the interacting Fermi–gas model, and the distorting nucleon–nucleus optical potential in a local density approximation. The distorting incoming and outgoing nucleon scattering wave functions are calculated in the eikonal approximation [Sm88, Br90]. By including the nonlocal couplings explicitly, they obtained an estimate for the range of validity of the "standard" model of quasielastic proton scattering [Be82, Es84, Ho88, Sm88], which assumes a direct relation between the inclusive double differential cross section and the nuclear response function. In addition, Brieva and Love also illustrated the level of uncertainty associated with the choice of the effective NN interaction used in calculating inclusive observables. Their calculations indicated that experimental results could be understood in terms of the nuclear response function with an uncertainty of $\sim$10 %. At incident energies near 100 MeV and below, the nonlocal couplings are much more important and cannot reliably be neglected. The sensitivity of inclusive nucleon scattering to the choice of the effective NN interaction was also found to be non–negligible. It is interesting to note that the exact calculations of Brieva and Love [Br90] for the analyzing power, for incident proton

energies between 100 MeV and 300 MeV, are suppressed relative to the corresponding free NN values. Thus far, Horowitz and collaborators [Ho86, Mu87a, Ho88, Iq88, Ho91b, Ho97], have attributed the latter suppression to relativistic medium modifications of the NN interaction. The predictions of Brieva and Love have yet to be compared to quasielastic $(\vec{p},\vec{p}')$ data.

Hicks et al. [Hi93] compared quasielastic $(\vec{p},\vec{n})$ data (unpolarized double differential cross sections and analyzing powers) measured for ^{12}C and ^{54}Fe targets at 290 MeV for a laboratory angle of 20.4°, and at 420 MeV for a laboratory angle of 24.0°, to the nonrelativistic calculations of Brieva and Love [Br90]. Shell effects accounting for the reaction Q–value, and target recoil were shown to be important for predicting the correct position of the quasielastic peak [Ta91]. The $(\vec{p},n)$ analyzing power data at the quasielastic peak are in fair agreement with these nonrelativistic predictions. The calculations do not, however, properly describe the analyzing power data for $(\vec{p},p')$ reactions in the quasielastic region.

2.6.4 Nonrelativistic random–phase approximation of the nuclear response

Based on a random–phase approximation calculation (RPA) in symmetric, infinite nuclear matter with one–pion exchange plus one–rho–meson exchange plus a contact interaction specified by the Landau–Migdal parameter g', the so–called $\pi + \rho + g'$ model, Alberico, Ericson and Molinari [Al82] predicted that, for momentum transfers larger than 1 fm^{-1} in the quasielastic region, the isovector nuclear responses to mesonic fields are expected to show an enhanced ratio of the spin–longitudinal to the spin–transverse nuclear response functions. However, analysis of a variety of $(\vec{p},\vec{p}')$ [Ca84, Re86, Fe88, Ha88, Ch90, Ch93] and $(\vec{p},\vec{n})$ [Mc92, Ta94, Ch93] data did not reveal the expected enhancement. Applications of the latter model [Al84], and the subsequent development of a random–phase approximation theory of the spin–isospin nuclear surface response by Alberico and collaborators [Al87, Al88], have failed to quantitatively describe the experimental data. Alberico et al. [Al82] suggest that the latter discrepancy could be attributed to distortion (mainly absorption) of the probe, finiteness of the nucleus, and a larger value of g'.

De Pace and Viviani [De93, De94] have calculated the spin–isospin responses within the continuum RPA framework. They employed an extension of the standard RPA to account for the spreading width of the single particle states through the inclusion of a complex and energy–

dependent nucleon self–energy. The nuclear responses were then used as the basic ingredient to calculate hadronic reactions in the Glauber theory framework. Both one– and two–step contributions to the multiple scattering series were taken into account. Predictions of the quasielastic peak position for (p,p') at 795 MeV scattering came out in the wrong position [Ch80]. The model of De Pace and Viviani could not consistently predict both (p,p') [Ch80] and (p,n) [Ta91] double differential cross sections at 795 MeV.

2.6.5 Nonrelativistic distorted wave models

Up to about 1989, the effects of distortion had been treated poorly (see Ref. [Ic89], and references therein). In most SISM [Al84, Re86] and local density approximation analyses [Sh86, Ok87], the effects of absorption had only been taken into account in terms of a Glauber approximation with straight line trajectories. The distortion of the trajectory and the spin reorientation during scattering were rarely included [Sm88]. There had been very few quantum mechanical calculations including distortions. Ichimura et al. [Ic89] developed the continuum random–phase approximation with the orthogonality condition (OCRPA) for calculations of spin–longitudinal and spin–transverse nuclear response functions. The model takes into account the finite size of the nucleus, the continuum nature of the single–particle states, and the damping of the particle states. Ichimura and collaborators compared their calculations of the ratio of the spin–longitudinal to the spin–transverse nuclear response functions to LAMPF data for quasielastic $^{40}\mathrm{Ca}(\vec{p},\vec{p}')$ scattering at 500 MeV, for various scattering angles [Ca84, Re86]. The combined effects of distortions, and the finiteness of the nucleus, reduced the ratio from the original SISM predictions [Es85a, Sh86]. The result is, however, still larger than the experimental ratio of unity.

Ichimura et al. [Ic94, Ni95] extended the model in Ref. [Ic89], to study the effects of Δ–isobars, the dependence on effective interactions, and the effects of distortion in scattering. This model provides a very poor description of the unpolarized inclusive cross section for $^{12}\mathrm{C}(p,n)$ at 495 MeV [Mc92, Ch93, Ta94]. The calculation not only fails to predict the location of the quasielastic peak correctly, but severely underestimates the unpolarized double differential cross section. It is seen that distortions reduce the ratio of spin–longitudinal to spin–transverse nuclear response functions, though the RPA makes the ratio too large. The experimental ratio

is reasonably well reproduced by free response functions (with no distortions and RPA correlations).

Taddeucci et al. [Ta94] compared their data for ratios of spin–longitudinal to spin–transverse nuclear response functions for quasielastic $(\vec{p},\vec{n})$ on ^{12}C and ^{40}Ca at 494 MeV (for scattering angles of 12.5°, 18° and 27°) to the calculations of Ichimura et al. [Ic89, Ic92a, Ni95]. Two cases were considered [Ta94]: calculations employing the full RPA response, and calculations where the residual interaction was set to zero (free response). The free response calculations gave a good description of the data at all three angles. While this result highlights the possible importance of distortion effects, the disagreement with the full RPA + DWIA ratios also suggests that some important physics is being missed by describing the reaction entirely in terms of single–particle responses.

McClelland [Mc92] and Chen [Ch93] compared their data for ratios of spin–longitudinal to spin–transverse nuclear response functions, for quasielastic $(\vec{p},\vec{n})$ on ^{12}C and ^{40}Ca at 495 MeV and 18°, to distorted wave calculations of Ichimura et al. [Ic89] with and without a random–phase approximation to the nuclear response. The data are in good agreement with calculations omitting the RPA calculations.

The experimental ratios of spin–longitudinal to spin–transverse nuclear response functions for quasielastic $(\vec{p},\vec{n})$ reactions at 346 MeV and 22° on ^{6}Li, ^{12}C, ^{40}Ca, and ^{208}Pb show no evidence of enhancement [Wa97], in contradiction with the calculations of Ichimura and collaborators [Ic94, Ni95].

In Ref. [Ic97], Ichimura investigated the effects of the finiteness of nuclear size, virtual Δ–excitation, removal of the universality ansatz, radial dependent effective masses, spreading widths of particle–hole states and correlations beyond RPA, on the response functions with RPA correlations. The extent to which distortions can be represented by the $N_{\rm eff}$ prescription [Ic92] for the extraction of response functions was also investigated. Ichimura concluded that distortion effects are not necessarily adequately represented by the $N_{\rm eff}$ prescription. Even considering the above mentioned effects and ambiguities, the large differences between theory and experiment could still not be explained.

The DWIA model of Chant and Roos [Ch77a, Ch83] has also been applied to analyze inclusive $(\vec{p},\vec{p}')$ unpolarized double differential cross sections and analyzing powers [Ch80, We85,

Ca95, Ca95a], as well as the depolarization parameter D_{nn} [Ma93], following the procedure of Wesick and collaborators [We85]. The calculations represent a quantum mechanical treatment of the scattering process, relying on the factorization approximation, and assuming the validity of the impulse approximation. Strong final state interactions are incorporated via scattering state wave functions which are solutions to the Schrödinger equation with complex, energy–dependent optical model potential (OMP) terms. The OMP parameters are generally fitted to elastic scattering data. Although the original DWIA model of Chant and Roos [Ch77a] was formulated to describe *exclusive* (p,pN) reactions (where N is either a proton or a neutron), the *inclusive* (p,p') observables are obtained by integrating the triple differential cross section, for (p,pN) scattering, over the solid angle of the unobserved nucleon N; the imaginary terms of the OMP for the associated nucleon are set to zero as there is no loss of flux if this particle is not observed [We85, Ca95, Ca95a]. For inclusive $(\vec{p},p')$ scattering on ^{4}He, ^{12}C, and ^{40}Ca at 200 MeV and 30° [Ma93, Ca95, Ca95a], these DWIA calculations provide a satisfactory description of the magnitude and the position of the double differential cross section and the depolarization parameter D_{nn} at the quasielastic peak. The DWIA calculations, however, overpredict the inclusive analyzing power data.

2.6.6 Relativistic plane wave impulse approximation (RPWIA)

Traditionally, reaction dynamics have been described in the framework of the Schrödinger equation using nonrelativistic or relativistic kinematics for intermediate energy reactions. More recently, however, considerable success has been obtained using the Dirac equation to describe elastic and inelastic proton scattering: see Chapter 1 for more detail.

A relativistic–plane–wave–mpulse–approximation (RPWIA) model for quasielastic proton scattering has been developed by Horowitz, Iqbal, and Murdock [Ho86, Mu87a, Ho88, Iq88, Ho91b, Ho97]. The RPWIA is based on a covariant form of the amplitudes describing the NN interaction, while the scattering is described through the use of the Dirac equation in infinite nuclear matter. In the nuclear medium the strong scalar potential enhances the lower two components of the four–component Dirac wave functions. Horowitz and Iqbal [Ho86, Iq88] developed a model in which this enhancement is parametrized by an effective mass m^* calculated in an eikonal approximation; this effective mass m^* is smaller than the free nucleon mass m,

due to the attractive scalar potential in the nuclear medium. These calculations were later extended by Horowitz and Murdock [Mu87a, Ho88, Ho91b, Ho97] to include averaging over Fermi–momentum distributions of the target nucleons.

The following experimental data have been compared to the RPWIA predictions of Horowitz and Murdock [Ho88]:

- Analyzing power data for quasielastic ^{208}Pb$(\vec{p},\vec{p}')$ scattering at 290 and 500 MeV (for scattering angles between 4° and 27°) [Ch88, Ch89a]: For free scattering, that is $m^* = m$, the calculations overpredict the analyzing power data, whereas the relativistic m^* calculations are in acceptable agreement with the analyzing power at the quasielastic peak. The successful prediction of A_y at both 290 and 500 MeV has been attributed to the relativistic m^* effect.

- Unpolarized double differential cross sections for quasielastic ^{208}Pb(p,p') scattering at 400 MeV (for scattering angles between 5° and 15°) [Sw89]: The calculations agree with the data only at large scattering angles. At smaller scattering angles the relativistic calculations are not in good agreement with the data.

- Complete sets of polarization transfer observables for quasielastic ^{54}Fe$(\vec{p},\vec{p}')$ scattering at 290 MeV and 20° [Ha88, Ha91]: The most striking feature of their data is the variation (mainly a decrease) of the polarization transfer observables as a function of excitation energy. This variation is reasonably well reproduced by the RPWIA calculations for $D_{s's}$ $D_{\ell'\ell}$, and $D_{s'\ell}$, but not for $-D_{\ell's}$. The calculations for P, A_y and D_{nn} do not, however, predict the observed slopes in the data. The enhancement of the lower Dirac component (relative to free m) at the quasielastic peak goes in the right direction for every spin observable, with the exception of D_{nn}, where there is essentially no relativistic effect. The reduction of P or A_y at the quasielastic peak is quantitatively reproduced by the RPWIA, in agreement with previous observations [Ca84, Ch88]. The reduction of P or A_y at present cannot be explained by any other mechanism, and appears to be a purely relativistic effect.

- The quenching of the analyzing power data relative to the values for free NN scattering, predicted by the RPWIA [Ho88], was also observed by Chan for ^{12}C$(\vec{p},\vec{p}')$ at 290 (at

29.5°) and 420 MeV (at 23.5°) [Ch89, Ch90]. However, the inclusion of relativistic m^* effects via the RPWIA failed to yield the correct variation of $D_{\ell' s}$ and $D_{s' \ell}$ as a function of energy loss at 420 MeV, and for $D_{s' s}$, it destroyed the good agreement obtained with Fermi motion alone [Ch90], that is for $m^* = m$.

- Unpolarized double differential cross sections and analyzing powers for quasielastic $^{12}C(\vec{p}, p')$ and $^{54}Fe(\vec{p}, p')$ scattering at 290 MeV (20.4°) and 420 MeV (24.0°) [Hi89]: The RPWIA adequately describes the shape, but not the absolute magnitude, of the double differential cross sections. Furthermore, the RPWIA model cannot consistently explain the enhancement (^{54}Fe data at 420 MeV) or suppression (^{54}Fe data at 290 MeV, and ^{12}C data at both 290 and 420 MeV) of the A_y data.

- Quasielastic $^{12}C(\vec{p}, n)$ analyzing power data at 300, 400, 494 and 795 MeV [Sa94]: The calculations with pseudoscalar πNN coupling reproduce the A_y values for 300 MeV and 795 MeV, while those with the pseudovector πNN coupling give a good description at 495 MeV. The data at 400 MeV, on the other hand, favour free NN scattering: pseudoscalar and pseudovector coupling yield identical results for free scattering (se Chapter 3).

- Unpolarized double differential cross sections and analyzing powers for quasielastic $^{12}C(\vec{p}, n)$ and $^{208}Pb(\vec{p}, n)$ at 494 and 795 MeV [Ta91a]: The relativistic m^*–based Fermi–gas model does a good job of describing the main features of inclusive spectra. Although the model fails to predict the absolute magnitude of the quasielastic peak, the angular dependence of the double differential cross sections is well reproduced. The angular dependence of the quasielastic analyzing power tracks well with free NN analyzing power.

- For quasielastic $(\vec{p}, p')$ and $(\vec{p}, n)$ analyzing power data at 392 MeV and 400 MeV respectively [Ot97b], on a variety of targets between ^2H and ^{nat}Pb, the reduction in the $(\vec{p}, p')$ data [relative to free scattering] and the enhancement in the $(\vec{p}, n)$ data [relative to free scattering], are simultaneously reproduced by pseudovector πNN coupling in the RPWIA model of Horowitz and Murdock [Ho88].

To summarize, the most striking feature of the RPWIA model is that the analyzing power and induced polarization for the inclusive $(\vec{p}, p')$ reaction are predicted to be substantially reduced compared to conventional nonrelativistic calculations. The smaller effective mass of nucleons in

the nuclear medium is responsible for this reduction. Such a reduction is observed in experiments performed at bombarding energies ranging from 200 to 500 MeV. The RPWIA model has, however, had mixed success in describing complete sets of quasielastic polarization transfer observables.

2.6.7 Relativistic random–phase approximation

Horowitz and Piekarewicz [Ho94, Ho94a] have developed a relativistic random phase approximation to infinite nuclear matter for calculating complete sets of quasielastic $(\vec{p},\vec{n})$ polarization transfer observables. A reduced value of the nucleon mass in the nuclear medium induces important dynamical changes in the residual isovector interaction relative to its nonrelativistic counterpart. As a result, good agreement is found for all polarization transfer observables, including the ratio of spin–longitudinal and spin–transverse nuclear response functions, when compared to the quasielastic ^{40}Ca$(\vec{p},\vec{n})$ of Chen et al. [Ch93] at 495 MeV and $|\vec{q}| = 1.72$ fm^{-1}. In contrast, the ratio of spin–longitudinal and spin–transverse nuclear response functions is underpredicted at $|\vec{q}| = 1.2$ fm^{-1} and overpredicted at $|\vec{q}| = 2.5$ fm^{-1}. Horowitz and Piekarewicz [Ho94] suggest that the inclusion of distortions could remedy the latter shortcomings. For most polarization transfer observables, except for D_{nn}, the relativistic RPA model [Ho94] gives slightly better agreement with data compared to the original RPWIA model [Ho88]. This is also the case for the ratio of spin–longitudinal to spin transverse nuclear response functions.

Hicks et al. [Hi89] compared quasielastic $(\vec{p},\vec{n})$ data (unpolarized double differential cross sections and analyzing powers) for ^{12}C and ^{54}Fe targets at 290 MeV and 420 MeV to the relativistic RPA model of Horowitz and Piekarewicz [Ho94]. The relativistic model, which has been successful in predicting ~30% suppression of A_y for the $(\vec{p},p')$ reaction, does not properly describe the $(\vec{p},n)$ analyzing power data.

The relativistic RPA results for quasielastic $(\vec{p},\vec{n})$ scattering can be summarized as follows [Ho94a]: Everything else being equal, a relativistic calculation will have less of an enhancement in the longitudinal to transverse ratio than a nonrelativistic calculation with the same interaction. Thus, relativity helps the agreement between theory and experiment, but it may not be the only effect one needs to consider. However, this relativistic effect must be considered along with other possible effects from full distortions, multistep contributions, problems with the RPA

approximations, etc.

2.6.8 Other models of quasielastic scattering

The failure of all the above–mentioned nonrelativistic and relativistic models to consistently predict complete sets of quasielastic $(\vec{p},\vec{p}')$ and $(\vec{p},\vec{n})$ polarization transfer observables, as well as the correct ratio of spin–longitudinal to spin–transverse nuclear response functions at different momentum transfers, questions the validity of the conventional meson–exchange picture of the NN interaction for describing quasielastic proton scattering. A number of suggestions have been made as to how the theoretical discrepancies may be remedied. Brown and Wambach [Br94] have offered an alternative explanation for the lack of enhancement, in the ratio of the spin–longitudinal to spin–transverse nuclear response functions, by invoking a rescaling of the ρ–meson mass in the nuclear medium. The experimental results seem to confirm the suppression at low energy loss. Yet, the data do not support the rapid variation with energy loss suggested by the model. Specifically, the rescaling model predicts a ratio of ~ 1 at the position of the quasielastic peak, while the data remain constant at a ratio ~ 0.6.

Bertsch, Frankfurt, and Strikman [Be93] have suggested that the answer may be found in the modification of the gluon properties in the nucleus, suppressing the pion field at distances below 0.5 fm.

Ericson [Er94], on the other hand, points out that the s–wave interaction of pions in the nuclear medium has a complex behaviour: It is appreciably repulsive for space–like pions, but it becomes small for on–shell pions. The latter behaviour has consequences for a number of physical quantities, such as the quark condensate in nuclei, and the effective pion mass. It may also offer an explanation for the discrepancy observed between theory and experiment, where the s–wave part has been ignored up to now.

Brown and collaborators [Br95] have proposed a solution to the problem based on arguments of partial restoration of chiral symmetry with density.

2.7 Concluding remarks

Of all the models reviewed in Sec. 2.6, the most successful models, for describing quasielastic $(\vec{p},\vec{p}')$ and $(\vec{p},\vec{n})$ polarization transfer observables, as well as the ratio of spin–longitudinal to spin–transverse response functions, have been the relativistic plane wave impulse approximation and relativistic random–phase approximation. In particular, for quasielastic $(\vec{p},p')$ scattering, the relativistic models predict the observed quenching of the analyzing power relative to the free analyzing power. To date, all nonrelativistic models fail to predict the latter suppression: an alternative explanation, for the observed suppression in the $(\vec{p},p')$ analyzing powers, has been suggested by Brieva and Love [Br90], who developed a nonrelativistic model including nonlocal couplings in the nuclear response, and the full off–shell behaviour of the NN interaction.

Although relativistic models cannot successfully describe all polarization transfer observables, of all the models considered thus far, they (relativistic models) seem to be the most encouraging. Rather than abandon the original RPWIA in favour of more sophisticated relativistic models, the approach, in the next chapter, is to critically review the underlying assumptions and input parameters of the RPWIA, and to perform more refined calculations so as to reveal the limitations of the model.

Chapter 3

Relativistic plane wave model

3.1 Introduction

Chapter 2 summarizes the current status of the measurement and interpretation of inclusive $(\vec{p},\vec{p}')$ and $(\vec{p},\vec{n})$ polarization transfer observables at the quasielastic peak. This chapter focuses on a relativistic Dirac–based plane wave description of quasielastic $(\vec{p},\vec{p}')$ and $(\vec{p},\vec{n})$ polarization observables.

Recall, from Chapter 2, that quasielastic scattering is the dominant reaction mechanism for nuclear excitation at moderate momentum transfers ($|\vec{q}\,| > 0.5$ fm^{-1}). It is considered to be a single–step, surface–peaked reaction, whereby an incoming proton knocks out a single bound nucleon in the target nucleus while the remainder of the nucleons act as "spectators". This process is characterized by a broad bump in the excitation spectrum, the centroid of which nearly corresponds to free NN kinematics, and a width resulting from the initial Fermi motion of the target nucleon. At the momentum transfers of interest ($|\vec{q}\,| > 1$ fm^{-1}), shell effects are unimportant, and the quasielastic peak is well separated from discrete states in the excitation spectrum. At the high excitation energies of interest, one nucleus looks like another. Essentially one is probing intrinsic properties of nuclear matter rather than details of the structure of a given nucleus. Hence, the quasielastic response is a fundamental property of nuclear matter. The primary difference between free NN scattering and quasielastic proton scattering is due to the presence of the nuclear medium in the latter. Consequently, deviations of the polarization transfer observables from the corresponding free NN values are expected to contain information on nuclear medium modifications of the free NN interaction. Hence, quasielastic scattering offers the possibility to study how the fundamental two–body nucleon–nucleon (NN) interaction is modified by the nuclear medium.

In recent years several elastic and inelastic proton–nucleus spin observables have been successfully analyzed using relativistic models based on the Dirac equation (see Chapter 2). This success, together with the fact that all nonrelativistic Schrödinger–based models [Es85, Sm85, Ha91] completely fail to successfully describe the analyzing power for quasielastic $(\vec{p},\vec{p}')$ scattering at 500 MeV from ^{40}Ca and ^{208}Pb [Ho86, Ho88], lead to the development of the **R**elativistic (Dirac) **P**lane **W**ave **I**mpulse **A**pproximation (**RPWIA**) for quasielastic proton–nucleus scattering [Ho86, Mu87a, Ho88, Iq88]. The relativistic NN amplitudes are based on a Lorentz–invariant parametrization of the standard five Fermi invariants (the so–called SVPAT form), and the target nucleus is treated as a Fermi–gas. For both of the above–mentioned nuclei, the RPWIA predictions have been spot on, while all nonrelativistic models overestimate the experimental values by $\approx 40\%$. The success of the RPWIA is attributed to the inclusion of nuclear medium effects (often referred to as relativistic effects) which are naturally incorporated as an enhancement of the lower components of projectile and target nucleon Dirac spinors resulting from strong scalar potentials. This amounts to replacing free nucleon masses in the Dirac plane waves with effective projectile and target nucleon masses within the context of relativistic mean field theory [Se86]. *Besides being strongly motivated by empirical evidence, one of the main advantages of the RPWIA model is that it is relatively simple, and hence, allows one to separately disentangle the effects of various model parameters without being swamped by unnecessary complexities.*

Despite the successful prediction of the analyzing power at 500 MeV, however, most of the other five polarization transfer observables allowed by parity and time–reversal invariance, namely $D_{nn}, D_{s's}, D_{\ell'\ell}, D_{s'\ell}$ and $D_{\ell's}$ (the primed and unprimed subscripts refer to outgoing and incoming spin directions, respectively: see Appendix G) favour relativistic predictions based on free nucleon masses. This inconsistency requires some deeper investigation. Note, however, that the original RPWIA predictions were based on crude assumptions and unrefined input. For example, a 10% uncertainty in effective mass values can translate to a 30% effect on certain polarization transfer observables (see Sec. 3.2.2).

Rather than abandon the original RPWIA in favour of more sophisticated relativistic models, my approach is to critically review the underlying assumptions and input parameters, and to perform more refined, and improved, calculations so as to reveal the limitations of the model.

The most important refinements to the original RPWIA include more sophisticated calculations of effective masses for both projectile and target nucleons, and also the implementation of a relativistic meson–exchange model for the NN amplitudes. For consistency, the latter model is also used to generate microscopic relativistic optical potentials required for the calculation of effective nucleon masses. Furthermore, contrary to the previously used SVPAT parametrization of the NN amplitudes, the meson–exchange model allows one to consider corrections to the RPWIA due to explicit treatments of exchange contributions to medium–modified NN amplitudes. Indeed, it has been suggested (although not explicitly shown) that a proper treatment of exchange is crucial for predictions of polarization transfer observables at energies lower than 200 MeV, whereas exchange effects are believed to be negligible at 500 MeV. For the first time, the importance of medium–modified exchange contributions is investigated via quasielastic $(\vec{p},\vec{p}')$ and $(\vec{p},\vec{n})$ scattering.

In the past, concern has been expressed about ambiguities in the SVPAT parametrization of the NN scattering operator. For example, replacing a pseudoscalar with a pseudovector πNN vertex yields identical matrix elements for free NN scattering. Hence, free NN scattering does not distinguish between these two different forms of πNN coupling. In the nuclear medium, however, certain quasielastic polarization transfer observables could be extremely sensitive to the different πNN vertices. To date, however, no experimental evidence has resolved this ambiguity. Previous attempts to study this ambiguity [Ho88], for quasielastic proton scattering, were extremely crude and therefore yielded unreliable results. With a meson–exchange model, however, one is able to distinguish between pseudoscalar and pseudovector forms of the πNN vertex. Indeed, one of the aims of the project is to identify observables which are sensitive to this ambiguity. Comparison with experimental data could shed light on the preferred type of πNN coupling.

Previous RPWIA studies were mainly concerned with relativistic effects on quasielastic polarization transfer observables at energies higher than 300 MeV [Ho86, Mu87a, Ho88, Iq88]. The question now arises as to how important these effects are at lower energies. Contrary to initial intuition, relativistic effects are expected to become even more important as the incident proton energy is lowered [Cl85, Wa85]: the magnitudes of the real parts of the Dirac scalar and vector optical potentials, which additively contribute to polarization transfer observables, both increase, and this may enhance relativistic effects on certain polarization transfer observables.

The effects of spin–orbit distortions on polarization transfer observables are also considered. Within the eikonal approximation, the effect of the spin–orbit potential is to rotate both initial and final state spinors, and in this way directly affects the polarization transfer observables. Previous studies of spin–orbit distortions [Ho86] focused on quasielastic $(\vec{p},\vec{p}')$ scattering at incident energies of 500 and 800 MeV. In this project, however, the effects of spin–orbit distortions on quasielastic $(\vec{p},\vec{p}')$ polarization transfer observables at incident energies ranging from $\sim$100 to $\sim$500 MeV, and for target nuclei between ^{12}C and ^{208}Pb, are investigated.

Since this project is partially motivated by current experimental interest in the measurement of quasielastic $(\vec{p},\vec{p}')$ and $(\vec{p},\vec{n})$ polarization transfer observables at NAC (National Accelerator Centre, South Africa), IUCF (Indiana University Cyclotron Center, USA), and RCNP (Research Centre for Nuclear Physics, Japan), the primary focus is on incident proton energies ranging from 135 to 420 MeV.

Both quasielastic $(\vec{p},\vec{p}')$ and $(\vec{p},\vec{n})$ scattering are considered, the reason being that these reactions probe different parts of the NN interaction: Whereas $(\vec{p},\vec{p}')$ scattering probes both isovector and isoscalar parts of the NN interaction, $(\vec{p},\vec{n})$ charge–exchange reactions sample only the isovector components, particularly those directly related to pion exchange [Wa94, Ho94]. Furthermore, since the Lorentz character of the isovector amplitudes is totally different from the isoscalar amplitudes, one expects quasielastic $(\vec{p},\vec{p}')$ and $(\vec{p},\vec{n})$ polarization transfer observables to yield different, but complementary, information about nuclear medium modifications of the NN interaction.

Besides modifying the free NN interaction, the effect of the nuclear medium is also to distort the incoming and outgoing plane waves. The effect of these distortions is to reduce the unpolarized double differential cross section relative to its plane–wave value. However, since polarization transfer observables are effectively ratios of linear combinations of polarized double differential cross sections (see Appendix G), one expects the effects of distortions to largely cancel, thus enhancing sensitivity to nuclear medium–modifications of the NN amplitudes. Thus, relative to unpolarized double differential cross sections, polarization transfer observables are expected to be less sensitive to distortions. Hence, a plane–wave model (such as the RPWIA) is expected to provide an adequate description of the polarization transfer observables. It is for these reasons that one mainly focuses on the description of *polarization transfer observables*,

rather than unpolarized double differential cross sections. In addition, comparison of theoretical predictions of *complete sets* of polarization transfer observables, namely P, A_y, D_{nn}, $D_{s's}$, $D_{\ell'\ell}$, $D_{\ell's}$and $D_{s'\ell}$, to experimental data will provide very stringent tests on the validity of the RPWIA.

The RPWIA formalism is presented in Sec. 3.2. Refined calculations of effective masses for both projectile and target nucleons are discussed in Sec. 3.2.2, the Fermi–gas model of the target nucleus is described in Sec. 3.2.3, and two different parametrizations of the NN interaction are presented in Sec. 3.2.4, namely a Lorentz–invariant parametrization based on the standard five relativistic invariants (the so-called SVPAT form), and the relativistic Horowitz–Love–Franey (HLF) meson–exchange model. In Sec. 3.2.7 expressions are derived for the polarization transfer observables in terms of the invariant scattering matrix elements. The differences between $(\vec{p},\vec{p}')$ and $(\vec{p},\vec{n})$ reactions, in terms of the isospin content of the NN amplitudes and the reaction Q–values, are discussed in Sec. 3.2.8.

Thereafter, for a ^{40}Ca target at a three–momentum transfer of 1.97 fm^{-1}, and incident energies below 500 MeV, the sensitivity of complete sets of quasielastic $(\vec{p},\vec{p}')$ and $(\vec{p},\vec{n})$ polarization transfer observables is investigated, both qualitatively and quantitatively, within the framework of the RPWIA, to medium effects, pseudoscalar versus pseudovector forms of the πNN vertex, exchange contributions to the NN amplitudes, and also spin–orbit distortions (Secs. 3.2.10 – 3.3.5). In Sec. 3.4, predictions based on the RPWIA model, are compared to published data. The generation of new Horowitz–Love–Franey meson–exchange parameters, between 80 and 195 MeV, is discussed in Sec. 3.3.3. The summary and conclusions are presented in Sec. 3.5.

3.2 RPWIA formalism

The formalism for the **R**elativistic **P**lane **W**ave **I**mpulse **A**pproximation (**RPWIA**) is described in Refs. [Ho86, Mu87a, Ho88, Iq88]. However, since the RPWIA forms the core of this chapter, for completeness, the formalism is presented, and new or refined aspects are discussed in detail. For the purpose of this project, natural units (i.e. $\hbar = c = 1$) are used [La90], and the conventions of Bjorken and Drell [Bj64] are adopted.

The RPWIA model is strongly motivated by a large number of experimental observations.

This is discussed in the next section.

3.2.1 Experimental basis

Although it may, at first, seem rather simple and extremely crude to model the quasielastic proton–nucleus scattering process in terms of a plane–wave formalism, the RPWIA is strongly motivated by the following empirical evidence (see Chapter 2):

- The centroid of the quasielastic peak in the unpolarized double differential cross section roughly corresponds to free NN kinematics, i.e. the peak position is located at an energy transfer of approximately $\frac{|\vec{q}|^2}{2m}$, where m is the free nucleon mass, and $|\vec{q}\,|$ is the three–momentum transfer. The width of the quasielastic peak is attributed to the initial momentum distribution of the struck target nucleon (see Sec. I.9 in Appendix I).
- Most of the polarization transfer observables at the quasielastic peak correspond to those for free NN scattering.
- At momentum transfers between 1 and 2 fm^{-1}, the quasielastic peak is well separated from low–lying discrete states and resonances in the excitation spectrum.
- Shell effects seem to be irrelevant at the high excitation energies of interest.

The experimental evidence, in turn, suggests that:

- The mechanism for quasielastic scattering is a single–step process, whereby a projectile nucleon knocks out a single bound nucleon in a target nucleus while the remainder of the nucleons remain inert.
- Polarization transfer observables are insensitive to distortions.
- Multiple scattering effects are negligible for polarization transfer observables.
- Collective excitations are not important.
- A Fermi–gas model, which totally ignores shell effects, should provide an adequate first–order description of the target nucleus.

- Deviations of the polarization transfer observables from the corresponding free values could possibly be related to medium modifications of the free NN interaction.

The above mentioned empirical evidence strongly suggests that the process of quasielastic scattering can be depicted schematically by Fig. 3.1, where $\{\vec{k}_{1(2)}, s_{1(2)}\}$ and $\{\vec{k}'_{1(2)}, s'_{1(2)}\}$ denote respectively the initial and final laboratory momenta and spins of the projectile nucleon (subscript 1) and target nucleon (subscript 2) involved in the collision process. The lambdas (λ_i) are the five Dirac matrices listed in Table 3.2 and represent the relativistic prescription for the free NN amplitudes (see Sec. 3.2.4). Nuclear medium modifications (also referred to as relativistic effects in the RPWIA) are incorporated via effective masses for the projectile (m_1^*) and target (m_2^*) nucleons. These effective masses, which come about in a natural way in the Dirac–based formalism, serve to distort the incoming and scattered plane waves, and also correct the free NN interaction for nuclear medium effects. The calculation and role of these effective masses will be discussed in subsequent sections.

3.2.2 Effective nucleon masses

For a proper description of the NN interaction in quasielastic proton scattering, medium effects of the surrounding nucleus have to be incorporated. These are treated as distortions of the Dirac free–particle wave function by the nuclear scalar potential and, as distortions are generally larger on low–energy particle waves, they deserve some special attention in the present analysis. The concept of an effective mass for a Dirac particle in the nuclear medium was introduced in the relativistic **M**ean **F**ield **T**heory (**MFT**) of the Walecka model [Se86]. For quasielastic proton–nucleus scattering, the effective masses of both projectile and target nucleons, m_1^* and m_2^* respectively, play a vital role in determining the nuclear medium (or relativistic) effects on scattering observables. Original RPWIA calculations [Ho86, Mu87a, Ha88, Ho88, Iq88] relied on rather crude values of the effective masses. However, some observables are extremely sensitive to small variations in the effective mass, and hence, much emphasis is placed on generating more refined values of the effective masses. To illustrate this point, Figs. 3.2 and 3.3 plot the polarization transfer observables (see Sec. 3.2.7) for different *projectile* effective masses between $0.7\,m \leq m_1^* \leq 1.0\,m$ (m being the free nucleon mass) for quasielastic $(\vec{p},\vec{p}\,')$ and $(\vec{p},\vec{n})$ scattering, respectively, from a ^{40}Ca target nucleus at an incident laboratory kinetic energy

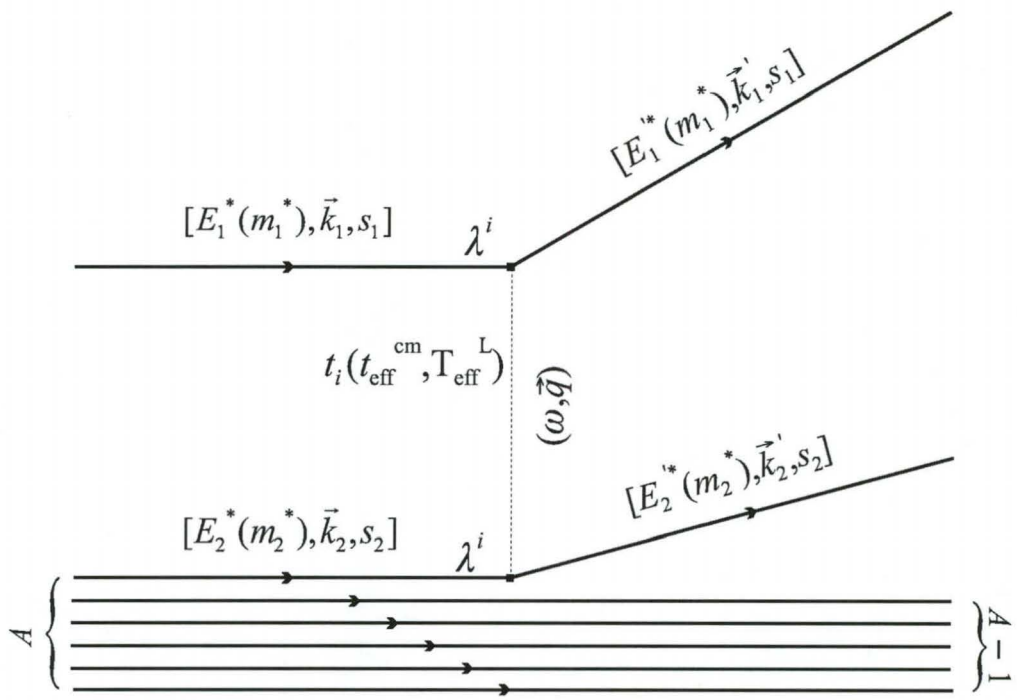

Figure 3.1: Schematic diagram of the Relativistic Plane Wave Impulse Approximation (RPWIA) for quasielastic inclusive proton–nucleus scattering. The index i is summed over the five Lorentz–invariant amplitudes listed in Table 3.2. Nuclear medium modifications of the NN amplitudes are incorporated via effective nucleon masses m_1^* and m_2^* for the projectile and ejectile, respectively. The remainder of the notation is defined in the text.

of 200 MeV: the effective mass of the target nucleon is kept fixed at $m_2^* = 0.795\,m$ (see Table 3.1). These predictions are based on a relativistic SVPAT parametrization of the NN amplitudes, with a pseudoscalar coupling for the pion: the meaning of this jargon, as well as the details of these calculations, are discussed in Secs. 3.2.4 to 3.2.9. Note the extreme sensitivity of certain polarization transfer observables to 10% variations in the effective nucleon mass. Hence, it is important to use refined values of these effective masses when testing the validity of the RPWIA.

The generation of projectile and ejectile effective masses is discussed in the next section. The Dirac equation with relativistic scalar $S(r)$ and time–like vector $V(r)$ spherical potentials resembles the free–particle Dirac equation, with $S(r)$ adding effectively to the mass m of a free nucleon [see Eq. (A.17) in Appendix A with S(r)=$\not{S}$(r), V(r)=U_v^0(r), and U_v^r(r)=U_t^r(r)=0]:

$$\{-i\boldsymbol{\alpha}\cdot\boldsymbol{\nabla}+\beta[m+S(r)]-[E-V(r)]\}\psi^{\pm}_{\vec{K},s}(\vec{r}\,)=0 \tag{3.1}$$

where the subscripts $(\pm)$ correspond to $(\frac{\text{incoming}}{\text{outgoing}})$ distorted waves. In the eikonal approximation the wave function $\psi^{\pm}_{\vec{K},s}(\vec{r}\,)$ is given by [Am83]

$$\psi^{\pm}_{\vec{K},s}(\vec{r}\,)=\sqrt{\frac{E+m}{2m}}\begin{pmatrix} 1 \\ \dfrac{\boldsymbol{\sigma}\cdot\vec{K}}{E-V(r)+m+S(r)} \end{pmatrix} e^{\vec{K}\cdot\vec{r}}e^{iW^{\pm}(\vec{r}\,)}\chi_s \tag{3.2}$$

where the eikonal phase factor (or Hamilton's characteristic function) $W^{\pm}(\vec{r}\,)$ is written in integral form as $[\vec{r}\equiv(\vec{b},z)]$

$$W^{\pm}(\vec{b},z)=-\frac{m}{|\vec{K}|}\int_{\mp\infty}^{z}dz'\{V_c(\vec{b},z')+V_{\rm SO}(\vec{b},z')(\boldsymbol{\sigma}\cdot\vec{b}\times\vec{K}-i|\vec{K}|z')\} \tag{3.3}$$

with $\vec{b}$ the impact parameter, and the z–axis is chosen along the direction of the average momentum $\vec{K}$:

$$\vec{K}=\frac{1}{2}(\vec{k}+\vec{k}')\,, \tag{3.4}$$

defined in terms of the initial $(\vec{k})$ and final $(\vec{k}')$ momenta in the laboratory frame. V_c(r) and $V_{\rm SO}$(r) denote Dirac–equation–based central and spin–orbit potentials produced via the transformation of the Dirac equation (3.1) to an equivalent Schrödinger equation (see Appendix A). Note that in the semi–classical eikonal approximation the path of the scattered proton is approximated by a straight line through the nucleus (in direction z with impact parameter b). The

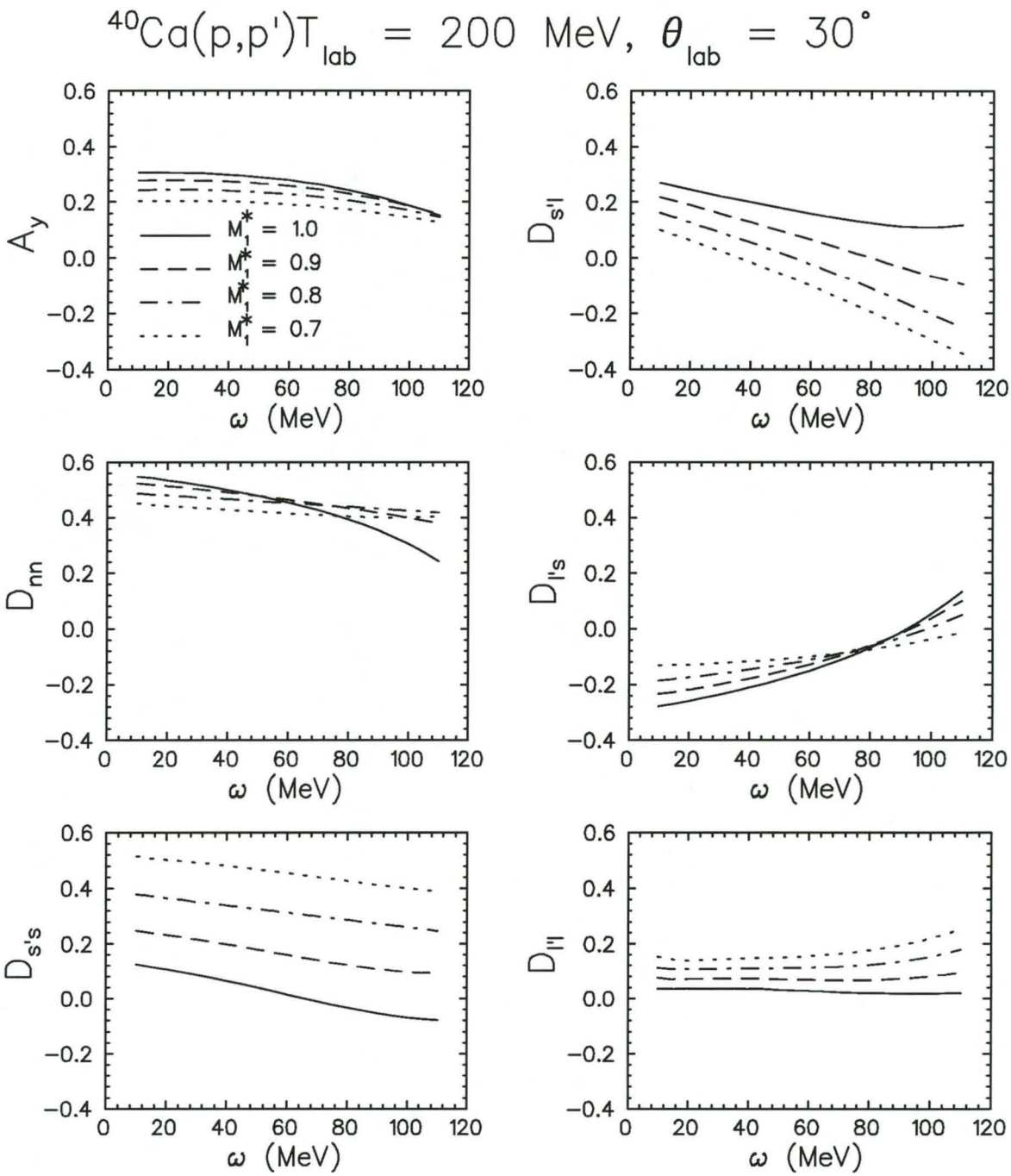

Figure 3.2: The sensitivity of complete sets of quasielastic ^{40}Ca$(\vec{p},\vec{p}\,')$ polarization transfer observables to 10% variations in the projectile effective mass M_1^*, where $M_1^* = \frac{m_1^*}{m}$. The incident laboratory energy is 200 MeV and the laboratory scattering angle is 30°.

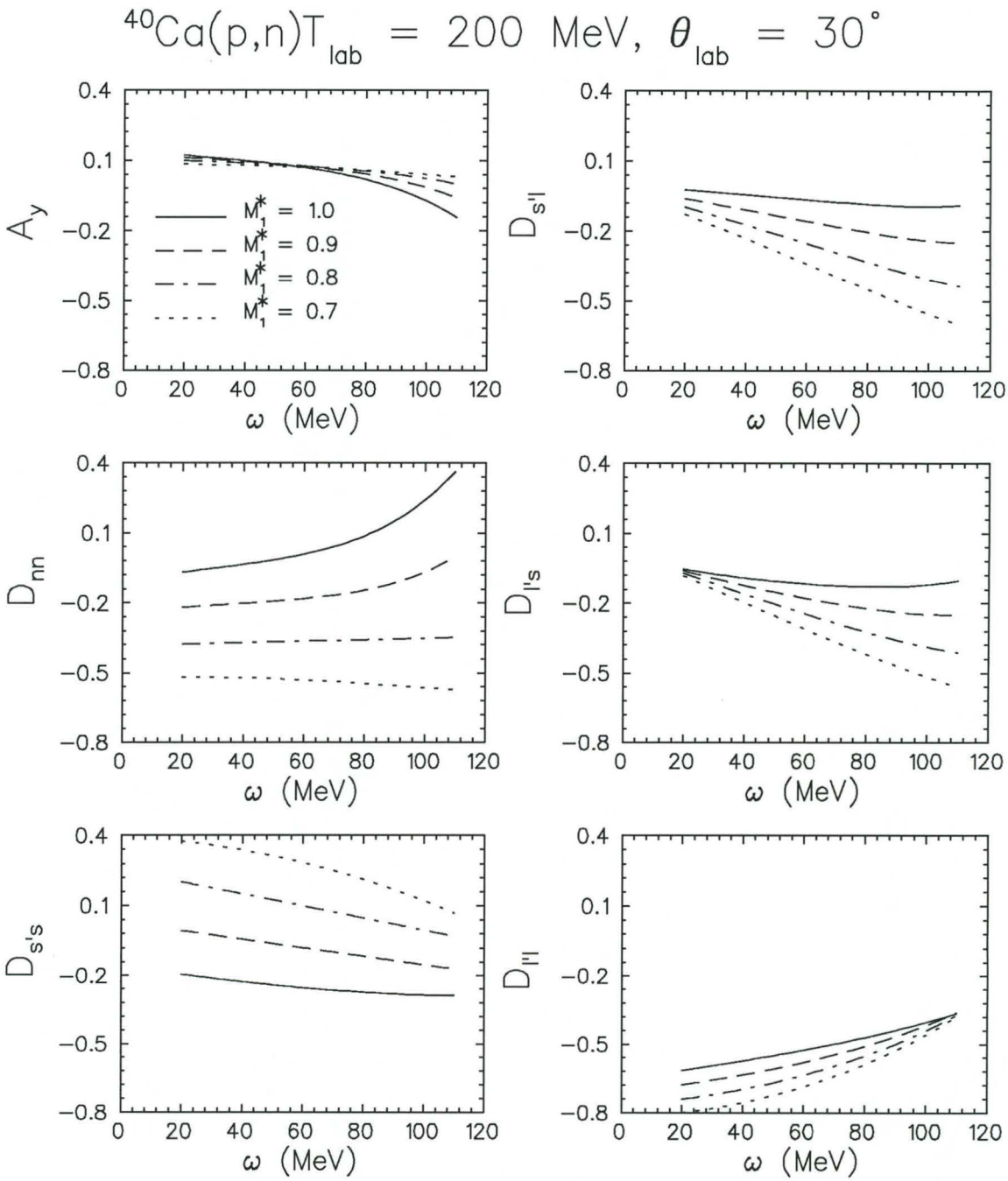

Figure 3.3: The sensitivity of complete sets of quasielastic ^{40}Ca$(\vec{p},\vec{n})$ polarization transfer observables to 10% variations in the projectile effective mass m_1^*, where $M_1^* = \frac{m_1^*}{m}$. The incident laboratory energy is 200 MeV and the laboratory scattering angle is 30°

effect of the nuclear medium is to distort the free–particle wave functions via the phase factor $e^{iW(\vec{b},z)}$.

If, on account of the mean–field theory of the Walecka model, the Dirac fields in Eq. (3.1) are replaced by their mean values [Se86]:

$$S(r) \rightarrow \langle S \rangle \quad \text{and} \quad V(r) \rightarrow \langle V \rangle \, ,$$

one obtains a truly free–particle Dirac equation with, however, an effective mass:

$$m^* = m + \langle S \rangle \, . \tag{3.5}$$

The mean vector field $\langle V \rangle$ simply shifts the energies of all particles by a fixed amount and does not affect the scattering process. To incorporate effective masses in the Dirac scattering wave functions for subsequent calculations of polarization transfer observables, $\langle S \rangle$ needs to be evaluated in accordance with the circumstances of the specific nuclear reaction. The procedure of Horowitz and Iqbal [Ho86, Mu87a, Iq88] is essentially followed, and the mean scalar potential is taken to be

$$\langle S \rangle = \frac{\int d\vec{r} \; S(r) \; \mathrm{w}(r)}{\int d\vec{r} \; \mathrm{w}(r)} \, , \tag{3.6}$$

where $S(r)$ represents the *real* part of the scalar potential, and the weighting function $\mathrm{w}(r)$ expresses the probability that both projectile and target nucleons are present at position r in a spherically symmetric nucleus, that is

$$\mathrm{w}(r) = \rho(r) \; T(r) \, , \tag{3.7}$$

with $\rho(r)$ the baryon density, and $T(r)$ the probability that the incoming nucleon will *not* be absorbed before reaching position r.

Since the imaginary component of the optical potential contributes to absorption of the beam, the probability for the beam being transmitted through the nucleus along an impact parameter $\vec{b}$, becomes:

$$\begin{aligned} T(b) &= |\exp\left[iW^+(b, z=\infty)\right]|^2 \\ &= \exp\left[(-2 \; \mathrm{Im} \; \mathrm{W}^+(b, z=\infty)\right] \, , \end{aligned} \tag{3.8}$$

where ImW indicates the imaginary part of W in Eq. (3.3). For simplicity, the spin–orbit and Darwin terms in Eq. (3.3) are omitted, thus yielding

$$T(b) = \exp\left[\frac{4m}{|\vec{K}|} \int_0^\infty dz \; \mathrm{Im} \, V_c(b,z)\right] \, . \tag{3.9}$$

The effects of spin–orbit distortion on polarization transfer observables will be considered in Sec. 3.2.10. Calculations of $T(b)$ show generally that, because of proton absorption in the nuclear interior, mainly the surface of the nucleus contributes to $\langle S \rangle$. In terms of cylindrical co-ordinates z and b, Eq. (3.6) is written as:

$$\langle S \rangle = \frac{\int db\, b\, T(b) \int dz\, S(b,z)\rho(b,z)}{\int db\, b\, T(b) \int dz\, \rho(b,z)} \tag{3.10}$$

such that an explicit evaluation requires an appropriate nuclear density function $\rho(r)$ [sometimes called the baryon density function] and Dirac potentials. Horowitz and Iqbal use the functions $S(r)$ and $\rho(r)$ of Kobos and Cooper [Ko85] to calculate m_1^* for the incoming protons, both functions being of Woods-Saxon form. For m_2^* of the target nucleon they use directly a mean scalar field for nuclear matter in Eq. (3.5), which relies on the assumption that $S(r) = \alpha\rho(r)$, but with constant α extracted from infinite nuclear matter. In the present project, apart from averaging scalar potentials as expressed by Eq. (3.10) [for eventually calculating both m_1^* and m_2^*], my aim is to employ the most recent and refined functions for the Dirac optical potentials and nuclear densities. For the purpose of calculating effective masses for the target nucleons m_2^*, I consider the work of Horowitz, Murdock and Serot [Ho91a], who analyze the mutual interaction of nucleons in a nucleus by relativistic fields describing the exchange of mesons as in the Walecka model [Se86], and perform selfconsistent Dirac–Hartree calculations to obtain the fields: they only considered spherically symmetrical closed–shell nuclei, which restricted the meson fields to the zero component of the vector field $V^0(r)$ and the scalar field $\phi(r)$: note that both $V^0(r)$ and $\phi(r)$ are *real* fields. The resulting field equation for the baryons yields a Dirac equation with $-g_s\phi(r)$ as the scalar potential, adding to the baryon mass, where g_s is the scalar meson coupling constant. In the present case one considers $-g_s\phi(r)$ to be the scalar potential for the struck nucleon and, therefore, in the mean field approximation, its effective mass becomes:

$$m_2^* = m - g_s\langle\phi\rangle\ . \tag{3.11}$$

The computer code TIMORA, of Horowitz and Murdock [Ho91a], is used to calculate, in a selfconsistent Dirac–Hartree formulation, the potentials $\phi(r)$ and $V^0(r)$ for a specific nucleus, as well as the scalar and baryon density functions $\rho_s(r)$ and $\rho_B(r)$. After averaging $\phi(r)$ via Eq. (3.10) with $\rho(r) = \rho_B(r)$, one calculates m_2^* from Eq. (3.11).

The calculation of m_1^* from Eq. (3.5) requires a scalar optical potential $S(r)$ for the projectile

nucleon. This potential is obtained by folding the components of a NN interaction t–matrix with the scalar density $\rho_s(r)$ for the specific nucleus: the code FOLDER [Ho91a] is used. There are two parametrizations for the NN scattering amplitudes, namely the Horowitz–Love–Franey model [Ho85] discussed in Sec. 3.2.4 with its separation of direct and exchange amplitudes, and a parametrization by McNeil, Ray and Wallace which uses complex Gaussian functions and treats the full amplitude as a direct term [Ho91a]. The former is preferred for proton energies below 400 MeV, while parameter sets exist at higher energies for the latter choice. For the t–matrix (below 400 MeV) one applies, for consistency, the same Horowitz–Love–Franey NN interaction which is to be used for calculating the polarization transfer observables in Sec. 3.2.7, and include pseudovector coupling for the pion, which formerly [Mc83] yielded by far the best agreement with phenomenological Dirac optical potentials. The *real* parts of the scalar potentials are then averaged according to Eq. (3.10) and consequently used to extract the m_1^* values via Eq. (3.5).

Table 3.1 lists various effective nucleon mass values for quasielastic proton scattering from the nuclei ^{12}C, ^{16}O, ^{40}Ca, ^{54}Fe and ^{208}Pb, at incident laboratory energies of 135, 200, 300, 400 and 500 MeV. Note that $M^* = \dfrac{m^*}{m}$, where m is the free nucleon mass. The subscript **SC** refers to effective masses based on **S**elf–**C**onsistent optical potentials: the scalar optical potential, used for extracting m_1^*, is obtained by folding the NN t–matrix with a scalar density generated via the self–consistent Dirac–Hartree procedure, and the bound scalar potential, used for calculating m_2^*, is generated via the self–consistent Dirac–Hartree procedure. For comparison, the effective masses (subscripted by **CP**) calculated with recent global phenomenological optical potentials developed by **C**oo**P**er et al. [Co92] are shown: they fitted proton elastic scattering data in the energy range 20 – 1040 MeV for targets ^{12}C, ^{16}O, ^{40}Ca, ^{90}Zr and ^{208}Pb. Table 3.1 also lists the M^*–values reported by **H**orowitz and **M**urdock [Ho88] and which are subscripted by **HM**: the M^*_{HM}–values at 300 MeV are taken from Ref. [Ha88]. The sensitivity of the polarization transfer observables to the **SC**, **CP** and **HM** effective masses will be discussed in Sec. 3.3. The general trends exhibited by the more refined SC– and CP–effective masses are now analyzed. Firstly, for scattering from a specific nucleus, the effective masses of both projectile and target nucleons increase with projectile laboratory kinetic energy T_{lab}, the increase for the projectile being larger. This can be explained as follows: as T_{lab} increases, more reaction channels generally open for projectile absorption inside the nucleus, manifesting itself as an increase in the imaginary part of the optical potential. This decreases the projectile's

Table 3.1: Effective masses $M^* = \frac{m^*}{m}$, average impact parameters $\langle b \rangle$, Fermi momenta k_F, and effective number of struck nucleons A_{eff} for various nuclei and laboratory kinetic energies. The meaning of the various subscripts is defined in the text.

Target nucleus	T_{lab} (MeV)	M^*_{1SC}	M^*_{2SC}	M^*_{1CP}	M^*_{2CP}	M^*_{1HM}	M^*_{2HM}	$\langle b \rangle$ (fm)	k_F (fm^{-1})	A_{eff}
^{12}C	135	0.762	0.762	0.836	0.754			2.109	1.059	4.210
^{12}C	200	0.795	0.768	0.853	0.775	0.850	0.840	2.136	1.050	4.443
^{12}C	300	0.832	0.772	0.868	0.792			2.162	1.042	4.482
^{12}C	400	0.862	0.786	0.883	0.807	0.860	0.840	2.243	1.020	4.156
^{12}C	500	0.890	0.799	0.892	0.814	0.910	0.870	2.331	0.996	3.636
^{16}O	135	0.847	0.779	0.828	0.765			2.409	1.029	4.875
^{16}O	200	0.839	0.781	0.846	0.782			2.421	1.026	5.311
^{16}O	300	0.855	0.786	0.862	0.798			2.458	1.017	5.302
^{16}O	400	0.870	0.796	0.871	0.809			2.529	1.000	5.016
^{16}O	500	0.893	0.809	0.885	0.815			2.631	0.976	4.330
^{40}Ca	135	0.836	0.778	0.810	0.749			3.434	1.024	6.736
^{40}Ca	200	0.832	0.784	0.832	0.771	0.82	0.81	3.484	1.014	7.277
^{40}Ca	300	0.847	0.787	0.851	0.789			3.510	1.008	7.496
^{40}Ca	400	0.864	0.798	0.865	0.799	0.83	0.80	3.599	0.989	7.133
^{40}Ca	500	0.892	0.817	0.879	0.810	0.90	0.85	3.759	0.955	5.973
^{54}Fe	135	0.819	0.757	0.796	0.722			3.753	1.055	6.494
^{54}Fe	200	0.817	0.766	0.819	0.748			3.822	1.041	7.066
^{54}Fe	300	0.833	0.770	0.840	0.769	0.86	0.85	3.850	1.034	7.378
^{54}Fe	400	0.853	0.783	0.855	0.781			3.948	1.012	7.044
^{54}Fe	500	0.885	0.805	0.874	0.794			4.123	0.974	5.811
^{208}Pb	135	0.828	0.835	0.807	0.767			6.929	0.986	7.670
^{208}Pb	200	0.845	0.831	0.842	0.801	0.82	0.82	6.880	0.922	9.572
^{208}Pb	300	0.860	0.825	0.866	0.822			6.808	0.934	11.140
^{208}Pb	400	0.885	0.836	0.885	0.839	0.86	0.83	6.913	0.911	11.033
^{208}Pb	500	0.916	0.857	0.896	0.850	0.88	0.85	7.114	0.868	9.146

transmission $T(b)$ through the inner nucleus and shifts the region of proton scattering to the nuclear surface, where the magnitudes of all nuclear potentials start to decline substantially. Therefore, as T_{lab} increases, both $\langle\phi\rangle$ and the magnitude of the real part of $\langle S\rangle$ decrease and, with S(r) being negative, this leads to an increase of both m_1^* and m_2^*, according to Eqs. (3.5) and (3.11) respectively. In addition, it is known that, as T_{lab} increases, the magnitude of the real part of the Dirac optical potential function $S(r)$ decreases at all r [Mc83]. This leads to a further reduction in $\langle S\rangle$ and consequently, a further increase in m_1^*. The last three columns in Table 3.1 list respectively:

- the mean impact parameter $\langle b\rangle$, which is calculated by replacing S(r) with b in Eq. (3.6),
- the Fermi momentum $k_F = (\frac{3}{2}\pi^2\langle\rho_B\rangle)^{\frac{1}{3}}$, which is calculated by replacing S(r) with $\rho_B(r)$ in Eq. (3.6),
- the effective number of struck nucleons (in the nuclear surface) A_{eff}, which is calculated from

$$A_{\text{eff}} = A\,\frac{\int db\; b\, T(b) \int dz\; \rho(b,z)}{\int dz\; \rho(b,z)}\;. \tag{3.12}$$

The effective masses m_1^* and m_2^* do not vary significantly with the mass number of the target nucleus. Also note, that the effective number of nucleons A_{eff} acting as scatterers does not increase much with nuclear size. This means that for heavier target nuclei, the scattering becomes more surface peaked and resembles more of a free NN interaction in which the remaining (heavy) nucleus plays a minor role. This is also reflected by the m_1^*–values for ^{208}Pb, where the effective masses are close to the free–mass value. On the other hand, the lightest nucleus ^{12}C, is penetrated more by the incident beam and, on average, a third of all the nucleons partake in the scattering. Thus, contrary to initial intuition, medium effects are better studied by scattering protons on light nuclei: this is illustrated by the relatively large differences between effective masses for ^{12}C and the free–mass value. Furthermore, one also sees that the effective number of target nucleons A_{eff} is mainly concentrated in the nuclear surface. This is due to the fact that, for each nucleus, the average impact parameter $\langle b\rangle$ is relatively close to the value of the nuclear radius $R = r_0 A^{\frac{1}{3}}$, with $r_0 = 1.2$ fm.

The effect of these M^*–values on polarization transfer observables will be discussed in Sec. 3.3. In Sec. 3.2.1 the choice of a Fermi–gas model for the target nucleus was motivated. In the

following section, the latter model is discussed in more detail.

3.2.3 Fermi–gas model of the target nucleus

At the large momentum transfers ($|\vec{q}| > 1$ fm^{-1}) and excitation energies ($\omega \approx \frac{|\vec{q}|^2}{2m}$) of interest, nuclear shell effects seem to be unimportant: the experimental polarization transfer observables are virtually identical for quasielastic $(\vec{p},\vec{p}')$ scattering from ^{12}C and ^{16}O at 290 MeV [Ch89], and for $(\vec{p},\vec{n})$ scattering from ^{2}H, ^{6}Li, ^{12}C, ^{40}Ca and ^{208}Pb at 346 MeV [Sa96, Wa96, Wa97]. Hence, it seems reasonable to treat the nucleus as a system of noninteracting nucleons in a very large volume where one applies periodic boundary conditions for the wave functions, thus yielding plane waves. This model of the nucleus is referred to as the Fermi–gas model. The distribution of the plane wave states is represented by a sphere in momentum space whose radius is the Fermi momentum k_F. Recall, from Sec. 3.2.2, that the Fermi momentum k_F is directly related to the average nuclear or baryon density via

$$k_F = (\frac{3}{2}\pi^2\langle\rho_B\rangle)^{\frac{1}{3}} . \tag{3.13}$$

When the bombarding nucleon transfers momentum $\vec{q}$ and energy ω to a target nucleon, the initial momentum $\vec{k}_2$ of the nucleon (before being struck) is limited to (See Sec. I.7 in Appendix I)

$$|\vec{k}_{\rm min}| \leq |\vec{k}_2| \leq |\vec{k}_{\rm max}| \tag{3.14}$$

where

$$k_{\rm min} = |\vec{k}_{\rm min}| = \max\{|\frac{|\vec{q}|}{2} - \frac{\omega}{2}\left(1 - \frac{4m_2^{*2}}{\omega^2 - |\vec{q}|^2}\right)^{\frac{1}{2}}|\,, 0\} \tag{3.15}$$

and

$$k_{\rm max} = |\vec{k}_{\rm max}| = \min\{\frac{|\vec{q}|}{2} + \frac{\omega}{2}\left(1 - \frac{4m_2^{*2}}{\omega^2 - |\vec{q}|^2}\right)^{\frac{1}{2}}\,, k_F\} . \tag{3.16}$$

Due to the Fermi motion of the target nucleons, all polarization transfer observables need to be averaged over the Fermi distribution of the target–nucleon momenta $\vec{k}_2$ (see Sec. 3.2.7).

Nonrelativistically, the energy– and momentum–transfer are related by (See Sec. I.9 in Appendix I)

$$\begin{aligned} \omega &= \frac{(\vec{k}_2 + \vec{q})^2}{2m} - \frac{|\vec{k}_2|^2}{2m} \\ &= \frac{|\vec{q}|^2}{2m} - \frac{\vec{k}_2 \cdot \vec{q}}{m} \end{aligned} \tag{3.17}$$

where m is the free nucleon mass. The first term gives the energy loss of the centroid of the quasielastic peak which corresponds to free NN scattering from a stationary target nucleon, i.e. $\vec{k}_2 = 0$. The second term indicates how the width of the peak (FWHM) is related to the momentum of the struck nucleon [Fe71, Ne88].

In the Fermi–gas model, the ground state of the nucleus is a Fermi sea with all states below k_F occupied. When quasielastic scattering takes place, the struck nucleon is removed from the Fermi sea, and the recoiled ejectile also remains above the Fermi sea. No scattering takes place for either $|\vec{k}'_1| \leq k_F$ or $|\vec{k}'_2| \leq k_F$. This effect is called Pauli blocking, and becomes important when $|\vec{q}| < 2k_F$ [Be82, Wa93].

For quasielastic scattering the Fermi–gas model relates the inclusive unpolarized double differential cross section for quasielastic proton–nucleus scattering to the probability of exciting a target nucleon from an occupied state within the Fermi sphere to an unoccupied state outside the Fermi sphere, with momentum and energy being conserved in the transition [Fe71, Ne88].

For a relativistic description of quasielastic proton scattering, one requires relativistic NN amplitudes as input. These amplitudes form the subject of the next section.

3.2.4 Relativistic NN amplitudes

Most calculations of scattering observables require some form of empirical input, such as, for example, the experimental NN scattering amplitudes. In direct nuclear reaction theory most models make use of the impulse approximation which essentially relates scattering observables to the free NN scattering amplitudes. Normally this approximation is valid for incident beam energies much larger than the binding energy of the target nucleons, so that the binding energy can be neglected, and the interaction is considered to be between free nucleons [Ja70]. Although the validity of the impulse approximation, as used in low to medium energy nuclear reaction

models is questionable, it is nevertheless used due to the lack of any better approximation. However, for quasielastic proton scattering it has already been emphasized (see Chapter 2, and also Sec. 3.2.1 in this chapter) that direct experimental evidence supports the idea of a projectile interacting with a single, essentially free, target nucleon. Hence, the impulse approximation should be valid for quasielastic scattering.

The free NN amplitudes are normally extracted from free NN scattering experiments via suitable phase shift analyses, such as the well–known Arndt phases [Ar86]. In the following two sections, relativistic parametrizations of the free NN scattering data will be presented.

Relativistic representation of the NN amplitudes

The nonrelativistic **McNeil–Ray–Wallace** (**MRW**) [Mc83a, Mu87a] parametrization of the on–shell NN scattering operator f, which is consistent with rotation, parity, time-reversal and isospin invariance, is given by (see Appendix G in Sec. G.4):

$$(2i|\vec{k}_{cm}|)^{-1} f \equiv A + B\boldsymbol{\sigma}_1 \cdot \boldsymbol{\sigma}_2 + i|\vec{q}\,|C(\boldsymbol{\sigma}_1 \cdot \hat{n} + \boldsymbol{\sigma}_2 \cdot \hat{n}) + |\vec{q}\,|^2 D\boldsymbol{\sigma}_1 \cdot \hat{q}\boldsymbol{\sigma}_2 \cdot \hat{q} + E\boldsymbol{\sigma}_1 \cdot \hat{z}\boldsymbol{\sigma}_2 \cdot \hat{z} \quad (3.18)$$

where f is a 4×4 operator in the spin space of both initial and final nucleons. The subscript cm refers to the NN centre–of–mass frame, the coefficients A, B, C, D and E are complex functions of the three–momentum transfer $|\vec{q}\,| = |\vec{k}'_{cm} - \vec{k}_{cm}|$ and collision energy $E_{cm} = \sqrt{|\vec{k}_{cm}|^2 + M^2}$, and are obtained from phase shift analyses. Introducing the isospin dependence via (see Appendix B)

$$A = A_0 + A_1 \boldsymbol{\tau}_1 \cdot \boldsymbol{\tau}_2, \quad B = B_0 + B_1 \boldsymbol{\tau}_1 \cdot \boldsymbol{\tau}_2, \quad \text{etc.} \quad (3.19)$$

yields the following parametrizations for the nonrelativistic pp (or nn) and pn scattering operators, f^{pp} (or f^{nn}) and f^{pn}, respectively (see Appendix B), namely

$$\begin{aligned}(2i|\vec{k}_{cm}|)^{-1} f^{pp} \equiv\ & (A_0 + A_1) + (B_0 + B_1)\boldsymbol{\sigma}_1 \cdot \boldsymbol{\sigma}_2 + i|\vec{q}\,|(C_0 + C_1)(\boldsymbol{\sigma}_1 \cdot \hat{n} + \boldsymbol{\sigma}_2 \cdot \hat{n}) + \\ & |\vec{q}\,|^2 (D_0 + D_1)\boldsymbol{\sigma}_1 \cdot \hat{q}\boldsymbol{\sigma}_2 \cdot \hat{q} + (E_0 + E_1)\boldsymbol{\sigma}_1 \cdot \hat{z}\boldsymbol{\sigma}_2 \cdot \hat{z} \quad (3.20)\end{aligned}$$

with an identical expression for $(2i|\vec{k}_{cm}|)^{-1} f^{nn}$, and

$$\begin{aligned}(2i|\vec{k}_{cm}|)^{-1} f^{pn} \equiv\ & (A_0 - A_1) + (B_0 - B_1)\boldsymbol{\sigma}_1 \cdot \boldsymbol{\sigma}_2 + i|\vec{q}\,|(C_0 - C_1)(\boldsymbol{\sigma}_1 \cdot \hat{n} + \boldsymbol{\sigma}_2 \cdot \hat{n}) + \\ & |\vec{q}\,|^2 (D_0 - D_1)\boldsymbol{\sigma}_1 \cdot \hat{q}\boldsymbol{\sigma}_2 \cdot \hat{q} + (E_0 - E_1)\boldsymbol{\sigma}_1 \cdot \hat{z}\boldsymbol{\sigma}_2 \cdot \hat{z}\,. \quad (3.21)\end{aligned}$$

The scattering amplitudes for particular spin directions are found by operating on the initial and final Pauli spinors. The orthogonal directions $\hat{z}$, $\hat{q}$ and $\hat{n}$ are defined as

$$\hat{z} = \hat{k}_a \qquad \hat{q} = \hat{k}_{cm} - \hat{k}'_{cm} \qquad \hat{n} = \hat{q} \times \hat{z} \tag{3.22}$$

where

$$\vec{k}_a = \frac{1}{2}(\vec{k}_{cm} + \vec{k}'_{cm}) \, . \tag{3.23}$$

The scattering matrix is normalized such that the polarized differential cross section for free NN scattering is given by

$$\frac{d\sigma}{d\Omega} = |\langle \chi^\dagger_{s'_1} \chi^\dagger_{s'_2} | f | \chi^\dagger_{s_1} \chi^\dagger_{s_2} \rangle|^2 \tag{3.24}$$

where the χ's represent the usual Pauli spinors for the different spin projections of the incident and scattered particles.

The preceding phenomenology can be parametrized in a form which displays the proper Lorentz–transformation character. The nonrelativistic scattering operator $\frac{f}{2ik_{cm}}$ is replaced by a relativistic scattering operator $\mathcal{F}$, where $\mathcal{F}(E_{cm}, |\vec{q}\,|)$ is a 4×4⊗4×4 matrix with 256 components in the Dirac spinor space of the two interacting nucleons. The relation between the nonrelativistic and relativistic scattering matrices is given by [Mc83a]:

$$\begin{aligned}(2i|\vec{k}_{cm}|)^{-1} \chi^\dagger_{s'_1} \chi^\dagger_{s'_2} f(E_{cm}, |\vec{q}\,|) \chi_{s_1} \chi_{s_2} \\ = \bar{U}(\vec{k}'_{cm}, s'_1) \bar{U}(-\vec{k}'_{cm}, s'_2) \mathcal{F}(E_{cm}, |\vec{q}\,|) U(\vec{k}_{cm}, s_1) U(-\vec{k}_{cm}, s_2)\end{aligned} \tag{3.25}$$

where $U(\vec{k}_{cm}, s)$ is a Dirac 4-component positive–energy (nucleon) spinor given by

$$U(\vec{k}_{cm}, s) = \sqrt{\frac{E+m}{2m}} \begin{pmatrix} I \\ \dfrac{\boldsymbol{\sigma} \cdot \vec{k}_{cm}}{E+m} \end{pmatrix} \chi_s \, . \tag{3.26}$$

χ is a two–component Pauli spinor of projection s, $\boldsymbol{\sigma}$ represents the Pauli spin matrices, and E is given by

$$E = \sqrt{|\vec{k}\,|^2 + m^2} \tag{3.27}$$

where m is the free nucleon mass. The Dirac spinors U are normalized such that

$$\bar{U} \, U = 1 \, . \tag{3.28}$$

This normalization is used by Bjorken and Drell [Bj64] and differs from that used in the Walecka model [Se86], namely $U^\dagger U = 1$. Again, there is an isospin label for $\mathcal{F}$, with $\mathcal{F}^{pp}$ for pp scattering and $\mathcal{F}^{pn}$ for pn scattering. Note that $\mathcal{F}$ is an operator in the two–particle Dirac space; it has 256 components when taken between all combinations of nucleon and antinucleon spinors at a given $|\vec{q}\,|$ and E_{cm}. Just as symmetries reduce the number of possible independent spin matrix elements of f to five (see Appendix G), parity, time–reversal, and isospin invariance reduce the number of independent amplitudes of $\mathcal{F}$ to 44, for on–shell kinematics [Tj85]. Hence, there can be many different operators $\mathcal{F}$ with the same five on–shell matrix elements, but different $4\times4\bigotimes4\times4$ matrix structures. These different structures will give different negative energy spinor matrix elements of $\mathcal{F}$. The information contained in the measurement of the free NN amplitudes, which are related to the five complex Wolfenstein parameters, determines only a small number of the components of $\mathcal{F}$, and so some assumptions need to be made about the form of $\mathcal{F}$ in Eq. (3.25). A convenient parametrization, which was originally introduced in the relativistic impulse approximation, is given by [Mc83a]

$$\mathcal{F}(E_{cm}, |\vec{q}\,|) = \sum_{i=1}^{5} F_i(E_{cm}, |\vec{q}\,|)\lambda_i^{(1)} \cdot \lambda_i^{(2)} \tag{3.29}$$

where the superscripts (1) and (2) refer to the projectile and target nucleons respectively. The i's stand for the five Dirac matrices listed in Table 3.2, and the dot product implies that the Lorentz indices are contracted. With Eq. (3.29), the right hand side of Eq. (3.25) can now be written as a sum of five terms:

$$\begin{aligned}(2i|\vec{k}_{cm}|)^{-1}\chi^\dagger_{s'_1}\chi^\dagger_{s'_2} f(E_{cm}, |\vec{q}\,|)\chi_{s_1}\chi_{s_2} &= F_S(\bar{U}_{1'}U_1)(\bar{U}_{2'}U_2) + F_V(\bar{U}_{1'}\gamma^\mu U_1)(\bar{U}_{2'}\gamma_\mu U_2) \\ +F_T(\bar{U}_{1'}\sigma^{\mu\nu}U_1)(\bar{U}_{2'}\sigma_{\mu\nu}U_2) &+ F_A(\bar{U}_{1'}\gamma^5\gamma^\mu U_1)(\bar{U}_{2'}\gamma^5\gamma_\mu U_2) + F_P(\bar{U}_{1'}\gamma^5 U_1)(\bar{U}_{2'}\gamma^5 U_2)\ .\end{aligned} \tag{3.30}$$

The scattering matrix in Eq. (3.29) is usually referred to as the **SVPAT** (**S**calar–**V**ector–**P**seudoscalar–**A**xialvector–**T**ensor) parametrization of the relativistic NN amplitudes.

With explicit expressions for the Dirac spinors and the γ matrices, the right hand side of Eq. (3.30) can be written in terms of the independent set of spin operators and Pauli spinors, and the coefficients can be identified with those of the right hand side of Eq. (3.18). In this way, the five SVPAT amplitudes (F_S, F_V, F_P, F_A, F_T) and the Wolfenstein amplitudes (A, B, C, D, E) can be written as linear combinations of one another. Hence, one can derive a 5×5 nonsingular matrix $\mathcal{O}(E_{cm}, |\vec{k}_a|, |\vec{q}\,|)$ which gives the MRW (centre–of–mass) amplitudes in

Table 3.2: Dirac matrix types parametrizing the free NN amplitudes.

$$\mathcal{F}(E_{cm}, |\vec{q}\,|) = \sum_{i=1}^{5} F_i(E_{cm}, |\vec{q}\,|)\lambda_i^{(1)} \cdot \lambda_i^{(2)}$$

i	λ_i
S (scalar)	1
V (vector)	γ_μ
P (pseudoscalar)	γ_5
A (axial–vector)	$\gamma_5\gamma_\mu$
T (tensor)	$\sigma_{\mu\nu}$

terms of the F_i invariants [Mc83a, Mu87a]:

$$\begin{pmatrix} A \\ B \\ C \\ D \\ E \end{pmatrix} = \begin{pmatrix} & & \\ & \mathcal{O}(E_{cm}, |\vec{k}_a|, |\vec{q}\,|) & \\ & & \end{pmatrix} \begin{pmatrix} F_S \\ F_V \\ F_T \\ F_P \\ F_A \end{pmatrix} . \tag{3.31}$$

Explicit expressions for the individual matrix elements of the 5×5 matrix are given in the paper by McNeil, Ray and Wallace [Mc83a].

For application to quasielastic scattering, the commonly used SVPAT parametrization is limited in that it does not address the exchange behaviour of the NN amplitudes in the nuclear medium, and is also rather crude in distinguishing between different forms of the πNN vertex (see Sec. 3.2.6). These shortcomings are, however, overcome by using a relativistic meson–exchange model of the NN amplitudes. The next section is devoted to a discussion of such a model.

Relativistic Horowitz–Love–Franey model

In principle, the NN t–matrix can be obtained via solution of the Bethe–Salpeter equation, where the on–shell NN amplitudes are matrix elements of this t–matrix. However, the complexity of this approach gives limited physical insight into the resulting amplitudes. An alternative approach is to fit the amplitudes directly with some phenomenological form, rather than generating the t–matrix from a microscopic interaction. Although the microscopic approach is certainly more fundamental, the advantage of phenomenological fits lies in their simple analytical form, which allows them to be conveniently incorporated in calculations requiring the NN t–matrix as input: see for example, the studies of elastic proton–nucleus scattering [Mu87a, Mu87b] and proton knockout reactions [Co89, Ma90, Ma93, Ma94, Ik95, Ma96a] based on the impulse approximation.

The NN t–matrix employed in this work is based on the relativistic meson–exchange described in Refs. [Ho85, Ho88, Ho91a], and will be referred to as the **H**orowitz–**L**ove–**F**raney (**HLF**) model. Essentially this model parametrizes the NN t–matrix in terms of a number of Yukawa–type meson exchanges in first–order Born approximation, such that both direct and exchange NN diagrams are considered separately. The corresponding Feynman diagrams for the HLF model are shown Fig. 3.4. The HLF model is used to investigate the importance of exchange effects, and also to study the consequences of different forms of the πNN vertex on quasielastic polarization transfer observables at various incident energies. Furthermore, this model is also used to generate microscopic optical potentials as already discussed in Sec. 3.2.2.

The meson–nucleon coupling constants and meson–nucleon form factors are adjusted to fit the relativistic NN amplitudes in Eq. (3.25). The fit provides a simple analytical form with a physical basis in the one–boson exchange mechanism. However, the price one pays for this simplicity is that:

- the coupling constants have a systematic and small energy dependence,
- the cutoff parameters vary dramatically from one energy to another,
- and, the meson–nucleon coupling constants and cutoff parameters are complex.

Horowitz [Ho85] emphasized that the (small) imaginary couplings are a purely phenomenological

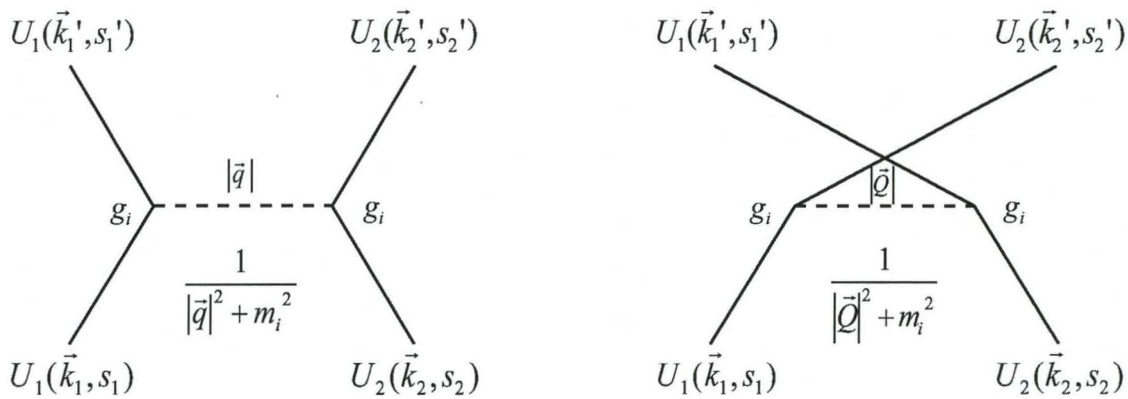

Figure 3.4: Feynman diagrams for the direct and exchange terms in the Horowitz–Love–Franey meson–exchange model. The notation is defined in the text.

means of obtaining the imaginary amplitudes, that is, they have no physical significance. The real coupling constants, on the other hand, agree with those obtained from one–boson exchange potentials. The mesons have different isospins and Lorentz types [Scalar (S), Vector (V), Tensor (T), Pseudoscalar (P) and Axial–vector (A)] such that there exists a simple relationship between individual Lorentz–invariant amplitudes and mesons exchanged. This relationship is lacking in the nonrelativistic Love–Franey model [Lo81a, Hi90], where the NN interaction is represented by an arbitrary sum of Yukawa functions.

The formalism for the HLF model is now presented. The intention is to parametrize the righthand side of Eq. (3.25) in terms of a set of meson–exchanges for both the direct and exchange amplitudes depicted by the Feynman diagrams in Fig. 3.4. For a meson of spin zero and mass m, one uses the nonrelativistic limit of the Klein–Gordon propagator [Bj64] (valid when the recoil kinetic energies of the nucleons are neglected relative to their rest mass energies) so that the mesons have propagators of the form

$$\frac{1}{|\vec{q}\,|^2 + m^2}\,, \tag{3.32}$$

where $\vec{q}$ is the three–momentum transfer, and the meson–nucleon vertices have the following monopole form factors

$$\frac{1}{1 + \frac{|\vec{q}\,|^2}{\Lambda^2}}\,, \tag{3.33}$$

with *separate* masses and cutoff parameters for the real and imaginary parts of the amplitude denoted by m, $\bar{m}$ and Λ, $\bar{\Lambda}$ respectively. From Feynman rules [Bj64, Sa67], the NN–meson vertex factor is

$$g_i\left(\frac{1}{1 + \frac{|\vec{q}\,|^2}{\Lambda_i^2}}\right)\, \lambda^{L(i)}(\vec{\tau}\,)^{T_i}\,, \tag{3.34}$$

where $L(i)\ \epsilon\ \{\mathrm{S, V, T, A, P}\}$, and $T_i = (0,1)$ is the isospin of the i^{th} meson. If one denotes the total isospin of the two–nucleon state by T, then the T = 0 scattered wave is symmetric for interchange of both spatial and spin coordinates, so that there is a relative (+) sign between the direct and exchange diagrams in Fig. 3.4. For T =1 scattering, the wave function is antisymmetric for interchange of both spatial and spin coordinates, and hence, there is a relative (−) sign between the diagrams. Then, up to an overall kinematic factor, the contribution of (real)

meson i to the i^{th} (real) amplitude is [Bj64, Sa67, Br76]

$$\bar{U}_{1'}\bar{U}_{2'}\mathcal{F}_i U_1 U_2 \propto \frac{g_i^2}{m_i^2+|\vec{q}\,|^2}\left(\frac{1}{1+\frac{|\vec{q}\,|^2}{\Lambda_i^2}}\right)^2 \bar{U}_{1'}\lambda^{L(i)}U_1\bar{U}_{2'}\lambda^{L(i)}U_2\{\boldsymbol{\tau}_1\cdot\boldsymbol{\tau}_2\}^{T_i}$$
$$+\ (-1)^T\frac{g_i^2}{m_i^2+|\vec{Q}\,|^2}\left(\frac{1}{1+\frac{|\vec{Q}\,|^2}{\Lambda_i^2}}\right)^2 \bar{U}_{2'}\lambda^{L(i)}U_1\bar{U}_{1'}\lambda^{L(i)}U_2\{\boldsymbol{\tau}_1\cdot\boldsymbol{\tau}_2\}^{T_i} \tag{3.35}$$

where the magnitude of the direct three–momentum transfer $|\vec{q}\,|$ is expressed in terms of the centre–of–mass scattering angle θ_{cm} (see Appendix D)

$$|\vec{q}\,| = 2|\vec{k}_{cm}\,|\sin(\frac{\theta_{cm}}{2})\,, \tag{3.36}$$

and $|\vec{Q}\,|$ is the magnitude of the exchange three–momentum transfer (see Appendix D)

$$|\vec{Q}\,| = \sqrt{4|\vec{k}_{cm}|^2-|\vec{q}\,|^2}\,. \tag{3.37}$$

The momentum of a nucleon in the centre–of–mass frame is (see Appendix D)

$$2|\vec{k}_{cm}\,| = \sqrt{2T_{\rm lab}M} \tag{3.38}$$

where T_{lab} is the incident laboratory kinetic energy of the projectile. The meaning of $\{\boldsymbol{\tau}_1\cdot\boldsymbol{\tau}_2\}^{T_i}$ is given by Eqs (3.52) and (3.53) (see also Appendix B). The imaginary part of the i^{th} amplitude has the same form as Eq. (3.35), except that the real values g_i, m_i and Λ_i are replaced by the corresponding imaginary values $\bar{g}_i$, $\bar{m}_i$ and $\bar{\Lambda}_i$, respectively.

The first term in Eq. (3.35) is already of the form of the righthand side of Eq. (3.30) from which one can identify the contributions to the F_i's in that expression. The second term is not of this form because of the different order of spinors in the product. However, it can be rewritten with a Fierz transformation [Br76, Na90]

$$(\bar{U}_{2'}\lambda^L\bar{U}_1)(\bar{U}_{1'}\lambda^L\bar{U}_2) = \sum_{L'} C_{LL'}(\bar{U}_{1'}\lambda^{L'}\bar{U}_1)(\bar{U}_{2'}\lambda^{L'}\bar{U}_2) \tag{3.39}$$

where

$$C_{LL'} = \frac{1}{8}\begin{pmatrix} 2 & 2 & 1 & -2 & 2 \\ 8 & -4 & 0 & -4 & -8 \\ 24 & 0 & -4 & 0 & 24 \\ -8 & -4 & 0 & -4 & 8 \\ 2 & -2 & 1 & 2 & 2 \end{pmatrix} \tag{3.40}$$

with the rows and columns labeled in the order (S, V, T, A, P). Hence Eq. (3.30) is rewritten as

$$\bar{U}_{1'}\bar{U}_{2'}\mathcal{F}_i U_1 U_2 \propto \frac{g_i^2}{m_i^2+|\vec{q}\,|^2}\left(\frac{1}{1+\frac{|\vec{q}\,|^2}{\Lambda_i^2}}\right)^2\{\boldsymbol{\tau}_1\cdot\boldsymbol{\tau}_2\}^{T_i}\bar{U}_{1'}\lambda^{L(i)}U_1\bar{U}_{2'}\lambda^{L(i)}U_2$$

$$+\ (-1)^T\frac{g_i^2}{m_i^2+|\vec{Q}\,|^2}\left(\frac{1}{1+\frac{|\vec{Q}\,|^2}{\Lambda_i^2}}\right)^2\{\boldsymbol{\tau}_1\cdot\boldsymbol{\tau}_2\}^{T_i}\sum_{L'}C_{L(i)L'}\bar{U}_{1'}\lambda^{L'}U_1\bar{U}_{2'}\lambda^{L'}U_2 \tag{3.41}$$

and the identification of the contributions to the invariants F_S, F_V, F_T, F_A and F_P can now be made. Note, that while a meson always contributes to the F_i invariant of the same Lorentz type in the direct term, all the other meson types appear in the exchange term. With the normalization in Eq. (3.28), the kinematic factor (which differs from the factor presented in Ref. [Ho85]: see Ref. [Mu87a] and Appendix A in Ref. [Mu87b]) needed to give the free spinor matrix elements in Eqs. (3.25) and (3.29) is

$$\frac{im^2}{2E_{cm}|\vec{k}_{cm}|} \tag{3.42}$$

where the NN centre–of–mass energy E_{cm} is defined in terms of the NN centre–of–mass momentum $\vec{k}_{cm}$ and the nucleon mass m, namely

$$E_{cm} \;=\; \sqrt{|\vec{k}_{cm}|^2+m^2}\,. \tag{3.43}$$

Combining all of these factors, the total contribution to the invariant F_L, in Eqs. (3.29) and (3.30), from all of the N mesons exchanged is the sum of direct and exchange terms, namely

$$F_L = \frac{im^2}{2E_{cm}k_{cm}}[F_L^D(|\vec{q}\,|)+F_L^X(|\vec{Q}\,|)] \tag{3.44}$$

$$F_L^D(|\vec{q}\,|) = \sum_{i=1}^{N}\delta_{L,L(i)}\{\boldsymbol{\tau}_1\cdot\boldsymbol{\tau}_2\}^{T_i}f^i(|\vec{q}\,|) \tag{3.45}$$

$$F_L^X(|\vec{Q}\,|) = (-1)^T\sum_{i=1}^{N}C_{L(i),L}\{\boldsymbol{\tau}_1\cdot\boldsymbol{\tau}_2\}^{T_i}f^i(|\vec{Q}\,|) \tag{3.46}$$

$$f^i(x) = f_R^i(x) - if_I^i(x) \tag{3.47}$$

$$f_R^i(x) = \frac{g_i^2}{x^2+m_i^2}\left(1+\frac{x^2}{\Lambda_i^2}\right)^{-2} \tag{3.48}$$

$$f_I^i(x) = \frac{\bar{g}_i^2}{x^2 + \bar{m}_i^2}(1 + \frac{x^2}{\bar{\Lambda}_i^2})^{-2}\,, \tag{3.49}$$

where x represents either $|\vec{q}\,|$ or $|\vec{Q}\,|$. The invariant amplitudes for pp and pn scattering are:

$$F_i(pp) \;=\; F_i(T=1) \tag{3.50}$$

$$F_i(pn) \;=\; \frac{1}{2}[F_i(T=1) \;+\; F_i(T=0)]\,. \tag{3.51}$$

The meaning of $\{\boldsymbol{\tau}_1 \cdot \boldsymbol{\tau}_2\}^{T_i}$ is explained in Appendix B: for the $T=1$ amplitudes

$$(\boldsymbol{\tau}_1 \cdot \boldsymbol{\tau}_2)^{T_i} \;=\; \left\{ \begin{array}{l} 1 \;\text{ for the exchange of }\; T_i = 0 \;\;\text{(isoscalar) mesons} \\ \\ 1 \;\text{ for the exchange of }\; T_i = 1 \;\;\text{(isovector) mesons} \end{array} \right\} \tag{3.52}$$

and, for $T=0$ amplitudes

$$(\boldsymbol{\tau}_1 \cdot \boldsymbol{\tau}_2)^{T_i} \;=\; \left\{ \begin{array}{l} 1 \;\text{ for the exchange of }\; T_i = 0 \;\;\text{(isoscalar) mesons} \\ \\ -3 \;\text{ for the exchange of }\; T_i = 1 \;\;\text{(isovector) mesons} \end{array} \right\}\,. \tag{3.53}$$

The original HLF parameter sets exist only at incident proton energies of 135, 200, 300 and 400 MeV [Ho85, Mu87a]. More technical detail on the types of mesons and fitting procedure for extracting the HLF parameters can be found in Sec. 3.3.3.

In relativistic quantum mechanics, most scattering observables are usually expressed in terms of invariant scattering matrix elements. The next section focuses on the invariant scattering matrix elements for quasielastic proton–nucleus scattering.

3.2.5 Invariant scattering matrix elements

Using the conventions of Bjorken and Drell [Bj64], the invariant matrix element for the quasielastic proton-scattering process, depicted in Fig. 3.1, is given by [Ho86, Mu87a, Ho88, Iq88] (see also Appendix E)

$$\mathcal{M} = \sum_{i=1}^{T} \bar{U}(m_1^*, \vec{k}_1', s_1')\lambda_i U(m_1^*, \vec{k}_1, s_1) t_i(\theta_{\text{eff}}^{cm}, T_{\text{eff}}^{L}) \bar{U}(m_2^*, \vec{k}_2', s_2')\lambda^i U(m_2^*, \vec{k}_2, s_2) \tag{3.54}$$

where the nucleon Dirac spinors $U(m^*, \vec{k}, s)$ are given by

$$U(m^*, \vec{k}, s) = \sqrt{\frac{E^* + m^*}{2m^*}} \begin{pmatrix} I \\ \dfrac{\boldsymbol{\sigma} \cdot \vec{k}}{E^* + m^*} \end{pmatrix} \chi_s \tag{3.55}$$

and are normalized such that

$$\bar{U}(m^* = m, \vec{k}, s)\, U(m^* = m, \vec{k}, s) \;=\; 1\,. \tag{3.56}$$

χ is a two–component Pauli spinor of projection s, $\boldsymbol{\sigma}$ represents the Pauli spin matrices, and E^* is given by

$$E^* = \sqrt{|\vec{k}\,|^2 + m^{*2}} \tag{3.57}$$

where m^* is the effective nucleon mass defined in Sec. 3.2.2. The invariant functions $t_i(\theta_{\rm eff}^{cm}, T_{\rm eff}^L)$ are related to the invariant amplitudes $F_i(\theta_{\rm eff}^{cm}, T_{\rm eff}^L)$, introduced in Sec. 3.2.4, via (see Appendix F)

$$t_i(\theta_{\rm eff}^{cm}, T_{\rm eff}^L) = \frac{-\,8\pi\, i |\vec{k}_{\rm eff}| E_{\rm eff}}{m^2} F_i(\theta_{\rm eff}^{cm}, T_{\rm eff}^L) \tag{3.58}$$

where $|\vec{k}_{\rm eff}|E_{\rm eff}$ is an invariant flux factor [Gr94]. This relation enforces the normalization condition expressed by Eqs. (3.24), (3.25) and (3.28). The kinematic quantities $T_{\rm eff}^L$, $|\vec{k}_{\rm eff}|$ and $E_{\rm eff}$ are the effective laboratory momentum, kinetic energy and total energy of the projectile in the frame where the target nucleon is at rest (see Appendix I):

$$T_{\rm eff}^L = \frac{E_1 E_2 - \vec{k}_1 \cdot \vec{k}_2 - m^2}{m}\,, \tag{3.59}$$

$$E_{\rm eff} = T_{\rm eff}^L + m = \sqrt{|\vec{k}_{\rm eff}|^2 + m^2} \tag{3.60}$$

where k_2 is the target–nucleon momentum, which ranges between $k_{\rm min}$ and $k_{\rm max}$ defined by Eqs. (3.15) and (3.16), and $|\vec{k}_1|$ is expressed in terms of the incident laboratory kinetic energy $T_{\rm lab}$

$$|\vec{k}_1| = \sqrt{(T_{\rm lab} + m_1)^2 - m_1^2}\,. \tag{3.61}$$

For each momentum $\vec{k}_2$ and azimuthal angle ϕ between $\vec{q}$ and $\vec{k}_2$, the NN amplitudes t_i are evaluated at the effective laboratory kinetic energy $T_{\rm eff}^L$ and NN centre–of–mass scattering angle $\theta_{\rm eff}^{cm}$ (see Appendix I)

$$\theta_{\rm eff}^{cm} = 2\,\sin^{-1}\!\left(\frac{|\vec{q}\,|^2 - \omega^2}{2mT_{\rm eff}^L}\right)^{\frac{1}{2}} \tag{3.62}$$

where the momentum transfer $\vec{q}$ is

$$\vec{q} = \vec{k}_1 - \vec{k}'_1 = \vec{k}'_2 - \vec{k}_2 \tag{3.63}$$

and energy transfer ω is

$$\omega = E^*_1 - E'^*_1 = E'^*_2 - E^*_2 \,. \tag{3.64}$$

The starred quantities are defined in the NN laboratory system as

$$\begin{aligned} E^*_1 &= \sqrt{|\vec{k}_1|^2 + m^{*2}_1} \\ E'^*_1 &= \sqrt{|\vec{k}'_1|^2 + m^{*2}_1} \\ E^*_2 &= \sqrt{|\vec{k}_2|^2 + m^{*2}_2} \\ E'^*_2 &= \sqrt{|\vec{k}'_2|^2 + m^{*2}_2} \,. \end{aligned} \tag{3.65}$$

In practice, a large table of relativistic amplitudes, calculated from the summer 1986 Arndt phase shifts (with the Coulomb interaction removed), is interpolated quadratically every 25 MeV on $T^L_{\rm eff}$ (from 25 MeV to 1200 MeV) and linearly every 5° on $\theta^{cm}_{\rm eff}$ (from 5° to 175°).

In the next section, the ambiguities exhibited by the relativistic SVPAT parametrization of the NN scattering operator are discussed.

3.2.6 Pseudoscalar versus pseudovector forms of the πNN vertex

In the past, concern has been expressed about ambiguities in the form of the relativistic NN scattering operator $\mathcal{F}$ given by Eq. (3.29) [Ma82, Se86, Ho88, Ho91b]. The form shown in Table 3.2 is sufficient to parametrize the free NN amplitudes. However, as already mentioned in Sec. 3.2.4, there are many operators with the same five on–shell matrix elements, but different $4\times4\bigotimes4\times4$ matrix structures. Furthermore, recall that the impulse approximation assumes the same form (see Table 3.2) for both free and medium–modified NN scattering.

The question now arises as to how the medium–modified scattering matrix, and consequently the polarization transfer observables, change when other forms of $\mathcal{F}$, different to that specified

in Eq. (3.29), are used. Once again, it is stressed, that although the different forms of $\mathcal{F}$ must parametrize the same free NN observables, one may expect differences in the medium–modified polarization transfer observables.

One of the major ambiguities concerns the choice of the πNN vertex in the amplitudes [Ma82, Se86, Mu87a, Ho88, Ho91a]. One could use either a pseudoscalar vertex, which simply uses the five amplitudes in Table 3.2, or a pseudovector vertex. The pion is a pseudoscalar particle with negative intrinsic parity. Hence the Lagrangian density for pion–nucleon interactions must contain a term which couples the pseudoscalar pion field $\boldsymbol{\pi}$ to the pseudoscalar density $\bar{\psi}\gamma_5\boldsymbol{\tau}\psi$ [Se86], where $\boldsymbol{\tau}$ is the usual isospin operator [Se86]. However, the other commonly used form contains a term which couples the derivative of the pseudoscalar pion field $\partial^\mu\boldsymbol{\pi}$ [which is a pseudovector quantity] to the pseudovector density $\bar{\psi}\gamma_5\gamma_\mu\boldsymbol{\tau}\psi$.

Elastic proton–nucleus spin observables at energies higher than 400 MeV show no difference between pseudoscalar and pseudovector couplings of the pion. At lower energies, however, the differences become larger and the pseudovector coupling is more compatible with the strength and energy dependence of the real scalar and vector optical potentials [Ho85]. On the other hand, crude calculations of quasielastic $(\vec{p},\vec{p}')$ polarization transfer observables at 290 and 420 MeV [Hi94] suggest a pseudoscalar form. However, various theoretical arguments [Se86] support the pseudovector form. At this stage, however, no overwhelming experimental evidence seems to clearly resolve this ambiguity, and hence, one of the aims of this thesis is to search for quasielastic polarization transfer observables that are sensitive to pseudoscalar or pseudovector forms of the πNN coupling.

One can only talk about pseudoscalar (PS) or pseudovector (PV) forms of the πNN interaction within the context of a Yukawa–type meson–exchange model, such as the HLF model. Calculations of quasielastic proton–nucleus polarization transfer observables by Horowitz and Murdock [Ho88] assumed that the $\bar{U}\gamma^5 U$ amplitudes in Eq. (3.30) were solely due to pion exchange. In this case the transition from a pseudoscalar to a pseudovector πNN coupling was made via the following substitution in Table 3.2:

$$\lambda_{ps} = \gamma_5 \longrightarrow \lambda_{pv} = \pm\frac{q_\mu\gamma^\mu\gamma_5}{2m}\,, \tag{3.66}$$

where q^μ is the four–momentum transfer. As noted above, this substitution does not change the NN amplitudes obtained from fitting free NN data, because the *free* spinors U in Eq. (3.30)

satisfy [using the notation $U_i(m_i^*) = U(m_i^*, \vec{k}_i, s_i)$]

$$[\bar{U}_1'(m)\lambda_{pv}U_1(m)]\,[\bar{U}_2'(m)\lambda_{pv}U_2(m)] = [\bar{U}_1'(m)\lambda_{ps}U_1(m)]\,[\bar{U}_2'(m)\lambda_{ps}U_2(m)]\,, \qquad (3.67)$$

thus giving the same free NN data: indeed, the PV πNN coupling in Eq. (3.66) is defined to yield the same free NN amplitudes as PS coupling. In a nuclear medium, the corresponding equality is

$$[\bar{U}_1'(m_1^*)\lambda_{pv}U_1(m_1^*)]\,[\bar{U}_2'(m_2^*)\lambda_{pv}U_2(m_2^*)] = M_1^*M_2^*[\bar{U}_1'(m_1^*)\lambda_{ps}U_1(m_1^*)]\,[\bar{U}_2'(m_2^*)\lambda_{ps}U_2(m_2^*)]\,, \qquad (3.68)$$

such that the pseudoscalar and pseudovector amplitudes are no longer equal, but differ by a factor $M_1^*M_2^*$ [recall that $M^* = \frac{m^*}{m}$]. This approximation is acceptable if one assumes that all the amplitudes are direct, and exchange contributions are negligibly small: recall that the Fierz matrix allows all mesons in Table 3.4 to contribute to each type of NN exchange amplitude. Furthermore, the SVPAT amplitudes do not explicitly incorporate the meson mediators of the NN force, such as the long range pions, for example, and hence, the SVPAT parametrization represents a fairly crude way of treating the different "pion" couplings: the relativistic SVPAT NN amplitudes are merely obtained via a matrix relation from a Wolfenstein–type parametrization of the Arndt phase shifts [see Eq. (3.31)].

A more appropriate way, to distinguish between PS and PV forms of the πNN vertex, would be to use the HLF model (or any meson–exchange model for the NN interaction) where the direct invariants in Eq. (3.30) are expressed as linear combinations of the five exchange invariants via the Fierz matrix [see Eq. (3.39)], such that the exchange terms from the "pion" contribute to each type of invariant. Analogous to Eq. (3.68), the transition from a pseudoscalar to a pseudovector πNN vertex, within the HLF model, is made by performing the following substitution in all direct and exchange terms in Eq. (3.41) containing the "pion":

$$g_\pi^2 \longrightarrow g_\pi^2 M_1^* M_2^*\,. \qquad (3.69)$$

Horowitz [Ho85] points out that the values of the pion coupling are virtually energy independent and agree with the corresponding values for one–boson–exchange–potentials. Hence, the substitution in Eq. (3.69) should give a fairly accurate description of the pseudovector form of the πNN vertex: this is one of the main motivations for using the HLF model.

The ultimate test for the validity of the more refined version of the RPWIA, is to compare model predictions of observables to all available experimental data. The following section is concerned with explicit expressions for the scattering observables of interest.

3.2.7 Scattering observables

Expressions for the (unpolarized and polarized) double differential cross section and polarization transfer observables, for quasielastic $(\vec{p},\vec{p}\,')$ scattering, are now derived in terms of the invariant scattering matrix $\mathcal{M}$ in Eq. (3.54). The corresponding $(\vec{p},\vec{n})$ scattering observables will be discussed in Sec. 3.2.8.

Double differential cross section

The general expression for the differential cross section to scatter from initial spin state $j = s_1$ to final spin state $i' = s_1'$ with particle 2 unobserved is [Bj64, Mu87a, Ho88, Gr92] (also see Sec. E.4 in Appendix E):

$$d\sigma_{j\to i'} = \frac{1}{|\vec{v}_1 - \vec{v}_2|}\,\frac{m_1^{*2}}{E_1^*\,E_1'^*}\,\frac{d\,\vec{k}_1'}{(2\pi)^3}\int \frac{d\,\vec{k}_2'}{(2\pi)^3}\,\frac{m_2^{*2}}{E_2^*\,E_2'^*}(2\pi)^4\,\delta^4\,(k_1' + k_2' - k_1 - k_2)\,\frac{1}{2}\sum_{s_2,\,s_2'}\mathcal{M}^*\,\mathcal{M}$$

where, analogous to electron–proton scattering discussed in Sec. E.5.1 in Appendix E, and using Eq. (3.54), one can express the quantity $\sum_{s_2,\,s_2'}\mathcal{M}^*\,\mathcal{M}$ as a contraction of a projectile–tensor $P_{m\,n}$ with a target–tensor $T^{m\,n}$, that is

$$\begin{aligned}\sum_{s_2,\,s_2'}\mathcal{M}^*\,\mathcal{M} &= \sum_{s_2,\,s_2'}|\mathcal{M}|^2 \\ &= t_m(\theta_{\rm eff}^{cm},T_{\rm eff}^L)\;t_n(\theta_{\rm eff}^{cm},T_{\rm eff}^L)^*\;P_{m\,n}\,T^{m\,n}\end{aligned} \tag{3.70}$$

where

$$P_{m\,n} = [\bar{U}(m_1^*,\vec{k}_1',s_1')\lambda_m U(m_1^*,\vec{k}_1,s_1)]\,[\bar{U}(m_1^*,\vec{k}_1',s_1')\lambda_n U(m_1^*,\vec{k}_1,s_1)]^* \tag{3.71}$$

$$= [\bar{U}(m_1^*,\vec{k}_1',s_1')\lambda_m U(m_1^*,\vec{k}_1,s_1)]\,[\bar{U}(m_1^*,\vec{k}_1,s_1)\lambda_n U(m_1^*,\vec{k}_1',s_1')] \tag{3.72}$$

and

$$T^{i\,j} = [\bar{U}(m_2^*,\vec{k}_2',s_2')\lambda^m U(m_2^*,\vec{k}_2,s_2)]\,[\bar{U}(m_2^*,\vec{k}_2',s_2')\lambda^n U(m_2^*,\vec{k}_2,s_2)]^* \tag{3.73}$$

$$= [\bar{U}(m_2^*,\vec{k}_2',s_2')\lambda^m U(m_2^*,\vec{k}_2,s_2)]\,[\bar{U}(m_2^*,\vec{k}_2,s_2)\lambda^n U(m_2^*,\vec{k}_2',s_2')]\,. \tag{3.74}$$

Note that since the spinors are parametrized by effective masses m_1^* and m_2^* [see Eq. (3.55)] and not the free mass m, the usual Feynman "$\frac{m}{E}$" factors and the δ function in the formula for $d\sigma$

are in terms of the E^*'s. The approximate incident flux in nuclear matter is taken to be [Gr92] (also see Appendix E)

$$|\vec{v}_1 - \vec{v}_2| \approx \frac{|\vec{k}_1|}{E_1^*} \tag{3.75}$$

and, furthermore, one also makes use of the fact that [Bj64]

$$d\vec{k}_1' = |\vec{k}_1'|\, E_1'\, dE_1'\, d\Omega_1' \,. \tag{3.76}$$

Note that there is no star (*) on E_1' in Eq. (3.76), since one is interested in the differential *free* energy for the cross section, that is, free nucleons are eventually detected. The integral over $\vec{k}_2'$ selects the value

$$\vec{k}_2' = \vec{k}_1 + \vec{k}_2 - \vec{k}_1' \tag{3.77}$$

from the 3–space part of the energy–momentum–conserving delta function. Finally, since the target is treated as a Fermi–gas, the Fermi motion averaging is done over the possible values of $\vec{k}_2$. Hence, the polarized double differential cross section for quasielastic proton scattering can now be expressed as

$$\frac{d\sigma_{j\to i'}}{d\Omega_1'\, dE_1'} = \frac{|\vec{k}_1'|}{|\vec{k}_1|}\frac{m_1^{*2}\, E_1'}{E_1'^*}\int_{k_{\min}}^{k_{\max}} \frac{d\vec{k}_2}{\frac{4}{3}\pi\, k_F^3}\frac{m_2^{*2}}{E_2^*\, E_2'^*}\frac{\delta\,(E_1^* + E_2^* - E_2'^* - E_1'^*)}{(2\pi)^2}\frac{1}{2}\sum_{s_2,\, s_2'} \mathcal{M}^*\,\mathcal{M}$$

where $k_{\min}$ and $k_{\max}$ are defined by Eqs. (3.15) and (3.16). The factor $\frac{4}{3}\pi\, k_F^3$ represents the volume of a Fermi–sphere in momentum space, and ensures that the double differential cross section is normalized per target nucleon, i.e. one calculates the double differential cross section for scattering from a *single* target nucleon. The integral over $d\vec{k}_2$ yields:

$$\int_{k_{\min}}^{k_{\max}} d\vec{k}_2\,\frac{\delta\,(E_1^* + E_2^* - E'^*_2 - E'^*_1)}{E'^*_2} = \int_{k_{\min}}^{k_{\max}} d|\vec{k}_2|\,\frac{|\vec{k}_2|}{|\vec{q}\,|}\int d\phi\Big|_{\chi=\chi_0} \tag{3.78}$$

where the angle χ between $\vec{k}_2$ and $\vec{q}$ is fixed by the energy–conserving delta function, yielding

$$\cos\chi = \cos\chi_0 = \frac{|\vec{q}\,|^2 + 2\omega\; E_2^*}{2|\vec{k}_2|\,|\vec{q}\,|}\,. \tag{3.79}$$

[See Appendix J for the explicit evaluation of the integral on the lefthand side of Eq. (3.78).] This gives the following expression for the polarized double differential cross section

$$\frac{d\sigma_{j\to i'}}{d\Omega_1'\, dE_1'} = \frac{|\vec{k}_1'|}{|\vec{k}_1|}\frac{m_1^{*2}\, E_1'}{E_1'^*}\int_0^{2\pi} d\phi\int_{k_{\min}}^{k_{\max}}\frac{d|\vec{k}_2|}{\frac{4}{3}\pi\, k_F^3}\,\frac{|\vec{k}_2|\, E_2'^*}{|\vec{q}\,|}\,\frac{m_2^{*2}}{E_2^*\, E_2'^*}\,\frac{1}{(2\pi)^2}\frac{1}{2}\sum_{s_2,\, s_2'}\mathcal{M}^*\mathcal{M}\Big|_{\chi=\chi_0} \,. \tag{3.80}$$

Defining

$$\Theta\left(|\vec{k}_2|\right) = \frac{|\vec{k}_1'|}{|\vec{k}_1|}\, m_1^{*2}\, \frac{E_1'}{E_1'^*}\, \frac{1}{\frac{4}{3}\pi\, k_F^3}\, \frac{m_2^{*2}}{E_2^*\, E_2'^*}\, \frac{|\vec{k}_2|\, E_2'^*}{|\vec{q}\,|}\,, \tag{3.81}$$

the formula simplifies to

$$\frac{d\sigma_{j\to i'}}{d\Omega_1'\, dE_1'} = \int_0^{2\pi} d\phi \int_{k_{\min}}^{k_{\max}} d|\vec{k}_2|\, \Theta\left(|\vec{k}_2|\right) \frac{1}{2} \sum_{s_2, s_2'} \mathcal{M}^* \mathcal{M} \Big|_{\chi=\chi_0}\,. \tag{3.82}$$

To get the unpolarized double differential cross section, one must average Eq. (3.82) over initial spins s_1 and sum over final spins s_1', that is

$$\left.\frac{d\bar{\sigma}}{d\Omega_1'\, dE_1'}\right|_{\text{unpol}} = \int_0^{2\pi} d\phi \int_{k_{\min}}^{k_{\max}} d|\vec{k}_2|\, \Theta\left(|\vec{k}_2|\right) \frac{1}{4} \sum_{s_1, s_1', s_2, s_2'} \mathcal{M}^* \mathcal{M} \Big|_{\chi=\chi_0}\,. \tag{3.83}$$

The additional factor of $\frac{1}{2}$ comes from averaging over the initial spins. In the next section expressions for the quasielastic proton scattering polarization transfer observables are written down in terms of appropriate combinations of the polarized double differential cross sections given by Eq. (3.82).

Polarization transfer observables

The general expressions for the polarization transfer observables for free NN scattering are derived in Appendix G. For quasielastic proton–nucleus scattering the expressions for the polarization transfer observables are similar to those for free scattering, the only differences being that one now deals with a relativistic scattering matrix $\mathcal{M}$, and one needs to integrate over the momenta of the target nucleon. First the initial and final laboratory coordinate frames are defined in terms of the initial ($\vec{k}_1$) and final ($\vec{k}_1'$) momenta in the laboratory frame, as shown in Fig. 3.5,

$$\begin{aligned} \hat{n} &= \frac{\vec{k}_1 \times \vec{k}_1'}{|\vec{k}_1 \times \vec{k}_1'|} \\ \hat{\ell} &= \hat{k}_1 \\ \hat{s} &= \hat{n} \times \hat{k}_1 \end{aligned} \tag{3.84}$$

and

$$\begin{aligned} \hat{n}' &= \hat{n} \\ \hat{\ell}' &= \hat{k}_1' \\ \hat{s} &= \hat{n} \times \hat{k}_1' \end{aligned} \tag{3.85}$$

where $\hat{n}$ is the "normal" spin direction, $\hat{\ell}$ ($\hat{\ell}'$) is the initial (final) "longitudinal" spin orientation, and $\hat{s}$ ($\hat{s}'$) the "sideways" spin orientation. Expressions for the analyzing power A_y and the polarization transfer observables $D_{i'j}$ are now written down for an incident proton scattering from a single target proton; identical expressions also hold for the corresponding observables for an incident proton scattering from a single target neutron. The resulting $(\vec{p},\vec{p}')$ observables are then taken as appropriate averages of the pp and pn observables. Recall, from Appendix G, that the induced polarization per target proton $P(pp)$, which is also equal to the analyzing power per target proton $A_y(pp)$ in this simple model of quasielastic scattering, is calculated by summing over the initial spin of the projectile, but not its final spin. Hence (see Eq. (G.154) in Appendix G)

$$
\begin{aligned}
A_y(pp) &= \frac{\frac{d\sigma}{d\Omega_1' dE_1'}(pp,\hat{s}_f=\hat{n}) - \frac{d\sigma}{d\Omega_1' dE_1'}(pp,\hat{s}_f=-\hat{n})}{\frac{d\sigma}{d\Omega_1' dE_1'}(pp,\hat{s}_f=\hat{n}) + \frac{d\sigma}{d\Omega_1' dE_1'}(pp,\hat{s}_f=-\hat{n})} \\
&= \frac{\int d|\vec{k}_2|\, d\phi\, \Theta(|\vec{k}_2|)\, \frac{1}{4} \sum_{s_1,s_2,s_2'} \{\mathcal{M}^*\mathcal{M}(\hat{s}_f=\hat{n}) - \mathcal{M}^*\mathcal{M}(\hat{s}_f=-\hat{n})\}}{\int d|\vec{k}_2|\, d\phi\, \Theta(|\vec{k}_2|)\, \frac{1}{4} \sum_{s_1,s_2,s_2'} \{\mathcal{M}^*\mathcal{M}(\hat{s}_f=\hat{n}) + \mathcal{M}^*\mathcal{M}(\hat{s}_f=-\hat{n})\}} \qquad (3.86) \\
&= \frac{\int d|\vec{k}_2|\, d\phi\, \Theta(|\vec{k}_2|)\, \frac{1}{4} \sum_{s_1,s_2,s_2'} \{\mathcal{M}^*\mathcal{M}(\hat{s}_f=\hat{n}) - \mathcal{M}^*\mathcal{M}(\hat{s}_f=-\hat{n})\}}{\frac{d\bar{\sigma}(pp)}{d\Omega_1' dE_1'}|_{\text{unpol}}}
\end{aligned}
$$

where $\frac{d\bar{\sigma}(pp)}{d\Omega_1' dE_1'}|_{\text{unpol}}$ is given by Eq. (3.83) with proton–proton SVPAT amplitudes as input. Note that the notation $\hat{s}_f = s_1'$ is introduced to refer to the spin orientation of the *ejectile* in the rest frame of the nucleon.

The polarization transfer observables per target proton, which express the "probability" for initial spin direction $\hat{j}$ going to final spin direction $\hat{i}'$, are defined as (see Eq. (G.155) in Appendix G)

$$
\begin{aligned}
D_{i'j}(pp) &= \frac{\frac{d\sigma}{d\Omega_1' dE_1'}(pp,\hat{j}\to\hat{i}') - \frac{d\sigma}{d\Omega_1' dE_1'}(pp,\hat{j}\to-\hat{i}') - \frac{d\sigma}{d\Omega_1' dE_1'}(pp,-\hat{j}\to\hat{i}') + \frac{d\sigma}{d\Omega_1' dE_1'}(pp,-\hat{j}\to-\hat{i}')}{\frac{d\sigma}{d\Omega_1' dE_1'}(pp,\hat{j}\to\hat{i}') + \frac{d\sigma}{d\Omega_1' dE_1'}(pp,\hat{j}\to-\hat{i}') + \frac{d\sigma}{d\Omega_1' dE_1'}(pp,-\hat{j}\to\hat{i}') + \frac{d\sigma}{d\Omega_1' dE_1'}(pp,-\hat{j}\to-\hat{i}')} \qquad (3.87) \\
&= \frac{\int d|\vec{k}_2|\, d\phi\, \Theta(|\vec{k}_2|)\, \frac{1}{4} \sum_{s_2,s_2'} \{\mathcal{M}^*\mathcal{M}(\hat{j}\to\hat{i}') - \mathcal{M}^*\mathcal{M}(\hat{j}\to-\hat{i}') - \mathcal{M}^*\mathcal{M}(-\hat{j}\to\hat{i}') + \mathcal{M}^*\mathcal{M}(-\hat{j}\to-\hat{i}')\}}{\int d|\vec{k}_2|\, d\phi\, \Theta(|\vec{k}_2|)\, \frac{1}{4} \sum_{s_2,s_2'} \{\mathcal{M}^*\mathcal{M}(\hat{j}\to\hat{i}') + \mathcal{M}^*\mathcal{M}(\hat{j}\to-\hat{i}') + \mathcal{M}^*\mathcal{M}(-\hat{j}\to\hat{i}') + \mathcal{M}^*\mathcal{M}(-\hat{j}\to-\hat{i}')\}}
\end{aligned}
$$

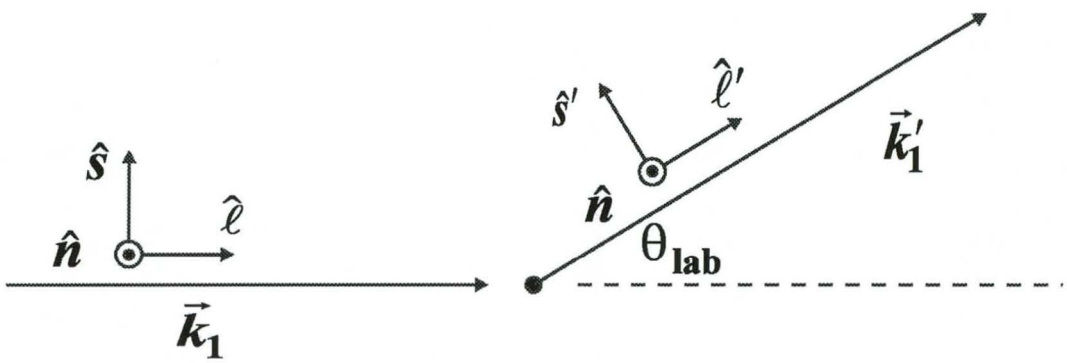

Figure 3.5: The initial and final laboratory coordinate frames used for defining the polarization transfer observables

where $\hat{j}$ and $\hat{i}'$ refer to the *projectile* and *ejectile* spin orientations in the rest frame of the nucleons. The denominator is merely the unpolarized cross section, so that

$$D_{i'j}(pp) = \frac{\int d|\vec{k}_2|\, d\phi\, \Theta\left(|\vec{k}_2|\right) M_{i'j}}{\left.\frac{d\bar{\sigma}(pp)}{d\Omega_1' dE_1'}\right|_{\text{unpol}}} \tag{3.88}$$

where

$$\begin{aligned} M_{i'j} = \frac{1}{4} \sum_{s_2, s_2'} \{ & \mathcal{M}^* \mathcal{M}\left(\hat{s}_i = \hat{j},\, \hat{s}_j = \hat{i}'\right) - \mathcal{M}^* \mathcal{M}\left(\hat{s}_i = \hat{j},\, \hat{s}_j = -\hat{i}'\right) \\ & - \mathcal{M}^* \mathcal{M}\left(\hat{s}_i = -\hat{j},\, \hat{s}_f = \hat{i}'\right) + \mathcal{M}^* \mathcal{M}\left(\hat{s}_i = -\hat{j},\, \hat{s}_f = -\hat{i}'\right)\} . \end{aligned} \tag{3.89}$$

Note that the notation $\hat{s}_i = s_1$ is introduced to refer to the spin orientation of the *projectile* in the rest frame of the nucleon.

Now to get the (p, p') double differential cross section per nucleus one uses the effective number of nucleons (see Table 3.1) A_{eff} extracted via the eikonal weighting procedure described in Sec. 3.2.2. The effective number of protons Z_{eff} and neutrons N_{eff} participating in the quasielastic scattering process are then assumed to be

$$Z_{\text{eff}} = \frac{Z}{A} A_{\text{eff}} \quad \text{and} \quad N_{\text{eff}} = \frac{N}{A} A_{\text{eff}} . \tag{3.90}$$

such that the double differential cross section for inclusive quasielastic (p, p') scattering from Z_{eff} protons and N_{eff} neutrons is given by

$$\frac{d\bar{\sigma}}{d\Omega_1' dE_1'} = Z_{\text{eff}} \frac{d\bar{\sigma}(pp)}{d\Omega_1' dE_1'} + N_{\text{eff}} \frac{d\bar{\sigma}(pn)}{d\Omega_1' dE_1'} \tag{3.91}$$

where $\dfrac{d\bar{\sigma}(pn)}{d\Omega_1' dE_1'}$ is given by Eq. (3.83) evaluated using the proton–neutron SVPAT amplitudes. Similarly, the analyzing power A_y is given by

$$A_y = \left[Z_{\text{eff}} \frac{d\bar{\sigma}(pp)}{d\Omega_1' dE_1'} A_y(pp) + N_{\text{eff}} \frac{d\bar{\sigma}(pn)}{d\Omega_1' dE_1'} A_y(pn) \right] / \frac{d\bar{\sigma}}{d\Omega_1' dE_1'} \tag{3.92}$$

$$= \left[Z \frac{d\bar{\sigma}(pp)}{d\Omega_1' dE_1'} A_y(pp) + N \frac{d\bar{\sigma}(pn)}{d\Omega_1' dE_1'} A_y(pn) \right] / \frac{d\bar{\sigma}}{d\Omega_1' dE_1'} \tag{3.93}$$

and the polarization transfer observables $(D_{i'j})$ are given by

$$D_{i'j} = \left[Z_{\text{eff}} \frac{d\bar{\sigma}(pp)}{d\Omega_1' dE_1'} D_{i'j}(pp) + N_{\text{eff}} \frac{d\bar{\sigma}(pn)}{d\Omega_1' dE_1'} D_{i'j}(pn) \right] / \frac{d\bar{\sigma}}{d\Omega_1' dE_1'} \tag{3.94}$$

$$= \left[Z \frac{d\bar{\sigma}(pp)}{d\Omega_1' dE_1'} D_{i'j}(pp) + N \frac{d\bar{\sigma}(pn)}{d\Omega_1' dE_1'} D_{i'j}(pn) \right] / \frac{d\bar{\sigma}}{d\Omega_1' dE_1'} . \tag{3.95}$$

Note that the $\frac{A_{\text{eff}}}{A}$ factors in the numerators and denominators of Eqs. (3.92) and (3.94) cancel, and hence, the polarization transfer observables are not affected by the distortions (contained in A_{eff}). The latter is only valid for the plane–wave formalism where the eikonal approximation is used to calculate values for A_{eff}. This justifies, to some extent, the claim that polarization transfer observables are relatively insensitive to distortions effects.

3.2.8 Distinguishing between quasielastic (p, p') and (p, n) scattering

In this section, one considers how to distinguish between quasielastic $(\vec{p}, \vec{p}')$ and $(\vec{p}, \vec{n})$ reactions in terms of isospin content and reaction Q–values. The quasielastic $(\vec{p}, \vec{n})$ reaction probes only the isovector parts of the NN interaction, whereas the $(\vec{p}, \vec{p}')$ polarization transfer observables sample both isovector and isoscalar components, and since the Lorentz character of the isovector amplitudes is totally different from the isoscalar amplitudes, one expects quasielastic $(\vec{p}, \vec{p}')$ and $(\vec{p}, \vec{n})$ polarization transfer observables to provide different, but complementary, information on the medium–modified NN interaction.

Isoscalar and isovector scattering amplitudes

The observables for quasielastic $(\vec{p}, \vec{p}')$ scattering are given by Eqs. (3.91) – (3.95). For this reaction, an incident proton can scatter from either protons or neutrons in the nucleus, and hence the isoscalar (p, p') observables [*isospin transfer is zero*] are given by sum of the corresponding pp and pn observables: Recall that the polarized double differential cross section for quasielastic (p, p') scattering is obtained by weighting the pp and pn polarized double differential cross sections with Z_{eff} and N_{eff} respectively.

For charge–exchange $(\vec{p}, \vec{n})$ scattering, on the other hand, the incident protons either transfer charge to a target neutron and emerge as a neutron or else knock a neutron out of the nucleus. The direct amplitude corresponds to the incident proton exchanging its charge through the interaction with a neutron in the nucleus, whereas the exchange amplitude corresponds to the neutron being knocked out. To identify the charge–exchange amplitude, one calculates the matrix elements of Eq. (3.18) for $p_1 + n_2 \longrightarrow n_1 + p_2$ and $n_1 + p_2 \longrightarrow p_1 + n_2$ scattering.

With Eqs. (B.2) and (B.3) in Appendix B, for $p_1 + n_2 \longrightarrow n_1 + p_2$ scattering it follows that

$$(2i|\vec{k}_{cm}|)^{-1} < p_1\, n_2|\, f\, |n_1\, p_2 > \equiv 2[A_1 + B_1 \boldsymbol{\sigma}_1 \cdot \boldsymbol{\sigma}_2 + i|\vec{q}\,|C_1(\boldsymbol{\sigma}_1 \cdot \hat{n} + \boldsymbol{\sigma}_2 \cdot \hat{n}) + |\vec{q}\,|^2 D_1 \boldsymbol{\sigma}_1 \cdot \hat{q}\boldsymbol{\sigma}_2 \cdot \hat{q} + E_1 \boldsymbol{\sigma}_1 \cdot \hat{z}\boldsymbol{\sigma}_2 \cdot \hat{z}] \tag{3.96}$$

with an identical expression for $n_1 + p_2 \longrightarrow p_1 + n_2$ scattering. Note that the charge–exchange amplitude given by Eq. (3.96) is also equal to the difference between the amplitudes for $p + p \longrightarrow p + p$ scattering [see Eq. (3.20)] and $p_1 + n_2 \longrightarrow p_1 + n_2$ scattering [see Eq. (3.21)], that is [By78, Gl83, Fe92]

$$\begin{aligned} < p_1\, n_2|\, f\, |n_1\, p_2 > &= < p\, p|\, f\, |p\, p > - < p_1\, n_2|\, f\, |p_2\, n_2 > \\ &= f^{pp} - f^{pn}\,. \end{aligned} \tag{3.97}$$

In an analogous fashion, the relativistic isovector (p, n) amplitudes can be written as the difference between the relativistic SVPAT pp and pn amplitudes:

$$F_i^{(p,n)} = F_i^{(pp)} - F_i^{(pn)}\,. \tag{3.98}$$

Hence, for (p, n) scattering, one uses Eq. (3.98) for the amplitudes in Eq. (3.54), and also sets $Z_{\rm eff} = 0$ in Eqs. (3.91) - (3.95).

Reaction Q–value and energy transfer

The conservation of energy for a nuclear reaction of the form $A(a, b)B$ may be written as [Si90]

$$E_\alpha + E_a + E_A = E_\beta + E_b + E_B \tag{3.99}$$

where E_α and E_β are kinetic energies of the entrance and exit channels, E_a and E_A, E_b and E_B are particle intrinsic energies in the entrance and exit channels respectively. If both a and b are elementary particles (e.g. nucleons in the case of medium–energy nuclear physics), then the intrinsic energies E_a and E_b may be expressed in terms of the particle rest masses, $E_a = m_a\, c^2$ and $E_b = m_b\, c^2$, where c is the speed of light. Intrinsic energies of the nuclei A and B are functions of their rest masses and excitation energies E_A^* and E_B^*:

$$\begin{aligned} E_A &= m_A\, c^2 + E_A^* \\ E_B &= m_B\, c^2 + E_B^*\,. \end{aligned} \tag{3.100}$$

The energy transfer ω is defined as the difference between the relative particle motion kinetic energies in the entrance and exit channels:

$$\omega = E_\alpha - E_\beta \, . \tag{3.101}$$

From the law of energy conservation, expressed by Eq. (3.99), Eq. (3.101) can be rewritten as

$$\omega = E_B^* - E_A^* - Q_{gs} \tag{3.102}$$

where the ground state Q–value is defined as

$$Q_{gs} = (m_a + m_A - m_b - m_B)\, c^2 \, . \tag{3.103}$$

For quasielastic proton–nucleus scattering, the target nucleus is in its ground state, that is

$$E_A^* \; = \; 0 \, , \tag{3.104}$$

and, hence Eq. (3.102) becomes

$$\begin{aligned} \omega \; &= \; E_B^* - Q_{gs} \\ &= \; \omega' - Q_{gs} \end{aligned} \tag{3.105}$$

where $\omega' \; = \; E_B^*$ is the excitation energy ω (or energy transfer) defined in Eq. (3.64). From Eq. (3.103) one sees that $Q = 0$ for (p,p') scattering, and hence $\omega' = \omega$, whereas for (p,n) scattering $Q < 0$, and hence $\omega' \neq \omega$. Note that for the RPWIA all polarization transfer observables are calculated as a function of ω'. However, experimental observables are plotted as a function of ω. For comparison with experiment, one merely shifts the ω' values of the (p,n) scattering observables by $-Q_{gs}$ to obtain the correct ω.

3.2.9 Calculational procedure

One now considers how the theoretical expressions for the observables are converted to numbers which can be ultimately compared to experimental data, thus testing the validity of the RPWIA.

All kinematic quantities in the RPWIA formalism are completely specified from the following input, namely

- the laboratory kinetic energy $T_{\rm lab}$ of the projectile proton,

- the laboratory scattering angle $\theta_{\rm lab}$ of the detected ejectile nucleon,
- the free nucleon mass m,
- the effective projectile and target nucleon effective masses, m_1^* and m_2^* respectively,
- the Fermi momentum k_F,
- the range of energy transfers ω spanning the quasielastic peak.

The exact expressions for all kinematic quantities of interest are derived in Appendix I. Note that the energy–transfer ω is not calculated from Eq. (3.64), but is chosen to span the quasielastic peak of interest, that is

$$\omega_{\rm min} \leq \omega_i \leq \omega_{\rm max} \tag{3.106}$$

where ω_i represents one of N values of ω spanning the quasielastic peak, namely

$$\omega = \omega_i = \omega_{\rm min} + i\Delta\omega \tag{3.107}$$

with

$$\Delta\omega = \frac{\omega_{\rm max} - \omega_{\rm min}}{N} \tag{3.108}$$

and i ranges from 0 to N. Without hindsight or access to experimental data, one may ask the question as to how one chooses values for $\omega_{\rm min}$ and $\omega_{\rm max}$ which span the allowed phase space and, hence, span the quasielastic bump in the excitation spectrum. Recall, from Sec. I.9 in Appendix I, that the centroid of the quasielastic peak corresponds to scattering from a single target nucleon at rest ($\vec{k}_2 = 0$), and the position of the centroid is approximately given by

$$\omega = \frac{|\vec{q}\,|^2}{2m} \tag{3.109}$$

where, from Eqs. (D.1) and (D.8) [see Appendix D] and Eq. (G.140) [see Appendix G], for a given laboratory scattering angle $\theta_{\rm lab}$, the magnitude of the three–momentum transfer $|\vec{q}\,|$ is approximately given by

$$|\vec{q}\,| = \sqrt{2T_{\rm lab}m}\,\sin\theta_{\rm lab}\,. \tag{3.110}$$

With the centroid of the quasielastic peak known from Eq. (3.109), the values of $\omega_{\rm min}$ and $\omega_{\rm max}$ can be chosen arbitrarily to the left and right of centroid respectively. This procedure at least

gives one a method for choosing the initial values of $\omega_{\min}$ and $\omega_{\max}$. For each value of ω [within the range specified by Eq. (3.106)], one integrates the observables over the momenta of the target nucleons [$\int d|\vec{k}_2|$], corrects for Pauli blocking as discussed in Sec. 3.2.3, and integrates over the azimuthal angle [$\int d\phi$]: for each value of $|\vec{k}_2|$ [with the range specified by Eqs. (3.14, (3.15) and (3.16)], the integral over ϕ [$0 \leq \phi \leq 2\pi$] is performed.

Finally, the units of the polarized and unpolarized double differential cross sections, given by Eqs. (3.82) and (3.83)respectively, are considered. The unit of the relativistic SVPAT amplitudes t_i is GeV^{-2}, and hence the unit of the invariant matrix elements squared is

$$\mathrm{GeV}^{-4} \;=\; 10^{-12}\,\mathrm{MeV}^{-4}\,. \tag{3.111}$$

The unit of the factor preceding $\sum \mathcal{M}^*\mathcal{M}$ in Eqs. (3.82) and (3.83) is $(\hbar c)^2\,\mathrm{MeV} = (\mathrm{MeV})^3\,\mathrm{fm}^2$: note, that due to the fact that natural units are adopted, the "$\hbar c$" factor is not explicitly shown in Eqs. (3.82) and (3.83). Hence the unit of the double differential cross section is

$$10^{-12}\,\mathrm{fm}^2\,\mathrm{MeV}^{-1}\,\mathrm{sr}^{-1} \tag{3.112}$$

where the steradian (sr) serves as a reminder that the double differential cross section is normalized per unit solid angle Ω. Making use of the fact that

$$1\,\mathrm{fm}^2 \;=\; 10\ \text{millibarns} \;=\; 10\,\mathrm{mb} \tag{3.113}$$

one can rewrite Eq. (3.112) as

$$10^{-12} \times 10\,\mathrm{mb}\,\mathrm{MeV}^{-1}\,\mathrm{sr}^{-1}\,. \tag{3.114}$$

Hence, the double differential cross sections are expressed in the usual units of $\mathrm{mb}\,\mathrm{MeV}^{-1}\,\mathrm{sr}^{-1}$.

Besides studying the sensitivity of polarization transfer observables to nuclear medium effects, different forms of the πNN vertex, and exchange contributions to the NN amplitudes (see Sec. 3.3.2), the importance of spin–orbit distortions on the observables is also investigated. The subject of spin–orbit distortions is discussed in the following section.

3.2.10 Spin–orbit distortions

The inclusion of spin–orbit distortions at the *centroid of the quasielastic peak* in the expressions for polarization transfer observables is discussed in detail in Ref. [Ho86]. The main aspects of this paper are briefly reviewed.

In calculating the nucleon transmission probability $T(b)$ in Sec. 3.2.2, only the central part of the (effective Schrödinger) optical potential is used. Within the eikonal approximation, the inclusion of a spin–orbit component adds an additional distortion factor $e^{-iW_{so}(r)}$ to the incoming Dirac wave function [See Eq. (3.2)] with:

$$W_{so} = \mathbf{R}(\vec{b}\,) \cdot \boldsymbol{\sigma}\,, \tag{3.115}$$

where

$$\mathbf{R}(\vec{b}\,) = mb \int_{-\infty}^{z} dz\, V_{so}(b,z) \hat{b} \times \hat{k}\,, \tag{3.116}$$

and $\vec{b}$ is the impact parameter, now as a vector.

The spin–orbit distortion manifests itself as a spin rotation operator,

$$\mathcal{R}(\vec{b}) = e^{-i\mathbf{R}(\vec{b}\,) \cdot \boldsymbol{\sigma}}\,, \tag{3.117}$$

on the initial state vector, which identifies $\mathbf{R}(\vec{b}\,)$ of Eq. (3.116) as the effective (complex) rotation angle in spin space. The treatment of this rotation is simplified by some approximations: Firstly, if the projectile scatters halfway through the nucleus [z = 0 in Eq. (3.116)], then one can express the spin–orbit effect as a rotation of the final state vector using the same $\mathbf{R}(\vec{b}\,)$ of Eq. (3.117) with only a sign change. This is due to the fact that, in the corresponding eikonal integral for the final state, the same function V_{so}, being even in z, is now integrated from $z = 0$ to $+\infty$. Secondly, b in $\mathbf{R}(\vec{b}\,)$ of Eq. (3.116) is taken as the reaction average $\langle b \rangle$ obtained in Sec. 3.2.2.

Consider now the angular average of $\mathbf{R}$ over the whole nucleus: First, in the special case where the projectile particle traverses the nucleus along a straight line (laboratory scattering angle $\theta = 0$), there is complete cylindrical symmetry with respect to the incoming beam direction. Therefore, the net contribution to $\langle \mathbf{R} \rangle$ equals zero, because the contributions of each pair of opposing directions of $\vec{b}$ cancel. However, in the general case of a non–zero scattering angle θ, contributions to the $\mathbf{R}$–integral [Eq. (3.116)] from two opposing directions of $\vec{b}$, one on the "inside" and one on the "outside" of the scattering bend, will be clearly different because of the different path lengths traversed through the nucleus. Keeping in mind that $\mathbf{R}(\vec{b})$ is always perpendicular to $\vec{b}$ [see Eq. (3.116)] and considering its components parallel and normal to the scattering plane separately, it becomes clear that the resultant rotation will only have a non–zero normal component, R_n.

Hence for $\theta \neq 0$, the distortion effect of V_{so} will be a space rotation of both the initial and final state vectors around an axis normal to the scattering plane. This is alternatively equivalent to a rotation on only the Pauli spin matrices; therefore the expressions for the polarization transfer observables [See Appendix G]:

$$D_{i'j} = \frac{\mathrm{Tr}(\sigma_i M \sigma_j M^\dagger)}{\mathrm{Tr}(MM^\dagger)} , \tag{3.118}$$

remain of similar form, except for the replacements: $\sigma_i \to \sigma_i^R$ and $\sigma_j \to \sigma_j^R$, where:

$$\sigma_i^R = e^{-iR_n^* \sigma_n} \sigma_i e^{+iR_n \sigma_n} ,$$

$$\sigma_j^R = e^{+iR_n \sigma_n} \sigma_j e^{-iR_n^* \sigma_n} . \tag{3.119}$$

For the small rotation angles (presently $|R_n| \leq 0.2$) the rotation can be expanded to first order in σ_n. This leads, by means of the commutation relations among the components of $\boldsymbol{\sigma}$ to linear combinations among the $D_{i'j}$'s to form the new polarization transfer observables with spin–orbit distortion (see Ref. [Ho86] for explicit expressions).

Fig. 3.6 presents graphically the amount of spin–orbit distortion on all six polarization transfer observables ($A_y, D_{nn}, D_{s's}, D_{\ell'\ell}, D_{s'\ell}$ and $D_{\ell's}$) as a function of the five chosen incident laboratory energies; these have been calculated for $m_1^* = m_2^* = m$, at the centroid of the quasielastic peak for $(\vec{p}, \vec{p}\,')$ scattering by ^{40}Ca, at a fairly large momentum transfer of 1.97 fm^{-1}. The graphs show that the spin–orbit distortion is indeed not a negligible factor; although being fairly constant with laboratory energy T_{lab}, the relative values increase as T_{lab} decreases. At low energies ($T_{lab} \leq 200$ MeV) the spin–orbit effect becomes comparable with other phenomenological effects (relativity and the form of the πNN vertex) investigated in Sec. 3.3.

Fig. 3.7 presents the spin–orbit distortion of the polarization transfer observables as a function of nuclear mass. These are calculated for $m_1^* = m_2^* = m$ at the centroid of the quasielastic peak and at a fixed incident laboratory energy $T_{lab} = 200$ MeV. The general increase of spin–orbit distortions with nuclear size agrees with the natural expectation. The very small distortion effect on the D_{nn}–values deserves some physical explanation: If the spin rotation angle $\mathbf{R}$ were completely real, this rotation with its axis perpendicular to the scattering plane ($\mathbf{R} = \mathbf{R}_n$) would have no effect on D_{nn}, which relates polarization components which are also perpendicular to the scattering plane. However, due to the small absorptive part of the optical potential, $\mathbf{R}$ has

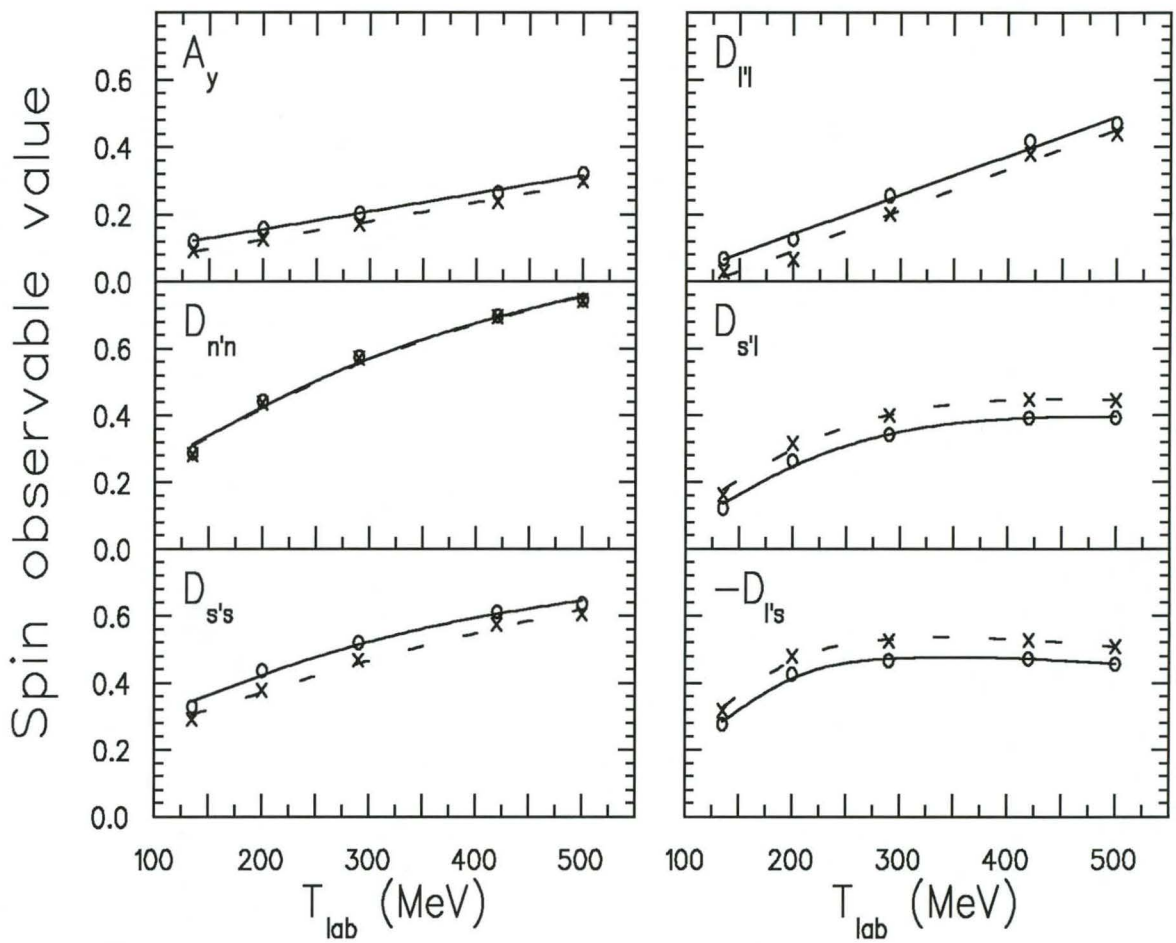

Figure 3.6: Spin–orbit distortion of the $(\vec{p}, \vec{p}\,')$ polarization transfer observables $\mathrm{D}_{i'j}$ as a function of the incident laboratory kinetic energy T_{lab}; these have been calculated for $m_1^* = m_2^* = m$, at the centroid of the quasielastic peak, for scattering by ^{40}Ca, at a fairly large momentum transfer of 1.97 fm^{-1}. For each observable the open circles and crosses refer to the respective undistorted and spin–orbit distorted values. The solid and dashed lines serve merely to guide the eye.

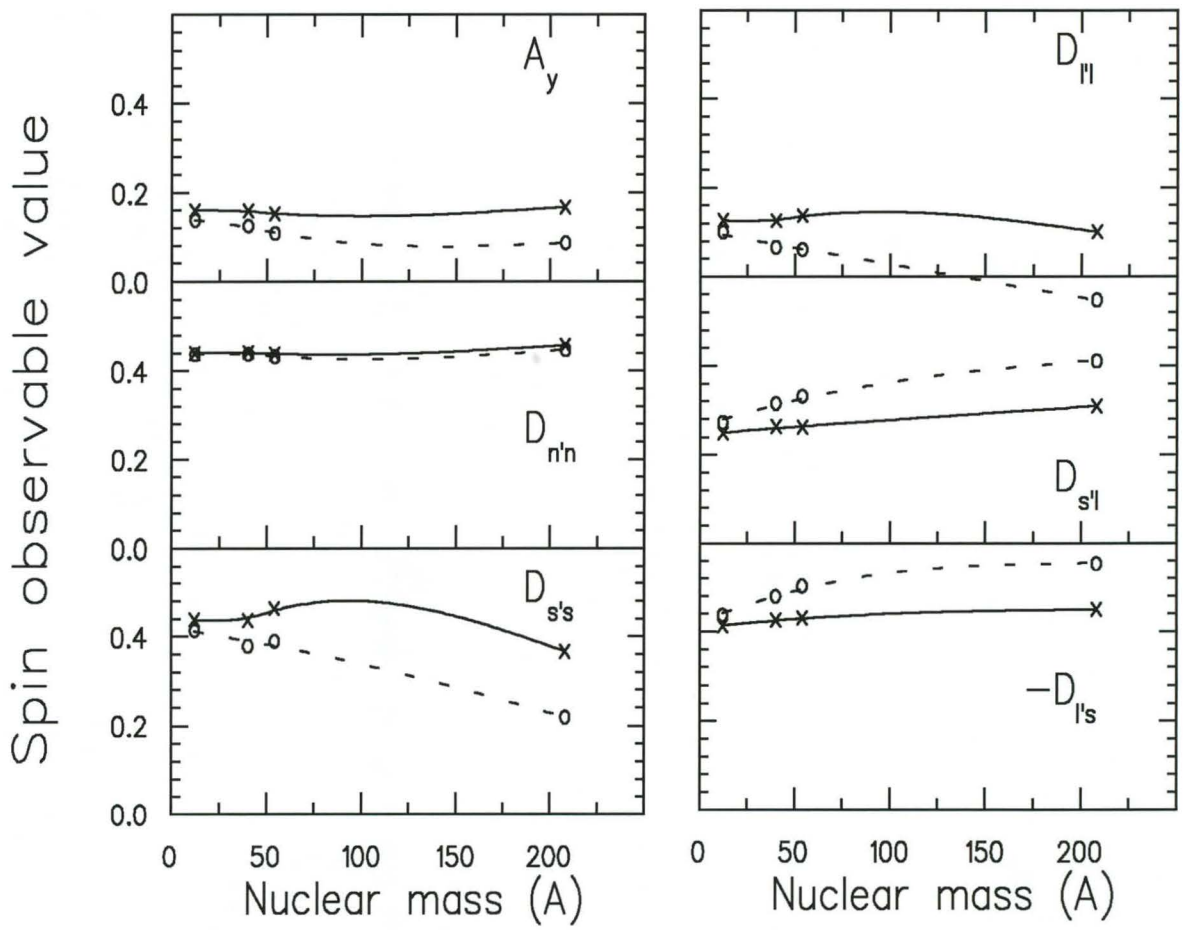

Figure 3.7: The same as Fig. 3.6, except that the spin–orbit distortion is now plotted as function of the mass number A of the target nucleus at a fixed incident laboratory kinetic energy $T_{\rm lab} = 200$ MeV.

a small imaginary part (typically $R = \pm 0.15 \pm 0.05i$), which leads to a generally non–unitary rotation operator $\mathcal{R}$ for Eq. (3.116), in which case D_{nn} might be slightly affected. The explicit expression for the spin–orbit distortion of D_{nn} (Eqs. (40) and (41) in Ref. [Ho86]) also displays this dependence on only the imaginary part of **R**.

The insensitivity of D_{nn} to spin–orbit distortion enhances, however, its value as a probe for studying medium–modifications of the free NN interaction (see Sec. 3.3).

3.3 Sensitivity of spin observables to RPWIA model parameters

The aim of this section is to investigate the sensitivity of complete sets of inclusive quasielastic $(\vec{p}, \vec{p}')$ and $(\vec{p}, \vec{n})$ polarization transfer observables to model parameters of the RPWIA discussed in Sec. 3.2. One starts by comparing calculations of polarization transfer observables, based on the new, more refined, effective masses, to corresponding calculations based on the original, more crude, effective masses of Horowitz and Murdock [Ho88].

3.3.1 Sensitivity to different types of effective masses

From Table 3.2, one observes that the largest differences between the more refined effective masses, M^*_{SC} and M^*_{CP}, and the original effective masses (M^*_{HM}), occur at 300 MeV for ^{54}Fe. For $|\vec{q}\,| = 1.36$ fm^{-1}, our M^*_{SC} and M^*_{CP}–based RPWIA calculations are compared with those using the cruder M^*_{HM}–values [Ha88].

The results, for the spin observables calculated at the centroid of the quasielastic peak, are shown in Table 3.3: one uses the SVPAT parametrization of the NN amplitudes (as opposed to the HLF model), and a PS coupling for the πNN vertex. Using the more refined effective masses, namely $M^*_{1SC} = 0.833$ and $M^*_{2SC} = 0.770$ or $M^*_{1CP} = 0.849$ and $M^*_{2CP} = 0.0.769$, compared to the cruder values used by Haüsser et al. [Ha88], $M^*_{1HM} = 0.86$ and $M^*_{2HM} = 0.85$, yields differences of up to 30% in some spin observables, the most sensitive observables being $D_{s's}$ and A_y, and the least sensitive $D_{\ell's}$. These large variations illustrate the importance of using the more refined effective masses, M^*_{SC} and/or M^*_{CP}. Note that the HLF model serves as input for calculations of both M^*_{SC} effective masses *as well as* the relativistic NN amplitudes.

Table 3.3: Values of the spin observables at the centroid of the quasielastic peak for $^{54}\mathrm{Fe}(\vec{p},\vec{p}')T_{\mathrm{lab}} = 300$ MeV at $|\vec{q}\,| = 1.36$ fm^{-1}, for the different types of effective masses listed in Table 3.1.

Type of mass	A_y	D_{nn}	$D_{s's}$	$D_{\ell'\ell}$	$D_{s'\ell}$	$D_{\ell's}$
M	0.418	0.602	0.105	0.140	0.207	0.194
M^*_{HM}	0.317	0.582	0.366	0.232	0.347	0.394
M^*_{SC}	0.278	0.550	0.459	0.249	0.319	0.392
M^*_{CP}	0.280	0.546	0.454	0.244	0.310	0.383

Hence, for reasons of consistency, one rather uses the M^*_{SC} instead the M^*_{CP}–values for the investigations to follow.

3.3.2 Qualitative investigations

Due to the Fermi motion of the target nucleons, all quasielastic polarization transfer observables need to be averaged over the momenta of the target nucleons. This also means that the NN scattering amplitudes must be evaluated over a wide range of effective laboratory kinetic energies T^L_{eff} (see Sec. 3.2.5). Unfortunately, at the time of this investigation, published HLF parameter sets existed only at incident proton energies of 135, 200, 300, 400 and 500 MeV [Ho85, Mu87a]. Thus, to make use of this limited input, for a quasielastic proton–nucleus reaction at a specific incident energy, one *considers only the HLF parameter set closest to the incident laboratory kinetic energy for all* T^L_{eff}. Hence, this investigation is merely *qualitative* and serves only to give an initial "feel" for the sensitivities of observables to model parameters: *the reader is cautioned against drawing any quantitative conclusions.* If, however, one sees that certain observables exhibit enhanced sensitivity to model parameters, then it will be worthwhile performing a similar, but quantitative study. The results of this section have been published in Refs. [Hi94, Hi95].

In this section, the sensitivity of polarization transfer observables is explored with respect to pseudoscalar versus pseudovector πNN coupling, relativistic or medium effects, and exchange contributions to the HLF NN amplitudes. Typical trends are illustrated for incident protons

scattering from a ^{40}Ca nucleus at laboratory energies 135, 200, 290 and 420 MeV. At each energy, the scattering angle is chosen to correspond to a laboratory momentum transfer of 1.97 fm^{-1} for free NN scattering, such that the quasielastic peak is centered at $\omega \approx 80$ MeV. The momentum transfer and incident energies (specifically 290 and 420 MeV) are chosen to correspond to experimental data [Ch90], and also due to the availability of HLF parameters sets (at 135, 200, 300 and 400 MeV) at approximately these incident energies.

The results are presented in graphical form, in Figs. 3.8 to 3.11, to highlight a specific tendency: each figure is a set of six graphs for the six independent polarization transfer observables (A_y, $D_{nn}, D_{s's}, D_{\ell'\ell}, D_{s'\ell}$ and $D_{\ell's}$) , all on the same scale. The solid and open circles denote the calculated values, whereas the solid lines serve only to guide the eye along a particular calculated data set. Although these graphs speak for themselves, a few comments will be made.

The notation $D^{PS}_{i'j}(M^*)$ and $D^{PV}_{i'j}(M^*)$ is introduced to refer to polarization transfer observables calculated using a **P**seudo**S**calar (**PS**) and a **P**seudo**V**ector (**PV**) coupling for the "pion", both calculated with the effective masses M^*_{SC} listed in Table 3.1.

Pseudoscalar versus pseudovector πNN coupling

One starts by studying the sensitivity of quasielastic $(\vec{p}, \vec{p}\,')$ and $(\vec{p}, \vec{n})$ polarization transfer observables to PS versus PV treatments of the πNN vertex. Most RPWIA quasielastic calculations to date have been based on the SVPAT parametrization of the NN amplitudes (as opposed to the HLF model) and, consequently, ignore exchange contributions to the medium–modified NN amplitudes. The inclusion of medium–modified exchange amplitudes plays a crucial role when considering a PV form of the πNN vertex and hence the SVPAT parametrization and HLF model will yield different results for this coupling of the pion. Note that, per construction, both HLF and SVPAT amplitudes, and hence polarization transfer observables, are identical for a PS coupling, that is,

$$D^{PS-SVPAT}_{i'j}(M^* \text{ or } M) = D^{PS-HLF}_{i'j}(M^* \text{ or } M) \tag{3.120}$$

and, for free nucleon masses M, it follows from Eq. (3.68) with $M^* = M$, that both PS and PV couplings yield identical polarization transfer observables

$$D^{PV}_{i'j}(M) = D^{PS}_{i'j}(M) \, . \tag{3.121}$$

PV versus PS calculations for both the HLF model and a direct SVPAT parametrization of the NN amplitudes are compared using the M^*_{SC} effective masses listed in Table 3.1. Fig. 3.8 compares for all $(\vec{p},\vec{p}\,')$ [solid- and open triangles] and $(\vec{p},\vec{n})$ [solid- and open circles] polarization transfer observables $D_{i'j}$, the values of $|D^{PV}_{i'j}(M^*) - D^{PS}_{i'j}(M^*)|$ based on a direct SVPAT parametrization (solid circles and triangles) and the HLF model (open circles and triangles) of the NN amplitudes.

Over the entire energy range, all the quasielastic $(\vec{p},\vec{n})$ polarization transfer observables are clearly much more sensitive to different forms of the pion coupling, compared to the corresponding $(\vec{p},\vec{p}\,')$ polarization transfer observables, D_{nn} being by far the most sensitive observable. Contrary to $(\vec{p},\vec{p}\,')$ scattering, both $(\vec{p},\vec{n})$ polarization transfer observables $D_{s'_s}$ (except at 200 MeV) and $D_{\ell'_s}$ depend substantially on the πNN coupling terms. Furthermore, it is particularly noticeable that, in contrast to the $(\vec{p},\vec{p}\,')$ observables, at *high energies* the direct SVPAT parametrization and the HLF model give significantly different results for the $(\vec{p},\vec{n})$ observables D_{nn}, $D_{s'_s}$ and $D_{\ell'_s}$; all three these observables clearly point to the necessity of a meson–exchange model for the NN interaction in order to correctly distinguish between PS and PV couplings of the pion. At 200 MeV $|D^{PV}_{i'j}(M^*) - D^{PS}_{i'j}(M^*)|$ exhibits maximum and minimum sensitivity for $D_{s'_s}$ for the SVPAT parametrization and HLF model respectively. On the other hand, A_y is totally insensitive to these differences.

One can conclude that the widely used relativistic SVPAT parametrization of NN amplitudes must be employed with caution when polarization transfer observables, based on the PV form of the πNN vertex, are calculated: rather, one must use a meson–exchange model, such as the HLF model, which explicitly treats exchange contributions of the NN amplitudes in the nuclear medium.

Relativistic or medium M^* effects for a pseudoscalar πNN vertex

The PS form of the πNN vertex is chosen, and the difference between effective mass M^* and free mass M calculations of the polarization transfer observables is studied. Fig. 3.9 displays the energy variation of $|D^{PS}_{i'j}(M^*) - D_{i'j}(M)|$ values which serves as a measure of the sensitivity to relativistic or medium effects of the specific polarization transfer observable $D_{i'j}$. The solid and open circles represent the $(\vec{p},\vec{p}\,')$ and $(\vec{p},\vec{n})$ results respectively. The hatched areas display

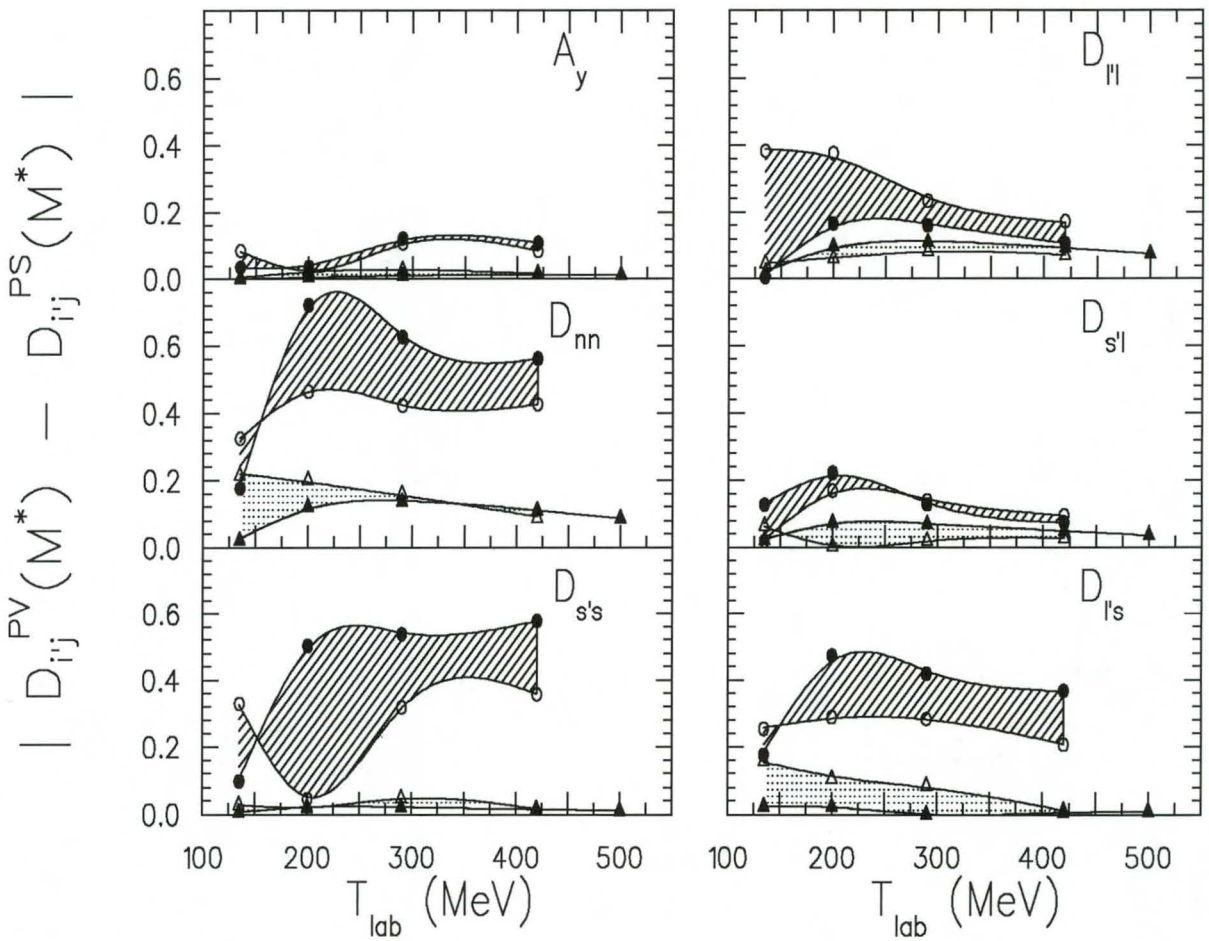

Figure 3.8: The difference, $|D^{PV}_{i'j}(M^*) - D^{PS}_{i'j}(M^*)|$, between quasielastic $(\vec{p},\vec{p}')$ and $(\vec{p},\vec{n}')$ polarization transfer observables $D_{i'j}$ calculated with a pseudovector (PV) and a pseudoscalar (PS) πNN vertex, as a function of laboratory kinetic energy, and *at the centroid of the quasielastic peak*. The solid circles [triangles] represent $(\vec{p},\vec{n})$ [$(\vec{p},\vec{p}')$] calculations based on the relativistic SVPAT parametrization of the NN amplitudes, whereas the open circles [triangles] represent $(\vec{p},\vec{n})$ [$(\vec{p},\vec{p}')$] calculations based on the HLF model. The solid lines serve merely to guide the eye.

the differences between the $(\vec{p},\vec{p}')$ and $(\vec{p},\vec{n})$ results. For $(\vec{p},\vec{n})$ scattering, one sees that D_{nn} and $D_{\ell'\ell}$ are the most sensitive observables to medium effects. At energies lower than 200 MeV, D_{nn} exhibits minimum and maximum sensitivity to relativistic effects for $(\vec{p},\vec{n})$ and $(\vec{p},\vec{p}\,')$ scattering, respectively.

Relativistic or medium M^* effects for a pseudovector πNN vertex

Next, the PV form of the πNN vertex is chosen, and the difference between effective mass M^* and free mass M calculations of the polarization transfer observables is studied. Fig. 3.10 displays the energy variation of $|D_{i'j}^{PV}(M^*) - D_{i'j}(M)|$ values which serves as a measure of the sensitivity to relativistic or medium effects of the specific polarization transfer observable $D_{i'j}$. These calculations are based on the PV implementation of the πNN coupling given by Eq. (3.69). The solid and open circles represent the $(\vec{p},\vec{p}')$ and $(\vec{p},\vec{n})$ results respectively. The hatched areas display the differences between the $(\vec{p},\vec{p}')$ and $(\vec{p},\vec{n})$ results. Over the entire energy range $D_{\ell'\ell}$ is extremely sensitive to relativistic M* effects. In addition, for $(\vec{p},\vec{n})$ scattering at energies above 200 MeV, D_{nn} is much more sensitive to relativistic effects than the celebrated "relativistic signature" exhibited by A_y at 500 MeV [Ho88]. At energies lower than 200 MeV, D_{nn} exhibits minimum and maximum sensitivity to relativistic effects for $(\vec{p},\vec{n})$ and $(\vec{p},\vec{p}\,')$ scattering, respectively.

Note that the nuclear medium effects differ for PS and PV forms of the πNN vertex. This emphasizes the need for data in order to distinguish between the different couplings.

Exchange contributions

Exchange is a fundamental phenomenon and in principle should be included in all calculations of $(\vec{p},\vec{n})$ and $(\vec{p},\vec{p}')$ polarization transfer observables. The HLF model allows one to consider corrections to the RPWIA due to explicit treatments of medium–modified NN exchange amplitudes.

Calculations of elastic scattering polarization transfer observables at laboratory energies of 500 MeV and higher seem to indicate that exchange contributions are not significant [Mc83]. However, Ref. [Mu87a] claims that a proper treatment of exchange is crucial for predicting

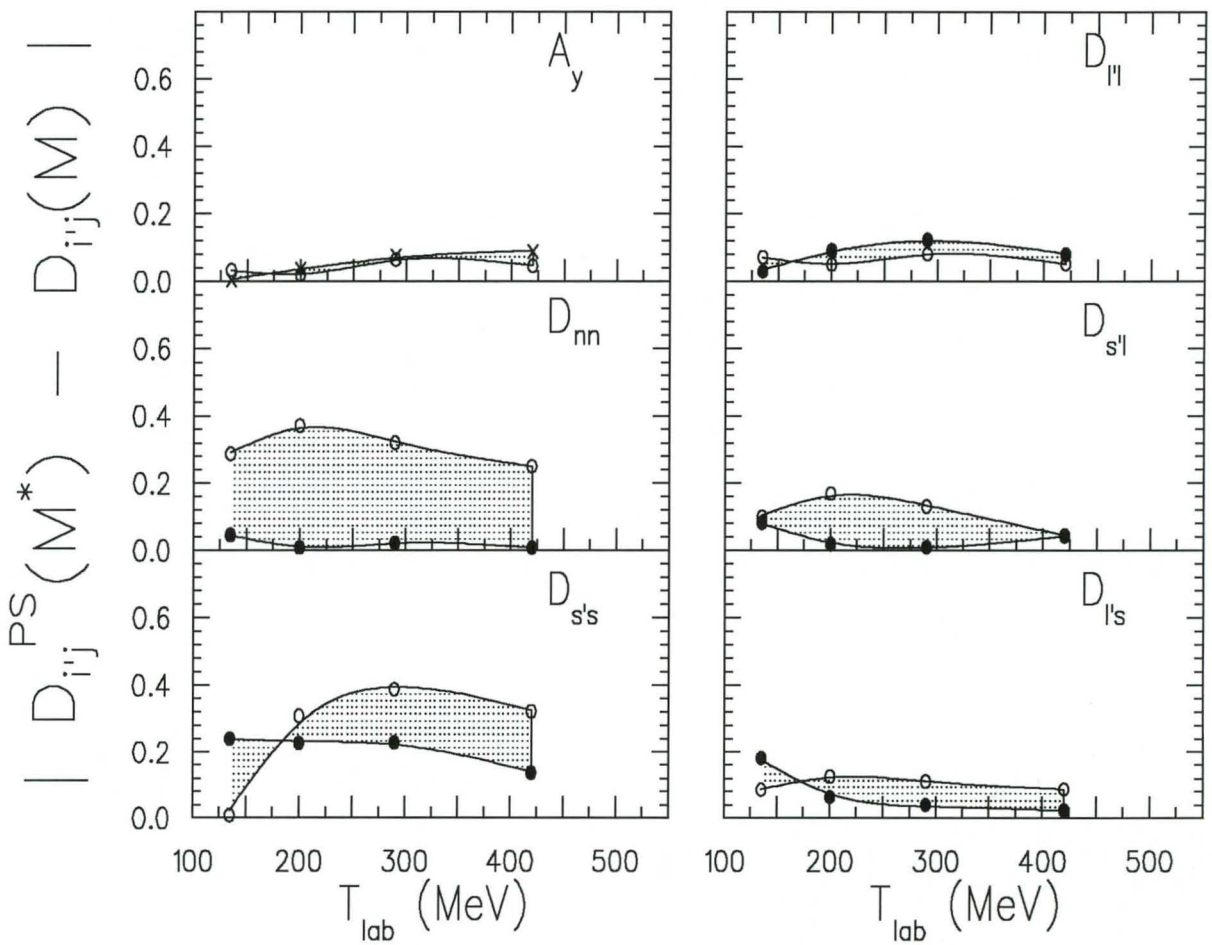

Figure 3.9: The values of $|D_{i'j}^{PS}(M^*) - D_{i'j}(M)|$, based on the HLF model, for $(\vec{p}, \vec{n})$ (open circles) and $(\vec{p}, \vec{p}\,')$ (solid circles and crosses) scattering, are plotted in precisely the same way as in Fig. 3.8

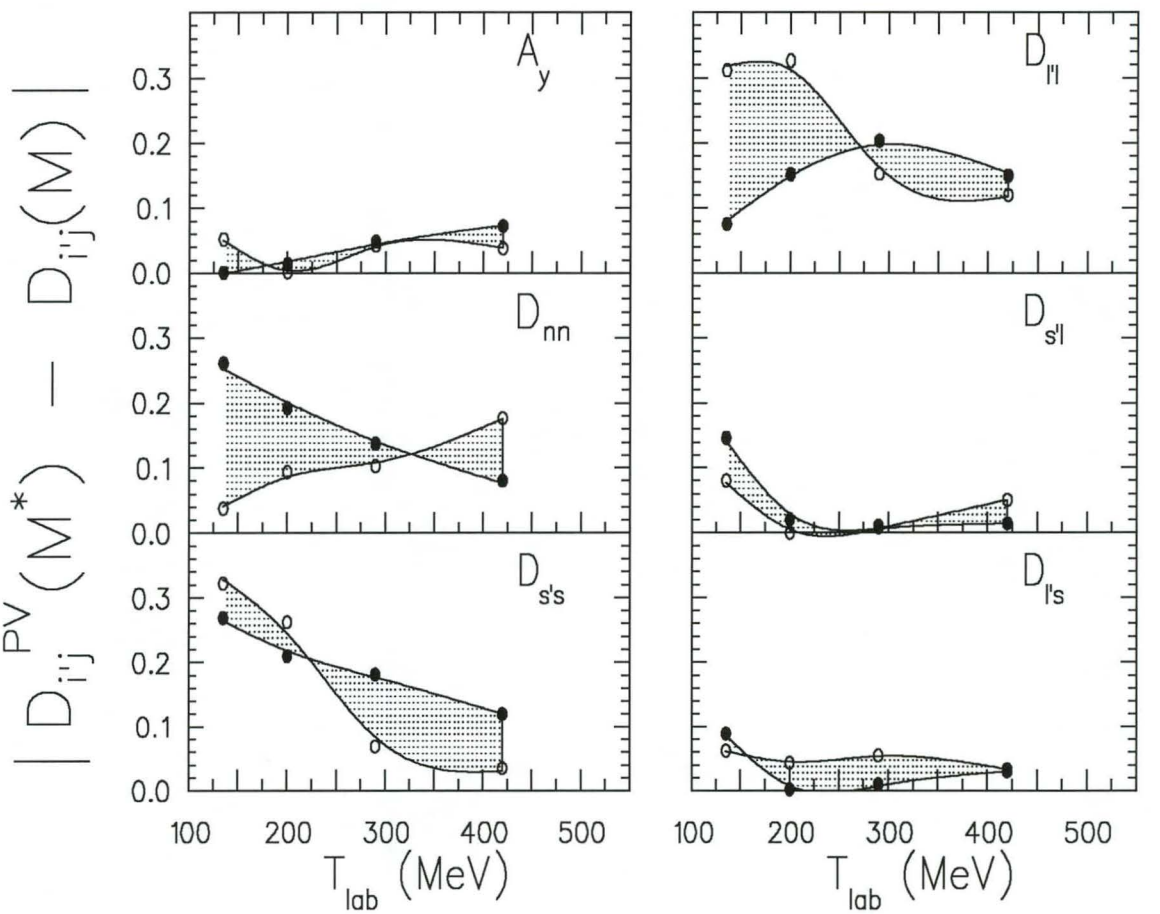

Figure 3.10: The values of $|D_i^{PV}{}_{,j}(M^*) - D_{i\,,j}(M)|$, based on the HLF model, for $(\vec{p},\vec{n})$ (open circles) and $(\vec{p},\vec{p}\,')$ (solid circles) scattering, are plotted in precisely the same way as in Fig. 3.8

elastic scattering polarization transfer observables at large scattering angles and/or low energies. Consequently, for the first time, the importance of exchange for *quasielastic proton–nucleus scattering* is studied in the 135 to 500 MeV range.

For illustrative purposes, one chooses the PV form of the πNN vertex and the difference $|D_{i\,'j}^{PV}(M^*)_{\rm Full} - D_{i\,'j}(M)_{\rm Direct}|$ is plotted, in Fig. 3.11, as a function of incident laboratory energy at the centroid of the quasielastic peak. These difference plots serve as a measure of the importance of exchange contributions to the polarization transfer observables. The subscript "full" refers to the direct plus exchange amplitudes given by Eq. (3.44), whereas the subscript "direct" refers to amplitudes where the exchange contributions are ignored, i.e. $F_i^X(q) = 0$ in Eq. (3.44). The solid and open circles in Fig. 3.11 represent the absolute differences between the latter calculations for both quasielastic $(\vec{p}, \vec{p}\,')$ and $(\vec{p}, \vec{n})$ scattering, respectively.

As expected, at low energies the exchange terms contribute significantly and, for quasielastic $(\vec{p}, \vec{n})$ scattering, these terms are generally more pronounced than for $(\vec{p}, \vec{p}\,')$ reactions. Note the extreme importance of exchange effects on D_{nn}. In addition, at *higher energies* the contributions of exchange become important again for some $(\vec{p}, \vec{n})$ polarization transfer observables, e.g. $D_{\ell'\ell}$ and $D_{s'\ell}$. Thus, one concludes that in practice one cannot neglect exchange, not even at 500 MeV, when calculating medium–modified NN amplitudes and the resulting polarization transfer observables.

Summary of qualitative study

The sensitivity of both quasielastic $(\vec{p}, \vec{p}\,')$ and $(\vec{p}, \vec{n})$ polarization transfer observables has been investigated with respect to PS versus PV forms of the πNN vertex, relativistic medium effects, and exchange contributions to the NN amplitudes. The tendencies displayed in the figures speak for themselves. Generally the $(\vec{p}, \vec{n})$ polarization transfer observables D_{nn}, $D_{s's}$ and $D_{\ell'\ell}$ exhibit the highest sensitivities to all these effects over the whole energy range. Relative to the above–mentioned observables, A_y is insensitive to all these effects (for both reactions). It was stressed that the commonly used SVPAT form does not correctly treat the PV form of the πNN vertex: one should rather use a meson–exchange model, such as the HLF model, for this purpose. It has also been shown that medium–modifications of the NN amplitudes depend on the choice of the πNN vertex. It has also been shown that, contrary to former expectations,

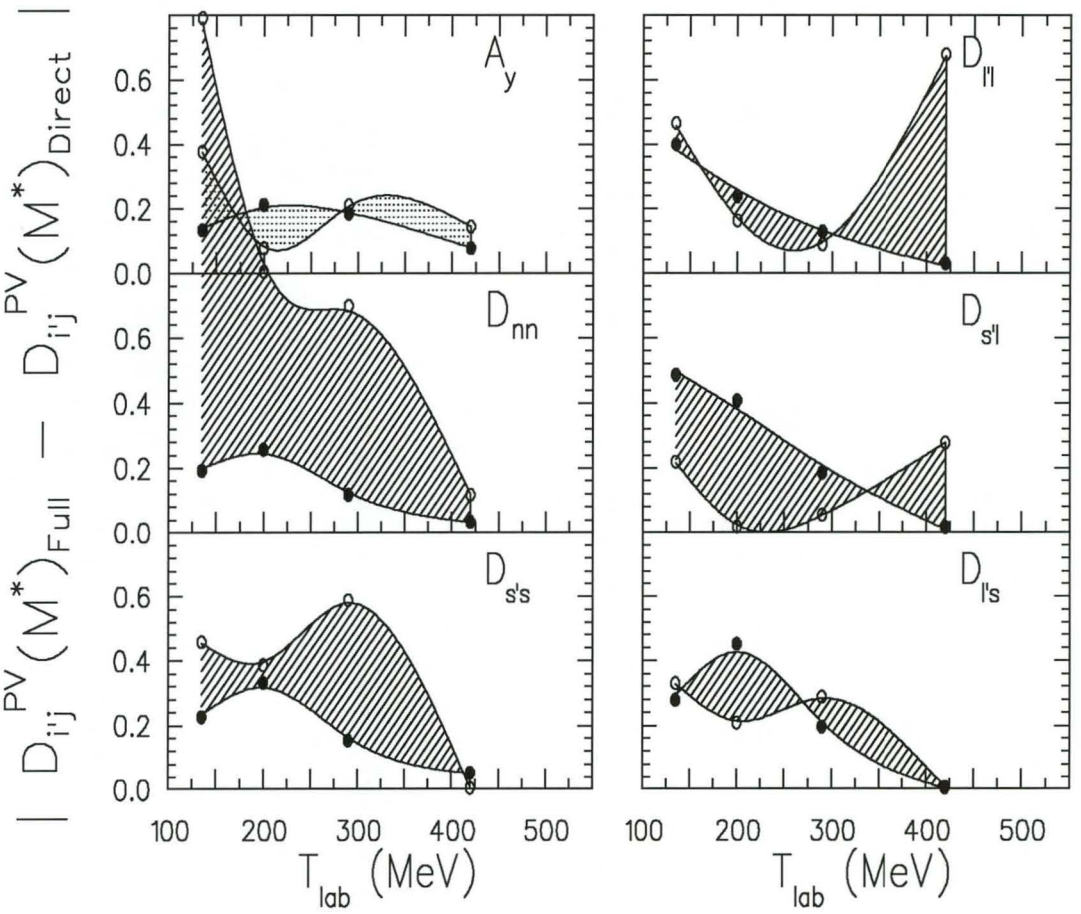

Figure 3.11: The values of $|D_{i'j}^{PV}(M^*)_{Full} - D_{i'j}^{PV}(M^*)_{Direct}|$ are presented again similarly as in Figs. 3.8 – 3.10. Open circles represent $(\vec{p}, \vec{n})$ scattering, whereas solid circles represent $(\vec{p}, \vec{p}')$ scattering. The subscripts "Direct" and "Full" refer to calculations where the exchange terms have been neglected and included respectively.

exchange contributions cannot be neglected over the *entire* 135 to 500 MeV range.

The next step is to make quantitative predictions of the sensitivities of polarization transfer observables to RPWIA model parameters. However, recall that due to the Fermi motion of the target nucleons, quantitative calculations require NN scattering amplitudes at a range of effective laboratory kinetic energies $T_{\rm eff}^{L}$ (see Sec. 3.2.5). Unfortunately, published HLF parameter sets exist only at incident proton energies of 135, 200, 300 and 400 and 500 MeV [Ho85, Mu87a]. Hence, to perform a similar, but quantitative investigation, it is necessary to generate new HLF parameter sets.

Next, the acquisition of new HLF parameters at incident proton energies ranging from 80 to 200 MeV is discussed, as well as the implementation of a recent energy-dependent parametrization by Maxwell [Ma96] between 200 and 500 MeV.

3.3.3 New HLF parameter sets

Recently Maxwell [Ma96] published an energy dependent parametrization of the HLF model between 200 and 500 MeV (see next section). However, calculations of polarization transfer observables of interest also require HLF parameters lower than 200 MeV. The lack of parameters in the latter range (except at 135 and 200 MeV), necessitated the generation of new HLF parameters between 80 and 200 MeV in 5 MeV intervals.

A procedure similar to that of Horowitz [Ho85] is followed, whereby the free SVPAT amplitudes are parametrized in terms of the exchange of the 10 mesons listed in Table 3.4. For each meson there are 6 parameters:

- a real NN–meson coupling constant g_i^2
- a real cutoff parameter Λ_i^2
- real mass of the meson m_i
- an imaginary NN–meson coupling constant $\bar{g}_i^2$
- an imaginary cutoff parameter $\bar{\Lambda}_i^2$
- imaginary mass of the meson $\bar{m}_i$.

Table 3.4: Mesons associated with the Horowitz–Love–Franey model.

Meson exchanged	Isospin of meson	Type of Coupling
π	1	pseudoscalar
η	0	pseudoscalar
σ	0	scalar
ω	0	vector
t_1	1	tensor
a_1	1	axial–vector
δ	1	scalar
ρ	1	vector
t_0	0	tensor
a_o	0	axial–vector

Thus in total there are 60 parameters at each energy. Not all parameters, however, are varied to fit data. For example, the real meson masses m_i correspond to the experimental values [Ho85]. The real coupling constants g_i^2 and cutoff parameters Λ_i^2 are varied to simultaneously fit the real T = 1 and T = 0 SVPAT amplitudes. For the imaginary amplitudes, the meson masses $\bar{m}_i$ are chosen to be the same as those in Ref. [Ho85], whereas $\bar{g}_i^2$ and $\bar{\Lambda}_i^2$ are varied so as to fit the imaginary T = 1 and T = 0 SVPAT amplitudes.

Fits are compared to the summer 1986 amplitudes of Arndt and Roper [Ar86] for centre–of–mass scattering angles ranging from 0° – 90° in 5° steps. The fitting procedure is based on the Oak Ridge and Oxford minimization routine described in Ref. [Me66]. The quality of fits can be best judged by comparing HLF–based (dotted lines) to experimental data (solid lines) of free NN spin observables, as shown in Figs. 3.12 – 3.17; for illustrative purposes one considers laboratory energies 80, 160 and 200 MeV. The expressions for the observables ($\frac{d\sigma}{d\Omega}$, P, D, A_{yy}, A, R), in terms of the ABCDE amplitudes in Eq. (3.31), are defined in Appendix C. The new parameter sets yield fits of comparable quality to the original 200 HLF parameter–fits: for example, compare the fits at 80 and 160 MeV to the original fit at 200 MeV (depicted by the dashed lines in Figs. 3.16 and 3.17, and also published in Ref. [Ho85]). All parameter sets between 80 and 200 MeV produce fits of similar quality to the original fits of Horowitz [Ho85].

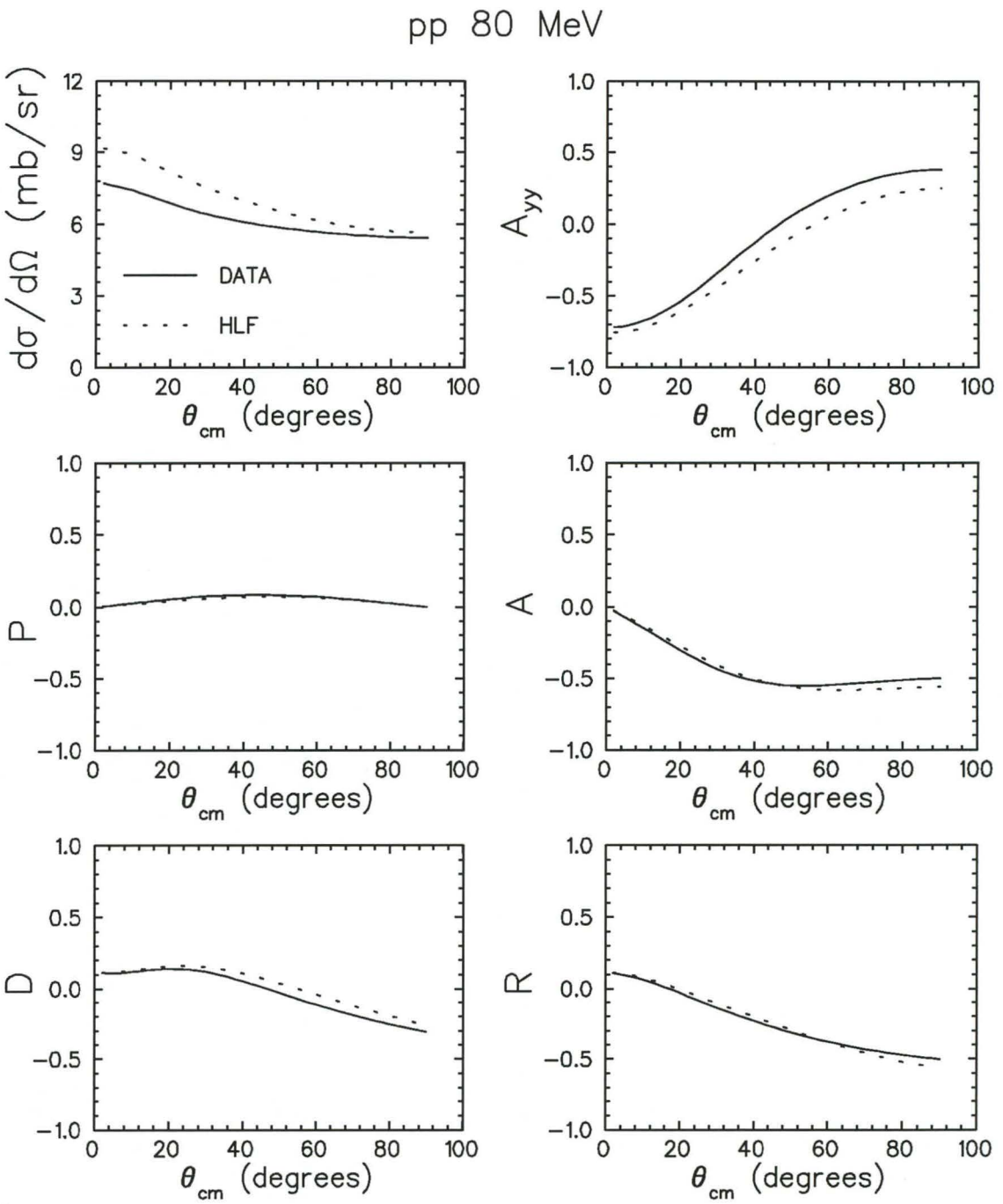

Figure 3.12: pp observables (using the notation of Ref. [Br78]) at an incident laboratory kinetic energy of 80 MeV, versus the centre–of–mass scattering angle. The solid lines show the observables calculated directly from the Arndt amplitudes, while the dotted lines are based on the new HLF parameters. The observables are defined in Appendix C.

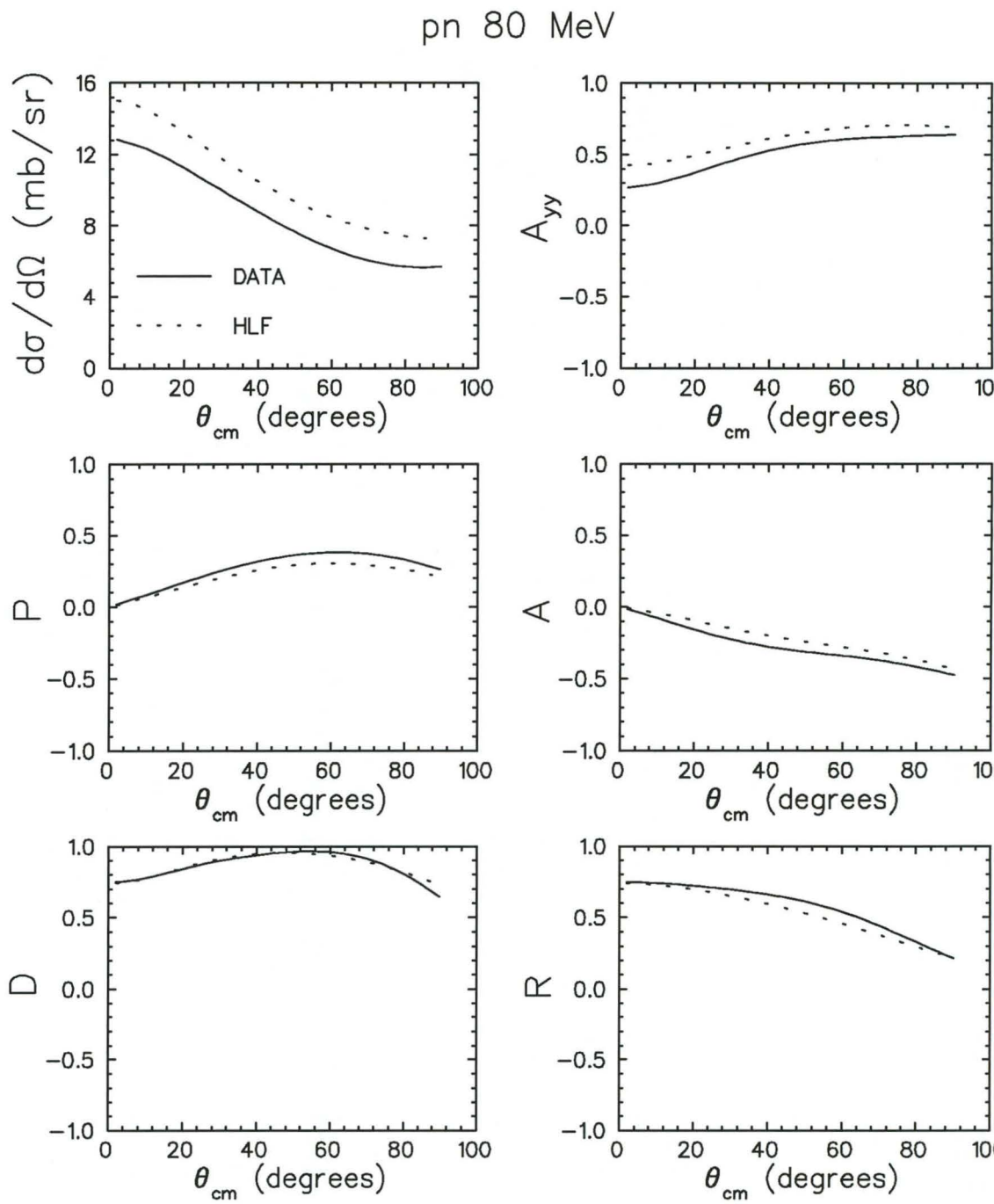

Figure 3.13: pn observables (using the notation of Ref. [Br78]) at an incident laboratory kinetic energy 80 of MeV, versus the centre–of–mass scattering angle. The solid lines show the observables calculated directly from the Arndt amplitudes, while the dotted lines are based on the new HLF parameters. The observables are defined in Appendix C.

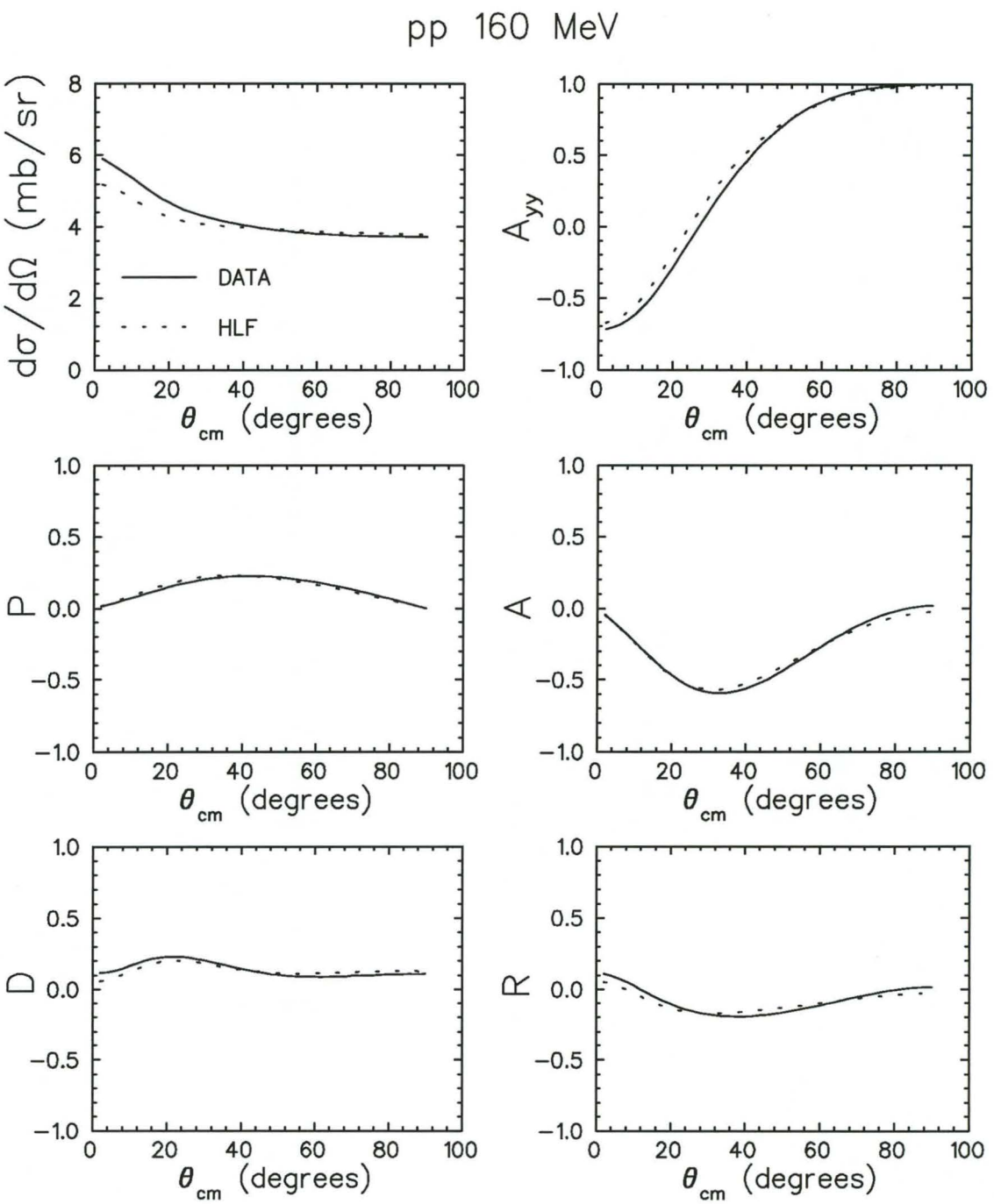

Figure 3.14: pp observables (using the notation of Ref. [Br78]) at an incident laboratory kinetic energy of 160 MeV, versus the centre–of–mass scattering angle. The solid lines show the observables calculated directly from the Arndt amplitudes, while the dotted lines are based on the new HLF parameters. The observables are defined in Appendix C.

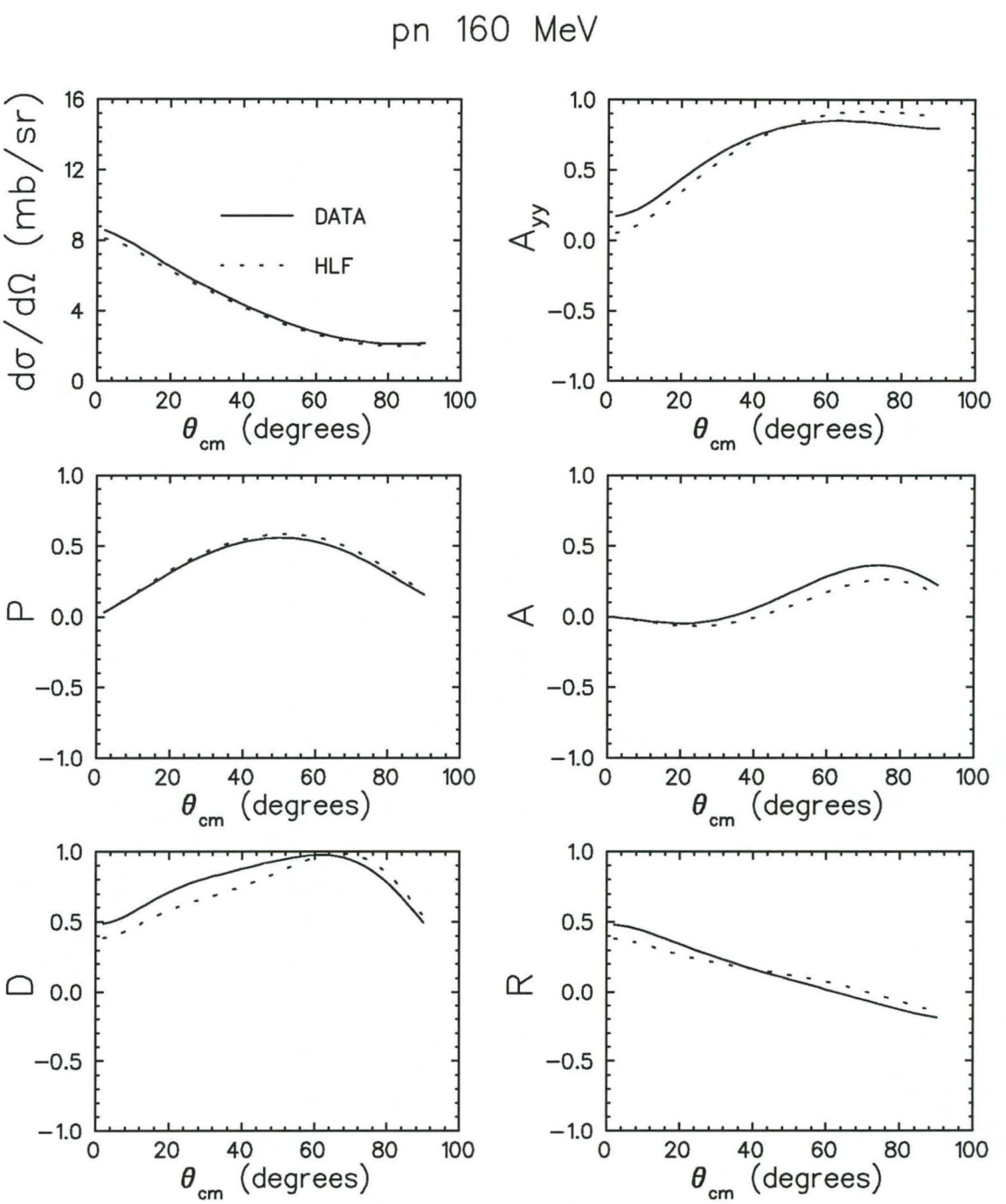

Figure 3.15: pn observables (using the notation of Ref. [Br78]) at an incident laboratory kinetic energy of 160 MeV, versus the centre–of–mass scattering angle. The solid lines show the observables calculated directly from the Arndt amplitudes, while the dotted lines are based on the new HLF parameters. The observables are defined in Appendix C.

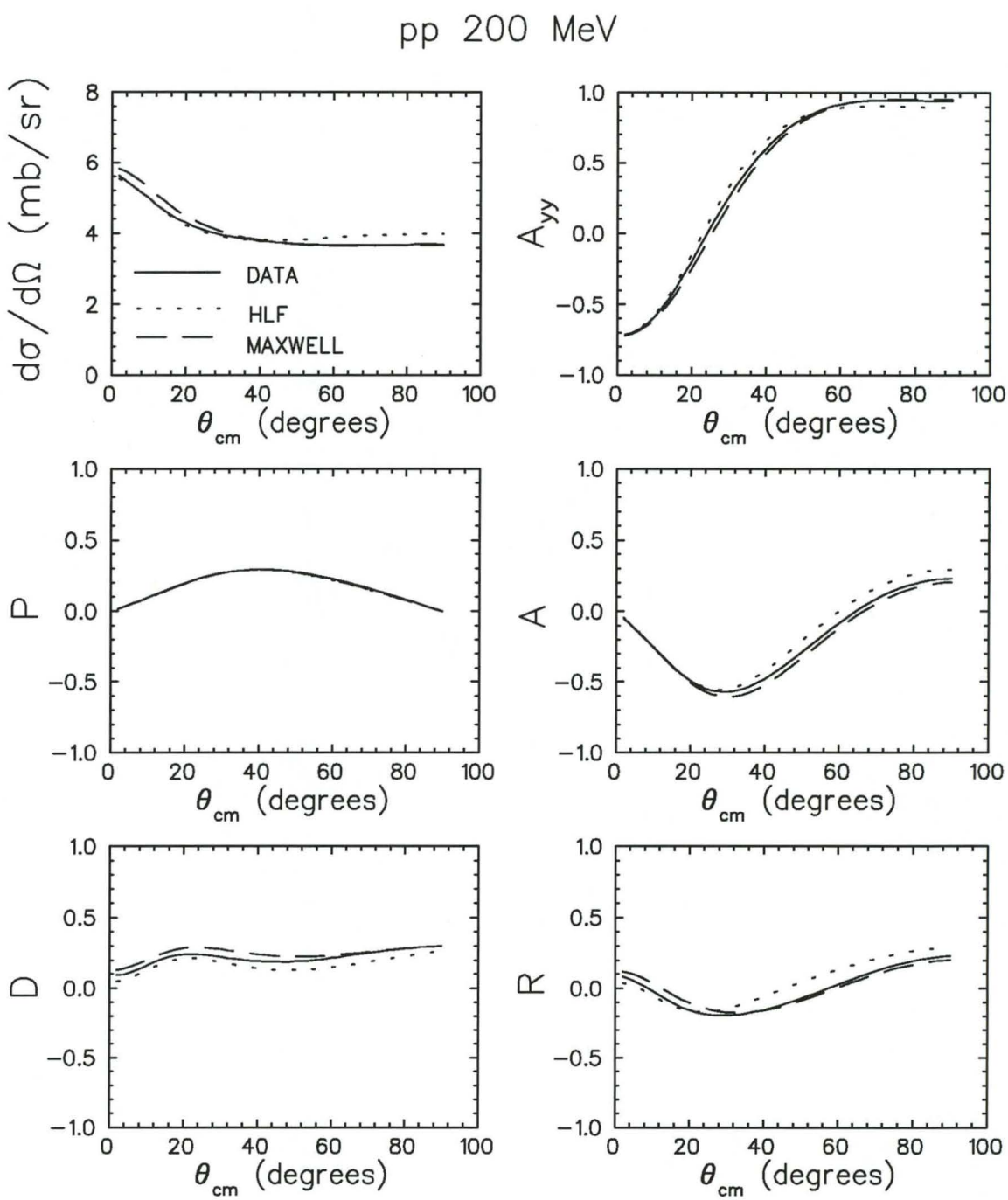

Figure 3.16: pp observables (using the notation of Ref. [Br78]) at an incident laboratory kinetic energy of 200 MeV, versus the centre–of–mass scattering angle. The solid lines show the observables calculated directly from the Arndt amplitudes, while the dotted lines are based on the original HLF parameters. The dashed lines use the Maxwell parameters [Ma96]. The spin observables are defined in Appendix C.

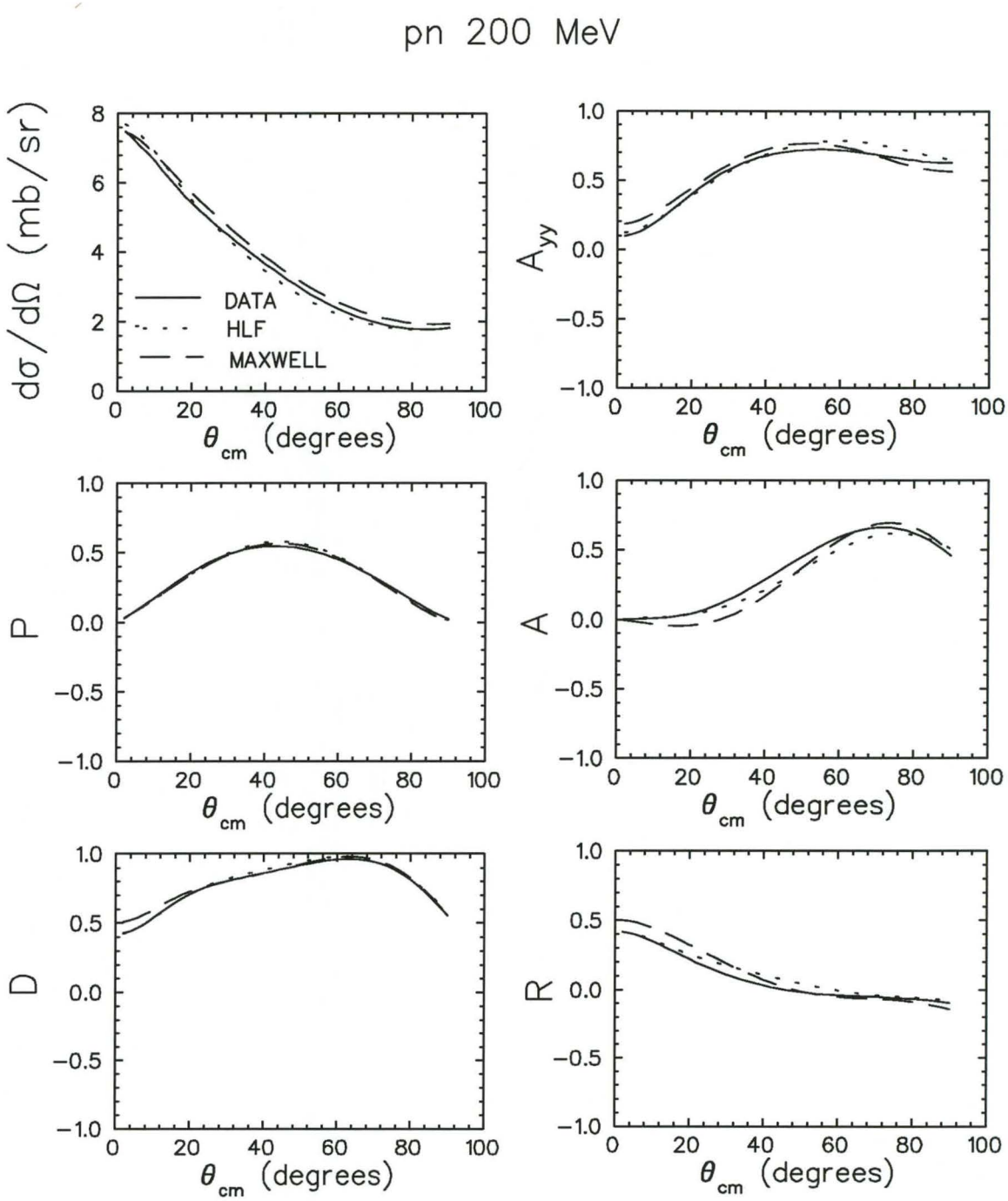

Figure 3.17: pn observables (using the notation of Ref. [Br78]) at an incident laboratory kinetic energy of 200 MeV, versus the centre–of–mass scattering angle. The solid lines show the observables calculated directly from the Arndt amplitudes, while the dotted lines are based on the original HLF parameters. The dashed lines use the Maxwell parameters [Ma96]. The observables are defined in Appendix C.

The new HLF parameter sets, including the original parameters [Ho85], are listed in Appendix H. Note that the coupling constants are not identical to those in Ref. [Ho85]: a correction has been applied in accordance with Ref. [Mu87b].

Next, an energy–dependent parametrization of the relativistic SVPAT amplitudes for NN scattering, between 200 and 500 MeV, is discussed.

3.3.4 Energy–dependent Maxwell parametrization

The HLF model has been successfully applied in studies of both elastic proton–nucleus scattering and the $(p, 2p)$ reaction [Mu87a, Co89, Ma90, Ma93, Ma94, Ik95], but suffers from the disadvantage that the various amplitudes are fitted separately to NN data at each laboratory kinetic energy, rather than as functions of energy. Not only is this inconvenient from a numerical point of view, since it necessitates interpolation between the energies used in the fit, but it also rules out any meaningful systematic comparison of the NN amplitudes at different energies, since these fits at are not related to one another. Note that, in this regard, the cutoff parameters in the HLF model vary quite dramatically from one energy to the next. However, since the NN amplitudes themselves vary quite smoothly and undramatically with energy, one might expect that a fit could be found in which the individual coupling constants and cutoff parameters also vary smoothly with energy.

Motivated by the above–mentioned considerations, Maxwell [Ma96] published a new Lorentz covariant parametrization of the NN amplitudes (in the HLF model) with energy–dependent coupling constants and cutoff parameters.

Maxwell generated two parametrizations: one with the energy dependence confined to the coupling constants:

$$g^2(T_{\rm rel}) = g_0 + g_1\, T_{\rm rel} + g_2\, T_{\rm rel}^2 \tag{3.122}$$

and the other with energy dependence in *both* coupling constants (same as above) and cutoff parameters:

$$\Lambda(E) = \Lambda_0(1 + \gamma\, T_{\rm rel})\,. \tag{3.123}$$

These parameters are used in both real and imaginary parts of the amplitudes, such that

$$T_{\rm rel} \equiv \frac{T_{\rm lab} - T_0}{T_0} \tag{3.124}$$

where $T_{\rm lab}$ is the laboratory kinetic energy and $T_0 = 200$ MeV. The parameters Λ_0, γ, g_1 and g_2 are extracted from fits to the summer 1994 Arndt amplitudes over the laboratory kinetic energies ranging from 200 to 500 MeV in 100 MeV intervals and over centre–of–mass scattering angles between 5° and 175° in 5° steps.

Although the parametrization given by *both* Eqs. (3.122) and (3.123) gives better fits than the parametrization given *solely* by Eq. (3.122), both reproduce the empirical amplitudes reasonably well. In contrast to the earlier work by Horowitz, a single χ^2 minimization is carried out over the *full energy range* considered, namely 200, 300, 400 and 500 MeV. The parameter sets are published in Tables 1 and 2 of Ref. [Ma96]. The Maxwell parameters produce observables of comparable quality to our parameter–fits at 200 MeV; see for example Figs. 3.16 and 3.17 where the dashed line corresponds to the Maxwell parameters at 200 MeV.

In the next section, the new HLF parameters, ranging from 80 to 195 MeV, are used, as well as the energy–dependent parametrization of Maxwell between 200 and 500 MeV, to quantitatively study the sensitivities of quasielastic polarization transfer observables to nuclear medium effects.

3.3.5 Quantitative investigations

The aim of this section is to quantitatively study the sensitivity of complete sets of quasielastic $(\vec{p},\vec{p}')$ and $(\vec{p},\vec{n})$ polarization transfer observables to relativistic or medium (M^*) effects, PS versus PV forms of the πNN vertex, and exchange contributions to the NN amplitudes. Most of these results have been published in Ref. [Hi97, Hi98]. This quantitative study is made possible by the recent availability of HLF parameters between 80 and 500 MeV, that is, the new HLF parameters between 80 and 195 MeV, and the Maxwell parametrization, with both energy–dependent coupling constants and cutoff parameters, between 200 and 500 MeV. For a momentum transfer of 1.97 fm^{-1} and a ^{40}Ca target, the effective laboratory kinetic energies (which range between 80 and 500 MeV) limit calculations of quasielastic polarization transfer observables to incident laboratory energies between 135 and 300 MeV.

As in Sec. 3.3.2, the results are presented as "difference " graphs in Figs. 3.19 – 3.22: the solid and open circles denote our calculated values, whereas the solid lines serve merely to guide the eye. The shaded areas accentuate differences between $(\vec{p},\vec{p}')$ and $(\vec{p},\vec{n})$ predictions. Based on the findings of Sec. 3.3.2, only calculations using the HLF model for the NN interaction, rather than a direct SVPAT parametrization, are considered.

Theoretical uncertainty

Recall that, per construction, the PS(M^*)–HLF and PS(M^*)–SVPAT polarization transfer observables are identical. However, the HLF parameter–fits are not perfect and, hence, slight differences occur. Furthermore, the Fermi–averaging procedure involves integrating over at least a 100 NN amplitudes, such that slight differences on individual amplitudes could add constructively, thus translating to relatively large differences after the integration. Therefore, before performing a quantitative investigation, it is important to know what the theoretical uncertainty is on the various polarization transfer observables: this is indicated by $|D_{i'j}^{PS-HLF}(M^*) - D_{i'j}^{PS-SVPAT}(M^*)|$ and displayed in Fig. 3.18. For the energies and momentum transfers under consideration, these differences are smaller than 0.04 and will not change any of the conclusions of the subsequent sections. Values of the statistical experimental errors are typically about $\pm$ 0.03 [Ch90]. Hence, one can hope to experimentally distinguish between different model calculations only when the absolute differences presented are significantly larger than 0.06.

Pseudoscalar versus pseudovector πNN coupling

The solid and open circles in Fig. 3.19 denote the values of $|D_{i'j}^{PV}(M^*) - D_{i'j}^{PS}(M^*)|$ for quasielastic $(\vec{p},\vec{p}\,')$ and $(\vec{p},\vec{n})$ scattering, respectively. For $(\vec{p},\vec{n})$ scattering, D_{nn}, $D_{s's}$, and $D_{\ell'\ell}$ are the most sensitive observables over the entire energy range. Generally, the sensitivities of the $(\vec{p},\vec{n})$ polarization transfer observables completely overshadow the corresponding $(\vec{p},\vec{p}')$ observables. Measurements of D_{nn} for both $(\vec{p},\vec{n})$ and $(\vec{p},\vec{p}')$ scattering, particularly at low energies, would be extremely useful in shedding light on the preferred form of the πNN vertex.

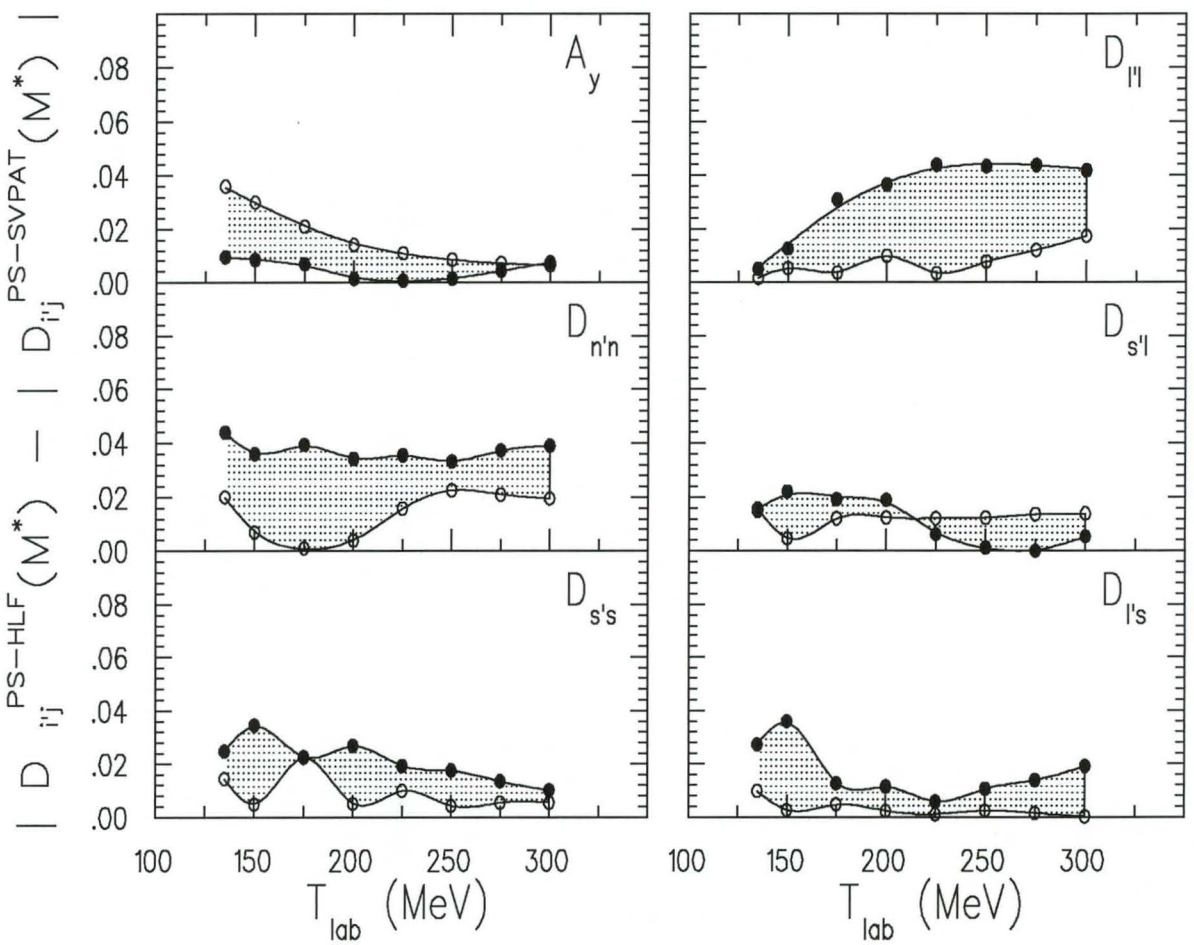

Figure 3.18: The difference, $|D_{i'j}^{PS-HLF}(M^*) - D_{i'j}^{PS-SVPAT}(M^*)|$, for $(\vec{p},\vec{p}')$ [solid circles] and $(\vec{p},\vec{n})$ [open circles] polarization transfer observables $D_{i'j}$ based on a direct SVPAT parametrization of the NN amplitudes and those based on the HLF model, as a function of laboratory energy, and *at the quasielastic peak*. All calculations use the PS form of the πNN vertex, and the solid lines serve merely to guide the eye.

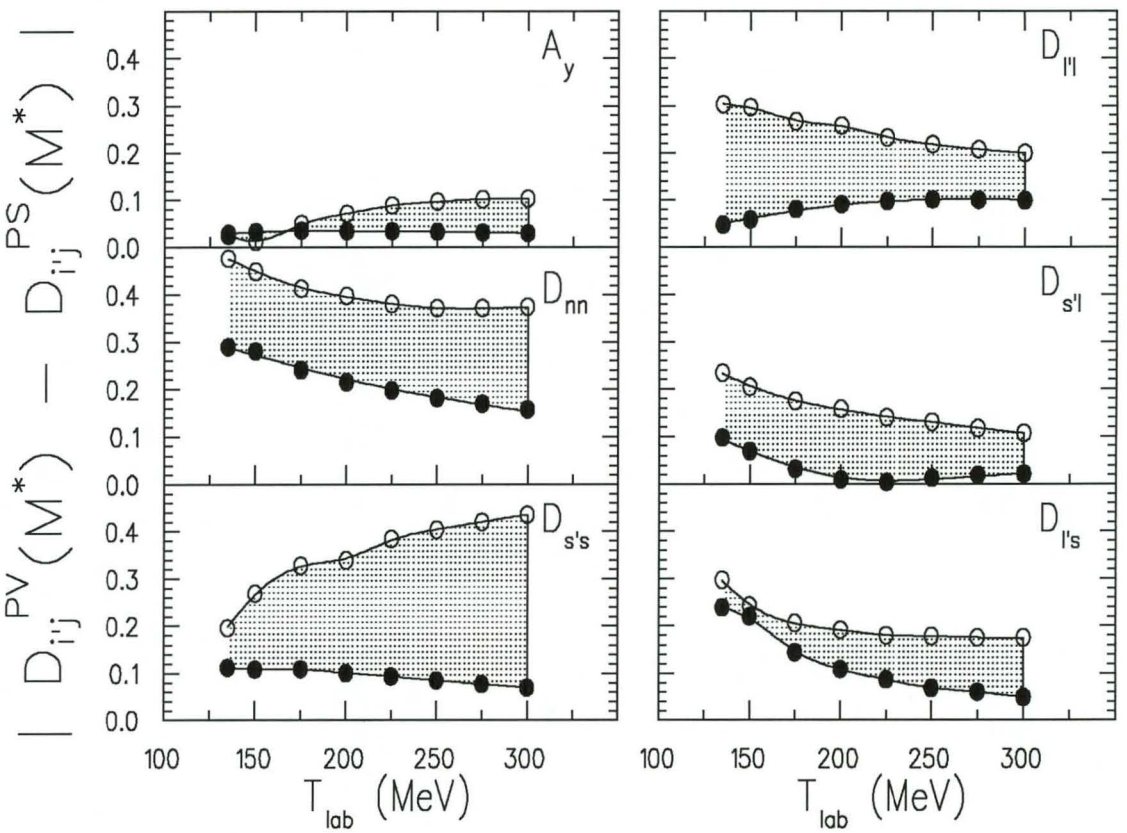

Figure 3.19: The difference, $|D^{PV}_{i'j}(M^*) - D^{PS}_{i'j}(M^*)|$, between the polarization transfer $(\vec{p}, \vec{n}\,')$ observables $D_{i'j}$ calculated with a pseudovector (PV) and a pseudoscalar (PS) term in the NN interaction, respectively, as a function of laboratory energy, and *at the quasielastic peak*. Open circles represent $(\vec{p}, \vec{n})$ scattering, whereas solid circles represent $(\vec{p}, \vec{p}\,')$ scattering. All calculations are based on the HLF model of the NN amplitudes. The solid lines serve merely to guide the eye.

Relativistic or medium M^* effects for a pseudoscalar πNN vertex

The PS form of the πNN vertex is chosen, and the difference between effective–mass (M^*) and free–mass (M) calculations is studied. The solid and open circles in Fig. 3.20 represent the values of $|D_{i'j}^{PS}(M^*) - D_{i'j}(M)|$ for quasielastic $(\vec{p},\vec{p}\,')$ and $(\vec{p},\vec{n})$ scattering, respectively. Compared to $(\vec{p},\vec{p}\,')$ scattering, the $(\vec{p},\vec{n})$ polarization transfer observables D_{nn}, $D_{s'\ell}$ and $D_{s'\ell}$ are more sensitive to relativistic M^* effects over the entire energy range. At higher energies for $(\vec{p},\vec{p}\,')$ scattering, D_{nn}, $D_{s's}$ and $D_{\ell's}$ observables are insensitive to medium effects and yield results similar to free NN scattering. These results are consistent with complete sets of quasielastic $(\vec{p},\vec{p}')$ polarization transfer observables measured for ^{12}C at 290 MeV and $|\vec{q}\,| = 1.97$ fm^{-1} [Ch90]: the data show that most of the proton–nucleus observables are virtually identical to the corresponding free NN polarization transfer observables. Note that D_{nn} exhibits maximum and minimum sensitivity to medium effects for $(\vec{p},\vec{p}')$ and $(\vec{p},\vec{n})$ scattering respectively.

Relativistic or medium M^* effects for a pseudovector πNN vertex

The PV form of the πNN vertex is chosen, and the difference between effective–mass (M^*) and free–mass (M) calculations is studied. The solid and open circles in Fig. 3.21 represent the values of $|D_{i'j}^{PV}(M^*) - D_{i'j}(M)|$ for quasielastic $(\vec{p},\vec{p}\,')$ and $(\vec{p},\vec{n})$ scattering, respectively. Compared to $(\vec{p},\vec{n})$ scattering, the $(\vec{p},\vec{p}\,')$ polarization transfer observables D_{nn}, $D_{s's}$ and $D_{\ell'\ell}$ are more sensitive to relativistic M^* effects over the entire energy range. This is totally the opposite effect compared to the case for PS coupling. At higher energies all the $(\vec{p},\vec{n})$ observables are insensitive to medium effects and yield results similar to free NN scattering. These results are consistent with A_y and D_{nn} measured at 186 MeV [Wa94], and also with preliminary RCNP data [Sa96, Wa96, Wa97]. The latter group measured complete sets of quasielastic $(\vec{p},\vec{n})$ polarization transfer observables for ^{2}H, ^{6}Li, ^{12}C, ^{40}Ca and ^{208}Pb at an incident energy of 346 MeV and a momentum transfer of 1.7 fm^{-1}: their data show that most of the proton–nucleus observables are virtually identical to the corresponding free NN polarization transfer observables (see section on "Comparison to data"). One sees that the effect of the nuclear medium, for both $(\vec{p},\vec{n})$ and $(\vec{p},\vec{p}\,')$, depends crucially on whether a PS or PV form of the pion coupling is used. Hopefully experimental data will shed light on the type of coupling favoured. Note the enhanced sensitivity of both D_{nn} and $D_{s's}$ at low energies for both $(\vec{p},\vec{n})$ and $(\vec{p},\vec{p}\,')$ scattering.

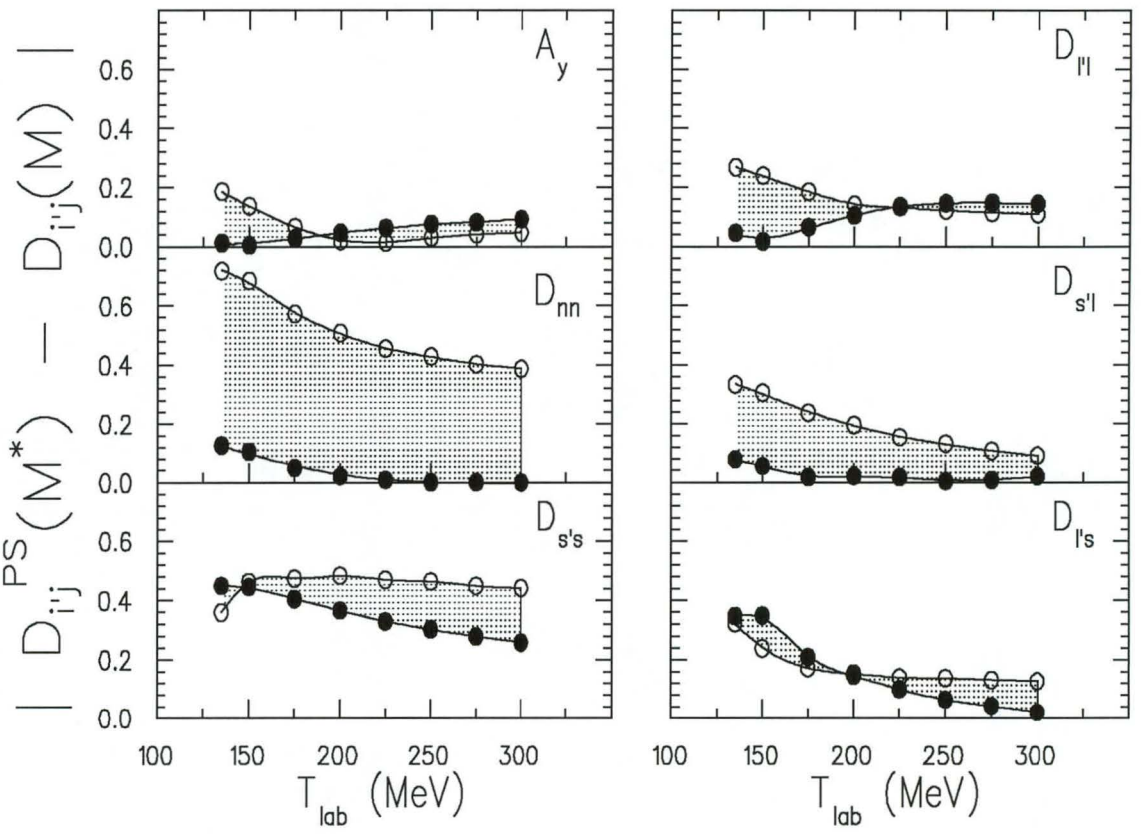

Figure 3.20: The values of $|D_i^{PS}{}_{i'j}(M^*) - D_{i\ i'j}(M)|$, based on the HLF model, for $(\vec{p}, \vec{n})$ (open circles) and $(\vec{p}, \vec{p}\,')$ (solid circles) scattering, are plotted in precisely the same way as in Fig. 3.19

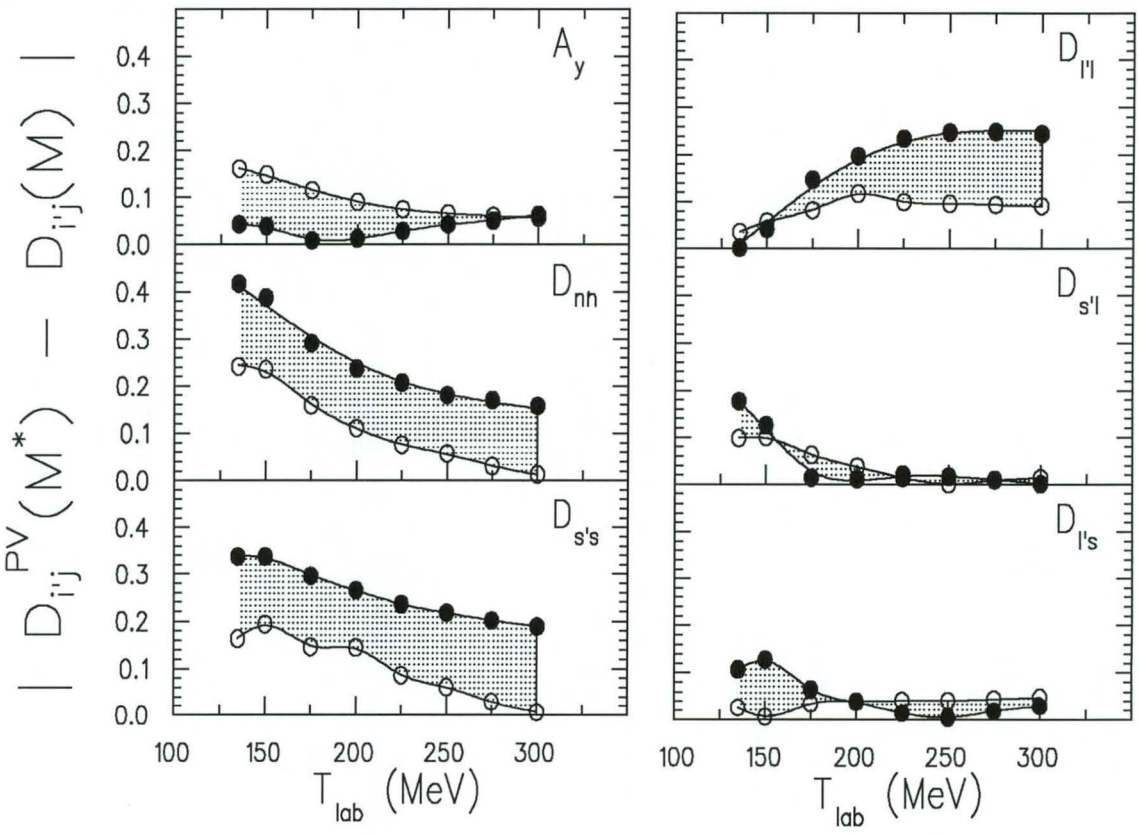

Figure 3.21: The values of $|D_{i'j}^{PV}(M^*) - D_{i'j}(M)|$, based on the HLF model, for $(\vec{p},\vec{n})$ (open circles) and $(\vec{p},\vec{p}\,')$ (solid circles) scattering, are plotted in precisely the same way as in Fig. 3.19

Exchange contributions

For illustrative purposes, the pseudovector form of the πNN vertex is chosen, and the difference $|D_i^{PV}{}_{'j}(M^*)_{\text{Full}} - D_{i\,'j}(M)_{\text{Direct}}|$ is plotted as a function of incident laboratory energy at the centroid of the quasielastic peak. These difference plots serve as a measure of the importance of exchange contributions to the polarization transfer observables. The subscript "Full" refers to the direct plus exchange amplitudes given by Eq. (3.44), whereas the subscript "Direct" refers to amplitudes where the exchange contributions are ignored, i.e. $F_i^X(q) = 0$ in Eq. (3.44). The solid and open circles in Fig. 3.22 represent the absolute differences between the latter calculations for both quasielastic $(\vec{p}, \vec{p}\,')$ and $(\vec{p}, \vec{n})$ scattering, respectively. Contrary to initial intuition, one sees that for some polarization transfer observables the exchange contributions become more important at higher energies. Generally, the $(\vec{p}, \vec{p}\,')$ observables are more sensitive to exchange contributions compared to the corresponding $(\vec{p}, \vec{n})$ observables. In particular, A_y and $D_{\ell'\ell}$ for $(\vec{p}, \vec{p}\,')$ scattering are sensitive to exchange contributions over the entire energy range. Note the extreme sensitivity of D_{nn} at low energies and $D_{\ell'\ell}$ at higher energies for $(\vec{p}, \vec{n})$ scattering. Hence, as in the qualitative study of exchange effects, one concludes that exchange cannot be neglected, even at higher energies.

Sensitivity studies of unpolarized double differential cross sections

Thus far sensitivity studies of only polarization transfer observables have been considered. For completeness the investigation is extended to include unpolarized double differential cross sections for quasielastic $(\vec{p}, \vec{p}\,')$ and $(\vec{p}, \vec{n})$ scattering. Although a simple plane wave treatment often describes qualitative features, such as the shape and the centroid of the quasielastic peak, it usually fails to describe the absolute unpolarized double differential cross section. Strictly speaking, one should rather consider a full distorted wave treatment in the incident and exit channels: The question of distortions is dealt with in Chapter 4. The inclusion of distorted waves, however, masks the effects of nuclear medium–modifications and different forms of the πNN vertex, thus preventing one from disentangling the various effects. However, handwaving arguments suggest that since polarization transfer observables are effectively ratios of polarized double differential cross sections, the effects of distortions largely cancel, thus enhancing relativistic or medium effects. Hence a plane wave description should be sufficient for studies

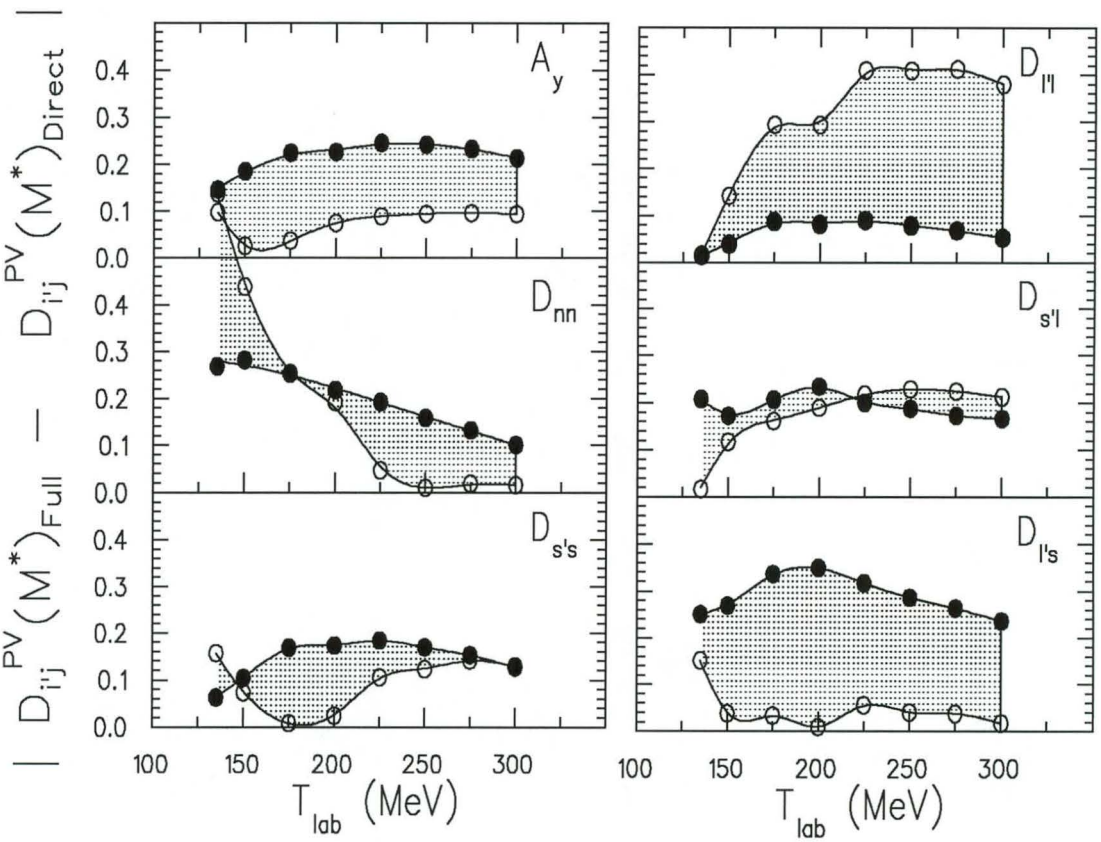

Figure 3.22: The values of $|D_{i'j}^{PV}(M^*)_{Full} - D_{i'j}^{PV}(M^*)_{Direct}|$ are plotted in precisely the same way as in Fig. 3.11. Open circles represent $(\vec{p}, \vec{n})$ scattering, whereas solid circles represent $(\vec{p}, \vec{p}')$ scattering. The subscripts "Direct" and "Full" refer to calculations where the exchange terms have respectively been neglected and included respectively.

of polarization observables. The RPWIA does, however, incorporate central distortions in an approximate way: Recall that the effects of central distortions are incorporated in the effective number of nucleons A_{eff} calculated via the transmission probability $T(b)$ [see Eq. (3.9)] within the eikonal approximation.

Before embarking on a full relativistic distorted–wave treatment, it is instructive to study the sensitivity of the unpolarized double differential cross sections to medium modifications of the NN interaction, different forms of the πNN vertex, and exchange contributions. For sake of convenience, the unpolarized double differential cross section is often referred to as merely the cross section, and the notation $\frac{d^2\sigma}{d\Omega\, dE}$ is used instead of $\frac{d\bar{\sigma}}{d\Omega_1' dE_1'}$ [see Eq. (3.83)].

The theoretical uncertainty on the cross section is approximately ± 0.1 mb sr^{-1} MeV^{-1} and is displayed in Fig. 3.23(a). Hence, a cross section may be classified as sensitive to a particular effect when the difference curves are greater than 0.2 mb sr^{-1} MeV^{-1}. Using the notation of previous sections, Figs. 3.23(b) to 3.23(e) display the sensitivities of $(\vec{p}, \vec{p}')$ and $(\vec{p}, \vec{n})$ cross sections to nuclear medium effects, different forms of the pion coupling, and exchange contributions to the NN amplitudes. The cross section is only sensitive to PS medium effects, whereas most of the other sensitivities are of the same order, if not smaller, than the theoretical uncertainty. We, therefore, conclude that cross section data are insensitive to the parameters under investigation, and once again, stress the importance of polarization transfer observables in isolating and studying various nuclear medium effects.

3.4 Comparison to data

The RPWIA calculations, based on the HLF model, are now compared to published experimental data. The availability of HLF parameter sets between 80 and 500 MeV limits this comparison to the following world (published) data:

- ^{12}C$(\vec{p}, \vec{n})$ $T_{\text{lab}} = 186$ MeV at 20°: $\frac{d^2\sigma}{d\Omega\, dE}$, A$_y$ and D$_{nn}$ [Wa93, Wa94],
- ^{12}C$(\vec{p}, \vec{p}')$ $T_{\text{lab}} = 290$ MeV at 29.5° ($|\vec{q}\,| = 1.97$ fm^{-1}): $\frac{d^2\sigma}{d\Omega\, dE}$, A$_y$, D$_{nn}$, D$_{s's}$, D$_{l'l}$, D$_{s'l}$ and D$_{l's}$[Ch90],

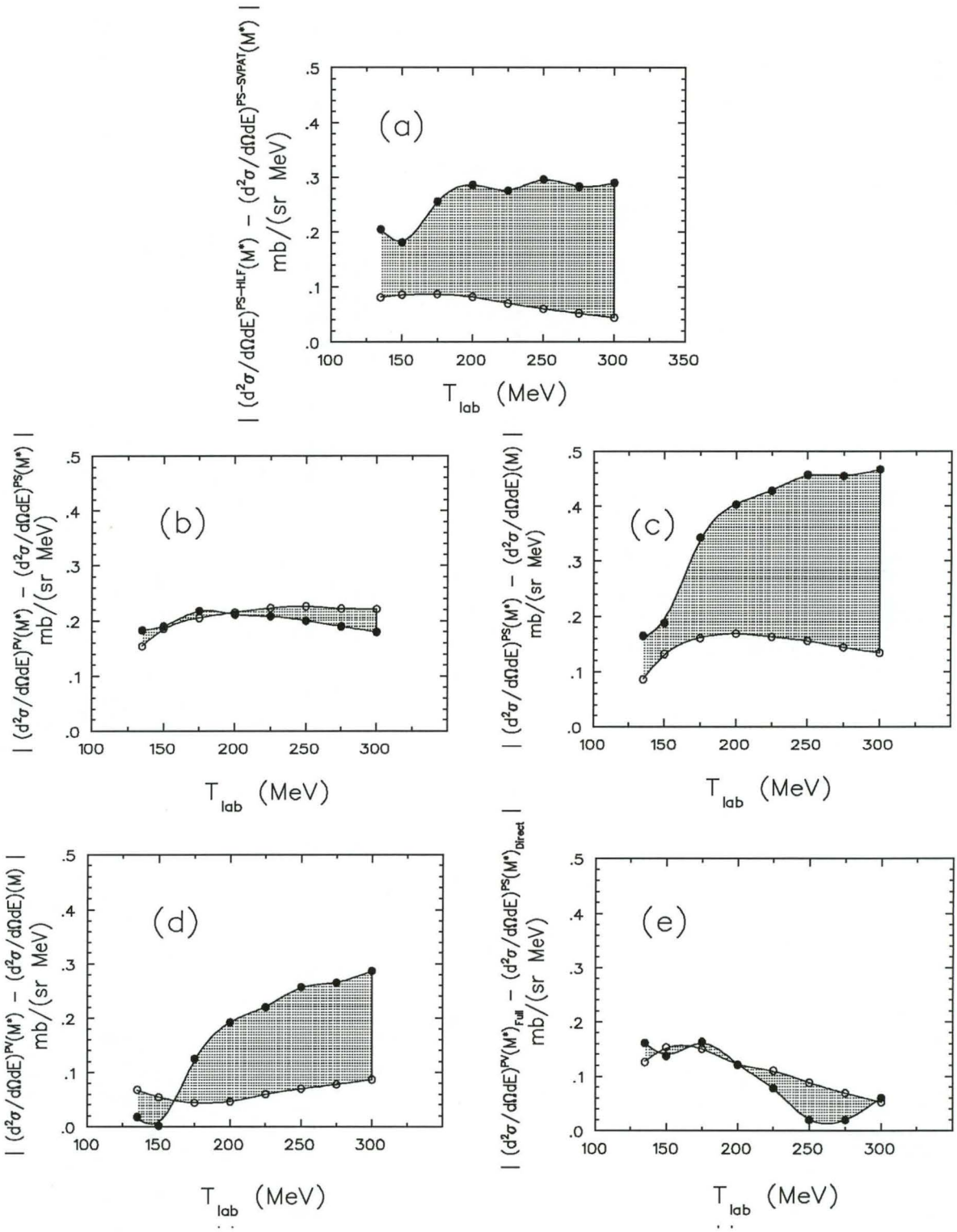

Figure 3.23: The sensitivity of quasielastic $(\vec{p},\vec{p}\,')$ and $(\vec{p},\vec{n})$ unpolarized double differential cross sections $(\frac{d\sigma}{d^2\Omega\, dE})$ in mb sr^{-1} MeV^{-1} to (a) the theoretical uncertainty in the HLF parameters, (b) PS versus PV forms of the πNN vertex, (c) PS medium effects, (d) PV medium effects, and (e) exchange contributions. The figures are plotted as a function of laboratory energy *at the quasielastic peak*. Open circles represent $(\vec{p},\vec{n})$ scattering, whereas solid circles represent $(\vec{p},\vec{p}\,')$ scattering. The notation is identical to that used in Figs. 3.19 – 3.22, except that $\frac{d\bar{\sigma}}{d\Omega_1' dE_1'}$ is now replaced by $\frac{d^2\sigma}{d\Omega\, dE}$. The solid lines serve merely to guide the eye.

- and, ^{54}Fe$(\vec{p},\vec{p}')$ $T_{\rm lab} = 290$ MeV at 20° ($|\vec{q}\,| = 1.97$ fm^{-1}): $\frac{d^2\sigma}{d\Omega\, dE}$, P, A_y, D_{nn}, $D_{s's}$, $D_{l'l}$, $D_{s'l}$ and $D_{l's}$ [Ha88].

A number of experiments [Wa94, Li94, Ca95, Ha98], partially motivated by our work [Hi94, Hi95], have been proposed [see Chapter 2] and preliminary data are now available in some cases. However, these data are not published, and so I refrain from a comparison to our model predictions.

Results are displayed in Figs. 3.24 – 3.28 and exclude spin–orbit distortions. The effect of spin–orbit distortions must be inferred from Figs. 3.6 – 3.7 discussed in Sec. 3.2.10. The solid lines indicate free mass (M) calculations [Free M], dotted lines represent PV effective mass (M^*) calculations based on the HLF model [PV(M^*)–HLF], dashed lines display PS effective mass (M^*) calculations based on the HLF–model [PS(M^*)–HLF], and dashed-dotted lines show PS effective mass (M^*) calculations based on a direct SVPAT parametrization of the Arndt phases [PS(M^*)–SVPAT]. The difference between the PS(M^*)–SVPAT and PS(M^*)–HLF calculations gives an indication of the theoretical uncertainty attributed to HLF model parameters. The RPWIA model predictions are now compared to the above–mentioned published data.

3.4.1 ^{12}C$(\vec{p},\vec{n})$ for $T_{\rm lab} = 186$ MeV at 20°

Figs. 3.24 and 3.25 display calculations for ^{12}C$(\vec{p},\vec{n})$ $T_{\rm lab} = 186$ MeV at 20° ($|\vec{q}\,| = 1.1$ fm^{-1}). The data are from Ref. [Wa93, Wa94] and the centroid of the quasielastic peak is located at $\omega \approx 50$ MeV. Note that, as explained in Sec. 3.2.8, the energy transfer ω includes the reaction Q–value of -18.6 MeV. In Fig. 3.24, one sees that the PS medium–modified calculation describes the overall shape and magnitude of the quasielastic peak surprisingly well. The PV M^*–based calculation underpredicts the cross section, but still describes the qualitative features of the quasielastic peak. The free mass prediction describes the shape, but fails to account for the correct position of the peak. Fig. 3.25 shows that D_{nn} clearly favours a PV treatment of the πNN coupling, whereas A_y fails to distinguish between PS and PV forms of the coupling. This illustrates the importance of measuring more than one polarization transfer observable when studying various effects. Note, however, that the free mass calculations do just as well as the PV(M^*) in describing the data. The largest difference for the latter predictions occurs for $D_{\ell'\ell}$; unfortunately the theoretical uncertainty is also the largest for this observable. Hence, for

all practical purposes, the PV(M^*) calculations are identical to the free mass calculations. It would be interesting to see whether this is verified experimentally by comparing *complete sets* of ^{12}C$(\vec{p},\vec{n})$ to ^{2}H$(\vec{p},\vec{n})$ polarization transfer observables at 186 MeV.

3.4.2 ^{12}C$(\vec{p},\vec{p}')$ for $T_{\rm lab} = 290$ MeV at 29.5°

Figs. 3.26 and 3.27 display calculations for ^{12}C$(\vec{p},\vec{n})$ $T_{\rm lab} = 290$ MeV at 29.5° ($|\vec{q}\,| = 1.97$ fm^{-1}). The data are from Ref. [Ch90] and the centroid of the quasielastic peak is located at $\omega \approx 80$ MeV. From Fig. 3.26 one sees that the data do not have simple Lorentzian shapes [Wa94]. The data exhibit more strength at high and low ω–values of the quasielastic peak, thus indicating modes of excitation not covered by the simple Fermi–gas model.

From Fig. 3.27, one sees that D_{nn}, $D_{s's}$, $D_{s'\ell}$ and $D_{\ell' s}$ correspond to the free mass predictions, whereas $D_{\ell'\ell}$ favours a PS form of the πNN vertex. None of the calculations predict A_y correctly. However, the inclusion of spin–orbit distortion moves most of the M^*–based polarization transfer observables (see Figs. 3.6 – 3.7), including A_y, closer to the data. Once again, as in Ref. [Ho88], the effect of relativity is to quench A_y for quasielastic $(\vec{p},\vec{p}')$ scattering relative to the free mass values. This quenching effect is not observed for quasielastic $(\vec{p},\vec{n})$ scattering. Furthermore, one sees that all the M^*–based calculations fail to describe the $D_{s's}$ data.

3.4.3 ^{54}Fe$(\vec{p},\vec{p}')$ for $T_{\rm lab} = 290$ MeV at 20°

Fig. 3.28 displays calculations for ^{54}Fe$(\vec{p},\vec{p}')T_{\rm lab} = 290$ MeV at 20° ($|\vec{q}\,| = 1.36$ fm^{-1}). The data are from Ref. [Ha88] and the centroid of the quasielastic peak is located at $\omega \approx 40$ MeV. This small momentum transfer was deliberately chosen so as to introduce some sensitivity to the nuclear response function resulting from Random–Phase–Approximation (RPA) correlations. Hence, in principle, one does not expect the RPWIA calculations to reproduce the data. Nevertheless, it is instructive to compare our model predictions to these data. The most striking features of all the experimental polarization transfer observables, compared to corresponding observables at larger momentum transfers, are the pronounced slopes versus energy transfer ω. The RPWIA calculations of Ref. [Ha88] are crude since they use $M^* \approx 0.86$ rather than the M^*_{SC}–values quoted in Table 3.1. As discussed in Sec. 3.3.1 this difference can cause a variation

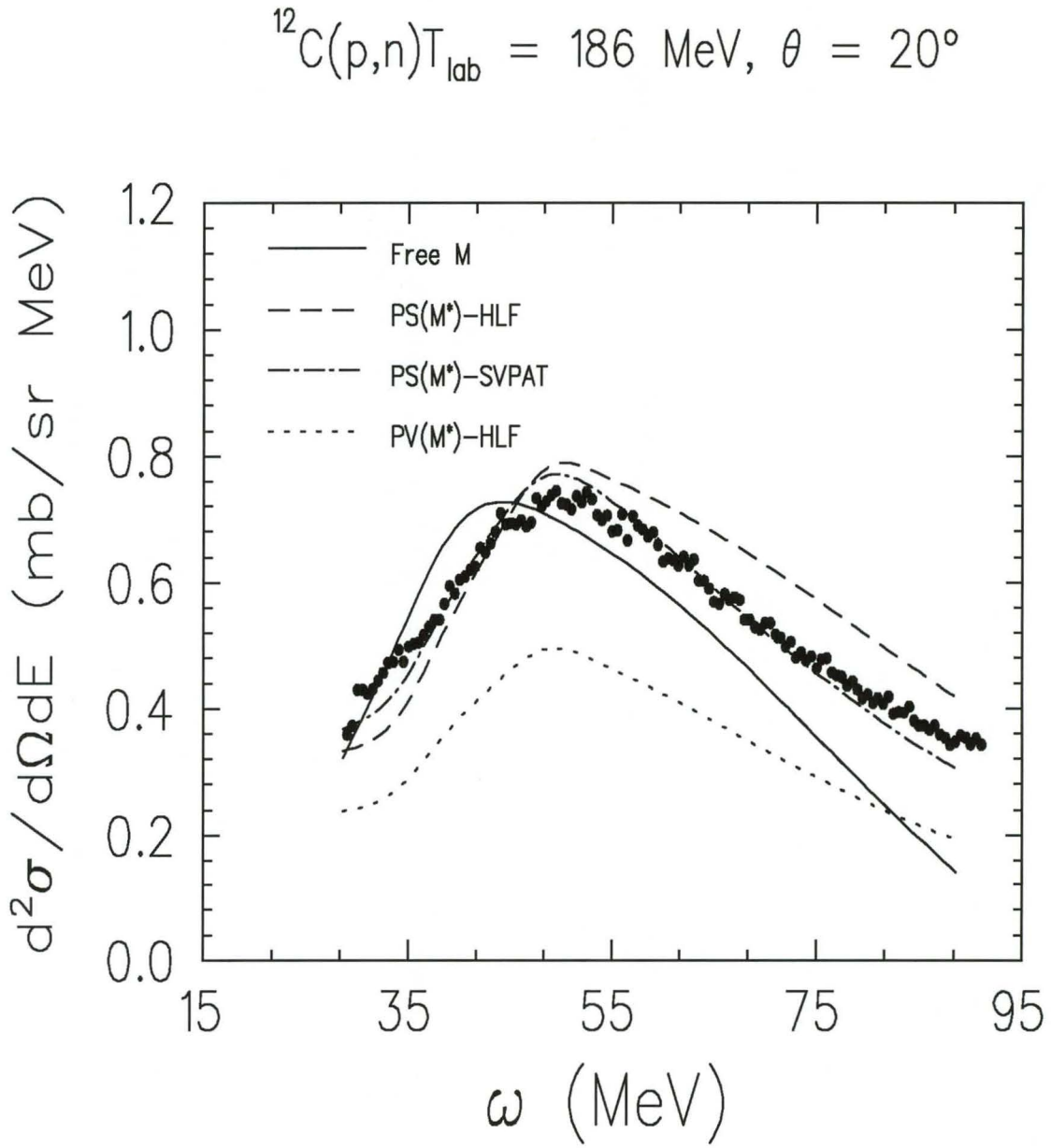

Figure 3.24: Unpolarized double differential cross section as a function of transferred energy ω over the quasielastic peak for $^{12}C(\vec{p},\vec{n})$ at 186 MeV and θ_{lab}=20°. The centroid of the quasielastic peak is at $\omega \approx 50$ MeV. Data are from Ref. [Wa94]. The solid lines indicate free mass (M) calculations [Free M], dotted lines represent effective mass (M^*) PV calculations based on the HLF model [PV(M^*)–HLF], dashed lines display effective mass (M^*) PS calculations based on the HLF–model [PS(M^*)–HLF], and dashed-dotted lines show effective mass (M^*) calculations based on a direct SVPAT parametrization of the Arndt phases [PV(M^*)–SVPAT].

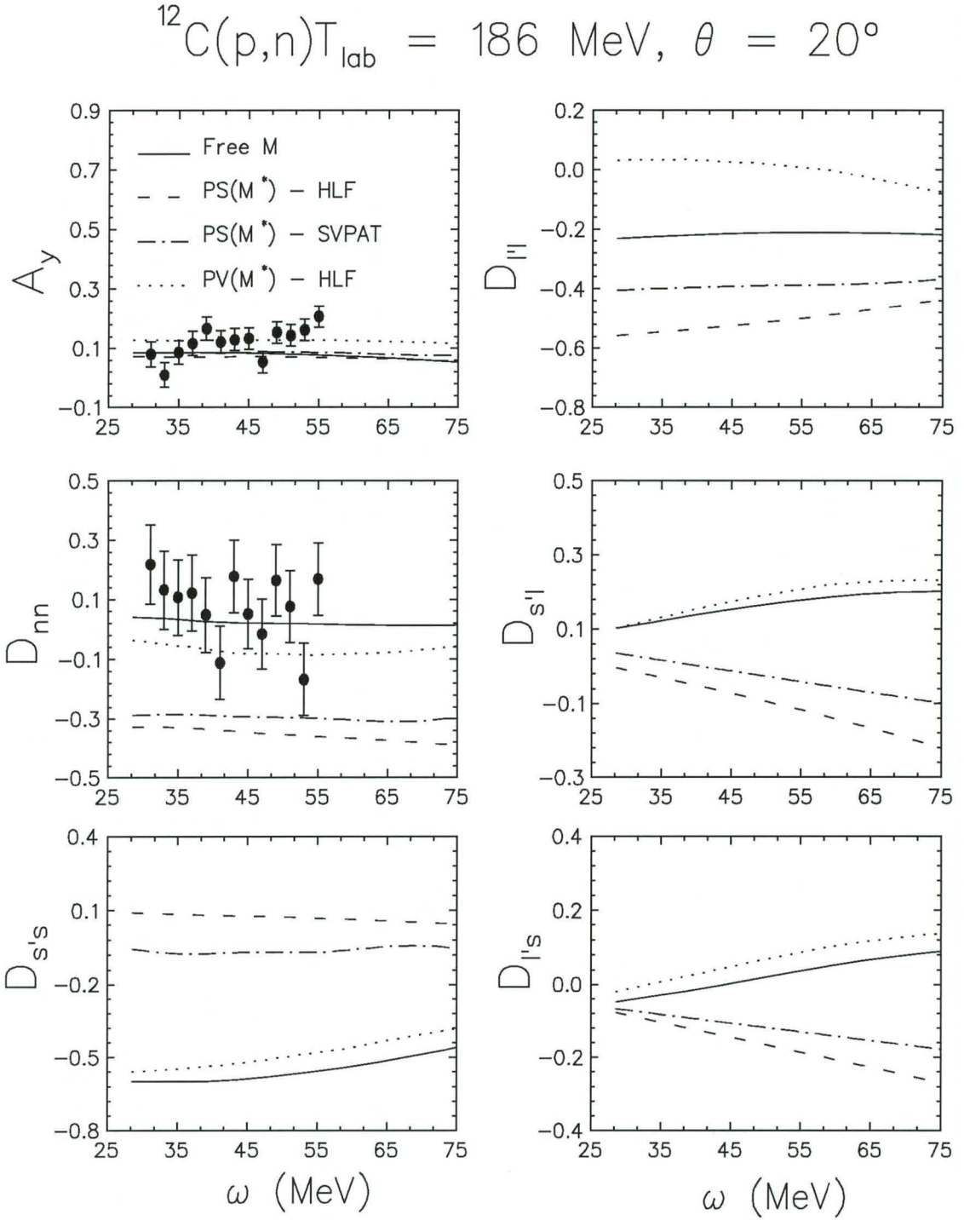

Figure 3.25: Polarization transfer observables as a function of transferred energy ω over the quasielastic peak for $^{12}C(\vec{p},\vec{n})$ at 186 MeV and θ_{lab}=20°. The centroid of the quasielastic peak is at $\omega \approx 50$ MeV. Data are from Ref. [Wa94]. The solid lines indicate free mass (M) calculations [Free M], dotted lines represent effective mass (M^*) PV calculations based on the HLF model [PV(M^*)–HLF], dashed lines display effective mass (M^*) PS calculations based on the HLF–model [PS(M^*)–HLF], and dashed-dotted lines show effective mass (M^*) calculations based on a direct SVPAT parametrization of the Arndt phases [PV(M^*)–SVPAT].

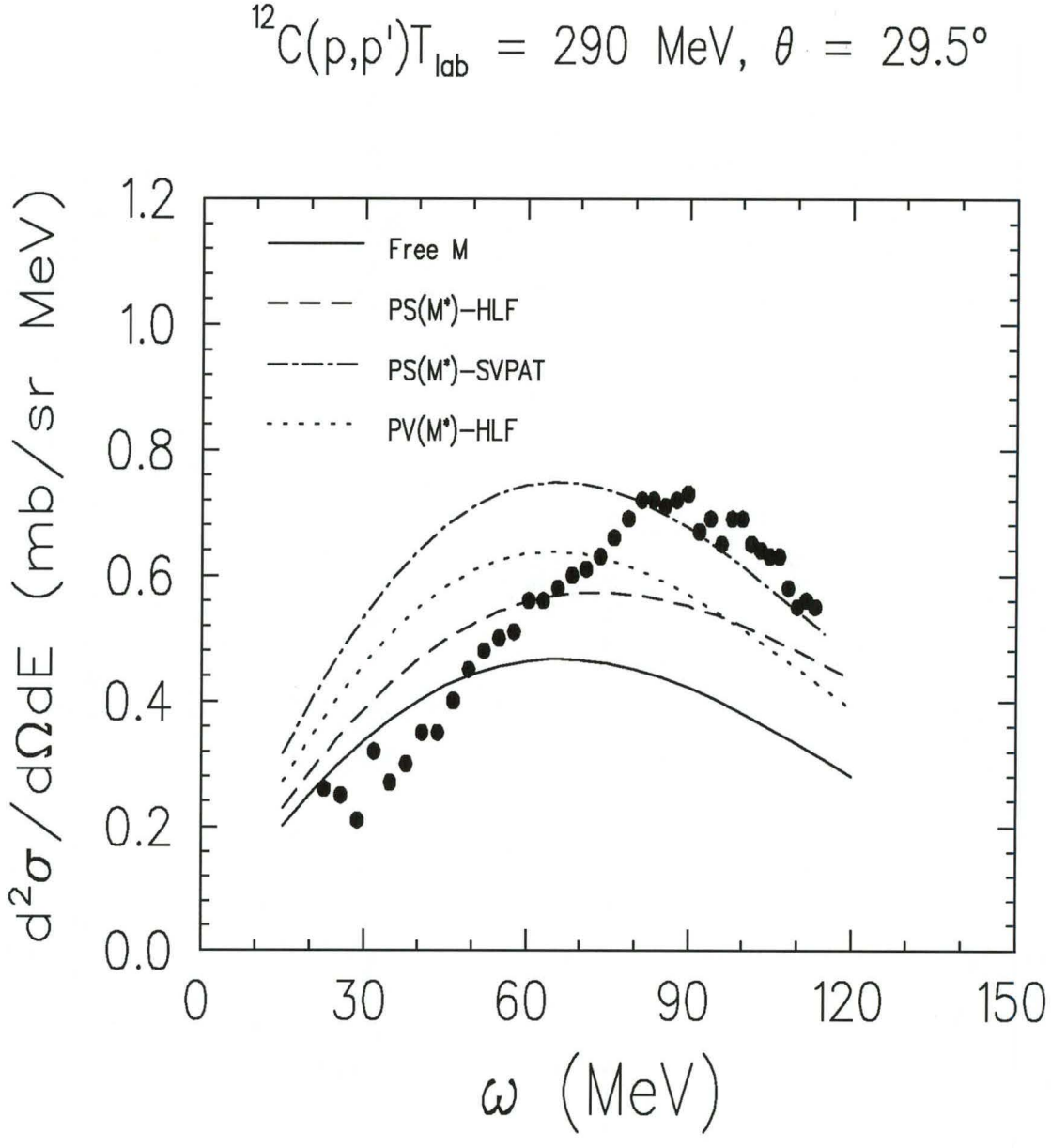

Figure 3.26: Unpolarized double differential cross section as a function of transferred energy ω over the quasielastic peak for $^{12}C(\vec{p},\vec{p}')$ at 290 MeV and θ_{lab}=29.5°. The centroid of the quasielastic peak is at $\omega \approx 80$ MeV. Data are from Ref. [Ch90], where P and A_y refer to induced polarization and analyzing power respectively. The solid lines indicate free mass (M) calculations [Free M], dotted lines represent effective mass (M^*) PV calculations based on the HLF model [PV(M^*)–HLF], dashed lines display effective mass (M^*) PS calculations based on the HLF–model [PS(M^*)–HLF], and dashed-dotted lines show effective mass (M^*) calculations based on a direct SVPAT parametrization of the Arndt phases [PV(M^*)–SVPAT].

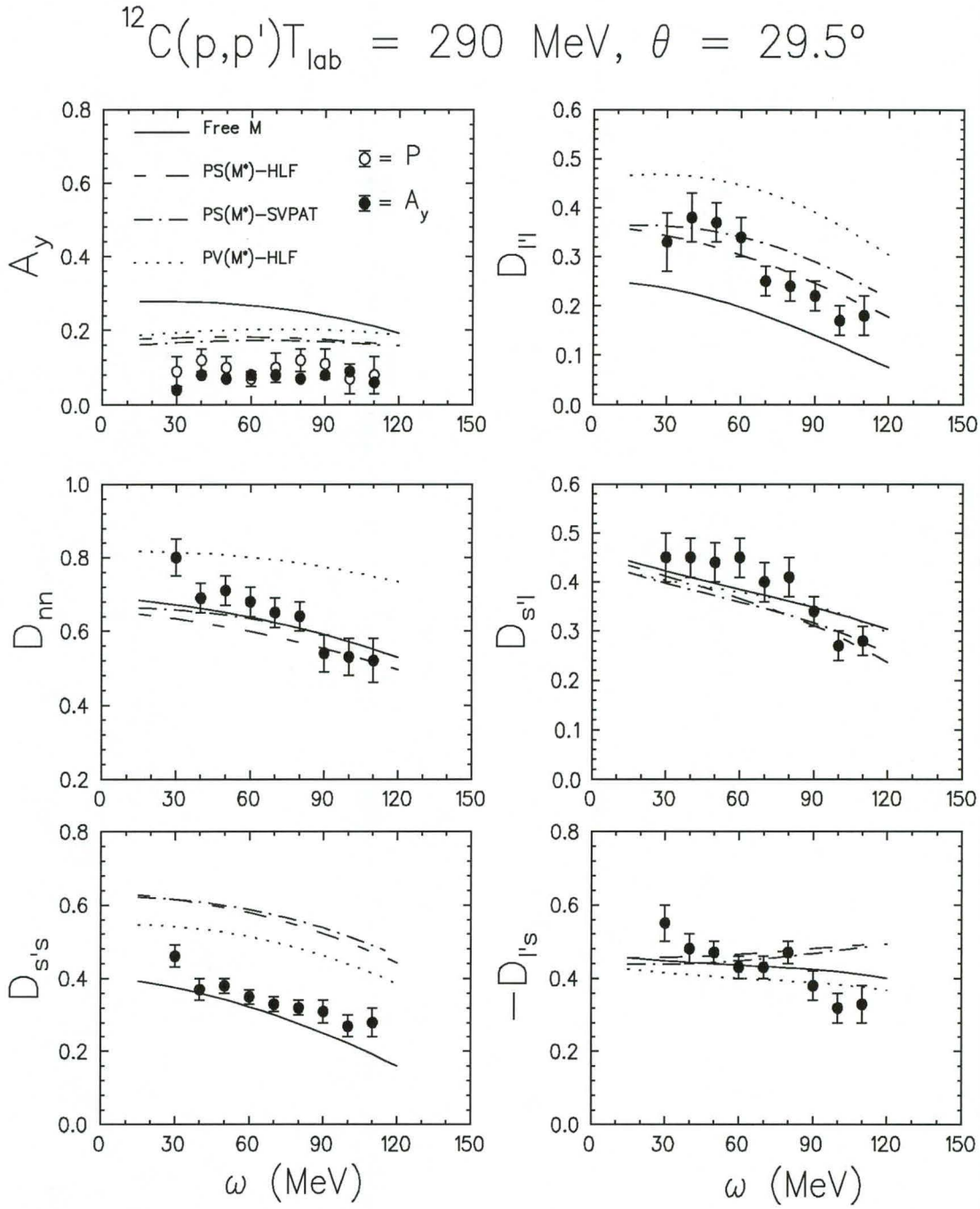

Figure 3.27: Polarization transfer observables as a function of transferred energy ω over the quasielastic peak for $^{12}C(\vec{p},\vec{p}')$ at 290 MeV and θ_{lab}=29.5°. The centroid of the quasielastic peak is at $\omega \approx 80$ MeV. Data are from Ref. [Ch90], where P and A_y refer to induced polarization and analyzing power respectively. The solid lines indicate free mass (M) calculations [Free M], dotted lines represent effective mass (M^*) PV calculations based on the HLF model [PV(M^*)–HLF], dashed lines display effective mass (M^*) PS calculations based on the HLF–model [PS(M^*)–HLF], and dashed-dotted lines show effective mass (M^*) calculations based on a direct SVPAT parametrization of the Arndt phases [PV(M^*)–SVPAT].

of up to 30% in some of the polarization transfer observables. Once again, the quenching of the data relative to the free NN values is evident. With the inclusion of spin–orbit distortions both M^*–based PS and PV calculations reproduce A_y and P at the centroid of the quasielastic peak: recall that the RPWIA model does not distinguish between A_y and P. With the exception of $D_{s's}$, the effective mass PS calculations correspond to the complete data set at the quasielastic peak. This good agreement is rather surprising in view of the above-mentioned limitations of the RPWIA model. Compared to the $^{12}C(\vec{p},\vec{p}')$ $T_{\rm lab} = 290$ MeV data the free mass calculations do much worse and only agree for D_{nn}. Note that the RPWIA fails to reproduce the slopes of D_{nn}, A_y and P. Reference [Ha88] indicates that these slopes are well reproduced by the nonrelativistic RPA slab model. For the other polarization transfer observables the slopes can be attributed to Fermi–motion averaging. It would be interesting to see whether the success of the effective mass PS calculations persists for larger momentum transfers at 290 MeV.

3.5 Summary and conclusions

In recent years considerable attention has been devoted to the measurement and interpretation of inclusive $(\vec{p},\vec{p}')$ and $(\vec{p},\vec{n})$ polarization transfer observables at the quasielastic peak. At moderate momentum transfers ($|\vec{q}| > 0.5$ fm^{-1}) quasielastic scattering (QES) becomes the dominant mechanism for nuclear excitation. It is considered to be a single-step process whereby a projectile knocks out a single bound nucleon in a target nucleus while the remainder of the nucleons remain inert. This process is characterized by a broad bump in the excitation spectrum, the centroid of which nearly corresponds to free NN scattering, and a width resulting from the initial momentum distribution of the struck nucleon. These reactions offer a means to study how the fundamental NN interaction is modified by the surrounding nuclear medium, and to probe the structure of the nucleus by seeing how it responds to large energy–, momentum–, spin– and isospin–transfer.

The failure of all nonrelativistic Schrödinger–based models to describe the quasielastic $(\vec{p},\vec{p}')$ analyzing power at 500 MeV led to the development of the Relativistic (Dirac) Plane Wave Impulse Approximation (RPWIA), where the NN amplitudes are based on the Lorentz–invariant parametrization of the standard five Fermi invariants (the so–called SVPAT form), and the target nucleus is treated as a Fermi–gas. Medium effects are incorporated by replacing free nucleon

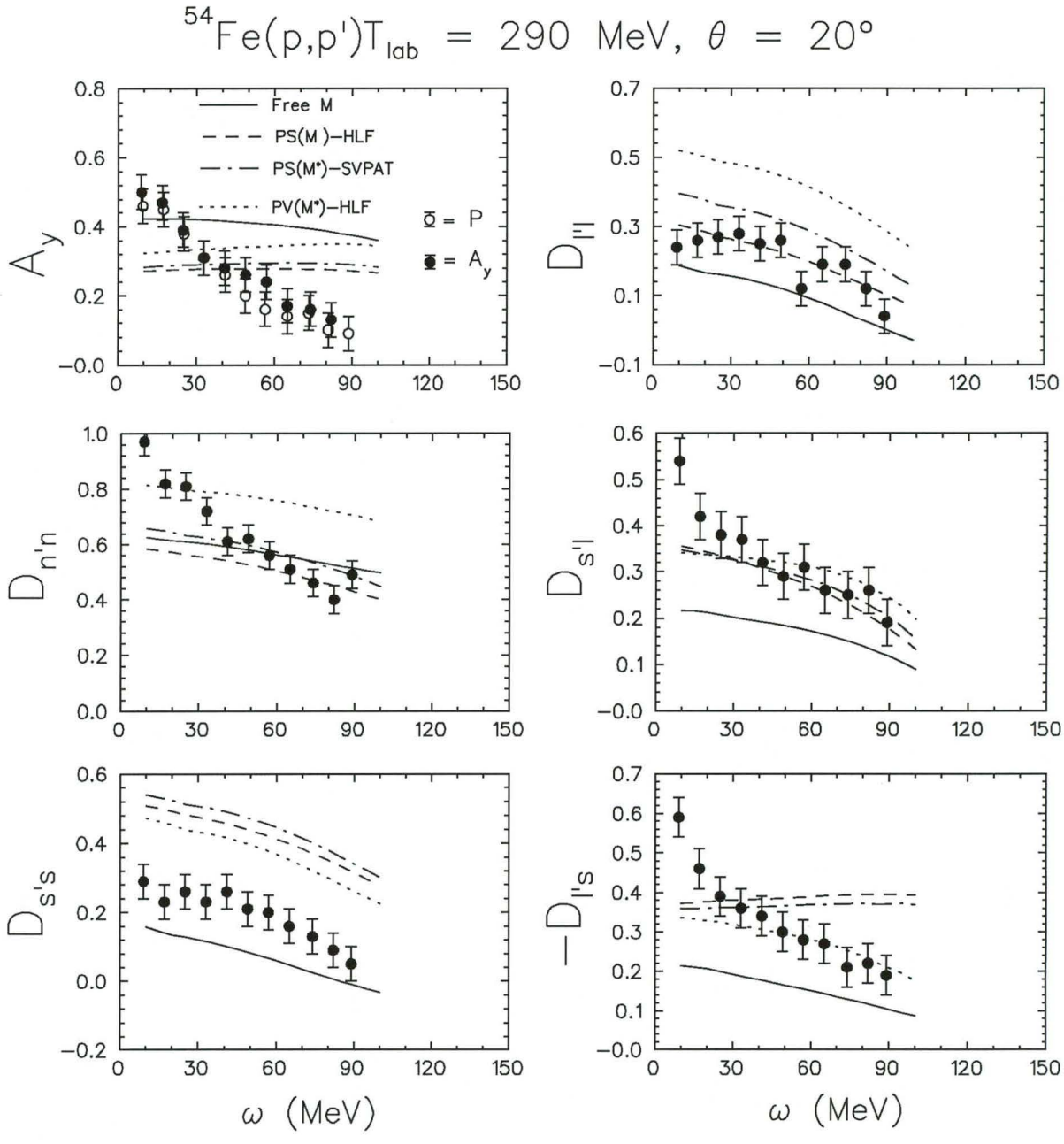

Figure 3.28: Polarization transfer observables for a range of transferred energy ω over the quasielastic peak for ^{54}Fe$(\vec{p},\vec{p}')$ 290 MeV and $\theta_{\rm lab}$=20°. The centroid of the quasielastic peak is at $\omega \approx 40$ MeV. Data are from Ref. [Ha88], where P and A_y refer to induced polarization and analyzing power respectively. The solid lines indicate free mass (M) calculations [Free M], dotted lines represent effective mass (M^*) PV calculations based on the HLF model [PV(M^*)–HLF], dashed lines display effective mass (M^*) PS calculations based on the HLF–model [PS(M^*)–HLF], and dashed-dotted lines show effective mass (M^*) calculations based on a direct SVPAT parametrization of the Arndt phases [PV(M^*)–SVPAT].

masses in the Dirac spinors with effective nucleon masses in the context of relativistic mean field theory.

The original RPWIA predictions [Ho88] gave mixed, but encouraging results. However, these calculations were based on crude assumptions and unrefined effective masses. For example, a 10% uncertainty in effective mass values translates into 30% effects on some polarization transfer observables. Rather than abandon the RPWIA in favour of more sophisticated relativistic models, the approach, in this chapter, has been to critically review the approximations, and to perform more refined calculations of effective masses so as to reveal the limitations of the model.

The much–used SVPAT form is limited in that it does not address the exchange behaviour of the NN amplitudes in the nuclear medium, and is rather crude in distinguishing between pseudoscalar and pseudovector forms of the πNN vertex. Instead, one uses the phenomenological Horowitz–Love–Franey (HLF) model which parametrizes the relativistic SVPAT amplitudes as a sum of Yukawa–like meson exchanges where both direct and exchange diagrams are considered separately. Both projectile and target nucleon effective masses are evaluated in accordance with the circumstances of the specific reaction, and consequently the averaging procedure relies on the proton transmission probability (calculated in the eikonal approximation), relativistic nuclear scalar and vector potentials, as well as relativistic scalar and baryon densities. The scalar fields needed for calculation of the *target* effective nucleon masses, as well as the scalar and baryon densities, are based on a self–consistent Dirac–Hartree formulation. On the other hand, the scalar potentials required for evaluating the *projectile* effective nucleon mass, and in addition the vector potentials needed for calculating effective Dirac–equation–based central and spin–orbit potentials, are obtained by folding components of the HLF t–matrix with the scalar and baryon densities. An attractive feature of this approach is the consistent use of the HLF model for calculating both effective masses and relativistic SVPAT NN scattering amplitudes.

For a ^{40}Ca target at $|\vec{q}\,| = 1.97$ fm^{-1}, and incident energies between 135 and 500 MeV, the sensitivity of complete sets of quasielastic $(\vec{p},\vec{p}\,')$ and $(\vec{p},\vec{n})$ polarization transfer observables (A_y, D_{nn}, $D_{s's}$, $D_{l'l}$, $D_{s'l}$ and $D_{l's}$) is systematically investigated to study medium effects, pseudoscalar versus pseudovector forms of the πNN vertex, exchange contributions to the NN amplitudes, and also spin–orbit distortions.

Although the Fermi motion of the target nucleons necessitates the input of NN amplitudes

over a wide range of effective laboratory kinetic energies $T_{\rm eff}^L$, the small number of published HLF parameters limited the initial investigation in that the Fermi–averaging procedure considered only the HLF parameter set closest to the incident laboratory kinetic energy for all $T_{\rm eff}^L$. Hence, this study was merely *qualitative* and served only to give an initial "feel" for the sensitivities of polarization transfer observables to model parameters. The tendencies displayed in Figs. 3.8 to 3.11 speak for themselves. This study shows that certain $(\vec{p},\vec{p}')$ and $(\vec{p},\vec{n})$ polarization transfer observables are extremely sensitive to the effects of the nuclear medium and pseudoscalar versus pseudovector forms of the πNN vertex. It was also shown that, contrary to former expectations, exchange contributions cannot be neglected over the *entire* 135 to 195 MeV range. Our qualitative investigation highlights the need for a meson–exchange model (such as the HLF model), instead of the usual SVPAT parametrization of the relativistic NN amplitudes, when studying the effects of the nuclear medium and different forms of the πNN vertex. The results of this investigation have been published in Refs. [Hi94, Hi95, Hi97, Hi98].

Although the qualitative investigation emphasized the value of certain polarization transfer observables in studying nuclear medium effects, it failed to give an indication of the expected statistical uncertainty required by experiments for distinguishing between the various model predictions. Furthermore, the lack HLF parameter sets between 80 and 500 MeV prevented such a *quantitative* study. Hence, to perform a quantitative investigation, it was necessary to generate new HLF parameters between 80 and 195 MeV in 5–MeV intervals, and also utilize the recent energy–dependent parametrization of Maxwell between 200 and 500 MeV.

Regarding pseudoscalar versus pseudovector forms of the πNN vertex, it was shown that most of the $(\vec{p},\vec{n})$ polarization transfer observables completely overshadow the corresponding $(\vec{p},\vec{p}')$ observables, whereas D_{nn} exhibits extreme sensitivity for both reactions. Measurements of D_{nn} for both $(\vec{p},\vec{n})$ and $(\vec{p},\vec{p}')$ scattering, particularly at low energies, would be extremely useful in shedding light on the preferred form of the πNN vertex. Medium effects are extremely sensitive to the type of πNN vertex: for a pseudoscalar πNN vertex, the $(\vec{p},\vec{n})$ polarization transfer observables D_{nn}, $D_{s'\ell}$ and $D_{\ell' s}$ are much more sensitive to medium effects, whereas the opposite occurs for a pseudovector pion coupling. It was emphasized that most observables exhibit maximum sensitivity to medium effects at energies lower than 200 MeV. With respect to exchange contributions, it was shown that some $(\vec{p},\vec{p}')$ and $(\vec{p},\vec{n})$ polarization transfer observables are extremely sensitive to these effects, even at higher energies.

The effect of spin–orbit distortions on polarization transfer observables was also considered at the centroid of the quasielastic peak. The inclusion of spin–orbit distortions leads to a space rotation of both initial and final state spinors. Averaging this effect over the whole nucleus leads to a net rotation along an axis perpendicular to the scattering plane which directly affects the polarization transfer observables. Spin–orbit distortions become more important as the incident energy is lowered and the nuclear mass is increased. These effects are comparable to the nuclear medium effects under investigation, and hence must be included when eventually comparing RPWIA calculations to data.

As with the original RPWIA calculations [Ho88], comparison with the small amount of available data still gives mixed, but encouraging results. The $(\vec{p},\vec{p}')$ data favour a pseudoscalar coupling for the pion, whereas the limited $(\vec{p},\vec{n})$ spin observable data suggest a pseudovector form. The latter ambiguity can perhaps be attributed to the simple Born approximation embodied by the phenomenological HLF model. Hence calculations based on more sophisticated models of the NN interaction would be useful.

The so–called relativistic signature for quasielastic $(\vec{p},\vec{p}')$ scattering at 500 MeV, which manifests itself as a reduction of the data compared to free–mass predictions, still persists at 290 MeV for protons scattering from ^{12}C and ^{54}Fe nuclei. To date all nonrelativistic models fail to predict this quenching effect. Note, however, that this so–called "relativistic signature" is much smaller than medium–effects predicted for other polarization transfer observables at lower energies. For $^{12}\mathrm{C}(\vec{p},\vec{n})$ scattering a sizeable medium effect is predicted for A_y at $|\vec{q}\,| \approx 1.97$ fm^{-1}. However at $|\vec{q}\,| \approx 1.1$ fm^{-1} our calculations show no sensitivity to medium effects as is confirmed by the limited IUCF data set [Wa94]. Therefore, it would be interesting to measure A_y for a range of angles on a ^{12}C target.

For both $(\vec{p},\vec{p}')$ and $(\vec{p},\vec{n})$ scattering the number of observables that exhibit maximum sensitivity to the above–mentioned effects, increase as the incident beam energy is lowered. In general, there is a lack of complete sets of polarization data for quasielastic $(\vec{p},\vec{p}')$ and $(\vec{p},\vec{n})$ scattering at medium energies. In particular, at energies lower than 200 MeV there exists absolutely no complete data set. Ideally one should measure the complete sets of polarization transfer observables for both the complementary $(\vec{p},\vec{p}')$ and $(\vec{p},\vec{n})$ reactions for the same target, energy– and momentum–transfer. At these low energies the quasielastic bump in the $(\vec{p},\vec{p}')$

excitation spectrum is less prominent and can only be seen for scattering from targets lighter than ^{40}Ca (see Chapter 2). On the other hand, for $(\vec{p},\vec{n})$ scattering, despite the fact that the unpolarized double differential cross section is approximately a factor 2 smaller than the corresponding $(\vec{p},\vec{p}')$ cross section, the quasielastic peak is fairly prominent (in terms of signal–to–background ratio) as evidenced by the IUCF data at 186 MeV [Wa94]. Hence, it would be interesting to measure complete sets of quasielastic $(\vec{p},\vec{n})$ polarization transfer observables at energies lower than 200 MeV. However, the data are so scarce that measurements of any individual polarization transfer observable for a range of targets, for example ^{2}H, ^{12}C, ^{16}O, ^{40}Ca, at low energies will also provide invaluable guidance in developing and refining theoretical models of quasielastic scattering.

Although the RPWIA seems to accurately describe the gross features of the quasielastic peak for $(\vec{p},\vec{n})$, it fails to predict the $(\vec{p},\vec{p}')$ peak position in the excitation spectrum. A number of effects, which have been neglected, could remedy the situation. For example, multiple scattering effects become sizeable in heavy nuclei and large scattering angles, which greatly increase the width of the peak [Ho88]. Furthermore, although signatures of low–lying collective states and giant resonances disappear at the large excitation energies of interest, the nucleus continues to respond collectively through the residual particle–hole interaction. This collectivity manifests itself in gross features of the spectrum, such as shifts in the position of the quasielastic peak and deviations of polarization transfer observables from the free values [Sm88]. Hence, one can improve the simple Fermi–gas treatment of the nucleus by considering a relativistic random–phase approximation to infinite nuclear matter as done by Horowitz and Piekarewicz [Ho94]. Essentially this description takes into account the interactions between the nucleons in the medium at the mean–field level. Furthermore, nonrelativistic Schrödinger–based DWIA calculations suggest that distortion effects appreciably affect the shape and position of the quasielastic peak [Ic89]. As a result, Horowitz and Piekarewicz suggest that the inclusion of distortions via a full relativistic distorted wave treatment may yield a good description of the polarization transfer observable data. The effect of distortions will be considered in Chapter 4.

Finally, it would be interesting to extend the quantitative RPWIA investigation to 500 MeV and to compare predictions to the 500 MeV $(\vec{p},\vec{p}')$ Los Alamos data [Ca84, Re86], where the effects of distortions on the polarization transfer observables are expected to be small (compared to distortion effects at lower energies). This would require additional HLF parameters between

500 and 800 MeV due to the effective laboratory kinetic energies used in the Fermi–averaging procedure.

Chapter 4

Relativistic distorted wave model

4.1 Introduction

In the previous chapter, it was concluded that the relativistic plane wave impulse approximation (RPWIA) does not provide a consistent description of *both* $(\vec{p},\vec{p}')$ and $(\vec{p},\vec{n})$ polarization transfer observables at the quasielastic peak: the $(\vec{p},\vec{p}')$ data favour a pseudoscalar coupling for the pion, whereas the $(\vec{p},\vec{n})$ data suggest a pseudovector form.

It has been suggested [Ho94, Ho97, Hi98] that the latter inconsistency could be attributed to the use of the five SVPAT invariants, rather than a more appropriate general Lorentz–invariant representation [Tj85, Tj87] of the NN amplitudes. Although the SVPAT approximation has worked surprisingly well for relativistic descriptions of elastic scattering [Mu87a, Mu87b] and proton–knockout reactions [Ik95], the RPWIA analysis in Chapter 3 suggests that this approach may be too simplistic for inclusive quasielastic reactions. The Ph.D project of Brandon van der Ventel (currently in progress at the University of Stellenbosch) addresses the latter issue.

It has also been suggested [Ho94, Ho97, Hi98] that the explicit inclusion of full relativistic distortions in the incident and exit channels could remedy the above–mentioned inconsistency. Until now, the effects of relativistic distortions have been treated poorly. In the RPWIA, for example, distortion effects are incorporated via effective nucleon masses due to medium modifications of the NN interaction, and also via effective numbers of protons and neutrons, $Z_{\rm eff}$ and $N_{\rm eff}$ respectively, partaking in the scattering process. The effect of the latter distortions is to reduce the value of double differential cross sections relative to their plane–wave values. However, for polarization transfer observables, which are effectively ratios of linear combinations of polarized double differential cross sections, the distortions cancel (see Sec 3.2.7 in Chapter 3), thus enhancing sensitivity to nuclear medium–modifications of the NN amplitudes. In principle,

however, one knows that, besides modifying the NN interaction, the effect of the nuclear medium is also to distort the incoming and outgoing plane waves. These distortions could have large effects on certain polarization transfer observables. For example, Ichimura and collaborators, have shown that, based on the nonrelativistic distorted wave impulse approximation, distortions significantly influence the polarization transfer observables for inclusive $(\vec{p},\vec{p}')$ scattering at 500 MeV [Ic94].

To our knowledge, no relativistic distorted wave calculations have ever been done for inclusive proton–nucleus inelastic scattering. The aim of this chapter, therefore, is to develop the theoretical framework for calculating complete sets of quasielastic proton–nucleus polarization transfer observables based on the **R**elativistic **D**istorted **W**ave **I**mpulse **A**pproximation (**RDWIA**). In Sec. 4.4, it will be shown that, for the RDWIA model, all the inclusive scattering observables of interest can be expressed in terms of the contraction of a projectile distorted nucleon tensor with a spin–independent nuclear polarization tensor for the target nucleus. The projectile distorted nucleon tensor, defined in Sec. 4.4, contains information about the spin projections and full relativistic distortions of the projectile and ejectile scattering wave functions (also called distorted wave functions). Partial wave analyses of the relativistic distorted wave functions are discussed in detail in Sec. 4.3. Compared to the RPWIA model (discussed in Chapter 3), whereby relativistic effects are included via effective nucleon masses in the free Dirac spinors, the RDWIA implicitly incorporates relativistic effects via the Dirac scattering wave functions which are solutions to the Dirac equation containing relativistic potentials. The spin–independent nuclear polarization tensor, on the other hand, which contains information about the nuclear response, can be evaluated to any level of sophistication, depending on the choice of model for the target nucleus. For simplicity, only the following three models are considered for describing the target nucleus: relativistic Fermi–gas model, relativistic mean–field approximation, and the local density approximation.

For the formulation of the RDWIA model, the normalization procedure of Serot and Walecka [Se86] is adopted for the Dirac wave functions (see also Sec. E.6 in Appendix E), instead of the Bjorken and Drell normalization [Bj64, Gr92] employed in Chapter 3 for the RPWIA. The concepts of nuclear response functions and nuclear polarization tensors are now introduced in the following section.

4.2 Nuclear response functions

One can extract information about physical systems via the analysis (both theoretical and experimental) of their response to a diversity of external probes [Fe71, Gr91]. The aim of this section is to develop the theoretical framework for calculating the nuclear response for inclusive quasielastic proton–nucleus scattering, for a variety of models of the target nucleus. In Sec. 4.2.3, the concept of a nuclear response function is introduced via a generalization of the simpler electromagnetic response for inclusive electron–nucleus scattering (discussed in Sec. 4.2.1). Although a general framework is developed for calculating nuclear response functions to any level of sophistication, for the purpose of this project, only the following three models of the nuclear response are considered: the relativistic free Fermi–gas model (FGM), relativistic mean–field approximation (MFA), and the local density approximation (LDA). The FGM and MFA have already been encountered in Chapter 3, but not within the context of nuclear response functions discussed in this chapter. The LDA, on the other hand, represents an improvement over the FGM and MFA.

In order to fully understand the complicated structure of the nuclear response, one starts by considering the simpler electromagnetic response of the nucleus. The discussion of electron scattering from nucleons and nuclei, in the next section, is considerably more detailed than would seem warranted, however, this detail is supplied so as to provide a familiar context for the treatment of inclusive nuclear proton–nucleus inelastic scattering in Sec. 4.4.

4.2.1 Electromagnetic response of a nucleus

In this section, the concept of the electromagnetic response of a *nucleus* is introduced, via a generalization of the proton electromagnetic response for electron–proton scattering. It is convenient to start by defining the invariant scattering amplitude for electron–proton scattering as (see Appendix E)

$$M_{fi} = e^2[\bar{u}(p_f, s_f)\gamma_\nu u(p_i, s_i)\frac{1}{(q)^2 + i\epsilon}\bar{u}(P_f, S_f)\gamma^\nu u(P_i, S_i) \tag{4.1}$$

where the four–momentum q is defined as

$$q = p_i - p_f = P_f - P_i = (\omega, \vec{q}\,), \tag{4.2}$$

and, $p_i = (\epsilon_i, \vec{p}_i)$, $p_f = (\epsilon_f, \vec{p}_f)$ [$P_i = (E_i, \vec{P}_i)$, $P_f = (E_f, \vec{P}_f)$] are the initial and final electron [proton] four–momenta, respectively. The free Dirac spinor for the incident electron $u(p_i, s_i)$, for example, is given by

$$u(\vec{p}, s) = \sqrt{\frac{\epsilon_i + m}{2\epsilon_i}} \begin{pmatrix} I \\ \\ \dfrac{\boldsymbol{\sigma} \cdot \vec{p}}{\epsilon_i + m} \end{pmatrix} \chi_s \tag{4.3}$$

with normalization (see Sec. E.6 of Appendix E)

$$u^\dagger u \;=\; 1\,, \tag{4.4}$$

where χ_s is the Pauli spinor for spin projection s in the rest frame of the electron. An expression similar to Eq. (4.3) exists for the proton. Note that the normalization in Eq. (4.4) differs from the conventional normalization of Bjorken and Drell [Bj64], $\bar{u}\,u \;=\; 1$, adopted in Chapter 3.

The definition of M_{fi} in Eq. (4.1) is virtually identical to Eq. (E.58) in Appendix E, with the exception that the exchange term in the latter equation is ignored (electrons and protons are not identical particles), and the dummy index ν is used instead of μ.

Adopting the normalization in Eq. (4.4), and following a procedure similar to that presented in Sec. E.5 of Appendix E, the unpolarized (indicated by a bar over the sigma below) differential cross section for electron–proton scattering in the plane–wave Born approximation is given by

$$d\bar{\sigma} \;=\; \frac{1}{v_{\rm rel}} \frac{4\alpha^2}{(q^2)^2}\, L_{\mu\nu}\, S^{\mu\nu}\, \delta(\epsilon_f + E_f - \epsilon_i - E_i)\, d\vec{p}_f \tag{4.5}$$

where the electron electromagnetic tensor $L_{\mu\nu}$ is defined by

$$L_{\mu\nu} \;=\; \frac{1}{2} \sum_{s_f, s_i} [\,\bar{u}(p_f, s_f)\gamma_\nu u(p_i, s_i)\,]\,[\,\bar{u}(p_f, s_f)\gamma_\mu u(p_i, s_i)\,]^* \tag{4.6}$$

$$\;=\; \frac{1}{2} \sum_{s_f, s_i} [\,\bar{u}(p_i, s_i)\gamma_\mu u(p_f, s_f)\,]\,[\,\bar{u}(p_f, s_f)\gamma_\nu u(p_i, s_i)\,] \tag{4.7}$$

and $v_{\rm rel}$ is the magnitude of the velocity of the incident electron relative to the target proton. In going from Eq. (4.6) to Eq. (4.7), Eq. (E.64) in Appendix E has been used. Similarly, the corresponding proton electromagnetic tensor $S_{\mu\nu}$ is defined by

$$S^{\mu\nu} \;=\; \frac{1}{2} \sum_{S_f, S_i} [\,\bar{u}(P_f, S_f)\gamma^\nu u(P_i, S_i)\,]\,[\,\bar{u}(P_f, S_f)\gamma^\mu u(P_i, S_i)\,]^* \tag{4.8}$$

$$\;=\; \frac{1}{2} \sum_{S_f, S_i} [\,\bar{u}(P_i, S_i)\gamma^\mu u(P_f, S_f)\,]\,[\,\bar{u}(P_f, S_f)\gamma^\nu u(P_i, S_i)\,]\,. \tag{4.9}$$

Eqs. (4.7) and (4.9) are readily evaluated via application of the usual well–known trace techniques described in Sec. E.5.1 of Appendix E.

For an electron scattering from a *nucleus* (as opposed to scattering from a single proton, as just discussed), the unpolarized differential cross section is obtained via a generalization of Eqs. (4.5) to (4.9), giving [Ai83, We93, Pi95]

$$d\bar{\sigma} \;=\; \frac{1}{v_{\rm rel}}\frac{4\alpha^2}{(q^2)^2}L_{\mu\nu}W^{\mu\nu}d\vec{p}_f \tag{4.10}$$

where $L_{\mu\nu}$ is the electron tensor already defined by Eq. (4.7), and $W^{\mu\nu}$ is the electromagnetic response of the nucleus defined by

$$W^{\mu\nu} \;=\; -\frac{1}{\pi}\,{\rm Im}\,[\,\Pi^{\mu\nu}(\vec{q},\vec{q}\,;\omega)\,] \tag{4.11}$$

where

$$\Pi^{\mu\nu}(\vec{q},\vec{q}\,';\omega) \;=\; \int d\vec{x}\; e^{-i\vec{q}\cdot\vec{x}} \int d\vec{y}\; e^{+i\vec{q}\,'\cdot\vec{y}}\;\Pi^{\mu\nu}(\vec{x},\vec{y},\omega)\;, \tag{4.12}$$

and the full interacting electromagnetic polarization tensor $\Pi^{\mu\nu}(\vec{x},\vec{y};\omega)$ (also called the current–current correlation function) is defined by [Fe71, Ne88, Gr91, We93, Pi95]

$$\Pi^{\mu\nu}(x,y) \;=\; \frac{1}{i} < \psi_i|\, T[\,\hat{\bar{\psi}}(x)\Gamma^\mu\hat{\psi}(x)\;\hat{\bar{\psi}}(y)\Gamma^\nu\hat{\psi}(y)\,]\,|\psi_i> \;. \tag{4.13}$$

T denotes the usual time–ordered product, $\hat{\psi}_\alpha(x)$ and $\hat{\bar{\psi}}_\alpha(y)$ represent the Heisenberg fields (for which explicit expressions will be given at a later stage for different models of the nucleus), $|\psi_i>$ represents the initial interacting ground state of the target in the Heisenberg picture, and for simplicity the electromagnetic interaction vertex Γ^μ is taken to be [Gr92]

$$\Gamma^\mu \;=\; \gamma^\mu\;. \tag{4.14}$$

[Note that for an electron scattering from a *pointlike* proton, the electromagnetic interaction vertex Γ^μ is given by Eq. (4.14).] It is convenient to express the full interacting polarization tensor, in Eq. (4.13), in terms of the full interacting nucleon propagator (or Green's function) $G_{\alpha\beta}(x,y)$, defined as

$$\begin{aligned} iG_{\alpha\beta}(x,y) \;&=\; <\Psi_i|\,T[\hat{\psi}_\alpha(x)\hat{\bar{\psi}}_\beta(y)]\,|\Psi_i> \\ &=\; \theta(x_0-y_0)\;<\Psi_i|\,\hat{\psi}_\alpha(x)\hat{\bar{\psi}}_\beta(y)\,|\Psi_i> \\ &\quad -\,\theta(y_0-x_0)\;<\Psi_i|\,\hat{\psi}_\beta(y)\hat{\bar{\psi}}_\alpha(x)\,|\Psi_i>\,, \end{aligned} \tag{4.15}$$

such that one can make use of well–known many–body techniques, such as the Feynman rules [Se86], to express the interacting propagators in order–by–order expansions of the coupling constants and the free noninteracting nucleon propagators $G^0_{\alpha\beta}(x,y)$ defined in Sec. 4.2.2. In Sec. 4.2.2, different models for the interacting nucleon propagator $G_{\alpha\beta}(x,y)$ will be considered.

Applying Wick's theorem [Fe71, Gr91, Gr96] to Eq. (4.13), one can express the polarization tensor in terms of the interacting nucleon propagator [defined in Eq. (4.15)] as

$$\begin{aligned} i\Pi^{\mu\nu}(x,y) &= \sum_{\alpha,\beta,\delta,\epsilon=1}^{4} < \Psi_i|\, T[\hat{\bar{\psi}}_\alpha(x)\, \gamma^\mu_{\alpha\beta}\, \hat{\psi}_\beta(x)\, \hat{\bar{\psi}}_\delta(y)\, \gamma^\nu_{\delta\epsilon}\, \hat{\psi}_\epsilon(y)\,]\, |\Psi_i> \\ &= \sum_{\alpha,\beta,\delta,\epsilon=1}^{4} [\, i\, G_{\beta\delta}(x,y)\,]\, [-i\, G_{\epsilon\alpha}(y,x)\,]\, \gamma^\mu_{\alpha\beta}\, \gamma^\nu_{\delta\epsilon} \\ &= \sum_{\alpha,\beta,\delta,\epsilon=1}^{4} G_{\epsilon\alpha}(y,x)\, \gamma^\mu_{\alpha\beta}\, G_{\beta\delta}(x,y)\, \gamma^\nu_{\delta\epsilon} \\ &= \mathrm{Tr}\,[\, G(y,x)\, \gamma^\mu\, G(x,y)\gamma^\nu\,]\,. \end{aligned} \tag{4.16}$$

Comparing Eqs. (4.5) and (4.10), one sees that the differential cross section for electron–nucleus scattering can be obtained via a generalization of Eq. (4.5) for electron–proton scattering, by means of the following replacement:

$$S^{\mu\nu}\delta(\epsilon_f + E_f - \epsilon_i - E_i) \longrightarrow W^{\mu\nu}\,. \tag{4.17}$$

To show that this is a suitable generalization, one starts by expressing the electromagnetic response of the nucleus $W^{\mu\nu}$ in terms of the matrix elements of nuclear many–body current operators in momentum space. Assuming translational invariance in time, the momentum–space representation of Eq. (4.13) is given by [We93]

$$\Pi^{\mu\nu}(\vec{q},\vec{q}\,';\omega) = \int d\,(x_0 - y_0)\, e^{i\omega}(x_0 - y_0) \int d\,\vec{x}\; e^{-i\vec{q}\cdot\vec{x}} \int d\,\vec{y}\,'\; e^{+i\vec{q}\,'\cdot\vec{y}}\, \Pi^{\mu\nu}(x,y)\,. \tag{4.18}$$

From the usual definition of a time–ordered product, and using Eq. (4.14), Eq. (4.13) is expressed as

$$\begin{aligned} i\Pi^{\mu\nu}(x,y) &= < \psi_i|\, T[\hat{\bar{\psi}}(x)\gamma^\mu\hat{\psi}(x)\, \hat{\bar{\psi}}(y)\gamma^\nu\hat{\psi}(y)\,]\, |\psi_i> \\ &= \theta(x_0 - y_0) < \psi_i|\, \bar{\psi}(x)\gamma^\mu\hat{\psi}(x)\, \hat{\bar{\psi}}(y)\gamma^\nu\hat{\psi}(y)\, |\psi_i> \\ &\quad - \theta(y_0 - x_0) < \psi_i|\, \hat{\bar{\psi}}(y)\gamma^\nu\hat{\psi}(y)\, \bar{\psi}(x)\gamma^\mu\hat{\psi}(x)\, |\psi_i> \\ &= \theta(x_0 - y_0) < \psi_i|\, \hat{J}^\mu_H(x)\, \hat{J}^\nu_H(y)\, |\psi_i> \\ &\quad - \theta(y_0 - x_0) < \psi_i|\, \hat{J}^\nu_H(y)\, \hat{J}^\mu_H(x)\, |\psi_i> \end{aligned} \tag{4.19}$$

where the nuclear current operator $\hat{J}^{\mu}_{H}(x)$ is defined as

$$\hat{J}^{\mu}_{H}(x) \;=\; \bar{\psi}(x)\gamma^{\mu}\hat{\psi}(x)\;, \tag{4.20}$$

and, the subscript "H" refers to the Heisenberg picture. The explicit time–dependence of the Heisenberg current operators is given by [Fe71, Gr96]

$$\begin{aligned} \hat{J}^{\mu}_{H}(x) \;= \hat{J}^{\mu}_{H}(\vec{x},x_0) \;&= e^{i\hat{H}x_0}\,\hat{J}^{\mu}_{H}(\vec{x},0)e^{-i\hat{H}x_0} \\ &= e^{i\hat{H}x_0}\,\hat{J}^{\mu}_{H}(\vec{x})e^{-i\hat{H}x_0} \end{aligned} \tag{4.21}$$

where $\hat{H}$ denotes the full interaction Hamilton operator. Inserting a complete set of Heisenberg eigenstates $|\psi_n>$, of the full Hamilton operator, between the current operators in Eq. (4.19), and using Eq. (4.21), gives

$$\begin{aligned} i\Pi^{\mu\nu}(x,y) \;=\; & \sum_n [\theta(x_0-y_0) < \psi_i|e^{i\hat{H}x_0}\;\hat{J}^{\mu}_{H}(\vec{x})\;e^{-i\hat{H}x_0}|\psi_n >< \psi_n|e^{i\hat{H}y_0}\;\hat{J}^{\nu}_{H}(\vec{y})\;e^{-i\hat{H}y_0}|\psi_i > \\ & - \theta(y_0-x_0) < \psi_i|e^{i\hat{H}y_0}\;\hat{J}^{\nu}_{H}(\vec{y})\;e^{-i\hat{H}y_0}|\psi_n >< \psi_n|e^{i\hat{H}x_0}\;\hat{J}^{\mu}_{H}(\vec{x})\;e^{-i\hat{H}x_0}|\psi_i >] \\ =\; & \sum_n [\theta(x_0-y_0)e^{-i(E_n-E_i)(x_0-y_0)} < \psi_i|\;\hat{J}^{\mu}_{H}(\vec{x})\;|\psi_n >< \psi_n|\;\hat{J}^{\nu}_{H}(\vec{y})\;|\psi_i > \\ & - \theta(y_0-x_0)e^{i(E_n-E_i)(x_0-y_0)} < \psi_i|\;\hat{J}^{\nu}_{H}(\vec{y})\;|\psi_n >< \psi_n|\;\hat{J}^{\mu}_{H}(\vec{x})\;|\psi_i >]\;. \end{aligned} \tag{4.22}$$

Inserting Eq. (4.22) into Eq. (4.18), and using the following identity [Fe71, Ne88]

$$\int_{-\infty}^{\infty} d\,x_0\; e^{i(\omega\,-\,\epsilon_\alpha)t}\;\theta(\pm x_0) \;=\; \pm\,\frac{i}{\omega\mp\epsilon_\alpha\pm i\eta} \tag{4.23}$$

gives

$$\begin{aligned} \Pi^{\mu\nu}(\vec{q},\vec{q}\,';\omega) \;=\; & \frac{1}{i}\sum_n \int d\,\vec{x}\; e^{-i\vec{q}\cdot\vec{x}} \int d\,\vec{y}\; e^{i\vec{q}\,'\cdot\vec{y}} \\ & \times [\frac{+i}{\omega-(E_n-E_0)+i\eta} < \psi_i|\;\hat{J}^{\mu}_{H}(\vec{x})\;|\psi_n >< \psi_n|\;\hat{J}^{\nu}_{H}(\vec{x})\;|\psi_i > \\ & - \frac{i}{\omega+(E_n-E_0)-i\eta} < \psi_i|\;\hat{J}^{\nu}_{H}(\vec{y})\;|\psi_n >< \psi_n|\;\hat{J}^{\mu}_{H}(\vec{y})\;|\psi_i >] \end{aligned} \tag{4.24}$$

and, with $\vec{q}\,' = \vec{q}$, one gets

$$\Pi^{\mu\nu}(\vec{q},\vec{q};\omega) \;=\; \sum_n \{\; \frac{[\,J^{\mu}_{ni}(\vec{q}\,)]^*\;J^{\nu}_{ni}(\vec{q}\,)}{\omega-(E_n+E_0)+i\eta} \;-\; \frac{[\,J^{\nu}_{ni}(-\vec{q}\,)]^*\;J^{\mu}_{ni}(-\vec{q}\,)}{\omega+(E_n+E_0)-i\eta}\;\} \tag{4.25}$$

where

$$J^{\nu}_{ni}(\vec{q}\,) \;=\; \int d\,\vec{x}\; e^{i\vec{q}\cdot\vec{x}} < \psi_n|\;\hat{J}^{\nu}_{H}(\vec{x})\;|\psi_i > \;. \tag{4.26}$$

Using the following symbolic identity in Eq. (4.25), namely

$$\frac{1}{\omega \pm i\eta} = \mathrm{P}\frac{1}{\omega} \mp i\pi\delta(\omega) , \tag{4.27}$$

where "P" denotes the Cauchy principal value, and taking the imaginary part of the latter, yields

$$\begin{aligned} \frac{1}{\pi}\mathrm{Im}[\,\Pi^{\mu\nu}(\vec{q},\vec{q};\omega)\,] &= \sum_n \{ -[\,J^{\mu}_{ni}(\vec{q}\,)\,]^* \, J^{\nu}_{ni}(\vec{q}\,)\,\delta(\omega - E_n + E_i) \\ &\quad - [\,J^{\nu}_{ni}(-\vec{q}\,)\,]^* \, J^{\mu}_{ni}(-\vec{q}\,)\,\delta(\omega + E_n + E_i)\} . \end{aligned} \tag{4.28}$$

For inelastic inclusive electron scattering, the energy transferred to the nucleus,

$$\omega_n = E_n - E_i \tag{4.29}$$

is always greater than zero, and thus one can neglect the second term Eq. (4.28). Hence, with the definition of the electromagnetic response of the nucleus $W^{\mu\nu}$ given by Eq. (4.11), one can now write the electromagnetic response of the nucleus $W^{\mu\nu}$ as [Ho94, Pi95]

$$W^{\mu\nu} = -\frac{1}{\pi}\mathrm{Im}[\,\Pi^{\mu\nu}(\vec{q},\vec{q}\,;\omega)\,] = \sum_n [\,J^{\mu}_{ni}(\vec{q}\,)\,]^* \, J^{\nu}_{ni}(\vec{q}\,)\,\delta(\omega - E_n + E_i) . \tag{4.30}$$

The latter form of the electromagnetic response function is often quoted in the literature [Fe71, Ne88, Ho94, Pi95].

It is now shown that Eq. (4.30) reduces to Eq. (4.9) for the special case of electron–proton scattering. One starts by evaluating the non–vanishing matrix elements of the current operators in coordinate space, namely

$$J^{\nu}_{ni}(\vec{x}\,) = < \psi_n | \, \hat{\bar{\psi}}^{(+)}(\vec{x})\gamma^{\nu}\hat{\psi}^{(-)}(\vec{x}\,) \, |\psi_i > \tag{4.31}$$

where the nucleon field operators associated with the scattering process are given by [Se86]

$$\begin{aligned} \hat{\bar{\psi}}^{(+)}(\vec{x}, x_0 = 0) &= \frac{1}{\sqrt{V}} \sum_{\vec{k}\,',s} \hat{a}^{\dagger}_{\vec{k}\,',s}\,\bar{u}(\vec{k}\,',s)e^{-i\vec{k}\,'\cdot\vec{x}} \\ \hat{\psi}^{(-)}(\vec{x}, x_0 = 0) &= \frac{1}{\sqrt{V}} \sum_{\vec{k},s} \hat{a}_{\vec{k}s}\,u(\vec{k},s)e^{+i\vec{k}\cdot\vec{x}} . \end{aligned} \tag{4.32}$$

[*Note: the above field operators represent the discretized version of those defined in Sec. E.3 of Appendix E.*] The nucleon creation and annihilation operators, $\hat{a}^{\dagger}_{\vec{k}s}$ and $\hat{a}_{\vec{k}s}$, satisfy the usual anticommutation relation

$$\{\hat{a}_{\vec{k},s}\hat{a}^{\dagger}_{\vec{k}s'}\} = \delta_{\vec{k},\vec{k}\,'}\delta_{s,s'} \tag{4.33}$$

where the vacuum state $|0>$ is defined by

$$\hat{a}_{\vec{k}s}|0> = 0 \qquad \text{for all } \vec{k}, s \tag{4.34}$$

and the initial and final proton scattering states are given by

$$\begin{aligned} |\psi_i> &= |\vec{P}_i\ S_i> = \hat{a}^\dagger_{\vec{P}_i\ S_i}|0> \\ |\psi_n> &= |\vec{P}_f\ S_f> = \hat{a}^\dagger_{\vec{P}_f\ S_f}|0> \ . \end{aligned} \tag{4.35}$$

With Eqs. (4.35), (4.32) and (4.31) in Eq. (4.26), one gets

$$\begin{aligned} J^\nu_{ni}(\vec{q}\,) &= \frac{1}{V}\int d\vec{x}\ e^{i\vec{q}\cdot\vec{x}} \sum_{\vec{k}'s'}\sum_{\vec{k}s} \bar{u}(\vec{k}\,',s')\gamma^\nu u(\vec{k},s) e^{i(\vec{k}-\vec{k}\,')\cdot\vec{y}} \\ &\quad \times <0|\hat{a}_{\vec{P}_f S_f}\hat{a}^\dagger_{\vec{k}\,'s'}\hat{a}_{\vec{k}s}\hat{a}^\dagger_{\vec{P}_i S_i}|0> \ . \end{aligned} \tag{4.36}$$

Using the anticommutation relation in Eq. (4.33), Eq. (4.36) becomes

$$\begin{aligned} J^\nu_{ni}(\vec{q}\,) &= \frac{1}{V}\int d\vec{x}\ e^{i(\vec{q}+\vec{k}-\vec{k}\,')\cdot\vec{x}} \sum_{\vec{k}'s'}\sum_{\vec{k}s'} \bar{u}(\vec{k}\,',s')\gamma^\nu u(\vec{k},s)\ \delta_{\vec{P}_f,\vec{k}'}\ \delta_{S_f,s'}\ \delta_{\vec{P}_i,\vec{k}}\ \delta_{S_i,s} \\ &= \delta_{\vec{q},\vec{P}_f-\vec{P}_i}\ \bar{u}(\vec{P}_f,S_f)\gamma^\nu u(\vec{P}_i,S_i) \ . \end{aligned} \tag{4.37}$$

Similarly, for $[\,J^\mu_{ni}(\vec{q}\,)\,]^*$, and making use of Eq. (E.64) in Appendix E, one gets

$$[\,J^\mu_{ni}(\vec{q}\,)\,]^* = \delta_{\vec{q},\vec{P}_f-\vec{P}_i}\ \bar{u}(\vec{P}_i,S_i)\gamma^\mu u(\vec{P}_f,S_f) \ . \tag{4.38}$$

Inserting Eqs. (4.37) and (4.38) into Eq. (4.30), and replacing

$$\sum_n \qquad \text{with} \qquad \frac{1}{2}\sum_{S_f S_i}\int d\vec{P}_f \ , \tag{4.39}$$

that is, averaging over initial spins (which accounts for the factor $\frac{1}{2}$), summing over final spins, and integrating over final momenta, one gets

$$\begin{aligned} W^{\mu\nu} &= -\frac{1}{\pi}\mathrm{Im}[\,\Pi^{\mu\nu}(\vec{q},\vec{q};\omega)\,] \\ &= \frac{1}{2}\sum_{S_f S_i}[\,\bar{u}(\vec{P}_i,S_i)\gamma^\mu u(\vec{P}_i+\vec{q},S_f)\,]\,[\,\bar{u}(\vec{P}_i+\vec{q},S_f)\gamma^\nu u(\vec{P}_i,S_i]\ \delta(\omega-E_n+E_i) \\ &= S^{\mu\nu}\ \delta(\omega-E_n+E_i) \end{aligned} \tag{4.40}$$

where $S^{\mu\nu}$ is now identical to the proton tensor defined in Eq. (4.9). Thus, it has been shown that, in the special case of electron–proton scattering, the electromagnetic response of the

target nucleus for electron–nucleus scattering $W^{\mu\nu}$ reduces to the well–known proton tensor $S^{\mu\nu}$. Hence, one concludes that the electromagnetic response of the target nucleus $W^{\mu\nu}$ in Eq. (4.30) is a suitable generalization of the proton tensor in Eq. (4.9). Moreover, it has also been shown that the electromagnetic response of the nucleus is given by the imaginary part of the polarization tensor $\Pi^{\mu\nu}(\vec{q},\vec{q}\,;\omega)$ [see Eq. (4.11)]: The polarization tensor is a fundamental many–body quantity which can be systematically computed using well–known many–body techniques, such as, for example, Feynman diagrams.

4.2.2 Models of the electromagnetic polarization tensor

Thus far, the inelastic electron–nucleus differential cross section has been expressed as the contraction of an electron electromagnetic tensor for the projectile with the imaginary part of the electromagnetic polarization tensor for the target nucleus [see Eqs. (4.10) and (4.11)], where the latter can be systematically computed using well–known many–body techniques. Next, various models, of increasing sophistication, are considered for calculating the electromagnetic polarization tensor for inclusive electron–nucleus inelastic scattering.

Relativistic free Fermi–gas model (FGM)

One starts by deriving an expression for the polarization tensor based on the relativistic Fermi–gas model (FGM), which treats the nuclear ground state as a system of noninteracting fermions at finite density.

Proceeding as in Sec. E.3 of Appendix E, and expanding the fermion field operators $\hat{\psi}(x)$ and $\hat{\bar{\psi}}(x)$ in normal modes, with periodic boundary conditions in a large box of volume V [Se86], namely

$$\begin{aligned}\hat{\psi}(x) &= \frac{1}{\sqrt{V}}\sum_{\vec{k}s}[\hat{a}_{\vec{k}s}\,u(\vec{k},s)e^{-ik\cdot x}+\hat{b}^{\dagger}_{\vec{k}s}\,v(\vec{k},s)e^{ik\cdot x}]\\ \hat{\bar{\psi}}(x) &= \frac{1}{\sqrt{V}}\sum_{\vec{k}s}[\hat{a}^{\dagger}_{\vec{k}s}\,\bar{u}(\vec{k},s)e^{ik\cdot x}+\hat{b}_{\vec{k}s}\,\bar{v}(\vec{k},s)e^{-ik\cdot x}]\end{aligned} \tag{4.41}$$

where the Dirac unit spinors are defined in Sec. E.3 of Appendix E, and are normalized according

to Eq. (4.4). Note that in the limit of an infinitely large box

$$\frac{1}{V}\sum_{\vec{k}} \longrightarrow \frac{1}{(2\pi)^{3/2}}\int d\vec{k}\,, \tag{4.42}$$

and one recovers the continuum versions of the field operators given in Sec. E.3 of Appendix E. The only nonvanishing anticommutation relations are

$$\begin{aligned} \{\hat{a}_{\vec{k}s}, \hat{a}^{\dagger}_{\vec{k}'s'}\} &= \delta_{\vec{k},\vec{k}'}\,\delta_{s,s'} \\ \{\hat{b}_{\vec{k}s}, \hat{b}^{\dagger}_{\vec{k}'s'}\} &= \delta_{\vec{k},\vec{k}'}\,\delta_{s,s'} \end{aligned} \tag{4.43}$$

where $\hat{a}^{\dagger}_{\vec{k}s}$ and $\hat{a}_{\vec{k}s}$ are identified with nucleon creation and annihilation operators, and likewise, $\hat{b}^{\dagger}_{\vec{k}s}$ and $\hat{b}_{\vec{k}s}$ are identified with antinucleon creation and annihilation operators, respectively. In accordance with Serot and Walecka [Se86], the noninteracting ground state $|\Psi_0>$ of the target nucleus is identified as containing positive–energy nucleon levels filled to some Fermi wave number k_F and containing no antiparticles, that is

$$\begin{aligned} \hat{b}_{\vec{k}s}|\Psi_0> &= 0 \qquad \text{for all } \vec{k} \\ \hat{a}^{\dagger}_{\vec{k}s}|\Psi_0> &= 0 \qquad \text{for all } \vec{k} < k_F \\ \hat{a}_{\vec{k}s}|\Psi_0> &= 0 \qquad \text{for all } \vec{k} > k_F\,. \end{aligned} \tag{4.44}$$

Analogous to Eq. (4.16), except that $|\psi_i>$ in now replaced by $|\Psi_0>$, the polarization tensor for the free Fermi–gas model is expressed in terms of the free noninteracting nucleon propagator $G^0_{\alpha\beta}(x,y)$, instead of the full interacting nucleon propagator $G_{\alpha\beta}(x,y)$ defined in Eq. (4.15), that is [Se86]

$$i\Pi^{\mu\nu}_{\rm FGM}(x,y) = {\rm Tr}\,[\,G^0(y,x)\,\gamma^{\mu}\,G^0(x,y)\gamma^{\nu}\,] \tag{4.45}$$

where $G^0_{\alpha\beta}(x,y)$ is defined in terms of the free fields in Eq. (4.41), namely

$$\begin{aligned} iG^0_{\alpha\beta}(x,y) &= <\Psi_0|\,T[\hat{\psi}_{\alpha}(x)\hat{\bar{\psi}}_{\beta}(y)]\,|\Psi_0> \\ &= \theta(x_0-y_0)\;<\Psi_0|\,\hat{\psi}_{\alpha}(x)\hat{\bar{\psi}}_{\beta}(y)\,|\Psi_0> \\ &\quad -\theta(y_0-x_0)\;<\Psi_0|\,\hat{\psi}_{\beta}(y)\hat{\bar{\psi}}_{\alpha}(x)\,|\Psi_0>\,, \end{aligned} \tag{4.46}$$

and the subscript "FGM" refers to the fact that one is dealing with the relativistic Fermi–gas model. In order to explicitly evaluate the FGM electromagnetic response of the nucleus, which is just the imaginary part of the polarization tensor, an explicit form for the free nucleon

propagator is required. Assuming translational invariance, the Fourier transform of Eq. (4.45) is [Se86]

$$\begin{aligned} i\Pi^{\mu\nu}_{\rm FGM}(\vec{q},\omega) &= \int d^4(x-y)\; e^{+iq\cdot(x-y)}\; i\Pi^{\mu\nu}_{\rm FGM}(x-y) \\ &= \int d^4(x-y)\; e^{+iq\cdot(x-y)}\; {\rm Tr}\,[\, G^0(y-x)\;\gamma^\mu\; G^0(x-y)\gamma^\nu\,]\,. \end{aligned} \tag{4.47}$$

Substitution of the fermion fields, given by Eq. (4.41), into Eq. (4.46), and making use of Eqs. (4.42) – (4.44), plus the integral representation of the Heaviside step function

$$\theta(x_0-y_0) \;=\; i\int \frac{d\omega}{2\pi}\;\frac{e^{-i\omega(x_0-y_0)}}{\omega+i\epsilon}\,, \tag{4.48}$$

where ϵ is a positive infinitesimal, leads to

$$iG^0_{\alpha\beta}(x-y) \;=\; i\int \frac{d^4k}{(2\pi)^4} G^0_{\alpha\beta}(k) e^{-ik\cdot(x-y)}\,, \tag{4.49}$$

from which the free nucleon propagator in momentum space is identified as

$$\begin{aligned} G^0_{\alpha\beta}(k) \;=\; & \frac{1}{2E_k}\,\{(\gamma_\mu K^\mu + M)_{\alpha\beta}\,[\,\frac{\theta(|\vec{k}\,|-k_F)}{k_0-E_k+i\epsilon} \;+\; \frac{\theta(k_F-|\vec{k}\,|)}{k_0-E_k-i\epsilon}\,] \\ & -\,(\gamma_\mu \tilde{K}^\mu + M)_{\alpha\beta}\,[\,\frac{1}{k_0+E_k-i\epsilon}\,]\} \end{aligned} \tag{4.50}$$

where

$$\begin{aligned} \gamma_\mu K^\mu &= E_k\gamma^0 \;-\; \vec{\gamma}\cdot\vec{k} \\ \gamma_\mu \tilde{K}^\mu &= -E_k\gamma^0 \;-\; \vec{\gamma}\cdot\vec{k}\,. \end{aligned} \tag{4.51}$$

The three terms in Eq. (4.50) are interpreted as follows:

- the first term corresponds to nucleon propagation above the Fermi surface.
- the second term describes the propagation of "holes" inside the Fermi sea, just as in the nonrelativistic propagator [Fe71].
- the third term allows for the propagation of "holes" in the infinite Dirac sea, which are to be interpreted as antinucleons.

Finally, the polarization tensor in momentum space is evaluated by substituting Eq. (4.49) in Eq. (4.47), and making use of the fact that

$$\int d^4x\; e^{-i(k-p)\cdot x} \;=\; (2\pi)^4\;\delta^4(k-p) \tag{4.52}$$

thus yielding

$$i\Pi^{\mu\nu}_{\mathrm{FGM}}(\vec{q},\omega) \;=\; \int \frac{d^4k}{(2\pi)^4}\,\mathrm{Tr}\left[\,G^0(k)\,\gamma^\mu\,G^0(k+q)\,\gamma^\nu\,\right]. \tag{4.53}$$

The latter expression represents the electromagnetic polarization tensor for the case where the nucleus is treated as a relativistic free Fermi–gas of nucleons.

Relativistic mean–field approximation (MFA)

One can improve the relativistic free Fermi–gas description of the target nucleus by taking into account, at least at the mean–field level, the interaction between the nucleons in the nucleus. In a relativistic mean–field–approximation (MFA) of the Walecka model [Se86], the propagation of a nucleon through the surrounding nuclear medium is modified by the presence of constant scalar ϕ_0 and time–like vector V_0 mean–fields. These potentials induce a shift in the mass and energy of a nucleon in the nuclear medium, respectively. In the relativistic MFA, the Heisenberg field operator $\hat{\psi}(x)$ in Eq. (4.41) is replaced by [Se86]:

$$\hat{\psi}(\vec{x},x_0) \;=\; \frac{1}{\sqrt{\Omega}}\sum_{\vec{k}s}\left[\,A_{\vec{k}s}U(\vec{k},s)e^{i(\vec{k}\cdot\vec{x}-\epsilon_k^{(+)}x_0)} \;+\; B^\dagger_{\vec{k}s}V(\vec{k},s)e^{-i(\vec{k}\cdot\vec{x}+\epsilon_k^{(-)}x_0)}\,\right] \tag{4.54}$$

where

$$\epsilon_k^{(\pm)} \;=\; g_vV_0 \;\pm\; E_k^* \tag{4.55}$$

and

$$\begin{aligned} E_k^* \;&=\; \sqrt{|\vec{k}\,|^2+M^{*2}} \\ M^* \;&=\; M \;-\; g_s\phi_0\,. \end{aligned} \tag{4.56}$$

Ω is the volume of the system, and g_s and g_v are the meson–nucleon scalar and vector coupling constants, respectively. Here, $A^\dagger_{\vec{k}s}$ and $A_{\vec{k}s}$ are the creation and annihilation operators for quasinucleons, whereas $B^\dagger_{\vec{k}s}$ and $B_{\vec{k}s}$ correspond to creation and annihilation operators for quasi–antinucleons, respectively, which satisfy the usual anticommutation relations. The word "quasinucleon (quasi–antinucleon)" refers to a nucleon (antinucleon) whose mass, energy, and Dirac wave function are modified by the constant scalar ϕ_0 and time–like vector potentials V_0.

The nuclear ground state $|F>$, within the relativistic MFA, is defined as

$$\begin{aligned} \hat{B}_{\vec{k}s}|F> &= 0 \qquad \text{for all } \vec{k} \\ \hat{A}^{\dagger}_{\vec{k}s}|F> &= 0 \qquad \text{for all } \vec{k} < k_F \\ \hat{A}_{\vec{k}s}|F> &= 0 \qquad \text{for all } \vec{k} > k_F \, . \end{aligned} \tag{4.57}$$

The mean–field quasinucleon and quasi–antinucleon Dirac spinors, U and V respectively, are given by [Se86]

$$U(\vec{k},s) = \sqrt{\frac{E^*_k + M^*}{2E^*_k}} \begin{pmatrix} I \\ \\ \dfrac{\vec{\sigma}\cdot\vec{k}}{E^*_k + M^*} \end{pmatrix} \chi_s \tag{4.58}$$

$$V(\vec{k},s) = \sqrt{\frac{E^*_k + M^*}{2E^*_k}} \begin{pmatrix} \dfrac{\vec{\sigma}\cdot\vec{k}}{E^*_k + M^*} \\ \\ I \end{pmatrix} \chi_s \, . \tag{4.59}$$

Analogous to Eq. (4.46), the coordinate space representation of the mean–field nucleon propagator (indicated by the superscript "MF") is defined as

$$iG^{MF}_{\alpha\beta}(x,y) = <F|\, T[\hat{\psi}_\alpha(x)\hat{\bar{\psi}}_\beta(y)]\, |F> \, . \tag{4.60}$$

With the mean-field field operator defined in Eq. (4.54), the derivation of the MFA nucleon propagator $G^{MF}_{\alpha\beta}(k)$ in momentum space proceeds in a similar fashion to the derivation of the free nucleon propagator given by Eq. (4.50), and gives

$$\begin{aligned} G^{MF}_{\alpha\beta}(k) = \frac{1}{2E^*_k} \{ &(\gamma_\mu K^{*\mu} + M)_{\alpha\beta} \left[\frac{\theta(|\vec{k}\,| - k_F)}{k_0 - g_v V_0 - E^*_k + i\epsilon} + \frac{\theta(k_F - |\vec{k}\,|)}{k_0 - g_v V_0 - E^*_k - i\epsilon} \right] \\ &- (\gamma_\mu \tilde{K}^{*\mu} + M)_{\alpha\beta} \left[\frac{1}{k_0 - g_v V_0 + E^*_k - i\epsilon} \right] \} \end{aligned} \tag{4.61}$$

where

$$\begin{aligned} \gamma_\mu K^{*\mu} &= E^*_k \gamma^0 - \vec{\gamma}\cdot\vec{k} \\ \gamma_\mu \tilde{K}^{*\mu} &= -E^*_k \gamma^0 - \vec{\gamma}\cdot\vec{k} \end{aligned} \tag{4.62}$$

and

$$k^{*\mu} = (k^0 - g_v V^0, \vec{k}\,) \, . \tag{4.63}$$

Thus, in the mean–field approximation, the interacting propagator in Eq. (4.61) takes a form that is similar to the free propagator in Eq. (4.50), the only difference being that k^0 and E_k are replaced by $k^0 - g_v V^0$ and E_k^*, respectively. As in Eq. (4.50) for the FGM, the three terms in Eq. (4.61) are easily interpreted as follows:

- the first term corresponds to quasinucleon propagation above the Fermi surface.
- the second term describes the propagation of quasinucleon "holes" inside the Fermi sea.
- the third term allows for the propagation of "holes" in the infinite Dirac sea, which are to be interpreted as quasi–antinucleons.

With the mean–field propagator defined in Eq. (4.61), and following a procedure analogous to that outlined in the previous section, the resulting mean–field polarization tensor is given by [Ch77, Ho84, Ku85, Li89, Ma82, Ho90, We93, Ho94, Pi95]

$$i\Pi^{\mu\nu}_{MF}(\vec{q},\omega) \;=\; \int \frac{d^4k}{(2\pi)^4} \mathrm{Tr}\left[\, G^{MF}(k)\, \gamma^\mu\, G^{MF}(k+q)\, \gamma^\nu \,\right]. \tag{4.64}$$

Note that, in computing the response, one integrates over the four–momenta of the nucleons, and hence, the contribution from the constant vector potential V_0 in Eq. (4.61) can be eliminated by a simple change of variables. *Formally, then, the mean–field response is identical to that of the relativistic free Fermi–gas with, however, an effective mass M^* instead of a free mass M.*

Local density approximation (LDA)

One can improve the mean–field approximation of the electromagnetic polarization tensor by considering a local density approximation (LDA) [We87, Ho90, We93, Pi95] of the Walecka model. The latter approximation assumes that, at an average momentum transfer, the response of the nucleus is just the sum of the responses of its volume elements, each characterized by a local Fermi wave number $k_F(r)$, and a local effective mass $M^*(r)$, and treated as nuclear matter with these parameters. Hence, for the electromagnetic polarization tensor, the transition from the MFA to the LDA is made via the following replacement:

$$\Pi^{\mu\nu}_{MF}(\vec{q},\omega) \;\longrightarrow\; \Pi^{\mu\nu}_{LDA}(\vec{q},\vec{q}\,';\omega) \tag{4.65}$$

where

$$\Pi^{\mu\nu}_{LDA}(\vec{q},\vec{q}\,';\omega) = \int d\vec{R}\, e^{-i(\vec{q}-\vec{q}\,')\cdot\vec{R}}\, \Pi^{\mu\nu}_{LDA}[\left(|\frac{\vec{q}+\vec{q}\,'}{2}|\right),\omega\,;k_F(R),M^*(R)\,] \tag{4.66}$$

and

$$\begin{aligned} M^*(R) &= M - g_s\phi_0(R) \\ k_F(R) &= [\frac{3}{2}\pi^2\rho_B(R)]^{\frac{1}{3}}\,. \end{aligned} \tag{4.67}$$

$\phi_0(r)$ and $\rho_B(r)$ represent the local scalar field and baryon density, respectively, which are generated selfconsistently via the Dirac–Hartree approximation [Ho91a]. The exact meaning of

$$\Pi^{\mu\nu}_{LDA}[\left(|\frac{\vec{q}+\vec{q}\,'}{2}|\right),\omega\,;k_F(R),M^*(R)\,]$$

will become clearer when analytical expressions are derived for the nuclear polarization propagator in Sec. 4.2.3. For calculations of scattering observables in coordinate space (see Sec. 4.4), the Fourier transform of Eq. (4.66) is required, namely [*Recall that the imaginary part of the polarization tensor is directly related to the double differential cross section*]

$$\Pi^{\mu\nu}_{LDA}(\vec{r},\vec{r}\,';\omega) = \int \frac{d\vec{q}}{(2\pi)^3}\, e^{+i\vec{q}\cdot\vec{r}} \int \frac{d\vec{q}\,'}{(2\pi)^3}\, e^{-i\vec{q}\,'\cdot\vec{r}\,'} \Pi^{\mu\nu}_{LDA}(\vec{q},\vec{q}\,';\omega)\,. \tag{4.68}$$

Eq. (4.68), together with Eq. (4.66), can be simplified via the following change of variables

$$\begin{aligned} \vec{q} &\longrightarrow \tilde{q} \\ \vec{q}\,' &\longrightarrow \tilde{Q} \end{aligned} \tag{4.69}$$

where

$$\begin{aligned} \vec{q} &= \tilde{q} + \tilde{Q} \\ \vec{q}\,' &= \tilde{q} - \tilde{Q} \end{aligned} \tag{4.70}$$

thus yielding the electromagnetic polarization tensor of the nucleus within the local density approximation, namely

$$\Pi^{\mu\nu}_{LDA}(\vec{r},\vec{r}\,';\omega) = \int \frac{d\tilde{q}}{(2\pi)^3}\, e^{i\tilde{q}\cdot(\vec{r}-\vec{r}\,')}\, \Pi^{\mu\nu}_{LDA}[\tilde{q},\omega\,;\, k_F(|\frac{\vec{r}+\vec{r}\,'}{2}|), M^*(|\frac{\vec{r}+\vec{r}\,'}{2}|)]\,. \tag{4.71}$$

Relativistic random phase approximation (RPA)

In the previous three sections, different models (relativistic free Fermi–gas model, relativistic mean–field approximation, and the local density approximation) were presented for evaluating the electromagnetic response of the nucleus for electron–nucleus scattering. One can improve these models by considering, for example, the nuclear response in a relativistic random–phase approximation (RPA). The RPA is not considered in this thesis: for more information on the RPA, the interested reader is referred to Refs. [Pi95, We87, Ho90, Ho94, We93, Ki95].

4.2.3 Nuclear response of a nucleus

Thus far, the primary focus has been on *electromagnetic* response functions for electrons scattering from nuclei. However, for calculations of quasielastic proton–nucleus scattering observables, one is interested in calculating *nuclear* response functions (see Sec. 4.4).

For simplicity, one starts by generalizing Eq. (4.5), for electron–proton scattering, to the case of nuclear nucleon–nucleon scattering. This is done by replacing the electromagnetic interaction vertex, $\Gamma^\mu = \gamma^\mu$, with the relativistic SVPAT interaction vertices for NN scattering (see Sec. 3.2.4 in Chapter 3), that is

$$\Gamma^\mu = \gamma^\mu \quad \text{is replaced by} \quad \lambda^\alpha = \{\, 1, \gamma^\mu, \sigma^{\mu\nu}, i\gamma^5, \gamma^\mu\gamma^5 \,\} \tag{4.72}$$

where

$$\bar{\lambda}^\alpha \equiv \gamma^0 (\lambda^\alpha)^\dagger \gamma^0 = \lambda^\alpha \,. \tag{4.73}$$

Note that in Chapter 3, one used γ^5, rather than $i\gamma^5$, for the πNN vertex: both γ^5 and $i\gamma^5$ yield identical results for the polarization transfer observables. Following a procedure similar to that presented in Sec. E.5 of Appendix E, and making use of the identity [Bj64]

$$[\, \bar{u}(p_f, s_f)\, \lambda^\alpha\, u(p_i, s_i)\,]^\dagger \;=\; \bar{u}(p_i, s_i)\, \lambda^\alpha\, u(p_f, s_f)\,, \tag{4.74}$$

the unpolarized differential cross section for nucleon–nucleon scattering in the plane–wave Born approximation is written as

$$d\bar{\sigma} \;=\; \frac{1}{v_{\rm rel}}\, \frac{1}{(2\pi)^2} \sum_{\alpha\beta} t^\alpha\, (t^\beta)^*\, L_{\alpha\beta}\, S^{\alpha\beta}\, d\vec{p}_f \tag{4.75}$$

where t^{α} represents the relativistic SVPAT NN scattering amplitudes, and, analogous to Eq. (4.6), the projectile nucleon tensor $L_{\alpha\beta}$ is defined by [compare to Eq. (3.71) for the invariant matrix element $\mathcal{M}$ in Chapter 3]

$$L_{\alpha\beta} = \frac{1}{2} \sum_{s_f,s_i} [\,\bar{u}(p_f,s_f)\lambda_{\alpha}u(p_i,s_i)\,]\,[\,\bar{u}(p_f,s_f)\lambda_{\beta}u(p_i,s_i)\,]^{*} \tag{4.76}$$

and, the nuclear response function of the target nucleon $S^{\alpha\beta}$ is given by [compare to Eq. (3.73) for the invariant matrix element $\mathcal{M}$ in Chapter 3]

$$S^{\alpha\beta} = \frac{1}{2} \sum_{S_f,S_i} [\,\bar{u}(P_f,S_f)\lambda^{\alpha}u(P_i,S_i)\,]\,[\,\bar{u}(P_f,S_f)\lambda^{\beta}u(P_i,S_i)\,]^{*}\,. \tag{4.77}$$

For a nucleon scattering from a *nucleus*, the unpolarized differential cross section is obtained via a generalization of Eqs. (4.75) – (4.77), giving {compare to Eqs. (4.10), (4.12) and (4.7) for electron–nucleus scattering} [Ho94]

$$d\bar{\sigma} = \frac{1}{v_{\rm rel}} \frac{1}{(2\pi)^2} \sum_{\alpha\beta} t^{\alpha}\,(t^{\beta})^{*}\,L_{\alpha\beta}\,S^{\alpha\beta}\,d\vec{p}_f \tag{4.78}$$

where $L_{\alpha\beta}$ is the nucleon tensor already given by Eq. (4.76), and $S^{\alpha\beta}$ is the nuclear response of the nucleus given by [compare to Eq. (4.30) for electron–nucleus scattering]:

$$\begin{aligned} S^{\alpha\beta}(\vec{q},\vec{q}\,;\omega) &= -\frac{1}{\pi}\,{\rm Im}[\,\Pi^{\alpha\beta}(\vec{q},\vec{q}\,;\omega)\,] \\ &= \sum_{n} [\,J^{\alpha}_{ni}(\vec{q}\,)\,]^{*}\,J^{\beta}_{ni}(\vec{q}\,)\,\delta(\omega - E_n + E_i) \end{aligned} \tag{4.79}$$

where

$$J^{\alpha}_{ni}(\vec{q}\,) = \int d\vec{x}\; e^{i\vec{q}\cdot\vec{x}} < \psi_n|\;\hat{J}^{\alpha}_{H}(\vec{x}\,)\;|\psi_i > \tag{4.80}$$

and the nuclear current operator is given by

$$\hat{J}^{\alpha}_{H}(\vec{x}\,) = \hat{\bar{\psi}}(\vec{x}\,)\,\lambda^{\alpha}\,\hat{\psi}(\vec{x}\,)\,. \tag{4.81}$$

Note that, compared to electromagnetic electron–nucleus scattering, the nuclear response functions for nucleon–nucleus scattering are more complicated due to the mixing of many different Lorentz structures of the NN interaction.

Analytical expressions for the nuclear polarization tensor

As in the case for electron–nucleus scattering, the polarization tensor can be evaluated for a variety of models. In this section, analytical expressions are derived for the imaginary parts of the nuclear scalar polarization, based on the relativistic free Fermi–gas model, relativistic mean–field approximation, and the local density approximation, for which

$$\lambda^{\alpha} = \lambda^{\beta} = 1 \,. \tag{4.82}$$

A similar approach can be followed to derive expressions for all the components of the nuclear polarization tensor $\Pi^{\alpha\beta}$.

First, the relativistic mean–field approximation is considered. The corresponding expressions for the free Fermi–gas model can be obtained as a special case of the mean–field results. The expressions with the local density approximations, on the other hand, are obtained via a simple generalization of the mean–field results.

Within the relativistic mean–field approximation, the nuclear polarization tensor is obtained via a generalization of Eq. (4.64), namely

$$i\,\Pi^{\alpha\beta}_{MF}(\vec{q},\omega) = \int \frac{d^4k}{(2\pi)^4} \mathrm{Tr}\,[\,G^{MF}(k)\;\lambda^{\alpha}\;G^{MF}(k+q)\;\lambda^{\beta}\,] \tag{4.83}$$

where the mean–field nucleon propagator $G^{MF}(k)$ is given by Eq. (4.61), and λ^{α} and λ^{β} are given by Eq. (4.72).

For the reaction kinematics of interest, namely incident laboratory energies smaller than 500 MeV, and space–like momentum transfers (for which $q^2_{\mu} < 0$), the production of nucleon–antinucleon pairs is kinematically forbidden, and hence, the last term in Eq. (4.61) can be omitted, thus yielding

$$\widetilde{G}^{MF}_{\alpha\beta}(k) = \frac{1}{2E^*_k}\,\{\,(\gamma_{\mu}K^{*\mu}+M)_{\alpha\beta}\,[\,\frac{\theta(|\vec{k}\,|-k_F)}{k_0-g_vV_0-E^*_k+i\epsilon}+\frac{\theta(k_F-|\vec{k}\,|)}{k_0-g_vV_0-E^*_k-i\epsilon}\,] \tag{4.84}$$

where the tilde serves as a reminder of the omission of antinucleon propagation. Note, however, that virtual nucleon–antinucleon pairs can be produced, and play an important role in the RPA response. The latter, however, does not form part of this project, and, for more detail, the interested reader is referred to Refs. [Ku85, Se86, Li89, Ho90, Ho94]. For simplicity, and to illustrate the approach, analytical expressions are now derived for the imaginary part of only

the nuclear scalar polarization. Essentially, the procedures outlined in Refs. [Ho84, Li89] are followed. Inserting Eq. (4.84) into Eq. (4.83), and taking $\lambda^\alpha = \lambda^\beta = 1$, yields the following expression for the nuclear scalar polarization:

$$\begin{aligned} i\widetilde{\Pi}^{s\,s}_{MF}(q) &= \int \frac{d^4k}{(2\pi)^4}\,[\,\frac{1}{2E^*_k 2E^*_{k+q}}\,]\,\mathrm{Tr}[(\not{k}^* + M^*)(\not{k}^* + \not{q}^* + M^*)] \\ &\quad \times [\,\frac{\theta(|\vec{k}\,| - k_F)}{k_0 - g_v V_0 - E^*_k + i\epsilon} + \frac{\theta(k_F - |\vec{k}\,|)}{k_0 - g_v V_0 - E^*_k - i\epsilon}\,] \\ &\quad \times [\,\frac{\theta(|\vec{k}+\vec{q}\,| - k_F)}{k_0 + q_0 - g_v V_0 - E^*_{k+q} + i\epsilon} + \frac{\theta(k_F - |\vec{k}+\vec{q}\,|)}{k_0 + q_0 - g_v V_0 - E^*_{k+q} - i\epsilon}\,]\,. \end{aligned} \tag{4.85}$$

Using the usual trace techniques [Bj64, Gr92], as well as Eqs. (4.56) and (4.63), Eq. (4.85) is readily evaluated, giving

$$\mathrm{Tr}[(\not{k}^* + M^*)(\not{k}^* + \not{q}^* + M^*)] = 4[\,(k_0 - g_v V_0)^2 - |\vec{k}\,|^2 + (k_0 - g_v V_0)(q_0 - g_v V_0) - \vec{k}\cdot\vec{q} + M^{*2}\,] \tag{4.86}$$

After elimination of the constant vector potential V_0 in Eq. (4.85), by a simple change of variables, the integral over k_0 is evaluated via contour integration, giving

$$\begin{aligned} i\widetilde{\Pi}^{s\,s}_{MF}(q) &= \int \frac{d\vec{k}}{(2\pi)^3}\,[\,\frac{1}{2E^*_k 2E^*_{k+q}}\,] \times 4\,[\,(E^*_{k+q} - q_0)^2 - |\vec{k}\,|^2 + (E^*_{k+q} - q_0)q_0 - \vec{k}\cdot\vec{q} + M^{*2}\,] \\ &\quad \times (2\pi i)\,\{\,\frac{\theta(|\vec{k}\,| - k_F)\theta(k_F - |\vec{k}+\vec{q}\,|)}{E^*_{k+q} - q_0 - E^*_k + i\epsilon} - \frac{\theta(k_F - |\vec{k}\,|\,\theta(|\vec{k}+\vec{q}\,| - k_F)}{E^*_{k+q} - q_0 - E^*_k - i\epsilon}\,\}\,. \end{aligned} \tag{4.87}$$

Now recall that scattering observables are eventually expressed in terms of nuclear response functions, which are given by the imaginary part of the polarization tensor [see Eq. (4.79)]. Using the relation [Bj64, Ne88]

$$\mathrm{Im}(\frac{1}{\omega \pm i\epsilon}) = \mp\,\delta(\omega) \tag{4.88}$$

the imaginary part of the nuclear scalar polarization in Eq. (4.88) is identified, namely

$$\mathrm{Im}\,[\,\widetilde{\Pi}^{s\,s}_{MF}(q)\,] = \widetilde{\Pi}^{I1}_{MF}(q) + \widetilde{\Pi}^{I2}_{MF}(q) \tag{4.89}$$

where

$$\begin{aligned} \widetilde{\Pi}^{I1}_{MF}(q) &= -\int \frac{d\vec{k}}{(2\pi)^3}\,[\,\frac{1}{2E^*_k 2E^*_{k+q}}\,] \times 4\,[\,(E^*_{k+q} - q_0)^2 - |\vec{k}\,|^2 + (E^*_{k+q} - q_0)q_0 - \vec{k}\cdot\vec{q} + M^{*2}\,] \\ &\quad \times \delta(E^*_{k+q} - q_0 - E^*_k)\,[\,\theta(k_F - |\vec{k}\,|)\theta(|\vec{k}+\vec{q}\,| - k_F)\,] \end{aligned} \tag{4.90}$$

and

$$\begin{aligned} \widetilde{\Pi}^{I2}_{MF}(q) &= -\int \frac{d\vec{k}}{(2\pi)^3}\,[\,\frac{1}{2E^*_k 2E^*_{k+q}}\,] \times 4\,[\,(E^*_{k+q} - q_0)^2 - |\vec{k}\,|^2 + (E^*_{k+q} - q_0)q_0 - \vec{k}\cdot\vec{q} + M^{*2}\,] \\ &\quad \times \pi\delta(E^*_{k+q} - q_0 - E^*_k)\,[\,\theta(|\vec{k}\,| - k_F)\theta(k_F - |\vec{k}+\vec{q}\,|)\,]\,. \end{aligned} \tag{4.91}$$

First $\widetilde{\Pi}^{I1}_{MF}(q)$ in Eq. (4.90) is evaluated. Using the fact that

$$E^{*2}_k = |\vec{k}\,|^2 + M^{*2}\,, \tag{4.92}$$

one can write

$$\begin{aligned} E^{*2}_{k+q} &= (\vec{k}+\vec{q})^2 + M^{*2} \\ &= E^{*2}_k + 2|\vec{k}\,|\,|\vec{q}\,|\cos\theta + |\vec{q}\,|^2 \end{aligned} \tag{4.93}$$

which implies that

$$\cos\theta = \frac{E^{*2}_{k+q} - E^{*2}_k - |\vec{q}\,|^2}{2|\vec{k}\,||\vec{q}\,|}\,. \tag{4.94}$$

Introducing the following change of variables

$$\begin{aligned} |\vec{k}\,| &\longrightarrow E^*_k \\ \cos\theta &\longrightarrow E^*_{k+q}\,, \end{aligned} \tag{4.95}$$

one can rewrite

$$\begin{aligned} \int d\vec{k} &= \int_0^{k_F} |\vec{k}\,|^2 dk \int_0^{\pi} \sin\theta\, d\theta \int_0^{2\pi} d\phi \\ &= 2\pi \int_0^{k_F} |\vec{k}\,|^2 dk \int_{-1}^{1} d(\cos\theta) \end{aligned} \tag{4.96}$$

in Eq. (4.90), as

$$d\vec{k} = \frac{2\pi}{|\vec{q}\,|} \int E^*_k\, dE^*_k \int E^*_{k+q}\, dE^*_{k+q}\,. \tag{4.97}$$

The constraint that $|\cos\theta| \leq 1$ is incorporated via a Heaviside step function. From Eq. (4.94), it follows that

$$|\cos\theta| \leq 1 \implies \theta[\,|4\vec{k}\,|^2\,|\vec{q}\,|^2 - (E^{*2}_{k+q} - E^{*2}_k - |\vec{q}\,|^2)^2\,]\,. \tag{4.98}$$

Finally, with Eqs. (4.97) and (4.98), and performing the integral $\int d\,E^*_{k+q}$ in Eq. (4.90), yields

$$\begin{aligned} \widetilde{\Pi}^{I1}_{MF}(q) &= -\frac{1}{8\pi|\vec{q}\,|}\,(4M^{*2} - q^2_\mu) \int d\,E^*_k\,\theta(E^*_F - E^*_k)\,\theta(q_0 + E^*_k - E^*_F) \\ &\quad \times \theta(-E^{*2}_k q^2_\mu - M^{*2}|\vec{q}\,|^2 - E^*_k\, q_0\, q^2_\mu - \frac{q^4_\mu}{4})\,. \end{aligned} \tag{4.99}$$

Next, $\Pi^{I2}_{MF}(q)$ in Eq. (4.91) is evaluated. With the transformation of variables

$$\vec{k} \longrightarrow \vec{k} + \vec{q}\,, \tag{4.100}$$

Eq. (4.91) can be rewritten as

$$\Pi^{I2}_{MF}(q) = -\int \frac{d\vec{k}}{(2\pi)^3}[\frac{1}{2E^*_{k-q}2E^*_k}] \times 4[(E^*_k - q_0)^2 - |\vec{k} - \vec{q}\,|^2 + (E^*_k - q_0)q_0 - (\vec{k} - \vec{q}) \cdot \vec{q} + M^{*2}] \times \delta(E^*_k - q_0 - E^*_{k-q})[\theta(|\vec{k} - \vec{q}\,| - k_F)\theta(k_F - |\vec{k}\,|)] \,. \quad (4.101)$$

Analogous to the procedure outlined from Eqs. (4.92) to (4.94), and with the following change of variables

$$\begin{aligned} |\vec{k}\,| &\longrightarrow E^*_k \\ \cos\theta &\longrightarrow E^*_{k-q} \end{aligned} \quad (4.102)$$

one can rewrite

$$\begin{aligned} \int d\vec{k} &= \int_0^{k_F} |\vec{k}\,|^2 dk \int_0^{\pi} \sin\theta \, d\theta \int_0^{2\pi} d\phi \\ &= 2\pi \int_0^{k_F} |\vec{k}\,|^2 dk \int_{-1}^{1} d(\cos\theta) \end{aligned} \quad (4.103)$$

in Eq. (4.101), as

$$d\vec{k} = -\frac{2\pi}{|\vec{q}\,|} \int E^*_k \, dE^*_k \int E^*_{k-q} \, dE^*_{k-q} \,. \quad (4.104)$$

As before, the constraint $|\cos\theta| \leq 1$ is incorporated via a Heaviside step function, that is

$$|\cos\theta| \leq 1 \implies \theta[|4\vec{k}\,|^2|\vec{q}\,|^2 - (E^{*2}_k - E^{*2}_{k-q} + |\vec{q}\,|^2)^2] \,. \quad (4.105)$$

Finally, with Eqs. (4.104) and (4.105), and performing the integral $\int dE^*_{k+q}$ in Eq. (4.101), yields

$$\widetilde{\Pi}^{I2}_{MF}(q) = \frac{1}{8\pi|\vec{q}\,|}(4M^{*2} - q^2_\mu) \int dE^*_k \, \theta(-q_0 + E^*_k - E^*_F) \, \theta(E^*_F - E^*_k) \times \theta(-E^{*2}_k q^2_\mu - M^{*2}|\vec{q}\,|^2 + E^*_k \, q_0 \, q^2_\mu - \frac{q^4_\mu}{4}) \,. \quad (4.106)$$

The step function in the above equation implies that the energy of the scattered nucleon is larger than the Fermi energy, that is,

$$E^*_k - q_0 \geq E^*_F \,. \quad (4.107)$$

However, this is unphysical, since the initial energy is smaller that the Fermi energy, that is

$$E^*_k < E^*_F \quad (4.108)$$

and hence Eq. (4.107) does not hold. Therefore, Eq. (4.106) is omitted from Eq. (4.89), and, hence, the expression for the imaginary part of the polarization tensor is now given by Eq. (4.99):

$$\begin{aligned}\widetilde{\Pi}^{I1}_{MF}(q) &= -\frac{1}{8\pi|\vec{q}\,|}\,(4M^{*2}-q_\mu^2)\int d\,E_k^*\,\theta(E_F^*-E_k^*)\,\theta(q_0+E_k^*-E_F^*) \\ &\quad\times\theta(-E_k^{*2}q_\mu^2-M^{*2}|\vec{q}\,|^2-E_k^*q_0q_\mu^2-\frac{q_\mu^4}{4})\,. \end{aligned} \tag{4.109}$$

Finally, integration over E_k^* in the latter equation, gives:

$$\mathrm{Im}[\,\widetilde{\Pi}^{s\,s}_{MF}(q)\,] \;=\; \widetilde{\Pi}^{I1}_{MF} \;=\; \frac{1}{8\pi|\vec{q}\,|}\,(4M^{*2}-q_\mu^2)\,(E_u-E_d) \tag{4.110}$$

where the θ functions imply the following integration limits:

$$\begin{aligned} E_u \;=\; E_F^* &= \sqrt{|\vec{k}\,|^2+M^{*2}} \\ E_d &= \min[\,E_F^*, E_{max}\,] \\ E_{max} &= \max[\,M^*, E_F^*-q_0, E_r\,] \\ E_r &= \frac{1}{2}[\,|\vec{q}\,|\sqrt{1-\frac{4M^{*2}}{q_\mu^2}}-q_0\,]\,. \end{aligned} \tag{4.111}$$

Eq. (4.110) is identical to the corresponding expressions in Refs. [Ho84, Li89, We93], with the exception that Ref. [Ho84] uses a different metric.

For the free Fermi–gas model, the imaginary part of the polarization tensor is obtained by replacing M^* by M in Eqs. (4.110) and (4.111). The corresponding results for the local density approximations are obtained by replacing M^* by $M^*(r)$ in Eqs. (4.110) and (4.111) and by making use of the LDA prescription in Eqs. (4.65) and (4.66).

Following a procedure analogous to the one just sketched for the nuclear scalar polarization, one can derive analytical expressions for all the components of the polarization tensor $\Pi^{\alpha\beta}$. Analytical expressions for some of the components of the polarization tensor can be found in Refs. [Ho84, Li89, We93, Ki95].

4.3 Relativistic distorted wave functions

The aim of this section is to derive partial wave expansions for relativistic distorted wave functions, which are scattering solutions to the Dirac equation, with scalar and time–like vector

potentials, for incoming and outgoing boundary conditions. The latter boundary conditions refer to the asymptotic behaviour of the scattering wave functions. For outgoing boundary conditions, the asymptotic form of the scattering wave function is that of an incident plane wave plus outgoing (scattered) spherical waves (see also Sec. 4.3.4), whereas for incoming boundary conditions, the asymptotic form is that of an outgoing plane wave plus incoming spherical waves. The term "distorted wave", used for scattering wave functions, refers to distortion away from the corresponding plane waves due to the presence of scattering potentials. The relativistic distorted waves will eventually be used for calculations of polarization transfer observables based on the relativistic distorted wave impulse approximation to be discussed in Sec. 4.4.

Before deriving partial wave expansions for relativistic distorted waves, some of the underlying principles are illustrated by considering the simplest case of a partial wave analysis for nonrelativistic Schrödinger–based scattering wave functions. The discussion of the nonrelativistic distorted waves is considerably more detailed than would seem warranted, however, this detail is supplied so as to provide a familiar context for developing the partial wave expansions of the relativistic distorted waves. Also note, at this stage, that both nonrelativistic and relativistic distorted wave functions are usually generated in the nucleon–nucleus centre–of–mass frame, and hence, most of the associated kinematic quantities (unless otherwise specified) are defined in the latter reference frame.

4.3.1 Partial wave analysis of nonrelativistic spin–dependent plane waves

For simplicity, the wave functions for a nonrelativistic free spin–$\frac{1}{2}$ particle are considered. By nonrelativistic free particle wave functions, one means the solutions to the Schrödinger equation for zero scattering potentials. The unnormalized wave function for a nonrelativistic free particle, with momentum $\vec{k}$ in the projectile–nucleus centre–of–mass system, spin projection s along an arbitrary quantization axis in the rest frame of the projectile, and outgoing boundary conditions [indicated by a superscript $(+)$ below], is given by [Sa83]

$$\psi^{(+)}_{\vec{k}\,s}(\vec{r}) \;=\; e^{+i\vec{k}\cdot\vec{r}}\chi_s\,. \tag{4.112}$$

The spin functions χ_s, with spin projections $s = \pm\frac{1}{2}$ along an arbitrary quantization axis in the rest frame of the projectile, are related to the usual basis spin functions (for which the

quantization axis is directed along the $+\hat{z}$–axis in the rest frame of the particle), namely

$$\begin{aligned} \chi_{s_z=\frac{1}{2}} &= \begin{pmatrix} 1 \\ 0 \end{pmatrix} \\ \chi_{s_z=-\frac{1}{2}} &= \begin{pmatrix} 0 \\ 1 \end{pmatrix} \end{aligned} \tag{4.113}$$

via the following relationship [Sa85, Va88]

$$\chi_s = \sum_{s_z} \chi_{s_z} \, D^{\frac{1}{2}}_{s_z\, s}(\alpha, \beta, \gamma) \tag{4.114}$$

where $D^{\frac{1}{2}}_{s_z\, s}(\alpha, \beta, \gamma)$ is the well–known Wigner D–function, and (α, β, γ) are the Euler rotation angles specifying the arbitrary quantization axis (relative to the $\hat{z}$–axis). Explicit expressions for the basis spin functions in the rotated coordinate system (where the $\hat{z}$–axis is rotated to an arbitrary quantization axis for which $s = \pm\frac{1}{2}$) are given by [Va88]

$$\begin{aligned} \chi_{s=\frac{1}{2}} &= \begin{pmatrix} \cos(\frac{\beta}{2})\, e^{-i\frac{(\alpha+\gamma)}{2}} \\ \\ \sin(\frac{\beta}{2})\, e^{i\frac{(\alpha-\gamma)}{2}} \end{pmatrix} \\ \chi_{s=-\frac{1}{2}} &= \begin{pmatrix} -\sin(\frac{\beta}{2})\, e^{-i\frac{(\alpha-\gamma)}{2}} \\ \\ \cos(\frac{\beta}{2})\, e^{i\frac{(\alpha+\gamma)}{2}} \end{pmatrix} . \end{aligned} \tag{4.115}$$

Consider, for example, the quantization axis directed along the $\hat{x}$–axis of a righthanded coordinate system, for which $(\alpha = 0,\ \beta = \frac{\pi}{2},\ \gamma = 0)$. Then, the expressions in Eq. (4.115) yield

$$\begin{aligned} \chi_{s=\frac{1}{2}} &= \frac{1}{\sqrt{2}} \begin{pmatrix} 1 \\ 1 \end{pmatrix} \\ \chi_{s=-\frac{1}{2}} &= \frac{1}{\sqrt{2}} \begin{pmatrix} -1 \\ 1 \end{pmatrix} . \end{aligned} \tag{4.116}$$

On the other hand, for the quantization axis directed along the $\hat{y}$–axis, with ($\alpha = \frac{\pi}{2}$, $\beta = \frac{\pi}{2}$, $\gamma = 0$), Eq. (4.115) yields

$$\begin{aligned} \chi_{s=\frac{1}{2}} &= \frac{1}{\sqrt{2}} e^{-i\frac{\pi}{4}} \begin{pmatrix} 1 \\ i \end{pmatrix} \\ \chi_{s=-\frac{1}{2}} &= e^{-i\frac{\pi}{4}} \frac{1}{\sqrt{2}} \begin{pmatrix} -1 \\ i \end{pmatrix} . \end{aligned} \tag{4.117}$$

The first step toward obtaining a partial wave expansion for Eq. (4.112), is to expand the spin–independent part of the plane–wave ($e^{i\vec{k}\cdot\vec{r}}$) in terms of the spherical harmonics $Y_{L\,M}$ as basis functions [Ne66, Sa83, Sa85], that is

$$e^{i\vec{k}\cdot\vec{r}} = \frac{4\pi}{kr} \sum_{L\,M} i^L \, u_L(kr) \, Y^*_{L\,M}(\hat{k}) \, Y_{L\,M}(\hat{r}) \tag{4.118}$$

where the radial part $u_L(kr)$ is related to the spherical Bessel function $j_L(kr)$ via

$$u_L(kr) = (kr) \, j_L(kr) \tag{4.119}$$

and $k = |\vec{k}\,|$. Substitution of Eqs. (4.118) and (4.114) into Eq. (4.112) gives

$$e^{+i\vec{k}\cdot\vec{r}} \chi_s = \frac{4\pi}{kr} \sum_{L\,M\,s_z} i^L \, u_L(kr) \, Y^*_{L\,M}(\hat{k}) \, Y_{L\,M}(\hat{r}) \, D^{\frac{1}{2}}_{s_z\,s}(\alpha,\beta,\gamma) \, \chi_{s_z} \, . \tag{4.120}$$

Next, eigenstates $|\, L\,M >$ of $\mathbf{L}^2$ and $\hat{L}_z$ are coupled with eigenstates $|\, \frac{1}{2}\, s_z >$ of $(\frac{1}{2}\boldsymbol{\sigma})^2$ and $\frac{1}{2}\sigma_z$, to construct eigenstates $|\, J\, \frac{1}{2}\, L\, \mu >$. Denoting $Y_{LM}(\hat{r})\chi_{s_z}$ by $< \hat{r}\,|L\,M\,\frac{1}{2}\,s_z >$, the unitary transformations connecting the $|\, J\, \frac{1}{2}\, L\, \mu >$ and $|L\,M\,\frac{1}{2}\,s_z >$ representations, namely [Br62]

$$|L\,\frac{1}{2}\,J\,\mu > = \sum_{M\,s_z} |L\,M\,\frac{1}{2}\,s_z >< L\,M\,\frac{1}{2}\,s_z|L\,\frac{1}{2}\,J\,\mu > \tag{4.121}$$

$$|L\,M\,\frac{1}{2}\,s_z > = \sum_{J\,(\mu)} |L\,\frac{1}{2}\,J\,\mu >< L\,\frac{1}{2}\,J\,\mu|L\,M\,\frac{1}{2}\,s_z > , \tag{4.122}$$

define the Clebsch–Gordon coefficients

$$< L\,M\,\frac{1}{2}\,s_z|L\,\frac{1}{2}\,J\,\mu > = < L\,\frac{1}{2}\,J\,\mu|L\,M\,\frac{1}{2}\,s_z > \, . \tag{4.123}$$

For brevity, one usually writes $< L\,M\,\frac{1}{2}\,s_z|J\,\mu >$ for $< L\,M\,\frac{1}{2}\,s_z|L\,\frac{1}{2}\,J\,\mu >$. The values of J are restricted by the triangular condition

$$L + \frac{1}{2} \geq J \geq |L - \frac{1}{2}|$$

where J ranges from $L+\frac{1}{2}$ down to $L-\frac{1}{2}$ in integer steps. Furthermore, since $\hat{J}_z = \hat{L}_z + \frac{1}{2}\sigma_z$, the Clebsch–Gordon coefficient vanishes for $\mu \neq M + s_z$, and hence the sum over μ in Eq. (4.122) is purely formal, and, in fact, the sum is only over J. Substitution of the righthand side of Eq. (4.122) for $Y_{LM}(\hat{r})\chi_{s_z} = < \hat{r}|L\,M\,\frac{1}{2}\,s_z >$ in Eq. (4.120), and subsequent application of Eq. (4.121), yields the following partial wave expansion for Eq. (4.112)

$$\begin{aligned} \psi^{(+)}_{\vec{k}\,s}(\vec{r}) &= e^{+i\vec{k}\cdot\vec{r}}\chi_s \\ &= \frac{4\pi}{kr}\sum_{s_z} D^{\frac{1}{2}}_{s_z\,s}(\alpha,\beta,\gamma)\sum_{L\,J\,M} i^L < L\,M\,\frac{1}{2}\,s_z|J\,\mu > \\ &\quad \times Y^*_{L\,M}(\hat{k})\,u_L(kr)\,\mathcal{Y}_{L\,J\,\mu}(\hat{r}) \end{aligned} \tag{4.124}$$

where (from the properties of Clebsch–Gordon coefficients) one sees that $\mu = M + s_z$, and the functions $\mathcal{Y}_{LJ\mu}(\hat{r})$, called the spinor spherical harmonics, defined as [Va88]

$$\begin{aligned} \mathcal{Y}_{LJ\mu}(\hat{r}) &= \sum_{s'_z\,(M')} < L\,M'\,\frac{1}{2}\,s'_z|J\,\mu > Y_{L\,M'}(\hat{r})\chi_{s'_z} \\ &= \sum_{s'_z} < L\,\mu - s'_z\,\frac{1}{2}\,s'_z|J\,\mu > Y_{L\,\mu-s'_z}(\hat{r})\chi_{s'_z}\,, \end{aligned} \tag{4.125}$$

have been constructed from the spherical harmonics (eigenfunctions of $\mathbf{L}^2$ and $\hat{L}_z$) and the basis spin functions χ_{s_z} (eigenfunctions of $(\frac{1}{2}\boldsymbol{\sigma})^2$ and $\frac{1}{2}\sigma_z$) in accordance with the coupling scheme of two angular momenta outlined above. Note that, since the spinor spherical harmonics are eigenfunctions of $\mathbf{J}^2$, $\hat{J}_z$, $\mathbf{L}^2$ and $(\frac{1}{2}\boldsymbol{\sigma})^2$, where

$$\mathbf{J}^2 = (\mathbf{L} + \frac{1}{2}\boldsymbol{\sigma})^2\,, \tag{4.126}$$

they satisfy the following eigenvalue relations:

$$\mathbf{L}^2\mathcal{Y}_{LJ\mu}(\hat{r}) = L(L+1)\,\mathcal{Y}_{LJ\mu}(\hat{r}) \tag{4.127}$$

$$\begin{aligned} \boldsymbol{\sigma}\cdot\mathbf{L}\;\mathcal{Y}_{LJ\mu}(\hat{r}) &= [\,J(J+1) - L(L+1) - \frac{3}{4}\,]\,\mathcal{Y}_{LJ\mu}(\hat{r}) \\ &= \left\{ \begin{array}{c} L\,\mathcal{Y}_{LJ\mu}(\hat{r}) \;\text{ for J = L + } \frac{1}{2} \\ \\ -(L+1)\,\mathcal{Y}_{LJ\mu}(\hat{r}) \;\text{ for J = L - } \frac{1}{2} \end{array} \right\}. \end{aligned} \tag{4.128}$$

For comparison to partial wave analyses in Refs. [Ch83, Sa83], the expression in Eq. (4.124) can be recast in the following form

$$\begin{aligned} \psi^{(+)}_{\vec{k}\,s}(\vec{r}) &= e^{+i\vec{k}\cdot\vec{r}}\chi_s \\ &= \sum_{s_z} D^{\frac{1}{2}}_{s_z\,s}(\alpha,\beta,\gamma) \sum_{s'_z} \psi^{(+)}_{s'_z\,s_z}(\vec{k},\vec{r})\chi_{s'_z} \end{aligned} \tag{4.129}$$

where

$$\begin{aligned} \psi^{(+)}_{s'_z\,s_z}(\vec{k},\vec{r}) &= \frac{4\pi}{kr}\sum_{L\,J\,M} < L\,M\,\frac{1}{2}\,s_z|J\,\mu > < L\,\mu - s'_z\,\frac{1}{2}\,s'_z|J\,\mu > \\ &\quad \times i^L\,u_L(kr)\,Y^*_{L\,M}(\hat{k})\,Y_{L\,\mu-s'_z}(\hat{r})\ . \end{aligned} \tag{4.130}$$

In addition to the plane waves with outgoing boundary conditions given by Eq. (4.129), calculations of scattering observables usually require the hermitian conjugate of a scattering wave function with incoming boundary conditions (see Sec. 4.4). The latter wave functions are now considered. Once again, the simplest case of a spin–dependent plane wave with incoming boundary conditions [indicated by the superscript $(-)$ below] is considered. The latter wave function is related to the scattering wave function in Eq. (4.129), with outgoing boundary conditions, via the following relation [Sa83, Sa85, Va88, Gr89]

$$\psi^{(-)}_{\vec{k}'\,s'}(\vec{r}) = \Theta[\,\psi^{(+)}_{\vec{k}'\,s'}(\vec{r})\,] \tag{4.131}$$

where $\vec{k}'$ is the momentum of the ejectile in the nucleon–nucleus centre–of–mass system, s' is the spin projection along an arbitrary quantization axis in the rest frame of the ejectile, and Θ is the usual time–reversal operator, defined such that [Sa83, Va88]

$$\begin{aligned} \Theta\,[\,\chi_{s'_z}\,] &= (-)^{\frac{1}{2}-s'_z}\chi_{-s'_z} \\ \Theta\,[\,D^{\frac{1}{2}}_{s_z\,s'}(\alpha,\beta,\gamma)\chi_{s'_z}\,] &= \Theta\,[\,e^{-is_z\alpha}\,d^{\frac{1}{2}}_{s_z\,s'}(\beta)\,e^{-is'\gamma}\chi_{s'_z}\,] = e^{+is_z\alpha}\,d^{\frac{1}{2}}_{s_z\,s'}(\beta)\,e^{+is'\gamma}(-)^{\frac{1}{2}-s'_z}\chi_{-s'_z} \\ \psi^{(-)}_{s'_z\,s_z}(\vec{k}',\vec{r}) &= \Theta\,[\,\psi^{(+)}_{s'_z\,s_z}(\vec{k}',\vec{r})\,] = (-)^{s_z-s'_z}\,\psi^{(+)}_{-s'_z\,-s_z}(-\vec{k}',\vec{r})^* \end{aligned} \tag{4.132}$$

where $d^{\frac{1}{2}}_{s_z\,s'}(\beta)$ is a real function, with explicit expressions given by [Va88]

$$\begin{aligned} d^{\frac{1}{2}}_{\frac{1}{2}\,\frac{1}{2}}(\beta) &= \cos(\frac{\beta}{2}) \\ d^{\frac{1}{2}}_{\frac{1}{2}\,-\frac{1}{2}}(\beta) &= -\sin(\frac{\beta}{2}) \\ d^{\frac{1}{2}}_{-\frac{1}{2}\,\frac{1}{2}}(\beta) &= \sin(\frac{\beta}{2}) \\ d^{\frac{1}{2}}_{-\frac{1}{2}\,-\frac{1}{2}}(\beta) &= \cos(\frac{\beta}{2})\ . \end{aligned} \tag{4.133}$$

Now, as already mentioned, for the calculation of scattering observables (see Sec. 4.4), one requires the hermitian conjugate of the scattering wave function with incoming boundary conditions, i.e. $\psi^{(-)\dagger}_{\vec{k}'\,s'}(\vec{r})$. With Eqs. (4.129) — (4.131), and using the relations in Eq. (4.132), one can write

$$\begin{aligned}\psi^{(-)\dagger}_{\vec{k}'\,s'}(\vec{r}) &= \{\,\Theta[\,\psi^{(+)}_{\vec{k}'\,s'}(\vec{r})\,]\,\}^{\dagger} \\ &= \sum_{s_z} D^{\frac{1}{2}}_{s_z\,s'}(\alpha',\beta',\gamma') \sum_{s'_z}(-)^{\frac{1}{2}-s'_z}\,\psi^{(-)\dagger}_{s'_z\,s_z}(\vec{k}',\vec{r})\chi^{\dagger}_{-s'_z}\end{aligned} \tag{4.134}$$

where

$$\psi^{(-)\dagger}_{s'_z\,s_z}(\vec{k}',\vec{r}) = (-)^{s_z-s'_z}\,\psi^{(+)}_{-s'_z\,-s_z}(-\vec{k}',\vec{r}) \tag{4.135}$$

and, from Eq. (4.130),

$$\begin{aligned}\psi^{(+)}_{-s'_z\,-s_z}(-\vec{k}',\vec{r}) &= \frac{4\pi}{k'r}\sum_{L\,J\,M} < L\,M\,\frac{1}{2}\,-s_z|J\,\mu >< L\,\mu+s'_z\,\frac{1}{2}\,-s'_z|J\,\mu > \\ &\quad \times i^{L}\,u_L(k'r)\,Y^{*}_{L\,M}(-\hat{k}')\,Y_{L\,\mu+s'_z}(\hat{r})\,.\end{aligned} \tag{4.136}$$

The Euler rotation angles in Eq. (4.134) are labeled with primes $'$, so as to distinguish them from the Euler angles used for wave functions with outgoing boundary conditions. Using the relation [Sa85, Va88, Si90]

$$Y_{L\,M}(-\hat{k}') = (-)^{L}\,Y_{L\,M}(\hat{k}') \tag{4.137}$$

in Eq. (4.136), gives

$$\begin{aligned}\psi^{(+)}_{-s'_z\,-s_z}(-\vec{k}',\vec{r}) &= \frac{4\pi}{k'r}\sum_{L\,J\,M} < L\,M\,\frac{1}{2}\,-s_z|J\,\mu >< L\,\mu+s'_z\,\frac{1}{2}\,-s'_z|J\,\mu > \\ &\quad \times i^{-L}\,u_L(k'r)\,Y^{*}_{L\,M}(\hat{k}')\,Y_{L\,\mu+s'_z}(\hat{r})\,.\end{aligned} \tag{4.138}$$

The partial wave expansions for the spin–dependent plane waves, with outgoing and incoming boundary conditions, given by Eq. (4.129) [with Eq. (4.130)] and Eq. (4.134) [with Eqs. (4.135) and (4.138)] respectively, are simplified considerably for the choice of projectile and ejectile reference frames in Fig. 4.1. The unprimed and primed coordinate systems are convenient for describing the kinematics and spin projections for projectile and ejectile nucleons respectively, in the incoming and outgoing nucleon–nucleus centre–of–mass frames. First, simplifications to Eqs. (4.129) and Eq. (4.130), for the choice of the initial (unprimed) reference frame in Fig. 4.1,

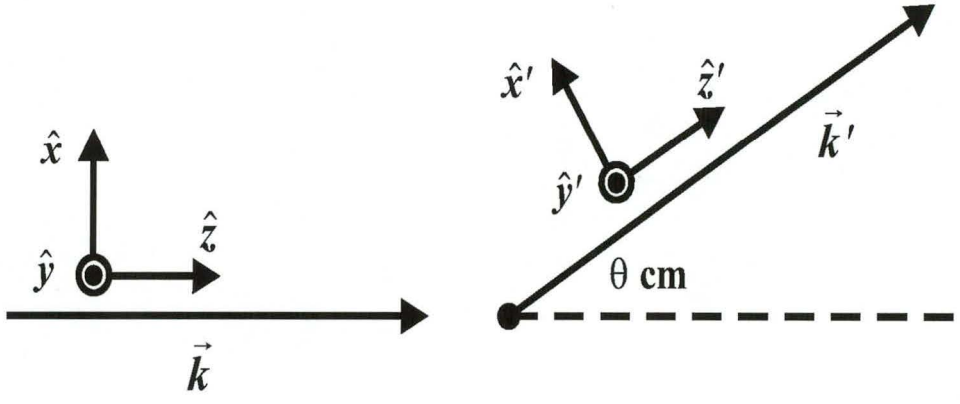

Figure 4.1: The initial (unprimed) and final (primed) nucleon–nucleus centre–of–mass reference frames used for defining the kinematics and spins of the projectile and ejectile distorted wave functions. θ_{cm} denotes the scattering angle in the nucleon–nucleus centre–of–mass frame.

are discussed. The direction of the momentum of the projectile (in the projectile–nucleus centre–of–mass system), described by a wave function with outgoing boundary conditions, is chosen along the $+\hat{z}$–axis, i.e. $\hat{k} \equiv \hat{z}$. For the latter choice, the spherical harmonics $Y^*_{LM}(\hat{k})$ become

$$Y^*_{LM}(\hat{k}) = Y_{L0}(\theta_{\hat{k}} = 0, \phi_{\hat{k}} = 0) = \sqrt{\frac{2L+1}{4\pi}}\,\delta_{M0} \tag{4.139}$$

and, since $M + s_z = \mu$ (in the Clebsch–Gordon coefficient $< L\,M\,\frac{1}{2}\,s_z|J\,\mu >$) in Eq. (4.130), the delta function δ_{M0} implies that

$$\mu = s_z\,. \tag{4.140}$$

Consequently, Eqs. (4.129) and (4.130) can be written as

$$\begin{aligned}\psi^{(+)}_{\vec{k}\,s}(\vec{r}) &= e^{+i\vec{k}\cdot\vec{r}}\chi_s \\ &= \sum_{s_z} D^{\frac{1}{2}}_{s_z\,s}(\alpha,\beta,\gamma) \sum_{s'_z} \psi^{(+)}_{s'_z\,s_z}(\vec{k},\vec{r})\chi_{s'_z}\end{aligned} \tag{4.141}$$

where

$$\begin{aligned}\psi^{(+)}_{s'_z\,s_z}(\vec{k},\vec{r}) &= \frac{4\pi}{kr}\sum_{L\,J\,M} < L\,0\,\frac{1}{2}\,s_z|J\,s_z >< L\,s_z - s'_z\,\frac{1}{2}\,s'_z|J\,s_z > \\ &\quad \times i^L\,u_L(kr)\sqrt{\frac{2L+1}{4\pi}}\,Y_{L\,s_z-s'_z}(\hat{r})\,.\end{aligned} \tag{4.142}$$

Next, simplifications to Eqs. (4.134), (4.135), and (4.138), for the choice of the outgoing (primed) reference frame in Fig. 4.1, are considered, where the momentum of the ejectile (in the ejectile–nucleus centre–of–mass system) is directed along the $+\hat{z}'$–axis , i.e. $\hat{k}' \equiv \hat{z}'$. The primed system is obtained via an anticlockwise rotation of the unprimed system through an angle of θ_{cm} around the $\hat{y}$–axis. For the latter rotation, the spherical harmonics (dependent on $\hat{k}$) in the primed coordinate system, are given by [Sa85, Va88]

$$Y^*_{LM}(\hat{k}') = \sqrt{\frac{2L+1}{4\pi}}\,P_L(\cos\theta_{cm})\,\delta_{M0} \tag{4.143}$$

where P_L denotes the well–known Legendre polynomials, and θ_{cm} is the scattering angle between the incident and outgoing momenta, $\vec{k}$ and $\vec{k}'$, in the nucleon–nucleus centre–of–mass frame. Note that, since $M + (-s_z) = \mu$ (in the Clebsch–Gordon coefficient $< L\,M\,\frac{1}{2}\,-s_z|J\,\mu >$) in Eq. (4.138), the delta function δ_{M0} implies that

$$\mu = -s_z\,. \tag{4.144}$$

Hence, Eq. (4.138), for incoming boundary conditions, can be written as

$$\psi^{(+)}_{-s'_z\,-s_z}(-\vec{k}',\vec{r}) = \frac{4\pi}{k'r}\sum_{L\,J} < L\,0\,\frac{1}{2}\,-s_z|J\,-s_z > < L\,-s_z+s'_z\,\frac{1}{2}\,-s'_z|J\,-s_z > \times i^{-L}\,u_L(k'r)\sqrt{\frac{2L+1}{4\pi}}\,P_L(\cos\theta_{cm})\,Y_{L\,-s_z+s'_z}(\hat{r})\,. \tag{4.145}$$

Substitution of the latter equation into Eqs. (4.135) and (4.134), and application of Eq. (4.114) to rotate the $+\hat{z}$ quantization axis to the $+\hat{z}'$–axis, followed by an additional rotation of the $+\hat{z}'$ quantization axis to an arbitrary direction in the primed coordinate system, yields the final expression for the hermitian conjugate of the nonrelativistic plane wave with incoming boundary conditions, namely

$$\psi^{(-)\dagger}_{\vec{k}'\,s'}(\vec{r}) = \sum_{s'_z} D^{\frac{1}{2}}_{s'_z\,s'}(\alpha',\beta',\gamma')\sum_{\sigma} D^{\frac{1}{2}}_{\sigma\,s'_z}(\alpha=0,\beta=\theta_{cm},\gamma=0) \times \sum_{\delta}(-)^{\frac{1}{2}-\delta}\,(-)^{\sigma-\delta}\,\psi^{(+)}_{-\delta\,-\sigma}(-\vec{k}',\vec{r})\,\chi^{\dagger}_{-\delta} \tag{4.146}$$

where

$$\psi^{(+)}_{-\delta\,-\sigma}(-\vec{k}',\vec{r}) = \frac{4\pi}{k'r}\sum_{L\,J} < L\,0\,\frac{1}{2}\,-\sigma|J\,-\sigma > < L\,-\sigma+\delta\,\frac{1}{2}\,-\delta|J\,-\sigma > \times i^{-L}\,u_L(k'r)\sqrt{\frac{2L+1}{4\pi}}\,P_L(\cos\theta_{cm})\,Y_{L\,-\sigma+\delta}(\hat{r})\,. \tag{4.147}$$

The Wigner D–function $D^{\frac{1}{2}}_{\sigma\,s'_z}(\alpha=0,\beta=\theta_{cm},\gamma=0)$ rotates the spin quantization axis from the $+\hat{z}$–axis to the $+\hat{z}'$–axis, which involves an anticlockwise rotation of the unprimed system through an angle of θ_{cm} around the $\hat{y}$–axis, and the Wigner D–function $D^{\frac{1}{2}}_{s'_z\,s'}(\alpha',\beta',\gamma')$ rotates the $+\hat{z}'$–axis quantization axis to any arbitrary direction, specified by the Euler angles (α',β',γ'), in the primed system. For quantization along the $\hat{x}$, $\hat{y}$ and $\hat{z}$–axes, the values of the latter Euler angles are

- $(\alpha'=0,\beta'=0,\gamma'=0)$ for quantization along the $+\hat{z}'$–axis,
- $(\alpha'=0,\beta'=\frac{\pi}{2},\gamma'=0)$ for quantization along the $+\hat{x}'$–axis,
- and, $(\alpha'=\frac{\pi}{2},\beta'=\frac{\pi}{2},\gamma'=0)$ for quantization along the $+\hat{y}'$–axis.

4.3.2 Partial wave analysis of nonrelativistic distorted wave functions

In this section, a partial wave analysis is considered for distorted wave solutions of the Schrödinger equation with central, spin–orbit and Coulomb scattering potentials. The partial wave expansions for the distorted wave functions with outgoing and incoming boundary conditions, denoted by the superscripts $(+)$ and $(-)$ respectively, are virtually identical to the corresponding plane waves discussed in Sec. 4.3.1, with the exception that [Mc68, Sa83]:

$$u_L(kr) \;=\; (kr)j_L(kr) \quad \text{is replaced by} \quad u_{LJ}(kr)e^{i\sigma_L} \tag{4.148}$$

in Eqs. (4.141) and (4.142) for outgoing boundary conditions, and Eqs. (4.146) and (4.147) for incoming boundary conditions, where σ_L denotes the usual Coulomb phase shifts [Mc68, Mu87a]. The radial wave functions $u_{L\,J}(kr)$ are solutions to the radial Schrödinger equation with central, spin–orbit and Coulomb scattering potentials, $V(r)$, $V_C(r)$ and $V_{so}(r)$ respectively, namely [Mc68]

$$\left\{ \frac{d^2}{d^2r} + k^2 - \frac{2\mu}{\hbar^2}[V(r) + V_c(r) + \frac{\hbar^2}{2}\begin{pmatrix} L \\ -L-1 \end{pmatrix} U_{so}(r)] - \frac{L(L+1)}{r^2} \right\} u_{LJ}(kr) = 0 \tag{4.149}$$

where μ is the reduced mass, and k is the incident momentum of the nucleon in the nucleon–nucleus centre–of–mass system. Note that, due to the presence of spin–orbit potentials, the radial wave functions depend on both quantum numbers L and J.

With the substitution advocated by Eq. (4.148), the partial wave expansion for a distorted wave, with outgoing boundary conditions, is given by [compare to Eqs. (4.141) and (4.142)]

$$\psi^{(+)}_{\vec{k}\,s}(\vec{r}) \;=\; \sum_{s_z} D^{\frac{1}{2}}_{s_z\,s}(\alpha,\beta,\gamma) \sum_{s'_z} \psi^{(+)}_{s'_z\,s_z}\,\chi_{s'_z}(\vec{k},\vec{r}) \tag{4.150}$$

where

$$\begin{aligned} \psi^{(+)}_{s'_z\,s_z}(\vec{k},\vec{r}) \;=\; & \frac{4\pi}{kr} \sum_{L\,J\,M} < L\,0\,\frac{1}{2}\,s_z|J\,s_z > < L\,s_z - s'_z\,\frac{1}{2}\,s'_z|J\,s_z > \\ & \times i^L\,e^{i\sigma_L}\,u_{L\,J}(kr)\sqrt{\frac{2L+1}{4\pi}}\,Y_{L\,s_z-s'_z}(\hat{r}) \end{aligned} \tag{4.151}$$

and the corresponding distorted wave, with incoming boundary conditions, is given by [compare to Eqs. (4.146) and (4.147)]

$$\psi^{(-)\dagger}_{\vec{k}'\,s'}(\vec{r}) = \sum_{s'_z} D^{\frac{1}{2}}_{s'_z\,s'}(\alpha',\beta',\gamma') \times \sum_{\sigma} D^{\frac{1}{2}}_{\sigma\,s'_z}(\alpha=0,\beta=\theta_{cm},\gamma=0) \sum_{\delta} (-)^{\frac{1}{2}-\delta}\,(-)^{\sigma-\delta}\,\psi^{(+)}_{-\delta\,-\sigma}(-\vec{k}',\vec{r})\,\chi^{\dagger}_{-\delta} \tag{4.152}$$

where

$$\psi^{(+)}_{-\delta\,-\sigma}(-\vec{k}',\vec{r}) = \frac{4\pi}{k'r}\sum_{L\,J} < L\,0\,\frac{1}{2}\,-\sigma|J\,-\sigma > < L\,-\sigma+\delta\,\frac{1}{2}\,-\delta|J\,-\sigma > \times i^{-L}\,e^{i\sigma_L}\,u_{L\,J}(k'r)\sqrt{\frac{2L+1}{4\pi}}\,P_L(\cos\theta_{cm})\,Y_{L\,-\sigma+\delta}(\hat{r})\,. \tag{4.153}$$

4.3.3 Partial wave analysis of relativistic plane waves

Based on the partial wave analysis of the nonrelativistic distorted wave functions discussed in Secs. 4.3.1 and 4.3.2, the corresponding partial wave expansions are derived for the relativistic nucleon plane waves with outgoing and incoming boundary conditions. By relativistic plane waves, one means the solutions to the Dirac equation for zero potentials, that is (see Appendix A)

$$[\boldsymbol{\alpha}\cdot\mathbf{k}+\beta m]\psi_{\vec{k}\,s}(\vec{r}) = E\,\psi_{\vec{k}\,s}(\vec{r}) \tag{4.154}$$

where $\mathbf{k}$ is the momentum operator, $\vec{k}$ is the momentum vector of the incident nucleon in the projectile–nucleus centre–of–mass system, and E is the energy of the incident nucleon in the projectile–nucleus centre–of–mass system (given by Eq. [(A.2) in Appendix A].

For outgoing boundary conditions [indicated by the superscript (+) below], the solution to the free Dirac equation in Eq. (4.154) is given by [Bj64, Se86, Gr90]

$$\psi^{(+)}_{\vec{k}\,s}(\vec{r}) = u(\vec{k},s)\,e^{+i\vec{k}\cdot\vec{r}} \tag{4.155}$$

where the free nucleon Dirac spinor

$$u(\vec{k},s) = \sqrt{\frac{E+m}{2E}}\begin{pmatrix} I \\ \\ \dfrac{\boldsymbol{\sigma}\cdot\mathbf{k}}{E+m} \end{pmatrix}\chi_s \tag{4.156}$$

where χ_s is a Pauli spinor for projection $s = \pm\frac{1}{2}$ along an arbitrary quantization axis in the rest frame of the nucleon, I is a 2×2 unit matrix, and the Dirac spinors are normalized according to Eq. (4.4). The normalization of the Dirac spinors in Eq. (4.156) corresponds to the normalization adopted in relativistic many–body calculations [Se86], and differs from the one used by Bjorken and Drell [Bj64, Gr90] (see Sec. E.6 in Appendix E). Using the partial wave expansion for $e^{+i\vec{k}\cdot\vec{r}}\chi_s$, given by Eq. (4.124), one can write down the partial wave expansion of a Dirac plane wave, with outgoing boundary conditions, as

$$\psi^{(+)}_{\vec{k}\,s}(\vec{r}) = 4\pi\sqrt{\frac{E+m}{2E}}\begin{pmatrix} I \\ \\ \dfrac{\boldsymbol{\sigma}\cdot\mathbf{k}}{E+m} \end{pmatrix}\sum_{s_z} D^{\frac{1}{2}}_{s_z\,s}(\alpha,\beta,\gamma)$$
$$\times \sum_{L\,J\,M} i^L < L\,M\,\frac{1}{2}\,s_z|J\,\mu > Y^*_{L\,M}(\hat{k})\,j_L(kr)\,\mathcal{Y}_{L\,J\,\mu}(\hat{r})\,. \qquad (4.157)$$

Note that, compared to the two–component Schrödinger plane waves, the Dirac plane waves for a nucleon, are four–component spinors. Using the operator relations given by Eqs. (A.26) and (A.27) in Appendix A, as well as the following relation for the spinor spherical harmonics (with "good" parity and total angular momentum J) [Bj64, Al73, Gr90]

$$(\boldsymbol{\sigma}\cdot\frac{\mathbf{r}}{r})\;\;\mathcal{Y}_{LJ\mu}(\hat{r}) = -\mathcal{Y}_{L'J\mu}(\hat{r}) \qquad (4.158)$$

where L' is the "other" L with the same J, defined as

$$L' = 2J - L = \left\{\begin{array}{l} L+1 \;\text{ for J = L + }\frac{1}{2} \\ \\ L-1 \;\text{ for J = L - }\frac{1}{2} \end{array}\right\}, \qquad (4.159)$$

one can derive the following relation

$$\boldsymbol{\sigma}\cdot\mathbf{k}\;\;[j_L(kr)\mathcal{Y}_{LJ\mu}(\hat{r})] = ik\left\{\begin{array}{l} (\dfrac{dj_L(x)}{dx} - L\dfrac{j_L(x)}{x})\mathcal{Y}_{L'J\mu} \;\text{ for J = L + }\dfrac{1}{2} \\ \\ (\dfrac{dj_L(x)}{dx} + (L+1)\dfrac{j_L(x)}{x})\mathcal{Y}_{L'J\mu} \;\text{ for J = L - }\dfrac{1}{2} \end{array}\right\}. \qquad (4.160)$$

where $x = kr$. Using the following recurrence relations [Ab70], for the spherical Bessel functions, in Eq. (4.160)

$$\frac{L+1}{x}j_L(x) + \frac{dj_L(x)}{dx} = j_{L-1}(x)$$

$$\frac{L}{x} j_L(x) - \frac{dj_L(x)}{dx} = j_{L+1}(x) \tag{4.161}$$

yields

$$\frac{\boldsymbol{\sigma}\cdot\mathbf{k}}{E+m}\,[j_L(kr)\mathcal{Y}_{LJ\mu}(\hat{r})] = \frac{i\,k}{E+m}\left\{\begin{array}{l} -j_{L+1}(kr) \text{ for J} = \text{L} + \frac{1}{2} \\ \\ j_{L-1}(kr) \text{ for J} = \text{L} - \frac{1}{2} \end{array}\right\}\mathcal{Y}_{L'J\mu} \tag{4.162}$$

$$= \frac{i\,k}{E+m}\,\tilde{j}_{L'}(kr)\,\mathcal{Y}_{L'J\mu} \tag{4.163}$$

where $\tilde{j}_{L'}(kr)$ is defined by the Eq. (4.162). Substitution of Eq. (4.163) into Eq. (4.157), gives the following partial wave expansion for a Dirac nucleon plane wave with outgoing boundary conditions [Ro84, Sh84, Ro87]

$$\psi^{(+)}_{\vec{k},s}(\vec{r}) = 4\pi\sqrt{\frac{E+m}{2E}}\sum_{s_z} D^{\frac{1}{2}}_{s_z\,s}(\alpha,\beta,\gamma)\sum_{L\,J\,M} i^L < L\,M\,\frac{1}{2}\,s_z|J\,\mu > Y^*_{L\,M}(\hat{k})$$
$$\times\left(\begin{array}{c} j_L(kr)\,\mathcal{Y}_{LJ\mu}(\hat{r}) \\ \\ \frac{k}{E+m}\,i\,\tilde{j}_{L'}(kr)\,\mathcal{Y}_{L'J\mu}(\hat{r}) \end{array}\right) \tag{4.164}$$

where L' is the "other" L with the same J, defined in Eq. (4.159). For comparison to relativistic partial wave expansions in Ref. [Ik95], Eq. (4.164) can be recast in the following form

$$\psi^{(+)}_{\vec{k},s}(\vec{r}) = \sqrt{\frac{E+m}{2E}}\sum_{s_z} D^{\frac{1}{2}}_{s_z\,s}(\alpha,\beta,\gamma)\sum_{s'_z}\psi^{(+)}_{s'_z\,s_z}(\vec{k},\vec{r})\,\chi_{s'_z} \tag{4.165}$$

where

$$\psi^{(+)}_{s'_z\,s_z}(\vec{k},\vec{r}) = 4\pi\sum_{L\,J\,M} i^L < L\,M\,\frac{1}{2}\,s_z|J\,\mu > Y^*_{L\,M}(\hat{k})$$
$$\times\left(\begin{array}{c} < L\,\mu - s'_z, \frac{1}{2}\,s'_z|J\,\mu > j_L(kr)\,Y_{L\,\mu-s'_z}(\hat{r})\,I \\ \\ < L'\,\mu - s'_z, \frac{1}{2}\,s'_z|J\,\mu > (\frac{k}{E+m})\,i\,\tilde{j}_{L'}(kr)\,Y_{L'\,\mu-s'_z}(\hat{r})\,I \end{array}\right) \tag{4.166}$$

and the Euler rotation angles specify the rotation from the $+\hat{z}$ quantization axis to an arbitrary quantization axis in the rest frame of the projectile, and $L' = 2J - L$.

Now, with the choice of coordinate axes in Fig. 4.1, and analogous to the discussion in Sec. 4.3.1 (except that, instead of working with two–component spinors, one now works with Dirac four–component spinors), the partial wave expansion for a Dirac plane wave, with outgoing boundary conditions, is once again given by Eq. (4.165), except that $\psi^{(+)}_{s'_z\, s_z}(\vec{k},\vec{r})$ in Eq. (4.166) now becomes

$$\psi^{(+)}_{s'_z\, s_z}(\vec{k},\vec{r}) = 4\pi \sum_{L\,J\,M} i^L \sqrt{\frac{2L+1}{4\pi}} < L\,0\,\frac{1}{2}\,s_z|J\,s_z > \times \begin{pmatrix} < L\,s_z - s'_z\,\frac{1}{2}\,s'_z|J\,s_z > \; j_L(kr)\; Y_{L\,s_z-s'_z}(\hat{r})\, I \\ \\ < L'\,s_z - s'_z\,\frac{1}{2}\,s'_z|J\,s_z > \; (\frac{k}{E+m})\; i\,\tilde{j}_{L'}(kr)\; Y_{L'\,s_z-s'_z}(\hat{r})\, I \end{pmatrix} \quad (4.167)$$

Similarly, for the ejectile reference frame in Fig. 4.1, the partial wave expansion for a Dirac plane wave, with incoming boundary conditions [indicated by a superscript $(-)$ below], is given by

$$\psi^{(-)\dagger}_{\vec{k}'\,s'}(\vec{r}) = \sqrt{\frac{E+m}{2E}} \sum_{s'_z} D^{\frac{1}{2}}_{s'_z\,s'}(\alpha',\beta',\gamma') \sum_{\sigma} D^{\frac{1}{2}}_{\sigma\,s'_z}(\alpha=0,\beta=\theta_{cm},\gamma=0) \times \sum_{\delta} (-)^{\frac{1}{2}-\delta}\,(-)^{\sigma-\delta}\,\chi^{\dagger}_{\delta}\,[\,\psi^{(+)}_{-\delta\,-\sigma}(\vec{k}',\vec{r})^*\,]^{\dagger} \quad (4.168)$$

where

$$[\,\psi^{(+)}_{-\delta\,-\sigma}(\vec{k}',\vec{r})^*\,]^{\dagger} = 4\pi \sum_{L\,J\,M} i^{-L} \sqrt{\frac{2L+1}{4\pi}} P_L(\cos\theta) < L\,0\,\frac{1}{2}\,-\sigma|J\,-\sigma > (\,\Psi_1\,,\Psi_2\,)\,,$$

$$\Psi_1 = < L\,-\sigma+\delta\,\frac{1}{2}\,-\delta|J\,-\sigma > \; j_L(k'r) Y_{L\,-\sigma+\delta}(\hat{r})\, I\,, \quad (4.169)$$

$$\Psi_2 = < L'\,-\sigma+\delta\,\frac{1}{2}\,-\delta|J\,-\sigma > \; (\frac{k}{E+m}) i\tilde{j}_{L'}(k'r) Y_{L'\,-\sigma+\delta}(\hat{r})\, I\,, \quad (4.170)$$

and θ_{cm} is the scattering angle in the nucleon–nucleus centre–of–mass system. The Wigner D–function $D^{\frac{1}{2}}_{\sigma\,s'_z}(\alpha=0,\beta=\theta_{cm},\gamma=0)$ rotates the spin quantization axis from the $+\hat{z}$–axis to the $+\hat{z}'$–axis, which involves an anticlockwise rotation of the unprimed system through an angle of θ_{cm} around the $\hat{y}$–axis, and the Wigner D–function $D^{\frac{1}{2}}_{s'_z\,s'}(\alpha',\beta',\gamma')$ rotates the $+\hat{z}'$–axis quantization axis to any arbitrary direction, specified by the Euler angles (α',β',γ'), in the primed system of the ejectile.

4.3.4 Partial wave analysis of relativistic distorted wave functions

Based on the partial wave analysis of the relativistic nucleon plane waves discussed in the previous section, partial wave expansions are now derived for relativistic distorted waves $\psi_{\vec{k}\,s}(\vec{r})$, which are solutions to the Dirac equation with nuclear scalar $S(r)$ and time–like vector potentials $V(r)$ (see Appendix A for the meaning of the terminolgy associated with the different types of relativistic potentials), as well as the usual Coulomb potential $V_c(r)$, that is

$$\{\, \boldsymbol{\alpha}\cdot\mathbf{k} + \beta m + S(r) + V(r) + V_c(r) \,\}\, \psi_{\vec{k}\,s}(\vec{r}) \;=\; E\, \psi_{\vec{k}\,s}(\vec{r}) \tag{4.171}$$

where the symbols have already been defined in Sec. 4.3.3,

Now, with the choice of coordinate axes in Fig. 4.1, and analogous to the discussions in Secs. 4.3.2 (except that, instead of working with two–component spinors, one now works with Dirac four–component spinors) and 4.3.3, the partial wave expansion for a relativistic Dirac distorted wave, with outgoing boundary conditions, is given by

$$\psi^{(+)}_{\vec{k},s}(\vec{r}) \;=\; \sqrt{\frac{E+m}{2E}} \sum_{s_z} D^{\frac{1}{2}}_{s_z\, s}(\alpha,\beta,\gamma) \sum_{s'_z} \psi^{(+)}_{s'_z\, s_z}(\vec{k},\vec{r})\, \chi_{s'_z} \tag{4.172}$$

with

$$\begin{aligned}\psi^{(+)}_{s'_z\, s_z}(\vec{k},\vec{r}) \;=\; & \frac{4\pi}{kr} \sum_{L\,J\,M} i^L\, e^{i\delta^C_{L\,J}} \sqrt{\frac{2L+1}{4\pi}} < L\,0\,\frac{1}{2}\,s_z | J\,s_z > \\ & \times \begin{pmatrix} < L\,s_z - s'_z, \tfrac{1}{2}\,s'_z | J\,s_z > \; g_{L\,J}(kr) Y_{L\,s_z - s'_z}(\hat{r})\, I \\ \\ < L'\,s_z - s'_z, \tfrac{1}{2}\,s'_z | J\,s_z > \; i\, f_{L'\,J}(kr) Y_{L'\,s_z - s'_z}(\hat{r})\, I \end{pmatrix}\end{aligned} \tag{4.173}$$

where $L' = 2J - L$, and the Euler rotation angles specify the rotation from the $+\hat{z}$ quantization axis to an arbitrary quantization axis in the rest frame of the projectile. The normalization of the relativistic distorted waves is chosen to match the Dirac plane wave (in the absence of Coulomb effects) in Eq. (4.155), and $\delta^C_{L\,J}$ is the relativistic Coulomb phase (see the next section). In the following two sections the upper and lower radial wave functions, $g_{L\,J}(kr)$ and $f_{L'\,J}(kr)$ respectively, are shown to be solutions to Schrödinger–like radial differential equations which can be solved using standard techniques.

Similarly, for the ejectile reference frame in Fig. 4.1, the partial wave expansion for a relativistic Dirac distorted wave, with incoming boundary conditions, is given by

$$\begin{aligned}\psi^{(-)\dagger}_{\vec{k}'\,s'}(\vec{r}) &= \sqrt{\frac{E+m}{2E}} \sum_{s'_z} D^{\frac{1}{2}}_{s'_z\,s'}(\alpha',\beta',\gamma') \sum_{\sigma} D^{\frac{1}{2}}_{\sigma\,s'_z}(\alpha=0,\beta=\theta_{cm},\gamma=0) \\ &\quad \times \sum_{\delta} (-)^{\frac{1}{2}-\delta}\,(-)^{\sigma-\delta}\,\chi^{\dagger}_{\delta}\,[\,\psi^{(+)}_{-\delta\,-\sigma}(\vec{k}',\vec{r})^{*}\,]^{\dagger} \qquad (4.174)\end{aligned}$$

where

$$\begin{aligned}[\,\psi^{(+)}_{-\delta\,-\sigma}(\vec{k}',\vec{r})^{*}\,]^{\dagger} &= \frac{4\pi}{k'r} \sum_{L\,J\,M} i^{-L}\,e^{i\delta^{C}_{L\,J}} \sqrt{\frac{2L+1}{4\pi}} P_{L}(\cos\theta_{cm}) \\ &\quad \times <L\,0\,\frac{1}{2}\,-\sigma|J\,-\sigma>\,(\,\Psi_1\,,\Psi_2\,)\,, \qquad (4.175)\end{aligned}$$

$$\Psi_1 = <L\,-\sigma+\delta\,\frac{1}{2}\,-\delta|J\,-\sigma>\,g_{L\,J}(k'r)Y_{L\,-\sigma+\delta}(\hat{r})\,I\,, \qquad (4.176)$$

$$\Psi_2 = <L'\,-\sigma+\delta\,\frac{1}{2}\,-\delta|J\,-\sigma>\,i\,f_{L\,J}(k'r)Y_{L'\,-\sigma+\delta}(\hat{r})\,I\,, \qquad (4.177)$$

and, θ_{cm} is the scattering angle in the nucleon–nucleus centre–of–mass system. The Wigner D–function $D^{\frac{1}{2}}_{\sigma\,s'_z}(\alpha=0,\beta=\theta_{cm},\gamma=0)$ rotates the spin quantization axis from the $+\hat{z}$–axis to the $+\hat{z}'$–axis, which involves an anticlockwise rotation of the unprimed system through an angle of θ_{cm} around the $\hat{y}$–axis, and the Wigner D–function $D^{\frac{1}{2}}_{s'_z\,s'}(\alpha',\beta',\gamma')$ rotates the $+\hat{z}'$–axis quantization axis to any arbitrary direction, specified by the Euler angles (α',β',γ'), in the primed system of the ejectile.

Next, the generation of the upper and lower radial distorted wave functions, $g_{L\,J}$ and $f_{L\,J}$ respectively, introduced in Sec. 4.3.4, is discussed. For simplicity, only the radial solutions in Eqs. (4.172) and (4.173) [for outgoing boundary conditions] are considered, for the special case where the spin of the projectile is quantized along the $+\hat{z}$–axis in Fig. 4.1, that is $\alpha = \beta = \gamma = 0$, and the Wigner D–function in Eq. (4.172) reduces to [Va88]

$$D^{\frac{1}{2}}_{s_z\,s}(\alpha=0,\beta=0,\gamma=0) = \delta_{s_z\,s}\,. \qquad (4.178)$$

With the latter simplification, Eq. (4.172) can now be written as

$$\psi^{(+)}_{\vec{k}\,s_z} = \sum_{L\,J} \begin{pmatrix} \psi^{u}_{L\,J}(\vec{r}) \\ \\ \psi^{\ell}_{L\,J}(\vec{r}) \end{pmatrix} \qquad (4.179)$$

where the upper and lower component wave functions, indicated by the superscripts u and ℓ respectively, are given by

$$\psi^u_{L\,J}(\vec{r}) = \zeta\, g_{L\,J}(kr)\, \mathcal{Y}_{LJ\mu}(\hat{r}) \tag{4.180}$$

$$\psi^\ell_{L\,J}(\vec{r}) = \zeta\, i\, f_{L'\,J}(kr)\, \mathcal{Y}_{L'J\mu}(\hat{r})\,, \tag{4.181}$$

$L' = 2J - L$ and ζ is defined as

$$\zeta = \sqrt{\frac{E+m}{2E}}\frac{4\pi}{kr} i^L e^{i\delta^C_{L\,J}} < L\,0\,\frac{1}{2}\,s_z | J\,s_z > \sqrt{\frac{2L+1}{4\pi}}\,. \tag{4.182}$$

Upper radial wave functions

The aim of this section is to show how to generate the upper component radial wave function $g_{L\,J}(kr)$ in Eq. (4.180). Following the procedure outlined in Sec. A.3 of Appendix A, one starts by defining the auxiliary wave function $\phi^u_{L\,J}(\vec{r})$, such that

$$\psi^u_{L\,J}(\vec{r}) = K(r)\, \phi^u_{L\,J}(\vec{r}) \tag{4.183}$$

$$= \zeta\, g_{L\,J}(kr)\, \mathcal{Y}_{LJ\mu}(\hat{r}) \tag{4.184}$$

where ζ is given by Eq. (4.182),

$$K(r) = \sqrt{A(r)} \tag{4.185}$$

and

$$A(r) = \frac{E + m + S(r) + V(r) - V_c(r)}{E + m}\,. \tag{4.186}$$

Substitution of Eq. (4.183) into Eq. (4.171) yields the following Schrödinger–like equation for $\phi^u_{L\,J}(\vec{r})$

$$[\mathbf{k}^2 + U_{\rm eff} + U_{\rm so}\boldsymbol{\sigma}\cdot\mathbf{L}]\phi^u_{L\,J}(\vec{r}) = (E^2 - m^2)\,\phi^u(\vec{r}) \tag{4.187}$$

where the equivalent central and spin–orbit potentials, $\mathrm{U_{eff}}(r)$ and $\mathrm{U_{so}}(r)$ respectively, are given by

$$U_{\rm eff}(r) = U_{\rm Central}(r) + U_{\rm Darwin}(r) \tag{4.188}$$

with

$$U_{\text{Central}}(r) = 2EV(r) + 2mS(r) + 2EV_c(r) - [V(r)]^2 + [S(r)]^2 - [V_c(r)]^2 - 2V_c(r)V(r)$$

$$U_{\text{Darwin}}(r) = [-\frac{1}{2r^2A}(\frac{\partial}{\partial r}(r^2\frac{\partial A}{\partial r})) + \frac{3}{4A^2}(\frac{\partial A}{\partial r})^2] \tag{4.189}$$

and

$$U_{so}(r) = -\frac{1}{2\,E\,r\,A}(\frac{\partial A}{\partial r});. \tag{4.190}$$

Recall that E is the total energy (including rest mass energy) of the projectile nucleon in the projectile–nucleus centre–of–mass system, and is given by Eq. (A.2) in Appendix A. From Eqs. (4.183), (4.184) and (4.185), one can write down the following expression for $\phi^u_{L\,J}(\vec{r})$

$$\phi^u_{L\,J}(\vec{r}) = \zeta\,\frac{g_{L\,J}(kr)}{\sqrt{A(r)}}\,\mathcal{Y}_{LJ\mu}(\hat{r})\,. \tag{4.191}$$

Substitution of the latter into Eq. (4.187), using the fact that [Va88]

$$\begin{aligned}\mathbf{k} &= \frac{\hbar}{i}\boldsymbol{\nabla}\\ \nabla^2 &= \frac{1}{r^2}\frac{\partial}{\partial r}[r^2\frac{\partial}{\partial r}] - \frac{1}{r^2}\mathbf{L}^2(\theta,\phi)\,,\end{aligned} \tag{4.192}$$

and making use of Eqs. (4.127) and (4.128), yields the following differential equation for the upper component radial wave function [Ro84] for a fixed L

$$\left\{\frac{d^2}{d^2r} + k^2 - U_{\text{eff}}(r) - \begin{pmatrix} L \\ -L-1 \end{pmatrix} U_{so}(r) - \frac{L(L+1)}{r^2}\right\}\frac{g^{\pm}_L(kr)}{\sqrt{A(r)}} = 0 \tag{4.193}$$

where $k = |\vec{k}| = \sqrt{E^2 - m^2}$ is the momentum of the projectile in the projectile–nucleus centre–of–mass system, and the + and − superscripts refer to solutions for J $= L + \frac{1}{2}$ and J $= L - \frac{1}{2}$ respectively. Note that Eq. (4.193) has the same structure as the conventional radial Schrödinger equation [compare to Eq. (4.149)]. The similarity is even greater if one ignores the quadratic Coulomb term in $U_{\text{eff}}(r)$ and also the Coulomb contributions to A(r) in Eq. (4.186). With these approximations the asymptotic Coulomb functions take on the simpler nonrelativistic forms which are far more convenient to handle numerically, and δ^C_{LJ} reduces to the usual Coulomb phase σ_L defined in Ref. [Mc68]. Rost et al. [Ro84] have shown that these approximations are very accurate for intermediate–energy proton-nucleus scattering. Note,

however, that for calculations of the distorted radial wave functions in this project, $V_c(r)$ has been included in Eq. (4.186) for $A(r)$, and $[V_c(r)]^2$ has been ignored in Eq. (4.189) for the central potential.

The outgoing boundary conditions are incorporated by specifying that the radial wave function must reduce to the incident wave $(kr)\, j_L(kr)$ when there is no interaction, and must be such that only the outgoing spherical wave is modified by the potential. These boundary conditions are satisfied in the exterior (i.e. where the nuclear potentials are negligible) by the expression

$$F_L(kr) \; + \; C_L^{\pm} \, [G_L(kr) \; + \; i \, F_L(kr)] \tag{4.194}$$

where $\mathrm{F}_L(\mathrm{kr})$ and $\mathrm{G}_L(\mathrm{kr})$ are the normal regular and irregular Coulomb wave functions, respectively, used in conventional scattering theory [Mc68].

The radial equation Eq. (4.193) is solved numerically, using a Numerov algorithm [Ko86], by integrating it from the origin (with arbitrary complex normalization) up to a matching radius R_M beyond which a potential U(r) is negligible. There is such a distance if

$$r\, U(r) \quad \longrightarrow \quad 0 \quad \text{as} \quad r \quad \longrightarrow \quad \infty \, . \tag{4.195}$$

This condition is satisfied by the short range nuclear forces, but not by the Coulomb potential. The Coulomb potential is never negligible, and serves to distort (deviate from plane wave) the wave function at infinity. Hence the inner solution $\frac{g_L^{\pm}}{\sqrt{A(r)}}$ is matched to the outer solution [Eq. (4.194) containing the Coulomb wave functions] at $r \geq R_M$:

$$D_L^{\pm} \, \frac{g_L^{\pm}(kr)}{\sqrt{A(r)}} = F_L(kr) + C_L^{\pm}[G_L(kr) + iF_L(kr)] \, , \tag{4.196}$$

where $\mathrm{D}_L^{\pm}$ and $\mathrm{C}_L^{\pm}$ represent the normalization and scattering amplitudes respectively. The coefficients $\mathrm{C}_L^{\pm}$ are usually generated by evaluating $\mathrm{g}_L^{\pm}$ at two values of the radius r, R_1 and R_2, larger than R_M. Defining

$$R_L^{\pm} = \frac{g_L^{\pm}(kR_1) \, \sqrt{A(R_2)}}{g_L^{\pm}(kR_2) \, \sqrt{A(R_1)}} \tag{4.197}$$

where R_1 and R_2 are well outside the range of the nuclear potential, it follows from Eq. (4.196) that

$$C_L^{\pm} \; = \; \frac{F_L(kR_2) \; - \; R_L^{\pm} F_L(kR_1)}{[R_L^{\pm} \, G_L(kR_1) \; - \; G_L \, (kR_2)] - i \, [F_L \, (kR_2) \; - \; R_L^{\pm} \, F_L(kR_1)]} \, . \tag{4.198}$$

Hence, the scattering amplitudes $C_L^{\pm}$'s can be determined, regardless of the normalization in Eq. (4.196). Note that Eq. (4.198) is only an approximate method for numerically matching *both* the inner wave functions *and* their derivatives to the corresponding asymptotic quantities. For computing radial wave functions and the associated Dirac distorted waves the normalization $D_L^{\pm}$ must be known. From Eq. (4.196), the normalization $D_L^{\pm}$ is given by

$$D_L^{\pm} = \left\{ \frac{\sqrt{A(r)}[F_L + C_L^{\pm}(G_L + i F_L)]}{g_L^{\pm}} \right\}_{r=R_M} . \tag{4.199}$$

Lower radial wave functions

The lower component radial wave functions $f_L^{\pm}$ can be obtained from the upper component radial wave functions $g_L^{\pm}$ via the relation [Gr90, Ro84]

$$\frac{f_L^{\pm}(kr)}{\sqrt{A(r)}} = (E + m + S - V - V_c)^{-1} \left\{ \frac{dg_L^{\pm}}{dr} + \frac{1}{r} \begin{pmatrix} -L-1 \\ L \end{pmatrix} \right\} \frac{g_L^{\pm}(kr)}{\sqrt{A(r)}} . \tag{4.200}$$

However, as pointed out in Ref. [Ro84], the functions $g_L^{\pm}$ and $f_L^{\pm}$ oscillate rapidly for large values of the orbital angular momentum L at intermediate energies and, consequently, Eq. (4.200) is numerically inconvenient to apply directly. To overcome this numerical problem, a procedure is employed which is analogous to the one followed in the previous section (for the upper radial wave functions) to derive the following radial differential equation for the lower component radial wave function, for a fixed L,

$$\left\{ \frac{d^2}{d^2r} + k^2 - \tilde{U}_{\text{eff}}(r) - \begin{pmatrix} -L-2 \\ L-1 \end{pmatrix} \tilde{U}_{\text{so}}(r) - \frac{L'(L'+1)}{r^2} \right\} \frac{f_L^{\pm}(kr)}{\sqrt{A(r)}} = 0 \tag{4.201}$$

where $\tilde{U}_{\text{eff}}(r)$ and $\tilde{U}_{\text{so}}(r)$ are functions of $A(r)$ [defined in Eq. (A.36) in Appendix A] given by

$$A(r) = \frac{E - m - S(r) - V(r) - V_c(r)}{E - m} \tag{4.202}$$

and $L' = 2J - L$.

Following a procedure analogous to the previous section (for the upper radial wave functions), and using the Coulomb function recurrence relations [Ab70], instead of those for the spherical Bessel functions in Eq. (4.161), determines the lower component matching conditions for $r \geq R_M$, namely [Ro84]

$$\tilde{D}_L^{\pm} \frac{f_L^{\pm}(kr)}{\tilde{A}_L^{\pm}} = \tilde{F}_L(kr) + C_L^{\pm}[\tilde{G}_L(kr) + i\tilde{F}_L(kr)] \tag{4.203}$$

where

$$\tilde{F}_L = \frac{k}{E+M} \left\{ \begin{array}{l} \frac{\eta}{L+1} F_L - \sqrt{1 + (\frac{\eta}{L+1})^2} F_{L+1} \quad \text{for J} = \text{L} + \frac{1}{2} \\ -\frac{\eta}{L} F_L - \sqrt{1 + (\frac{\eta}{L})^2} F_{L-1} \quad \text{for J} = \text{L} - \frac{1}{2} \end{array} \right\} \tag{4.204}$$

and, $\tilde{D}_L^{\pm}$ and $\text{C}_L^{\pm}$ represent the normalization and scattering amplitudes respectively. The parameter η is the usual Coulomb parameter given by $\eta = \frac{Ze^2E}{k}$ [Ro84]. The same equation holds for $\tilde{G}_L$ in terms of G_L and $G_{L\pm1}$. The fact that the scattering amplitudes $C_L^{\pm}$ in Eqs. (4.203) and (4.196) must be identical, provides a consistency check on the numerical accuracy of the lower component radial wave functions. Note that, as expected, Eq. (4.204) reduces to Eq. (4.163) in the limit of zero potentials.

4.3.5 Numerical accuracy of the relativistic distorted waves

The computer code HOOVER, of Horowitz and Murdock [Ho91a], was modified to generate the upper and lower component distorted waves via the methods discussed in Sec. 4.3.4. A number of stringent numerical tests were performed to check the implementation and numerical accuracy of our relativistic distorted waves. The latter wave functions will eventually serve as input for distorted wave calculations of quasielastic polarization transfer observables (see Sec. 4.4). The various numerical checks are now discussed in the following subsections.

Focusing effects of optical potentials

Partial wave studies of optical–model wave functions reveal that there is a region called the "focus" where a nucleon is most likely to be found on the side of the nucleus furthest away from the incident beam [Ei59, Mc59, Au61, Mc62, Am63, Am66, Mc68, Au70]. In classical language this focus is due to the constructive interference among two or three partial waves grazing the nuclear surface [Ei59]. The aim of this section is to attempt to reproduce the quantum mechanical focusing effects, reported by McCarthy [Mc62, Mc68] and Amos [Am66], by explicitly calculating nonrelativistic distorted wave functions at incident proton and neutron energies below 30 MeV. Exact duplication of the focusing effects will provide stringent numerical

tests for the accuracy of the following quantities in our nonrelativistic partial wave expansions discussed in Secs. 4.3.1 and 4.3.2:

- the Clebsch–Gordan coefficients,
- the Legendre polynomials $P_L(\cos\theta)$,
- the spherical harmonics $Y_{L\,M}(\cos\theta)$,
- the spinor spherical harmonics $\mathcal{Y}_{LJ\mu}(\hat{r})$,
- the partial wave summations, yielding the distorted wave functions,
- the Numerov algorithm, used for generating the radial wave functions,
- and, the Coulomb phases σ_L.

Of course, these checks will also provide confirmation of the correctness of the latter quantities in the partial wave expansions for the relativistic distorted waves discussed in Secs. 4.3.3 and 4.3.4.

The above–mentioned focusing effects are now investigated by following the procedure described in Ref. [Mc62], where the distorted wave functions are solutions of the traditional Schrödinger equation, namely

$$\{\,\frac{\hbar^2}{2\mu}\,\boldsymbol{\nabla}^2\;+\;E-\;V(r)\;-\;V_c\,\}\chi^{(+)}(\vec{r})\;=\;0 \tag{4.205}$$

where E, given by Eq. (A.2) in Appendix A, is the total energy of the projectile nucleon in the nucleon–nucleus centre–of–mass frame, μ is the reduced mass of the nucleon–nucleus system, V_c is the Coulomb potential, and $V(r)$ is the central optical potential parametrized by

$$V(r)\;=\;(V_0\;+i\,W_0)\,[\,1\;+\;e^{\frac{(r-R)}{a}}\,]^{-1} \tag{4.206}$$

where $R\;=\;r_0\;A^{\frac{1}{3}}$, and the parameters depend on the energy of the incident nucleon and the type of target nucleus. Note that there are only four parameters: the real and imaginary well depths V_0 and W_0, the radius parameter R_0 and the surface thickness parameter a.

Neglecting the spin of the incident nucleon, and making use of the following identity in Eq. (4.118) [Sa85]

$$\sum_L Y_{LM}(\hat{r})\, Y^*_{LM}(\hat{k}) \;=\; [\frac{2\,L\,+\,1}{4\,\pi}]\, P_L(\hat{k}\cdot\hat{r})\,, \tag{4.207}$$

where P_L refers to the usual Legendre polynomials, yields the following partial wave expansion for the scattering wave function $\chi^{(+)}(\vec{r})$ in Eq. (4.205), namely

$$\chi^{(+)}(\vec{r}) \;=\; \sum_{L=0}^{\infty} \psi_L(kr)\; P_L(\cos\theta) \tag{4.208}$$

where

$$\psi_L(kr) \;=\; i^L\,(2L+1)\,\frac{u_L}{kr}\,e^{i\sigma_L}\,, \tag{4.209}$$

and $u_L(kr)$ is the solution of the radial Schrödinger equation

$$\left\{\frac{d^2}{d^2r} \;+\; k^2 \;-\; \frac{2\mu}{\hbar^2}\,[V(r)+V_c(r)] \;-\; \frac{L(L+1)}{r^2}\right\} u_L(kr) \;=\; 0\,, \tag{4.210}$$

where k is the incident momentum of the nucleon in the nucleon–nucleus centre–of–mass system, and σ_L is the usual Coulomb phase shift [Mc68]. Following the methods discussed in Sec. 4.3.4 (for obtaining the upper radial wave functions), one can solve Eq. (4.210), thus yielding the radial wave function $u_L(kr)$. The radial differential equation is solved numerically using the procedure discussed in Sec. 4.3.4 (for the upper radial wave functions).

For the scattering of 30 MeV neutrons (zero Coulomb potentials and Coulomb phase shifts) and 5 MeV protons from ^{12}C, the magnitudes $|\psi_L(kr)\,|$ and phases $\phi_L(kr)$ for the most important partial waves contributing to Eq. (4.208), are calculated, where

$$\begin{aligned} \text{phase}\{\psi_L(kr)\} \;&=\; \text{phase}\{i^L\} + \text{phase}\{u_L(kr)\} && (4.211)\\ &=\; \frac{L\pi}{2} + \phi_L(kr)\,. && (4.212) \end{aligned}$$

More detail can be found in Refs. McCarthy [Mc62, Mc68]. Figs. 4.2 and 4.3 display the phase angles $\phi_L(kr)$ and the magnitudes $|\psi_L(kr)\,|$ of the first four partial waves, for the scattering of 30 MeV neutrons and 5 MeV protons from ^{12}C, respectively. The optical–model parameters used in both cases are $V_0 = -40$ MeV, $W_0 = -8$ MeV, $r_0 = 1.2$ fm and $a = 0.5$ fm. Figs. 4.2 and 4.3 are identical to Figs. 1 and 2 in Ref. [Mc62], respectively, thus confirming the correctness of our numerical approach. Next, an attempt is made to reproduce the focusing effect discussed

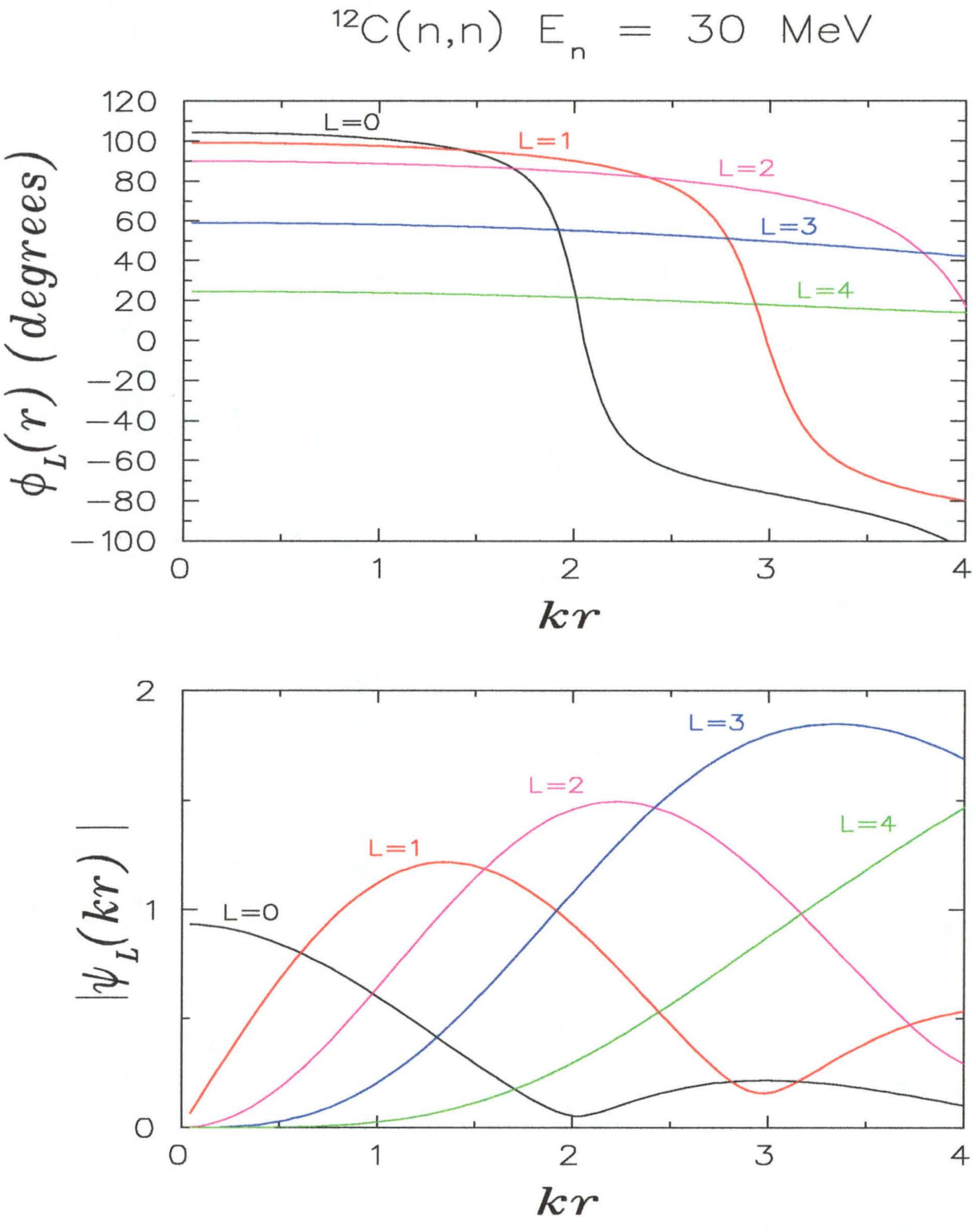

Figure 4.2: The phase angles $\phi_L(kr)$ and the magnitudes $|\psi_L(kr)|$ of the first four partial waves for the elastic scattering of 30 MeV neutrons on ^{12}C. The optical–model parameters are given in the text.

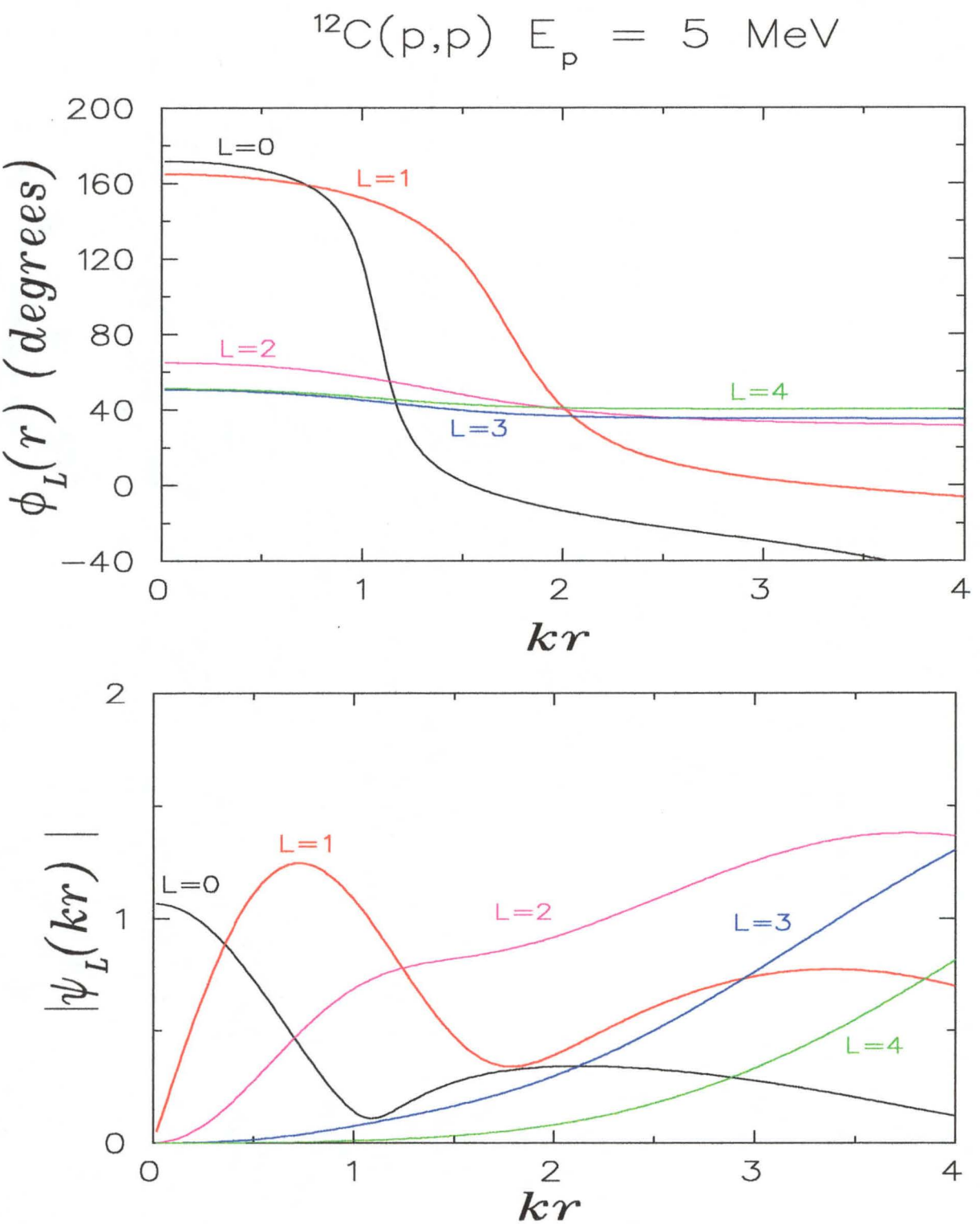

Figure 4.3: The phase angles $\phi_L(kr)$ and the magnitudes $|\psi_L(kr)|$ of the first four partial waves for the elastic scattering of 5 MeV protons on ^{12}C. The optical–model parameters are given in the text.

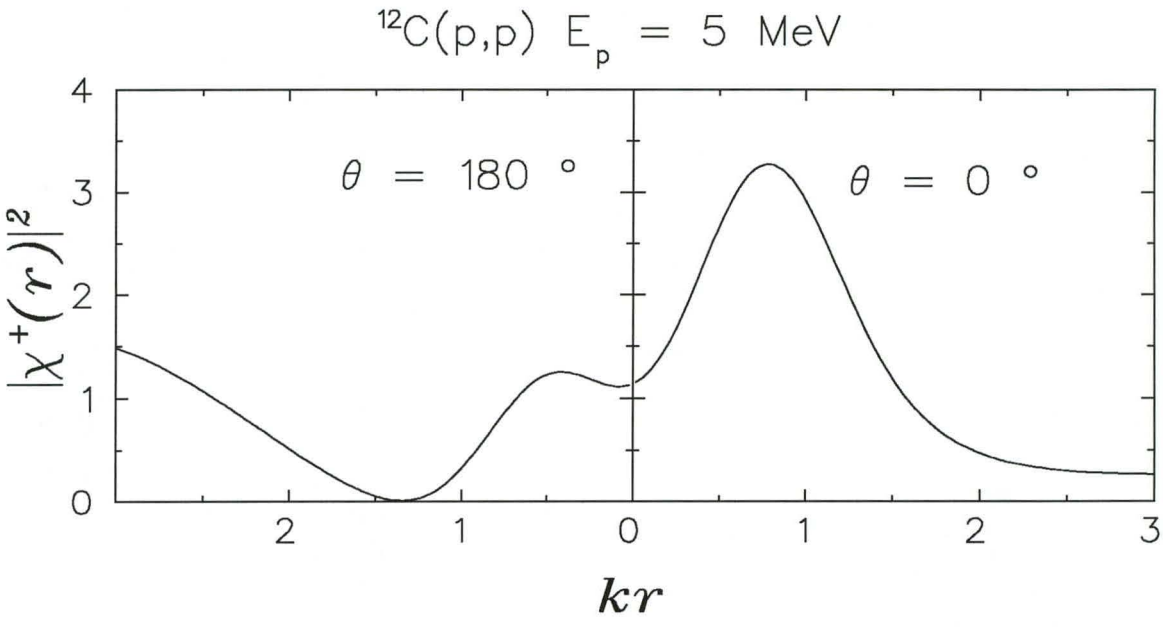

Figure 4.4: The square of the magnitude of the optical–model wave function $|\chi^{(+)}(\vec{r})|^2$, for the scattering of 5 MeV protons from ^{12}C, on the scattering axis. The optical–model parameters are given in the text.

by McCarthy in Refs. [Mc62, Mc68], by summing the first 8 partial waves for the scattering of 5 MeV protons from ^{12}C, and plotting $|\chi^{(+)}(\vec{r})|^2$ on the scattering axis defined by $\theta = 0$ (forward scattering) and $\theta = \pi$ (backward scattering) in Eq. (4.208), that is, along the trajectory of the projectile through the centre of a nucleus. The focus appears as a large peak in Fig. 4.4, and is identical to Fig. 4 in Ref. [Mc62]. Another way of displaying the focus in Fig. 4.4 is to plot $|\chi^{(+)}(\vec{r})|$ in the scattering plane for $\phi \leq \theta \leq \pi$ and $\phi = 0$ [Am66], that is, one only considers scattering in one half of the scattering plane. The focus appears as an intense spot in Fig. 4.5.

One of the most spectacular illustrations of the focusing effect of optical potentials, is observed in Figs. 4.6 and 4.7, for the scattering of 24 MeV neutrons from ^{118}Sn, where the optical–model parameters are $V_0 = -40$ MeV, $W_0 = -11$ MeV, $r_0 = 1.25$ fm and $a = 0.7$ fm. Fig. 4.6 plots the phase variation of the distorted wave function $\chi^{(+)}(\vec{r})$as a function of the impact parameter, defined as the perpendicular distance of the projectile from the scattering axis, where lines of equal phase are plotted at intervals of 100°. The result, in Fig. 4.6, is identical to Fig. 12 in Ref. [Am66]. As in Fig. 4.5, Fig. 4.7 plots the magnitude $|\chi^{(+)}(\vec{r})|$ of the distorted

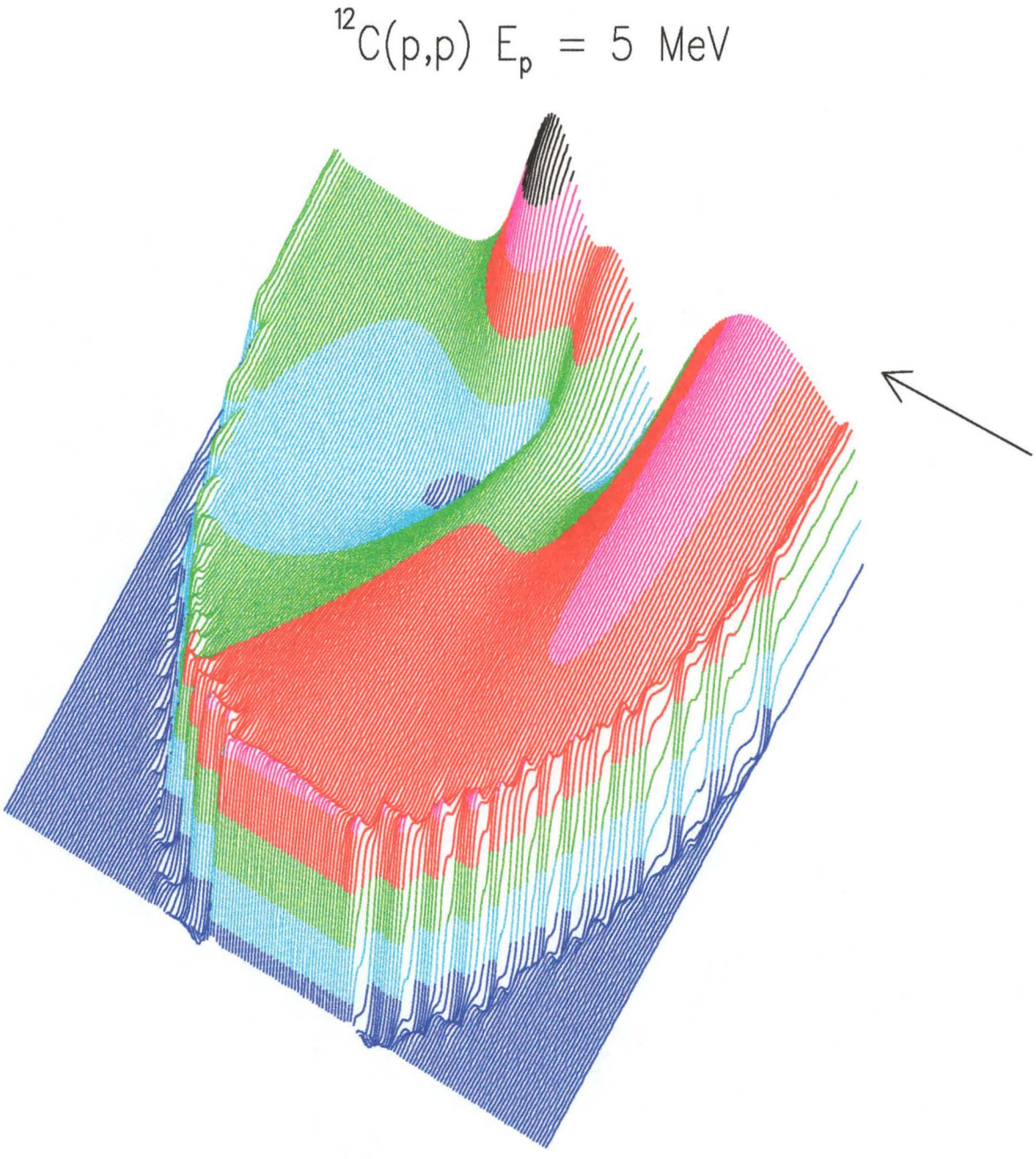

Figure 4.5: The magnitude of the optical–model wave function $|\chi^{(+)}(\vec{r})|$, for the scattering of 5 MeV protons from ^{12}C using the parameters specified in the text. The direction of the incident beam is indicated by the arrow, and the focus is indicated by the most pronounced region.

wave function, which is identical to Fig. 11 in Ref. [Am66], thus providing confidence in our numerical procedures.

Plane wave limit of relativistic distorted waves

In this section, it is checked whether the relativistic distorted waves in Eq. (4.179) reduce to the Dirac nucleon plane wave solutions in Eq. (4.164) for zero relativistic potentials in the Dirac equation given by Eq. (4.171). A free incident nucleon is considered with spin projections $s_z = \pm\frac{1}{2}$, along the $\hat{z}$ quantization axis, in the rest frame of the nucleon, for which the relativistic plane wave solutions are given by [see Eq. (E.34) in Appendix E, and also Eqs. (4.155) and (4.156)]

$$\psi^{(+)}_{\vec{k},s_z=+\frac{1}{2}}(\vec{r}) = \sqrt{\frac{E+m}{2E}} \begin{pmatrix} 1 \\ 0 \\ \dfrac{k_z}{E+m} \\ \dfrac{k_x+ik_y}{E+m} \end{pmatrix} e^{i\vec{k}\cdot\vec{r}} \tag{4.213}$$

$$\psi^{(+)}_{\vec{k},s_z=-\frac{1}{2}}(\vec{r}) = \sqrt{\frac{E+m}{2E}} \begin{pmatrix} 0 \\ 1 \\ \dfrac{k_x-k_y}{E+m} \\ \dfrac{-ik_z}{E+m} \end{pmatrix} e^{i\vec{k}\cdot\vec{r}} \tag{4.214}$$

where

$$\vec{k}\cdot\vec{r} = (kr)\,\cos\alpha \tag{4.215}$$

such that

$$\cos\alpha = \cos\theta_k\,\cos\theta_r + \sin\theta_k\,\sin\theta_r\,\cos(\phi_k-\phi_r) \tag{4.216}$$

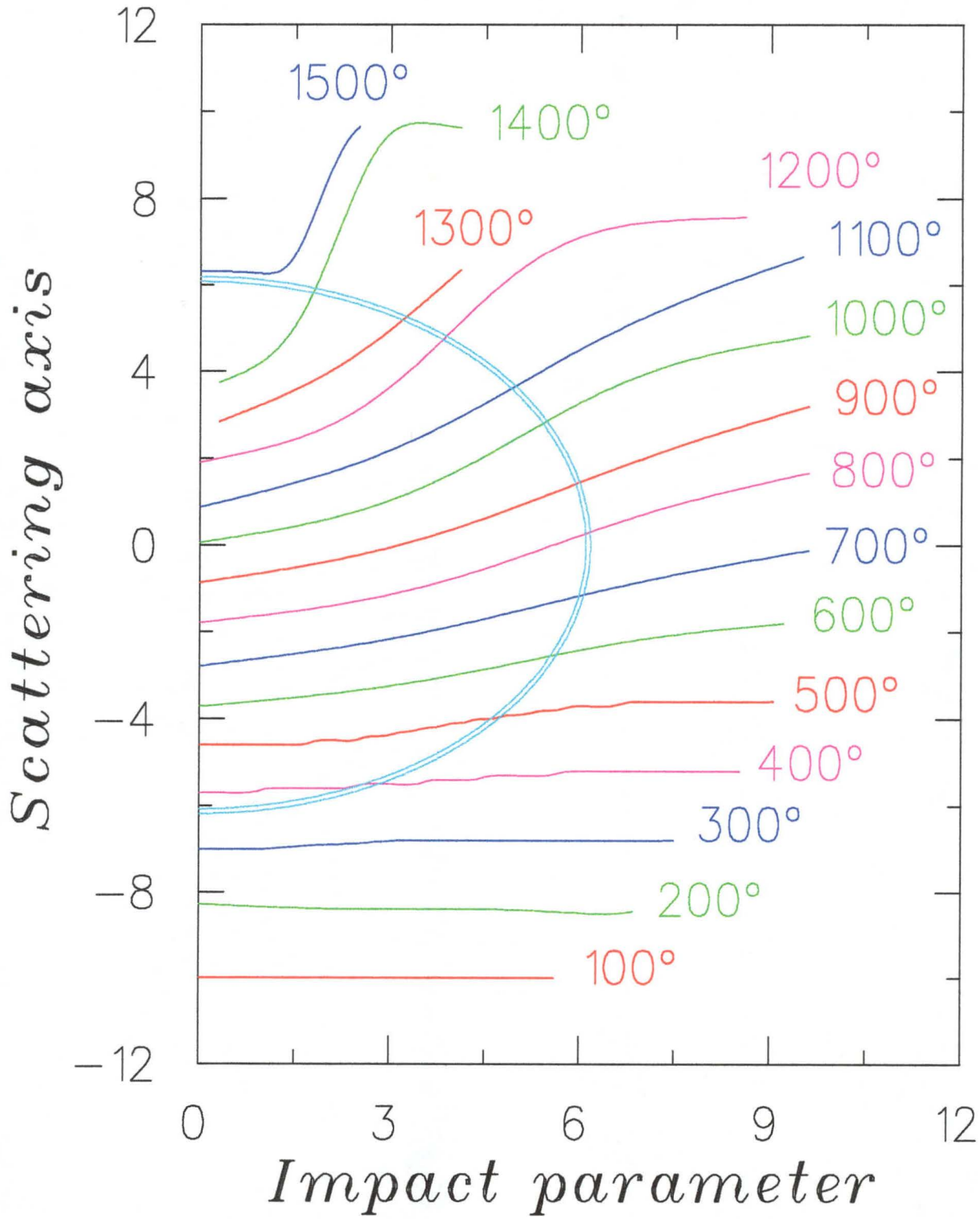

Figure 4.6: The phase variation of the optical–model wave function $\chi^{(+)}(\vec{r})$ for the scattering of 24 MeV neutrons from ^{118}Sn, using the optical–model parameters specified in the text. The incident direction is that for increasing phase value. The double line indicates the approximate radius of the ^{118}Sn nucleus.

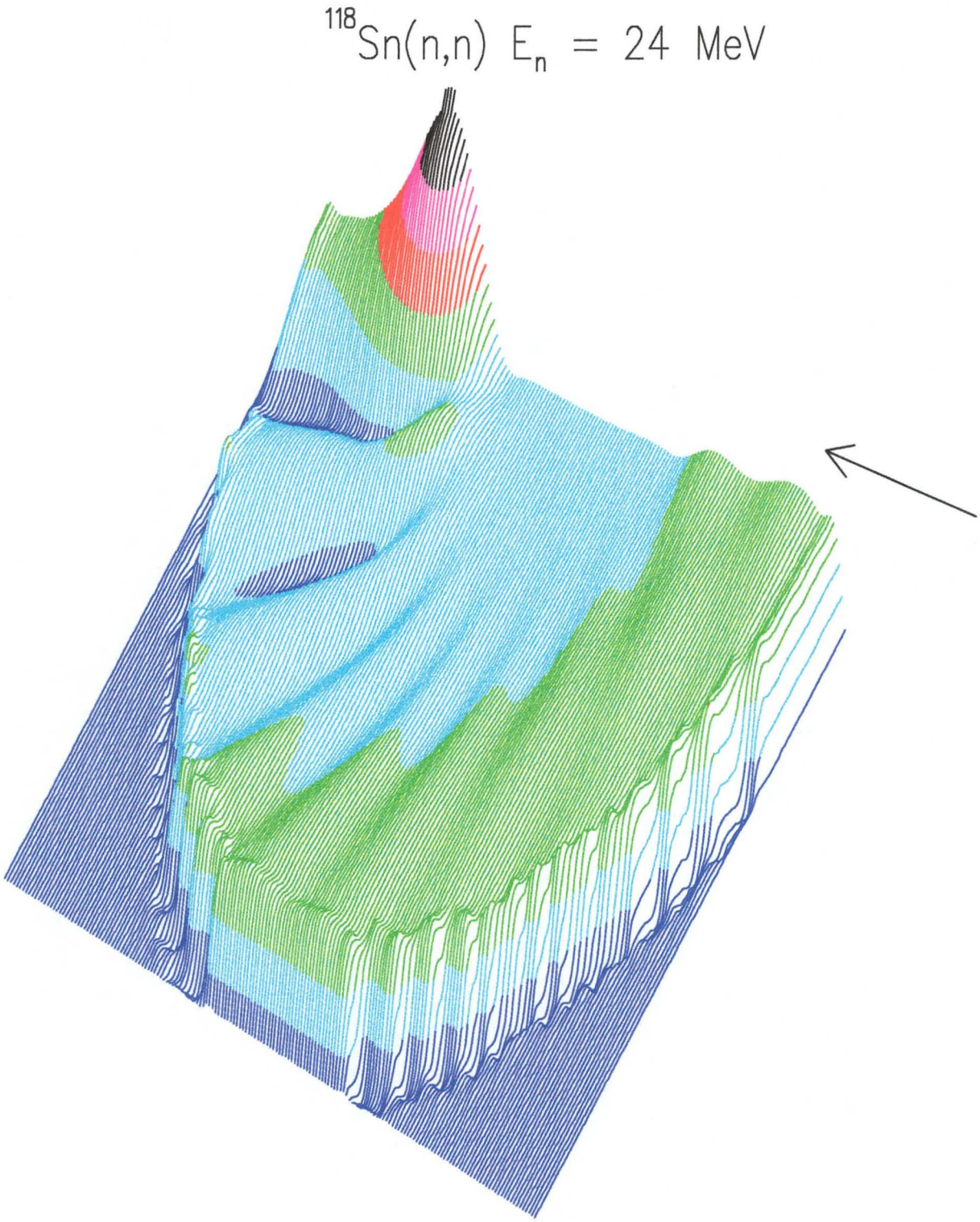

Figure 4.7: The magnitude of the optical–model wave function $|\chi^{(+)}(\vec{r})|$ for the scattering of 24 MeV neutrons from ^{118}Sn, using the parameters specified in the text. The direction of the incident beam is indicated by the arrow, and the focus is indicated by the most pronounced region.

for $(\theta_k, \phi_k) \equiv \hat{k}$ and $(\theta_r, \phi_r) \equiv \hat{r}$.

First, it has been verified numerically that Eqs. (4.213) and (4.214) are identical to Eq. (4.165) [Eq. (4.166)] for the spin–up and spin–down projections along the $\hat{z}$ quantization axis. This ensures that the partial wave summations for the upper and lower components are correct, and also that the spherical Bessel functions are correctly generated from the usual recursion relations [Ab70]. Thereafter, it has been verified numerically that Eq. (4.179) reduces to Eqs. (4.213) and (4.214) for the two different spin projections.

Scattering amplitudes

As an additional check for correctness of the upper and lower component distorted wave functions, another stringent numerical test is discussed. As already mentioned in Sec. 4.3.4, for non–zero potentials in Eqs. (4.193) and (4.201), the scattering amplitudes $C_L^{\pm}$ obtained from both the upper and lower component matching conditions in Eqs. (4.196) and (4.203) respectively, must be identical. This provides a check on the numerical accuracy of the lower component radial wave functions, as well as the associated matching conditions. To check whether the above–mentioned scattering amplitudes are equal, the elastic scattering spin observables ($\frac{d\sigma}{d\Omega}$, A_y, Q) [see Sec. G.6 in Appendix G] based on the scattering amplitudes generated from Eqs. (4.196) and (4.203) as input, are directly compared: expressions for the observables in terms of the scattering amplitudes $C_L^{\pm}$ were obtained from Refs. [Mc68, Mu87a, Ho91a].

Results are presented in Fig. 4.8 for elastic scattering of 200 MeV protons on ^{40}Ca using the microscopic Dirac optical potentials of Ref. [Mu87b, Ho91a]. The solid and dashed curves are calculated using the scattering amplitudes $C_L^{\pm}$ generated from Eqs. (4.196) and (4.203). Note that from about 50°, in the nucleon–nucleus centre–of–mass system, the spin observables differ slightly. This difference increases as the centre-of-mass scattering increases. It is found that the latter discrepancy is related to the fact that the scattering amplitudes for partial waves with orbital angular momentum larger than $L = 30$ are different for upper and lower component matchings. The latter, in turn, is related to the fact that the upper and lower relativistic radial wave functions are matched to the asymptotic *nonrelativistic* Coulomb wave functions, and also due to the fact that the scattering amplitudes were generated via the approximate matching conditions given by Eq. (4.198). Note, however, that since Rost et. al. [Ro84] were

only concerned with scattering angles smaller than 30°, the above–mentioned discrepancies did not show up in their work.

The above–mentioned shortcomings are addressed by

- matching the inner radial solutions to full relativistic Coulomb wave functions [Ro60, Gr90, Co95], instead of the usual nonrelativistic Coulomb wave functions,
- matching the inner upper radial wave functions and their derivatives to the corresponding asymptotic expressions at the matching radius R_M, instead of using the approximation advocated by Eq. (4.198), that is [Mc68]

$$\frac{(g_L^{\pm}/\sqrt{A(r)})'}{(g_L^{\pm}/\sqrt{A(r)})} = \frac{(F_L)' + C_L^{\pm}[(G_L)' + i(F_L)']}{(F_L) + C_L^{\pm}[(G_L) + i(F_L)]} \tag{4.217}$$

which yields the following expression for $C_L^{\pm}$ [instead of Eq. (4.198)]

$$C_L^{\pm} = \frac{(g_L^{\pm}/\sqrt{A(r)})\,(F_L)' - (g_L^{\pm}/\sqrt{A(r)})'\,(F_L)}{(g_L^{\pm}/\sqrt{A(r)})'(G_L) - (g_L^{\pm}/\sqrt{A(r)})(G_L)' + i[(g_L^{\pm}/\sqrt{A(r)})'(F_L) - (g_L^{\pm}/\sqrt{A(r)})(F_L)']}\,, \tag{4.218}$$

where the primed quantities indicate first order radial derivatives. An identical expression also exists for the scattering amplitudes generated from the lower component matching conditions [Ro84].

Results are presented in Fig. 4.9 for elastic scattering of 200 MeV protons on ^{40}Ca using the global Dirac optical potentials of Ref. [Ha90]. The solid and dashed curves are calculated using the scattering amplitudes $C_L^{\pm}$ generated from Eqs. (4.196) and (4.203). Note that the spin observables are identical, and don't exhibit the unphysical large–angle behaviour observed in Fig. 4.8. The latter result confirms the accuracy of the numerical procedures used for generating the relativistic upper and lower component radial wave functions.

4.4 Relativistic distorted wave impulse approximation

In this section, the **R**elativistic **D**istorted **W**ave **I**mpulse **A**pproximation (**RDWIA**) formalism, for calculating inclusive proton–nucleus inelastic polarization transfer observables, is developed.

The basic ingredients of the RPWIA are:

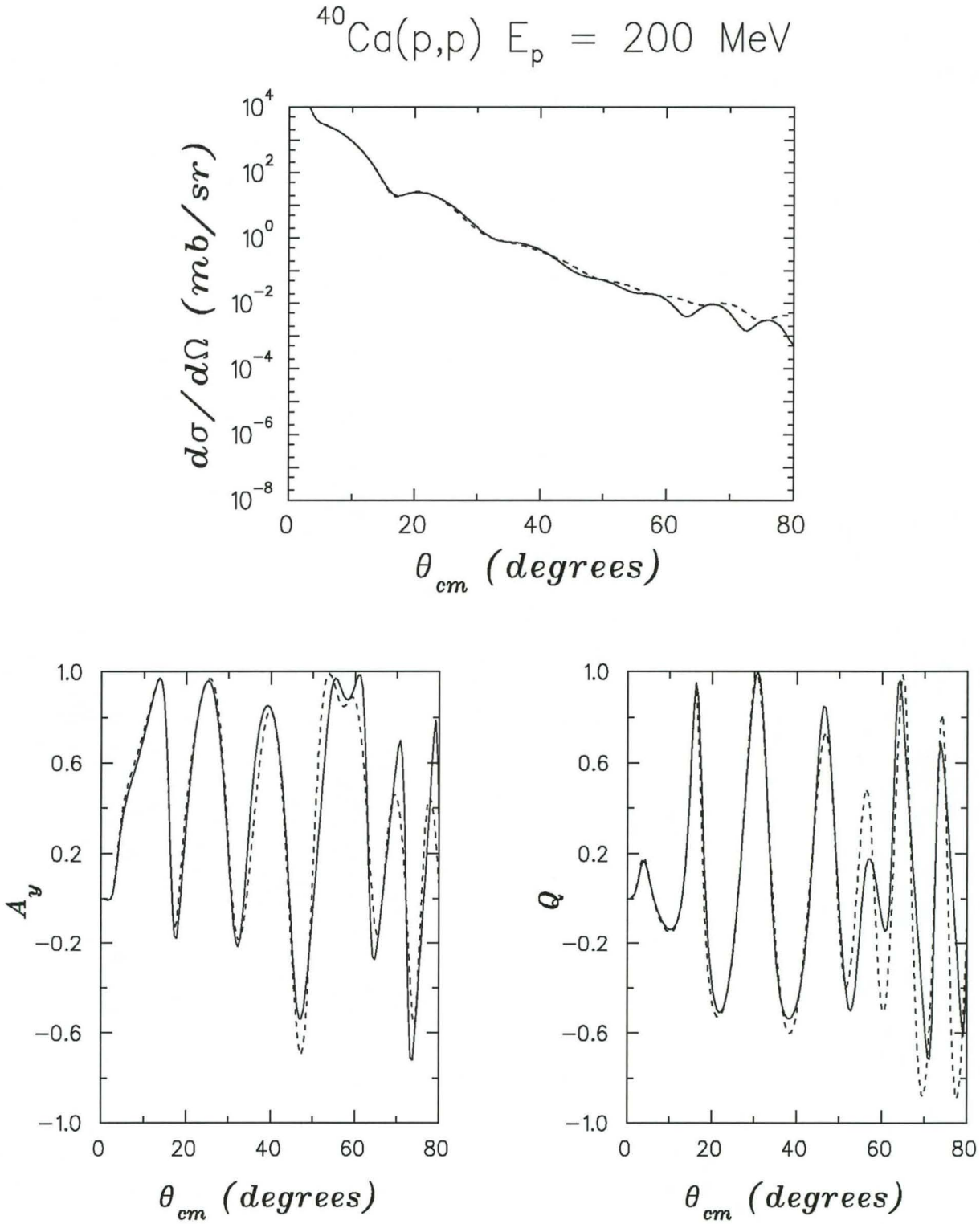

Figure 4.8: Elastic scattering spin observables [differential cross section ($\frac{d\sigma}{d\Omega}$), analyzing power (A_y) and spin rotation function (Q)] for protons scattering from ^{40}Ca at 200 MeV, calculated using the global optical potential parameters from Refs. [Mu87b,Ho91a]. The solid and dashed curves are calculated using the scattering amplitudes $C_L^{\pm}$ obtained from both the upper and lower component matching conditions in Eqs. (4.196) and (4.203) respectively.

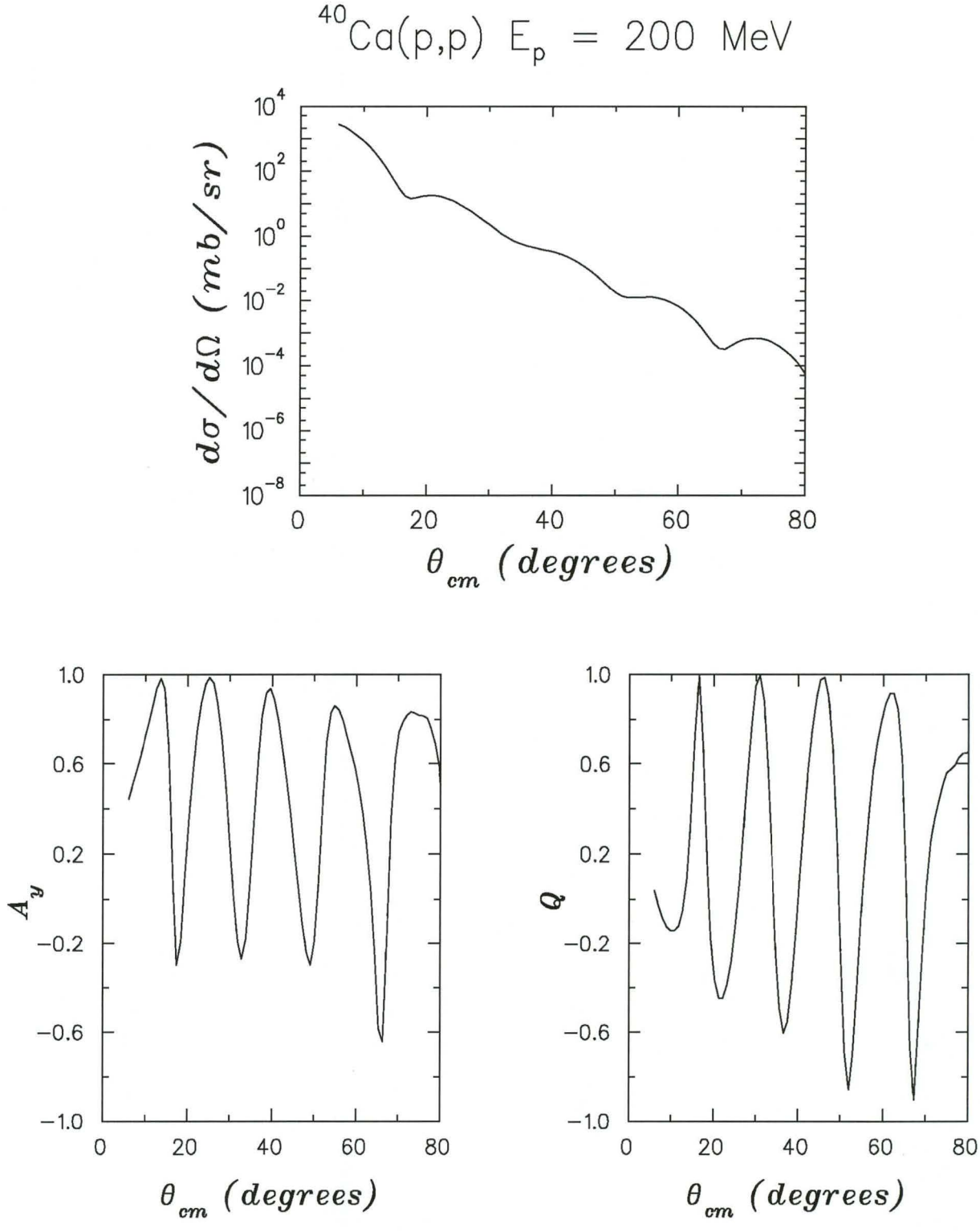

Figure 4.9: Elastic scattering spin observables [differential cross section ($\frac{d\sigma}{d\Omega}$), analyzing power (A_y) and spin rotation function (Q)], for protons scattering from ^{40}Ca at 200 MeV, calculated using the global optical potential parameters from Refs. [Ha90]. The solid and dashed curves, which are identical, are calculated using the scattering amplitudes $C_L^{\pm}$ obtained from both the upper and lower component matching conditions in Eqs. (4.196) and (4.203) respectively.

- the relativistic SVPAT NN scattering amplitudes defined in Sec. 3.2.4 of Chapter 3,
- the relativistic nuclear response functions introduced in Sec. 4.2,
- and, relativistic distorted wave functions discussed in Sec. 4.3.

Essentially, the RDWIA differs from the RPWIA developed in Chapter 3, as follows:

- the mean–field Dirac spinors for the projectile and ejectile nucleons, given by Eq. (3.55) in Chapter 3, are replaced by the relativistic projectile and ejectile distorted wave functions (discussed in Sec. 4.3.4), which are solutions to the Dirac equation with relativistic spherical scalar and time–like vector potentials. Consequently, the projectile and ejectile mean–field Dirac spinors, $U(m_1^*, \vec{k}_1, s_1)$ and $\bar{U}(m_1^*, \vec{k}_1', s_1')$ respectively, in the invariant matrix in Eq. (3.54) of Chapter 3, are replaced by the relativistic distorted waves $\psi^{(+)}_{\vec{k},s}(\vec{r})$ and $\psi^{(-)\dagger}_{\vec{k}'\,s'}(\vec{r})$, respectively: $\psi^{(+)}_{\vec{k},s}(\vec{r})$ is a relativistic distorted wave with outgoing boundary conditions [given by Eqs. (4.172) and (4.173)], and $\psi^{(-)\dagger}_{\vec{k}'\,s'}(\vec{r})$ is a relativistic distorted wave with incoming boundary conditions [given by Eqs. (4.174) – (4.177)]. Note that the RDWIA does not incorporate relativistic effects via effective masses of the projectile and ejectile nucleons. Instead, the relativistic effects are fully incorporated in the Dirac distorted waves which are solutions to the Dirac equation containing relativistic potentials.
- compared to the RPWIA formulated in momentum space, the RDWIA formalism is developed in coordinate space; this is due to the fact that the relativistic distorted waves are conventionally generated in coordinate space.
- compared to the Fermi–gas model (FGM) and mean–field approximation (MFA) descriptions of the target nucleus in the RPWIA, a general framework is developed in which the nuclear response can be treated to any level of sophistication in the RDWIA; the nuclear response is related to the nuclear polarization tensor, which can be systematically computed using well–known many–body techniques (see Sec. 4.2). For the purpose of this project, nuclear response functions, based on the relativistic free Fermi–gas model, relativistic mean field approximation, and the local density approximation, are considered. As in the RPWIA, the latter two models incorporate relativistic effects via effective masses of the target nucleons.

The RDWIA is similar to the RPWIA in that both formalisms employ the impulse approximation, that is the off–shell NN scattering matrix is replaced by the on–shell free NN scattering matrix. The impulse approximation is generally valid at energies where the mean free path of the incident nucleon is long compared to the size of the nucleus, and wavelength is short compared to the average distance between nucleons in the nucleus. This is usually the case at the intermediate bombarding energies of interest (between 100 and 500 MeV). Also recall, that the empirically observed features of quasielastic proton–nucleus scattering (see Chapter 2), suggest that the interaction be modelled via a free NN interaction, and hence, the impulse approximation should be valid.

In the following section, the RDWIA transition amplitude $T_{n0}^{s's}$ for inelastic proton–nucleus scattering is considered.

4.4.1 Relativistic transition amplitude

In order to calculate polarization transfer observables within the framework of the relativistic distorted wave impulse approximation, it is necessary to define the appropriate transition amplitude. As in Ref. [Ro87], the RDWIA transition amplitude, for proton–nucleus *inelastic scattering to discrete states*, is taken to be

$$\begin{aligned} T_{n0}^{s's} &= \sum_{j=1}^{A} \int d^4x'\, d^4y'_j\, d^4x\, d^4y_j [\bar{\psi}^{(-)}_{k's'}(x') \otimes \bar{\phi}_n(y_1, ..., y'_j, ..., y_A)] \\ &\quad \times [< x'y'_j|\widetilde{\hat{t}}|xy_j >] [\psi^{(+)}_{k\,s}(x) \otimes \phi_0(y_1, ..., y_j, ..., y_A)] \end{aligned} \tag{4.219}$$

where

- the symbol $\otimes$ indicates a kronecker (or direct) product, defined by Eq. (G.3) in Appendix G, and the products of square brackets refer to normal multiplication. In the section that follows, the symbol $\otimes$ for the kronecker–product is often omitted, although it is obviously implied throughout the discussion that follows.
- $\psi^{(+)}_{k\,s}(x)$ is the relativistic distorted wave function of the projectile proton, with outgoing boundary conditions [indicated by the superscript (+)], asymptotic incoming four momentum $k = [E_k\,, \vec{k}\,]$ in the proton–nucleus centre–of–mass system, and spin projection s along an arbitrary quantization axis in the rest frame of the projectile (see Sec. 4.3.4).

- $\bar{\psi}^{(-)}_{k'\,s'}(x') = \psi^{(-)\dagger}_{k'\,s'}(x')\gamma^0$, where $\psi^{(-)}_{k'\,s'}(x')$ is the relativistic distorted wave function of the ejectile nucleon, with incoming boundary conditions [indicated by the superscript $(-)$], asymptotic outgoing four momentum $k' = [E_{k'}\,,\,\vec{k}']$ in the nucleon–nucleus centre–of–mass system, and spin projection s' along an arbitrary quantization axis in the rest frame of the ejectile (see Sec. 4.3.4).

- $\phi_0(y_1,...,y_j,...,y_A)$ is the initial many–body ground state of the nucleus, and is a function of all A constituent target nucleons.

- $\phi_n(y_1,...,y_j,...,y_A)$ is the final many–body excited state of the nucleus, and is a function of all A constituent target nucleons.

- $\hat{t}$ is the relativistic NN interaction which drives the transition, and the tilde in $< x'y'_j|\hat{t}|xy_j >$ indicates explicit treatment of nucleon exchange, that is, the coordinate space matrix elements of $\hat{t}$ are antisymmetrized.

Introducing a complete set of four–momentum eigenstates, the transition amplitude in Eq. (4.219) can be written as

$$T^{s's}_{n0} = \sum_{j=1}^{A}\int \frac{d^4p'_0\,d^4p_0\,d^4p'_j\,d^4p_j}{(2\pi)^4(2\pi)^4(2\pi)^4(2\pi)^4} d^4x'\,d^4y'_j\,d^4x\,d^4y_j\,\bar{\psi}^{(-)}_{k'\,s'}(x')\,\bar{\phi}_n(y_1,...,y'_j,...,y_A)$$
$$\times e^{-ip'_0\cdot x'}\,e^{-ip'_j\cdot y'_j} < p'_0p'_j|\widetilde{\hat{t}}|p_0p_j > e^{ip_0\cdot x}\,e^{ip_j\cdot y_j}\,\psi^{(+)}_{k\,s}(x)\,\phi_0(y_1,...,y_j,...,y_A)\,. \quad (4.220)$$

Exploiting the harmonic time–dependence of the initial and final scattering and bound state wave functions, by assuming that they are solutions of the fixed energy Dirac equation, the time and energy integrations are readily performed, yielding

$$T^{s's}_{n0} = \sum_{j=1}^{A}\int \frac{d\vec{p}_0\,'\,d\vec{p}_0\,d\vec{p}_j\,'\,d\vec{p}_j}{(2\pi)^3(2\pi)^3(2\pi)^3(2\pi)^3} d\vec{x}\,'\,d\vec{y}_j\,'\,d\vec{x}\,d\vec{y}_j\,\bar{\psi}^{(-)}_{\vec{k}'\,s'}(\vec{x}\,')\,\bar{\phi}_n(\vec{y}_1,...,\vec{y}_j\,',...,\vec{y}_A)\,e^{i\vec{p}_0\,'\cdot\vec{x}\,'}\,e^{i\vec{p}_j\,'\cdot\vec{y}_j\,'}$$
$$\times < p'_0p'_j|\widetilde{\hat{t}}|p_0p_j > e^{-i\vec{p}_0\cdot\vec{x}}\,e^{-i\vec{p}_j\cdot\vec{y}_j}\,\psi^{(+)}_{\vec{k}\,s}(\vec{x}\,)\,\phi_0(\vec{y}_1,...,\vec{y}_j,...,\vec{y}_A)\,. \quad (4.221)$$

The impulse approximation is invoked by assuming that the off–shell NN t–operator $\hat{t}$ can be replaced by the on–shell t–operator $\hat{t}_{NN}$, which is a function of the relativistic Mandelstam invariants (see Sec. E.5.1 in Appendix E)

$$\begin{aligned} s &= p_0 + p_j &&= p_0\,' + p_j\,' \\ t &= p_0 - p_0\,' &&= p_j\,' - p_j \\ u &= p_0 - p_j\,' &&= p_0\,' - p_j\,. \end{aligned} \quad (4.222)$$

As an additional approximation, one assumes that the explicit dependence of $\hat{t}_{NN}$ on s is ignored, and $\hat{t}_{NN}$ is evaluated at a fixed value s_0, taken from the asymptotic four–momentum in some appropriate frame such as the nucleon–nucleus centre–of–mass frame, Breit frame or "optimal frame" [Sm88, Ha91, Fe92, Ic92]. The customary choice for s_0, in impulse approximation calculations, is the Breit–frame energy, but in this project nuclear recoil is ignored, so s_0 is taken to be the incident laboratory kinetic energy $T_{\rm lab}$. One also makes the approximation that, in the nonrelativistic limit, $t^2 \approx -\vec{q}\cdot\vec{q}$ [Si90], where $\vec{q}$ is the local three–momentum in the chosen reference frame, namely the nucleon–nucleus centre–of–mass system. Furthermore, for the relativistic on–shell NN amplitudes, one adopts the Horowitz–Love–Franey model, discussed in Sec. 3.2.4 of Chapter 3, for which the antisymmetrized matrix elements of the t–operator $\hat{t}_{NN}$ are given by [Mu87a]

$$\begin{aligned} < p_0' p_j' | \widetilde{\hat{t}_{NN}} | p_0 p_j > &= (2\pi)^3 \, \delta^3(\vec{p}_0\,' + \vec{p}_j\,' - \vec{p}_0 - \vec{p}_j) \\ &\quad \times \sum_\beta [\, t_\beta^D(T_{\rm lab}, |\vec{q}\,|) + t_\beta^X(T_{\rm lab}, |\vec{Q}\,|) \,] \, \lambda_\beta^{(1)} \cdot \lambda_\beta^{(2)} \end{aligned} \tag{4.223}$$

where the superscripts (1) and (2) refer to the projectile and target nucleon respectively, the i's stand for the five Dirac matrices listed in Table 3.2 (see Sec. 3.2.4 in Chapter 3), and the dot product implies that the Lorentz indices are contracted. The direct and exchange three–momenta, $\vec{q}$ and $\vec{Q}$ respectively, are given by

$$\begin{aligned} \vec{q} &= \vec{p}_0 - \vec{p}_0\,' &&= \vec{p}_j\,' - \vec{p}_j \\ \vec{Q} &= \vec{p}_0 - \vec{p}_j\,' &&= \vec{p}_0\,' - \vec{p}_j \, . \end{aligned} \tag{4.224}$$

where all quantities are defined in the nucleon–nucleus centre–of–mass system. The t_β functions are related to the usual relativistic SVPAT F_β amplitudes of the HLF model via [see Appendix F, and Eq. 3.58 in Chapter 3]

$$t_\beta^{D,X} = \frac{-8\pi i |\vec{k}_{cm}| E_{cm}}{m^2} F_\beta^{D,X} \tag{4.225}$$

where the momentum and energy of the projectile in the NN centre–of–mass system, $|\vec{k}_{cm}|$ and E_{cm} respectively, are given by (see Appendix D)

$$\begin{aligned} |\vec{k}_{cm}| &= \frac{1}{2}\sqrt{2\, T_{\rm lab}\, M} \\ E_{cm} &= \sqrt{|\vec{k}_{cm}|^2 + m^2} \, . \end{aligned} \tag{4.226}$$

Substitution of Eq. (4.223) into Eq. (4.221), and subsequent integration over $\vec{p}_j\,'$, gives

$$\begin{aligned} T_{n0}^{s's} &= \sum_{j=1}^{A}\sum_{\beta}\int d\vec{x}\,'\,d\vec{y}_j\,'\,d\vec{x}\,d\vec{y}_j\,\bar{\psi}^{(-)}_{\vec{k}'\,s'}(\vec{x}\,')\,\bar{\phi}_n(\vec{y}_1,...,\vec{y}_j\,',...,\vec{y}_A) \\ &\times\{\int \frac{d\vec{p}_0\,'\,d\vec{p}_0\,d\vec{p}_j}{(2\pi)^3(2\pi)^3(2\pi)^3(2\pi)^3} e^{i\vec{p}_0\,'\cdot\vec{x}\,'}\,e^{i(\vec{p}_0+\vec{p}_j-\vec{p}_0\,')\cdot\vec{y}_j\,'}\,[\,t_\beta^D(T_{\rm lab},|\vec{q}\,|)+t_\beta^X(T_{\rm lab},|\vec{Q}\,|)\,] \\ &\times\lambda_\beta^{(1)}\cdot\lambda_\beta^{(2)}\,e^{-i\vec{p}_0\cdot\vec{x}}\,e^{-i\vec{p}_j\cdot\vec{y}_j}\}\,\psi^{(+)}_{\vec{k}\,s}(\vec{x}\,)\,\phi_0(\vec{y}_1,...,\vec{y}_j,...,\vec{y}_A)\,. \end{aligned} \tag{4.227}$$

Making use of the following relationships [see Eq. (4.224)]

$$\begin{aligned} \vec{p}_0\,' &= \vec{p}_0 - \vec{q} \\ \vec{p}_0\,' &= \vec{p}_j + \vec{Q} \end{aligned} \tag{4.228}$$

in the first and second terms of Eq. (4.227) respectively, the $\vec{p}_0$ integrations in Eq. (4.227) are replaced by

$$\int d\vec{p}_0\,' \longrightarrow \int d\vec{q} \quad \text{and} \quad \int d\vec{p}_0\,' \longrightarrow \int d\vec{Q}\;(\,\vec{Q}\longrightarrow -\vec{Q}\,) \tag{4.229}$$

in the first and second terms respectively, thus giving

$$\begin{aligned} T_{n0}^{s's} &= \sum_{j=1}^{A}\sum_{\beta}\int d\vec{x}\,'\,d\vec{y}_j\,'\,d\vec{x}\,d\vec{y}_j\;\bar{\psi}^{(-)}_{\vec{k}'\,s'}(\vec{x}\,')\,\bar{\phi}_n(\vec{y}_1,...,\vec{y}_j\,',...,\vec{y}_A) \\ &\times\{\int \frac{d\vec{p}_0\,d\vec{p}_j\,d\vec{q}}{(2\pi)^3(2\pi)^3(2\pi)^3(2\pi)^3} e^{i(\vec{p}_0-\vec{q})\cdot\vec{x}\,'}\,e^{i(\vec{p}_j+\vec{q})\cdot\vec{y}_j\,'}\,t_\beta^D(T_{\rm lab},|\vec{q}\,|)\,e^{-i\vec{p}_0\cdot\vec{x}}\,e^{-i\vec{p}_j\cdot\vec{y}_j} \\ &\times\int \frac{d\vec{p}_0\,d\vec{p}_j\,d\vec{Q}}{(2\pi)^3(2\pi)^3(2\pi)^3(2\pi)^3} e^{i(\vec{p}_j-\vec{Q})\cdot\vec{x}\,'}\,e^{i(\vec{p}_0+\vec{Q})\cdot\vec{y}_j\,'}\,t_\beta^X(T_{\rm lab},|\vec{Q}\,|)\,e^{-i\vec{p}_0\cdot\vec{x}}\,e^{-i\vec{p}_j\cdot\vec{y}_j}\} \\ &\times\lambda_\beta^{(1)}\cdot\lambda_\beta^{(2)}\,\psi^{(+)}_{\vec{k}\,s}(\vec{x}\,)\,\phi_0(\vec{y}_1,...,\vec{y}_j,...,\vec{y}_A)\,. \end{aligned} \tag{4.230}$$

Doing the momentum integrals in Eq. (4.230) yields

$$\begin{aligned} T_{n0}^{s's} &= \sum_{j=1}^{A}\sum_{\beta}\int d\vec{x}\,'\,d\vec{y}_j\,'\,d\vec{x}\,d\vec{y}_j\,\bar{\psi}^{(-)}_{\vec{k}'\,s'}(\vec{x}\,')\,\bar{\phi}_n(\vec{y}_1,...,\vec{y}_j\,',...,\vec{y}_A)\,\{t_\beta^D(|\vec{x}\,'-\vec{y}_j\,'|)\delta^3(\vec{x}\,'-\vec{x}\,)\delta^3(\vec{y}_j\,'-\vec{y}_j)\} \\ &+\{t_\beta^X(|\vec{x}\,'-\vec{y}_j\,'|)\delta^3(\vec{y}_j\,'-\vec{x}\,)\delta^3(\vec{x}\,'-\vec{y}_j)\}\,\lambda_\beta^{(1)}\cdot\lambda_\beta^{(2)}\,\psi^{(+)}_{\vec{k}\,s}(\vec{x}\,)\,\phi_0(\vec{y}_1,...,\vec{y}_j,...,\vec{y}_A) \end{aligned} \tag{4.231}$$

where

$$\begin{aligned} t_\beta^D(|\,\vec{x}-\vec{y}\,|) &= \frac{1}{(2\pi)^3}\int d\,\vec{q}\,\,t_\beta^D(|\vec{q}\,|)\,e^{-i\vec{q}\cdot(\vec{x}-\vec{y})} \\ t_\beta^X(\,|\vec{x}-\vec{y}\,|) &= \frac{1}{(2\pi)^3}\int d\,\vec{Q}\,\,t_\beta^D(|\vec{Q}\,|)\,e^{-i\vec{Q}\cdot(\vec{x}-\vec{y})}\,. \end{aligned} \tag{4.232}$$

Performing the remaining coordinate space integrals gives

$$\begin{aligned} T_{n0}^{s's} &= \sum_{j=1}^{A}\sum_{\beta}\int d\vec{x}'\, d\vec{y}_j{}'\, \bar{\psi}^{(-)}_{\vec{k}'\,s'}(\vec{x}')\, \bar{\phi}_n(\vec{y}_1,...,\vec{y}_j{}',...,\vec{y}_A)\, \lambda_\beta^{(1)}\cdot\lambda_\beta^{(2)} \\ &\quad \{t_\beta^D(|\,\vec{x}'-\vec{y}_j{}'\,|)\, \psi^{(+)}_{\vec{k}\,s}(\vec{x}')\, \phi_0(\vec{y}_1,...,\vec{y}_j{}',...,\vec{y}_A) \\ &\quad + t_\beta^X(|\,\vec{x}'-\vec{y}_j{}'\,|)\psi^{(+)}_{\vec{k}\,s}(\vec{y}_j{}')\, \phi_0(\vec{y}_1,...,\vec{x}',...,\vec{y}_A)\}\,. \end{aligned} \tag{4.233}$$

Since $\vec{x}'$ and $\vec{y}_j{}'$ are merely integration variables, Eq. (4.233) can also be written as

$$\begin{aligned} T_{n0}^{s's} &= \sum_{j=1}^{A}\sum_{\beta}\int d\vec{x}\, d\vec{y}_j\, [\bar{\psi}^{(-)}_{\vec{k}'\,s'}(\vec{x})\otimes\bar{\phi}_n(\vec{y}_1,...,\vec{y}_j,...,\vec{y}_A)]\,[\lambda_\beta^{(1)}\otimes\lambda_\beta^{(2)}] \\ &\quad \{t_\beta^D(|\vec{x}-\vec{y}_j|)\,[\psi^{(+)}_{\vec{k}\,s}(\vec{x})\otimes\phi_0(\vec{y}_1,...,\vec{y}_j,...,\vec{y}_A)] \\ &\quad + t_\beta^X(|\vec{x}-\vec{y}_j|)\,[\psi^{(+)}_{\vec{k}\,s}(\vec{y}_j)\otimes\phi_0(\vec{y}_1,...,\vec{x},...,\vec{y}_A)]\}\,. \end{aligned} \tag{4.234}$$

The latter equation is identical to Eq. (2.3) in Ref. [Ro87]. Note that the second term in Eq. (4.234) has exchanged the labels $\vec{x}$ and $\vec{y}$, and thus treats the explicit exchange of projectile and target nucleon. Application of the following identity (twice)

$$(A\otimes B)\,(C\otimes D) \;=\; (A\,C)\otimes(B\,D) \tag{4.235}$$

to Eq. (4.234), allows one to write Eq. (4.234) as:

$$\begin{aligned} T_{n0}^{s's} &= \sum_{j=1}^{A}\sum_{\beta}\int d\vec{x}\, d\vec{y}_j \\ &\quad \{[\bar{\psi}^{(-)}_{\vec{k}'\,s'}(\vec{x})\,\lambda_\beta\,\psi^{(+)}_{\vec{k}\,s}(\vec{x})]\,[\bar{\phi}_n(\vec{y}_1,...,\vec{y}_j,...,\vec{y}_A)\lambda^\beta\,\phi_0(\vec{y}_1,...,\vec{y}_j,...,\vec{y}_A)]\,t_\beta^D(|\vec{x}-\vec{y}_j|) \\ &\quad + [\bar{\psi}^{(-)}_{\vec{k}'\,s'}(\vec{x})\,\lambda_\beta\,\psi^{(+)}_{\vec{k}\,s}(\vec{y}_j)]\,[\bar{\phi}_n(\vec{y}_1,...,\vec{y}_j,...,\vec{y}_A)\,\lambda^\beta\,\phi_0(\vec{y}_1,...,\vec{x},...,\vec{y}_A)] \\ &\quad \times t_\beta^X(|\vec{x}-\vec{y}_j|)\}\,. \end{aligned} \tag{4.236}$$

The plane–wave limit of Eq. (4.236) for free NN scattering is now investigated, for which

$$\begin{aligned} A &= 1 \\ \psi^{(+)}_{\vec{k}\,s}(\vec{x}) &= u(\vec{k},s)\, e^{-i\vec{k}\cdot\vec{x}} \\ \bar{\psi}^{(-)}_{\vec{k}'\,s'}(\vec{x}) &= \bar{u}(\vec{k}',s')\, e^{+i\vec{k}'\cdot\vec{x}} \end{aligned} \tag{4.237}$$

where the free–nucleon Dirac spinor is given by Eq. (4.156), with normalization $u^\dagger u = 1$, and all kinematic quantities are now defined in the NN centre–of–mass system. Analogous to

Eq. (4.236), the elementary free NN amplitude is now given by

$$
\begin{aligned}
t_{NN} \;=\; & \sum_{\beta} \int d\vec{x}\, d\vec{y} \\
& \{ [\bar{\psi}^{(-)}_{\vec{k}_1' s_1'}(\vec{x})\, \lambda_\beta\, \bar{\psi}^{(+)}_{\vec{k}_1 s_1}(\vec{x})]\, [\bar{\psi}^{(-)}_{\vec{k}_2' s_2'}(\vec{y})\, \lambda_\beta\, \bar{\psi}^{(+)}_{\vec{k}_2 s_2}(\vec{y})]\, t^D_\beta(|\vec{x}-\vec{y}|) \\
& + [\bar{\psi}^{(-)}_{\vec{k}_1' s_1'}(\vec{x})\, \lambda_\beta\, \bar{\psi}^{(+)}_{\vec{k}_1 s_1}(\vec{y})]\, [\bar{\psi}^{(-)}_{\vec{k}_2' s_2'}(\vec{y})\, \lambda_\beta\, \bar{\psi}^{(+)}_{\vec{k}_2 s_2}(\vec{x})]\, t^X_\beta(|\vec{x}-\vec{y}|) \} \qquad (4.238)
\end{aligned}
$$

where subscripts 1 (2) and $1'$ ($2'$) refer to the projectile (initial target nucleus) and ejectile (final target nucleus) respectively. Substitution of Eqs. (4.237) and (4.232) into Eq. (4.238), and performing the coordinate space integrals, gives

$$
t_{NN} \;=\; \sum_{\beta} [\bar{u}(\vec{k}_1', s_1')\lambda_\beta u(\vec{k}_1, s_1)]\, [t^D_\beta(|\vec{q}\,|) + t^X_\beta(|\vec{Q}\,|,]\, [\bar{u}(\vec{k}_2', s_2')\lambda^\beta u(\vec{k}_2, s_2)]\,, \qquad (4.239)
$$

which is identical to the invariant scattering matrix element $\mathcal{M}$ defined in Eq. (3.54) (with $m^* = m$) of Chapter 3. Thus, it is gratifying to see that, in the plane–wave limit of free NN scattering, our expression for the relativistic distorted wave transition amplitude for inelastic proton–nucleus scattering, given by Eq. (4.236), reduces to the well–known expression for the invariant matrix element $\mathcal{M}$, given by Eq. (3.54) in Chapter 3, for the free NN amplitude.

In the next section, expressions for complete sets of polarization transfer observables, for inclusive proton–nucleus scattering for the RDWIA model, are derived.

4.4.2 Polarized double differential cross sections

The aim of this section is to derive expressions for polarized double differential cross sections for inclusive proton–nucleus inelastic scattering for the RDWIA model: One is eventually interested in calculating polarization transfer observables which, as shown in Sec. 3.2.7 of Chapter 3, are ratios of linear combinations of polarized double differential cross sections. Following standard references [Bj64, Gr92] (see also Appendix E), and adopting the normalization procedure of Serot and Walecka [Se86] given by Eq. (4.4) for the Dirac wave functions, the differential cross section for proton–nucleus inelastic scattering is given by

$$
d\sigma_{s's} \;=\; \frac{1}{|\vec{v}-\vec{v}_0|}\, |T^{s's}_{n0}|^2\, \frac{d\vec{k}\,'}{(2\pi)^3}\, \frac{d\vec{k}_n}{(2\pi)^3}\, \delta^4(k' + k_n - k - k_0) \qquad (4.240)
$$

where

- $\vec{v}$ and $\vec{v}_0$ are the velocities of the projectile and target nucleus respectively,
- $\vec{k}$ and $\vec{k}\,'$ are three–momenta of the projectile and ejectile respectively,
- and $\vec{k}_0$ and $\vec{k}_n$ are three–momenta of the initial and final target nucleus respectively.

For inclusive proton–nucleus inelastic scattering, one must sum over final states n (where $\sum_n$ also implies integrating over final momenta $\vec{k}_n$) of the final nucleus. Following the procedure outlined in Sec. E.5.1 of Appendix E, namely, integrating over the three-momenta $\vec{k}_n$, and writing

$$d\vec{k}\,' \;=\; |\vec{k}\,'|^2\, d|\vec{k}\,'|\, d\Omega' \;=\; |\vec{k}\,'|\, E_{k'}\, dE_{k'}\, d\Omega' \,, \tag{4.241}$$

Eq. (4.240) can be rewritten as

$$d\sigma_{s's} \;=\; \frac{1}{(2\pi)^2}\frac{1}{|\,\vec{v}-\vec{v}_0\,|}\sum_n |\,T_{n0}^{s's}\,|^2\, |\vec{k}\,'|\, E_{k'}\, dE_{k'}\, d\Omega'\, \delta(E_{k'}+E_n-E_k-E_0) \tag{4.242}$$

where the E_k and $E_{k'}$ denote the projectile and ejectile nucleon energies, E_0 and E_n denote the initial and final energies of the target nucleus, and s' and s denote spin projections along quantization axes (to be specified in Sec. 4.4.4) in the rest frames of the ejectile and projectile respectively. The formula given by Eq. (4.242) is valid in any Lorentz system. However, for calculations of observables, it is necessary to choose a specific reference frame. Now since the relativistic distorted waves, discussed in Sec. 4.3, are traditionally generated in the nucleon–nucleus centre–of–mass system, one adopts the latter reference frame for explicitly calculating the polarization transfer observables. The nucleon–nucleus centre–of–mass system is defined by

$$\vec{k} \;+\; \vec{k}_0 \;=\; \vec{k}\,' \;+\; \vec{k}_n \;=\; 0\,. \tag{4.243}$$

which implies that the scattering four–momenta are given by

$$\begin{aligned} k &= (E_k,\, \vec{k}) \\ k_0 &= (E_0,\, -\vec{k}) \\ k' &= (E_{k'},\, \vec{k}\,') \\ k_n &= (E_n,\, -\vec{k}\,')\,. \end{aligned} \tag{4.244}$$

Conservation of energy is expressed by

$$\sqrt{|\vec{k}|^2+m^2}+\sqrt{|\vec{k}|^2+m_t^2} \;=\; \sqrt{|\vec{k}\,'|^2+m^2}+\sqrt{|\vec{k}\,'|^2+m_t^2}\,, \tag{4.245}$$

where m and m_t refer to the masses of the nucleon and target nucleus respectively. From Eqs. (4.244) and (4.245), one sees that

$$|\vec{k}| = |\vec{k}'| = p \quad \text{(say)}\,, \tag{4.246}$$

and hence the total energy in the proton–nucleus centre–of–mass system is given by

$$\begin{aligned} E_{cm} &= E_k + E_0 \\ &= \sqrt{p^2 + m^2} + \sqrt{p^2 + m_t^2}\,. \end{aligned} \tag{4.247}$$

Next, an expression for the flux factor $\dfrac{1}{|\vec{v} - \vec{v}_0|}$ in Eq. (4.242), in the nucleon–nucleus centre–of–mass system, is derived. One starts by writing

$$\frac{1}{|\vec{v} - \vec{v}_0|} = \frac{E_k\, E_0}{E_k\, E_0\, |\vec{v} - \vec{v}_0|} \tag{4.248}$$

where

$$E_k E_0\, |\vec{v} - \vec{v}_0| \tag{4.249}$$

is the Lorentz invariant flux factor (only in collinear frames) which, using Eqs. (4.244) and (4.246), is given by [Gr94]

$$\begin{aligned} E_k\, E_0\, |\vec{v} - \vec{v}_0| &= \sqrt{(k \cdot k_0)^2 - m^2\, m_t^2} \\ &= \sqrt{(E_k\, E_0 + p^2)^2 - (E_k^2 - p^2)(E_0^2 - p^2)} \\ &= p\, E_{cm}\,. \end{aligned} \tag{4.250}$$

Substitution of Eq. (4.248) [with Eq. (4.250)] into Eq. (4.242), yields

$$d\sigma_{s's} = \frac{1}{(2\pi)^2} \frac{E_k\, E_0}{p\, E_{cm}} \sum_n |\, T_{n0}^{s's}\,|^2\, p\, E_{k'}\, d\, E_{k'}\, d\Omega'\, \delta(E_{k'} + E_n - E_k - E_0) \tag{4.251}$$

and the resulting polarized double differential cross section, for inclusive proton–nucleus inelastic scattering, is given by

$$\left(\frac{d\sigma_{s's}}{d\Omega'\, d\, E_{k'}}\right)_{cm} = \frac{1}{(2\pi)^2} \frac{E_k E_0}{E_k + E_0} E_{k'} \sum_n |\, T_{n0}^{s's}\,|^2\, \delta(E_{k'} + E_n - E_k - E_0) \tag{4.252}$$

where the explicit expression for $T_{n0}^{s's}$, with the relativistic distorted wave impulse approximation, is given by Eq. (4.236).

4.4.3 Zero–range no–exchange approximation

In this section, additional approximations are invoked, so as to simplify the expression for the transition amplitude in Eq. (4.236). Firstly, the explicit treatment of nucleon exchange is ignored, which means that Eq. (4.236) can be written as

$$T_{n0}^{s's} = \sum_{j=1}^{A}\sum_{\beta}\int d\vec{x}\, d\vec{y}_j\, [\bar{\psi}^{(-)}_{\vec{k}'\,s'}(\vec{x})\,\lambda_\beta\,\psi^{(+)}_{\vec{k}\,s}(\vec{x})] \\ [\bar{\phi}_n(\vec{y}_1,...,\vec{y}_j,...,\vec{y}_A)\lambda^\beta\,\phi_0(\vec{y}_1,...,\vec{y}_j,...,\vec{y}_A)]\,t_\beta(|\vec{x}-\vec{y}_j|) \tag{4.253}$$

where

$$t_\beta(|\,\vec{x}-\vec{y}\,|) = \frac{1}{(2\pi)^3}\int d\,\vec{q}\,t_\beta(T_{\rm lab},|\vec{q}\,|)\,e^{-i\vec{q}\cdot(\vec{x}-\vec{y})} \tag{4.254}$$

and the t_β's are related to the relativistic SVPAT NN amplitudes via [see Eq. (4.225)]

$$t_\beta(T_{\rm lab},|\vec{q}\,|) = \frac{-8\pi i|\vec{k}_{cm}|E_{cm}}{m^2}F_\beta(T_{\rm lab},|\vec{q}\,|)\,, \tag{4.255}$$

where $T_{\rm lab}$ is the laboratory kinetic energy of the projectile, and $\vec{q}$ is the three–momentum transfer given by Eq. (4.224) in the nucleon–nucleus centre–of–mass system. Eq. (4.253) is identical to Eq. (9) in Ref. [Sh84]. An additional approximation is made by assuming that NN interaction is a zero–range interaction, that is [Ik95]

$$t_\beta(|\vec{x}-\vec{y}_j|) \approx t_\beta(T_{\rm lab},|\vec{q}\,|)\,\delta(\vec{x}-\vec{y}_j)\,. \tag{4.256}$$

Substitution of Eq. (4.256) in Eq. (4.253) yields the following expression for the transition amplitude

$$T_{n0}^{s's} = \sum_{j=1}^{A}\sum_{\beta}t_\beta(T_{\rm lab},|\vec{q}\,|)\int d\vec{y}_j\,[\bar{\psi}^{(-)}_{\vec{k}'\,s'}(\vec{y}_j)\,\lambda_\beta\,\psi^{(+)}_{\vec{k}\,s}(\vec{y}_j)] \\ [\bar{\phi}_n(\vec{y}_1,...,\vec{y}_j,...,\vec{y}_A)\lambda^\beta\,\phi_0(\vec{y}_1,...,\vec{y}_j,...,\vec{y}_A)]\,. \tag{4.257}$$

Using second quantization for the target space matrix elements, one replaces

$$[\bar{\phi}_n(\vec{y}_1,...,\vec{y}_j,...,\vec{y}_A)\lambda^\beta\,\phi_0(\vec{y}_1,...,\vec{y}_j,...,\vec{y}_A)] \tag{4.258}$$

by the second quantized form (see Sec. 4.2.1 and Appendix E),

$$[<\phi_n(\vec{y}_1,...,\vec{y}_j,...,\vec{y}_A)\,|\,\hat{\bar{\psi}}(\vec{y}_j)\,\lambda^\beta\,\hat{\psi}(\vec{y}_j)\,|\,\phi_0(\vec{y}_1,...,\vec{y}_j,...,\vec{y}_A)>] \tag{4.259}$$

where

- $|\phi_0> = |\phi_0(\vec{y}_1,...,\vec{y}_j,...,\vec{y}_A)> = \phi_0(\vec{y}_1,...,\vec{y}_j,...,\vec{y}_A)$, is the initial interacting ground state in the Heisenberg picture

- $<\phi_n| = <\phi_n(\vec{y}_1,...,\vec{y}_j,...,\vec{y}_A)| = \bar{\phi}_n(\vec{y}_1,...,\vec{y}_j,...,\vec{y}_A)$, is the excited state of the nucleus with excitation energy

$$\omega = E_n - E_0 \,, \tag{4.260}$$

- $\hat{\psi}(\vec{y}_j)$ is a nucleon field operator in the Heisenberg picture, the form of which depends on the model of the target nucleus. For example, for a Fermi–gas model, the field operator is given by Eq. (4.41), and within the mean–field approximation, the field operator is given by Eq. (4.54).

- $\hat{\bar{\psi}}(\vec{y}_j)\,\lambda^\beta\,\hat{\psi}(\vec{y}_j)$ is the nuclear current operator.

Substitution of Eqs. (4.259) and (4.257) into Eqs. (4.252) yields the following expression for the inclusive polarized double differential cross section [compare to Eq. (3.82), with Eqs. (3.70) – (3.74), in Chapter 3]

$$\begin{aligned}\left(\frac{d\sigma_{s's}}{d\Omega'\,dE_{k'}}\right)_{cm} &= K\sum_{i,j=1}^{A}\sum_{\alpha,\beta} t_\alpha(T_{\rm lab},|\vec{q}\,|)^*\,t_\beta(T_{\rm lab},|\vec{q}\,|) \\ &\quad\times\int dy_j\,dy_i\,H^{s's}_{\alpha\beta}(\vec{k},\vec{k}';\vec{y}_j,\vec{y}_i)\,S^{\alpha\beta}(\vec{y}_j,\vec{y}_i)\end{aligned} \tag{4.261}$$

where the kinematic factor K is given by

$$K = \frac{1}{(2\pi)^2}\,\frac{E_k\,E_0}{E_k + E_0}\,E_{k'}\,. \tag{4.262}$$

The projectile distorted nucleon tensor $H^{s's}_{\alpha\beta}(\vec{k},\vec{k}';\vec{y}_j,\vec{y}_i)$ is defined by [compare to Eqs. (3.71) and (3.72) in Chapter 3]

$$H^{s's}_{\alpha\beta}(\vec{k},\vec{k}';\vec{y}_j,\vec{y}_i) = [\bar{\psi}^{(-)}_{\vec{k}'\,s'}(\vec{y}_i\,)\,\lambda_\alpha\,\psi^{(+)}_{\vec{k}\,s}(\vec{y}_i\,)]^*\,[\bar{\psi}^{(-)}_{\vec{k}'\,s'}(\vec{y}_j\,)\,\lambda_\beta\,\psi^{(+)}_{\vec{k}\,s}(\vec{y}_j\,)] \tag{4.263}$$

where $\psi^{(+)}_{\vec{k}\,s}(\vec{y}_i\,)$ is the relativistic distorted wave function of the projectile proton, with outgoing boundary conditions, given by Eqs. (4.172) and (4.173) [with $\delta^C_{L\,J}$ replaced by σ_L], and $\bar{\psi}^{(-)}_{\vec{k}'\,s'}(\vec{y}_i\,) = \psi^{(-)\dagger}_{\vec{k}'\,s'}(\vec{y}_i\,)\gamma^0$, where $\psi^{(-)\dagger}_{\vec{k}'\,s'}(\vec{y}_i\,)$ is the hermitian conjugate of the relativistic distorted wave function of the ejectile nucleon, with incoming boundary conditions, given by Eqs. (4.174) –

(4.177) [with δ^C_{LJ} replaced by σ_L]. The spin–independent nuclear response $S^{\alpha\beta}(\vec{y}_i, \vec{y}_j)$ is defined as [compare to Eqs. (3.73) and (3.74) in Chapter 3]

$$S^{\alpha\beta}(\vec{y}_i, \vec{y}_j) = \int \frac{d\vec{q}}{(2\pi)^3} e^{-i\vec{q}\cdot\vec{y}_i} \frac{d\vec{q}'}{(2\pi)^3} e^{+i\vec{q}'\cdot\vec{y}_j} S^{\alpha\beta}(\vec{q}, \vec{q}'; \omega) \tag{4.264}$$

where

$$S^{\alpha\beta}(\vec{q}, \vec{q}'; \omega) = \sum_n [J^\alpha_{n0}(\vec{q})]^* J^\beta_{n0}(\vec{q}') \, \delta[\omega - (E_n - E_0)] \tag{4.265}$$

(*Note that the summation* $\sum_n$ *in Eq. (4.265) contains the summation over final spins, thus yielding a spin–independent quantity*) with

$$J^\alpha_{n0}(\vec{q}) = \int d\vec{y}_i < \phi_n \mid \hat{J}^\alpha_H \mid \phi_0 > \tag{4.266}$$

where the nuclear current operator is given by

$$\hat{J}^\alpha_H = \hat{\bar{\psi}}(\vec{x}) \lambda^\alpha \psi(\vec{x}) \tag{4.267}$$

and the subscript "H" refers to the fact that the field operators $\hat{\psi}(\vec{x})$ are defined in the Heisenberg picture. Comparison of Eq. (4.265) with Eq. (4.79) enables one to identify the nuclear response $S^{\alpha\beta}(\vec{q}, \vec{q}'; \omega)$ with the imaginary part of the nuclear polarization tensor $\Pi^{\alpha\beta}(\vec{q}, \vec{q}'; \omega)$ defined in Sec. 4.2.3, namely

$$S^{\alpha\beta}(\vec{q}, \vec{q}' \, ; \omega) = -\frac{1}{\pi} \mathrm{Im} [\Pi^{\alpha\beta}(\vec{q}, \vec{q}' \, ; \omega)] \, . \tag{4.268}$$

As stressed in Sec. 4.2.1, the advantage of expressing the nuclear response in terms of the nuclear polarization tensor, is that the latter can be computed using well–known many–body techniques. As an improvement of the relativistic mean–field treatment of the nuclear response in Chapter 3, one adopts a local density approximation (LDA), as discussed in Secs. 4.2.2 and 4.2.3, which corresponds to taking

$$\Pi^{\alpha\beta}_{LDA}(\vec{y}_j, \vec{y}_i \, ; \omega) = \int \frac{d\tilde{q}}{(2\pi)^3} e^{i\tilde{q}\cdot(\vec{y}_i - \vec{y}_j)} \Pi^{\alpha\beta}_{LDA}[\tilde{q}, \omega \, ; \, k_F(|\frac{\vec{y}_i + \vec{y}_j}{2}|), M^*(|\frac{\vec{y}_i + \vec{y}_j}{2}|)] \tag{4.269}$$

where $\Pi^{\mu\nu}_{LDA}(\vec{y}_j, \vec{y}_i \, ' \, ; \omega)$, given by Eq. (4.68) for electromagnetic electron scattering, is generalized to $\Pi^{\alpha\beta}_{LDA}(\vec{y}_j, \vec{y}_i \, ' \, ; \omega)$ for nuclear proton scattering, for which λ^α is given by Eq. (4.72).

For inclusive $(\vec{p},\vec{p}\,')$ scattering, the polarized double differential cross section in Eq. (4.261) is written as (see Sec. 3.2.8 in Chapter 3)

$$\begin{aligned}\left(\frac{d\sigma_{s's}}{d\Omega'\,dE_{k'}}\right)_{cm} &= K\,[\sum_{i,j=1}^{Z}\sum_{\alpha,\beta} t_\alpha^{pp}(T_{\rm lab},|\vec{q}\,|)^*\; t_\beta^{pp}(T_{\rm lab},|\vec{q}\,|) \\ &\quad + \sum_{i,j=1}^{N}\sum_{\alpha,\beta} t_\alpha^{pn}(T_{\rm lab},|\vec{q}\,|)^*\; t_\beta^{pn}(T_{\rm lab},|\vec{q}\,|)\,] \\ &\quad \times \int d\,y_j\; d\,y_i\; H_{\alpha\beta}^{s's}(\vec{k},\vec{k}';\vec{y}_j,\vec{y}_i)\; S^{\alpha\,\beta}(\vec{y}_j,\vec{y}_i)\;, \end{aligned} \tag{4.270}$$

where t_β^{pp} and t_β^{pn} are related to $F_\beta(pp)$ and $F_\beta(pn)$ in Eqs. (3.50) and (3.51) in Chapter 3, respectively, via Eq. (4.225).

For inclusive $(\vec{p},\vec{n})$ scattering, on the other hand, the relativistic SVPAT NN amplitudes t_β in Eq. (4.261), are replaced by (see Sec. 3.2.8 in Chapter 3)

$$t_\beta^{pp}(T_{\rm lab},|\vec{q}\,|) \;-\; t_\beta^{pn}(T_{\rm lab},|\vec{q}\,|) \tag{4.271}$$

where t_β^{pp} and t_β^{pn} are related to $F_\beta(pp)$ and $F_\beta(pn)$ in Eqs. (3.50) and (3.51) in Chapter 3, respectively, via Eq. (4.225). In addition, for inclusive $(\vec{p},\vec{n})$ scattering, the relativistic distorted waves for the ejectile neutron are generated with $V_c(r) = 0$ and $\sigma_L = 0$ in the relevant expressions.

4.4.4 Polarization transfer observables

With the polarized double differential cross sections given by Eq. (4.261), one is now in a position to write down expressions for the quasielastic polarization transfer observables for the RDWIA model.

The general formula for the polarization transfer observables, $D_{i'j}$, namely $\mathrm{A}_y = \mathrm{D}_{0'n}$, D_{nn}, $\mathrm{D}_{s's}$, $\mathrm{D}_{\ell'\ell}$, $\mathrm{D}_{s'\ell}$ and $\mathrm{D}_{\ell's}$, is given by (See Appendix G, and also Sec. 3.2.7 in Chapter 3)

$$D_{i'j} = \frac{\frac{d\sigma}{d\Omega' dE_{k'}}(\hat{j}\to\hat{i}') - \frac{d\sigma}{d\Omega' dE_{k'}}(\hat{j}\to-\hat{i}') - \frac{d\sigma}{d\Omega' dE_{k'}}(-\hat{j}\to\hat{i}') + \frac{d\sigma}{d\Omega' dE_{k'}}(-\hat{j}\to-\hat{i}')}{\frac{d\sigma}{d\Omega' dE_{k'}}(\hat{j}\to\hat{i}') + \frac{d\sigma}{d\Omega' dE_{k'}}(\hat{j}\to-\hat{i}') + \frac{d\sigma}{d\Omega' dE_{k'}}(-\hat{j}\to\hat{i}') + \frac{d\sigma}{d\Omega' dE_{k'}}(-\hat{j}\to-\hat{i}')} \tag{4.272}$$

where $\hat{j}$ refers to an arbitrary quantization axis in the rest frame of the projectile nucleon, which is chosen to be the unprimed $x\,y\,z$ reference frame in Fig. 4.1, $\hat{i}'$ refers to an arbitrary

spin quantization axis in the primed $x'\,y'\,z'$ reference frame in Fig. 4.1, and

$$(i'\,j) \;\epsilon\; \{\,(0'\,n),\,(n\,n),\,(s'\,s),\,(\ell'\,\ell),\,(s'\,\ell),\,(\ell'\,s)\,\}\,. \tag{4.273}$$

The different polarization transfer observables are distinguished by the choice of spin projections along different quantization axes in the incoming and outgoing reference frames in Fig. 4.1, in the expression for the polarized double differential cross section given by Eq. (4.261). The only quantity in Eq. (4.261) that contains information about the projectile and ejectile spin projections, is the projectile distorted nucleon tensor defined in Eq. (4.263). The spin projections in the latter tensor are, in turn, determined by different choices of the Wigner D–functions in Eqs. (4.172) and (4.174), for the projectile and ejectile relativistic distorted waves respectively.

For each polarization transfer observable, $\mathrm{A}_y \;=\; \mathrm{D}_{0'n},\; \mathrm{D}_{nn},\; \mathrm{D}_{s's},\; \mathrm{D}_{\ell'\ell},\; \mathrm{D}_{s'\ell}$ and $\mathrm{D}_{\ell's}$, Table 4.1 lists the values of the Euler angles and spin indices for the Wigner D–functions, $D^{\frac{1}{2}}_{s_z\,s}(\alpha,\beta,\gamma)$ [in Eq. (4.172)] and $D^{\frac{1}{2}}_{s_z\,s}(\alpha',\beta',\gamma')$ [in Eq. (4.174)], for each of the polarized double differential cross sections [given by Eq. (4.261)] comprising the polarization transfer observables $D_{i'\,j}$ defined by Eqs. (4.272) and (4.273) . The Wigner D–functions $D^{\frac{1}{2}}_{s_z\,s}(\alpha,\beta,\gamma)$ are given by [Va88]

$$D^{\frac{1}{2}}_{s_z\,s}(\alpha,\beta,\gamma) \;=\; e^{-is_z\alpha}\,d^{\frac{1}{2}}_{s_z\,s}(\beta)\,e^{-is\gamma}\,, \tag{4.274}$$

where explicit expressions for the $d^{\frac{1}{2}}_{s_z\,s}(\beta)$ functions, which are real, are given in Eq. (4.133).

4.4.5 Kinematics

A brief discussion is now given of the kinematic quantities relevant to calculating the various polarized double differential cross sections, which constitute the polarization transfer observables, for a range of excitation energies ω spanning the quasielastic peak (see also Sec.3.2.9 in Chapter 3).

The upper and lower radial components of the relativistic distorted waves, with outgoing boundary conditions [Eqs. (4.172) and (4.173)], are obtained via solutions of Eqs. (4.193) and (4.201) respectively, for which the magnitude of the incident momentum of the projectile, $|\vec{k}\,|$, in the projectile–nucleus centre–of–mass frame, is given by

$$|\vec{k}\,| \;=\; \sqrt{(E_k)^2 \;+\; m^2}\,. \tag{4.275}$$

Table 4.1: Values of the Euler angles and spin indices, for the Wigner D–functions, $D^{\frac{1}{2}}_{s_z\, s}(\alpha,\beta,\gamma)$ [in Eq. (4.172)] and $D^{\frac{1}{2}}_{s_z\, s}(\alpha',\beta',\gamma')$ [in Eq. (4.174)], for each of the polarized double differential cross sections [given by Eq. (4.261)] comprising the polarization transfer observables $D_{i'\,j}$ defined by Eqs. (4.272) and (4.273).

$D_{i'\,j}$	Quantization axis $\hat{j}$ for projectile spin	Quantization axis $\hat{i}\,'$ for ejectile spin	Projection of projectile spin along $\hat{j}$–axis	Form of $D^{\frac{1}{2}}_{s_z\, s}(\alpha,\beta,\gamma)$ in Eq. (4.172)	Projection of ejectile spin along $\hat{i}\,'$–axis	Form of $D^{\frac{1}{2}}_{s'_z\, s'}(\alpha',\beta',\gamma')$ in Eq. (4.174)
$D_{n'\,n}$	$\hat{j}=\hat{n}=\hat{y}$	$\hat{i}\,'=\hat{n}\,'=\hat{y}\,'$	$+\hat{y}$	$D^{\frac{1}{2}}_{s_z\,\frac{1}{2}}(\frac{\pi}{2},\frac{\pi}{2},0)$	$+\hat{y}\,'$	$D^{\frac{1}{2}}_{s'_z\,\frac{1}{2}}(\frac{\pi}{2},\frac{\pi}{2},0)$
			$-\hat{y}$	$D^{\frac{1}{2}}_{s_z\,-\frac{1}{2}}(\frac{\pi}{2},\frac{\pi}{2},0)$	$-\hat{y}\,'$	$D^{\frac{1}{2}}_{s'_z\,-\frac{1}{2}}(\frac{\pi}{2},\frac{\pi}{2},0)$
$D_{s'\,s}$	$\hat{j}=\hat{s}=\hat{x}$	$\hat{i}\,'=\hat{s}\,'=\hat{x}\,'$	$+\hat{x}$	$D^{\frac{1}{2}}_{s_z\,\frac{1}{2}}(0,\frac{\pi}{2},0)$	$+\hat{x}\,'$	$D^{\frac{1}{2}}_{s'_z\,\frac{1}{2}}(0,\frac{\pi}{2},0)$
			$-\hat{x}$	$D^{\frac{1}{2}}_{s_z\,-\frac{1}{2}}(0,\frac{\pi}{2},0)$	$-\hat{x}\,'$	$D^{\frac{1}{2}}_{s'_z\,-\frac{1}{2}}(0,\frac{\pi}{2},0)$
$D_{\ell'\,\ell}$	$\hat{j}=\hat{\ell}=\hat{z}$	$\hat{i}\,'=\hat{\ell}\,'=\hat{z}\,'$	$+\hat{z}$	$D^{\frac{1}{2}}_{s_z\,\frac{1}{2}}(0,0,0)$	$+\hat{z}\,'$	$D^{\frac{1}{2}}_{s'_z\,\frac{1}{2}}(0,0,0)$
			$-\hat{z}$	$D^{\frac{1}{2}}_{s_z\,-\frac{1}{2}}(0,0,0)$	$-\hat{z}\,'$	$D^{\frac{1}{2}}_{s'_z\,-\frac{1}{2}}(0,0,0)$
$D_{s'\,\ell}$	$\hat{j}=\hat{\ell}=\hat{z}$	$\hat{i}\,'=\hat{s}\,'=\hat{x}\,'$	$+\hat{z}$	$D^{\frac{1}{2}}_{s_z\,\frac{1}{2}}(0,0,0)$	$+\hat{x}\,'$	$D^{\frac{1}{2}}_{s'_z\,\frac{1}{2}}(0,\frac{\pi}{2},0)$
			$-\hat{z}$	$D^{\frac{1}{2}}_{s_z\,-\frac{1}{2}}(0,0,0)$	$-\hat{x}\,'$	$D^{\frac{1}{2}}_{s'_z\,-\frac{1}{2}}(0,\frac{\pi}{2},0)$
$D_{\ell'\,s}$	$\hat{j}=\hat{s}=\hat{x}$	$\hat{i}\,'=\hat{\ell}\,'=\hat{z}\,'$	$+\hat{x}$	$D^{\frac{1}{2}}_{s_z\,\frac{1}{2}}(0,\frac{\pi}{2},0)$	$+\hat{z}\,'$	$D^{\frac{1}{2}}_{s'_z\,\frac{1}{2}}(0,0,0)$
			$-\hat{x}$	$D^{\frac{1}{2}}_{s_z\,-\frac{1}{2}}(0,\frac{\pi}{2},0)$	$-\hat{z}\,'$	$D^{\frac{1}{2}}_{s'_z\,-\frac{1}{2}}(0,0,0)$
$D_{0'\,n}$ (A_y)	$\hat{j}=\hat{n}=\hat{y}$	$\hat{i}\,'=\hat{n}\,'=\hat{y}\,'$	$+\hat{y}$	$D^{\frac{1}{2}}_{s_z\,\frac{1}{2}}(\frac{\pi}{2},\frac{\pi}{2},0)$	$D^{\frac{1}{2}}_{s'_z\,s'}(\alpha',\beta',\gamma')$ is replaced by $\sum_{s'} D^{\frac{1}{2}}_{s'_z\,s'}(\alpha',\beta',\gamma')$	
			$-\hat{y}$	$D^{\frac{1}{2}}_{s_z\,-\frac{1}{2}}(\frac{\pi}{2},\frac{\pi}{2},0)$		

The energy of the projectile in the projectile–nucleus centre–of–mass frame E_k, is given by [see Eq. (A.2) in Appendix A]

$$E_k = \frac{m^2 c^4 + m_t c^2 (m c^2 + T_{lab})}{\sqrt{(m c^2 + m_t c^2)^2 + 2 m_t c^2 T_{lab}}} \tag{4.276}$$

where, m and m_t are the masses of the projectile proton and target nucleus, respectively. For a fixed energy transfer ω to the target nucleus, the energy of the ejectile nucleon in the ejectile–nucleus centre–of–mass frame, is given by

$$E_{k'} = E_k - \omega \, . \tag{4.277}$$

The upper and lower radial components of the relativistic distorted waves, with incoming boundary conditions [in Eqs. (4.174) – (4.177)], are obtained via solutions of Eqs. (4.193) and (4.201) respectively, for which the magnitude of the momentum of the ejectile $|\vec{k}'|$, in the ejectile–nucleus centre–of–mass frame, is given by

$$|\vec{k}'| = \sqrt{(E_{k'})^2 + m^2} \, . \tag{4.278}$$

Next, the magnitude of the momentum transfer $|\vec{q}|$, at which the SVPAT scattering amplitudes $t_\beta(T_{\rm lab}, |\vec{q}\,|)$ in Eq. (4.261) are evaluated, is specified. For a specific scattering angle θ_{cm}, in the ejectile–nucleus centre–of–mass system, shown in Fig. 4.1, the components of the momentum transfer are given by

$$\begin{aligned} q_x &= k_x - k'_x = 0 - |\vec{k}'| \sin\theta_{cm} = - |\vec{k}'| \sin\theta_{cm} \\ q_y &= k_y - k'_y = 0 \\ q_z &= k_z - k'_z = |\vec{k}'| - |\vec{k}'| \cos\theta_{cm} \end{aligned} \tag{4.279}$$

such that,

$$|\vec{q}| = \sqrt{(q_x)^2 + (q_z)^2} \, . \tag{4.280}$$

The explicit expressions for the kinematic factors $|\vec{k}_{cm}|$ and E_{cm}, relating the t_β–amplitudes to the F_β–amplitudes in Eq. (4.255), are given by Eq. (4.255).

Finally, the kinematic factor K in Eq. (4.262) is calculated via Eqs. (4.276) and (4.277), and E_0 is the rest mass energy of the ground state of the target nucleus, that is

$$E_0 = m_t c^2 \, . \tag{4.281}$$

4.5 Status of numerical program

To calculate quasielastic polarization transfer observables $D_{i'j}$, it is necessary to numerically evaluate the polarized double differential cross sections, given by Eq. (4.261), for different incident and outgoing nucleon spin projections. The latter cross sections, in turn, are expressed in terms of the contraction of a projectile distorted nucleon tensor $H^{s's}_{\alpha\beta}(\vec{k},\vec{k}';\vec{y}_j,\vec{y}_i)$ [see Eq. (4.263)], expressed in terms of relativistic distorted waves, with the imaginary part of a spin–independent nuclear polarization tensor $\Pi^{\alpha\beta}$ [see Eq. (4.268)].

Following the methods outlined in Sec. 4.3, the relativistic distorted waves, comprising the projectile distorted nucleon tensor, have already been generated, and checked for numerical accuracy (as discussed in Sec. 4.3.5).

I still need to evaluate the imaginary components of the nuclear polarization tensor $\Pi^{\alpha\beta}_{LDA}(\vec{y}_j,\vec{y}_i\,;\omega)$ within the local density approximation expressed by Eq. (4.269).

Perhaps, the most challenging problem, from a numerical point of view, that still needs to be tackled, is to evaluate the six–dimensional integral in Eq. (4.261). One could, for example, use the (time–consuming) Monte Carlo integration method employed by Ikebata [Ik95]. However, to achieve acceptable computing times, it seems that the integration technique developed by Chant and Roos would be more appropriate [Ch83].

The numerical evaluation of the above–mentioned nuclear polarization tensor, within the local density approximation, as well as the numerical evaluation of the six–dimensional integral in Eq. (4.261), will be addressed in future research projects.

4.6 Summary

In this chapter, the theoretical framework has been developed for calculating complete sets of quasielastic proton–nucleus polarization transfer observables based the **R**elativistic **D**istorted **W**ave **I**mpulse **A**pproximation (**RDWIA**).

For the simpler case of a zero–range NN interaction, and ignoring exchange effects, it was shown, in Sec. 4.4, that polarized double differential cross sections can be expressed as the

contraction between a projectile distorted nucleon tensor and a spin–independent nuclear polarization tensor for the target nucleus.

The projectile distorted nucleon tensor contains information about the spin projections and full relativistic distortions of the projectile and ejectile distorted wave functions. Compared to the distortion effects, incorporated via effective masses in the mean–field Dirac spinors in the RPWIA, the relativistic distorted wave functions are solutions to the Dirac equation with nuclear scalar $S(r)$ and time–like vector potentials $V(r)$. In Sec. 4.3, partial wave expansions for the relativistic distorted wave functions were derived, with incoming and outgoing boundary conditions.

The spin–independent nuclear polarization tensor, on the other hand, contains information about the nuclear response of the target nucleus, and is conveniently expressed in terms of the imaginary part of the nuclear polarization tensor which can be evaluated to any level of sophistication, depending on the choice of model for the nuclear response. In Sec. 4.2.3, the concept of nuclear response functions was introduced, via a generalization of the simpler electromagnetic response for inclusive electron–nucleus scattering discussed in Sec. 4.2.1. Although, a general framework was developed for calculating nuclear response functions to any level of sophistication, for the purpose of this project, I only focused on the following three models of the nuclear response: relativistic free Fermi–gas model (FGM), relativistic mean–field approximation (MFA), and the local density approximation (LDA). Furthermore, analytical expressions were derived for the imaginary parts of the nuclear scalar polarization for FGM and MFA models. Future theoretical work will involve deriving analytical expressions for all the components of the imaginary parts of the nuclear polarization tensor.

The next phase is to perform numerical calculations of the quasielastic polarization transfer observables based on the zero–range no–exchange approximation, discussed in Sec. 4.4.3, so as to get a first order feel for the effects of distortions.

APPENDICES

Appendix A

Relativistic optical potentials

A.1 Introduction

The aim of this appendix is to clarify the terminolgy associated with the various Dirac potential–types, and also to derive the most general form of the Dirac equation, which is consistent with rotational and parity invariance, for describing elastic proton–nucleus scattering. In Sec. A.3, the Schrödinger equivalent potentials, required for evaluating the transmission probability in Eq. (3.9) of Chapter 3 and for generating the relativistic distorted waves in Sec. 4.3 of Chapter 4, are discussed.

A.2 General form of Dirac equation for elastic scattering

A fundamental characteristic of the Dirac equation is that the Lorentz character of the potentials must be specified. Using the conventions of Bjorken and Drell [Bj64], the most general local, time–independent Dirac equation contains five tensor types of potentials: scalar, vector, pseudoscalar, axial–vector (also called pseudovector) and tensor. In this case the Dirac equation for the scattering of a charged spin–$\frac{1}{2}$ particle from an external potential is [Mi91]

$$\begin{aligned}\{c\boldsymbol{\alpha}\cdot\mathbf{p} + \beta[mc^2 + U^s(\mathbf{r}) + \gamma^\mu U^v_\mu(\mathbf{r}) \\ + \gamma^5 U^p(\mathbf{r}) + \gamma^\mu\gamma^5 U^a_\mu(\mathbf{r}) + \sigma^{\mu\nu}U^t_{\mu\nu}(\mathbf{r})]\}\psi(\vec{r}) = E\psi(\vec{r})\end{aligned} \tag{A.1}$$

where E is the energy of the incident (or scattered) nucleon in the nucleon–nucleus centre–of–mass system, and α, β, γ^μ, γ^5, and $\sigma^{\mu\nu}$ are the usual 4×4 Dirac matrices expressed as:

$$\gamma^\mu \;=\; (\gamma^0, \boldsymbol{\gamma})$$

$$\begin{aligned}
\boldsymbol{\gamma} &= \begin{pmatrix} 0 & \boldsymbol{\sigma} \\ -\boldsymbol{\sigma} & 0 \end{pmatrix} \\
\beta &= \gamma^0 = \begin{pmatrix} 1 & 0 \\ 0 & -1 \end{pmatrix} \\
\boldsymbol{\alpha} &= \gamma^0 \boldsymbol{\gamma} \\
\gamma^5 &= i\gamma^0\gamma^1\gamma^2\gamma^3 \\
\sigma^{\mu\nu} &= \frac{i}{2}(\gamma^\mu\gamma^\nu - \gamma^\nu\gamma^\mu) \, .
\end{aligned}$$

For any four–vector potential X^μ, where

$$X^\mu = (X^0, \vec{X}) = g^{\mu\nu} X_\nu \, ,$$

the Lorentz–invariant quantity $\gamma^\mu X_\mu$ is defined as

$$\gamma^\mu X_\mu = g_{\mu\nu}\gamma^\mu X^\nu = \gamma^0 X^0 - \vec{\gamma}\cdot\vec{X}$$

where the metric tensor $g_{\mu\nu} = g^{\mu\nu}$ is given by

$$g_{\mu\nu} = \begin{pmatrix} 1 & 0 & 0 & 0 \\ 0 & -1 & 0 & 0 \\ 0 & 0 & -1 & 0 \\ 0 & 0 & 0 & -1 \end{pmatrix} .$$

The potential subscripts **s**, **v**, **p**, **a** and **t** denote **s**calar, **v**ector, **p**seudoscalar, **a**xial-vector and **t**ensor respectively. Section A.2.1 clarifies the context of this nomenclature. The symbols **r** and $\vec{r}$ denote the coordinate operators and vectors of the nucleon respectively, and **p** is the the momentum operator. E is the total energy of the projectile nucleon in the nucleon–nucleus centre–of–mass frame [Mu87a, Mu87b, Si90]

$$E = \frac{m^2 c^4 + m_t c^2 (m c^2 + T_{\rm lab})}{\sqrt{(m c^2 + m_t c^2)^2 + 2 m_t c^2 T_{\rm lab}}} \qquad \text{(A.2)}$$

where m is the free rest mass energy, m_t is the mass of the target nucleus, and $\mathrm{T_{lab}}$ is the incident laboratory kinetic energy of the nucleon. Note that for generality one can consider the electromagnetic four–potential $A_\mu = (A^0, \vec{A})$ to be part of the four–potential $U^v_\mu = (U^0, \vec{U})$ in Eq. (A.1).

A.2.1 Nomenclature

For a covariant relativistic description of elastic proton–nucleus scattering, the nucleon–nucleus interaction potentials must be independent of the specific Lorentz frame. Hence, all potentials must transform like scalar quantities (tensors of rank zero) under a Lorentz transformation. Within the context of the Dirac equation, this condition restricts the most general local, time-independent potential to the five tensor types (scalar, vector, pseudoscalar, axial–vector/pseudovector and tensor) mentioned later on in Eq. (A.1). The context in which this nomenclature is used is now discussed.

Using the conventions of Bjorken and Drell [Bj64], any 4×4 matrix can be expanded in terms of the following 16 linearly independent 4×4 matrices $\Gamma^n_{\alpha\beta}$ [Gr90, Bj64]

$$\begin{aligned}
\Gamma^s &= 1 \\
\Gamma^v_\mu &= \gamma_\mu \\
\Gamma^p &= i\gamma^0\gamma^1\gamma^2\gamma^3 = \gamma^5 = \gamma_5 \\
\Gamma^a_\mu &= \gamma^5\gamma_\mu \\
\Gamma^t_{\mu\nu} &= \sigma_{\mu\nu} = \frac{i}{2}(\gamma_\mu\gamma_\nu - \gamma_\nu\gamma_\mu)
\end{aligned}$$

where the superscripts "*s, v, p, a, t*" refer respectively to "scalar", "vector", "pseudoscalar", "axial–vector" and "tensor". This nomenclature refers to the behaviour of the bilinear expressions

$$\bar{\psi}(x)\Gamma^n\psi(x) \qquad (n \,\epsilon\, \{s, v, p, a, t\}) \tag{A.3}$$

under a Lorentz transformation, where

$$x \equiv (ct, x, y, z) \tag{A.4}$$

and ψ is the solution to the time–dependent Dirac equation. The Lorentz transformation between the coordinates x^μ and $(x')^\mu$ for two observers in different inertial frames O and O' respectively, is given by

$$(x')^\nu = \sum_{\mu=0}^{3} a^\nu_\mu x^\mu \equiv a^\nu_\mu x^\mu \equiv (\hat{a}x)^\nu \,. \tag{A.5}$$

The transformation $\hat{S}(\hat{a})$ that guarantees form invariance of the Dirac equation, and enables observer O' to construct a wave function $\psi'(x')$ from the wave function $\psi(x)$ of observer O through $\psi'(x') = \hat{S}(\hat{a})\psi(x)$, such that both observers describe the same physical state, is given by [Gr90, Bj64]

$$\hat{S}(\hat{a})\gamma^{\mu}\hat{S}^{-1}(\hat{a})a^{\nu}{}_{\mu} = \gamma^{\nu} \tag{A.6}$$

or

$$\hat{S}(\hat{a})\gamma^{\mu}\hat{S}^{-1} = \gamma^{\nu}(\hat{a})a_{\nu}{}^{\mu}\,. \tag{A.7}$$

Using the fact that for all proper Lorentz transformations (det$|a|$=+1)

$$[\hat{S}(\hat{a}), \gamma_5] = 0 \tag{A.8}$$

and, for the parity operator $\mathbf{P}$ (an improper Lorentz transformation for which det$|a| = -1$) defined in Eq. (A.13),

$$\mathbf{P}\gamma_5 = \gamma_5\mathbf{P} \tag{A.9}$$

one can readily obtain the transformation properties of the following complete set of linearly independent bilinear covariants [Gr90, Bj64]

$$\bar{\psi}'(x')\Gamma^{s}\psi'(x') = \bar{\psi}'(x')\psi'(x') = \bar{\psi}(x)\psi(x)$$

(transforms like a Lorentz scalar)

$$\bar{\psi}'(x')\Gamma^{v}\psi'(x') = \bar{\psi}'(x')\gamma^{\nu}\psi'(x') = a^{\nu}{}_{\mu}\bar{\psi}(x)\gamma^{\mu}\psi(x)$$

(transforms like a Lorentz vector)

$$\bar{\psi}'(x')\Gamma^{p}\psi'(x') = \bar{\psi}'(x')\gamma^{5}\psi'(x') = \bar{\psi}(x)\gamma^{5}\psi(x)$$

(transforms like a Lorentz pseudoscalar)

$$\bar{\psi}'(x')\Gamma^{a}\psi'(x') = \bar{\psi}'(x')\gamma^{5}\gamma^{\nu}\psi'(x') = a^{\nu}{}_{\mu}\bar{\psi}(x)\gamma^{5}\gamma^{\mu}\psi(x)$$

(transforms like a Lorentz axial–vector)

$$\bar{\psi}'(x')\Gamma^{t}\psi'(x') = \bar{\psi}'(x')\sigma^{\mu\nu}\psi'(x') = a^{\mu}{}_{\alpha}a^{\nu}{}_{\beta}\bar{\psi}(x)\sigma^{\alpha\beta}\psi(x)$$

(transforms like a Lorentz tensor of rank 2) . (A.10)

The prefix "pseudo" in pseudoscalar indicates that $\bar{\psi}(x)\gamma^5\psi(x)$ transforms as a Lorentz scalar, but reverses its sign, under the improper Lorentz transformation of space reflection.

The most general way to construct Lorentz *scalar* potential terms in the Dirac equation is by contraction of the Γ^n's (n = s, v, p, a, t) with the corresponding coordinate space Dirac potentials thus forming the following scalar bilinear covariants

$$\begin{aligned}
&\bar{\psi}(x)U^s\psi(x)\\
&\bar{\psi}(x)\gamma^\mu U^v_\mu\psi(x)\\
&\bar{\psi}(x)\gamma^5 U^p\psi(x)\\
&\bar{\psi}(x)\gamma^5\gamma^\mu U^a_\mu\psi(x)\\
&\bar{\psi}(x)\sigma^{\mu\nu}U^t_{\mu\nu}\psi(x)
\end{aligned} \tag{A.11}$$

where the U^n's represent the various potential types specified later on in Eq. (A.1). Hence, it should be clear as to the context in which the *s, v, p, a, t* nomenclature is used, and why the terms

$$U^s(\mathbf{r}) + \gamma^\mu U^v_\mu(\mathbf{r}) + \gamma^5 U^p(\mathbf{r}) + \gamma^\mu\gamma^5 U^a_\mu(\mathbf{r}) + \sigma^{\mu\nu}U^t_{\mu\nu}(\mathbf{r}) \tag{A.12}$$

are treated with the same status as the Lorentz scalar rest mass m in Eq. (A.1) [i.e. lumped together with the mass term].

A.2.2 Parity and rotational invariance

The question now arises as to what is the most general form of Eq. (A.1) that is consistent with rotational invariance and parity conservation. This reduces to the requirement that each potential term in Eq. (A.1) must commute with the relativistic parity

$$\mathbf{P} = \gamma^0\mathbf{P}_{NR}, \tag{A.13}$$

and total angular momentum operators

$$\mathbf{J} = \mathbf{r}\times\mathbf{p}\begin{pmatrix} I & 0\\ 0 & I\end{pmatrix} + \frac{\hbar}{2}\begin{pmatrix}\boldsymbol{\sigma} & 0\\ 0 & \boldsymbol{\sigma}\end{pmatrix}. \tag{A.14}$$

The operator $\mathbf{P}_{NR}$ in Eq. (A.13) is the usual nonrelativistic parity operator whose operation upon a function of coordinates changes $\vec{r} \equiv (r,\theta,\phi)$ to $-\vec{r} \equiv (r,\pi-\theta,\phi+\pi)$. The matrix I in Eq. (A.14) is the 2×2 identity matrix, and $\boldsymbol{\sigma}$ represents the usual 2×2 Pauli spin matrices.

The requirement that **J** and **P** commute with each term of the Hamiltonian in Eq. (A.1) introduces simplifying restrictions on the potentials in Eq. (A.1). These restrictions are most simply imposed by introducing the spherical coordinate form for the angular momentum operator,

$$\mathbf{L} = \mathbf{r}\times\mathbf{p} = -i\hbar\{\hat{\mathbf{u}}_\phi \frac{\partial}{\partial\theta} - \frac{1}{\sin\theta}\hat{\mathbf{u}}_\theta \frac{\partial}{\partial\phi}\} \tag{A.15}$$

and the Pauli spin matrix,

$$\begin{aligned}\boldsymbol{\sigma} &= \hat{\mathbf{u}}_r\,\sigma_r + \hat{\mathbf{u}}_\theta\,\sigma_\theta + \hat{\mathbf{u}}_\phi\,\sigma_\phi \\ &= \hat{\mathbf{u}}_r\begin{pmatrix}\cos\theta & \sin\theta\, e^{-i\phi}\\ \sin\theta\, e^{i\phi} & -\cos\theta\end{pmatrix} + \hat{\mathbf{u}}_\theta\begin{pmatrix}-\sin\theta & -\cos\theta\, e^{-i\phi}\\ \cos\theta\, e^{i\phi} & \sin\theta\end{pmatrix} + \hat{\mathbf{u}}_\phi\begin{pmatrix}0 & -i\, e^{-i\phi}\\ i\, e^{i\phi} & 0\end{pmatrix}\end{aligned} \tag{A.16}$$

The unit vectors in the r, θ and ϕ directions, denoted by $\hat{\mathbf{u}}_r$, $\hat{\mathbf{u}}_\theta$ and $\hat{\mathbf{u}}_\phi$ respectively, are defined as [Me70]

$$\begin{aligned}\hat{\mathbf{u}}_r &= \sin\theta\cos\phi\,\hat{\mathbf{i}} + \sin\theta\sin\phi\hat{\mathbf{j}} + \cos\theta\,\hat{\mathbf{k}}\\ \hat{\mathbf{u}}_\phi &= -\sin\phi\,\hat{\mathbf{i}} + \cos\phi\,\hat{\mathbf{j}}\\ \hat{\mathbf{u}}_\theta &= \sin\theta\cos\phi\,\hat{\mathbf{i}} + \cos\theta\sin\phi\,\hat{\mathbf{j}} - \sin\theta\,\hat{\mathbf{k}}\end{aligned}$$

where $\hat{\mathbf{i}}$, $\hat{\mathbf{j}}$ and $\hat{\mathbf{k}}$ are the usual cartesian unit vectors along the x, y and z axes respectively. The commutation relations are calculated in a similar fashion to those presented in Exercise 9.4 and Sec. 12.4 of Ref. [Gr90]. Consequently, the most general Dirac equation consistent with good J^2, J_z, and **P** is thus [Mi91],

$$\begin{aligned}\{c\boldsymbol{\alpha}\cdot\mathbf{p} + \beta[mc^2 + U_s(r) + \gamma^0 U_v^0(r) + \gamma^0 V_c(r)\\ -\gamma^r U_v^r(r) - \gamma^0\gamma^r U_t^r(r)]\}\psi(\vec{r}) = E\psi(\vec{r})\end{aligned} \tag{A.17}$$

where the Coulomb potential $V_c(r)$ has been explicitly included.

Most calculations of elastic scattering spin observables usually only consider $U_s(r)$ and $U_v^0(r)$ and ignore all the other potential terms. The justification and consequences of the latter assumption are discussed in Sec. A.3.

A.3 Schrödinger–equivalent potentials

In this section it is shown how Schrödinger–equivalent potentials [Cl83, Cl85] are obtained by transforming the Dirac equation Eq. (A.17) to a second order Schrödinger–like differential

equation which can be solved using the standard procedures discussed in Ref. [Mc68].

Using the explicit forms for the α, β and γ matrices, and distinguishing between upper and lower components of ψ by writing

$$\psi(\vec{r}) = \begin{pmatrix} \psi^u(\vec{r}) \\ \psi^\ell(\vec{r}) \end{pmatrix} \tag{A.18}$$

where $\psi^u(\vec{r})$ and $\psi^\ell(\vec{r})$ are two–component–type Pauli wave functions, Eq. (A.17) can be written as a pair of coupled equations for the upper and lower wave functions, that is

$$\begin{aligned}[(m+U_s)-(E-U_v^0-V_c)]\psi^u(\vec{r}) \; + \\ [\boldsymbol{\sigma}\cdot\mathbf{p}-\boldsymbol{\sigma}\cdot\hat{r}(U_v^r+iU_t)]\psi^\ell(\vec{r})=0\end{aligned} \tag{A.19}$$

$$\begin{aligned}[-(m+U_s)-(E-U_v^0-V_c)]\psi^\ell(\vec{r}) \; + \\ [\boldsymbol{\sigma}\cdot\mathbf{p}-\boldsymbol{\sigma}\cdot\hat{r}(U_v^r-iU_t)]\psi^u(\vec{r})=0\end{aligned} \tag{A.20}$$

where all potentials are spherically symmetric, and natural units ($\hbar = c = 1$) are adopted. Solving Eq. (A.20) for $\psi^\ell(\vec{r})$ yields

$$\psi^\ell(\vec{r}) = \frac{1}{(E+m)A(r)}[\boldsymbol{\sigma}\cdot\mathbf{p}-\boldsymbol{\sigma}\cdot\hat{r}(U_v^r-iU_t)]\psi^u(\vec{r}) \tag{A.21}$$

where

$$A(r) = \frac{E+m+U_s(r)-U_v^0(r)-V_c(r)}{E+m}\,. \tag{A.22}$$

Substituting Eq. (A.21) into Eq. (A.19) gives an equation for $\psi^u(\vec{r})$, namely

$$[(E-U_v^0-V_c)^2-(m+U_s)^2-Q(r)]\psi^u(\vec{r})=0 \tag{A.23}$$

where

$$Q(r)=A(r)[\boldsymbol{\sigma}\cdot\mathbf{p}-\boldsymbol{\sigma}\cdot\hat{r}(U_v^r+iU_t)]\frac{1}{A(r)}[\boldsymbol{\sigma}\cdot\mathbf{p}-\boldsymbol{\sigma}\cdot\hat{r}(U_v^r-iU_t)]\,. \tag{A.24}$$

Carrying out the indicated algebra in Eq. (A.23), and making use of the following operator relations

$$(\boldsymbol{\sigma}\cdot\mathbf{A_{op}})(\boldsymbol{\sigma}\cdot\mathbf{B_{op}}) = \mathbf{A_{op}}\cdot\mathbf{B_{op}} + i\boldsymbol{\sigma}\cdot(\mathbf{A_{op}}\times\mathbf{B_{op}}) \tag{A.25}$$

$$\mathbf{p} = \frac{\hbar}{i}\boldsymbol{\nabla} \tag{A.26}$$

$$\mathbf{L} = \vec{r}\times\mathbf{p} \tag{A.27}$$

$$(\boldsymbol{\sigma}\cdot\mathbf{p}) = \frac{\sigma_r}{r}[\vec{r}\cdot\mathbf{p} + i\boldsymbol{\sigma}\cdot\mathbf{L}] \tag{A.28}$$

and vector identities for arbitrary scalar and vector functions, η and $\vec{A}$ respectively,

$$\begin{aligned}
\boldsymbol{\nabla}\cdot(\eta\vec{A}) &= \vec{A}\cdot(\boldsymbol{\nabla}\eta) + \eta(\boldsymbol{\nabla}\cdot\vec{A}) \\
\boldsymbol{\nabla}\times(\eta\vec{A}) &= (\boldsymbol{\nabla}\eta)\times\vec{A} + \eta(\boldsymbol{\nabla}\times\vec{A}) \\
(\boldsymbol{\nabla}\times\vec{r})\eta &= -(\vec{r}\times\boldsymbol{\nabla})\eta \\
\boldsymbol{\nabla}\cdot\hat{r} &= \frac{2}{r}
\end{aligned}$$

yields

$$\begin{aligned}
&\{\boldsymbol{\nabla}^2 + (E - U_v^0 - V_c)^2 - (m + U_s)^2 - (U_v^r)^2 - (U_t)^2 + \\
&[\frac{1}{rA}\frac{\partial A}{\partial r} - 2\frac{U_t}{r}](\boldsymbol{\sigma}\cdot\mathbf{L}) - \frac{2}{r}(iU_v^r + U_t) + \frac{1}{A}\frac{\partial A}{\partial r}(iU_v^r + U_t) + \\
&\frac{1}{r}[(\vec{r}\cdot\mathbf{p})(U_v^r - iU_t)] - [i\frac{1}{rA}\frac{\partial A}{\partial r} - 2\frac{U_v}{r}](\vec{r}\cdot\mathbf{p})\}\psi^u(\mathbf{r}) = 0\,.
\end{aligned} \tag{A.29}$$

This is an exact second order differential equation for ψ^u that can be interpreted as a Schrödinger-like equation with a nonlocal potential (due to first order derivatives of the potentials). To get an ordinary Schrödinger equation (i.e. with no first derivative terms) and a local 2×2 nucleon–nucleus potential that is useful for comparison with commonly used local nonrelativistic Schrödinger–based phenomenological potentials, one writes

$$\psi^u(\vec{r}) = K(r)\phi^u(\vec{r}) \tag{A.30}$$

where

$$K(r) = A^{\frac{1}{2}}e^{\int_0^r iU_v^r(r')dr'} \tag{A.31}$$

such that

$$K(r) \longrightarrow \infty \quad \text{as} \quad r \longrightarrow \infty\,.$$

Substituting Eqs. (A.30) and A.31 into Eq. (A.29) gives the following Schrödinger–like equation for $\psi^u(\vec{r})$

$$[\mathbf{p}^2 + U_{\text{eff}} + U_{\text{so}}\boldsymbol{\sigma}\cdot\mathbf{L}]\phi^u(\vec{r}) = [E^2 - m^2]\phi^u(\vec{r}) \tag{A.32}$$

with equivalent central $U_{\rm eff}(r)$ and spin-orbit $U_{\rm so}(r)$ potentials, also called **D**irac–**E**quation–**B**ased (**DEB**) potentials, given by

$$U_{\rm eff}(r) = U_{\rm Central}(r) + U_{\rm Darwin}(r) \tag{A.33}$$

where

$$\begin{aligned} U_{\rm Central}(r) &= [\, 2EU_v^0 + 2mU_s + 2EV_c - (U_v^0)^2 + (U_s)^2 - (V_c)^2 - 2V_cU_v^0 + (U_t)^2 \,] \\ &\quad + [\, -\frac{U_t}{A}(\frac{\partial A}{\partial r}) + 2\frac{U_t}{r} + \frac{\partial U_t}{\partial r} \,] \\ U_{\rm Darwin}(r) &= [\, -\frac{1}{2r^2A}(\frac{\partial}{\partial r}(r^2\frac{\partial A}{\partial r})) + \frac{3}{4A^2}(\frac{\partial A}{\partial r})^2 \,] \end{aligned} \tag{A.34}$$

and

$$U_{so}(r) = \frac{1}{2E}[\, -\frac{1}{rA}(\frac{\partial A}{\partial r}) + 2\frac{U_t}{r} \,]\,. \tag{A.35}$$

Note that, compared to the traditional Schrödinger equation, there is no reduced mass μ in Eq. (A.32). To obtain an effective Schrödinger equation for the lower component wave function $\psi^\ell(\vec{r})$, one proceeds analogously to the method outlined between Eqs. (A.21) and (A.34), except that

$$\psi^\ell(\vec{r}) = \mathcal{K}(r)\phi^\ell(\vec{r})$$

where

$$\mathcal{K}(r) = \mathcal{A}^{\frac{1}{2}} e^{\int_0^r iU_v^r(r')dr'}$$

and

$$\mathcal{A}(r) = \frac{E - m - U_s(r) - U_v^0(r) - V_c(r)}{E - m}\,. \tag{A.36}$$

The procedure yields a differential equation for $\phi^\ell(\vec{r})$ similar to Eq. (A.23), except that A(r) is now replaced by $\mathcal{A}$(r) in Eq. (A.34).

To summarize: a two-component reduction of Eq. (A.17) yields a Schrödinger–like differential equation, containing central, spin–orbit, and Darwin potentials, for both the upper and lower two components of the wave function.

Notice that the space–like part of the vector potential does not explicitly appear in the second order equation. More generally, it can be shown that when the spatial portion of the

vector potential in Eq. (A.17) is spherically symmetric it has no effect on elastic scattering [Ja83]. The only effect of the potential $U_v^T(r)$, and more precisely of its imaginary part, is to modify the amplitude of the wave functions $\phi^u(\vec{r})$ and $\phi^\ell(\vec{r})$ *inside* the nucleus. Examination of Eqs. (A.32) to (A.35) indicates that, at a minimum, one should consider $U_v^0(r)$ and $U_s(r)$ or $U_v^0(r)$ and $U_t(r)$ or $U_s(r)$ and $U_t(r)$ in order to obtaine the required central and spin-orbit potentials. Most calculations of elastic scattering spin observables choose $U_v^0(r)$ and $U_s(r)$, since these potential types appear in various mean field theories [Bo81, Bo82, Ei81, Ho81, Ho81a, Lo81, No81, Wa74, Ja81], and these potentials are also the largest terms in relativistic Brueckner-Hartree-Fock calculations [Ce82, Sh83] of the optical potential.

Finally, a number of important features of the DEB optical potentials are stressed:

- the central potential has explicit energy dependence,
- non–linear terms involving $U_v^0(r)$ and $U_s(r)$ are present,
- the spin–orbit potential occurs naturally,
- the spin–orbit and central terms are constrained by the choice of $U_v^0(r)$ and $U_s(r)$,
- Coulomb terms $V_c^2(r)$ and $U_v^0(r)V_c(r)$ are present.

These considerations lead, in the case of the large repulsive potential $U_v^0(r)$ and large attractive potential $U_s(r)$ usually found, to central and spin–orbit potentials of reasonable size. In addition, the real central potential exhibits a radial dependence which changes with energy in a manner similar to that of nonrelativistic microscopic calculations of the real central potential [Je77, Ma79, Br77, Br77a, Br78, Br78a, Ke80, Fr81].

Appendix B

Isospin dependence of NN amplitudes

The aim of this appendix is to derive isospin–dependent expressions for the f^{pp} and f^{nn} scattering operators given by Eqs. (3.20) and (3.21) in Sec. 3.2.4 of Chapter 3.

Recall that the requirement of charge independence of the NN interaction is equivalent to demanding that the interaction be an isoscalar (i.e. isospin invariant). The only isoscalars which may be constructed from the isospin operators $\boldsymbol{\tau}_1$ and $\boldsymbol{\tau}_2$ for particles one [projectile] and two [target] are the identity operator $\mathbf{1}$ and $\boldsymbol{\tau}_1 \cdot \boldsymbol{\tau}_2$. Hence, the isospin dependence of the nonrelativistic scattering operator f is introduced via the following substitution in Eq. (3.18).

$$A = A_0 + A_1 \boldsymbol{\tau}_1 \cdot \boldsymbol{\tau}_2, \quad B = B_0 + B_1 \boldsymbol{\tau}_1 \cdot \boldsymbol{\tau}_2, \qquad \text{etc.} \tag{B.1}$$

where the isospin operators $\boldsymbol{\tau}$ are identical to the usual Pauli spin operators $\boldsymbol{\sigma}$. In analogy with the ordinary spin operator $\boldsymbol{\sigma}$, the z–component of $\boldsymbol{\tau}$ is required to have two possible values, $+1$ and -1, which are related to the proton and neutron respectively. Defining the proton and neutron isospin wave functions[Wo90], $|p>$ and $|n>$ respectively, as

$$|p> \;=\; \begin{pmatrix} 1 \\ 0 \end{pmatrix}$$

$$|n> \;=\; \begin{pmatrix} 0 \\ 1 \end{pmatrix}$$

such that

$$\tau_z \, |p> \;=\; +|p>$$

$$\tau_z \, |n> \;=\; -|n>\,,$$

and using explicit forms of the isospin matrices, it follows that (where the subscripts 1 and 2 below refer to the projectile and initial target nucleon respectively)

$$\boldsymbol{\tau}_1 \cdot \boldsymbol{\tau}_2 |p>_1 \, |p>_2 \;=\; \boldsymbol{\tau}_1 \cdot \boldsymbol{\tau}_2 |p_1 \, p_2> \;=\; +|p_1 \, p_2>$$

$$\begin{aligned}
\boldsymbol{\tau}_1 \cdot \boldsymbol{\tau}_2 |n>_1 |n>_2 &= \boldsymbol{\tau}_1 \cdot \boldsymbol{\tau}_2 |n_1\, n_2> &= +|n_1\, n_2> \\
\boldsymbol{\tau}_1 \cdot \boldsymbol{\tau}_2 |p>_1 |n>_2 &= \boldsymbol{\tau}_1 \cdot \boldsymbol{\tau}_2 |p_1\, n_2> &= 2|n_1\, p_2> - |p_1\, n_2> \,. \qquad \text{(B.2)}
\end{aligned}$$

With the above relations it follows that the only non–zero matrix elements of $\boldsymbol{\tau}_1 \cdot \boldsymbol{\tau}_2$ are

$$\begin{aligned}
< p\, p|\, \boldsymbol{\tau}_1 \cdot \boldsymbol{\tau}_2 \, |p\, p> &= +1 \\
< n\, n|\, \boldsymbol{\tau}_1 \cdot \boldsymbol{\tau}_2 \, |n\, n> &= +1 \\
< p_1\, n_2|\, \boldsymbol{\tau}_1 \cdot \boldsymbol{\tau}_2 \, |p_1\, n_2> &= -1 \\
< n_1\, p_2|\, \boldsymbol{\tau}_1 \cdot \boldsymbol{\tau}_2 \, |n_1\, p_2> &= -1 \\
< n_1\, p_2|\, \boldsymbol{\tau}_1 \cdot \boldsymbol{\tau}_2 \, |p_1\, n_2> &= +2 \\
< p_1\, n_2|\, \boldsymbol{\tau}_1 \cdot \boldsymbol{\tau}_2 \, |n_1\, p_2> &= +2 \,. \qquad \text{(B.3)}
\end{aligned}$$

With Eq. (B.1) in Eq. (3.18) [from Chapter 3], and making use of the relations in Eq. (B.3) for $p + p \longrightarrow p + p$ scattering, it follows that

$$\begin{aligned}
(2i|\vec{k}_{cm}|)^{-1} f^{pp} &= (2i|\vec{k}_{cm}|)^{-1} < p\, p|\, f \, |p\, p> \\
&= (A_0 + A_1) + (B_0 + B_1)\boldsymbol{\sigma}_1 \cdot \boldsymbol{\sigma}_2 + i|\vec{q}\,|(C_0 + C_1)(\boldsymbol{\sigma}_1 \cdot \hat{n} + \boldsymbol{\sigma}_2 \cdot \hat{n}) \\
&\quad + |\vec{q}\,|^2 (D_0 + D_1)\boldsymbol{\sigma}_1 \cdot \hat{q}\boldsymbol{\sigma}_2 \cdot \hat{q} + (E_0 + E_1)\boldsymbol{\sigma}_1 \cdot \hat{z}\boldsymbol{\sigma}_2 \cdot \hat{z} \qquad \text{(B.4)}
\end{aligned}$$

and, for $n + n \longrightarrow n + n$ scattering, it follows that

$$\begin{aligned}
(2i|\vec{k}_{cm}|)^{-1} f^{nn} &= (2i|\vec{k}_{cm}|)^{-1} < n\, n|\, f \, |n\, n> \\
&= (A_0 + A_1) + (B_0 + B_1)\boldsymbol{\sigma}_1 \cdot \boldsymbol{\sigma}_2 + i|\vec{q}\,|(C_0 + C_1)(\boldsymbol{\sigma}_1 \cdot \hat{n} + \boldsymbol{\sigma}_2 \cdot \hat{n}) \\
&\quad + |\vec{q}\,|^2 (D_0 + D_1)\boldsymbol{\sigma}_1 \cdot \hat{q}\boldsymbol{\sigma}_2 \cdot \hat{q} + (E_0 + E_1)\boldsymbol{\sigma}_1 \cdot \hat{z}\boldsymbol{\sigma}_2 \cdot \hat{z} \,. \qquad \text{(B.5)}
\end{aligned}$$

Similarly, for $p_1 + n_2 \longrightarrow p_1 + n_2$ scattering, it follows that

$$\begin{aligned}
(2i|\vec{k}_{cm}|)^{-1} f^{pn} &= (2i|\vec{k}_{cm}|)^{-1} < p_1\, n_2|\, f \, |p_1\, n_2> \\
&= (A_0 - A_1) + (B_0 - B_1)\boldsymbol{\sigma}_1 \cdot \boldsymbol{\sigma}_2 + i|\vec{q}\,|(C_0 - C_1)(\boldsymbol{\sigma}_1 \cdot \hat{n} + \boldsymbol{\sigma}_2 \cdot \hat{n}) \\
&\quad + |\vec{q}\,|^2 (D_0 - D_1)\boldsymbol{\sigma}_1 \cdot \hat{q}\boldsymbol{\sigma}_2 \cdot \hat{q} + (E_0 - E_1)\boldsymbol{\sigma}_1 \cdot \hat{z}\boldsymbol{\sigma}_2 \cdot \hat{z} \qquad \text{(B.6)}
\end{aligned}$$

with an identical expression for $n_1 + p_2 \longrightarrow n_1 + p_2$ scattering.

Our next aim is to find the relationship between the isospin of NN amplitudes and the isospin of the exchanged mesons (see also Refs. [Br76, Wo90]).

Clearly the identity operator allows no change of τ_z at either vertex in the Feynman diagram depicted in Fig. 3.4 of Sec. 3.2.4 in Chapter 3, and hence represents the exchange of a neutral isoscalar meson (e.g. ω, σ). The operator $\boldsymbol{\tau}_1 \cdot \boldsymbol{\tau}_2$, however, does permit changes in the z–component of isospin at each vertex of ± 1 or 0, and must therefore correspond to the exchange of an isovector meson (e.g. π^+ π^0 π^- or ρ^+ ρ^0 ρ^-). For a given choice of the form of the interaction, matrix elements for the exchange of a meson of isospin $T_i = (0,\ 1)$, for NN states of isospin $T = (0,\ 1)$ are simply related. Considering only the isospin dependence of the matrix elements, one notes that, for the exchange of an isoscalar $T_i = 0$ meson [Br76, Wo90]:

$$< (t_1 t_2) T | \mathbf{1} | (t_1 t_2) T > \ = \ \left\{ \begin{array}{l} 1 \ \text{ for } \ T = 0 \\ \\ 1 \ \text{ for } \ T = 1 \end{array} \right\} \tag{B.7}$$

and, for the exchange of an isovector $T_i = 1$ meson [Br76, Wo90]

$$< (t_1 t_2) T | \boldsymbol{\tau}_1 \cdot \boldsymbol{\tau}_2 | (t_1 t_2) T > = \ 2T(T+1) - 3 \ = \ \left\{ \begin{array}{l} -3 \ \text{ for } \ T = 0 \\ \\ 1 \ \text{ for } \ T = 1 \end{array} \right\} \tag{B.8}$$

where t_1 and t_2 are the isospin projections of particles 1 and 2. From the above result, one sees that the operator $\boldsymbol{\tau}_1 \cdot \boldsymbol{\tau}_2$ is able to distinguish a two–nucleon state with isospin $T = 0$ from one with $T = 1$. In contrast, the identity operator has the same expectation value, unity, in both $T = 0$ and $T = 1$ states. Hence, with Eqs. (B.7) and (B.8), one obtains the isospin dependence, expressed by Eqs. (3.52) and (3.53) in Sec. 3.2.4 of Chapter 3, of the Horowitz–Love–Franey model of the NN interaction.

Appendix C

Relating NN observables to amplitudes

The aim of this appendix is to write down the relation between the NN spin observables ($\frac{d\sigma}{d\Omega}$, P, D, A_{yy}, A, R), plotted in Figs. 3.12 – 3.17 [see Chapter 3], and the McNeil–Ray–Wallace (MRW) amplitudes for NN scattering [see Eq. (3.18) in Chapter 3].

A convenient form of the NN scattering matrix, which respects parity and time-reversal invariance, is [Br78]

$$M(\vec{k}_f, \vec{k}_i) = \frac{1}{2}\{(a+b) + (a-b)\boldsymbol{\sigma}_1 \cdot \hat{n}\boldsymbol{\sigma}_2 \cdot \hat{n} + (c+d)\boldsymbol{\sigma}_1 \cdot \hat{m}\boldsymbol{\sigma}_2 \cdot \hat{m} + (c-d)\boldsymbol{\sigma}_1 \cdot \hat{\ell}\boldsymbol{\sigma}_2 \cdot \hat{\ell} + e(\boldsymbol{\sigma}_1 \cdot \hat{n} + \boldsymbol{\sigma}_2 \cdot \hat{n})$$

Here the amplitudes a, b, c, d and e are complex functions of two variables, e.g. the centre–of–mass system energy and scattering angle θ. The centre–of–mass basis vectors are:

$$\hat{\ell} = \frac{\vec{k}_f + \vec{k}_i}{|\vec{k}_f + \vec{k}_i|} \qquad \hat{m} = \frac{\vec{k}_f - \vec{k}_i}{|\vec{k}_f - \vec{k}_i|} \qquad \hat{n} = \frac{\vec{k}_i \times \vec{k}_f}{|\vec{k}_i \times \vec{k}_f|} \tag{C.1}$$

where $\vec{k}_i$ and $\vec{k}_f$ are vectors in the direction of the incident and scattered particle momenta in the centre–of–mass system. The Pauli spin matrices $\boldsymbol{\sigma}_1$ and $\boldsymbol{\sigma}_2$ act on the projectile and target nucleon wave functions, respectively. The amplitudes a, b, c, d and e are related to the A, B, C, D and E of the MRW scattering matrix $\mathcal{M}$ in Eq. (3.18) [see Chapter 3] via

$$\begin{pmatrix} a \\ b \\ c \\ d \\ e \end{pmatrix} = 2k_c i \begin{pmatrix} 1 & 1 & 0 & 0 & 0 \\ 1 & -1 & 0 & 0 & 0 \\ 0 & 2 & 0 & q^2 & 1 \\ 0 & 0 & 0 & q^2 & -1 \\ 0 & 0 & 2q & 0 & 0 \end{pmatrix} \begin{pmatrix} A \\ B \\ C \\ D \\ E \end{pmatrix} \tag{C.2}$$

The NN spin observables plotted in Figs. 3.12 – 3.17 (see Sec. 3.3.3 in Chapter 3) are defined in terms of the a, b, c, d and e amplitudes in Eq. (C.1) [Br78] as follows:

- Unpolarized differential cross section:

$$\bar{\sigma} = \frac{1}{2}\{|a|^2 + |b|^2 + |c|^2 + |d|^2 + |e|^2\} \tag{C.3}$$

- Polarization of scattered particle:

$$P = \mathrm{Re}(a^* e) \tag{C.4}$$

- Polarization correlation for initially unpolarized particles:

$$\sigma A_{yy} = \sigma C_{nn00} = \frac{1}{2}\{|a|^2 - |b|^2 - |c|^2 + |d|^2 + |e|^2\} \tag{C.5}$$

- Wolfenstein parameters or polarization transfer observables:

$$\sigma D = \sigma D_{l0m0} = \mathrm{Re}(b^* e) \tag{C.6}$$

$$\sigma A = \sigma D_{s'0k0} = -\mathrm{Re}(a^* b)\,\sin(\frac{\theta}{2}) + \mathrm{Re}(c^* d)\,\sin(\frac{-\theta}{2}) - \mathrm{Im}(b^* e)\,\cos(\frac{\theta}{2}) \tag{C.7}$$

$$\sigma R = \sigma D_{s'0s0} = -\mathrm{Re}(a^* b)\,\cos(\frac{\theta}{2}) + \mathrm{Re}(c^* d)\,\cos(\frac{-\theta}{2}) - \mathrm{Im}(b^* e)\,\sin(\frac{\theta}{2})\,. \tag{C.8}$$

Appendix D

Kinematics: Horowitz–Love–Franey model

The Horowitz–Love–Franey (HLF) model, discussed in Sec. (3.2.4) of Chapter 3, deals with the scattering of free–mass nucleons as opposed to the scattering of effective–mass nucleons for quasielastic proton–nucleus scattering. The aim of this appendix is to derive expressions for the kinematic quantities pertaining to the HLF model discussed in Sec. 3.2.4 of Chapter 3.

D.1 Projectile momentum in NN centre–of–mass system

Following a procedure analogous to that described in Sec. (I.10) of Appendix I, it is fairly straightforward to derive the following expression for the momentum of the incident nucleon in the NN centre–of–mass system (compare to Eq. (I.63) in Appendix I), namely

$$2|(\vec{k}\,)_{cm}| \;=\; \sqrt{2T_{\rm lab}\,m} \tag{D.1}$$

where m is the free nucleon rest mass, and $T_{\rm lab}$ is the laboratory kinetic energy of the projectile nucleon.

D.2 Direct and exchange three–momentum transfer

The aim of this section is to derive expressions for the nonrelativistic limit of the square of the direct four–momentum transfer $(q_\mu)^2$ and the square of the exchange four–momentum transfer $(Q_\mu)^2$, in the laboratory frame, for free NN scattering. One starts by deriving an expression for the nonrelativistic limit of the square of the direct four–momentum transfer $(q_\mu)^2$. From Eqs. (I.18), (I.14) [in Appendix I] and Eq. (3.64) [for the special case of free–mass scattering,

i.e. $m_1^* = m_2^* = m$] in Chapter 3, the square of the direct four–momentum transfer is given by

$$\begin{aligned}(q_\mu)^2 &= \omega^2 - |\vec{q}\,|^2 \\ &= (E_1 - E_1')^2 - (\vec{k}_1 - \vec{k}_1')^2 \,. \end{aligned} \tag{D.2}$$

Substitution of the relations

$$\begin{aligned}(E_1)^2 &= |\vec{k}_1|^2 + m^2 \\ (E_2)^2 &= |\vec{k}_2|^2 + m^2 \end{aligned} \tag{D.3}$$

in Eq. (D.2), and making use of the following Taylor expansions for the scattering energies (valid for $|\frac{|\vec{k}|}{m}| < 1$)

$$E = \sqrt{|\vec{k}|^2 + m^2} = m(1 + \frac{1}{2}\frac{|\vec{k}|^2}{m^2} + ...) \tag{D.4}$$

yields the nonrelativistic limit (i.e. $|\frac{\vec{k}}{m}| \ll 1$) of Eq. (D.2), namely

$$\begin{aligned}(q_\mu)^2 &= -(\vec{k}_1 - \vec{k}_1')^2 \\ &= -|\vec{q}\,|^2 \,. \end{aligned} \tag{D.5}$$

Following an argument similar to the one leading to Eq. (I.68) in Sec. I.11 of Appendix I, the following expression is obtained for the square of the direct four–momentum transfer

$$(q_\mu)^2 = -4|(\vec{k}\,)_{cm}|^2 \sin^2(\frac{\theta_{cm}}{2}) \tag{D.6}$$

where $\vec{k}_{cm}$ is the energy of the incident nucleon in the NN centre–of–mass system, and θ_{cm} is the centre–of–mass scattering angle. Combining Eqs. (D.5) and (D.6), one can now write down an expression for $|\vec{q}\,|$ in the nonrelativistic limit, namely

$$\begin{aligned}(q_\mu)^2 &= -|\vec{q}\,|^2 \\ &= -4|(\vec{k}\,)_{cm}|^2 \sin^2(\frac{\theta_{cm}}{2}) \,. \end{aligned} \tag{D.7}$$

which implies the following expression (in the nonrelativistic limit) for $|\vec{q}\,|$:

$$|\vec{q}\,| = 2|(\vec{k}\,)_{cm}| \sin(\frac{\theta_{cm}}{2}) \,. \tag{D.8}$$

Next, an expression for the nonrelativistic limit of the square of the exchange four–momentum transfer $(Q_\mu)^2$ is derived. To this end, one makes use of the fact that the exchange four–momentum transfer (often called the Mandelstam variable u) is an invariant quantity [Si90]),

that is

$$[(k_1 - k_2')_{cm}]_\mu \, [(k_1 - k_2')_{cm}]^\mu \;=\; [(k_1 - k_2')_{\rm lab}]_\mu \, [(k_1 - k_2')_{\rm lab}]^\mu \tag{D.9}$$

where the subscripts "cm" and "lab" refer to the laboratory– and NN centre–of–mass frames respectively. The centre–of–mass exchange four–momentum transfer is defined by

$$[(k_1 - k_2')_{cm}]^\mu \;=\; [\,(E_1)_{cm} - (E_2')_{cm}\,,\; (\vec{k}_1)_{cm} - (\vec{k}_2')_{cm}\,]\,, \tag{D.10}$$

and, the laboratory exchange four–momentum transfer Q_μ is given by

$$Q^\mu \;=\; [\,(k_1 - k_1')_{\rm lab}\,]^\mu \;=\; [\,W\,,\,\vec{Q}\,] \tag{D.11}$$

where

$$\begin{aligned} W &= E_1 - E_2' \\ \vec{Q} &= \vec{k}_1 - \vec{k}_2'\,. \end{aligned} \tag{D.12}$$

With Eqs. (D.10), (D.11) and (D.12), Eq. (D.9) can be written as

$$[(E_1)^{cm}_{\rm eff} - (E_2')^{cm}_{\rm eff}]^2 \;-\; [(\vec{k}_1)^{cm}_{\rm eff} - (\vec{k}_2')^{cm}_{\rm eff}]^2 \;=\; W^2 \;-\; |\vec{Q}\,|^2\,. \tag{D.13}$$

Making use of the fact that the NN centre–of–mass system (for scattering of free equal–mass nucleons) is defined by

$$\begin{aligned} (E_1)_{cm} \;=\; (E_1')_{cm} \;&=\; (E_2)_{cm} \;=\; (E_2')_{cm} \\ (\vec{k}_1)_{cm} + (\vec{k}_2)_{cm} \;&=\; 0 \\ |(\vec{k}_1)_{cm}| \;=\; |(\vec{k}_1')_{cm}| \;&=\; |(\vec{k}_2)_{cm}| \;=\; |(\vec{k}_2')_{cm}| \;=\; |(\vec{k})_{cm}| \quad \text{(say)} \end{aligned} \tag{D.14}$$

one can write Eq. (D.13) as

$$W^2 - |\vec{Q}\,|^2 \;=\; -4|(\vec{k}\,)_{cm}|^2 \cos^2(\frac{\theta_{cm}}{2})\,. \tag{D.15}$$

Following a discussion similar to the one leading to Eq. (D.7), it can be shown that the nonrelativistic limit of $(Q_\mu)^2$ is given by

$$(Q_\mu)^2 \;=\; -|\vec{Q}\,|^2 \tag{D.16}$$

From Eqs. (D.15) and (D.16) it follows that (in the nonrelativistic limit)

$$|\vec{Q}\,| \;=\; 2|(\vec{k}\,)_{cm}|\cos(\frac{\theta_{cm}}{2})\,. \tag{D.17}$$

Combining Eqs. (D.7) and (D.17) yields the following nonrelativistic relation between $|\vec{q}\,|$ and $|\vec{Q}\,|$:

$$|\vec{q}\,|^2 \;+\; |\vec{Q}\,|^2 \;=\; 4|(\vec{k}\,)_{cm}|^2\,. \tag{D.18}$$

Appendix E

Electron scattering

E.1 Introduction

In this appendix, a systematic derivation is given of the S–matrix element for electron–electron scattering within the framework of quantum field theory, thereby confirming the Feynman rules quoted in standard texts such as Bjorken and Drell [Bj64] and Greiner [Gr92]. It is also shown how the physical scattering cross section is related to the S–matrix element, and how one applies the well–known trace techniques to explicitly evaluate the unpolarized and polarized differential and double differential cross sections to lowest order.

E.2 Electromagnetic coupling and the S–matrix

The conventions and notation of Bjorken and Drell [Bj64] are adopted, and Heaviside–Lorentz [Gu91, Gr92], and natural units ($\hbar = c = 1$) are also used. Furthermore, it is also assumed that the reader is familiar with the canonical quantization procedure of local field theories [Sa67, Na90, Gu91, Ka93, Gr96].

In this section some of the background leading to the perturbation expansion of the S–matrix for quantum electrodynamics (QED) is given, that is, the theory of a charged spin–$\frac{1}{2}$ field (electrons) coupled to a massless spin–1 field (photons). This theory is ideally suited for a perturbative approach, since the electromagnetic coupling constant $\alpha = \frac{e^2}{4\pi\hbar c} \approx \frac{1}{137}$ is very small.

The classical Lagrangian of QED is given by

$$\mathcal{L} = \mathcal{L}_0^{\text{Dirac}} + \mathcal{L}_0^{\text{em}} + \mathcal{L}_{\text{int}} \tag{E.1}$$

with

$$\mathcal{L}_0^{\text{Dirac}} = \bar{\psi}(x)(\frac{1}{2}\gamma^\mu \overleftrightarrow{\partial}_\mu - m)\psi(x) , \tag{E.2}$$

$$\mathcal{L}_0^{\text{em}} = -\frac{1}{4}F_{\mu\nu}(x)F^{\mu\nu}(x) , \tag{E.3}$$

$$\mathcal{L}_0^{\text{int}} = -e\bar{\psi}(x)\gamma_\mu\psi(x)A^\mu , \tag{E.4}$$

where the interaction term $\mathcal{L}_0^{\text{int}}$ is introduced via substitution of the gauge invariant minimal–substitution–prescription

$$\partial_\mu \longrightarrow \partial_\mu + ieA_\mu . \tag{E.5}$$

$F_{\mu\nu}$ is the usual electromagnetic field strength tensor. The equations of motion follow from independent variation of the Lagrangian density with respect to the fields ψ, $\bar{\psi}$, and A^μ:

$$[\gamma^\mu i\{\partial_\mu + ieA_\mu(x)\} - m]\psi(x) = 0 , \tag{E.6}$$

$$\bar{\psi}(x)[\gamma^\mu i\{\overleftarrow{\partial}_\mu - ieA_\mu\} + m] = 0 , \tag{E.7}$$

$$\partial_\nu F^{\mu\nu}(x) = e\bar{\psi}(x)\gamma^\mu\psi(x) . \tag{E.8}$$

The associated Hamilton density is defined in the usual way

$$\mathcal{H} = \pi\dot{\psi} - \mathcal{L} \tag{E.9}$$

where the momentum conjugate π to the field ψ is given by

$$\pi = \frac{\partial\mathcal{L}}{\partial\dot{\pi}} . \tag{E.10}$$

Substituting Eq. (E.1) into Eq. (E.9), and using Eq. (E.10), gives the Hamilton density describing the interaction

$$\mathcal{H}_{\text{int}} = -\mathcal{L}_{\text{int}} = e\bar{\psi}(x)\gamma_\mu\psi(x)A^\mu(x) . \tag{E.11}$$

Quantizing this theory, and employing the usual normal-ordering prescription (denoted by : :), yields the interaction term of the Hamilton density operator, namely

$$\hat{\mathcal{H}}_{\text{int}} = -\hat{\mathcal{L}}_{\text{int}} = e{:}\bar{\hat{\psi}}(x)\gamma_\mu\hat{\psi}(x)A^\mu(x){:} \tag{E.12}$$

where the hat denotes quantized field operators in the Heisenberg picture. In order to evaluate cross sections for elementary scattering processes it is necessary to define the S–operator, the

matrix elements of which describe the probability amplitude for a system to make a transition from an initial to a final state under the influence of an interaction. Following standard texts [Sa67, Na90, Gu91, Ka93, Gr96], the perturbation series for the unitary S–operator in the interaction picture is

$$\hat{S} = \sum_{n=0}^{\infty} \frac{1}{n!}(-i)^n \int d^4x_1 ... d^4x_n \times \mathrm{T}[\hat{\mathcal{H}}_{\mathrm{int}}(t_1) ... \hat{\mathcal{H}}_{\mathrm{int}}(t_n)] \tag{E.13}$$

where T is the usual chronological or time–ordering operator. In order to carry out the perturbation expansion, it is convenient to express all operators in the interaction picture. The transition from the Heisenberg to the interaction picture is accomplished by the transformation

$$\hat{O}^I(t) = e^{i\hat{H}_0^S t} e^{-i\hat{H}t} \hat{O}^H(t) e^{i\hat{H}t} e^{-i\hat{H}_0^S t} \tag{E.14}$$

where the superscripts "I", "S" and "H" refer to the interaction, Schrödinger and Heisenberg pictures respectively, and the full Hamiltonian $\hat{H}$ is split into a noninteracting $\hat{H}_0$ and an interacting part $\hat{H}_{\mathrm{int}}$,

$$\hat{H} = \hat{H}_0 + \hat{H}_{\mathrm{int}} \,. \tag{E.15}$$

The Hamilton operator $\hat{H}$ and Hamilton density operator $\hat{\mathcal{H}}$ are related via

$$\hat{H} = \int d\vec{x}\, \hat{\mathcal{H}} \,. \tag{E.16}$$

With the transformation defined by Eq. (E.14), Eq. (E.12) retains its form, namely

$$\hat{\mathcal{H}}^I_{\mathrm{int}} = e{:}\bar{\hat{\psi}}^I(x)\gamma_\mu \hat{\psi}^I A^\mu_I(x){:} \,. \tag{E.17}$$

For the remainder of the discussion, it is assumed that all operators are in the interaction picture, unless otherwise specified, and hence the indices "I" are omitted.

E.3 Plane–wave expansions for spin–$\frac{1}{2}$ field operators

The aim of this section is to write down the plane–wave expansions of the spin–$\frac{1}{2}$ field operators and to define normalizations which are consistent with those of Bjorken and Drell [Bj64]. The momentum-space expansions for spin–$\frac{1}{2}$ Dirac fields in the interaction picture are [Gr96]

$$\hat{\psi}(x) = \hat{\psi}^+(x) + \hat{\psi}^-(x) \,, \tag{E.18}$$

where

$$\hat{\psi}^{+}(x) = \int \frac{d\vec{p}}{(2\pi)^{3/2}} \sqrt{\frac{m}{E_p}} \sum_s \hat{b}_{ps} u(p,s) e^{-ip\cdot x} , \tag{E.19}$$

$$\hat{\psi}^{-}(x) = \int \frac{d\vec{p}}{(2\pi)^{3/2}} \sqrt{\frac{m}{E_p}} \sum_s \hat{d}^{\dagger}_{ps} v(p,s) e^{ip\cdot x} , \tag{E.20}$$

and $E_p = |\vec{p}\,|^2 + m^2$. The corresponding expansions for the adjoint field operator are obtained via the relation

$$\bar{\psi}(x) = \psi^{\dagger}(x)\gamma^0 . \tag{E.21}$$

The properties of the positive and negative energy Dirac spinors, u and v respectively, are compactly written by introducing the following notation

$$\begin{aligned} w_1(\vec{p}\,) &= u(p,+s) \\ w_2(\vec{p}\,) &= u(p,-s) \\ w_3(\vec{p}\,) &= v(p,-s) \\ w_4(\vec{p}\,) &= v(p,+s) \end{aligned} \tag{E.22}$$

where the Dirac unit spinors $w_r(\vec{p}\,)$ satisfy the algebraic equation

$$(i\gamma^{\mu}\partial_{\mu} - \epsilon_r m) w_r(\vec{p}\,) . \tag{E.23}$$

The index r enumerates the four independent solutions of the free Dirac equation, where r = 1,2 denotes the solutions with positive energy $E = +\sqrt{|\vec{p}\,|^2 + m^2}$, and r = 3,4 denotes solutions with negative energy $E = -\sqrt{|\vec{p}\,|^2 + m^2}$. This is expressed by the sign function $\epsilon_r = +1$ for r = 1,2 and $\epsilon_r = -1$ for r = 3,4. With this notation, the plane–wave solutions of the free Dirac equation

$$(i\gamma^{\mu}\partial_{\mu} - m)\psi^{r}_{\vec{p}}(\vec{x},t) = 0 , \tag{E.24}$$

are given by [Bj64, Gr90]

$$\psi^{r}_{\vec{p}}(\vec{x},t) = (2\pi)^{-3/2} \sqrt{\frac{m}{E_p}} w_r(\vec{p}\,) e^{-i\epsilon_r(E_p t - \vec{p}\cdot\vec{x})} \tag{E.25}$$

where the Dirac unit spinors $w_r(\vec{p}\,)$ satisfy the following orthogonality and completeness properties [Gr96]:

$$w^{\dagger}_{r'}(\epsilon_{r'}\vec{p}\,) w_r(\epsilon_r \vec{p}\,) = \frac{E_p}{m}\delta_{rr'} , \tag{E.26}$$

$$\bar{w}_{r'}(\vec{p}\,)w_r(\vec{p}\,) = \epsilon_r\delta_{rr'}\,, \tag{E.27}$$

$$\sum_{r=1}^{4} w_{r\alpha}(\epsilon_r\vec{p}\,)w^{\dagger}_{r\beta}(\epsilon_r\vec{p}\,) = \frac{E_p}{m}\delta_{\alpha\beta}\,, \tag{E.28}$$

$$\sum_{r=1}^{4} \epsilon_r w_{r\alpha}(\vec{p}\,)\bar{w}_{r\beta}(\vec{p}\,) = \delta_{\alpha\beta}\,. \tag{E.29}$$

Eq. (E.26) guarantees that the plane waves in Eq. (E.25) have the correct normalization, namely

$$\int d\vec{x}\,\psi^{(r')\dagger}_{\vec{p}\,'}(x)\psi^{(r)}_{\vec{p}}(x) = \delta_{rr'}\delta^3(\vec{p}-\vec{p}\,')\,. \tag{E.30}$$

The normalization conditions given by Eqs. (E.26) and (E.27), yield the following expressions for the Dirac unit spinors

$$w_1(\vec{p}\,) = \sqrt{\frac{E_p+m}{2m}}\begin{pmatrix} 1 \\ 0 \\ \dfrac{p_z}{E_p+m} \\ \dfrac{p_x+ip_y}{E_p+m} \end{pmatrix} \tag{E.31}$$

$$w_2(\vec{p}\,) = \sqrt{\frac{E_p+m}{2m}}\begin{pmatrix} 0 \\ 1 \\ \dfrac{p_x-ip_y}{E_p+m} \\ \dfrac{-p_z}{E_p+m} \end{pmatrix} \tag{E.32}$$

$$w_3(\vec{p}\,) = \sqrt{\frac{E_p+m}{2m}}\begin{pmatrix} \dfrac{p_z}{E_p+m} \\ \dfrac{p_x+ip_y}{E_p+m} \\ 1 \\ 0 \end{pmatrix} \tag{E.33}$$

$$w_4(\vec{p}\,) = \sqrt{\frac{E_p+m}{2m}}\begin{pmatrix} \dfrac{p_x-ip_y}{E_p+m} \\ \dfrac{-p_z}{E_p+m} \\ 0 \\ 1 \end{pmatrix}. \tag{E.34}$$

The time–independent creation and annihilation operators in Eqs. (E.19) and (E.20) satisfy the usual equal–time anticommutation relations

$$\{\hat{b}_{ps}, \hat{b}^{\dagger}_{p's'}\} = \delta^3(\vec{p}-\vec{p}\,')\delta_{ss'}\,, \tag{E.35}$$

$$\{\hat{d}_{ps}, \hat{d}^{\dagger}_{p's'}\} = \delta^3(\vec{p}-\vec{p}\,')\delta_{ss'}\,, \tag{E.36}$$

whereas the anticommutators involving the remaining eight combinations of $\hat{b}$, $\hat{b}^\dagger$, $\hat{d}$ and $\hat{b}^\dagger$ vanish. The operators $\hat{b}^\dagger$ and $\hat{b}$ are associated with the creation and annihilation of particles, whereas the operators $\hat{d}^\dagger$ and $\hat{d}$ are associated with the creation and annihilation of antiparticles. Using these operators the Fock space can be constructed, starting from the vacuum state $|0>$, defined to be that state containing neither particles or antiparticles, that is

$$\hat{b}_{ps}|0> = 0 \tag{E.37}$$

$$\hat{d}_{ps}|0> = 0\,. \tag{E.38}$$

E.3.1 Feynman propagator for photons

The plane–wave expansions for the photon fields are not written down in this appendix. Quantization of the photon field is more complicated, and the interested reader is referred to Refs. [Sa67, Na90, Gu91, Ka93, Gr96]. For our purposes, however, it is sufficient to quote the expression for the Feynman propagator for photons, namely

$$\begin{aligned} iD_F^{\mu\nu}(x-y) &= \hat{A}^\mu(x)\hat{A}^\nu(y) \\ &= \langle 0|T[\hat{A}^\mu(x)\hat{A}^\nu(y)]|0\rangle \\ &= i\int \frac{d^4k}{(2\pi)^4} e^{-ik\cdot(x-y)} D_F^{\mu\nu}(k) \end{aligned} \tag{E.39}$$

where the momentum–space Feynman propagator in the Feynman gauge is given by

$$D_F^{\mu\nu}(k) = \frac{-g_{\mu\nu}}{k^2 + i\epsilon}\,. \tag{E.40}$$

E.4 Electron–electron scattering

In this section, the preceding theory is applied to evaluate the cross section for electron–electron scattering, also known as Møller scattering.

E.4.1 S–matrix elements

To explicitly evaluate a scattering process, one needs the matrix element of the S–operator taken between definite particle configurations. Consider Møller scattering for which two electrons with

four–momenta and spin (p_1, s_1) and (p_2, s_2) in the initial state, are scattered into the final state with $(p_{1'}, s_{1'})$ and $(p_{2'}, s_{2'})$.

One begins by defining single–particle fermion states of definite momentum within a box of volume V

$$|\vec{p}, s> = \sqrt{\frac{(2\pi)^3}{V}}\hat{b}^{\dagger}_{ps}|0> , \tag{E.41}$$

with normalization

$$<\vec{p}, s\,|\vec{p}, s\,'> = \frac{(2\pi)^3}{V}\delta^3(\vec{p}-\vec{p}\,')\,\delta_{s's} . \tag{E.42}$$

For momentum states, the latter normalization implies that

$$<\vec{p}\,|\vec{p}> = \frac{(2\pi)^3}{V}\delta^3(0) , \tag{E.43}$$

which means that one has an awkward definition for the number of states. However, this is interpreted to mean that one is actually calculating particle densities inside a large but finite box of length L and volume V; that is, one defines

$$\delta^3(\vec{p}) = \lim_{L\to\infty}[\frac{1}{(2\pi)^3}\int\int\int_{-L/2}^{L/2} dx\,dy\,dz\,e^{-i\vec{p}\cdot\vec{r}}] . \tag{E.44}$$

This implies that one takes the definition:

$$\delta^3(0) = \frac{V}{(2\pi)^3} \tag{E.45}$$

and, hence, Eq. (E.43) becomes

$$<\vec{p}\,|\vec{p}> = 1 . \tag{E.46}$$

One lets the volume V of the box tend to infinity only at the end of the calculation. The origin of this problem is that one is dealing with plane waves, rather than wave packets that are confined to a specific region of space and time. The price one pays for these nonlocalized plane waves is that one must carefully divide out infinite quantities proportional to time and the volume of space.

For Møller scattering, the initial state of the two–electron system (at time $t = -\infty$) is

$$|t = -\infty> = |e(p_1, s_1)\; e(p_2, s_2)> = \frac{(2\pi)^3}{V} \times \hat{b}^{\dagger}_{p_1 s_1}\hat{b}^{\dagger}_{p_2 s_2}|0> . \tag{E.47}$$

The probability amplitude for finding two electrons of four–momenta $p_{1'}$, $p_{2'}$ and spin orientations $s_{1'}$, $s_{2'}$ in the final state $|t = +\infty>$, is given by the S–matrix element

$$\begin{aligned} S_{fi} &= < e(p_{1'}, s_{1'})\ e(p_{2'}, s_{2'})|\ \hat{S}\ |e(p_1, s_1)\ e(p_2, s_2)> \\ &= \frac{(2\pi)^6}{V^2} \times < 0|\hat{b}_{p_{2'}s_{2'}} \hat{b}_{p_{1'}s_{1'}}\ \hat{S}\ \hat{b}^\dagger_{p_1 s_1} \hat{b}^\dagger_{p_2 s_2}|0> \end{aligned} \tag{E.48}$$

where use has been made of Eq. (E.47), and $\hat{S}$ is defined in Eq. (E.13). One only considers the case in which a scattering has taken place, and hence the initial and final states in Eq. (E.48) are different, that is

$$e(p_{1'}, s_{1'}),\ e(p_{2'}, s_{2'}) \neq e(p_1, s_1),\ e(p_2, s_2)\ . \tag{E.49}$$

For this case, the unit operator in the perturbation series of the S–operator in Eq. (E.13) [i.e, the term for which $n = 0$] does not contribute to the scattering process. The first correction term [term $n = 1$ in Eq. (E.13)] also does not contribute for the following reason: if one expresses $\mathcal{H}_{\text{int}}$ in Eq. (E.12) in terms of creation and annihilation operators via Eqs. (E.19) and (E.20), and the analogous expressions for the photon field operators [Gr96], then the photon creation and annihilation operators give zero when acting on the vacuum to the left and right respectively. Thus, the lowest order scattering (i.e. Born approximation) in the perturbation series given by Eq. (E.13) is to order e^2. Truncating the expansion at this term gives [Na90]

$$\begin{aligned} S_{fi} &= \frac{1}{2}(-ie)^2 \int d^4x_1\ d^4x_2 < 0|\hat{b}_{p_{2'}s_{2'}} \hat{b}_{p_{1'}s_{1'}} \\ &\quad \times T[:\bar{\psi}(x_1)\gamma_\mu\psi(x_1) : A^\mu(x_1) : \bar{\psi}(x_2)\gamma_\nu\psi(x_2) : A^\nu(x_2)] \\ &\quad \times \hat{b}^\dagger_{p_1 s_1} \hat{b}^\dagger_{p_2 s_2}|0> \times \frac{(2\pi)^6}{V^2}\ . \end{aligned} \tag{E.50}$$

This expression may at first seem rather complicated, however, one only needs to insert expansions for the field operators in Eq. (E.19) and (E.20), and then use Wick's theorem to reduce the expression to a simpler form. The matrix element has the following structure:

$$< 0|\hat{b}\,\hat{b} : (\hat{b}^\dagger + \hat{d})(\hat{b} + \hat{d}^\dagger) : \hat{A}^\mu(x_1)\ : (\hat{b}^\dagger + \hat{d})(\hat{b} + \hat{d}^\dagger) : \hat{A}^\nu(x_2)\ \hat{b}^\dagger\,\hat{b}^\dagger|0> \ . \tag{E.51}$$

One sees that $\hat{A}^\mu(x_1)$ can only be contracted with $\hat{A}^\nu(x_2)$, yielding the photon propagator given by Eq. (E.39) and (E.40). If one further contracts all fermion operators, one finds no contribution when operators from $\hat{\psi}(x_1)$ and $\hat{\bar{\psi}}(x_2)$ are paired. This is because here at least one contraction of an incoming with an outgoing electron operator occurs, and due to the condition expressed by

Eq. (E.49), one gets zero. The only nonzero contribution is obtained by contracting all operators of incoming and outgoing electrons with the field operators $\hat{\psi}$ and $\hat{\bar{\psi}}$. For example, one must contract $\hat{b}^{\dagger}_{p_1 s_1}$ with $\hat{\psi}(x_1)$ and $\hat{\psi}(x_2)$ in turn. Thus, applying Wick's theorem to Eq. (E.50), one gets

$$\frac{V^2}{(2\pi)^6} \times \langle 0|\hat{b}_{p_{2'}s_{2'}}\hat{b}_{p_{1'}s_{1'}} : \hat{\bar{\psi}}(x_1)\gamma_\mu\hat{\psi}(x_1) :: \hat{\bar{\psi}}(x_2)\gamma_\nu\hat{\psi}(x_2) : \hat{b}^{\dagger}_{p_1 s_1}\hat{b}^{\dagger}_{p_2 s_2}|0\rangle$$

$$= \hat{b}_{p_{2'}s_{2'}}\hat{b}_{p_{1'}s_{1'}} : \hat{\bar{\psi}}(x_1)\gamma_\mu\hat{\psi}(x_1) :: \hat{\bar{\psi}}(x_2)\gamma_\nu\hat{\psi}(x_2) : \hat{b}^{\dagger}_{p_1 s_1}\hat{b}^{\dagger}_{p_2 s_2}$$

A

$$+\hat{b}_{p_{2'}s_{2'}}\hat{b}_{p_{1'}s_{1'}} : \hat{\bar{\psi}}(x_1)\gamma_\mu\hat{\psi}(x_1) :: \hat{\bar{\psi}}(x_2)\gamma_\nu\hat{\psi}(x_2) : \hat{b}^{\dagger}_{p_1 s_1}\hat{b}^{\dagger}_{p_2 s_2}$$

$$+\hat{b}_{p_{2'}s_{2'}}\hat{b}_{p_{1'}s_{1'}} : \hat{\bar{\psi}}(x_1)\gamma_\mu\hat{\psi}(x_1) :: \hat{\bar{\psi}}(x_2)\gamma_\nu\hat{\psi}(x_2) : \hat{b}^{\dagger}_{p_1 s_1}\hat{b}^{\dagger}_{p_2 s_2}$$

$$+\hat{b}_{p_{2'}s_{2'}}\hat{b}_{p_{1'}s_{1'}} : \hat{\bar{\psi}}(x_1)\gamma_\mu\hat{\psi}(x_1) :: \hat{\bar{\psi}}(x_2)\gamma_\nu\hat{\psi}(x_2) : \hat{b}^{\dagger}_{p_1 s_1}\hat{b}^{\dagger}_{p_2 s_2} \,.$$

The contraction denoted by A, for example, can be simplified by substitution of Eq. (E.18) into the latter expression, and by applying the anticommutation relations given by Eqs. (E.35) and (E.36), thus yielding

$$\begin{aligned}
\hat{\psi}(x_2)\hat{b}^{\dagger}_{p_2 s_2} &= \langle 0|\hat{\psi}(x_2)\hat{b}^{\dagger}_{p_2 s_2}|0\rangle \\
&= \int \frac{d\vec{p}}{(2\pi)^{3/2}}\sqrt{\frac{m}{E_p}}\sum_s \langle 0|[\hat{b}_{ps}u(p,s)e^{-ip\cdot x_2} + \hat{d}^{\dagger}_{ps}v(p,s)e^{ip\cdot x_2}]\hat{b}^{\dagger}_{p_2 s_2}|0\rangle \\
&= \frac{1}{(2\pi)^{3/2}}\sqrt{\frac{m}{E_p}}u(p_2,s_2)e^{-ip_2\cdot x_2} \,.
\end{aligned} \tag{E.52}$$

Applying a similar procedure to the remaining contractions, gives

$$\begin{aligned}
&\frac{V^2}{(2\pi)^6}\times\langle 0|\hat{b}_{p_{2'}s_{2'}}\hat{b}_{p_{1'}s_{1'}} : \hat{\bar{\psi}}(x_1)\gamma_\mu\hat{\psi}(x_1) :: \hat{\bar{\psi}}(x_2)\gamma_\nu\hat{\psi}(x_2) : \hat{b}^\dagger_{p_1s_1}\hat{b}^\dagger_{p_2s_2}|0\rangle \\
&= [\sqrt{\frac{m}{E_{p_{1'}}}}\bar{u}(p_{1'},s_{1'})e^{ip_{1'}\cdot x_1}\gamma_\mu\sqrt{\frac{m}{E_{p_1}}}\bar{u}(p_1,s_1)e^{-ip_1\cdot x_1}] \\
&+ [\sqrt{\frac{m}{E_{p_{2'}}}}\bar{u}(p_{2'},s_{2'})e^{ip_{2'}\cdot x_2}\gamma_\nu\sqrt{\frac{m}{E_{p_2}}}\bar{u}(p_2,s_2)e^{-ip_2\cdot x_2}] \\
&- (1\longleftrightarrow 2) - (2'\longleftrightarrow 1') + (1\longleftrightarrow 2,\ 2'\longleftrightarrow 1') \,. \qquad \text{(E.53)}
\end{aligned}$$

If this result is inserted into Eq. (E.50) then, since the contraction of fermion operators for $t_1 > t_2$ and $t_1 < t_2$ is the same, one obtains

$$\begin{aligned}
S_{fi} \;=\; &\frac{1}{2}(-ie)^2\int d^4x_1\, d^4x_2\{\theta(t_1-t_2)<0|\hat{A}^\mu(x_1)\hat{A}^\nu(x_2)|0> + \theta(t_2-t_1)<0|\hat{A}^\nu(x_2)\hat{A}^\mu(x_1)|0>\} \\
&\sqrt{\frac{m}{E_{p_1}}}\sqrt{\frac{m}{E_{p_2}}}\sqrt{\frac{m}{E_{p'_1}}}\sqrt{\frac{m}{E_{p'_2}}}\,\frac{1}{V^2}\,[\bar{u}(p_{1'},s_{1'})\gamma_\mu u(p_1,s_1)e^{i(p_{1'}-p_1)\cdot x_1}\bar{u}(p_{2'},s_{2'})\gamma_\nu u(p_2,s_2)e^{i(p_{2'}-p_2)\cdot x_2} \\
&-(1\longleftrightarrow 2) - (2'\longleftrightarrow 1') + (1\longleftrightarrow 2,\ 2'\longleftrightarrow 1')] \,. \qquad \text{(E.54)}
\end{aligned}$$

Collecting together terms which differ only in the symbols used for integration or summation variables, finally leads to

$$\begin{aligned}
S_{fi} \;=\; &\frac{(-ie)^2}{V^2}\sqrt{\frac{m}{E_{p_1}}}\sqrt{\frac{m}{E_{p_2}}}\sqrt{\frac{m}{E_{p'_1}}}\sqrt{\frac{m}{E_{p'_2}}}\int d^4x_1 d^4x_2 < 0|T[\hat{A}^\mu(x_1)\hat{A}^\nu(x_2)]|0> \\
&[\bar{u}(p_{1'},s_{1'})\gamma_\mu\bar{u}(p_1,s_1)\bar{u}(p_{2'},s_{2'})\gamma_\nu\bar{u}(p_2,s_2)e^{i(p_{1'}-p_1)\cdot x_1}e^{i(p_{2'}-p_2)\cdot x_2} \\
&- \bar{u}(p_{2'},s_{2'})\gamma_\mu\bar{u}(p_1,s_1)\bar{u}(p_{1'},s_{1'})\gamma_\nu\bar{u}(p_2,s_2)e^{i(p_{2'}-p_1)\cdot x_1}e^{i(p_{1'}-p_2)\cdot x_2}] \,. \qquad \text{(E.55)}
\end{aligned}$$

Replacing the photon propagator $< 0|T[\hat{A}^\mu(x)\hat{A}^\nu(y)]|0 >= i\,D_F^{\mu\nu}(x-y)$ by the Fourier transform expressed in Eqs. (E.39) and (E.40), enables the integration over x_1 and x_2 to be easily carried out, yielding delta functions of four–momenta. Hence, the final result for the S–matrix element for Møller scattering, to order e^2 in Eq. (E.48), is

$$\begin{aligned}
S_{fi} \;=\; &\frac{(-ie)^2}{V^2}\sqrt{\frac{m}{E_{p_1}}}\sqrt{\frac{m}{E_{p_2}}}\sqrt{\frac{m}{E_{p'_1}}}\sqrt{\frac{m}{E_{p'_2}}}(2\pi)^4(p_{1'}+p_{2'}-p_1-p_2) \\
&\times[\bar{u}(p_{1'},s_{1'})\gamma_\mu u(p_1,s_1)iD_F^{\mu\nu}(p_{1'}-p_1)\bar{u}(p_{2'},s_{2'})\gamma_\nu u(p_2,s_2) \\
&- \bar{u}(p_{2'},s_{2'})\gamma_\mu\bar{u}(p_1,s_1)iD_F^{\mu\nu}(p_{1'}-p_2)\bar{u}(p_{1'},s_{1'})\gamma_\nu\bar{u}(p_2,s_2)] \,, \qquad \text{(E.56)}
\end{aligned}$$

where the photon propagator $D_F^{\mu\nu}(k)$ is given by Eq. (E.40). The minus sign in the second term of Eq. (E.56) is a consequence of the indistinguishability of the electrons and of the Fermi–Dirac statistics.

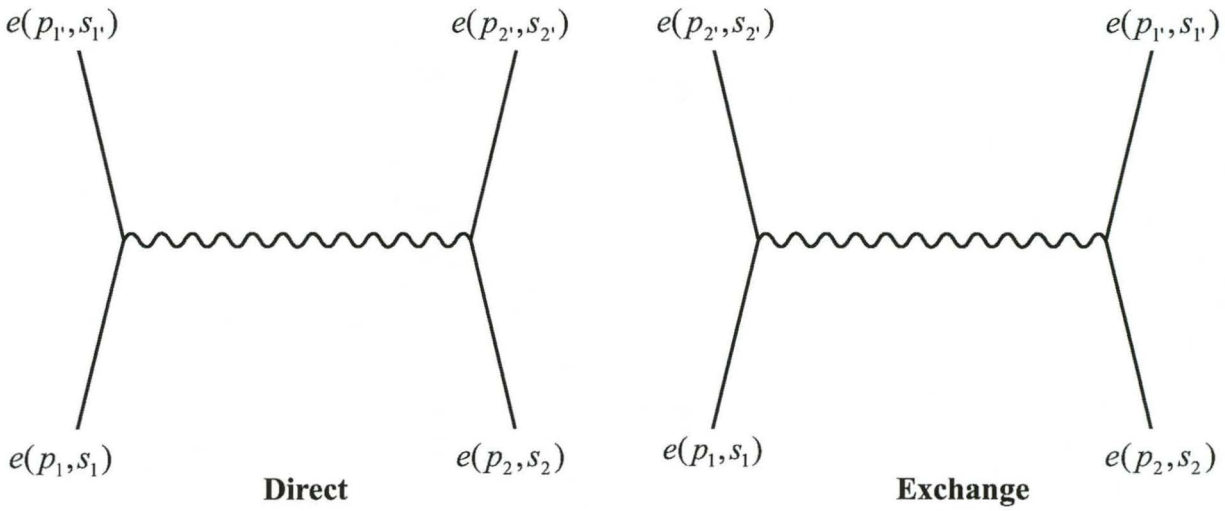

Figure E.1: Direct and exchange Feynman diagrams for electron–electron scattering.

The result in Eq. (E.56) is now compared to the corresponding expression obtained via application of the Feynman rules for Møller scattering as described in Bjorken and Drell [Bj64]. According to the latter reference, the lowest order Feynman (i.e. order e^2) diagrams for electron–electron scattering are the direct and exchange diagrams depicted in Fig. E.1: these are examples of "tree diagrams", that is, diagrams without loops.

Using Feynman rules (see Appendix B in Ref. [Bj64]) to write down the S–matrix element associated with the diagrams in Fig. E.1, yields an expression which is identical to Eq. (E.56). Thus, for Møller scattering, the validity of the Feynman rules quoted by Bjorken and Drell [Bj64] has been explicitly confirmed. Note that Eq. (E.56) is also identical to the corresponding S–matrix element for Møller scattering in section 3.3 of Ref. [Gr92].

E.5 Scattering cross sections

The connection between the S–matrix element and the physical scattering cross section is now presented. This topic is discussed in more detail in Greiner's book on "*Quantum Electrodynamics*" [Gr92]. Note that the latter reference uses Gaussian units, whereas Heaviside–Lorentz units [Gu91, Gr92] are considered here.

Starting from the scattering matrix element S_{fi} in Eq. (E.56), the Lorentz invariant amplitude M_{fi} is defined by extracting some kinematical factors. For the case of Møller scattering, the connection between S_{fi} and M_{fi} is given by [Bj64, Gr92]

$$S_{fi} = \frac{-i}{V^2}(2\pi)^4\sqrt{\frac{m}{E_{p_1}}}\sqrt{\frac{m}{E_{p_2}}}\sqrt{\frac{m}{E_{p_1'}}}\sqrt{\frac{m}{E_{p_2'}}}\delta^4(p_{1'}+p_{2'}-p_1-p_2)M_{fi} \tag{E.57}$$

where

$$\begin{aligned} M_{fi} = {} & e^2[\,\bar{u}(p_{1'},s_{1'})\gamma_\mu u(p_1,s_1)\frac{1}{(p_{1'}-p_1)^2+i\epsilon}\bar{u}(p_{2'},s_{2'})\gamma^\mu u(p_2,s_2) \\ & - \bar{u}(p_{2'},s_{2'})\gamma_\mu u(p_1,s_1)\frac{1}{(p_{1'}-p_2)^2+i\epsilon}\bar{u}(p_{1'},s_{1'})\gamma^\mu u(p_2,s_2)\,]\,. \end{aligned} \tag{E.58}$$

Following standard references [Bj64, Gr92], the differential scattering cross section, which is the number of transitions per unit time per unit volume divided by the flux of incident particles, is given by

$$d\sigma = \frac{1}{|\vec{v}_1-\vec{v}_2|}\left(\frac{m}{E_{p_1}}\right)\left(\frac{m}{E_{p_2}}\right)|M_{fi}|^2\frac{m d\vec{p}_{1'}}{E_{p_{1'}}(2\pi)^3}\frac{m d\vec{p}_{2'}}{E_{p_{2'}}(2\pi)^3}(2\pi)^4\delta^4(p_{1'}+p_{2'}-p_1-p_2) \tag{E.59}$$

where $E_p = \sqrt{|\vec{p}|^2+m^2}$, and $\vec{v}_1$ and $\vec{v}_2$ are velocities of the incident collinear particles. This expression is integrated (summed) over all the undetected momenta (spins) of the final particles. Note that Eq. (E.59) is divided into two parts: first the invariant amplitude M_{fi}, which is a Lorentz scalar and in which the physics lies, and second, the phase space and kinematical factors. The conservation of total energy and momentum is guaranteed by the factor $(2\pi)^4\delta^4(p_{1'}+p_{2'}-p_1-p_2)$. Furthermore, there are exactly four factors of the type $\frac{m}{E_p}$. In general, there occurs a factor $\frac{m}{E}$ for every external fermion line of the corresponding graph of the scattering process. The $\frac{d\vec{p}}{(2\pi)^3}$ phase–space factors give the density of final states within the momentum range $\vec{p}$ to $\vec{p}+\delta\vec{p}$. It is customary to express the relative velocities $|\vec{v}_1-\vec{v}_2|$ in Eq. (E.59) in a Lorentz "invariant" form (which is only invariant in collinear frames, such as

laboratory and centre–of–mass frames [Gr92, Ka93])

$$E_{p_1} E_{p_2} |\vec{v}_1 - \vec{v}_1| \; = \; \sqrt{(p_1 \cdot p_2)^2 - m^4} \tag{E.60}$$

where one has made use of $\vec{p}_1 = \dfrac{\vec{v}_1}{E_{p_1}}$ and $\vec{p}_2 = \dfrac{\vec{v}_2}{E_{p_2}}$.

E.5.1 Unpolarized cross sections

In this section an expression is derived for the unpolarized cross section for Møller scattering. If polarizations are not measured, then one has to average over the initial spins and sum over final spins in Eq. (E.59). Since the spin quantum numbers occur solely in the invariant amplitude squared, from Eq. (E.58) the spin–averaged squared invariant amplitude is defined as

$$\begin{aligned} \overline{|M_{fi}|^2} \; = \; & \frac{e^2}{4} \sum_{s_{1'} s_1} \sum_{s_{2'} s_2} | \, [\bar{u}(p_{1'}, s_{1'}) \gamma_\mu \bar{u}(p_1, s_1) \frac{1}{(p_{1'} - p_1)^2 + i\epsilon} \bar{u}(p_{2'}, s_{2'}) \gamma^\mu \bar{u}(p_2, s_2) \\ & - \bar{u}(p_{2'}, s_{2'}) \gamma_\mu \bar{u}(p_1, s_1) \frac{1}{(p_{1'} - p_2)^2 + i\epsilon} \bar{u}(p_{1'}, s_{1'}) \gamma^\mu \bar{u}(p_2, s_2)] \, |^2 \, , \end{aligned} \tag{E.61}$$

where the averaging over initial spins s_1 and s_2 is responsible for the factor $\frac{1}{4}$. To illustrate the application of the usual trace techniques in deriving explicit expressions for differential cross sections, the problem is simplified by ignoring the second term (i.e. the exchange term) in Eq. (E.61), and considering only the first term (i.e. the direct term). The latter is a good approximation for a small momentum transfer $(p_{1'} - p_1)$, that is, for forward scattering. Hence, one takes

$$\overline{|M_{fi}|^2} = \frac{e^2}{4} \sum_{s_{1'} s_1} \sum_{s_{2'} s_2} | \, [\bar{u}(p_{1'}, s_{1'}) \gamma_\mu u(p_1, s_1) \frac{1}{(p_{1'} - p_1)^2 + i\epsilon} \bar{u}(p_{2'}, s_{2'}) \gamma_\mu u(p_2, s_2) \, |^2 \, . \tag{E.62}$$

One starts by noting that terms of the form

$$\text{[adjoint spinor]} \times \text{[matrix]} \times \text{[spinor]} \tag{E.63}$$

are complex numbers, for which the operations of complex conjugation and taking the adjoint are identical, and hence

$$
\begin{aligned}
[\bar{u}(p_{1'},s_{1'})\gamma^{\mu}u(p_1,s_1)]^* &= [\bar{u}(p_{1'},s_{1'})\gamma^{\mu}u(p_1,s_1)]^{\dagger} \\
&= [u^{\dagger}(p_{1'},s_{1'})\gamma^0\gamma^{\mu}u(p_1,s_1)]^{\dagger} \\
&= \bar{u}(p_1,s_1)\gamma^0(\gamma^{\mu})^{\dagger}(\gamma^0)^{\dagger}u(p_{1'},s_{1'}) \\
&= \bar{u}(p_1,s_1)\gamma^{\mu}u(p_{1'},s_{1'}) \\
&= \sum_{\delta,\epsilon=1}^{4}\bar{u}_{\delta}(p_1,s_1)\gamma^{\mu}_{\delta\epsilon}u_{\epsilon}(p_{1'},s_{1'}) \qquad \text{(E.64)}
\end{aligned}
$$

where use has been made of the fact that [Bj64]

$$
\begin{aligned}
(\gamma^0)^{\dagger} &= \gamma^0 \\
(\gamma^0)^2 &= 1 \\
\gamma^0(\gamma^{\mu})^{\dagger}\gamma^0 &= \gamma^{\mu}\,.
\end{aligned}
$$

The spin sum in Eq. (E.62) is now evaluated:

$$
\begin{aligned}
&\sum_{s_{1'},s_1,s_{2'},s_2} |\,[\bar{u}(p_{2'},s_{2'})\gamma_{\mu}u(p_2,s_2)][\bar{u}(p_{1'},s_{1'})\gamma^{\mu}u(p_1,s_1)]\,|^2 \\
&= \sum_{s_{1'},s_1,s_{2'},s_2}\{\sum_{\mu=0}^{3}[\bar{u}(p_{2'},s_{2'})\gamma_{\mu}u(p_2,s_2)][\bar{u}(p_{1'},s_{1'})\gamma^{\mu}u(p_1,s_1)]\} \\
&\times\{\sum_{\nu=0}^{3}[\bar{u}(p_{2'},s_{2'})\gamma_{\nu}u(p_2,s_2)]^*[\bar{u}(p_{1'},s_{1'})\gamma^{\nu}u(p_1,s_1)]^*\} \\
&= \sum_{\mu,\nu=0}^{3}\sum_{s_{1'},s_1,s_{2'},s_2}\sum_{\alpha,\beta,\delta,\epsilon=1}^{4}\bar{u}_{\alpha}(p_{2'},s_{2'})\gamma_{\mu,\alpha\beta}u_{\beta}(p_2,s_2)\bar{u}_{\delta}(p_2,s_2)\gamma_{\nu,\delta\epsilon}u_{\epsilon}(p_{2'},s_{2'}) \\
&\times\sum_{\rho,\sigma,\tau,\lambda=1}^{4}\bar{u}_{\rho}(p_{1'},s_{1'})\gamma^{\mu}_{\rho\sigma}u_{\sigma}(p_1,s_1)\bar{u}_{\tau}(p_1,s_1)\gamma^{\nu}_{\tau\lambda}u_{\lambda}(p_{1'},s_{1'}) \quad \text{[using Eq. (E.64)]} \\
&= \sum_{\mu,\nu=0}^{3}\sum_{\alpha,\beta,\delta,\epsilon=1}^{4}\sum_{s_{2'}}\bar{u}_{\alpha}(p_{2'},s_{2'})\gamma_{\mu,\alpha\beta}[\sum_{s_2}u_{\beta}(p_2,s_2)\bar{u}_{\delta}(p_2,s_2)]\gamma_{\nu,\delta\epsilon}u_{\epsilon}(p_{2'},s_{2'}) \\
&\times\sum_{\rho,\sigma,\tau,\lambda=1}^{4}\sum_{s_{1'}}\bar{u}_{\rho}(p_{1'},s_{1'})\gamma^{\mu}_{\rho\sigma}[\sum_{s_1}u_{\sigma}(p_1,s_1)\bar{u}_{\tau}(p_1,s_1)]\gamma^{\nu}_{\tau\lambda}u_{\lambda}(p_{1'},s_{1'})\,. \qquad \text{(E.65)}
\end{aligned}
$$

The spin summations in the square brackets are evaluated using the identity [Bj64, Gr92]

$$
\sum_{s_2}u_{\beta}(p_2,s_2)\bar{u}_{\delta}(p_2,s_2) = \left(\frac{\not{p}+m}{2m}\right)_{\beta\delta} \qquad \text{(E.66)}
$$

yielding

$$
\sum_{s_{1'},s_1,s_{2'},s_2} |\,[\bar{u}(p_{2'},s_{2'})\gamma_{\mu}u(p_2,s_2)][\bar{u}(p_{1'},s_{1'})\gamma^{\mu}u(p_1,s_1)]\,|^2
$$

$$
\begin{aligned}
&= \sum_{\mu,\nu=0}^{3} \sum_{\alpha,\epsilon=1}^{4} \sum_{s_{2'}} \bar{u}_\alpha(p_{2'}, s_{2'}) u_\epsilon(p_{2'}, s_{2'}) (\gamma_\mu \frac{\not{p}_2 + m}{2m} \gamma_\nu)_{\alpha\epsilon} \\
&\times \sum_{\rho,\lambda=1}^{4} \sum_{s_{1'}} \bar{u}_\rho(p_{1'}, s_{1'}) u_\lambda(p_{1'}, s_{1'}) (\gamma^\mu \frac{\not{p}_1 + m}{2m} \gamma^\nu)_{\rho\lambda} \\
&= \sum_{\mu,\nu=0}^{3} \sum_{\alpha\epsilon=1}^{4} (\frac{\not{p}_{2'} + m}{2m})_{\epsilon\alpha} (\gamma_\mu \frac{\not{p}_2 + m}{2m} \gamma_\nu)_{\alpha\epsilon} \times \sum_{\rho,\lambda=1}^{4} (\frac{\not{p}_{1'} + m}{2m})_{\lambda\rho} (\gamma^\mu \frac{\not{p}_1 + m}{2m} \gamma^\nu)_{\rho\lambda} \\
&\quad \text{[applying Eq. (E.66) again]} \\
&= \sum_{\mu,\nu=0}^{3} \mathrm{Tr}[\frac{\not{p}_{2'} + m}{2m} \gamma_\mu \frac{\not{p}_2 + m}{2m} \gamma_\nu] \, \mathrm{Tr}[\frac{\not{p}_{1'} + m}{2m} \gamma^\mu \frac{\not{p}_1 + m}{2m} \gamma^\nu] \, . \qquad \text{(E.67)}
\end{aligned}
$$

With Eq. (E.67) in Eq. (E.62), the spin–averaged squared matrix element is now written as

$$\overline{|M_{fi}|^2} = \frac{e^2}{(q^2)^2} L^{\mu\nu} S_{\mu\nu} \qquad \text{(E.68)}$$

where $q = p_{1'} - p_1$ is the four–momentum transfer, and the projectile–tensor and target–tensor, $L^{\mu\nu}$ and $S_{\mu\nu}$ respectively, are defined as

$$L^{\mu\nu} = \frac{1}{2} \mathrm{Tr}[\frac{\not{p}_{1'} + m}{2m} \gamma^\mu \frac{\not{p}_1 + m}{2m} \gamma^\nu] \qquad \text{(E.69)}$$

$$S_{\mu\nu} = \frac{1}{2} \mathrm{Tr}[\frac{\not{p}_{2'} + m}{2m} \gamma_\mu \frac{\not{p}_2 + m}{2m} \gamma_\nu] \, . \qquad \text{(E.70)}$$

One has thus succeeded in expressing the invariant matrix element squared as the contraction of projectile and target tensors. Note that the factorization expressed by Eq. (E.68) is only valid as long as a single photon is exchanged in the scattering process: In general, for lowest order scattering processes depicted by Feynman diagrams similar to Fig. E.1, where only a single photon or meson is exchanged, the invariant matrix element squared can be written as the contraction of projectile and target tensors, yielding factorized expressions similar to Eq. (E.68).

By applying the usual trace theorems (see, for example, Appendix A of Bjorken and Drell [Bj64] and section 3.3 of Greiner's book on "Quantum Electrodynamics" [Gr92]), the projectile and target tensors are easily evaluated. Since traces of odd numbers of γ–matrices vanish, Eq. (E.69) is immediately simplified to

$$L^{\mu\nu} = \frac{1}{2} \frac{1}{4m^2} \mathrm{Tr}[\not{p}_1 \gamma^\mu \not{p}_1 \gamma^\nu + m^2 \gamma^\mu \gamma^\nu] \, . \qquad \text{(E.71)}$$

In order to make use of the trace theorems, Eq. (E.71) needs to be rewritten in terms of the "slash" notation. To this end, one introduces two unit four–vectors with a 1 for components μ

and ν respectively, and the other components are zero

$$A = (0, \underbrace{1}_{\text{component } \mu}, 0, 0)$$
$$B = (0, 0, \underbrace{1}_{\text{component } \nu}, 0) .$$

With this notation, and applying the usual trace theorems to the first term in Eq. (E.71), one can now write

$$\begin{aligned}
\mathrm{Tr}(\not{p}_{1'}\gamma^\mu \not{p}_1 \gamma^\nu) &= \mathrm{Tr}(\not{p}_{1'} \not{A} \not{p}_1 \not{B}) \\
&= p_{1'} \cdot A \mathrm{Tr}(\not{p}_1 \not{B}) - p_{1'} \cdot p_1 \mathrm{Tr}(\not{A} \not{B}) + p_{1'} \cdot B \mathrm{Tr}(\not{A} \not{p}_1) \\
&= 4(p_{1'} \cdot A)(p_1 \cdot B) - 4(p_{1'} \cdot p_1)(A \cdot B) + 4(p_{1'} \cdot B)(A \cdot p_1) \\
&= 4p_{1'}^\mu p_1^\nu - 4p_{1'} \cdot p_1 g^{\mu\nu} + 4p_{1'}^\nu p_1^\mu \qquad \text{(E.72)}
\end{aligned}$$

where the dot denotes a Lorentz contraction and $g^{\mu\nu}$ is the usual metric tensor. For the second term in Eq. (E.71) one gets

$$\mathrm{Tr}(\gamma^\mu \gamma^\nu) = \mathrm{Tr}(\not{A} \not{B}) = 4A \cdot B = 4g^{\mu\nu} . \qquad \text{(E.73)}$$

With Eqs. (E.72) and (E.73), the projectile tensor in Eq. (E.71) now reads

$$L^{\mu\nu} = \frac{1}{2}\frac{1}{m^2}[p_{1'}^\mu p_1^\nu + p_1^\mu p_{1'}^\nu - g^{\mu\nu}(p_{1'} \cdot p_1 - m^2)] \qquad \text{(E.74)}$$

with a similar expression for the target tensor in Eq. (E.70):

$$S_{\mu\nu} = \frac{1}{2}\frac{1}{m^2}[p_{2'\mu} p_{2\nu} + p_{2\mu} p_{2'\nu} - g_{\mu\nu}(p_{2'} \cdot p_2 - m^2)] . \qquad \text{(E.75)}$$

Substitution of Eqs. (E.74) and (E.75) into Eq. (E.68) and carrying out the implied summation over μ and ν yields

$$\begin{aligned}
\overline{|M_{fi}|^2} &= \frac{e^4}{4m^2(q^2)^2}[p_{1'}^\mu p_1^\nu + p_1^\mu p_{1'}^\nu - g^{\mu\nu}(p_{1'} \cdot p_1 - m^2)] \\
&\quad \times [(p_{2'})_\mu (p_2)_\nu + (p_2)_\mu (p_{2'})_\nu - g_{\mu\nu}(p_{2'} \cdot p_2 - m^2)] \\
&= \frac{e^4}{4m^2(q^2)^2}[(p_{1'} \cdot p_{2'})(p_1 \cdot p_2) + (p_{1'} \cdot p_2)(p_1 \cdot p_{2'}) + (p_1 \cdot p_{2'})(p_{1'} \cdot p_2) \\
&\quad + (p_1 \cdot p_2)(p_{1'} \cdot p_{2'}) - 2(p_1 \cdot p_{1'})(p_{2'} \cdot p_2 - m^2) - 2(p_2 \cdot p_{2'})(p_{1'} \cdot p_1 - m^2) \\
&\quad + 4(p_{1'} \cdot p_1 - m^2)(p_{2'} \cdot p_2 - m^2)] \\
&= \frac{e^4}{2m^2(q^2)^2}[(p_1 \cdot p_2)(p_{1'} \cdot p_{2'}) + (p_1 \cdot p_{2'})(p_{1'} \cdot p_2) \\
&\quad (p_1 \cdot p_{1'})m^2 - (p_2 \cdot p_{2'})m^2 + 2m^4] . \qquad \text{(E.76)}
\end{aligned}$$

The unpolarized differential cross section is now evaluated by replacing $|M_{fi}|^2$ in Eq. (E.59) with $\overline{|M_{fi}|^2}$:

$$d\bar{\sigma} = \frac{m^4}{\sqrt{(p_1 \cdot p_2)^2 - m^4}} \overline{|M_{fi}|^2} \frac{d\vec{p}_{1'}}{E_{p_{1'}}(2\pi)^3} \frac{d\vec{p}_{2'}}{E_{p_{2'}}(2\pi)^3} (2\pi)^4 \delta^4(p_{1'} + p_{2'} - p_1 - p_2) \tag{E.77}$$

where $\overline{|M_{fi}|^2}$ is given by Eq. (E.76), and the incident flux factor is defined in Eq. (E.60).

Next, the unpolarized differential cross section is explicitly evaluated for an electron scattering into a given solid–angle element $d\Omega'$, centred around the scattering angle θ, in any collinear reference frame. The unpolarized *double* differential cross section is also evaluated. Since only one scattered electron is observed, Eq. (E.77) needs to integrated over all final momentum variables, except for $\vec{p}_{1'}$ (which one takes to be the momentum of the detected electron). Using the fact that

$$|\vec{p}\,|d|\vec{p}\,| = EdE \tag{E.78}$$

which follows from

$$E_p^2 = |\vec{p}\,|^2 + M^2\,, \tag{E.79}$$

one starts by writing the volume element $d\vec{p}_{1'}$ in spherical coordinates

$$d\vec{p}_{1'} = |\vec{p}_{1'}|^2 d|\vec{p}_{1'}|d\Omega' = |\vec{p}_{1'}|E_{1'}dE_{1'}d\Omega' \tag{E.80}$$

where, for convenience, the notation $E_{1'} = E_{p_{1'}}$ has been introduced. Integrating over the $d\vec{p}_{2'}$ in Eq. (E.77), one obtains [Ai83, Gr94]

$$\int \frac{d\vec{p}_{2'}}{E_{2'}} \delta^4(p_{1'} + p_{2'} - p_1 - p_2) = \frac{1}{E_{2'}} \delta(E_{1'} + E_{2'} - E_1 - E_2)\,. \tag{E.81}$$

On the righthand side, $|\vec{p}_{2'}|$ and $E_{2'}$ are no longer independent variables, but are now related by

$$\vec{p}_{2'} = \vec{p}_1 + \vec{p}_2 - \vec{p}_{1'} \qquad \text{and} \qquad E_{2'} = \sqrt{|\vec{p}_{2'}|^2 + m^2}\,. \tag{E.82}$$

Eq. (E.77) can now be written as

$$d\bar{\sigma} = \frac{m^4}{\sqrt{(p_1 \cdot p_2)^2 - m^4}} \overline{|M_{fi}|^2} \frac{1}{(2\pi)^2} \frac{1}{E_{2'}} \delta(E_{1'} + E_{2'} - E_1 - E_2)|\vec{p}_{1'}|dE_{1'}d\Omega'\,. \tag{E.83}$$

This formula is valid in any Lorentz system. To explicitly evaluate the differential cross section, it is necessary to adopt a specific reference frame. For the purpose of this discussion all kinematic quantities are defined in the electron–electron centre–of–mass system, defined by [Ai83, Gr94]

$$\vec{p}_1 + \vec{p}_2 \;=\; \vec{p}_{1'} + \vec{p}_{2'} \;=\; 0\,. \tag{E.84}$$

For the scattering of two equal–mass particles, the centre–of–mass four–momenta are

$$\begin{aligned} p_1 \quad &= (E_1, \vec{p}\,) \quad &&= (E, \vec{p}\,) \\ p_2 \quad &= (E_2, -\vec{p}\,) \quad &&= (E, -\vec{p}\,) \\ p_{1'} \quad &= (E_{1'}, \vec{p}\,') \quad &&= (E, \vec{p}\,') \\ p_{2'} \quad &= (E_{2'}, -\vec{p}\,') \quad &&= (E, -\vec{p}\,') \end{aligned} \tag{E.85}$$

where

$$\begin{aligned} |\vec{p}\,| \;&=\; |\vec{p}\,'\,| \;=\; p \\ E_1 \;&=\; E_2 \;=\; E_{1'} \;=\; E_{2'} \;=\; E \end{aligned} \tag{E.86}$$

and p now stands for the magnitude of the three–momentum. Defining

$$E_{cm} \;=\; E_1 + E_2 \;=\; 2E \tag{E.87}$$

where the equality $E_1 = E_2 = E$ is valid only for equal mass scattering, that is $m_1 = m_2 = m$, and introducing the free variable

$$E' \;=\; E_{1'} + E_{2'} \tag{E.88}$$

[since $E_{1'} + E_{2'}$ is only constrained to be equal to $E_{cm} = E_1 + E_2$ after performing the integral over the energy–conserving delta function in Eq. (E.83)], and noting that [see Eqs. (E.78) and (E.79)]

$$E_{1'}dE_{1'} \;=\; E_{2'}dE_{2'} \;=\; pdp\,, \tag{E.89}$$

one can write

$$\begin{aligned} dE' \;&=\; \frac{p}{E_{1'}}dp + \frac{p}{E_{2'}}dp \\ &=\; \frac{E'}{E_{1'}E_{2'}}pdp \\ &=\; \frac{E'}{E_{2'}}dE_{1'}\,. \end{aligned} \tag{E.90}$$

Furthermore, in the centre–of–mass system, the flux factor in Eq. (E.60) reduces to

$$\sqrt{(p_1 \cdot p_2)^2 - m^4} \;=\; pE_{cm} \;. \tag{E.91}$$

With Eqs. (E.86), (E.90) and (E.91) in Eq. (E.83), one gets

$$d\bar{\sigma} \;=\; \frac{m^4}{(2\pi)^2 E' E_{cm}} \overline{|M_{fi}|^2} \delta(E' - E_{cm}) dE' d\Omega' \;. \tag{E.92}$$

From this one can write down an expression for the *double* differential cross section

$$\left(\frac{d\bar{\sigma}}{dE' d\Omega'}\right)_{cm} \;=\; \frac{m^4}{(2\pi)^2 E' E_{cm}} \overline{|M_{fi}|^2} \delta(E' - E_{cm}) \;. \tag{E.93}$$

The unpolarized differential cross section is obtained by integrating over E' in Eq. (E.92) to yield

$$\begin{aligned} \left(\frac{d\bar{\sigma}}{d\Omega'}\right)_{cm} &= \frac{m^4}{(2\pi)^2 E_{cm}^2} \overline{|M_{fi}|^2} \\ &= \frac{m^4}{16\pi^2 E^2} \overline{|M_{fi}|^2} \qquad \text{[from Eq. (E.87)]} \;. \end{aligned} \tag{E.94}$$

Next, $\overline{|M_{fi}|^2}$ in Eq. (E.76) for electron–electron scattering, at small momentum transfers, is explicitly evaluated. For this purpose, one introduces the Lorentz–invariant Mandelstam variables

$$\begin{aligned} s &= (p_1 + p_2)^2 &&= (p_{1'} + p_{2'})^2 \\ t &= (p_1 - p_{1'})^2 &&= (p_2 - p_{2'})^2 \\ u &= (p_1 - p_{2'})^2 &&= (p_{1'} - p_2)^2 \end{aligned} \tag{E.95}$$

which are related by

$$\begin{aligned} s + t + u &= m_1^2 + m_2^2 + m_{1'}^2 + m_{2'}^2 \\ &= 4m^2 \qquad \text{(for equal–mass scattering)} \;. \end{aligned} \tag{E.96}$$

In the centre–of–mass system the Mandelstam invariants have the values

$$\begin{aligned} s &= (p_1 + p_2)^2 &&= 4E^2 \\ t &= (p_{1'} - p_2)^2 &&= -(\vec{p}\,' - \vec{p}\,)^2 \\ & && = -2|\vec{p}\,|^2(1 - \cos\theta) \\ & && = -4|\vec{p}\,|^2 \sin\frac{\theta}{2} \end{aligned}$$

$$\begin{aligned} u &= (p_{2'} - p_1)^2 &&= -(-\vec{p}\,' - \vec{p}\,)^2 \\ &&&= -2|\vec{p}\,|^2(1+\cos\theta) \\ &&&= -4|\vec{p}\,|^2\cos\frac{\theta}{2}\,. \end{aligned} \tag{E.97}$$

The scalar products in Eq. (E.76) can be expressed in terms of the Mandelstam variables as follows

$$\begin{aligned} p_1\cdot p_2 &= p_{1'}\cdot p_{2'} &&= \frac{1}{2}(s-2m^2) \\ p_1\cdot p_{1'} &= p_2\cdot p_{2'} &&= -\frac{1}{2}(t-2m^2) \\ p_1\cdot p_{2'} &= p_{1'}\cdot p_2 &&= -\frac{1}{2}(u-2m^2) \end{aligned} \tag{E.98}$$

yielding

$$\overline{|M_{fi}|^2} = e^4\frac{1}{4}\frac{1}{2m^2}\frac{1}{t^2}[(s-2m^2)^2+(u-2m^2)^2+4m^2t]\,. \tag{E.99}$$

With Eqs. (E.99) and (E.97), and defining

$$\alpha = \frac{e^2}{4\pi}\,, \tag{E.100}$$

the explicit expression for the unpolarized differential cross section in Eq. (E.94) is now written as

$$\begin{aligned} \left(\frac{d\bar{\sigma}}{d\Omega'}\right)_{cm} = {} & \frac{\alpha^2}{8E^2|\vec{p}\,|^2(1-\cos\theta)^2} \\ & \times[(2E^2-m^2)^2+(|\vec{p}\,|^2(1+\cos\theta)+m^2)^2-2m^2|\vec{p}\,|^2(1-\cos\theta)]\,. \end{aligned} \tag{E.101}$$

E.5.2 Polarized cross sections

Thus far only unpolarized Møller scattering has been considered. In this section the generalization of the latter to the case for polarized Møller scattering is briefly discussed. More detail can be found in Greiner's book on "*Quantum Electrodynamics*" [Gr92].

Recall that a free electron is described by a Dirac spinor with positive energy, momentum p^μ and spin vector s^μ [Gr90, Gr92], denoted by $u(p,s)$, where

$$(\not{p} - m)_{\alpha\beta}u_\beta(p,s) = 0\,. \tag{E.102}$$

The four–spin vector s^μ is a Lorentz vector which, in the rest system of the particle, is defined as a unit vector

$$(s^\mu)_{\text{rest system}} = (s^\mu)_{RS} = (0, \hat{s}\,') \tag{E.103}$$

where $\hat{s}\,'$ refers to the quantization axis (also called spin orientation) in the rest frame of the particle. The components of s^μ in an arbitrary frame, in which the particle moves with momentum $\vec{p}$, are obtained by a Lorentz boost with the result

$$s^\mu = [\frac{\vec{p}\cdot\hat{s}\,'}{m}\,,\ \hat{s}\,' + \frac{\hat{s}\,'\cdot\vec{p}}{m(E+m)}\vec{p}\,]\,. \tag{E.104}$$

Because of the Lorentz invariance of the four–dimensional scalar product, it immediately follows that

$$s_\mu s^\mu = (s_\mu)_{RS}(s^\mu)_{RS} = -\hat{s}\,'\hat{s}\,' = -1\,, \tag{E.105}$$

and with

$$(p^\mu)_{\text{rest system}} = (p^\mu)_{RS} = (m, 0, 0, 0)\,,$$

it also follows that

$$p_\mu s^\mu = (p_\mu)_{RS}(s^\mu)_{RS} = 0\,. \tag{E.106}$$

In the rest frame, the unit spinors are eigenstates of the operator

$$\boldsymbol{\Sigma}\cdot\hat{s}\,'u(0, \pm\hat{s}\,') = \pm u(0, \pm\hat{s}\,') \tag{E.107}$$

where $\boldsymbol{\Sigma} = \gamma_5\gamma^0\vec{\gamma}$ is the "double" Pauli matrix

$$\boldsymbol{\Sigma} = \begin{pmatrix} 0 & \boldsymbol{\sigma} \\ -\boldsymbol{\sigma} & 0 \end{pmatrix}\,. \tag{E.108}$$

The covariant generalization of Eq. (E.107) is given by

$$\gamma_5 \not{s}\ u(p, \pm s) = \pm u(p, \pm s) \tag{E.109}$$

where an extra factor γ^0 is included in order to make this equation also valid for positron spinors. In order to take advantage of trace techniques in evaluating polarized cross sections, the spin projection operator $\hat{\Sigma}(s)$ is introduced

$$\hat{\Sigma}(s) = \frac{1}{2}(1 + \gamma_5\not{s}\ )\,, \tag{E.110}$$

with the property that [see Eq. (E.109)]

$$\begin{aligned}\hat{\Sigma}(s)u(p,+s) &= u(p,+s)\\ \hat{\Sigma}(s)u(p,-s) &= 0\\ \hat{\Sigma}(s)u(p,s') &= \delta_{s's}u(p,s)\ .\end{aligned} \tag{E.111}$$

Now consider, for example, the scattering of polarized electrons in which the final spin is measured. The polarized cross sections are obtained by following a procedure analogous to that described in Sec. E.5.1. The only difference now is that one does not average over the initial spins and sum over the final spins when evaluating the invariant amplitude squared. Once again, the double differential cross section and differential cross section are given by Eqs. (E.93) and (E.94), respectively, with, however, $\overline{|M_{fi}|^2}$ in Eq. (E.62) replaced by

$$|M_{fi}|^2 = e^2|\,[\bar{u}(p_{1'},s_{1'})\gamma_\mu u(p_1,s_1)\frac{1}{(p_{1'}-p_1)^2+i\epsilon}\bar{u}(p_{2'},s_{2'})\gamma_\nu u(p_2,s_2)\,|^2\ . \tag{E.112}$$

With Eqs. (E.64) and (E.111), this expression is rewritten as

$$\begin{aligned}|M_{fi}|^2 = \frac{e^2}{(q)^2}\sum_{\mu\nu=0}^{3}\sum_{s_{f'}s_{i'}}&\{[\bar{u}(p_{2'},s_{f'})\gamma_\mu\hat{\Sigma}(s_2)u(p_2,s_{i'})][\bar{u}(p_2,s_{i'})\gamma_\nu\hat{\Sigma}(s_{2'})u(p_{2'},s_{f'})]\\ &\times[\bar{u}(p_{1'},s_{f'})\gamma^\mu\hat{\Sigma}(s_1)u(p_1,s_{i'})][\bar{u}(p_1,s_{i'})\gamma^\nu\hat{\Sigma}(s_{1'})u(p_{1'},s_{1'})]\}\ ,\end{aligned} \tag{E.113}$$

which allows one to take advantage of trace techniques. Repeating the procedure between Eqs. (E.63) and (E.67) in Sec. E.5.1, the double sum over the spins can be transformed into traces yielding

$$\begin{aligned}|M_{fi}|^2 = \frac{e^2}{(q)^2}&\mathrm{Tr}[\gamma^\mu\frac{1+\gamma_5\not{s}_1}{2}\frac{\not{p}_1+m}{2m}\gamma^\nu\frac{1+\gamma_5\not{s}_{1'}}{2}\frac{\not{p}_{1'}+m}{2m}]\\ &\mathrm{Tr}[\gamma_\mu\frac{1+\gamma_5\not{s}_2}{2}\frac{\not{p}_2+m}{2m}\gamma_\nu\frac{1+\gamma_5\not{s}_{2'}}{2}\frac{\not{p}_{2'}+m}{2m}]\ .\end{aligned} \tag{E.114}$$

As in Sec. E.5.1, these traces can be evaluated in a specific reference frame via application of the usual trace techniques.

E.6 Alternative normalization for Dirac spinors

It is fairly common, in applications of the relativistic many–body problem, to adopt the normalization procedure of Serot and Walecka [Se86], which differs from that of Bjorken and Drell

given by Eqs. (E.26) and (E.27) in Sec. E.3, namely

$$w^{\dagger}_{r'}(\epsilon_{r'}\vec{p}\,)w_r(\epsilon_r\vec{p}\,) = \delta_{rr'}\,, \tag{E.115}$$

$$\bar{w}_{r'}(\vec{p}\,)w_r(\vec{p}\,) = \frac{m}{E_p}\epsilon_r\delta_{rr'} \tag{E.116}$$

With the above normalizations, the free Dirac unit spinors are given by Eqs. (E.31) – (E.34), with the exception that one needs to make the following substitution:

$$\sqrt{\frac{E_p+m}{2m}} \longrightarrow \sqrt{\frac{E_p+m}{2E_p}}\,. \tag{E.117}$$

To derive the unpolarized differential cross section for electromagnetic electron–proton scattering, one follows a procedure analogous to that discussed in Sec. E.4. With the normalizations of Serot and Walecka, there are, however, a few minor differences. First of all, the following replacement needs to be made in the S–matrix element of Eq. (E.57):

$$\frac{m}{E_p} \longrightarrow 1\,, \tag{E.118}$$

and , secondly, one must use the identity

$$\sum_s u_\beta(p_2,s_2)\bar{u}_\delta(p_2,s_2) = \left(\frac{\not{p}+m}{2E_p}\right)_{\beta\delta}\,. \tag{E.119}$$

instead of Eq. (E.66), when deriving the factorized form of the differential cross section in Eq. (E.68).

Appendix F

Relation between t_i and F_i amplitudes

The aim of this appendix is to derive the relationship expressed by Eq. (3.58) [in Sec. 3.2.5 of Chapter 3] between the invariant amplitudes t_i [Eq. (3.54) in Sec. 3.2.5] and F_i [Eqs. (3.29) and (3.30) in Sec. 3.2.4].

Following the procedure outlined in Sec. E.5 of Appendix E, one can write down the polarized differential cross section for NN scattering in the NN centre–of–mass frame, namely (compare to Eq. (E.94) for unpolarized Møller scattering)

$$\left(\frac{d\bar{\sigma}}{d\Omega'}\right)_{cm} = \frac{m^4}{16\pi^2 E_{cm}^2}|\mathcal{M}|^2 \tag{F.1}$$

where E_{cm} is the energy of the incident nucleon in the centre–of–mass frame, and the invariant matrix element $\mathcal{M}$ is defined by Eq. (3.54) in Sec. 3.2.5 of Chapter 3. Now let's assume that the invariant amplitudes t_i [Eq. (3.54) in Sec. 3.2.5] and F_i [Eqs. (3.29) and (3.30) in Sec. 3.2.4] are related via

$$t_i = \xi\, F_i \tag{F.2}$$

where ξ is the (complex) kinematic factor to be derived. With Eqs. (3.25) and (3.54) in Eq. (F.1), and making use of Eq. (3.25) in Sec. 3.2.4, one can write the following expression for the polarized NN differential cross section in the centre–of–mass system:

$$\left(\frac{d\bar{\sigma}}{d\Omega'}\right)_{cm} = |\xi|^2 \frac{m^4}{16\pi^2 E_{cm}^2} \frac{1}{4|\vec{k}_{cm}|^2} |\langle \chi_{1'}^\dagger \chi_{2'}^\dagger | f | \chi_1^\dagger \chi_2^\dagger \rangle|^2 \tag{F.3}$$

where f is the nonrelativistic scattering matrix given by Eq. (3.18). Now, from Eq. (3.24) one sees the nonrelativistic scattering matrix is normalized such that the polarized differential cross section is given by

$$\left(\frac{d\bar{\sigma}}{d\Omega'}\right)_{cm} = |\langle \chi_{1'}^\dagger \chi_{2'}^\dagger | f | \chi_1^\dagger \chi_2^\dagger \rangle|^2 \,. \tag{F.4}$$

To be consistent with the latter normalization, it follows from Eq. (F.3) that

$$\xi = \frac{-8\pi i E_{cm}|\vec{k}_{cm}|}{m^2} \tag{F.5}$$

and, hence, one can write Eq. (F.2) as

$$t_i = \frac{-8\pi i E_{cm}|\vec{k}_{cm}|}{m^2} F_i \, . \tag{F.6}$$

where $E_{cm}|\vec{k}_{cm}|$ is an invariant flux factor [Gr94]. Note that the phase factor $-i$ just ensures that the real (imaginary) SVPAT amplitudes are related to the real (imaginary) Wolfenstein amplitudes. The factor of $-i$ is excluded in the RPWIA of Horowitz and Murdock [Ho88]: for calculating observables, which involve terms of the form $t_i^* t_j$ (see Appendix K), one can omit this factor. For quasielastic proton–nucleus scattering discussed in Chapter 3, the latter expression is replaced by the corresponding expression in the effective laboratory frame, namely $E_{\rm eff}|\vec{k}_{\rm eff}|$, and hence Eq. (F.6) is written as

$$t_i(\theta_{\rm eff}^{cm}, T_{\rm eff}^{L}) = \frac{-8\pi i E_{\rm eff}|\vec{k}_{\rm eff}|}{m^2} F_i(\theta_{\rm eff}^{cm}, T_{\rm eff}^{L}) \, , \tag{F.7}$$

where $T_{\rm eff}^{L}$ and $\theta_{\rm eff}^{cm}$ are given by Eqs. (3.59) and (3.62) [in Chapter 3], respectively.

Appendix G

Polarization formalism

The aim of this appendix is to present the polarization formalism for the elastic scattering of nucleons by spin–zero nuclei, as well as for elastic nucleon–nucleon (NN) scattering. Before introducing the concepts of density– and scattering–matrices M, one first needs to consider a few mathematical preliminaries.

G.1 Mathematical preliminaries

Throughout the following section use is made of the following mathematical concepts:

- the inner product of two matrices U and V, which is defined as

$$< U, V > = \frac{1}{2} \mathrm{Tr}\,(U^{\dagger} V) \tag{G.1}$$

One can easily verify that this definition satisfies the requirements of an inner product:

$$\begin{aligned} &\text{(i)} && < U, V > = < V, U >^{*} \\ &\text{(ii)} && < U + V, W > = < U, W > + < V, W > \\ &\text{(iii)} && < kU, V > = \; k \; < U, V > \\ &\text{(iv)} && < V, V > \geq \; 0 \qquad \text{and} \\ & && < V, V > = \; 0 \qquad \text{if} \qquad V \; = \; 0 \end{aligned} \tag{G.2}$$

- the direct product of two matrices A and B, which is defined as

$$(A \otimes B)_{i \times j, k \times \ell} = A_{ik} \, B_{j\ell} \, . \tag{G.3}$$

- the direct product, which has the very useful property:

$$(A \otimes B)(C \otimes D) = AC \otimes BD \tag{G.4}$$

- the fact that any vector $\vec{\beta}$ transforms as

$$\beta_i = \sum_{j=1}^{3} (R)_{ij}\, \beta_j \tag{G.5}$$

under a rotation operator R, characterized by a 3×3 orthogonal matrix R.

- under a rotation the Pauli spin matrices σ_i transform according to:

$$D^{\dagger}(R)\, \sigma_i\, D(R) = \sum_{j=1}^{3} R_{ij}\, \sigma_j \tag{G.6}$$

where R is the rotation matrix that corresponds to the rotation of the physical system; e.g. if the rotation is around the $z-$axis, then

$$R = \begin{pmatrix} \cos\theta & -\sin\theta & 0 \\ \sin\theta & \cos\theta & 0 \\ 0 & 0 & 1 \end{pmatrix}. \tag{G.7}$$

- any 2×2 matrix can be expanded in terms of the following linearly independent matrices: the 2×2 unit matrix, I_2, together with the three Pauli spin matrices, that is

$$\begin{pmatrix} a & b \\ c & d \end{pmatrix} = A\, I_2 + B\, \sigma_x + C\, \sigma_y + D\, \sigma_z \tag{G.8}$$

where

$$\begin{aligned} A &= \frac{1}{2}(a+d) \\ B &= \frac{1}{2}(b+c) \\ C &= -\frac{i}{2}(c-b) \\ D &= \frac{1}{2}(a-d)\,. \end{aligned}$$

Based on the definition of the inner product in Eq. (G.1) one can easily verify that the set of 2×2 matrices

$$\mathcal{H} = \{I_2,\, \sigma_x,\, \sigma_y,\, \sigma_z\} \tag{G.9}$$

is orthonormal, that is

$$< S_i \, ; \, S_j > = \, \delta_{ij} \tag{G.10}$$

where

$$S_0 = I_2 \qquad \text{and} \qquad S_i = \sigma_i \, ; \qquad i = 1, \, 2, \, 3 \tag{G.11}$$

Consequently, the matrices indicated by $\mathcal{H}$ are orthonormal and span 2–dimensional space.

G.2 Polarization of incident beam of spin–$\frac{1}{2}$ particles

The aim of this section is to describe an incident beam of polarized spin–$\frac{1}{2}$ particles via the concept of a density matrix.

The polarization of an ensemble (or beam) of N spin–$\frac{1}{2}$ particles is defined as [Pa81, Hi90]

$$\vec{p} = \overline{\langle \boldsymbol{\sigma} \rangle} \tag{G.12}$$

where $\boldsymbol{\sigma}$ is the usual Pauli spin operator, and the overhead bar denotes the average of the underlying expectation value. Denoting the spin state of the nth particle of the ensemble by the Pauli spinor

$$\chi^n = \begin{pmatrix} a_1^n \\ a_2^n \end{pmatrix} \tag{G.13}$$

with normalization

$$|a_1^n|^2 + |a_2^n|^2 = 1 \, , \tag{G.14}$$

the polarization can now be written as

$$\begin{aligned} \vec{p} &= \overline{\langle \boldsymbol{\sigma} \rangle} \\ &= \tfrac{1}{N} \textstyle\sum_{n=1}^{N} \langle \chi^n | \boldsymbol{\sigma} | \chi^n \rangle \\ &= \tfrac{1}{N} \textstyle\sum_{n=1}^{N} \begin{pmatrix} a_1^{n*} & a_2^{n*} \end{pmatrix} \begin{pmatrix} \sigma_{11} & \sigma_{12} \\ \sigma_{21} & \sigma_{22} \end{pmatrix} \begin{pmatrix} a_1^n \\ a_2^n \end{pmatrix} \\ &= \textstyle\sum_{n=1}^{N} (|a_{1n}|^2 \sigma_{11} + |a_{2n}|^2 \sigma_{22} + a_{1n}^* a_2 \sigma_{12} + a_{2n}^* a_1 \sigma_{21}) \, . \end{aligned} \tag{G.15}$$

Introducing the spin density matrix ρ

$$\begin{aligned}\rho &= \frac{1}{N}\begin{pmatrix} \sum_{n=1}^{N}|a_{1n}|^2 & \sum_{n=1}^{N} a_1^n a_{2n*} \\ \sum_{n=1}^{N} a_{2n}a_{1n*} & \sum_{n=1}^{N}|a_{2n}|^2 \end{pmatrix} \\ &= \frac{1}{N}\sum_{n=1}^{N}\chi^n\chi^{n\dagger}\,, \end{aligned} \tag{G.16}$$

the polarization can now be written as

$$\vec{p} = \mathrm{Tr}(\rho\boldsymbol{\sigma}) \tag{G.17}$$

with the normalization in Eq. (G.14) translating to

$$\mathrm{Tr}(\rho) = 1\,. \tag{G.18}$$

"Tr" denotes the trace of a matrix, i.e. the sum of the diagonal elements of the corresponding matrix.

For a beam of polarized spin–$\frac{1}{2}$ particles it is convenient to express the density matrix in terms of its polarization $\vec{p}$. This is accomplished by expanding the density matrix in terms of a complete set of 2×2 matrices, namely the 2×2 unit matrix, $I = \bar{\sigma}$, and the usual Pauli spin matrices σ_i (i=1, 2, 3), that is

$$\rho = \sum_{\mu=0}^{3} c_\mu\sigma_\mu\,. \tag{G.19}$$

From the properties of the Pauli spin matrices it follows that

$$c_\mu = \frac{1}{2}\mathrm{Tr}(\rho\sigma_\mu) \tag{G.20}$$

and, hence, one can rewrite Eq. (G.19) as

$$\begin{aligned}\rho &= \tfrac{1}{2}[I + \mathrm{Tr}(\rho\boldsymbol{\sigma})\cdot\boldsymbol{\sigma}] \\ &= \tfrac{1}{2}[I + \vec{p}\cdot\boldsymbol{\sigma}]\,. \end{aligned} \tag{G.21}$$

G.3 Description of scattered polarized spin–$\frac{1}{2}$ particles

The aim of this section is to describe a scattered beam of polarized spin–$\frac{1}{2}$ particles for spin–$\frac{1}{2}$ particles scattering from spin–zero target nuclei.

First, two very important relationships pertaining to the elastic scattering of polarized spin–$\frac{1}{2}$ particles from a spin–zero target are derived, namely

- the relationship between the density matrices for the incident and scattered particles:

$$\rho^{\text{scatt}} = M\rho^{\text{inc}}M^{\dagger} \tag{G.22}$$

- the relationship between the differential cross section $\frac{d\sigma}{d\Omega}$ and the density matrices for the incident and scattered particles:

$$(\frac{d\sigma}{d\Omega}) = \frac{\text{Tr}\rho^{\text{scatt}}}{\text{Tr}\rho^{\text{inc}}} \, . \tag{G.23}$$

These relationships are easily generalized to the case of nucleon–nucleon scattering.

Per definition, the scattering matrix M, for the elastic scattering of spin–$\frac{1}{2}$ particles on a spin–zero target, is a 2×2 matrix which relates the scattered spin state to the initial spin state via

$$\chi^{\text{scatt}} = M\chi^{\text{inc}} \, . \tag{G.24}$$

With this definition, and making use of Eq. (G.16) for $N = 1$, the density matrix for the scattered beam becomes

$$\begin{aligned} \rho^{\text{scatt}} &= (\chi^{\text{scatt}})(\chi^{\dagger\text{scatt}}) \\ &= (M\chi^{\text{inc}})(\chi^{\dagger\text{inc}}M^{\dagger}) \\ &= M\rho^{\text{inc}}M^{\dagger} \, . \end{aligned} \tag{G.25}$$

where

$$\rho^{\text{inc}} = (\chi^{\text{inc}})(\chi^{\dagger\text{inc}}) \tag{G.26}$$

From conventional scattering theory [Ho92], the differential cross section $\frac{d\sigma}{d\Omega}$, for scattering through an area $r^2 d\Omega$ subtended by a detector, is defined as

$$\begin{aligned}(\frac{d\sigma}{d\Omega})d\Omega &= \frac{\text{number of particles scattered into } d\Omega \text{ per unit time}}{\text{number of incident particles crossing plane } \perp \text{ to incident direction per unit area per unit time}} \\ &= \frac{j_{\text{scatt}}}{j_{\text{inc}}} r^2 d\Omega \end{aligned} \tag{G.27}$$

where

$$\vec{j}_{\text{scatt/inc}} = \frac{\hbar}{\mu}\text{Im}(\psi^{\dagger}_{\text{scatt/inc}} \nabla \psi_{\text{scatt/inc}}) \tag{G.28}$$

refers to the asymptotic flux density of particles, and μ signifies the reduced mass of the system. If the direction of the incident beam is taken to be along the z-axis, then the incident and scattered wavefunctions, for a spin–$\frac{1}{2}$ particle, are [Pa81]

$$\psi_{\text{inc}} = e^{ikz}\chi^{\text{inc}} \tag{G.29}$$

and

$$\begin{aligned}\psi_{\text{scatt}} &= \frac{e^{ikr}}{r}\chi^{\text{scatt}} \\ &= \frac{e^{ikr}}{r} M \chi^{\text{inc}} \end{aligned} \tag{G.30}$$

Substitution of Eqs. (G.30) and (G.29) into Eq. (G.28), substitution of the latter into Eq. (G.27), and making use of Eqs. (G.25) and (G.16), yields the following expression for the differential cross section in terms of the incident and scattered density matrices

$$\begin{aligned}\frac{d\sigma}{d\Omega} &= \frac{\text{Tr}(\rho_{\text{scatt}})}{\text{Tr}(\rho_{\text{inc}})} \\ &= \frac{\text{Tr}(M\rho_{\text{inc}}M^{\dagger})}{\text{Tr}(\rho_{\text{inc}})} \quad \text{[from Eq. (G.25)]} . \end{aligned} \tag{G.31}$$

For an unpolarized incident beam

$$\rho_{\text{inc}} = \frac{1}{2}\begin{pmatrix} 1 & 0 \\ 0 & 1 \end{pmatrix} \tag{G.32}$$

since for this density matrix Eq. (G.17) yields zero polarization. This implies that the differential cross section Eq. (G.31) reduces to

$$(\frac{d\bar{\sigma}}{d\Omega}) = \frac{1}{2}\text{Tr}(MM^{\dagger}) \tag{G.33}$$

where the bar above the sigma indicates that this is an *unpolarized* differential cross section.

Next, a description is given for a beam of polarized spin–$\frac{1}{2}$ particles after scattering from a spin–zero nucleus. From Eqs. (G.17) and (G.25), the polarization of a scattered beam of spin–$\frac{1}{2}$ particles is defined to be

$$\begin{aligned} \vec{p}\,' &= \frac{\mathrm{Tr}(\rho_{\mathrm{scatt}}\boldsymbol{\sigma})}{\mathrm{Tr}(\rho_{\mathrm{scatt}})} \\ &= \frac{\mathrm{Tr}(\rho_{\mathrm{inc}})}{\mathrm{Tr}(\rho_{\mathrm{scatt}})}\frac{\mathrm{Tr}(M\rho_{\mathrm{inc}}M^{\dagger}\boldsymbol{\sigma})}{\mathrm{Tr}(\rho_{\mathrm{inc}})} . \end{aligned} \tag{G.34}$$

With Eqs. (G.31) and (G.31) this becomes

$$(\frac{d\sigma}{d\Omega})\vec{p}\,' = \frac{\mathrm{Tr}(M\rho_{\mathrm{inc}}M^{\dagger}\boldsymbol{\sigma})}{\mathrm{Tr}(\rho_{\mathrm{inc}})} . \tag{G.35}$$

Consequently, one can write down an expression for the i^{th} component of the polarization of the scattered beam [with normalization $\mathrm{Tr}(\rho) = 1$] as

$$\begin{aligned} (\frac{d\sigma}{d\Omega})p_i\,' &= \mathrm{Tr}(M\rho_{\mathrm{inc}}M^{\dagger}\sigma_i) \\ &= \mathrm{Tr}(M\tfrac{1}{2}[I + \textstyle\sum_{j=1}^{3} p_j\sigma_j]M^{\dagger}\sigma_i) \\ &= \tfrac{1}{2}[\mathrm{Tr}(MM^{\dagger}\sigma_i) + \textstyle\sum_{j=1}^{3} p_j\mathrm{Tr}(M\sigma_jM^{\dagger}\sigma_i)] \\ &= \tfrac{1}{2}\mathrm{Tr}(MM^{\dagger})[\frac{\mathrm{Tr}(MM^{\dagger}\sigma_i)}{\mathrm{Tr}(MM^{\dagger})} + \sum_{j=1}^{3} p_j\frac{\mathrm{Tr}(M\sigma_jM^{\dagger}\sigma_i)}{\mathrm{Tr}(MM^{\dagger})}] \\ &= (\frac{d\bar{\sigma}}{d\Omega})[D_{i'0} + \sum_{j=1}^{3} p_jD_{i'j}] \end{aligned}$$

where

$$D_{i'0} = \frac{\mathrm{Tr}(MM^{\dagger}\sigma_i)}{\mathrm{Tr}(MM^{\dagger})} \tag{G.36}$$

and the polarization transfer observables, which relate the i^{th} component of the scattered beam polarization to the j^{th} component of the initial beam polarization, are defined by

$$D_{i'j} = \frac{\mathrm{Tr}(M\sigma_jM^{\dagger}\sigma_i)}{\mathrm{Tr}(MM^{\dagger})} \tag{G.37}$$

and $(\frac{d\bar{\sigma}}{d\Omega})$ refers to the unpolarized cross section defined in Eq. (G.33). Eqs. (G.31) and (G.36) also hold for NN scattering, with the exception that the scattering matrix M and density matrix ρ_{inc} are 4×4 matrices instead of 2×2 matrices: this will be discussed in Sec. G.4.

Before writing down explicit expressions for the polarization transfer observables in terms of the scattering amplitudes, it is necessary to derive the form of the scattering matrix for spin–$\frac{1}{2}$ on spin–zero scattering, and also for NN scattering. The latter derivations can be found in Refs. [Pa81, Hi90]. However, in this appendix, an alternative approach is presented.

G.3.1 Scattering matrix

The aim of this section is to derive the most general form of the scattering matrix that is consistent with rotational, parity, and time–reversal invariance, for the scattering of polarized spin–$\frac{1}{2}$ particles from a spin–zero target nucleus.

In Sec. G.3 it was shown that the scattering matrix for spin–$\frac{1}{2}$ on spin–zero is two–dimensional. Using the basis of Eq. (G.9), the scattering matrix $M(\vec{k}, \vec{k}')$ can be written as:

$$M(\vec{k}, \vec{k}') = \alpha(\vec{k}, \vec{k}')\, I_2 + \sum_{i=1}^{3} \beta_i(\vec{k}, \vec{k}')\, \sigma_i \,, \tag{G.38}$$

where the kinematical quantities $\vec{k}$ and $\vec{k}'$ enter in the expansion coefficients of M, and denote the incoming and outgoing momenta in an *arbitrary reference frame* respectively. The discussion that follows is very general and is independent of a specific reference frame such as the conventional centre–of–mass and laboratory reference frames.

First, the consequences of imposing rotational invariance on the scattering matrix M are investigated. Let us now perform a rotation on the scattering matrix $M(\vec{k}, \vec{k}')$ to a *new scattering process* $M(\vec{\ell}, \vec{\ell}')$ *with the same collision energy and scattering angle.* Such a rotation implies that the incident and outgoing momenta $\vec{k}$ and $\vec{k}'$ are simultaneously rotated to new incident and outgoing momenta, $\vec{\ell}$ and $\vec{\ell}'$ respectively, indicated by

$$\begin{aligned} \vec{k} &\longrightarrow (R) \longrightarrow \vec{\ell} \\ \vec{k}' &\longrightarrow (R) \longrightarrow \vec{\ell}' \end{aligned} \tag{G.39}$$

where R denotes the rotation operation from $(\vec{k}, \vec{k}')$ to $(\vec{\ell}, \vec{\ell}')$. Let χ represent an arbitrary Pauli spin state, then the corresponding spinor in the rotated frame is given by:

$$\chi_R = D(R)\,\chi \tag{G.40}$$

where $D(R)$ represents a 2×2 rotation operator.

The original unrotated *scattering amplitude*, for scattering from an initial spin state χ_i to a final spin state χ_f, is

$$\chi_f^\dagger\, M(\vec{k}, \vec{k}')\, \chi_i \tag{G.41}$$

and the *scattering amplitude* in the rotated frame is

$$(\chi_f^\dagger)_R\, M(\vec{\ell}, \vec{\ell}')\, .(\chi_i)_R \tag{G.42}$$

Enforcing rotational invariance implies that

$$\chi_f^\dagger\, M(\vec{k}, \vec{k}')\, \chi_i = (\chi_f^\dagger)_R\, M(\vec{\ell}, \vec{\ell}')\, (\chi_i)_R\,. \tag{G.43}$$

With Eq. (G.40) this condition can be rewritten as

$$\chi_f^\dagger\, M(\vec{k}, \vec{k}')\, \chi_i = \chi_f^\dagger\, D^\dagger(R)\, M(\vec{\ell}, \vec{\ell}')\, D(R)\, \chi_i \tag{G.44}$$

and, consequently, rotational invariance can be restated as

$$M(\vec{k}, \vec{k}') = D^\dagger(R)\, M(\vec{\ell}, \vec{\ell}')\, D(R)\,. \tag{G.45}$$

Combining Eqs. (G.45) and (G.38), and making use of the fact that α and β_i are merely complex numbers, yields

$$\begin{aligned}\alpha(\vec{k}, \vec{k}') + \sum_{i=1}^{3} \beta_i(\vec{k}, \vec{k}')\, \sigma_i \;&=\; D^\dagger(R)\, \alpha(\vec{\ell}, \vec{\ell}')\, D(R) + \sum_{i=1}^{3} D^\dagger(R)\, \beta_i(\vec{\ell}, \vec{\ell}')\, \sigma_i\, D(R) \\ &=\; \alpha(\vec{\ell}, \vec{\ell}') + \sum_{i=1}^{3} \beta_i(\vec{\ell}, \vec{\ell}')\, D^\dagger(R)\, \sigma_i\, D(R)\,. \end{aligned} \tag{G.46}$$

Hence, one sees that rotational invariance imposes the following condition on the α coefficients in Eq. (G.38), namely

$$\alpha(\vec{k}, \vec{k}') = \alpha(\vec{\ell}, \vec{\ell}')\,. \tag{G.47}$$

Now for α to be invariant under a rotation, it can only be a function of quantities which are invariant under rotations, namely

$$\begin{aligned} |\vec{k}|^2 &= k^2 \\ |\vec{k}'|^2 &= k'^2 \\ \vec{k} \cdot \vec{k} &= k\,k' \cos\theta \end{aligned} \tag{G.48}$$

For elastic scattering $k = k'$, and hence one can restate the condition of rotational invariance on the α coefficients as

$$\alpha = \alpha\left(k^2, \cos\theta\right) . \tag{G.49}$$

Using the transformation property of the Pauli spin matrices expressed by Eq. (G.6), the second term in Eq. (G.46) becomes

$$\sum_{i=1}^{3} \beta_i\left(\vec{\ell}, \vec{\ell}'\right) D^{\dagger}\left(R\right) \sigma_i D\left(R\right) = \sum_{j=1}^{3} \left(\sum_{i=1}^{3} (R^T)_{ji}\, \beta_i\left(\vec{\ell}, \vec{\ell}'\right) \right) \sigma_j \ , \tag{G.50}$$

and since the Pauli spin matrices are linearly independent, rotational invariance imposes the following condition on the β coefficients, namely

$$\beta_j\left(\vec{k}, \vec{k}'\right) = \sum_{i=1}^{3} (R^T)_{ji}\, \beta_i\left(\vec{\ell}, \vec{\ell}'\right) . \tag{G.51}$$

According to Eq. (G.5) the latter condition implies that the β_i coefficients transform as the components of a vector, and hence one can write

$$\vec{\beta}\left(\vec{k}, \vec{k}'\right) = \begin{pmatrix} \beta_1\left(\vec{k}, \vec{k}'\right) \\ \beta_2\left(\vec{k}, \vec{k}'\right) \\ \beta_3\left(\vec{k}, \vec{k}'\right) \end{pmatrix} . \tag{G.52}$$

Consider a righthanded coordinate system defined by any orthonormal set of unit vectors, $\hat{X}$, $\hat{Z}$, $\hat{n}$. These unit vectors are usually defined in terms of the incident and outgoing nucleon momenta in either the centre–of–mass or laboratory system. At a later stage, a convenient set of orthonormal unit vectors is chosen in accordance with the reaction kinematics. At this stage, however, an arbitrary reference frame is chosen. Expanding the vector $\vec{\beta}\left(\vec{k}, \vec{k}'\right)$ in terms of this basis yields

$$\vec{\beta}\left(\vec{k}, \vec{k}'\right) = \beta_X\left(\vec{k}, \vec{k}'\right) \hat{X} + \beta_Z\left(\vec{k}, \vec{k}'\right) \hat{Z} + \beta_n\left(\vec{k}, \vec{k}'\right) \hat{n} . \tag{G.53}$$

The fact that $\vec{\beta}$ is a rotational vector function of $\vec{k}$ and $\vec{k}'$ implies that a rotation of $\vec{k}$ and $\vec{k}'$ will produce the same effect as a rotation of $\vec{\beta}$ itself [Ta72], therefore

$$\beta_i(\vec{k}, \vec{k}') = \beta_i(\vec{\ell}, \vec{\ell}') . \tag{G.54}$$

Hence, for elastic scattering, rotational invariance implies that

$$\beta_i = \beta_i(k^2, \cos\theta) . \tag{G.55}$$

Employing the notation

$$\vec{\sigma} = \sigma_X \hat{X} + \sigma_n \hat{n} + \sigma_Z \hat{Z} ,$$

Eq. G.38 can be rewritten as

$$M = \alpha(k^2, \cos\theta) + \vec{\beta}(k^2, \cos\theta) \cdot \vec{\sigma} \tag{G.56}$$

where

$$\vec{\beta} \cdot \vec{\sigma} \equiv \sum_{i=1}^{3} \beta_i \sigma_i .$$

Hence, the most *general form of M, consistent with rotational invariance*, for *elastic spin–$\frac{1}{2}$ on spin–0 scattering* is given by:

$$M = \alpha(k^2, \theta) + \beta_X(k^2, \theta)\, \vec{\sigma} \cdot \hat{X} + \beta_Z(k^2, \theta)\, \vec{\sigma} \cdot \hat{Z} + \beta_n(k^2, \theta)\, \vec{\sigma} \cdot \hat{n} . \tag{G.57}$$

For spin–$\frac{1}{2}$ on spin–zero scattering, it customary [Pa81, Hi90] to define the righthanded coordinate system $\hat{X}$, $\hat{Z}$, $\hat{n}$ in terms of the incident and outgoing nucleon momenta, $\vec{k}$ and $\vec{k}'$ respectively, in the *laboratory frame of the nucleon–nucleus system*:

$$\begin{aligned} \hat{X} &= \frac{\vec{k} - \vec{k}'}{|\vec{k} - \vec{k}'|} \\ \hat{Z} &= \frac{\vec{k} + \vec{k}'}{|\vec{k} + \vec{k}'|} \\ \hat{n} &= \frac{\vec{k} \times \vec{k}'}{|\vec{k} \times \vec{k}'|} . \end{aligned} \tag{G.58}$$

The unit vectors $\hat{X}$ and $\hat{Z}$ lie in the reaction plane, and the unit vector $\hat{n}$ is normal to the reaction plane.

Next, let us consider the form of the scattering matrix after imposing additional symmetries on the scattering process, namely

- **Parity invariance**

Under a parity transformation P, the momentum vectors transform as follows [Sa85]:

$$\begin{aligned} \vec{k} &\longrightarrow (P) \longrightarrow -\vec{k} \\ \vec{k}' &\longrightarrow (P) \longrightarrow -\vec{k}' . \end{aligned} \tag{G.59}$$

Hence, the unit vectors defined in Eq. (G.58) transform as

$$\begin{aligned} \hat{X} &\longrightarrow (P) \longrightarrow -\hat{X} \\ \hat{Z} &\longrightarrow (P) \longrightarrow -\hat{Z} \\ \hat{n} &\longrightarrow (P) \longrightarrow \hat{n} . \end{aligned} \tag{G.60}$$

The Pauli spin matrices are invariant under a parity transformation:

$$\vec{\sigma} \longrightarrow (P) \longrightarrow \vec{\sigma} . \tag{G.61}$$

Since k^2 and $\cos\theta$ are invariant under parity [see Eq. (G.48)], the expansion coefficients are also invariant under parity. Combining Eqs. (G.57) and (G.59) – (G.61) yields the *most general form of M consistent with rotational and parity invariance*, namely

$$M = \alpha\,(k^2,\,\theta) + \beta_n\,(k^2,\,\theta)\,\vec{\sigma}\cdot\hat{n} . \tag{G.62}$$

- **Time–Reversal invariance**

Under a time–reversal transformation T the momentum vectors transform as follows [Sa85]:

$$\begin{aligned} \vec{k} &\longrightarrow (T) \longrightarrow -\vec{k}' \\ \vec{k}' &\longrightarrow (T) \longrightarrow -\vec{k} . \end{aligned} \tag{G.63}$$

Hence, the unit vectors defined in Eq. (G.58) transform as

$$\begin{aligned} \hat{X} &\longrightarrow (T) \longrightarrow \hat{X} \\ \hat{Z} &\longrightarrow (T) \longrightarrow -\hat{Z} \\ \hat{n} &\longrightarrow (T) \longrightarrow -\hat{n} . \end{aligned} \tag{G.64}$$

The Pauli spin matrices change sign under a time–reversal transformation:

$$\vec{\sigma} \longrightarrow (T) \longrightarrow -\vec{\sigma} . \tag{G.65}$$

As can be seen from Eq. (G.48), the expansion coefficients are invariant under time–reversal.

Combining Eqs. (G.57 and (G.63) – (G.65) yields the *most general form of M consistent with rotational and time-reversal invariance*, namely

$$M = \alpha\,(k^2,\,\theta) + \beta_Z\,(k^2,\,\theta)\,\vec{\sigma}\cdot\hat{Z} + \beta_n\,(k^2,\,\theta)\,\vec{\sigma}\cdot\hat{n}\,. \tag{G.66}$$

- **Parity and Time–Reversal invariance**

Combining Eqs. (G.57), (G.62) and (G.66), one sees that the most *general form of M consistent with rotational, parity and time-reversal invariance is given by*

$$M = \alpha\,(k^2,\,\theta) + \beta_n\,(k^2,\,\theta)\,\vec{\sigma}\cdot\hat{n}\,. \tag{G.67}$$

Next, an analogous procedure is followed for the derivation of the scattering matrix for elastic NN scattering.

G.4 Scattering matrix for elastic NN scattering

The aim of this section is to derive the most general form of the scattering matrix that is consistent with rotational, parity, and time–reversal invariance for elastic NN scattering.

For NN scattering the scattering matrix which relates $\chi^{\rm scatt}$ to $\chi^{\rm inc}$, analogous to Eq. (G.24), is four–dimensional. This is due to the fact the both $\chi^{\rm scatt}$ and $\chi^{\rm inc}$ are a direct product of projectile and target nucleon Pauli spinors, that is, the spinors in Eq. (G.24) generalize to

$$\chi^{\rm scatt} = \chi_1^{\rm scatt} \otimes \chi_2^{\rm scatt} \tag{G.68}$$

and

$$\chi^{\rm inc} = \chi_1^{\rm inc} \otimes \chi_2^{\rm inc}\,. \tag{G.69}$$

where the subscripts "1" and "2" refer to projectile and target nucleons respectively. Hence the scattering matrix can be expanded in terms of sixteen linearly independent 4×4 matrices. For the projectile one has the following basis

$$\mathcal{H}_p = \{I_1,\,\sigma_x^1,\,\sigma_y^1,\,\sigma_z^1\} \tag{G.70}$$

and, similarly for the target, the basis is

$$\mathcal{H}_t = \{I_2,\, \sigma_x^2,\, \sigma_y^2,\, \sigma_z^2\} \tag{G.71}$$

where the σ's are the usual Pauli spin matrices. A suitable basis $\mathcal{H}$ for the combined space is then given by the direct product, defined in Eq. (G.3), of $\mathcal{H}_p$ and $\mathcal{H}_t$, that is

$$\mathcal{H} = \mathcal{H}_p \otimes \mathcal{H}_t \tag{G.72}$$

where

$$\begin{aligned}\mathcal{H} \;=\; \{&I_1 \otimes I_2,\; I_1 \otimes \sigma_x^2,\; I_1 \otimes \sigma_y^2,\; I_1 \otimes \sigma_z^2,\; \sigma_x^1 \otimes I_2,\; \sigma_y^1 \otimes I_2,\; \sigma_z^1 \otimes I_2,\; \sigma_x^1 \otimes \sigma_x^2,\; \sigma_x^1 \otimes \sigma_y^2,\; \sigma_x^1 \otimes \sigma_z^2,\\ &\sigma_y^1 \otimes \sigma_x^2,\; \sigma_y^1 \otimes \sigma_y^2,\; \sigma_y^1 \otimes \sigma_z^2,\; \sigma_z^1 \otimes \sigma_x^2,\; \sigma_z^1 \otimes \sigma_y^2,\; \sigma_z^1 \otimes \sigma_z^2\}\,.\end{aligned} \tag{G.73}$$

Consequently, one can now expand the NN scattering matrix M in terms of this basis, that is

$$\begin{aligned}M(\vec{k},\vec{k}') \;=\; &\alpha(\vec{k},\vec{k}')\, I_4 \;+\; \sum_{i=1}^{3} \beta_i(\vec{k},\vec{k}')\,(I_1 \otimes \sigma_i^2)\\ &+ \sum_{i=1}^{3} \gamma_i(\vec{k},\vec{k}')\,(\sigma_i^1 \otimes I_2) + \sum_{i,j=1}^{3} \mathcal{E}_{ij}(\vec{k},\vec{k}')\,(\sigma_i^1 \otimes \sigma_j^2)\end{aligned} \tag{G.74}$$

where

$$I_4 \;=\; I_1 \otimes I_2 \;\equiv\; 4 \times 4 \text{ unit matrix}\,. \tag{G.75}$$

First, the consequences of imposing rotational invariance on the scattering matrix M are investigated. Let us now perform a rotation on the scattering matrix $M(\vec{k},\vec{k}')$ to a *new scattering process* $M(\vec{\ell},\vec{\ell}')$ *with the same collision energy and scattering angle.* Such a rotation implies that the incident and outgoing momenta, $\vec{k}$ and $\vec{k}'$, are simultaneously rotated to new incident and outgoing momenta $\vec{\ell}$ and $\vec{\ell}'$ respectively:

$$\begin{aligned}\vec{k} \;&\longrightarrow (R) \longrightarrow\; \vec{\ell}\\ \vec{k}' \;&\longrightarrow (R) \longrightarrow\; \vec{\ell}'\end{aligned} \tag{G.76}$$

where R denotes the rotation operation. Let χ represent an arbitrary Pauli spin state (which is actually a direct product of arbitrary spin states for the projectile and target nucleons), then the corresponding spinor in the rotated frame is given by:

$$\chi_R = D(R)\,\chi \tag{G.77}$$

where $D(R)$ represents a 4×4 rotation operator.

Now, following a procedure which is analogous to that outlined between Eqs. (G.41) and (G.44), it follows that rotational invariance can be restated as

$$M(\vec{k}, \vec{k}') = D^{\dagger}(R)\, M(\vec{\ell}, \vec{\ell}')\, D(R). \tag{G.78}$$

Using the expansion for M in Eq. (G.74), the above condition can be restated as:

$$\begin{aligned} &\alpha(\vec{k},\vec{k}') + \sum_{i=1}^{3} \beta_i(\vec{k},\vec{k}')(I_1 \otimes \sigma_i^2) + \sum_{i=1}^{3} \gamma_i(\vec{k},\vec{k}')(\sigma_i^1 \otimes I_2) + \sum_{i,j=1}^{3} \epsilon_{i,j}(\vec{k},\vec{k}')(\sigma_i^1 \otimes \sigma_j^2) \\ &= \alpha(\vec{\ell},\vec{\ell}') + \sum_{i=1}^{3} \beta_i(\vec{\ell},\vec{\ell}')D^{\dagger}(R)(I_1 \otimes \sigma_i^2)D(R) + \sum_{i=1}^{3} \gamma_i(\vec{\ell},\vec{\ell}')D^{\dagger}(R)(\sigma_i^1 \otimes I_2)D(R) \\ &\qquad + \sum_{i,j=1}^{3} \epsilon_{i,j}(\vec{\ell},\vec{\ell}')D^{\dagger}(R)(\sigma_i^1 \otimes \sigma_j^2)D(R). \end{aligned} \tag{G.79}$$

Comparing the first terms on the left and right sides of this equation yields the condition on the α coefficients imposed by rotational invariance, namely

$$\alpha(\vec{k}, \vec{k}') = \alpha(\vec{\ell}, \vec{\ell}'). \tag{G.80}$$

Analogous to Eq. (G.47) this implies that

$$\alpha = \alpha(k^2, \cos\theta). \tag{G.81}$$

The operator $D(R)$ is a matrix which acts in the combined spinor space of the projectile and target nucleons. In Ref. [Sa85] it is shown that a rotation matrix that acts in a *direct product space*, can be written as the *direct product* of two *rotation matrices which act in the separate spaces*, that is

$$D(R) = D_1(R) \otimes D_2(R) \tag{G.82}$$

where $D_1(R)$ is a 2×2 rotation matrix which acts only in the spinor space of the projectile, and $D_2(R)$ is a 2×2 rotation matrix which acts only in the spinor space of the target. Note that the same rotation, R, appears as the arguments of D_1 and D_2. Substituting Eq. (G.82) in the second term on the righthand side of Eq. (G.79) gives

$$\sum_{i=1}^{3} \beta_i(\vec{\ell}, \vec{\ell}')\, D^{\dagger}(R)\, (I_1 \otimes \sigma_i^2)\, D(R) = \sum_{i=1}^{3} \beta_i(\vec{\ell}, \vec{\ell}')\, (D_1^{\dagger}(R) \otimes D_2^{\dagger}(R))\, (I_1 \otimes \sigma_i^2)\, (D_1(R) \otimes D_2(R))$$

Using Eq. (G.4) one can write

$$\sum_{i=1}^{3} \beta_i(\vec{\ell}, \vec{\ell}')\, D^{\dagger}(R)\,(I_1 \otimes \sigma_i^2)\, D(R) = \sum_{i=1}^{3} \beta_i(\vec{\ell}, \vec{\ell}')\,(I_1 \otimes D_2^{\dagger}(R)\,\sigma_i^2\, D_2(R)) \,. \tag{G.83}$$

Using the transformation property of the Pauli spin matrices expressed by Eq. (G.6), Eq. (G.83) becomes

$$\begin{aligned} \sum_{i=1}^{3} \beta_i(\vec{\ell}, \vec{\ell}')\, D^{\dagger}(R)\,(I_1 \otimes \sigma_i^2)\, D(R) &= \sum_{i,j=1}^{3} \beta_i(\vec{\ell}, \vec{\ell}')\, R_{ij}\,(I_1 \otimes \sigma_j^2) \\ &= \sum_{j=1}^{3} \left(\sum_{i=1}^{3} (R^T)_{ji}\, \beta_i(\vec{\ell}, \vec{\ell}') \right) I_1 \otimes \sigma_j^2 \,. \end{aligned} \tag{G.84}$$

Similarly, the third term on the right side of Eq. (G.79) can be written as

$$\begin{aligned} \sum_{i=1}^{3} \gamma_i(\vec{\ell}, \vec{\ell}')\, D^{\dagger}(R)\,(\sigma_i^1 \otimes I_2)\, D(R) &= \sum_{i=1}^{3} \gamma_i(\vec{\ell}, \vec{\ell}')\,(D_1^{\dagger}(R) \otimes D_2^{\dagger}(R))\,((\sigma)_i^1 \otimes I_2)\,(D_1(R) \otimes D_2(R)) \\ &= \sum_{j=1}^{3} \left(\sum_{i=1}^{3} (R^T)_{ji}\, \gamma_i(\vec{\ell}, \vec{\ell}') \right) (\sigma_j^1 \otimes I_2) \,. \end{aligned}$$

Comparing the left and right sides of Eqs. (G.84) and (G.84) yields the following two conditions resulting from rotational invariance:

$$\beta_i(\vec{k}, \vec{k}') = \sum_{\gamma=1}^{3} (R^T)_{ij}\, \beta_j(\vec{\ell}, \vec{\ell}') \tag{G.85}$$

and

$$\gamma_i(\vec{k}, \vec{k}') = \sum_{j=1}^{3} (R^T)_{ij}\, \gamma_j(\vec{\ell}, \vec{\ell}') \,. \tag{G.86}$$

According to Eq. (G.5), these two equations imply that β_i and γ_i transform as vectors, and so one can write

$$\vec{\beta}(\vec{k}, \vec{k}') = \begin{pmatrix} \beta_1(\vec{k}, \vec{k}') \\ \beta_2(\vec{k}, \vec{k}') \\ \beta_3(\vec{k}, \vec{k}') \end{pmatrix} \tag{G.87}$$

and

$$\vec{\gamma}(\vec{k}, \vec{k}') = \begin{pmatrix} \gamma_1(\vec{k}, \vec{k}') \\ \gamma_2(\vec{k}, \vec{k}') \\ \gamma_3(\vec{k}, \vec{k}') \end{pmatrix} \,. \tag{G.88}$$

Alternatively, one can work on the basis $\{\hat{X},\, \hat{Z},\, \hat{n}\}$ and write:

$$\vec{\beta}\,(\vec{k},\, \vec{k}') = \beta_X\,(\vec{k},\, \vec{k}')\,\hat{X} + \beta_Z\,(\vec{k},\, \vec{k}')\,\hat{Z} + \beta_n\,(\vec{k},\, \vec{k}')\,\hat{n} \tag{G.89}$$

and

$$\vec{\gamma}\,(\vec{k},\, \vec{k}') = \gamma_X\,(\vec{k},\, \vec{k}')\,\hat{X} + \gamma_Z\,(\vec{k},\, \vec{k}')\,\hat{Z} + \gamma_n\,(\vec{k},\, \vec{k}')\,\hat{n}\,. \tag{G.90}$$

Just as in the case for spin–$\frac{1}{2}$ on spin–zero scattering, it follows that expansion coefficients are only functions of k^2 and $\cos\theta$. Therefore, rotational invariance implies that

$$\vec{\beta}\,(k^2,\, \cos\theta) = \beta_X\,(k^2,\, \cos\theta)\,\hat{X} + \beta_Z\,(k^2,\, \cos\theta)\,\hat{Z} + \beta_n\,(k^2,\, \cos\theta)\,\hat{n} \tag{G.91}$$

and

$$\vec{\gamma}\,(k^2,\, \cos\theta) = \gamma_X\,(k^2,\, \cos\theta)\,\hat{X} + \gamma_Z\,(k^2,\, \cos\theta)\,\hat{Z} + \gamma_n\,(k^2,\, \cos\theta)\,\hat{n}\,. \tag{G.92}$$

Next, the last term on the righthand side of Eq. (G.79) is considered. Analogous to the ensuing discussion, one can write

$$\begin{aligned}
\sum_{i,\,j=1}^{3} \mathcal{E}_{ij}\,(\vec{\ell},\, \vec{\ell}')\,D^{\dagger}\,(R)\,(\sigma_i^1 \otimes \sigma_j^2)\,D\,(R) &= \sum_{i,\,j=1}^{3} \mathcal{E}_{ij}\,(\vec{\ell},\, \vec{\ell}')\,(D_1^{\dagger}\,(R) \otimes D_2^{\dagger}\,(R))\,(\sigma_i^1 \otimes \sigma_j^2)\,(D_1\,(R) \otimes D_2\,(R)) \\
&= \sum_{i,\,j=1}^{3} \mathcal{E}_{ij}\,(\vec{\ell},\, \vec{\ell}')\,(D_1^{\dagger}\,(R)\,\sigma_i^1\,D_1\,(R)) \otimes (D_2^{\dagger}\,(R)\,\sigma_j^2\,D_2\,(R)) \\
&= \sum_{i,\,j=1}^{3} \mathcal{E}_{ij}\,(\vec{\ell},\, \vec{\ell}')\,(R_{ik}\,\sigma_k^1 \otimes R_{j\ell}\,\sigma_\ell^2) \\
&= \sum_{i,\,j=1}^{3} \mathcal{E}_{ij}\,(\vec{\ell},\, \vec{\ell}')\,R_{ik}\,R_{j\ell}\,(\sigma_k^1 \otimes \sigma_\ell^2) \\
&= \sum_{i,\,j,\,k,\,\ell}^{3} ((R^T)_{ki}\,\mathcal{E}_{ij}\,(\vec{\ell},\, \vec{\ell}')\,R_{j\ell})\,(\sigma_k^1 \otimes \sigma_\ell^2)\,.
\end{aligned} \tag{G.93}$$

Therefore

$$\sum_{i,\,j=1}^{3} \mathcal{E}_{ij}\,(\vec{\ell},\, \vec{\ell}')\,D^{\dagger}\,(R)\,(\sigma_i^1 \otimes \sigma_j^2)\,D\,(R) = \sum_{k,\,\ell=1}^{3} \left(\sum_{i,\,j=1}^{3} (R^T)_{ki}\,\mathcal{E}_{ij}\,(\vec{\ell},\, \vec{\ell}')\,R_{j\,\ell} \right) (\sigma_k^1 \otimes \sigma_\ell^2)\,.$$

Comparing the last term on the lefthand side of Eq. (G.79) with the above equation, yields another condition imposed by rotational invariance, namely

$$\mathcal{E}_{ij}\,(\vec{k},\, \vec{k}') = \sum_{k,\,\ell=1}^{3} (R^T)_{ik}\,\mathcal{E}_{k\ell}\,(\vec{\ell},\, \vec{\ell}')\,R_{\ell j}\,. \tag{G.94}$$

This equation tells us that $\mathcal{E}_{ij}$ transforms as a matrix (second rank tensor) [Mo53]. Consequently, one may write

$$\mathcal{E} = \begin{pmatrix} \mathcal{E}_{11} & \mathcal{E}_{12} & \mathcal{E}_{13} \\ \mathcal{E}_{21} & \mathcal{E}_{22} & \mathcal{E}_{23} \\ \mathcal{E}_{31} & \mathcal{E}_{32} & \mathcal{E}_{33} \end{pmatrix} \tag{G.95}$$

where all the matrix elements are functions of k^2 and $\cos\theta$ in order to have rotational invariance.

The following aim is to write the matrix $\mathcal{E}$ in terms of the basis $\hat{X}$, $\hat{Z}$ and $\hat{n}$. Consider an arbitrary 3×3 matrix,

$$A = \begin{pmatrix} a & b & c \\ d & e & f \\ g & h & i \end{pmatrix}, \tag{G.96}$$

then

$$A = (a\ b\ c) \otimes \begin{pmatrix} 1 \\ 0 \\ 0 \end{pmatrix} + (d\ e\ f) \otimes \begin{pmatrix} 0 \\ 1 \\ 0 \end{pmatrix} + (g\ h\ i) \otimes \begin{pmatrix} 0 \\ 0 \\ 1 \end{pmatrix}. \tag{G.97}$$

Consider the first term:

$$\begin{aligned} (a\ b\ c) \otimes \begin{pmatrix} 1 \\ 0 \\ 0 \end{pmatrix} &= (a\ 0\ 0) \otimes \begin{pmatrix} 1 \\ 0 \\ 0 \end{pmatrix} + (0\ b\ 0) \otimes \begin{pmatrix} 1 \\ 0 \\ 0 \end{pmatrix} + (0\ 0\ c) \otimes \begin{pmatrix} 1 \\ 0 \\ 0 \end{pmatrix} \\ &= a\,(1\ 0\ 0) \otimes \begin{pmatrix} 1 \\ 0 \\ 0 \end{pmatrix} + b\,(0\ 1\ 0) \otimes \begin{pmatrix} 1 \\ 0 \\ 0 \end{pmatrix} + c\,(0\ 0\ 1) \otimes \begin{pmatrix} 1 \\ 0 \\ 0 \end{pmatrix} \end{aligned}$$

and define

$$\hat{x} = \begin{pmatrix} 1 \\ 0 \\ 0 \end{pmatrix}; \quad \hat{y} = \begin{pmatrix} 0 \\ 1 \\ 0 \end{pmatrix}; \quad \hat{z} = \begin{pmatrix} 0 \\ 0 \\ 1 \end{pmatrix}. \tag{G.98}$$

Then one can write

$$(a\ b\ c) \otimes \begin{pmatrix} 1 \\ 0 \\ 0 \end{pmatrix} = a\,\hat{x}^T \otimes \hat{x} + b\,\hat{y}^T \otimes \hat{x} + c\,\hat{z}^T \otimes \hat{x}\,. \tag{G.99}$$

For notational simplicity one disposes of the transpose symbol, T and just writes

$$\hat{x}^T \otimes \hat{x} \qquad \text{as} \qquad \hat{x} \otimes \hat{x}\,. \tag{G.100}$$

Using the same notation for the other terms in Eq. (G.97) gives

$$A = a\,(\hat{x} \otimes \hat{x}) + b\,(\hat{y} \otimes \hat{x}) + c\,(\hat{z} \otimes \hat{x}) + d\,(\hat{x} \otimes \hat{y}) + e\,(\hat{y} \otimes \hat{y}) + f\,(\hat{z} \otimes \hat{y}) + g\,(\hat{x} \otimes \hat{z}) + h\,(\hat{y} \otimes \hat{z}) + i\,(\hat{z} \otimes \hat{z}$$

One now does a basis transformation from the basis $\{\hat{x},\, \hat{y},\, \hat{z}\}$ to the basis, $\{\hat{X},\, \hat{Z},\, \hat{n}\}$. This will only affect the expansion coefficients, therefore

$$\begin{aligned} A \;=\; & A_1\,(\hat{X} \otimes \hat{X}) + A_2\,(\hat{Z} \otimes \hat{X}) + A_3\,(\hat{n} \otimes \hat{X}) + A_4\,(\hat{X} \otimes \hat{Z}) + A_5\,(\hat{Z} \otimes \hat{Z}) + A_6\,(\hat{n} \otimes \hat{Z}) \\ & + A_7\,(\hat{X} \otimes \hat{n}) + A_8\,(\hat{Z} \otimes \hat{n}) + A_9\,(\hat{n} \otimes \hat{n}) \end{aligned}$$

where each of the new expansion coefficients, A_i, are functions of a, b, c, d, e, f, g and h. Using this result one writes $\mathcal{E}$ as:

$$\mathcal{E} = \sum_{i,j=1}^{3} \mathcal{E}_{ij}\,(k^2,\, \cos\theta)\,\hat{e}_i \otimes \hat{e}_j \tag{G.101}$$

where

$$\hat{e}_1 = \hat{X};\ \hat{e}_2 = \hat{Z};\ \hat{e}_3 = \hat{n}\,. \tag{G.102}$$

Using Eq. (G.91), one writes the second term in Eq. (G.74) as

$$\vec{\beta}\,(k^2,\, \cos\theta) \cdot (I_1 \otimes \vec{\sigma}^1) \tag{G.103}$$

and similarly, using Eq. (G.92), one writes the third term in Eq. (G.74) as:

$$\vec{\gamma}\,(k^2,\, \cos\theta) \cdot (\vec{\sigma}^2 \otimes I_1)\,. \tag{G.104}$$

The last term in Eq. (G.74) requires a bit of manipulation. Let

$$\mathcal{E} \cdot (\vec{\sigma}^1 \otimes \vec{\sigma}^2) \equiv \sum_{i,j=1}^{3} \mathcal{E}_{ij}\,(\sigma_i^1 \otimes \sigma_j^2)\,. \tag{G.105}$$

This equation defines the "$\cdot$" operation on the LHS. $\mathcal{E}$ is now to be interpreted as a 3×3 matrix.

One has, however, an expansion for $\mathcal{E}$, given by Eq. (G.101). Therefore

$$\mathcal{E}\cdot(\vec{\sigma}'\otimes\vec{\sigma}^2)=\sum_{i,j=1}^{3}\mathcal{E}_{ij}\,(k_1^2\cos\theta)\,(\hat{e}_i\otimes\hat{e}_j)\cdot(\vec{\sigma}^1\otimes\vec{\sigma}^2)\,. \tag{G.106}$$

Using the definition of the '$\cdot$' operation, given in Eq. (G.105), one may write:

$$(\hat{e}_i\otimes\hat{e}_j)\cdot(\vec{\sigma}^1\otimes\vec{\sigma}^2)=\sum_{c,r=1}^{3}(\hat{e}_i\otimes\hat{e}_j)_{cr}\,(\sigma_c^1\otimes\sigma_r^2)\,. \tag{G.107}$$

Since $\hat{e}_i$ only has one row and $\hat{e}_j$ only one column, the direct product defined by Eq. (G.3) reduces to

$$(\hat{e}_i\otimes\hat{e}_j)_{cr}=(\hat{e}_i)_c(\hat{e}_j)_r \tag{G.108}$$

and, therefore,

$$\begin{aligned}(\hat{e}_i\otimes\hat{e}_j)\cdot(\vec{\sigma}^1\otimes\vec{\sigma}^2) &= \sum_{c,r=1}^{3}(\hat{e}_i)_c\,(\sigma_c^1\otimes I_2)\,(\hat{e}_j)_r\,(I_1\otimes\sigma_r^2)\\ &= (\vec{\sigma}'\otimes I_2)\cdot\hat{e}_i\,(I_1\otimes\vec{\sigma}^2)\cdot\hat{e}_j\,.\end{aligned}$$

Hence

$$\begin{aligned}\sum_{i,j=1}^{3}\mathcal{E}_{ij}\,(\sigma_i^1\otimes\sigma_j^2) &= \mathcal{E}\cdot(\vec{\sigma}^1\otimes\vec{\sigma}^2)\\ &= \sum_{i,j=1}^{3}\mathcal{E}_{ij}\,(k^2,\cos\theta)\,(\vec{\sigma}^1\otimes I_2)\cdot\hat{e}_i\,(I_1\otimes\vec{\sigma}^2)\cdot\hat{e}_j\,.\end{aligned}$$

Thus the *most general form of M, consistent with rotational invariance*, is given by

$$\begin{aligned}M &= \alpha\,(k^2,\cos\theta)I_1\otimes I_2+\vec{\beta}\,(k^2,\cos\theta)\cdot(\vec{\sigma}^1\otimes I_2)+\vec{\gamma}\,(k^2,\cos\theta)\cdot(I_1\otimes\vec{\sigma}^2)\\ &+ \sum_{i,j=1}^{3}\mathcal{E}_{ij}\,(k^2,\cos\theta)\,(\vec{\sigma}^1\otimes I_2)\cdot\hat{e}_i\,(I_1\otimes\vec{\sigma}^2)\cdot\hat{e}_j\end{aligned} \tag{G.109}$$

or written out explicitly

$$
\begin{aligned}
M \;=\; & \alpha\,(k^2,\cos\theta) I_1\otimes I_2 + \beta_X\,(k^2,\cos\theta)\,(\vec{\sigma}^1\otimes I_2)\cdot\hat{X} + \beta_Z\,(k^2,\cos\theta)\,(\vec{\sigma}^1\otimes I_2)\cdot\hat{Z} \\
& + \beta_n\,(k^2,\cos\theta)\,(\vec{\sigma}^1\otimes I_2)\cdot\hat{n} + \gamma_X\,(k^2,\cos\theta)\,(I_1\otimes\vec{\sigma}^2)\cdot\hat{X} + \gamma_Z\,(k^2,\cos\theta)\,(I_1\otimes\vec{\sigma}^2)\cdot\hat{Z} \\
& + \gamma_n\,(k^2,\cos\theta)\,(I_1\otimes\vec{\sigma}^2)\cdot\hat{n} + \mathcal{E}_{XX}\,(k^2,\cos\theta)\,(\vec{\sigma}^1\otimes I_2)\cdot\hat{X}\,(I_1\otimes\vec{\sigma}^2)\cdot\hat{X} \\
& + \mathcal{E}_{XZ}\,(k^2,\cos\theta)\,(\vec{\sigma}^1\otimes I_2)\cdot\hat{X}\,(I_1\otimes\vec{\sigma}^2)\cdot\hat{Z} + \mathcal{E}_{Xn}\,(k^2,\cos\theta)\,(\vec{\sigma}^1\otimes I_2)\cdot\hat{X}\,(I_1\otimes\vec{\sigma}^2)\cdot\hat{n} \\
& + \mathcal{E}_{ZX}\,(k^2,\cos\theta)\,(\vec{\sigma}^1\otimes I_2)\cdot\hat{Z}\,(I_1\otimes\vec{\sigma}^2)\cdot\hat{X} + \mathcal{E}_{ZZ}\,(k^2,\cos\theta)\,(\vec{\sigma}^1\otimes I_2)\cdot\hat{Z}\,(I_1\otimes\vec{\sigma}^2)\cdot\hat{Z} \\
& + \mathcal{E}_{Zn}\,(k^2,\cos\theta)\,(\vec{\sigma}^1\otimes I_2)\cdot\hat{Z}\,(I_1\otimes\vec{\sigma}^2)\cdot\hat{n} + \mathcal{E}_{nX}\,(k^2,\cos\theta)\,(\vec{\sigma}'\otimes I_2)\cdot\hat{n}\,(I_1\otimes\vec{\sigma}^2)\cdot\hat{X} \\
& + \mathcal{E}_{nZ}\,(k^2,\cos\theta)\,(\vec{\sigma}'\otimes I_2)\cdot\hat{n}\,(I_1\otimes\vec{\sigma}^2)\cdot\hat{Z} + \mathcal{E}_{nn}\,(k^2,\cos\theta)\,(\vec{\sigma}^1\otimes I_2)\cdot\hat{n}\,(I_1\otimes\vec{\sigma}^2)\cdot\hat{n}
\end{aligned}
$$

One therefore sees that *rotational invariance alone leaves 16 independent quantities.*

For NN scattering, it customary [Pa81, Hi90] to define the righthanded coordinate system $\hat{X}$, $\hat{Z}$, $\hat{n}$ in terms of the incident and outgoing nucleon momenta, $\vec{k}$ and $\vec{k}'$ respectively, in the *NN centre–of–mass system*:

$$
\begin{aligned}
\hat{X} &= \frac{\vec{k}-\vec{k}'}{|\vec{k}-\vec{k}'|} \\
\hat{Z} &= \frac{\vec{k}+\vec{k}'}{|\vec{k}+\vec{k}'|} \\
\hat{n} &= \frac{\vec{k}\times\vec{k}'}{|\vec{k}\times\vec{k}'|}\,.
\end{aligned}
$$

The unit vectors $\hat{X}$ and $\hat{Z}$ lie in the reaction plane and the unit vector $\hat{n}$ is normal to the reaction plane.

Now consider additional symmetries which may be imposed on the system. The argumentation is identical to that followed for the case of spin–$\frac{1}{2}$ on spin–zero scattering, and only the final results are quoted, namely

- the *most general form of M, consistent with invariance under rotations and parity is*:

$$\begin{aligned} M &= \alpha(k^2, \cos\theta) I_1 \otimes I_2 + \beta_n(k^2, \cos\theta)(\vec{\sigma}^1 \otimes I_2)\cdot\hat{n} + \gamma_n(k^2, \cos\theta)(I_1 \otimes \vec{\sigma}^2)\cdot\hat{n} \\ &+ \mathcal{E}_{XX}(k^2, \cos\theta)(\vec{\sigma}^1 \otimes I_2)\cdot\hat{X}(I_1 \otimes \vec{\sigma}^2)\cdot\hat{X} + \mathcal{E}_{XZ}(k^2, \cos\theta)(\vec{\sigma}^1 \otimes I_2)\cdot\hat{X}(I_1 \otimes \vec{\sigma}^2)\cdot\hat{Z} \\ &+ \mathcal{E}_{ZX}(k^2, \cos\theta)(\vec{\sigma}^1 \otimes I_2)\cdot\hat{Z}(I_1 \otimes \vec{\sigma}^2)\cdot\hat{X} + \mathcal{E}_{ZZ}(k^2, \cos\theta)(\vec{\sigma}^1 \otimes I_2)\cdot\hat{Z}(I_1 \otimes \vec{\sigma}^2)\cdot\hat{Z} \\ &+ \mathcal{E}_{nn}(k^2, \cos\theta)(\vec{\sigma}^1 \otimes I_2)\cdot\hat{n}(I_1 \otimes \vec{\sigma}^2)\cdot\hat{n} \end{aligned} \tag{G.110}$$

In this case one has *eight independent functions.*

- *the most general form of M, consistent with invariance under rotations and time–reversal is*:

$$\begin{aligned} M &= \alpha(k^2, \cos\theta) I_1 \otimes I_2 + \beta_Z(k^2, \cos\theta)(\vec{\sigma}^1 \otimes I_2)\cdot\hat{Z} + \beta_n(k^2, \cos\theta)(\vec{\sigma}^1 \otimes I_2)\cdot\hat{n} \\ &+ \gamma_Z(k^2, \cos\theta)(I_1 \otimes \vec{\sigma}^2)\cdot\hat{Z} + \gamma_n(k^2, \cos\theta)(I_1 \otimes \vec{\sigma}^2)\cdot\hat{n} + \mathcal{E}_{XX}(k^2, \cos\theta)(\vec{\sigma}^1 \otimes I_2)\cdot\hat{X} \\ &(I_1 \otimes \vec{\sigma}^2)\cdot\hat{X} + \mathcal{E}_{ZZ}(k^2, \cos\theta)(\vec{\sigma}^1 \otimes I_2)\cdot\hat{Z}(I_1 \otimes \vec{\sigma}^2)\cdot\hat{Z} + \mathcal{E}_{Zn}(k^2, \cos\theta)(\vec{\sigma}^1 \otimes I_2)\cdot\hat{Z} \\ &(I_1 \otimes \vec{\sigma}^2)\cdot\hat{n} + \mathcal{E}_{nZ}(k^2, \cos\theta)(\vec{\sigma}^1 \otimes I_2)\cdot\hat{n}(I_1 \otimes \vec{\sigma}^2)\cdot\hat{Z} + \mathcal{E}_{nn}(k^2, \cos\theta)(\vec{\sigma}^1 \otimes I_2)\cdot\hat{n} \\ &(I_1 \otimes \vec{\sigma}^2)\cdot\hat{n} \end{aligned} \tag{G.111}$$

In this case one has *10 independent functions.*

- imposing *rotational, parity and time–reversal invariance gives*:

$$\begin{aligned} M &= \alpha(k^2, \cos\theta) I_1 \otimes I_2 + \beta_n(k^2, \cos\theta)(\vec{\sigma}^1 \otimes I_2)\cdot\hat{n} + \gamma_n(k^2, \cos\theta)(I_1 \otimes \vec{\sigma}^2)\cdot\hat{n} \\ &+ \mathcal{E}_{XX}(k^2, \cos\theta)(\vec{\sigma}^1 \otimes I_2)\cdot\hat{X}(I_1 \otimes \vec{\sigma}^2)\cdot\hat{X} + \mathcal{E}_{ZZ}(k^2, \cos\theta)(\vec{\sigma}^1 \otimes I_2)\cdot\hat{Z}(I_1 \otimes \vec{\sigma}^2)\cdot\hat{Z} \\ &+ \mathcal{E}_{nn}(k^2, \cos\theta)(\vec{\sigma}^1 \otimes I_2)\cdot\hat{n}(I_1 \otimes \vec{\sigma}^2)\cdot\hat{n} \end{aligned} \tag{G.112}$$

In this case, there are *six independent functions.*

- imposing the fact that the projectile and target nucleons are indistinguishable

$$1 \rightleftharpoons 2 \tag{G.113}$$

yields

$$\vec{k} \longrightarrow -\vec{k}$$

$$\begin{aligned}
\vec{k}' &\longrightarrow -\vec{k}' \\
\hat{X} &\longrightarrow -\hat{X} \\
\hat{Z} &\longrightarrow -\hat{Z} \\
\hat{n} &\longrightarrow \hat{n}\,.
\end{aligned}$$

Also

$$\begin{aligned}
\vec{\sigma}^1 \otimes I_2 &\longrightarrow I_1 \otimes \vec{\sigma}^2 \\
I_1 \otimes \vec{\sigma}^2 &\longrightarrow \vec{\sigma}^1 \otimes I_2
\end{aligned}$$

Hence, if one demands that M is invariant under exchange of particles, it is clear that the functions in the second and third term in Eq. (G.112) must be equal.

Therefore the most *general form of M invariant under rotations, parity, time–reversal and exchange of nucleons* is then given by:

$$\begin{aligned}
M \;=\; & \alpha\,(k^2, \cos\theta) I_1 \otimes I_2 + \lambda_n\,(k^2, \cos\theta)\,[(\vec{\sigma}^1 \otimes I_2)\cdot\hat{n} + (I_1 \otimes \vec{\sigma}^2)\cdot\hat{n}] \\
& + \mathcal{E}_{XX}\,(k^2, \cos\theta)\,(\vec{\sigma}^1 \otimes I_2)\cdot\hat{X}\,(I_1 \otimes \vec{\sigma}^2)\cdot\hat{X} + \mathcal{E}_{ZZ}\,(k^2, \cos\theta)\,(\vec{\sigma}^1 \otimes I_2)\cdot\hat{Z}\,(I_1 \otimes \vec{\sigma}^2)\cdot\hat{Z} \\
& + \mathcal{E}_{nn}\,(k^2, \cos\theta)\,(\vec{\sigma}^1 \otimes I_2)\cdot\hat{n}\,(I_1 \otimes \vec{\sigma}^2)\cdot\hat{n} \qquad \text{(G.114)}
\end{aligned}$$

where $\lambda_n = \beta_n = \gamma_n$, and in this case there are only *five independent functions.*

Eq. (G.114) can be recast into several forms: for example, see Refs. [Br78], [Pa81] and [Hi90]. With the coordinate frame in Eq. (G.58), one can make the following connection between Eq.(G.114) and the scattering matrix derived in Refs. [Pa81, Hi90]:

$$\begin{aligned}
\alpha &\longleftrightarrow g_0 \\
\lambda_n &\longleftrightarrow h_0 \\
\mathcal{E}_{XX} &\longleftrightarrow h_X \\
\mathcal{E}_{ZZ} &\longleftrightarrow h_Z \\
\mathcal{E}_{nn} &\longleftrightarrow h_n\,. \qquad \text{(G.115)}
\end{aligned}$$

Another convenient form, which is used in Chapter 3, is the **McNeil–Ray–Wallace (MRW)** scattering matrix [Mc83a]:

$$\begin{aligned}(2\,i\,|\vec{k}_{cm}|)^{-1}\,M &= A + B\,(\vec{\sigma}^1 \otimes I_2)\cdot(I_1 \otimes \vec{\sigma}^2) + i\,|\vec{X}|\,C\,(\sigma_{1n} \otimes I_2 + I_1 \otimes \sigma_{2n}) \\ &\quad + D\,|\vec{X}|^2\,(\vec{\sigma}_1 \otimes I_2)\cdot\hat{X}\,(I_1 \otimes \vec{\sigma}^2)\cdot\hat{X} + E\,(\sigma_{1z} \otimes I_2)\,(I_1 \otimes \sigma_{2z})\,.\end{aligned}$$

The quantity k_{cm} refers to the centre–of–mass momentum, and A, B, C, D and E are five complex functions. With the notation

$$\sigma_{1z} \otimes I_2\,,$$

one means

$$(\vec{\sigma}^1 \otimes I_2)\cdot\hat{Z} \tag{G.116}$$

where $\hat{X}$, $\hat{Z}$ and $\hat{n}$ still represent the previously defined unit–vectors.

One now aims to express the MRW amplitudes in terms of the amplitudes in Eq. (G.114). The dot–product in the second term is expanded in terms of the basis $\{\hat{X},\,\hat{Z},\,\hat{n}\}$. Then

$$\begin{aligned}(2\,i\,k_{cm})^{-1}\,M &= A + B\,(\vec{\sigma}^1 \otimes I_2)\cdot\hat{X}\,(I_1 \otimes \vec{\sigma}^2)\cdot\hat{X} + B\,(\vec{\sigma}^1 \otimes I_2)\cdot\hat{Z}\,(I_1 \otimes \vec{\sigma}^2)\cdot\hat{Z} \\ &\quad + B\,(\vec{\sigma}^1 \otimes I_2)\cdot\hat{n}\,(I_1 \otimes \vec{\sigma}^2)\cdot\hat{n} + i\,|\vec{X}|\,C\,[(\vec{\sigma}' \otimes I_2)\cdot\hat{n} + (I_1 \otimes \vec{\sigma}^2)\cdot\hat{n}] \\ &\quad + D\,(\vec{\sigma}^1 \otimes I_2)\cdot\hat{X}\,(I_1 \otimes \vec{\sigma}^2)\cdot\hat{X} + E\,(\vec{\sigma}^1 \otimes I_2)\cdot\hat{Z}\,(I_1 \otimes \vec{\sigma}^2)\cdot\hat{Z}\,.\end{aligned}$$

Regrouping the terms yields

$$\begin{aligned}(2\,i\,k_{cm})^{-1}\,M &= A + i\,|\vec{X}|\,C\,[(\vec{\sigma}^1 \otimes I_2)\cdot\hat{n} + (I_1 \otimes \vec{\sigma}^2)\cdot\hat{n}] + (B+D)\,[(\vec{\sigma}^1 \otimes I_2)\cdot\hat{X}\,(I_1 \otimes \vec{\sigma}^2)\cdot\hat{X}] \\ &\quad + (B+E)\,[(\vec{\sigma}^1 \otimes I_2)\cdot\hat{Z}\,(I_1 \otimes \vec{\sigma}^2)\cdot\hat{Z}] + B\,[(\vec{\sigma}^1 \otimes I_2)\cdot\hat{n}\,(I_1 \otimes \vec{\sigma}^2)\cdot\hat{n}]\,.\end{aligned}$$

Comparison with Eq. (G.114), allows one to make the following identifications:

$$\begin{aligned}\alpha &\longleftrightarrow (2\,i\,k_{cm})\,A \\ \lambda_n &\longleftrightarrow (2\,i\,k_{cm})\,(i\,|\vec{X}|\,C) \\ \mathcal{E}_{XX} &\longleftrightarrow (2\,i\,k_{cm})\,(B + DX^2) \\ \mathcal{E}_{ZZ} &\longleftrightarrow (2\,i\,k_{cm})\,(B+E) \\ \mathcal{E}_{nn} &\longleftrightarrow (2\,i\,k_{cm})\,B\,.\end{aligned}$$

G.5 Observables for NN scattering

The expressions for the polarization transfer observables are now derived for the scattering of polarized spin–$\frac{1}{2}$ beams from unpolarized spin–$\frac{1}{2}$ targets.

G.5.1 Density matrix for incident channel

For spin–$\frac{1}{2}$ on spin–$\frac{1}{2}$ scattering, such as NN scattering, the combined spin–space of the incident and target particles is four–dimensional. This means that the density matrix for the incident channel ρ^{inc} can be expanded in terms of the 16 linearly independent matrices specified in Eq. (G.73). Hence, analogous to the procedure in Sec. G.2, one can write

$$\rho^{\text{inc}} = \sum_{\mu=1}^{16} C_\mu S_\mu \tag{G.117}$$

where $S_\mu \epsilon \mathcal{H}$ in Eq. (G.73). From the properties of the Pauli spin matrices, it follows that

$$\text{Tr}(S_\mu \, S_\nu) \; = \; 4\delta_{\mu\nu} \; . \tag{G.118}$$

This enables one to write

$$C_\mu = \frac{1}{4}\text{Tr}(\rho^{\text{inc}} S_\mu) \tag{G.119}$$

and consequently, using the notation defined in Sec. G.4,

$$\begin{aligned}
\rho^{\text{inc}} \; &= \; \frac{1}{4}\sum_{\mu=1}^{16}\text{Tr}(\rho^{\text{inc}}S_\mu)S_\mu = \frac{1}{4}\text{Tr}(\rho^{\text{inc}}I_4)I_4 + \frac{1}{4}\sum_{i=1}^{3}\text{Tr}(\rho^{\text{inc}}I_1\otimes\sigma_i^2)I_1\otimes\sigma_i^2 \\
&\quad + \frac{1}{4}\sum_{i=1}^{3}\text{Tr}(\rho^{\text{inc}}\sigma_i^1\otimes I_2)\sigma_i^1\otimes I_2 + \frac{1}{4}\sum_{i,j=1}^{3}\text{Tr}(\rho^{\text{inc}}\sigma_i^1\otimes\sigma_j^2)\sigma_i^1\otimes\sigma_j^2 \\
&= \; \frac{1}{4}\text{Tr}(\rho^{\text{inc}})[I_4 + \vec{P}_2^{\text{inc}}\cdot I_1\otimes\vec{\sigma}^2 + \vec{P}_1^{\text{inc}}\cdot\vec{\sigma}^1\otimes I_2 + \sum_{i,j=1}^{3}\overline{\langle\vec{\sigma}_i^1\otimes\vec{\sigma}_j^2\rangle}\vec{\sigma}_i^1\otimes\vec{\sigma}_j^2]
\end{aligned} \tag{G.120}$$

where, analogous to Eq. (G.34), the polarization of the projectile and initial target nucleons, $\vec{P}_1^{\text{inc}}$ and $\vec{P}_2^{\text{inc}}$ respectively, are defined as

$$\begin{aligned}
\vec{P}_1^{\text{inc}} \; &= \; \frac{\text{Tr}(\rho^{\text{inc}}\vec{\sigma}^1\otimes I_2)}{\text{Tr}(\rho^{\text{inc}})} \\
\vec{P}_2^{\text{inc}} \; &= \; \frac{\text{Tr}(\rho^{\text{inc}}I_2\otimes\vec{\sigma}^2)}{\text{Tr}(\rho^{\text{inc}})} \; .
\end{aligned} \tag{G.121}$$

The average value of the direct product $\vec{\sigma}_i^1 \otimes \vec{\sigma}_j^2$ is called the *polarization correlation function.* For the special case of an *incident polarized beam* scattering on an *unpolarized target*, Eq. (G.120) reduces to

$$\rho^{\text{inc}} = \frac{1}{4}\text{Tr}(\rho^{\text{inc}})[I_4 + \vec{P}_1^{\text{inc}} \cdot \vec{\sigma}^1 \otimes I_2] \,. \tag{G.122}$$

G.5.2 Differential cross section and analyzing power

Substituting Eq. (G.122) in Eq. (G.31) yields the differential cross section for the scattering of polarized nucleons from an unpolarized nucleon target:

$$\begin{aligned} (\frac{d\sigma}{d\Omega}) &= \frac{1}{4}\text{Tr}(MI_4M^\dagger) + \frac{1}{4}\vec{P}_1^{\text{inc}} \cdot \text{Tr}(M\vec{\sigma}^1 \otimes I_2 M^\dagger) \\ &= \bar{\sigma}(1 + \vec{P}_1^{\text{inc}} \cdot \vec{a}) \end{aligned} \tag{G.123}$$

where $\bar{\sigma}$ is the *unpolarized differential cross section*

$$\bar{\sigma} = \frac{1}{4}\text{Tr}(MI_4M^\dagger) \tag{G.124}$$

and the *asymmetry parameter* $\vec{a}$ is

$$\vec{a} = \frac{\text{Tr}(M\vec{\sigma}^1 \otimes I_2 M^\dagger)}{\text{Tr}(MI_4M^\dagger)} \,. \tag{G.125}$$

Using the explicit expression for M given by Eq. (G.114) and (G.115), with the right–handed coordinate system defined by Eq. (G.58) in the NN centre–of–mass system, and evaluating the traces (as described in Refs. [Pa81] and [Hi90]) yield the following expression for the unpolarized differential cross section in terms of the 5 complex amplitudes g_0, h_0, h_X, h_Z and h_n:

$$\bar{\sigma} = \bar{\sigma}(\theta) = |g_0|^2 + 2|h_0|^2 + |h_X|^2 + |h_Z|^2 + |h_n|^2 \,. \tag{G.126}$$

The right–hand side of Eq. (G.126) is a function of k^2 and $\cos\theta$. There is no dependence on the azimuthal angle ϕ of the direction $\vec{k}'$ of the scattered beam. This is a consequence of the lack of polarization of the incident beam.

Recall that $\hat{n}$ is the unit vector perpendicular to the plane containing the incident and outgoing momentum vectors $\vec{k}$ and $\vec{k}'$. Due to the various symmetries imposed on the scattering matrix M, the asymmetry parameter a, also called the *analyzing power* A_y, defined by

Eq. (G.128) is always perpendicular to the scattering plane, that is

$$\begin{aligned} \vec{a} &= a\hat{n} \\ &= A_y\hat{n} \end{aligned} \tag{G.127}$$

where

$$\bar{\sigma}\vec{a} = \bar{\sigma}a\hat{n} = 2\,\mathrm{Re}(g_0 + h_n)h_0^*\hat{n}\,. \tag{G.128}$$

Hence, Eq. (G.123) can be more explicitly written as

$$(\frac{d\sigma}{d\Omega}) = \sigma = \bar{\sigma}(\theta)(1 + a\vec{P}_1^{\mathrm{inc}} \cdot \hat{n})\,. \tag{G.129}$$

The physical meaning of the asymmetry parameter becomes clear if one considers "left" and "right" scattering of $\vec{k}'$ through an angle θ with respect to $\vec{k}$, in the plane of the page. In the case of $\vec{k}'$ in the left direction, a right–handed screw driven from $\vec{k}$ towards $\vec{k}'$ moves upwards, therefore, the corresponding $\hat{n}$ is perpendicular to the plane of the paper, and it points upwards. Similarly, in the case of $\vec{k}'$ in the right direction, $\hat{n}$ is still perpendicular to the plane of the paper, but it points downwards. Therefore, the directions of $\hat{n}$ in the two cases are exactly opposite to each other. If $\hat{n}$ describes the upward normal, then Eq. (G.129) can be written as

$$\begin{aligned} \sigma_L(\theta) &= \bar{\sigma}(\theta)(1 + a\vec{P}_1^{\mathrm{inc}} \cdot \hat{n}) \\ \sigma_R(\theta) &= \bar{\sigma}(\theta)(1 - a\vec{P}_1^{\mathrm{inc}} \cdot \hat{n}) \end{aligned} \tag{G.130}$$

where the subscripts "L" and "R" denote scattering to the left and right respectively. Combining these expressions yields

$$a\vec{P}_1^{\mathrm{inc}} \cdot \hat{n} = \frac{\sigma_L(\theta) - \sigma_R(\theta)}{\sigma_L(\theta) + \sigma_R(\theta)}\,. \tag{G.131}$$

For obvious reasons, the quantity $a\vec{P}_1^{\mathrm{inc}} \cdot \hat{n}$ is called the left–right asymmetry. This is exactly equal to the asymmetry parameter a for a fully polarized incident beam perpendicular to the scattering plane, i.e. $\vec{P}_1^{\mathrm{inc}} \cdot \hat{n} = 1$.

G.5.3 The polarization transfer observables

An expression for the polarization of a scattered nucleon beam is now derived in terms of the incident polarization and the so–called polarization transfer observables.

Analogous to Eq. (G.34), for spin–$\frac{1}{2}$ on spin–zero elastic scattering, one can write down the polarization of the scattered beam beam for NN scattering:

$$\begin{aligned} \vec{P}_1^{\text{scatt}} &= \frac{\text{Tr}(\rho^{\text{scatt}}\vec{\sigma}^1 \otimes I_2)}{\text{Tr}(\rho^{\text{scatt}})} \\ &= \frac{\text{Tr}(M\rho^{\text{inc}}M^\dagger\vec{\sigma}^1 \otimes I_2)}{\text{Tr}(\rho^{\text{inc}})} \frac{\text{Tr}(\rho^{\text{inc}})}{\text{Tr}(\rho^{\text{scatt}})} \\ &= \frac{\text{Tr}(M\rho^{\text{inc}}M^\dagger\vec{\sigma}^1 \otimes I_2)}{\text{Tr}(\rho^{\text{inc}})\sigma} \end{aligned} \tag{G.132}$$

where $\sigma = \frac{d\sigma}{d\Omega}$ is defined by Eq. (G.31). For the scattering of a polarized nucleon beam from an unpolarized nucleon target, Eq. (G.122) is used to rewrite the latter expression as:

$$\begin{aligned} \sigma P_{1i}^{\text{scatt}} &= \frac{1}{4}\text{Tr}(MI_4M^\dagger[\frac{\text{Tr}(MI_4M^\dagger\sigma_i^1 \otimes I_2)}{\text{Tr}(MI_4M^\dagger)} + \sum_{j=1}^{3} P_{1j}^{\text{inc}} \cdot \frac{\text{Tr}(M\sigma_j^1 \otimes I_2M^\dagger\sigma_i^1 \otimes I_2)}{\text{Tr}(MI_4M^\dagger)}] \\ &= \bar{\sigma}[D_{i'0} + \sum_{j=1}^{3} P_{1j}^{\text{inc}} D_{i'j}] \,. \end{aligned} \tag{G.133}$$

Analogous to Eq. (G.37), the polarization transfer observables $\text{D}_{i'j}$, which relate the i^{th} component of the scattered beam polarization to the j^{th} component of the initial beam polarization, are defined by

$$D_{i'j} = \frac{\text{Tr}(M\sigma_j^1 \otimes I_2M^\dagger\sigma_i^1 \otimes I_2)}{\text{Tr}(MI_4M^\dagger)} \tag{G.134}$$

and

$$D_{i'0} = \frac{\text{Tr}(MM^\dagger\sigma_i^1 \otimes I_2)}{\text{Tr}(MI_4M^\dagger)} \,. \tag{G.135}$$

Consider the special case of an unpolarized incident beam, i.e. $\vec{P}_1^{\text{inc}} = 0$. Then, using Eq. (G.124), one gets

$$\vec{P}_1^{\text{scatt}} = \vec{P} = \frac{\text{Tr}(MI_4M^\dagger\vec{\sigma}^1 \otimes I_2)}{\text{Tr}(MI_4M^\dagger)} \,. \tag{G.136}$$

Explicit evaluation of this equation (see for example, Ref. [Pa81]) gives the result

$$\text{Tr}(MI_4M^\dagger\vec{\sigma}^1 \otimes I_2) = \text{Tr}(M\vec{\sigma}^1 \otimes I_2M^\dagger I_4) \,. \tag{G.137}$$

Using this result, and comparing Eqs. (G.136) and (G.125) yields the important result that $\vec{P}^{\text{scatt}}$, for the case of an unpolarized incident nucleon scattering from an unpolarized nucleon

target, is equal to the asymmetry parameter $a\hat{n}$ (or analyzing power A_y), for scattering of a polarized nucleon beam from an unpolarized nucleon target, that is

$$\vec{P}_1^{\text{scatt}} = P\hat{n} = a\hat{n} = A_y \,, \tag{G.138}$$

where the quantity P is called the *induced polarization* and A_y is the analyzing power defined by Eqs. (G.125) and (G.127). The second term in Eq. (G.133) is evaluated in terms of the explicit expression for the scattering matrix M [Pa81, Hi90] yielding

$$\begin{aligned}
\frac{1}{4}\vec{P}_1^{\text{inc}} \cdot \text{Tr}(M\vec{\sigma}^1 \otimes I_2 M^\dagger \vec{\sigma}^1 \otimes I_2) \;=\; & [\,(|g_0|^2 + 2|h_0|^2 - |h_X|^2 - |h_Z|^2 + |h_n|^2)(\vec{P}_1^{\text{inc}} \cdot \hat{n})\,]\hat{n} \\
& + [\,(|g_0|^2 + |h_X|^2 - |h_Z|^2 + |h_n|^2)(\vec{P}_1^{\text{inc}} \cdot \hat{X}) \\
& + 2\,\text{Im}(h_0 g_0 - h_0 h_n)\vec{P}_1^{\text{inc}} \cdot \hat{Z})\,]\hat{X} \\
& + [\,(|g_0|^2 - |h_X|^2 + |h_Z|^2 - |h_n|^2)(\vec{P}_1^{\text{inc}} \cdot \hat{Z}) \\
& - 2\,\text{Im}(h_0 g_0 - h_0 h_n)(\vec{P}_1^{\text{inc}} \cdot \hat{X})\,]\hat{Z} \,.
\end{aligned} \tag{G.139}$$

Next, expressions for the traditional Wolfenstein parameters or polarization transfer observables $D_{i'j}$, used in Chapter 3, are obtained. The latter observables are defined in the NN laboratory system. Consequently, one needs to express the components of $\vec{P}^{\text{scatt}}$ [in Eq. (G.133)] along the scattered momentum ($\hat{\ell}'$) in the laboratory frame, along the perpendicular to this direction in the scattering plane ($\hat{s}'$), and along the direction $\hat{n}$ normal to the scattering plane, such that $\vec{s}'$, $\vec{\ell}'$ and $\vec{n}$ form the right–handed coordinate system shown in Fig. G.1. Similarly it is necessary to express the components of $\vec{P}^{\text{inc}}$ along the orthogonal directions $\vec{s}$, $\vec{\ell}$ and $\vec{n}$, shown in Fig. G.1, in the laboratory system. Recall that $\vec{k}$ and $\vec{k}'$ are the incident and outgoing nucleon momenta in the NN centre–of–mass frame, and θ is the scattering angle between $\vec{k}$ and $\vec{k}'$. For NN elastic, where $|\vec{k}| = |\vec{k}'|$, one can show by nonrelativistic kinematic considerations [Pa81] that the laboratory and centre–of–mass scattering angles are related by

$$\theta_{\text{lab}} = \frac{\theta_{\text{cm}}}{2} \,. \tag{G.140}$$

The relativistic relations between these scattering angles are found in Ref. [Br78]. Since the incident momentum $\vec{k}$ has the same direction in both the laboratory and the centre–of–mass system, and using the fact that for elastic NN scattering $|\vec{k}| = |\vec{k}'|$, one can show that the final momentum in the laboratory system points in the same direction as $\hat{Z} = \frac{\vec{k}+\vec{k}'}{|\vec{k}+\vec{k}'|}$ which one now relabels as $\hat{\ell}'$ (longitudinal along the final momentum) (refer to geometrical considerations in

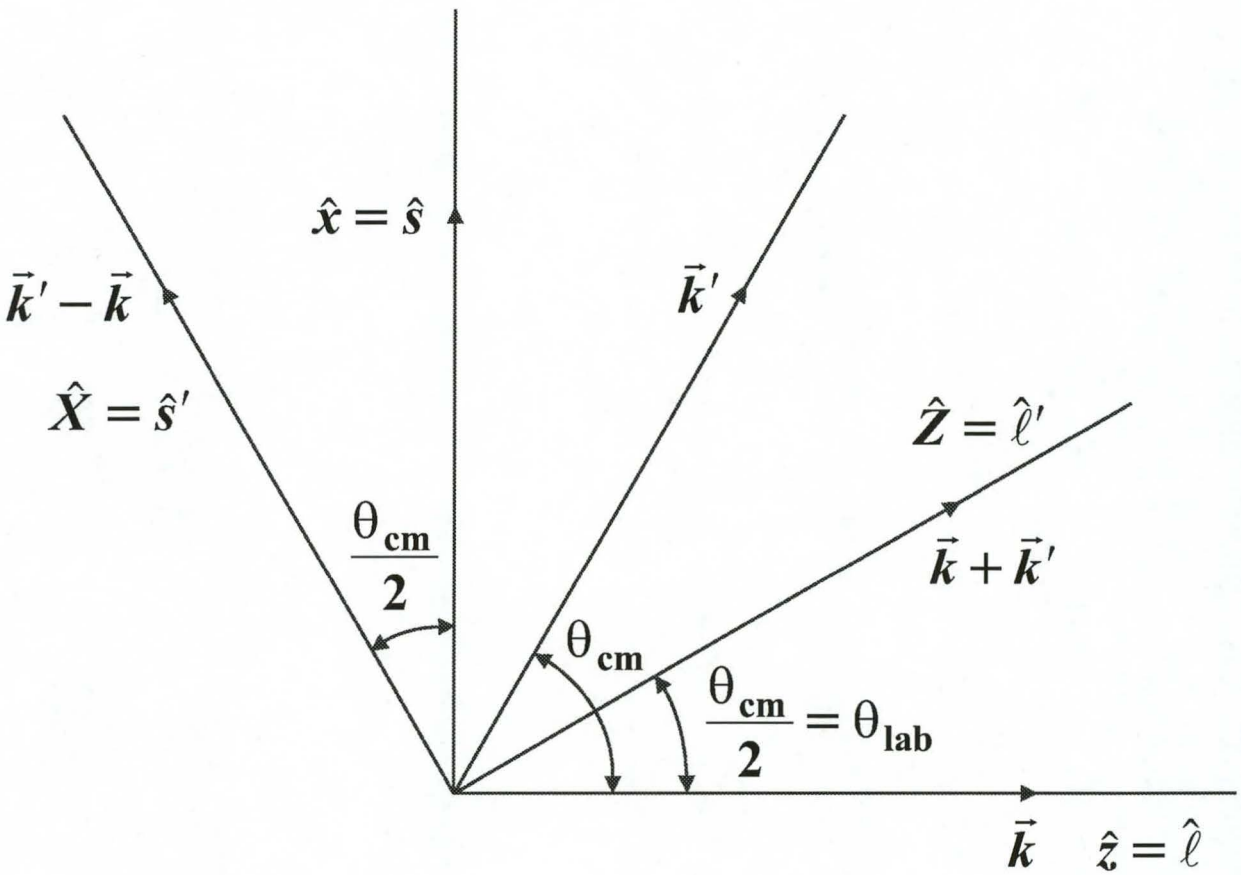

Figure G.1: Laboratory and centre–of–mass coordinate frames for describing polarization transfer observables for elastic NN scattering.

Fig. G.1). The perpendicular to this direction, namely $\hat{X}$, is now relabelled as $\hat{s}'$ (sideways). Note that the last term in Eq. (G.139) gives the component of $\vec{P}_1^{\rm scatt}$ in the direction $\hat{\ell}'$ and the second terms gives the component of $\vec{P}_1^{\rm scatt}$ in the direction $\hat{s}'$, both in the outgoing laboratory system. The first term together with Eq. (G.138), gives the component of $\vec{P}_1^{\rm scatt}$ in the direction normal ($\hat{n}$) to the scattering plane. However, the coefficients of the three terms in Eq. (G.139) contain components of $\vec{P}_1^{\rm inc}$ along the directions $\hat{X}$, $\hat{n}$, and $\hat{Z}$ in the NN centre–of–mass system. Our aim is to express the components of $\vec{P}_1^{\rm inc}$ along the right–handed coordinate system defined by $\hat{s} = \hat{x}$, $\hat{n} = \hat{y}$ and $\hat{\ell} = \hat{z} = \hat{k}$ in the incident laboratory system. This is achieved by expressing $(\vec{P}_1^{\rm inc} \cdot \hat{X})$ and $(\vec{P}_1^{\rm inc} \cdot \hat{Z})$ in Eq. (G.139) in terms of $(\vec{P}_1^{\rm inc} \cdot \hat{\ell})$ and $(\vec{P}_1^{\rm inc} \cdot \hat{s})$. From the geometry shown in Fig. G.1, it follows that

$$\begin{aligned} \vec{P}_1^{\rm inc} \cdot \hat{X} &= -(\vec{P}_1^{\rm inc} \cdot \hat{l})\sin(\theta_{\rm lab}) + (\vec{P}_1^{\rm inc} \cdot \hat{s})\cos(\theta_{\rm lab}) \\ \vec{P}_1^{\rm inc} \cdot \hat{Z} &= (\vec{P}_1^{\rm inc} \cdot \hat{l})\sin(\theta_{\rm lab}) + (\vec{P}_1^{\rm inc} \cdot \hat{s})\cos(\theta_{\rm lab}) \, . \end{aligned} \tag{G.141}$$

Substituting Eqs. (G.141), (G.136), (G.138) into Eq. (G.139), and then substituting the resultant expression into Eq. (G.133), yields

$$\begin{aligned} \frac{\sigma(\theta,\phi)}{\bar{\sigma}(\theta)} \vec{P}_1^{\rm scatt} &= (P + {\rm D}_{nn}\vec{P}^{\rm inc} \cdot \hat{n})\hat{n} + ({\rm D}_{\ell'\ell}\vec{P}^{\rm inc} \cdot \hat{\ell} + {\rm D}_{\ell' s}\vec{P}^{\rm inc} \cdot \hat{s})\hat{\ell}' \\ &\quad + ({\rm D}_{s'\ell}\vec{P}^{\rm inc} \cdot \hat{\ell} + {\rm D}_{s's}\vec{P}^{\rm inc} \cdot \hat{s})\hat{s}' \end{aligned} \tag{G.142}$$

where the polarization transfer observables ${\rm D}_{i'j}$, also defined by Eq. (G.134) (but with the NN scattering matrix M defined in the incident and outgoing laboratory systems), are explicitly written as

$$\begin{aligned} \bar{\sigma}(\theta)[1 - {\rm D}_{nn}] = \bar{\sigma}(\theta)[1 - {\rm D}] &= 2(|h_X|^2 + |h_Z|^2) \\ \bar{\sigma}(\theta){\rm D}_{s'\ell} = \bar{\sigma}(\theta){\rm A} &= -(|g_0|^2 + |h_X|^2 - |h_Z|^2 - |h_n|^2)\sin(\theta_{\rm lab}) \\ &\quad + 2{\rm Im}(h_0^* g_0 - h_0^* h_n)\cos(\theta_{\rm lab}) \\ \bar{\sigma}(\theta){\rm D}_{s's} = \bar{\sigma}(\theta){\rm R} &= (|g_0|^2 + |h_X|^2 - |h_Z|^2 - |h_n|^2)\cos(\theta_{\rm lab}) \\ &\quad + 2{\rm Im}(h_0^* g_0 - h_0^* h_n)\sin(\theta_{\rm lab}) \\ \bar{\sigma}(\theta){\rm D}_{\ell'\ell} = \bar{\sigma}(\theta){\rm A}' &= (|g_0|^2 - |h_X|^2 + |h_Z|^2 - |h_n|^2)\cos(\theta_{\rm lab}) \\ &\quad + 2{\rm Im}(h_0^* g_0 - h_0^* h_n)\sin(\theta_{\rm lab}) \\ \bar{\sigma}(\theta){\rm D}_{\ell' s} = -\bar{\sigma}(\theta){\rm R}' &= (|g_0|^2 - |h_X|^2 + |h_Z|^2 - |h_n|^2)\sin(\theta_{\rm lab}) \\ &\quad - 2{\rm Im}(h_0^* g_0 - h_0^* h_n)\cos(\theta_{\rm lab}) \, . \end{aligned} \tag{G.143}$$

The symbols D, A, R, A', and R' represent the so-called Wolfenstein parameters [Pa81, Hi90]. Combining Eqs. (G.129) and (G.143) yields the following matrix relation

$$\sigma(\theta,\phi)\begin{pmatrix} 1 \\ P^{\text{scatt}}_{1s'} \\ P^{\text{scatt}}_{1n} \\ P^{\text{scatt}}_{1\ell'} \end{pmatrix} = \bar{\sigma}(\theta)\begin{pmatrix} 1 & 0 & \mathrm{D}_{0n} & 0 \\ 0 & \mathrm{D}_{s'\ell} & 0 & \mathrm{D}_{s's} \\ \mathrm{D}_{n0} & 0 & \mathrm{D}_{nn} & 0 \\ 0 & \mathrm{D}_{\ell's} & 0 & \mathrm{D}_{\ell'\ell} \end{pmatrix}\begin{pmatrix} 1 \\ P^{\text{inc}}_{1s} \\ P^{\text{inc}}_{1n} \\ P^{\text{inc}}_{1\ell} \end{pmatrix} \tag{G.144}$$

where one has introduced the notation

$$\mathrm{D}_{0n} = A_y \text{ (analyzing power)} \qquad \mathrm{D}_{n0} = P \text{ (induced polarization)}\,. \tag{G.145}$$

The pictorial representation of the polarization transfer observables is depicted in Fig. G.2.

Next, expressions for the polarization transfer observables are derived in terms of the polarized differential cross section $\sigma_{\hat{j}\longrightarrow\hat{i}'}$. These expressions are used for calculating quasielastic polarization transfer observables in Chapter 3. From Eq. (G.142) the following expressions are obtained for the specified incoming and outgoing spin directions, namely

$$\begin{aligned}
\vec{P}^{\text{inc}}_1 = \hat{n} \longrightarrow \vec{P}^{\text{scatt}}_1 = \hat{n}: &\qquad \sigma_{\hat{n}\longrightarrow\hat{n}} = \bar{\sigma}P + \bar{\sigma}\mathrm{D}_{nn} \\
\vec{P}^{\text{inc}}_1 = \hat{n} \longrightarrow \vec{P}^{\text{scatt}}_1 = -\hat{n}: &\qquad -\sigma_{\hat{n}\longrightarrow-\hat{n}} = \bar{\sigma}P + \bar{\sigma}\mathrm{D}_{nn} \\
\vec{P}^{\text{inc}}_1 = -\hat{n} \longrightarrow \vec{P}^{\text{scatt}}_1 = \hat{n}: &\qquad \sigma_{-\hat{n}\longrightarrow\hat{n}} = \bar{\sigma}P - \bar{\sigma}\mathrm{D}_{nn} \\
\vec{P}^{\text{inc}}_1 = -\hat{n} \longrightarrow \vec{P}^{\text{scatt}}_1 = -\hat{n}: &\qquad -\sigma_{-\hat{n}\longrightarrow-\hat{n}} = \bar{\sigma}P - \bar{\sigma}\mathrm{D}_{nn}\,.
\end{aligned} \tag{G.146}$$

Combining these equations yields

$$\mathrm{D}_{nn} = \frac{\sigma_{\hat{n}\longrightarrow\hat{n}} - \sigma_{\hat{n}\longrightarrow-\hat{n}} - \sigma_{-\hat{n}\longrightarrow\hat{n}} + \sigma_{-\hat{n}\longrightarrow-\hat{n}}}{4\bar{\sigma}}\,. \tag{G.147}$$

Similarly, from Eq. (G.129) one obtains the following expressions for the specified incoming and outgoing spin directions

$$\begin{aligned}
\vec{P}^{\text{inc}}_1 = \hat{n} \longrightarrow \vec{P}^{\text{scatt}}_1 = \hat{n}: &\qquad \sigma_{\hat{n}\longrightarrow\hat{n}} = \bar{\sigma} + \bar{\sigma}\mathrm{A}_y \\
\vec{P}^{\text{inc}}_1 = \hat{n} \longrightarrow \vec{P}^{\text{scatt}}_1 = -\hat{n}: &\qquad \sigma_{\hat{n}\longrightarrow-\hat{n}} = \bar{\sigma} + \bar{\sigma}\mathrm{A}_y \\
\vec{P}^{\text{inc}}_1 = -\hat{n} \longrightarrow \vec{P}^{\text{scatt}}_1 = \hat{n}: &\qquad \sigma_{-\hat{n}\longrightarrow\hat{n}} = \bar{\sigma} - \bar{\sigma}\mathrm{A}_y \\
\vec{P}^{\text{inc}}_1 = -\hat{n} \longrightarrow \vec{P}^{\text{scatt}}_1 = -\hat{n}: &\qquad \sigma_{-\hat{n}\longrightarrow-\hat{n}} = \bar{\sigma} - \bar{\sigma}\mathrm{A}_y\,.
\end{aligned} \tag{G.148}$$

Combining these equations yields

$$4\bar{\sigma} = \sigma_{\hat{n}\longrightarrow\hat{n}} + \sigma_{\hat{n}\longrightarrow-\hat{n}} + \sigma_{-\hat{n}\longrightarrow\hat{n}} + \sigma_{-\hat{n}\longrightarrow-\hat{n}} \tag{G.149}$$

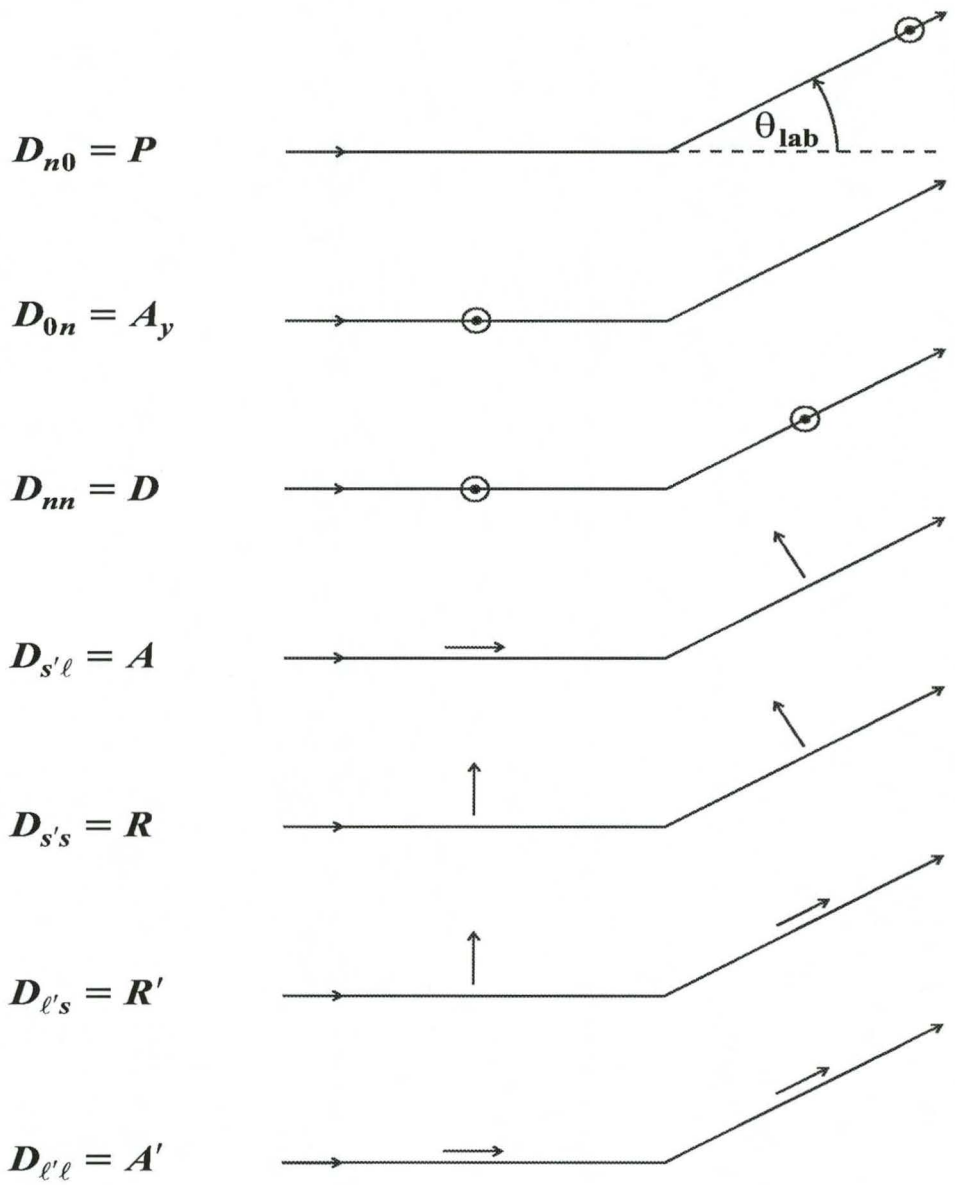

Figure G.2: Diagram illustrating the meaning of the NN polarization transfer observables. The spin directions before and after the scattering are represented in the incident and outgoing laboratory coordinate systems, defined by $(\hat{s}, \hat{n}, \hat{\ell})$ and $(\hat{s}', \hat{n}, \hat{\ell}')$ respectively. The spin direction associated with the incident proton indicates the state of polarization of the incident beam; and that associated with the outgoing proton indicates the component of the final polarization that is measured.

From Eqs. (G.147) and (G.149) one gets

$$\mathrm{D}_{nn} = \frac{\sigma_{\hat{n}\longrightarrow\hat{n}} - \sigma_{\hat{n}\longrightarrow-\hat{n}} - \sigma_{-\hat{n}\longrightarrow\hat{n}} + \sigma_{-\hat{n}\longrightarrow-\hat{n}}}{\sigma_{\hat{n}\longrightarrow\hat{n}} + \sigma_{\hat{n}\longrightarrow-\hat{n}} + \sigma_{-\hat{n}\longrightarrow\hat{n}} + \sigma_{-\hat{n}\longrightarrow-\hat{n}}} \,. \tag{G.150}$$

Combining Eqs. (G.146) and (G.148) yields an expression for A_y

$$\mathrm{A}_y = \frac{\sigma_{\hat{n}\longrightarrow\hat{n}} + \sigma_{\hat{n}\longrightarrow-\hat{n}} - \sigma_{-\hat{n}\longrightarrow\hat{n}} - \sigma_{-\hat{n}\longrightarrow-\hat{n}}}{\sigma_{\hat{n}\longrightarrow\hat{n}} + \sigma_{\hat{n}\longrightarrow-\hat{n}} + \sigma_{-\hat{n}\longrightarrow\hat{n}} + \sigma_{-\hat{n}\longrightarrow-\hat{n}}} \tag{G.151}$$

and, the induced polarization P

$$\mathrm{P} = \frac{\sigma_{\hat{n}\longrightarrow\hat{n}} - \sigma_{\hat{n}\longrightarrow-\hat{n}} + \sigma_{-\hat{n}\longrightarrow\hat{n}} - \sigma_{-\hat{n}\longrightarrow-\hat{n}}}{\sigma_{\hat{n}\longrightarrow\hat{n}} + \sigma_{\hat{n}\longrightarrow-\hat{n}} + \sigma_{-\hat{n}\longrightarrow\hat{n}} + \sigma_{-\hat{n}\longrightarrow-\hat{n}}} \,. \tag{G.152}$$

Recall that the induced polarization P is per definition the polarization that results from the scattering of an unpolarized beam from an unpolarized target. Defining the following spin–averaged polarization cross sections

$$\begin{aligned} \sigma_{0\longrightarrow\hat{n}} &= \frac{1}{2}(\sigma_{\hat{n}\longrightarrow\hat{n}} + \sigma_{-\hat{n}\longrightarrow\hat{n}}) \\ \sigma_{0\longrightarrow-\hat{n}} &= \frac{1}{2}(\sigma_{\hat{n}\longrightarrow-\hat{n}} + \sigma_{-\hat{n}\longrightarrow-\hat{n}}) \,, \end{aligned} \tag{G.153}$$

the induced polarization can be written as

$$P = \frac{\sigma_{0\longrightarrow\hat{n}} - \sigma_{0\longrightarrow-\hat{n}}}{\sigma_{0\longrightarrow\hat{n}} + \sigma_{0\longrightarrow-\hat{n}}} \,. \tag{G.154}$$

This is the form that is used in Chapter 3. Recall that $\mathrm{P} = A_y$, and hence the analyzing power is also given by Eq. (G.154). Following similar arguments that lead to Eq. (G.150), is straightforward to show that

$$\mathrm{D}_{i'j} = \frac{\sigma_{\hat{j}\longrightarrow\hat{i}'} - \sigma_{\hat{j}\longrightarrow-\hat{i}'} - \sigma_{-\hat{j}\longrightarrow\hat{i}'} + \sigma_{-\hat{j}\longrightarrow-\hat{i}'}}{\sigma_{\hat{j}\longrightarrow\hat{i}'} + \sigma_{\hat{j}\longrightarrow-\hat{i}'} + \sigma_{-\hat{j}\longrightarrow\hat{i}'} + \sigma_{-\hat{j}\longrightarrow-\hat{i}'}} \tag{G.155}$$

where $\hat{j} \in \{\hat{\ell}, \hat{n}, \hat{s}\}$ and $\hat{i}' \in \{\hat{\ell}', \hat{n}, \hat{s}'\}$.

G.6 Polarization observables for spin–$\frac{1}{2}$ on spin–zero scattering

The aim of this section is to derive explicit expressions for the spin observables for spin–$\frac{1}{2}$ on spin–zero scattering. For convenience, and analogous to the discussion on NN scattering, one uses the notation $\hat{s} = \hat{X}$ and $\hat{\ell} = \hat{Z}$ in Eq. (G.58), where $\{\hat{s},\ \hat{n},\ \hat{\ell}\}$ form a right–handed

coordinate system in the laboratory frame of the nucleon–nucleus system. Substituting the scattering matrix [Eq. (G.67)] into Eq. (G.37) yields

$$\begin{aligned} \mathrm{D}_{nn} &= 1 \\ \mathrm{D}_{s's} &= \mathrm{D}_{\ell'\ell} \\ \mathrm{D}_{\ell's} &= -\mathrm{D}_{s'\ell} \\ P^2 + \mathrm{D}_{s'\ell}^2 + \mathrm{D}_{s's}^2 &= 1 \,. \end{aligned} \tag{G.156}$$

The relations between the spin observables imply that, besides the usual unpolarized differential cross section,

$$\bar{\sigma} = |\alpha|^2 + |\beta_n|^2 \,, \tag{G.157}$$

one only needs two independent spin observables to completely describe elastic spin–$\frac{1}{2}$ on spin–zero scattering. These are chosen to be the induced polarization ($P = \mathrm{D}_{n0}$), which is also equal to the analyzing power ($\mathrm{A}_y = \mathrm{D}_{n0}$)

$$P = A_y = \mathrm{D}_{n0} = \frac{2\ \mathrm{Re}(\alpha\ \beta_n^*)}{|\alpha|^2 + |\beta_n|^2} \tag{G.158}$$

and, the spin–rotation function Q

$$Q = \mathrm{D}_{s'\ell} = \frac{2\ \mathrm{Im}(\alpha\ \beta_n^*)}{|\alpha|^2 + |\beta_n|^2} \,. \tag{G.159}$$

The nomenclature "spin–rotation function" becomes obvious when one expresses the scattered in terms of the incident beam polarization, via Eqs. (G.144) and (G.156), in the scattering plane only. This gives

$$\sigma \begin{pmatrix} P_{s'}^{\mathrm{scatt}} \\ P_{\ell'}^{\mathrm{scatt}} \end{pmatrix} = \bar{\sigma}(\theta) \begin{pmatrix} \mathrm{D}_{\ell'\ell} & -\mathrm{D}_{s'\ell} \\ \mathrm{D}_{s'\ell} & \mathrm{D}_{\ell'\ell} \end{pmatrix} \begin{pmatrix} P_s^{\mathrm{inc}} \\ P_\ell^{\mathrm{inc}} \end{pmatrix} \tag{G.160}$$

where the 2×2 matrix reminds one of a rotation in two dimensions. The analogy can be made more explicit by writing

$$\mathrm{D}_{\ell'\ell} = \sqrt{1 - P^2}\ \cos(\beta) \tag{G.161}$$

$$\mathrm{D}_{s'\ell} = \sqrt{1 - P^2}\ \sin(\beta) \tag{G.162}$$

where $\sqrt{1 - P^2}$ results from the normalization imposed by Eq. (G.156). Hence, one can write

$$\sigma \begin{pmatrix} P_{s'}^{\mathrm{scatt}} \\ P_{\ell'}^{\mathrm{scatt}} \end{pmatrix} = \bar{\sigma}(\theta) \begin{pmatrix} \sqrt{1 - P^2}\ \cos(\beta) & -\sqrt{1 - P^2}\ \sin(\beta) \\ \sqrt{1 - P^2}\ \sin(\beta) & \sqrt{1 - P^2}\ \cos(\beta) \end{pmatrix} \begin{pmatrix} P_s^{\mathrm{inc}} \\ P_\ell^{\mathrm{inc}} \end{pmatrix} \tag{G.163}$$

where it is clear that β is the rotation angle of the in–plane component of $\vec{P}^{\text{scatt}}$ (in the outgoing particle frame) with respect to the original in–plane $\vec{P}^{\text{inc}}$ (in the projectile frame): see Fig. G.3.

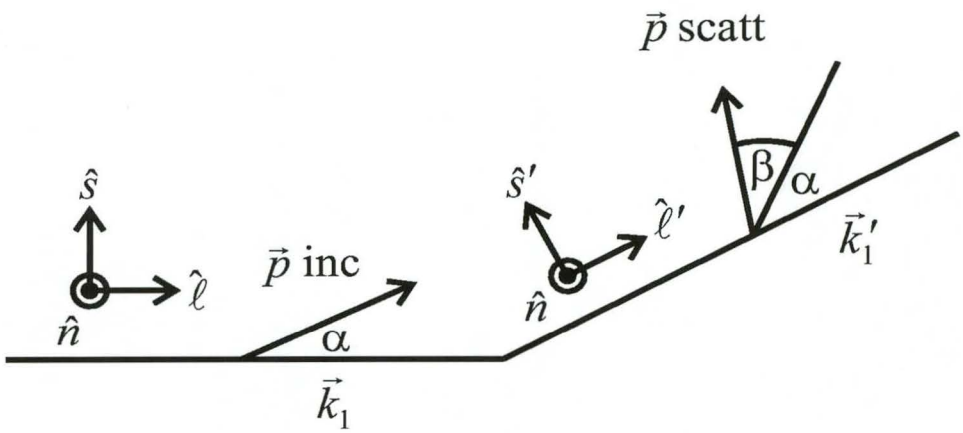

Figure G.3: The rotation angle β of the in–plane component of $\vec{P}^{\text{scatt}}$ (in the outgoing particle frame) with respect to the original in–plane $\vec{P}^{\text{inc}}$ (in the projectile frame).

Appendix H

Horowitz–Love–Franey (HLF) parameters

Real Relativistic Love–Franey parameters								
	80 MeV		**85 MeV**		**90 MeV**		**95 MeV**	
Meson	g^2	Λ	g^2	Λ	g^2	Λ	g^2	Λ
π	12.99	557.36	13.03	557.36	13.06	557.36	13.09	557.36
η	10.16	2500.00	10.18	2500.00	10.21	2500.00	10.23	2500.00
σ	-6.26	718.43	-6.28	718.43	-6.29	718.43	-5.31	2046.20
ω	11.54	630.78	11.57	630.78	11.59	630.78	10.45	693.98
t_1	-0.33	432.67	-0.33	432.67	-0.33	432.67	-1.25	341.07
a_1	-2.18	444.57	-2.18	444.57	-2.19	444.57	-4.15	358.28
δ	0.19	236.73	0.19	236.73	0.19	236.73	-1.71	236.73
ρ	-0.36	547.59	-0.36	547.59	-0.36	547.59	0.90	547.59
t_0	1.26	1322.82	1.26	1322.82	1.26	1322.82	2.03	1322.82
a_0	7.07	833.29	7.09	833.29	7.11	833.29	13.11	456.05

Real Relativistic Love–Franey parameters								
	100 MeV		105 MeV		110 MeV		115 MeV	
Meson	g^2	Λ	g^2	Λ	g^2	Λ	g^2	Λ
π	13.13	557.36	13.16	557.36	13.19	557.36	13.23	557.36
η	10.26	2500.00	10.29	2500.00	10.31	2500.00	10.34	2500.00
σ	-6.33	718.43	-5.62	2059.59	-6.36	718.43	-5.85	2071.98
ω	11.66	630.78	10.62	701.67	11.71	630.78	10.72	715.64
t_1	-0.34	432.67	-0.99	302.06	-0.34	432.67	-0.81	268.89
a_1	-2.19	444.57	-3.35	326.98	-2.21	444.57	-2.78	299.19
δ	0.19	236.73	-1.21	236.73	0.19	236.73	-0.77	236.73
ρ	-0.36	547.59	0.31	547.59	-0.36	547.59	-0.15	547.59
t_0	1.27	1322.82	1.65	1322.82	1.28	1322.82	1.38	1322.82
a_0	7.14	833.29	11.52	473.27	7.18	833.29	10.27	495.15

Real Relativistic Love–Franey parameters								
	120 MeV		**125 MeV**		**130 MeV**		**135 MeV**	
Meson	g^2	Λ	g^2	Λ	g^2	Λ	g^2	Λ
π	13.26	557.36	13.29	557.36	13.32	557.36	13.36	557.36
η	10.36	2500.00	10.39	2500.00	10.42	2500.00	10.44	2500.00
σ	-6.39	718.43	-5.97	2080.07	-6.42	718.43	-6.44	718.43
ω	11.77	630.78	10.71	722.62	11.83	630.78	11.86	630.78
t_1	-0.34	432.67	-0.67	240.29	-0.34	432.67	-0.34	432.67
a_1	-2.22	444.57	-2.39	274.61	-2.23	444.57	-2.24	444.57
δ	0.19	236.73	-0.48	236.73	0.19	236.73	0.19	236.73
ρ	-0.36	547.59	-0.49	547.59	-0.37	547.59	-0.37	547.59
t_0	1.28	1322.82	1.24	1322.82	1.29	1322.82	1.29	1322.82
a_0	7.22	833.29	9.33	539.93	7.25	833.29	7.27	833.29

Real Relativistic Love–Franey parameters								
	140 MeV		**145 MeV**		**150 MeV**		**155 MeV**	
Meson	g^2	Λ	g^2	Λ	g^2	Λ	g^2	Λ
π	13.39	557.36	13.42	557.36	13.46	557.36	13.49	557.36
η	10.47	2500.00	10.49	2500.00	10.52	2500.00	10.55	2500.00
σ	-6.45	718.43	-6.15	2095.58	-6.49	718.43	-6.20	2106.40
ω	11.89	630.78	10.57	774.17	11.95	630.78	10.39	813.35
t_1	-0.34	432.67	-0.45	188.33	-0.34	432.67	-0.35	162.73
a_1	-2.24	444.57	-1.83	230.76	-2.25	444.57	-1.64	214.51
δ	0.19	236.73	0.09	236.73	0.19	236.73	0.26	236.73
ρ	-0.37	547.59	-1.07	547.59	-0.37	547.59	-1.34	547.59
t_0	1.29	1322.82	0.94	1322.82	1.30	1322.82	0.82	1322.82
a_0	7.29	833.29	7.48	646.22	7.32	833.29	6.43	794.57

Real Relativistic Love–Franey parameters								
	160 MeV		**165 MeV**		**170 MeV**		**175 MeV**	
Meson	g^2	Λ	g^2	Λ	g^2	Λ	g^2	Λ
π	13.52	557.36	13.56	557.36	13.01	565.77	13.05	565.77
η	10.57	2500.00	10.59	2500.00	8.65	1386.82	8.67	1386.82
ω	-6.52	718.43	-6.29	1905.29	-6.13	970.28	-6.23	1018.63
σ	12.01	630.78	10.12	865.37	10.87	845.81	10.79	834.91
t_1	-0.35	432.67	-0.26	136.04	-0.03	240.22	-0.03	201.23
a_1	-2.27	444.57	-1.59	213.75	-1.11	406.53	-1.11	402.54
δ	0.19	236.73	0.18	236.73	0.55	1479.58	0.35	543.17
ρ	-0.37	547.59	-1.65	547.59	-0.56	917.19	-0.58	906.48
t_0	1.31	1322.82	0.73	1322.82	0.38	2919.12	0.33	3202.19
a_0	7.36	833.29	4.99	1760.26	2.029	1002.42	2.23	1249.44

Real Relativistic Love–Franey parameters								
	180 MeV		**185 MeV**		**190 MeV**		**195 MeV**	
Meson	g^2	Λ	g^2	Λ	g^2	Λ	g^2	Λ
π	13.08	565.77	13.11	565.77	13.14	565.77	13.17	565.77
η	8.69	1386.82	8.72	1386.82	8.74	1386.82	8.76	1386.82
σ	-6.19	988.30	-6.22	993.49	-6.26	997.58	-6.27	995.17
ω	10.88	842.48	10.89	841.47	10.90	843.93	10.93	844.59
t_1	-0.03	218.34	-0.03	213.42	-0.03	193.49	-0.03	194.51
a_1	-1.12	404.28	-1.12	403.69	-1.14	403.19	-1.14	403.15
δ	0.48	997.77	0.46	913.67	0.38	1173.05	0.39	1279.72
ρ	-0.56	917.19	-0.57	917.19	-0.59	917.19	-0.59	917.19
t_0	0.36	3098.55	0.36	3082.16	0.37	1858.35	0.37	1910.32
a_0	2.14	1067.39	2.17	1090.12	2.12	1262.96	2.11	1262.96

	Real parameters		Imaginary parameters	
	200 MeV		200 MeV	
Meson	g^2	Λ	g^2	Λ
π	13.20	565.77	-4.37	1099.19
η	8.78	1386.82	6.89	1162.15
σ	-6.31	1018.96	-2.91	591.32
ω	10.93	835.09	4.51	601.09
t_1	-0.03	200.00	0.25	1112.98
a_1	-1.13	403.56	0.78	673.62
δ	0.34	543.17	2.49	529.83
ρ	-0.59	917.19	-2.01	548.18
t_0	0.33	2500.00	-0.87	985.48
a_0	2.27	1262.96	-1.96	944.93

Imaginary Relativistic Love–Franey parameters								
	80 MeV		**85 MeV**		**90 MeV**		**95 MeV**	
Meson	g^2	Λ	g^2	Λ	g^2	Λ	g^2	Λ
π	-9.19	2057.95	-8.87	1861.55	-8.48	1681.12	-8.46	1880.35
η	4.53	1200.00	6.09	1200.00	6.52	1200.00	6.78	1200.00
σ	-6.37	535.34	-6.49	581.23	-5.89	549.09	-5.84	559.01
ω	9.22	523.11	8.61	508.75	8.37	517.86	8.23	526.24
t_1	0.97	670.20	0.83	564.99	0.83	635.37	0.87	707.65
a_1	4.38	793.31	4.86	969.94	3.98	825.05	4.01	903.05
δ	4.11	485.83	4.49	535.42	4.17	515.50	4.13	517.86
ρ	-3.25	470.00	-3.16	465.27	-3.21	482.82	-3.21	492.88
t_0	-2.46	849.90	-2.21	758.78	-2.09	780.02	-2.12	843.59
a_0	-5.42	1038.36	-5.40	1106.96	-4.76	990.52	-4.79	1031.28

Imaginary Relativistic Love–Franey parameters

Meson	100 MeV		105 MeV		110 MeV		115 MeV	
	g^2	Λ	g^2	Λ	g^2	Λ	g^2	Λ
π	-8.27	1869.74	-7.94	1676.27	-7.84	1771.34	-7.62	1705.51
η	7.00	1200.00	7.62	1200.00	7.85	1200.00	8.24	1200.00
σ	-5.62	557.74	-5.36	557.29	-5.11	548.05	-4.94	552.27
ω	8.02	531.74	7.63	531.12	7.48	541.01	7.19	540.03
t_1	0.85	746.27	0.79	736.16	0.84	870.21	0.81	894.46
a_1	3.78	855.09	3.54	871.29	3.36	870.18	3.26	902.06
δ	4.05	521.48	3.99	527.77	3.81	513.71	3.77	522.74
ρ	-3.19	504.24	-3.14	507.21	-3.12	517.58	-3.06	521.04
t_0	-2.06	873.51	-1.89	848.41	-1.91	934.08	-1.82	939.63
a_0	-4.59	1032.54	-4.28	999.48	-4.15	1011.53	-3.99	1025.31

Imaginary Relativistic Love–Franey parameters								
	120 MeV		**125 MeV**		**130 MeV**		**135 MeV**	
Meson	g^2	Λ	g^2	Λ	g^2	Λ	g^2	Λ
π	-7.44	1696.58	-7.23	1660.29	-6.80	1655.49	-6.82	1655.49
η	8.48	1200.00	8.76	1200.00	8.77	1200.00	8.79	1200.00
σ	-4.79	560.48	-4.65	565.26	-4.29	563.64	-4.30	563.64
ω	6.96	540.96	6.70	540.71	6.30	549.91	6.32	549.91
t_1	0.79	964.57	0.77	1001.41	0.73	1115.63	0.73	1115.63
a_1	3.19	958.82	3.11	1013.81	2.77	1013.61	2.78	1013.61
δ	3.70	527.63	3.66	535.32	3.44	531.29	3.45	531.29
ρ	-3.00	525.68	-2.94	529.32	-2.83	541.85	-2.84	541.85
t_0	-1.76	969.61	-1.69	983.74	-1.57	1031.49	-1.57	1031.49
a_0	-3.88	1045.93	-3.76	1062.27	-3.44	1056.91	-3.45	1056.91

Imaginary Relativistic Love–Franey parameters								
	140 MeV		145 MeV		150 MeV		155 MeV	
Meson	g^2	Λ	g^2	Λ	g^2	Λ	g^2	Λ
π	-6.84	1931.76	-6.59	1829.47	-6.41	1787.24	-6.35	1870.69
η	9.01	1200.00	9.04	1200.00	9.33	1200.00	10.25	1200.00
σ	-4.21	574.08	-4.07	576.93	-3.88	572.68	-3.66	562.06
ω	6.21	561.14	5.99	560.38	5.79	562.31	5.57	559.81
t_1	0.80	1456.08	0.76	1530.15	0.75	1768.09	0.81	3586.30
a_1	2.98	1217.98	2.79	1227.59	2.69	1278.78	2.83	1526.10
δ	3.35	531.25	3.28	532.82	3.19	532.23	3.08	529.42
ρ	-2.76	542.67	-2.71	546.77	-2.65	550.45	-2.59	552.17
t_0	-1.66	1238.59	-1.56	1225.43	-1.51	1282.86	-1.53	1409.26
a_0	-3.61	1200.93	-3.41	1178.08	-3.28	1192.62	-3.28	1273.06

Imaginary Relativistic Love–Franey parameters								
	160 MeV		**165 MeV**		**170 MeV**		**175 MeV**	
Meson	g^2	Λ	g^2	Λ	g^2	Λ	g^2	Λ
π	-6.07	1689.72	-5.89	1614.87	-5.79	1672.35	-5.54	1541.06
η	9.45	1200.00	9.49	1200.00	6.84	1162.15	6.94	1162.15
σ	-3.76	600.53	-3.69	613.00	-3.57	608.65	-3.42	601.89
ω	5.37	558.21	5.18	555.97	5.44	602.54	5.26	602.02
t_1	0.70	1886.72	0.67	1886.72	0.53	2026.61	0.49	2056.68
a_1	2.61	1573.79	2.52	1732.04	1.76	1159.38	1.57	1106.47
δ	3.07	538.98	3.02	542.34	2.73	506.17	2.67	506.75
ρ	-2.51	551.36	-2.44	552.37	-2.29	533.79	-2.24	535.62
t_0	-1.38	1453.56	-1.29	1513.89	-1.37	1648.34	-1.28	1551.67
a_0	-3.10	1247.90	-2.99	1253.36	-2.96	1340.47	-2.77	1281.49

Imaginary Relativistic Love–Franey parameters

Meson	180 MeV		185 MeV		190 MeV		195 MeV	
	g^2	Λ	g^2	Λ	g^2	Λ	g^2	Λ
π	-4.99	1313.76	-5.00	1313.77	-4.89	1348.25	-4.70	1295.95
η	6.87	1162.15	6.89	1162.15	7.08	1162.15	7.09	1162.15
σ	-3.19	596.09	-3.19	596.09	-3.06	590.41	-2.96	587.39
ω	4.92	601.47	4.93	601.47	4.83	608.08	4.69	610.49
t_1	0.37	1490.65	0.37	1490.65	0.38	2227.48	0.35	2344.25
a_1	1.17	901.87	1.18	901.87	1.17	973.85	1.06	932.59
δ	2.60	516.96	2.61	516.96	2.52	512.84	2.47	513.71
ρ	-2.15	542.44	-2.15	542.44	-2.09	542.19	-2.05	543.48
t_0	-1.08	1241.22	-1.08	1241.22	-1.08	1332.14	-1.03	1288.25
a_0	-2.37	1108.98	-2.38	1108.98	-2.35	1168.13	-2.23	1140.79

Appendix I

Kinematic relations: Quasielastic scattering

The aim of this appendix is to derive expressions for the kinematic quantities of interest for quasielastic proton–nucleus scattering discussed in Chapter 3. The following input parameters are required in order to completely specify all the kinematics:

- laboratory kinetic energy T_{lab} of the incident proton beam,
- laboratory scattering angle θ_{lab} of the detected ejectile nucleon,
- free nucleon mass m,
- effective projectile and target nucleon effective masses m_1^* and m_2^* respectively,
- maximum Fermi momentum k_F,
- the range of energy transfers ω spanning the quasielastic peak: ω is *not calculated* from other kinematic quantities, but is chosen to span the quasielastic peak of interest. So for the purposes of this appendix, one regards ω as known.

Given the above input, all the kinematic quantities of interest to quasielastic proton–nucleus scattering will now be derived, using natural units, i.e. $\hbar = c = 1$ will be used in this Appendix. Furthermore, as in Chapter 3, the following notation is used for the asymptotic (i.e. free) energies and momenta in the conventional *laboratory frame*:

1. E_1 and $\vec{k}_1$ refer to the energy and momentum of the projectile nucleon,
2. E_1' and $\vec{k}_1'$ refer to the energy and momentum of the ejectile nucleon,
3. E_2 and $\vec{k}_2$ refer to the initial energy and momentum of the target nucleon (before it has been struck),

4. E_2' and $\vec{k}_2'$ refer to the final energy and momentum of the target nucleon (after it has been struck).

I.1 Energy of asymptotic incident nucleon in laboratory frame

The aim of this section is to derive an expression for the energy E_1 of the asymptotic incident nucleon in the laboratory frame.

Energy E and momentum $\vec{k}$ together form the energy–momentum four–vector

$$k^\mu = (E, \vec{k}) \tag{I.1}$$

and are related via the well–known invariant expression [Go80, Gr87, Si90]

$$k_\mu k^\mu = E^2 - |\vec{k}|^2 = m^2 \tag{I.2}$$

where m is the rest mass of the particle under consideration. An expression for the relativistic kinetic energy T is derived by expanding

$$E = \sqrt{|\vec{k}|^2 + m^2} \tag{I.3}$$

in a Taylor series (valid for $|\frac{|\vec{k}|}{m}| < 1$):

$$\begin{aligned} E &= m(1 + \frac{1}{2}(\frac{|\vec{k}|}{m})^2 + \frac{3}{8}(\frac{|\vec{k}|}{m})^4 + ...) \\ &= m + T \end{aligned} \tag{I.4}$$

where T is the relativistic kinetic energy attributable to the relative motion of the system, and is given by

$$T = \frac{1}{2}(\frac{|\vec{k}|}{m})^2 + \frac{3}{8}(\frac{|\vec{k}|}{m})^4 + \ldots . \tag{I.5}$$

Given the kinetic energy of the incident nucleon in the laboratory frame T_{lab} of the proton–nucleus system, one can calculate the asymptotic (free) energy E_1 of the incident nucleon (in the laboratory frame of the proton–nucleus laboratory system) from Eq. (I.4), namely (using natural units)

$$E_1 = T_{\text{lab}} + m \tag{I.6}$$

where m is the rest mass of the nucleon.

I.2 Asymptotic projectile and ejectile momenta in lab frame

In this section, expressions are derived for the components of the asymptotic three–momenta of the projectile and ejectile nucleons in the laboratory frame.

The magnitude of the asymptotic incident three–momentum of the projectile follows from Eq. (I.2), that is

$$|\vec{k}_1| = \sqrt{(E_1)^2 - m^2} \tag{I.7}$$

where E_1 is given by Eq. (I.6). To find expressions for the components of $\vec{k}_1$ and $\vec{k}'_1$, it is necessary to specify the initial and final laboratory coordinate frames. Consistent with Sec. 3.2.7 in Chapter 3, the axes of the initial laboratory coordinate frame are defined as

$$\begin{aligned} \hat{z} &= \frac{\vec{k}_1 \times \vec{k}'_1}{|\vec{k}_1 \times \vec{k}'_1|} \,. \\ \hat{x} &= \hat{k}_1 \\ \hat{y} &= \hat{z} \times \hat{k}_1 \end{aligned} \tag{I.8}$$

and the final laboratory coordinate frame is defined as

$$\begin{aligned} \hat{z}' &= \hat{z} \\ \hat{x}' &= \hat{k}'_1 \\ \hat{y} &= \hat{z}' \times \hat{k}'_1 \,. \end{aligned} \tag{I.9}$$

With the x–axis defined along the direction of the incident beam, the x–, y– and z–components of $\vec{k}_1$ are written as

$$\begin{aligned} (k_1)_x &= |\vec{k}_1| \\ (k_1)_y &= 0 \\ (k_1)_z &= 0 \,. \end{aligned} \tag{I.10}$$

For an energy transfer of ω to the target nucleon, the energy E'_1 of the ejectile nucleon is obtained from Eq. (3.64) in Chapter 3, namely

$$E'_1 = E_1 - \omega \tag{I.11}$$

and the corresponding magnitude of the asymptotic three–momentum is given by Eq. (I.2), namely

$$|\vec{k}'_1| \;=\; \sqrt{(E'_1)^2 - m^2}\,. \tag{I.12}$$

From Fig. 3.5 in Chapter 3, the x–, y– and z–components of $\vec{k}'_1$ are written in terms of the laboratory scattering angle $\theta_{\rm lab}$ in the xy– or scattering plane, namely

$$\begin{aligned}(k'_1)_x &= |\vec{k}'_1|\cos\theta_{\rm lab}\\ (k'_1)_y &= |\vec{k}'_1|\sin\theta_{\rm lab}\\ (k'_1)_z &= 0\,.\end{aligned} \tag{I.13}$$

I.3 Three– and four–momentum transfer to the target nucleon

The aim of this section is to write down expressions for the three–momentum and four–momentum transfer for quasielastic proton–nucleus scattering in the laboratory frame.

The three–momentum transfer $\vec{q}$ is defined as

$$\vec{q} \;=\; \vec{k}_1 \;-\vec{k}'_1 \;=\; \vec{k}'_2 \;-\vec{k}_2 \tag{I.14}$$

and, from Eqs. (I.10) and (I.13), one can write down expressions for the x–, y– and z–components of $\vec{q}$, namely

$$\begin{aligned}q_x &= (k_1)_x \;-\; (k'_1)_x \;=\; |\vec{k}_1| \;-\; |\vec{k}'_1|\cos\theta_{\rm lab}\\ q_y &= (k_1)_y \;-\; (k'_1)_y \;=\; -|\vec{k}'_1|\sin\theta_{\rm lab}\\ q_z &= (k_1)_x \;-\; (k'_1)_z \;=\; 0\,.\end{aligned} \tag{I.15}$$

The magnitude of the three–momentum transfer $|\vec{q}\,|$ is then calculated from

$$|\vec{q}\,| \;=\; \sqrt{(q_x)^2 + (q_y)^2} \tag{I.16}$$

and the angle α between $\vec{q}$ and the Y–axis is given by (see Fig. I.1)

$$\alpha \;=\; \tan^{-1}[\,|\frac{q_x}{q_y}|\,]\,. \tag{I.17}$$

For a specific energy and three–momentum transfer, ω and $\vec{q}$ respectively, the four–momentum squared is defined as

$$q_\mu q^\mu \;=\; \omega^2 \;-\; |\vec{q}\,|^2\,. \tag{I.18}$$

I.4 Initial and final momenta of target nucleons in lab frame

The aim of this section is to derive expressions for the initial and final target–nucleon momenta, $\vec{k}_2$ and $\vec{k}'_2$ respectively, in the laboratory frame.

One starts by deriving expressions for the x–, y– and z–components of the momentum $\vec{k}_2$ of the target nucleon (before it has been struck) in the laboratory frame.

Consider the nucleon–nucleon scattering process depicted in Fig. I.1, where $\vec{k}_1$ and $\vec{k}'_1$ refer to the initial and final laboratory momenta of the projectile and ejectile nucleon respectively, and the laboratory scattering angle is denoted by θ_{lab}. The aim is to express $\vec{k}_2$ in terms of the following three angles (see Fig. I.1):

- α defined by Eq. (I.17): the angle between $\vec{q}$ and the negative y–axis (Y), i.e. $\angle$CAD,
- χ defined by Eq. (I.27): the angle between AB$'$ and AC,
- ϕ: the azumithal angle between CB and CB$'$.

From the geometry of the scattering process depicted in Fig. I.1 one can immediately write down expressions for the x–, y– and z–components of $\vec{k}_2$ with respect to the *initial* xyz frame, namely

$$\begin{aligned}
(k_2)_x &= \text{AG} \\
&= \text{AH} + \text{HG} \\
&= \text{AC}\sin\alpha + \text{CB}\cos\alpha \\
&= \text{AB}'\cos\chi\sin\alpha + \text{CB}'\cos\phi\cos\alpha \\
&= \text{AB}'\cos\chi\sin\alpha + \text{AB}'\sin\chi\cos\phi\cos\alpha \\
&= |\vec{k}_2|(\cos\chi\sin\alpha + \sin\chi\cos\phi\cos\alpha)\,, \qquad \text{(I.19)}
\end{aligned}$$

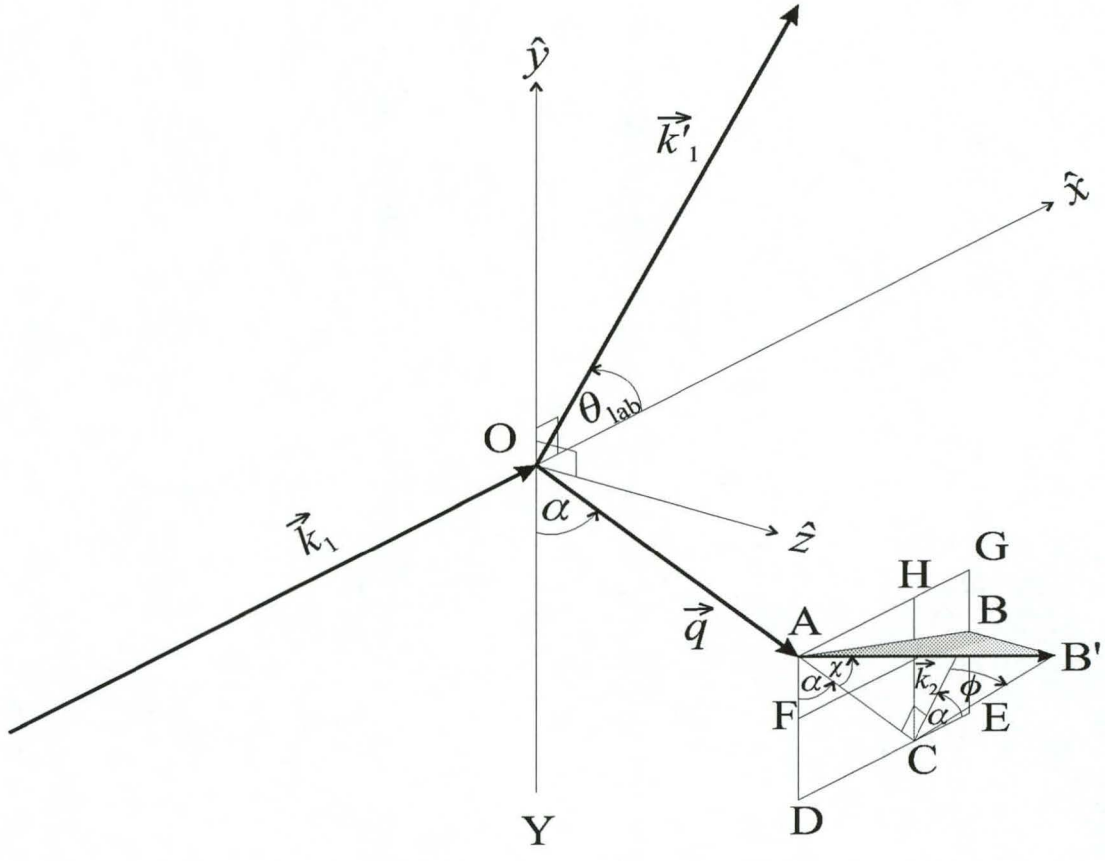

Figure I.1: Coordinate frame for derivation of expressions for the asymptotic laboratory momenta of the initial and final nucleons within a Fermi–gas model of the nucleus. The symbols are defined in the text.

$$
\begin{aligned}
(k_2)_y &= \mathrm{AF} \\
&= \mathrm{AD} - \mathrm{FD} \\
&= \mathrm{AC}\cos\alpha - \mathrm{BC}\sin\alpha \\
&= \mathrm{AB}'\cos\chi\cos\alpha - \mathrm{CB}'\cos\phi\sin\alpha \\
&= \mathrm{AB}'\cos\chi\cos\alpha - \mathrm{AB}'\sin\chi\cos\phi\sin\alpha \\
&= |\vec{k}_2|(\cos\chi\cos\alpha - \sin\chi\cos\phi\sin\alpha)\ , \qquad \text{(I.20)}
\end{aligned}
$$

$$
\begin{aligned}
(k_2)_z &= BB' \\
&= CB'\sin\phi \\
&= AB'\sin\chi\sin\phi \\
&= |\vec{k}_2|\sin\chi\sin\phi\ . \qquad \text{(I.21)}
\end{aligned}
$$

With Eqs. (I.14) and (I.15), one can also write down expressions for the x–, y– and z–components of the ejectile three–momentum $\vec{k}_2'$, namely

$$
\begin{aligned}
(k_2')_x &= (k_2)_x + (q)_x \\
(k_2')_y &= (k_2)_y + (q)_y \\
(k_2')_z &= (k_2)_z\ . \qquad \text{(I.22)}
\end{aligned}
$$

I.5 Scattering energies in medium–modified Dirac spinors

The aim of this section is to write down expressions for the scattering energies contained in the medium–modified Dirac spinors in Chapter 3.

The scattering energies E^* in the medium–modified Dirac spinors in the invariant matrix element $\mathcal{M}$ [see Eqs. (3.54) and (3.55) in Chapter 3] are given by expressions of the form of Eq. (I.3), with the exception that the free nucleon masses m are replaced by effective projectile and target nucleon masses, m_1^* and m_2^* respectively.

Hence, in the laboratory frame, one writes

$$\begin{aligned} E_1^* &= \sqrt{|\vec{k}_1|^2 + m_1^{*2}} \\ E'^*_1 &= \sqrt{|\vec{k}'_1|^2 + m_1^{*2}} \\ E_2^* &= \sqrt{|\vec{k}_2|^2 + m_2^{*2}} \\ E'^*_2 &= \sqrt{|\vec{k}'_2|^2 + m_2^{*2}} \end{aligned} \tag{I.23}$$

where all the three–momenta refer to the asymptotic (free) values.

I.6 Angle between target–nucleon momentum and $\vec{q}$

The aim of this section is to derive an expression for the angle between the target–nucleon momentum $\vec{k}_2$ and the three–momentum transfer $\vec{q}$ in the laboratory frame.

For an energy transfer ω to the target nucleon, the energy of the scattered target nucleon is

$$E'^*_2 = E_2^* + \omega \tag{I.24}$$

where E_2^* and E'^*_2 are defined by Eq. (I.23). Equivalently, for a three–momentum transfer of $\vec{q}$ to the target nucleon, the final momentum of the target nucleon is given by

$$\vec{k}'_2 = \vec{k}_2 + \vec{q} \tag{I.25}$$

and from Eq. (I.2) one can write down an expression for the final energy of the target nucleon, namely

$$(E'^*_2)^2 = (\vec{k}_2 + \vec{q}\,)^2 + m_2^{*2}\,. \tag{I.26}$$

Equating the square of Eq. (I.24) to Eq. (I.26) yields the following expression for the angle χ between the target–nucleon momentum $\vec{k}_2$ and the three–momentum transfer $\vec{q}$, namely

$$\cos\chi = \frac{q_\mu q^\mu + 2\omega E_2^*}{2|\vec{k}_2|\,|\vec{q}\,|}\,. \tag{I.27}$$

I.7 Minimum and maximum values of the target–nucleon momentum

For a Fermi–gas nucleus, the target–nucleon momentum of an individual nucleon ranges between zero and the maximum value k_F (see Sec. 3.2.3), that is

$$0 \leq |\vec{k}_2| \leq k_F \,. \tag{I.28}$$

However, imposing the additional constraint that the ejectile nucleon must be detected at a fixed laboratory scattering angle $\theta_{\rm lab}$ (i.e. the three–momentum transfer $\vec{q}$ is fixed) after the projectile collides with a target nucleon, places further restrictions on the permissible values of the momentum $\vec{k}_2$. The latter constraint is incorporated by virtue of the fact that in Eq. (I.27)

$$|\cos\chi| \leq 1 \tag{I.29}$$

which means that

$$\frac{q_\mu q^\mu + 2\omega E_2^*}{2|\vec{k}_2|\,|\vec{q}\,|} \geq -1 \tag{I.30}$$

and

$$\frac{q_\mu q^\mu + 2\omega E_2^*}{2|\vec{k}_2|\,|\vec{q}\,|} \leq +1 \,. \tag{I.31}$$

The constraints imposed by Eqs. (I.30) and (I.31) on the allowed values of $|\vec{k}_2|$ are now investigated.

One starts by considering the restrictions imposed by Eq. (I.30) on the allowed values of $|\vec{k}_2|$. Substitution of Eq. (I.23) into Eq. (I.30) yields

$$q_\mu q^\mu + 2|\vec{k}_2|\,|\vec{q}\,| \geq -2\omega\sqrt{|\vec{k}_2|^2 + m_2^{*2}} \,. \tag{I.32}$$

Squaring both sides, making use of Eq. (I.18), and multiplying all terms by $\dfrac{1}{4(q_\mu)^2}$, yields

$$(|\vec{k}_2| - \frac{|\vec{q}\,|}{2})^2 \leq \frac{\omega^2}{4}(1 - \frac{m_2^{*2}}{(q_\mu)^2}) \,. \tag{I.33}$$

This condition implies that

$$\big|\,|\vec{k}_2| - \frac{|\vec{q}\,|}{2}\,\big| \leq \frac{\omega}{2}\sqrt{1 - \frac{m_2^{*2}}{(q_\mu)^2}} \,. \tag{I.34}$$

There are two solutions for $|\vec{k}_2|$ which satisfy the above inequality, namely [Ma86a]

$$|\vec{k}_2| \leq \frac{|\vec{q}|}{2} + \frac{\omega}{2}\sqrt{1 - \frac{m_2^{*2}}{(q_\mu)^2}}\,, \tag{I.35}$$

and

$$|\vec{k}_2| \geq \frac{|\vec{q}|}{2} - \frac{\omega}{2}\sqrt{1 - \frac{m_2^{*2}}{(q_\mu)^2}}\,. \tag{I.36}$$

Next, the restrictions imposed by Eq. (I.31) on the allowed values of $|\vec{k}_2|$ are investigated. Substitution of Eq. (I.23) into Eq. (I.31) yields

$$q_\mu q^\mu - 2|\vec{k}_2|\,|\vec{q}\,| \leq -2\omega\sqrt{|\vec{k}_2|^2 + m_2^{*2}}\,. \tag{I.37}$$

Squaring both sides, making use of Eq. (I.18), and multiplying all terms by $\frac{1}{4(q_\mu)^2}$, yields

$$(|\vec{k}_2| + \frac{|\vec{q}|}{2})^2 \geq \frac{\omega^2}{4}(1 - \frac{m_2^{*2}}{(q_\mu)^2})\,. \tag{I.38}$$

This condition implies that

$$||\vec{k}_2| + \frac{|\vec{q}|}{2}| \geq \frac{\omega}{2}\sqrt{1 - \frac{m_2^{*2}}{(q_\mu)^2}}\,. \tag{I.39}$$

There is one solution for $|\vec{k}_2|$ which satisfies the above inequality, namely [Ma86a]

$$|\vec{k}_2| \geq -\frac{|\vec{q}|}{2}\frac{\omega}{2}\sqrt{1 - \frac{m_2^{*2}}{(q_\mu)^2}}\,. \tag{I.40}$$

Combining the restrictions encompassed by Eqs. (I.28), (I.35), (I.36) and (I.40) yields the following limits on the minimum and maximum values of the initial target–nucleon momentum, $|\vec{k}_2|_{\min}$ and $|\vec{k}_2|_{\max}$ respectively:

$$\begin{aligned} |\vec{k}_2|_{\min} &= \text{maximum}[\,\frac{|\vec{q}|}{2} - \frac{\omega}{2}\sqrt{1 - \frac{m_2^{*2}}{(q_\mu)^2}}\,, -\frac{|\vec{q}|}{2} + \frac{\omega}{2}\sqrt{1 + \frac{m_2^{*2}}{(q_\mu)^2}}\,, 0\,] \\ &= \text{maximum}[\,|\,\frac{|\vec{q}|}{2} - \frac{\omega}{2}\sqrt{1 - \frac{m_2^{*2}}{(q_\mu)^2}}\,|\,, 0\,] \end{aligned} \tag{I.41}$$

and

$$|\vec{k}_2|_{\max} = \text{minimum}[\,\frac{|\vec{q}|}{2} + \frac{\omega}{2}\sqrt{1 - \frac{m_2^{*2}}{(q_\mu)^2}}\,, k_F\,]\,. \tag{I.42}$$

I.8 Effective laboratory kinetic energy of the incident nucleon

The aim of this section is to derive an expression for the effective laboratory kinetic energy of the projectile nucleon. The effective NN laboratory frame is defined as that system whereby both the initial target–nucleon momentum and kinetic energy of the target nucleon are zero, that is

$$\begin{aligned} (\vec{k}_2)^L_{\text{eff}} &= 0 \\ (T_2)^L_{\text{eff}} &= 0 \,. \end{aligned} \tag{I.43}$$

To derive an expression for the effective incident laboratory kinetic in this system, one needs to find the transformation between the conventional laboratory system, where the target–nucleon momentum $\vec{k}_2$ is not zero, and the effective laboratory system defined by Eq. (I.43). To this end, one makes use of the fact that the square of the total four–momentum (often denoted by the Mandelstam variable s) is an invariant quantity [Si90], that is

$$(k_\mu)^L_{\text{eff}} \, (k^\mu)^L_{\text{eff}} = (k_\mu)_{\text{lab}} \, (k^\mu)_{\text{lab}} \,, \tag{I.44}$$

where the indices "L" and "eff " denote the effective laboratory frame and the subscript "lab" refers to the conventional laboratory frame. The total effective laboratory four–momentum is given by

$$(k^\mu)^L_{\text{eff}} = [\, E^L_{\text{eff}} \,, \, (\vec{k})^L_{\text{eff}} \,] \tag{I.45}$$

where

$$E^L_{\text{eff}} = (E_1)^L_{\text{eff}} + (E_2)^L_{\text{eff}} \tag{I.46}$$

and

$$\begin{aligned} (\vec{k})^L_{\text{eff}} &= (\vec{k}_1)^L_{\text{eff}} + (\vec{k}_2)^L_{\text{eff}} \\ &= (\vec{k}_1)^L_{\text{eff}} \qquad \text{[from Eq. (I.43)]} \,. \end{aligned} \tag{I.47}$$

The total laboratory four–momentum, on the other hand, is given by

$$(k^\mu)_{\text{lab}} = [\, E_{\text{lab}} \,, \, (\vec{k})_{\text{lab}} \,] \tag{I.48}$$

where

$$\begin{aligned} E_{\text{lab}} &= E_1 + E_2 \\ (\vec{k}\,)_{\text{lab}} &= \vec{k}_1 + \vec{k}_2 \end{aligned} \tag{I.49}$$

and

$$\begin{aligned} E_1 &= \sqrt{|\vec{k}_1|^2 + m^2} \\ E_2 &= \sqrt{|\vec{k}_2|^2 + m^2}\,. \end{aligned} \tag{I.50}$$

Expressions for the x–, y– and z–components of $\vec{k}_1$ and $\vec{k}_2$ are given by Eqs. (I.10) and (I.19) – (I.21) respectively. Note that, due to the Fermi–motion of the target nucleon (before it has been struck), $\vec{k}_2 \neq 0$. Substitution of Eqs. (I.45) and (I.48) in Eq. (I.44) yields

$$(E^L_{\text{eff}})^2 - |(\vec{k})^L_{\text{eff}}|^2 = (E_{\text{lab}})^2 - |(\vec{k})_{\text{lab}}|^2\,. \tag{I.51}$$

Substitution of Eqs. (I.46), (I.47), (I.49) and (I.50) into Eq. (I.51), and making use of the following relations

$$\begin{aligned} \{(E_1)^L_{\text{eff}}\}^2 &= |(\vec{k}_1)^L_{\text{eff}}|^2 + m^2 \\ (E_1)^L_{\text{eff}} &= T^L_{\text{eff}} + m^2 \\ (E_2)^L_{\text{eff}} &= (T_2)^L_{\text{eff}} + m^2 = m^2 \quad \text{[from Eq. (I.43)]} \end{aligned} \tag{I.52}$$

and

$$\begin{aligned} (E_1)^2 - |\vec{k}_1|^2 &= m^2 \\ (E_2)^2 - |\vec{k}_2|^2 &= m^2 \end{aligned} \tag{I.53}$$

yields an expression for T^L_{eff} in terms of the conventional laboratory quantities, namely

$$T^L_{\text{eff}} = \frac{E_1 E_2 - \vec{k}_1 \cdot \vec{k}_2 - m^2}{m}\,. \tag{I.54}$$

I.9 Nonrelativistic energy–momentum transfer relation

The aim of this section is to derive a nonrelativistic expression which relates energy– and momentum–transfer.

Consider a projectile nucleon scattering from a single target nucleon with momentum $\vec{k}_2$. Using the nonrelativistic relation between kinetic energy and three–momentum, namely

$$T = \frac{|\vec{k}|^2}{2m} \tag{I.55}$$

[*Note: this relationship follows directly from Eq. (I.5) for* $|\frac{\vec{k}}{m}| \ll 1$], and making use of the definition of the three–momentum transfer in Eq. (I.14), one can write down an expression for the nonrelativistic analogue of energy transfer ω, defined by Eq. (3.64) in Chapter 3, in terms of the three–momentum transfer $\vec{q}$

$$\begin{aligned} \omega &= \frac{|\vec{k}_2'|^2}{2m} - \frac{|\vec{k}_2|^2}{2m} \\ &= \frac{|\vec{k}_2 + \vec{q}\,|^2}{2m} - \frac{|\vec{k}_2|^2}{2m} \\ &= \frac{|\vec{q}|^2}{2m} + \frac{\vec{k}_2 \cdot \vec{q}}{2m}\,. \end{aligned} \tag{I.56}$$

The first term gives energy–transfer at the centroid of the quasielastic peak, which corresponds to free NN scattering from a stationary target nucleon (i.e. $|\vec{k}_2| = 0$). The second term indicates how the width of the quasielastic peak is related to the target–nucleon momentum $\vec{k}_2$ of the struck nucleon [Fe71, Ne88].

I.10 Momentum of incident nucleon in effective NN cm system

The aim of this section is to derive an expression for the momentum of the incident nucleon in the effective NN centre–of–mass system in terms of the effective laboratory kinetic energy $T_{\rm eff}^L$ given by Eq. (I.54). The effective NN centre–of–mass frame, for the elastic scattering of free equal–mass nucleons, is defined as that system whereby

$$\begin{aligned} (E_1)_{\rm eff}^{cm} &= (E_1')_{\rm eff}^{cm} = (E_2)_{\rm eff}^{cm} = (E_2')_{\rm eff}^{cm} \\ (\vec{k}_1)_{\rm eff}^{cm} + (\vec{k}_2)_{\rm eff}^{cm} &= 0 \\ |(\vec{k}_1)_{\rm eff}^{cm}| &= |(\vec{k}_1')_{\rm eff}^{cm}| = |(\vec{k}_2)_{\rm eff}^{cm}| = |(\vec{k}_2')_{\rm eff}^{cm}| = |(\vec{k})_{\rm eff}^{cm}| \quad \text{(say)} \end{aligned} \tag{I.57}$$

where the indices "*cm*" and "eff " are used to denote effective NN centre–of–mass frame. For the derivation of interest, one makes use of the fact that the square of the total four–momentum (often denoted by the Mandelstam variable s) is an invariant quantity [Si90], that is

$$(k_\mu)_{\rm eff}^L \, (k^\mu)_{\rm eff}^L = (k_\mu)_{\rm eff}^{cm} \, (k^\mu)_{\rm eff}^{cm} \tag{I.58}$$

where the indices "L" and "eff " denote the effective laboratory frame [defined by Eq. (I.43)]. The total effective laboratory four–momentum is defined by Eqs. (I.45) – (I.47), and the total four–momentum in the effective NN centre–of–mass system is defined by

$$(k^{\mu})^{cm}_{\rm eff} \;=\; [\, E^{cm}_{\rm eff} \;,\; (\vec{k})^{cm}_{\rm eff} \,] \tag{I.59}$$

where

$$\begin{aligned} E^{cm}_{\rm eff} &= (E_1)^{cm}_{\rm eff} \;+\; (E_2)^{cm}_{\rm eff} \\ (\vec{k}\,)^{cm}_{\rm eff} &= (\vec{k}_1)^{cm}_{\rm eff} \;+\; (\vec{k}_2)^{cm}_{\rm eff} \;. \end{aligned} \tag{I.60}$$

Substitution of Eqs. (I.45) and (I.59) into Eq. (I.58) yields

$$(E^{L}_{\rm eff})^2 \;-\; |(\vec{k})^{L}_{\rm eff}|^2 \;=\; (E^{cm}_{\rm eff})^2 \;-\; |(\vec{k})^{cm}_{\rm eff}|^2 \;. \tag{I.61}$$

From the definitions of the two reference frames expressed by Eqs. (I.57) and (I.43), and making use of the following relations in Eq. (I.61)

$$\begin{aligned} [(E_1)^{L}_{\rm eff}]^2 - |(\vec{k}_1)^{L}_{\rm eff}| &= m^2 \\ (E_1)^{L}_{\rm eff} &= (T)^{L}_{\rm eff} + m \\ (E_2)^{L}_{\rm eff} &= m \qquad \text{[from Eq. (I.43)]} \\ \{(E_1)^{cm}_{\rm eff}\}^2 &= |(\vec{k}_1)^{cm}_{\rm eff}| + m^2 \end{aligned} \tag{I.62}$$

yields the desired expression, namely

$$|(\vec{k})^{cm}_{\rm eff}|^2 \;=\; \frac{(T)^{L}_{\rm eff}\; m}{4} \;. \tag{I.63}$$

I.11 Effective NN centre–of–mass scattering angle

The aim of this section is to derive an expression for the effective NN centre–of–mass scattering angle, where the effective NN centre–of–mass frame is defined by Eq. (I.57). For the derivation of the effective centre–of–mass scattering angle $\theta^{cm}_{\rm eff}$, one makes use of the fact that the direct four–momentum transfer (often called the Mandelstam variable t) is an invariant quantity [Si90]), that is

$$[(k_1 - k_1')^{cm}_{\rm eff}]_{\mu}\; [(k_1 - k_1')^{cm}_{\rm eff}]^{\mu} \;=\; [(k_1 - k_1')_{\rm lab}]_{\mu}\; [(k_1 - k_1')_{\rm lab}]^{\mu} \tag{I.64}$$

where the indices "cm" and "eff " denote the effective NN centre–of–mass frame, and the subscript "lab" refers to the conventional laboratory frame. With the effective centre–of–mass four–momentum transfer given by

$$[(k_1 - k_1')^{cm}_{\text{eff}}]^{\mu} \;=\; [\,(E_1)^{cm}_{\text{eff}} - (E_1')^{cm}_{\text{eff}}\;,\; (\vec{k}_1)^{cm}_{\text{eff}} - (\vec{k}_1')^{cm}_{\text{eff}}\,] \tag{I.65}$$

and the laboratory four–momentum transfer

$$[\,(k_1 - k_1')_{\text{lab}}\,]^{\mu} \;=\; [\,E_1^* - E_1'^*\;,\; \vec{k}_1 - \vec{k}_1'\,]\,, \tag{I.66}$$

Eq. (I.64) can be written as

$$[(E_1)^{cm}_{\text{eff}} - (E_1')^{cm}_{\text{eff}}]^2 \;-\; [(\vec{k}_1)^{cm}_{\text{eff}} - (\vec{k}_1')^{cm}_{\text{eff}}]^2 \;=\; [E_1 - E_1']^2 \;-\; [\vec{k}_1 - \vec{k}_1']^2\,. \tag{I.67}$$

Making use of Eqs. (3.64) [from Chapter 3], (I.14) and (I.18) in Eq. (I.64), gives

$$(q_\mu)^2 \;=\; -4|(\vec{k}\,)^{cm}_{\text{eff}}|^2 \sin^2(\frac{\theta^{cm}_{\text{eff}}}{2}) \tag{I.68}$$

where θ^{cm}_{eff} is the angle between $(\vec{k}_1)^{cm}_{\text{eff}}$ and $(\vec{k}_1')^{cm}_{\text{eff}}$. Substitution of Eqs. (I.63) in Eq. (I.68) yields the desired expression for the effective NN centre–of–mass scattering angle θ^{cm}_{eff}:

$$\theta^{cm}_{\text{eff}} \;=\; 2\sin^{-1}\{\frac{|\vec{q}\,|^2 - \omega^2}{2mT^L_{\text{eff}}}\}\,. \tag{I.69}$$

Appendix J

Evaluation of the integral in Eq. (3.78)

The aim of this appendix is to evaluate the integral

$$I = \int_{k_{\min}}^{k_{\max}} d\vec{k}_2 \, \frac{\delta\left(E_1^* + E_2^* - E'^*_2 - E'^*_1\right)}{E'^*_2} \tag{J.1}$$

in Eq. (3.78) [Sec. 3.2.7 of Chapter 3].

In the initial laboratory frame [defined by Eq. (I.8) in Appendix I], the volume element $d\vec{k}_2$ is defined by

$$d\vec{k}_2 = d(k_2)_x \, d(k_2)_y \, d(k_2)_z \tag{J.2}$$

where the x, y, and z–components of $\vec{k}_2$ are given by Eqs. (I.19) – (I.21) in Appendix I. To evaluate the integral in Eq. (J.1), it is more convenient to express Eq. (J.2) in terms of the scattering angles χ and ϕ defined in Appendix I. This is achieved via the following transformation [Sp74, Sa90]:

$$\begin{aligned} d\vec{k}_2 &= d(k_2)_x \, d(k_2)_y \, d(k_2)_z \\ &= \left\{ \frac{\partial[(k_2)_x, (k_2)_y, (k_2)_z]}{\partial[|\vec{k}_2|, \chi, \phi]} \right\} d|\vec{k}_2| \, d\chi \, d\phi \end{aligned} \tag{J.3}$$

where the quantity in curly brackets is the Jacobian defined by

$$\frac{\partial[(k_2)_x, (k_2)_y, (k_2)_z]}{\partial[|\vec{k}_2|, \chi, \phi]} = \begin{vmatrix} \frac{\partial(k_2)_x}{\partial|\vec{k}_2|} & \frac{\partial(k_2)_x}{\partial\chi} & \frac{\partial(k_2)_x}{\partial\phi} \\ \frac{\partial(k_2)_y}{\partial|\vec{k}_2|} & \frac{\partial(k_2)_y}{\partial\chi} & \frac{\partial(k_2)_y}{\partial\phi} \\ \frac{\partial(k_2)_z}{\partial|\vec{k}_2|} & \frac{\partial(k_2)_z}{\partial\chi} & \frac{\partial(k_2)_z}{\partial\phi} \end{vmatrix} . \tag{J.4}$$

With Eqs. (I.19) – (I.21) for the x–, y– and z–components of $\vec{k}_2$, one gets the following expression for the Jacobian:

$$\frac{\partial[(k_2)_x,(k_2)_y,(k_2)_z]}{\partial[|\vec{k}_2|,\chi,\phi]} = |\vec{k}_2|^2 \sin\chi \,. \tag{J.5}$$

Substitution of Eq. (J.5) in Eq. (J.3) in Appendix I, yields

$$\begin{aligned} d\vec{k}_2 &= |\vec{k}_2|^2 \sin\chi \, d|\vec{k}_2| \, d\chi \, d\phi \\ &= |\vec{k}_2|^2 \, d|\vec{k}_2| \, d(\cos\chi) \, d\phi \,. \end{aligned} \tag{J.6}$$

Next, one writes down an expression for the effective energy of the recoil nucleon E'^*_2 in Eq. (J.1) in terms of the angle χ. From Eqs. (3.63) and (3.65) in Chapter 3, it follows that

$$\begin{aligned} E'^*_2 &= \sqrt{|\vec{k}'_2|^2 + m^{*2}_2} \\ &= \sqrt{(\vec{q}+\vec{k}_2)^2 + m^{*2}_2} \\ &= \sqrt{(E^*_2)^2 + |\vec{q}\,|^2 + 2|\vec{k}_2| \, |\vec{q}\,| \cos\chi} \end{aligned} \tag{J.7}$$

where χ is the angle between $\vec{q}$ and $\vec{k}_2$. Introducing the variable t defined by

$$t = \cos\chi \tag{J.8}$$

and, using Eqs. (J.6) and (J.7), one can rewrite Eq. (J.1) as

$$I = \int_{k_{\min}}^{k_{\max}} d|\vec{k}_2| \, |\vec{k}_2|^2 \, dt \, d\phi \, h_1(t) \, \delta[h_2(t)] \tag{J.9}$$

where

$$h_1(t) = (a_1 + a_2 t)^{-\frac{1}{2}} \tag{J.10}$$

$$h_2(t) = a_3 - (a_1 + a_2 t)^{\frac{1}{2}} \tag{J.11}$$

and

$$\begin{aligned} a_1 &= E^*_2 + |\vec{q}\,|^2 \\ a_2 &= 2|\vec{k}_2| \, |\vec{q}\,| \\ a_3 &= \omega + E^*_2 \,. \end{aligned} \tag{J.12}$$

Making use of the identity [Gr92]

$$\delta[f(x)] = \sum_k \frac{\delta(x - x_k)}{|\frac{df}{dx}|_{x_k}} \tag{J.13}$$

with x_k being the roots of $f(x)$ contained in the interval of integration, the integral in Eq. (J.1) yields

$$\begin{aligned} I &= \int_{k_{\min}}^{k\max} d\,|\vec{k}_2|\;|\vec{k}_2|^2\,dt\,d\phi\,h_1(t)\,\frac{\delta(t-t_0)}{|h_2'(t)|} \\ &= \int_{k_{\min}}^{k\max} d\,|\vec{k}_2|\,d\phi\,|\vec{k}_2|^2\,\frac{h_2'(t_0)}{|h_2'(t)|}\,. \end{aligned} \tag{J.14}$$

With the root of Eq. (J.11) given by

$$t_0 = \frac{(a_3)^2 - a_1}{a_2} \tag{J.15}$$

and, making use of Eqs. (J.10) and (J.11), one gets

$$\begin{aligned} h_1(t_0) &= \frac{1}{a_3} \\ |h_2'(t_0)| &= |-\frac{a_2}{2a_3}| = \frac{a_2}{2a_3}\,. \end{aligned} \tag{J.16}$$

Substitution of Eq. (J.10) into (J.14), and making use of Eq. (J.12) yields the desired expression, namely

$$I = \int_{k_{\min}}^{k\max} d\,|\vec{k}_2| \int_0^{2\pi} d\phi\,\frac{|\vec{k}_2|}{|\vec{q}\,|}\Bigg|_{\chi=\chi_0} \tag{J.17}$$

where, from Eqs. (J.15) and (J.12),

$$\cos\chi = t_0 = \frac{(q_\mu)^2 + 2\omega E_2^*}{2|\vec{k}_2|\;|\vec{q}\,|}\,. \tag{J.18}$$

Appendix K

Spins sums of invariant matrix elements

The aim of this section is to write down the explicit expressions for the spin sums in Eqs. (3.82), (3.86) and (3.83) in Sec. 3.2.7 of Chapter 3.

Analogous to the discussion in Sec. E.4 of Appendix E, the spin summations in Eqs. (3.82), (3.86) and (3.83) are readily evaluated using the identities

$$\sum_s U\left(m^*, \vec{k}, s\right) \bar{U}_2\left(m^*, \vec{k}_2, s\right) = \frac{\not{k} + m^*}{2m^*} \tag{K.1}$$

and

$$U\left(m^*, \vec{k}, s\right) \bar{U}\left(m^*, \vec{k}, s\right) = \frac{\not{k} + m^*}{2m^*} \left[\frac{1 + \gamma_5 \not{s}}{2}\right] \tag{K.2}$$

where the medium–modified Dirac spinors $U(m^*, \vec{k}, s)$ are defined by Eqs. (3.55) and (3.56) in Chapter 3, thus yielding

$$\sum_{s_1, s_1', s_2, s_2'} \mathcal{M}^* \mathcal{M} = \sum_{i,j=S}^{T} \mathrm{Tr}_1 \left\{\frac{\not{k}_1' + m_1^*}{2m_1^*} \lambda_j \frac{\not{k}_1 + m_1^*}{2m_1^*} \lambda_i\right\} \times$$

$$\mathrm{Tr}_2 \left\{\frac{\not{k}_2' + m_2^*}{2m_2^*} \lambda^j \frac{\not{k}_2 + m_2^*}{2m_2^*} \lambda^i\right\} t_i^* t_j \,, \tag{K.3}$$

$$\sum_{s_1', s_2, s_2'} \mathcal{M}^* \mathcal{M} = \sum_{i,j=S}^{T} \mathrm{Tr}_1 \left\{\frac{\not{k}_1' + m_1^*}{2m_1^*} \lambda_j \frac{\not{k}_1 + m_1^*}{2m_1^*} \left[\frac{1 + \gamma_5 \not{s}_i}{2}\right] \lambda_i\right\} \times$$

$$\mathrm{Tr}_2 \left\{\frac{\not{k}_2' + m_2^*}{2m_2^*} \lambda^j \frac{\not{k}_2 + m_2^*}{2m_2^*} \lambda^i\right\} t_i^* t_j \tag{K.4}$$

and

$$\sum_{s_2, s_2'} \mathcal{M}^* \mathcal{M} = \sum_{i,j=S}^{T} \mathrm{Tr}_1 \left\{\frac{\not{k}_1' + m_1^*}{2m_1^*} \left[\frac{1 + \gamma_5 \not{s}_f}{2}\right] \lambda_j \frac{\not{k}_1 + m_1^*}{2m_1^*} \left[\frac{1 + \gamma_5 \not{s}_i}{2}\right] \lambda_i\right\} \times$$

$$\mathrm{Tr}_2 \left\{\frac{\not{k}_2' + m_2^*}{2m_2^*} \lambda^j \frac{\not{k}_2 + m_2^*}{2m_2^*} \lambda^i\right\} t_i^* t_j \,, \tag{K.5}$$

where $s_i = s_1$ and $s_f = s_1'$ are the spin four–vectors of the projectile and ejectile respectively. Evaluating the traces in the above equations with a computer algebra program ("Mathematica") yields the following explicit expressions for the spin summations in Eqs. (K.3) and (K.4) (our results confirm the expressions of Horowitz and Murdock in Ref. [Ho88]: note that the corresponding expressions in Murdock's thesis [Mu87a] are not entirely correct):

$$\begin{aligned}\sum_{s_2, s_2', s_1, s_1'} \mathcal{M}^* \mathcal{M} \;=\; & t_S^* t_S (1 + K_1 \cdot P_1)(1 + K_2 \cdot P_2) + t_P^* t_P (1 - K_1 \cdot P_1)(1 - K_2 \cdot P_2) \\ & + 2 t_V^* t_V [2 - K_1 \cdot P_1 - K_2 \cdot P_2 + K_1 \cdot K_2 P_1 \cdot P_2 + K_1 \cdot P_2 K_2 \cdot P_1] \\ & + 2 t_A^* t_A [2 + K_1 \cdot P_1 + K_2 \cdot P_2 + K_1 \cdot K_2 P_1 \cdot P_2 + K_1 \cdot P_2 K_2 \cdot P_1] \\ & + 8 t_T^* t_T [3 - K_1 \cdot P_1 K_2 \cdot P_2 + 2 K_1 \cdot K_2 P_1 \cdot P_2 + K_1 \cdot P_2 K_2 \cdot P_1] \\ & + 2 \,\mathrm{Re}\,(t_V^* t_S - 6 t_T^* t_A)[K_1 \cdot K_2 + K_1 \cdot P_2 + K_2 \cdot P_1 + P_1 \cdot P_2] \\ & - 2 \,\mathrm{Re}\,(t_A^* t_P - 6 t_T^* t_V)[K_2 \cdot P_1 + K_1 \cdot P_2 - K_1 \cdot K_2 - P_1 \cdot P_2] \\ & + 4 \,\mathrm{Re}\,(t_A^* t_V - t_T^* t_S - t_T^* t_P)[K_1 \cdot K_2 P_1 \cdot P_2 - K_2 \cdot P_1 K_1 \cdot P_2] \end{aligned} \tag{K.6}$$

and

$$\begin{aligned}\sum_{s_1, s_2, s_2'} \mathcal{M}^* \mathcal{M} \;=\; & \mathrm{Im}\left[t_S^* t_V + 2 t_T^* t_A - \frac{m_1^*}{m_2^*}(t_A^* t_V + 2 t_T^* t_S)\right] \\ & \times \left\{(E_2^* + E_2'^*)\,\vec{k}_1 \times \vec{k}_1' + E_1^*\,\vec{k}_1' \times (\vec{k}_2 + \vec{k}_2') - E_1'^*\,\vec{k}_1 \times (\vec{k}_2 + \vec{k}_2')\right\} \cdot \frac{\hat{s}_f}{m_1^{*2}\, m_2^*}\end{aligned} \tag{K.7}$$

where

$$\begin{aligned} P_1 &= \frac{(k_1)^\mu}{m_1^*} = \frac{1}{m_1^*}[\,E_1^*, \vec{k}_1\,] \\ P_2 &= \frac{(k_2)^\mu}{m_2^*} = \frac{1}{m_2^*}[\,E_2^*, \vec{k}_2\,] \\ K_1 &= \frac{(k_1')^\mu}{m_1^*} = \frac{1}{m_1^*}[\,E_1', \vec{k}_1'\,] \\ K_2 &= \frac{(k_2')^\mu}{m_2^*} = \frac{1}{m_2^*}[\,E_2'^*, \vec{k}_2'\,] \end{aligned} \tag{K.8}$$

and all the kinematic quantities are defined in Appendix I. The quantity $\hat{s}_f$ represents the three–spin orientation of the ejectile in the rest frame of the nucleon. Note that the spin sum in

Eq. (K.7) [Sec. 3.2.7 of Chapter 3)], used for A_y in Eq. (3.86), is dominated by the interference of the vector and scalar amplitudes. Using "Mathematica" to evaluate the traces in Eq. (K.5), yields an expression with the following structure for spin transfer $\hat{j}$ to $\hat{i}'$, namely

$$\begin{aligned}\sum_{s_2,s_2'} \mathcal{M}^*\,\mathcal{M}(\hat{j}\longrightarrow\hat{i}') &= \Omega(\vec{k}_1,\vec{k}_1',\vec{k}_2,\vec{k}_2',s_j,s_i')\\ &= \Omega_1(X)+\Omega_2(X\,,\,Y\cdot s_j)+\Omega_3(X\,,\,Y\cdot s_i')\\ &\quad +\Omega_4(X\,,\,Y\cdot s_j\,,\,S\cdot s_i')+\Omega_5(X)(s_j\cdot s_i')\end{aligned} \tag{K.9}$$

where X represents the contraction of any two scattering momenta, Y represents any single scattering momentum, and the initial and final four–vector spins are given by $s_j = s_1$ and $s_i' = s_1'$ respectively. From Eq. (K.9), one sees that the Ω functions exhibit the following behaviour for the various spin transfers in Eq. (3.89)

$$\begin{aligned}\Omega_1(-\hat{j}\longrightarrow\hat{i}') &= \Omega_1(\hat{j}\longrightarrow\hat{i}')\\ \Omega_1(\hat{j}\longrightarrow-\hat{i}') &= \Omega_1(\hat{j}\longrightarrow\hat{i}')\\ \Omega_1(-\hat{j}\longrightarrow-\hat{i}') &= \Omega_1(\hat{j}\longrightarrow\hat{i}')\\ \Omega_2(-\hat{j}\longrightarrow\hat{i}') &= -\Omega_2(\hat{j}\longrightarrow\hat{i}')\\ \Omega_2(\hat{j}\longrightarrow-\hat{i}') &= \Omega_2(\hat{j}\longrightarrow\hat{i}')\\ \Omega_2(-\hat{j}\longrightarrow-\hat{i}') &= -\Omega_2(\hat{j}\longrightarrow\hat{i}')\\ \Omega_3(-\hat{j}\longrightarrow\hat{i}') &= \Omega_3(\hat{j}\longrightarrow\hat{i}')\\ \Omega_3(\hat{j}\longrightarrow-\hat{i}') &= -\Omega_3(\hat{j}\longrightarrow\hat{i}')\\ \Omega_3(-\hat{j}\longrightarrow-\hat{i}') &= -\Omega_3(\hat{j}\longrightarrow\hat{i}')\\ \Omega_4(-\hat{j}\longrightarrow\hat{i}') &= -\Omega_4(\hat{j}\longrightarrow\hat{i}')\\ \Omega_4(\hat{j}\longrightarrow-\hat{i}') &= -\Omega_4(\hat{j}\longrightarrow\hat{i}')\\ \Omega_4(-\hat{j}\longrightarrow-\hat{i}') &= \Omega_4(\hat{j}\longrightarrow\hat{i}')\\ \Omega_5(-\hat{j}\longrightarrow\hat{i}') &= -\Omega_5(\hat{j}\longrightarrow\hat{i}')\\ \Omega_5(\hat{j}\longrightarrow-\hat{i}') &= -\Omega_5(\hat{j}\longrightarrow\hat{i}')\\ \Omega_5(-\hat{j}\longrightarrow-\hat{i}') &= \Omega_5(\hat{j}\longrightarrow\hat{i}')\end{aligned} \tag{K.10}$$

where $\hat{j}$ and $\hat{i}'$ refer to the projectile and ejectile spin orientations in the rest frames of the respective nucleons. Substitution of Eq. (K.9) into Eq. (3.89), and making use of the properties

of the Ω_i's in Eq. (K.10), reveals that only the Ω_4 and Ω_5 functions contribute to the polarization transfer observables in Eq. (3.88), and the Ω_1, Ω_2 and Ω_3 terms all cancel out. Hence, for the purpose of calculating polarization transfer observables defined by Eqs. (3.87) – (3.89), Eq. (K.9) can be written as

$$\sum_{s_2, s_2'} \mathcal{M}^* \mathcal{M}(\hat{j} \longrightarrow \hat{i}') \;=\; \Omega_4(X\,,\, S\cdot s_j\,,\, S\cdot s_i') + \Omega_5(X)(s_j\cdot s_i') \tag{K.11}$$

where the explicit expressions for Ω_4 and Ω_5 are given by (after doing trace algebra in Eq. (K.5) and omitting the Ω_1, Ω_2 and Ω_3 terms defined in Eq. (K.9) [Ho88]

$$\begin{aligned}
4\Omega_4 \;=\;& t_S^* t_S(1+K_2\cdot P_2)s_i\cdot K_1 s_f\cdot P_1 + t_P^* t_P(1-K_2\cdot P_2)s_i\cdot K_1 s_f\cdot P_1 \\
&+ 2t_V^* t_V[s_i\cdot K_1 s_f\cdot K_2 P_1\cdot P_2 + s_f\cdot P_1 s_i\cdot K_2 K_1\cdot P_2 - s_f\cdot P_1 s_i\cdot K_1 K_2\cdot P_2 \\
&+(1-K_1\cdot P_1)(s_f\cdot K_2 s_i\cdot P_2 + s_i\cdot K_2 s_f\cdot P_2) + s_f\cdot P_2 s_i\cdot K_1 K_2\cdot P_1 + s_i\cdot P_2 s_f\cdot P_1 K_1\cdot K_2] \\
&+ 2t_A^* t_A[s_i\cdot K_1 s_f\cdot P_1 K_2\cdot P_2 - s_i\cdot K_1 s_f\cdot K_2 P_1\cdot P_2 - s_i\cdot K_1 s_f\cdot P_2 K_2\cdot P_1 \\
&+ (1+K_1\cdot P_1)(s_i\cdot K_2 s_f\cdot P_2 + s_f\cdot K_2 s_i\cdot P_2) - s_f\cdot P_1 s_i\cdot P_2 K_1\cdot K_1 - s_i\cdot K_2 s_f\cdot P_1 K_1\cdot P_2] \\
&- 8t_T^* t_T[s_i K_1 s_f\cdot P_1 + 2(s_i\cdot K_2 s_f\cdot P_2 + s_i\cdot P_2 s_f\cdot K_2)] \\
&+ 2\,\mathrm{Re}(t_V^* t_S + 2t_T^* t_A)[s_i\cdot K_1 s_f\cdot K_2 + s_f\cdot P_1 s_i\cdot K_2 + s_f\cdot P_2 s_i\cdot K_1 + s_i\cdot P_2 s_f\cdot P_1] \\
&+ 2\,\mathrm{Re}(t_A^* t_P + 2t_T^* t_V)[s_i\cdot K_1 s_f\cdot P_2 + s_f\cdot P_1 s_i\cdot K_2 - s_f\cdot K_2 s_i\cdot K_1 - s_i\cdot P_2 s_f\cdot P_1] \\
&+ 4\,\mathrm{Re}(t_A^* t_V)[s_i\cdot P_2 s_f\cdot K_2 - s_i\cdot K_2 s_f\cdot P_2] \\
&+4,\mathrm{Re}(t_T^* t_S)[(1+K_1\cdot P_1)(s_f\cdot K_2 s_i\cdot P_2 - s_i\cdot K_2 s_f\cdot P_2) \\
&- K_1\cdot K_2 s_f\cdot P_1 s_i\cdot P_2 + K_1\cdot P_2 s_i\cdot K_2 s_f\cdot P_1 + K_2\cdot P_1 s_i\cdot K_1 s_f\cdot P_2 - P_1\cdot P_2 s_i\cdot K_1 s_f\cdot K_2] \\
&+ 4\,\mathrm{Re}(t_T^* t_P)[(1-K_1\cdot P_1)(s_f\cdot K_2 s_i\cdot P_2 - s_f\cdot P_2 s_i\cdot K_2) + K_1\cdot K_2 s_f\cdot P_1 s_i\cdot P_2 \\
&- K_1\cdot P_2 s_i\cdot K_2 s_f\cdot P_1 - K_2\cdot P_1 s_i\cdot K_1 s_f\cdot P_2 - P_1\cdot P_2 s_i\cdot K_1 s_f\cdot K_2]
\end{aligned} \tag{K.12}$$

and

$$\begin{aligned}
4\Omega_4 \;=\;& -s_i\cdot s_f[t_S^* t_S(1+K_1\cdot P_1)(1+K_2\cdot P_2) - t_P^* t_P(1-K_1\cdot P_1)(1-K_2\cdot P_2) \\
&+ 2(t_V^* t_V - t_A^* t_A)(1+K_1\cdot K_2 P_1\cdot P_2 - K_1\cdot P_1 K_2\cdot P_2 + K_1\cdot P_2\cdot K_2\cdot P_1) \\
&- 8t_T^* t_T(K_1\cdot P_1 + K_2\cdot P_2) \\
&+ 2\,\mathrm{Re}(t_V^* t_S + 2t_T^* t_A)(K_1\cdot K_2 + K_1\cdot P_2 + K_2\cdot P_1 + P_1\cdot P_2) \\
&+ 4\,\mathrm{Re}(t_T^* t_P - t_S^* t_S)(K_1\cdot K_2 P_1\cdot P_2 - K_1\cdot P_2 K_2\cdot P_1) \\
&+ 2\,\mathrm{Re}(t_A^* t_P + 2t_T^* t_V)(K_1\cdot P_2 + K_2\cdot P_1 - K_1\cdot K_2 - P_1\cdot P_2)]\,.
\end{aligned} \tag{K.13}$$

In doing the trace algebra that lead to the above equations, one also made use of the fact that [see Sec. E.5.2 in Appendix E]

$$\begin{aligned} s_i \cdot P_1 &= \frac{1}{m_1^*}(s_1)^\mu\,(k_1)_\mu = 0 \\ s_f \cdot K_1 &= \frac{1}{m_1^*}(s_1')^\mu\,(k_1')_\mu = 0\,. \end{aligned} \tag{K.14}$$

Due to the properties of the Ω–functions, one can write down the following relations:

$$\begin{aligned} \sum_{s_2,s_2'} \mathcal{M}^*\,\mathcal{M}\,(\hat{s}_1=\hat{j},\,\hat{s}_1'=\hat{i}') &= -\sum_{s_2,s_2'} \mathcal{M}^*\,\mathcal{M}\,(\hat{s}_1=\hat{j},\,\hat{s}_1'=-\hat{i}') \\ &= -\sum_{s_2,s_2'} \mathcal{M}^*\,\mathcal{M}\,(\hat{s}_1=-\hat{j},\,\hat{s}_1'=\hat{i}') \\ &= \sum_{s_2,s_2'} \mathcal{M}^*\,\mathcal{M}\,(\hat{s}_1=-\hat{j},\,\hat{s}_1'=-\hat{i}') \end{aligned} \tag{K.15}$$

and, hence

$$\begin{aligned} M_{i'j} &= 4\sum_{s_2,s_2'} \mathcal{M}^*\,\mathcal{M}\,(\hat{s}_1=\hat{j},\,\hat{s}_1'=\hat{i}') \\ &= 4\,(\,\Omega_4 + \Omega_5\,)\,. \end{aligned} \tag{K.16}$$

The latter implies that the polarization transfer observable defined by Eqs. (3.87) and (3.88), can now be written in a simplified form as

$$D_{i'j}(pp) = \frac{\frac{d\sigma}{d\Omega_1'\,dE_1'}\,(pp,\hat{j}\to\hat{i}')}{\frac{d\bar{\sigma}}{d\Omega_1'\,dE_1'}\,|_{\rm unpol}}\,, \tag{K.17}$$

where this expression is only valid when the spin sum is given by Eq. (K.11), that is the functions Ω_1, Ω_2 and Ω_3 are canceled by virtue of the original definition [given by Eq. (3.87)] of the polarization transfer observables.

The question of how one distinguishes amongst the five polarization transfer observables allowed by parity and time–reversal invariance, namely $\mathrm{D}_{n0} = \mathrm{D}_{0n} = \mathrm{A}_y$, $\mathrm{D}_{nn}, \mathrm{D}_{s's}, \mathrm{D}_{\ell'\ell}, \mathrm{D}_{s'l}$ and $\mathrm{D}_{l's}$ (see Appendix G: the primed and unprimed subscripts refer to outgoing and incoming spin directions defined in Fig. 3.5 of Chapter 3) is discussed.

From Sec. E.5.2 in Appendix E one can write down the following expressions for the initial and final spin four–vectors s_i and s_f, namely [Gr92]

$$s_i = (s_i)^\mu = (s_1)^\mu = [\frac{\vec{k}_1 \cdot \hat{t}}{m_1^*} , \hat{t} + \frac{\hat{t} \cdot \vec{k}_1}{m_1^*(E_1^* + m_1^*)} \vec{k}_1] ,$$
$$s_f = (s_f)^\mu = (s_1')^\mu = [\frac{\vec{k}_1' \cdot \hat{t}'}{m_1^*} , \hat{t}' + \frac{\hat{t}' \cdot \vec{k}_1'}{m_1^*(E_1'^* + m_1^*)} \vec{k}_1'] , \tag{K.18}$$

where $\hat{t}$ and $\hat{t}'$ are the initial and final spin orientations in the rest frames of the projectile and ejectile nucleons respectively. From Eqs. (K.12) and (K.13) one sees that the spin–dependence of the polarization transfer observables is contained in the following terms:

$$s_i \cdot s_f = \frac{\vec{k}_1 \cdot \hat{t}\, \vec{k}_1' \cdot \hat{t}'}{(m_1^*)^2} - [\hat{t} \cdot \hat{t}' + \frac{\vec{k}_1 \cdot \hat{t}\, \vec{k}_1 \cdot \hat{t}'}{m_1^*(E_1^* + m_1^*)} + \frac{\vec{k}_1' \cdot \hat{t}\, \vec{k}_1' \cdot \hat{t}'}{m_1^*(E_1'^* + m_1^*)} + \frac{\vec{k}_1 \cdot \hat{t}\, \vec{k}_1' \cdot \hat{t}' \vec{k}_1 \cdot \vec{k}_1'}{(m_1^*)^2(E_1^* + m_1^*)(E_1'^* + m_1^*)}] \tag{K.19}$$

and

$$s_i \cdot K_1 = \frac{1}{m_1^*}[(\frac{\vec{k}_1 \cdot \hat{t}}{m_1^*})E_1'^* - \hat{t} \cdot \vec{k}_1' - \frac{\vec{k}_1 \cdot \hat{t}\vec{k}_1 \cdot \vec{k}_1'}{m_1^*(E_1^* + m_1^*)}] \tag{K.20}$$

$$s_i \cdot K_2 = \frac{1}{m_2^*}[(\frac{\vec{k}_1 \cdot \hat{t}}{m_1^*})E_2'^* - \hat{t} \cdot \vec{k}_2' - \frac{\vec{k}_1 \cdot \hat{t}\vec{k}_1 \cdot \vec{k}_2'}{m_1^*(E_1^* + m_1^*)}] \tag{K.21}$$

$$s_i \cdot P_2 = \frac{1}{m_2^*}[(\frac{\vec{k}_1 \cdot \hat{t}}{m_1^*})E_2^* - \hat{t} \cdot \vec{k}_2 - \frac{\vec{k}_1 \cdot \hat{t}\vec{k}_1 \cdot \vec{k}_2}{m_1^*(E_1^* + m_1^*)}] \tag{K.22}$$

$$s_f \cdot K_2 = \frac{1}{m_2^*}[(\frac{\vec{k}_1' \cdot \hat{t}'}{m_1^*})E_2'^* - \hat{t}' \cdot \vec{k}_2' - \frac{\vec{k}_1' \cdot \hat{t}'\vec{k}_1' \cdot \vec{k}_2'}{m_1^*(E_1'^* + m_1^*)}] \tag{K.23}$$

$$s_f \cdot P_1 = \frac{1}{m_1^*}[(\frac{\vec{k}_1' \cdot \hat{t}'}{m_1^*})E_1^* - \hat{t}' \cdot \vec{k}_1 - \frac{\vec{k}_1' \cdot \hat{t}'\vec{k}_1' \cdot \vec{k}_1}{m_1^*(E_1'^* + m_1^*)}] \tag{K.24}$$

$$s_f \cdot P_2 = \frac{1}{m_2^*}[(\frac{\vec{k}_1' \cdot \hat{t}'}{m_1^*})E_2^* - \hat{t}' \cdot \vec{k}_2 - \frac{\vec{k}_1' \cdot \hat{t}'\vec{k}_1' \cdot \vec{k}_2}{m_1^*(E_1'^* + m_1^*)}] \tag{K.25}$$

where one has made use of Eqs. (K.8) and (K.18) to write down general expressions for these spin–dependent quantities.

The aim of the following sections is to write down explicit expressions for the spin–dependent terms given by Eqs. (K.18) to (K.25) for each of the polarization transfer observables $D_{i'j}$. Before proceeding, one notes that the $(\hat{\ell}, \hat{s}, \hat{n})$ [Eq. (3.84) in Chapter 3)] and $(\hat{x}, \hat{y}, \hat{z})$ [Eq. (I.8) in Appendix I] reference systems are identical, and the $(\hat{\ell}', \hat{s}', \hat{n})$ [Eq. (3.85) in Chapter 3)] and $(\hat{x}', \hat{y}', \hat{z}')$ [Eq. (I.9) in Appendix I] reference frames are identical. Also recall, from Appendix E

that,

$$\begin{aligned} \vec{k}_1 &= (k_1)_x \hat{x} = |\vec{k}_1| \hat{\ell} \\ \vec{k}'_1 &= (k'_1)_x \hat{x}' = |\vec{k}'_1| \hat{\ell}' \, . \end{aligned} \tag{K.26}$$

Furthermore, the components of $\vec{k}_2$ and $\vec{k}'_2$ are always defined with respect to the initial frame $(\hat{\ell}, \hat{s}, \hat{n})$ displayed in Fig. 3.5 of Chapter 3.

K.1 Polarization transfer observable: $D_{s's}$

The polarization transfer observable $D_{s's}$ corresponds to the following choice of initial and final spin orientations in the rest frame of the nucleon in Eqs. (K.18) to (K.25):

$$\begin{aligned} \hat{t} &= \hat{s} \\ \hat{t}' &= \hat{s}' \, . \end{aligned} \tag{K.27}$$

Before, writing down explicit expressions for the spin–dependent terms in Eqs. (K.18) to (K.25), it is necessary to write derive explicit expressions for the following quantities:

$$\begin{aligned} \vec{k}_1 \cdot \hat{t} &= |\vec{k}_1| \hat{\ell} \cdot \hat{s} = 0 \\ \vec{k}_1 \cdot \hat{t}' &= |\vec{k}_1| \hat{\ell} \cdot \hat{s}' = (k_1)_x \cos(90 + \theta) = -(k_1)_x \sin(\theta_{\rm lab}) \\ \vec{k}'_1 \cdot \hat{t} &= |\vec{k}'_1| \hat{\ell}' \cdot \hat{s} = |\vec{k}'_1| \cos(90 - \theta) = |\vec{k}'_1| \sin(\theta_{\rm lab}) = (\vec{k}'_1)_y \\ \vec{k}'_1 \cdot \hat{t}' &= |\vec{k}'_1| \hat{\ell}' \cdot \hat{s}' = 0 \\ \vec{k}_2 \cdot \hat{t} &= |\vec{k}_2| \hat{k}_2 \cdot \hat{s} = (k_2)_y \\ \vec{k}_2 \cdot \hat{t}' &= |\vec{k}_2| \hat{k}_2 \cdot \hat{s}' = \vec{k}_2 \cdot [\sin(\theta_{\rm lab}) \hat{l} - \cos(\theta_{\rm lab}) \hat{s}] = (k_2)_x \sin(\theta_{\rm lab}) - (k_2)_y \cos(\theta_{\rm lab}) \\ \vec{k}'_2 \cdot \hat{t} &= |\vec{k}'_2| \hat{k}'_2 \cdot \hat{s} = (k'_2)_y \\ \vec{k}'_2 \cdot \hat{t}' &= |\vec{k}'_2| \hat{k}'_2 \cdot \hat{s}' = \vec{k}'_2 \cdot [\sin(\theta_{\rm lab}) \hat{l} - \cos(\theta_{\rm lab}) \hat{s}] = (k'_2)_x \sin(\theta_{\rm lab}) - (k'_2)_y \cos(\theta_{\rm lab}) \\ \hat{t} \cdot \hat{t}' &= \hat{s} \cdot \hat{s} = \cos(\theta_{\rm lab}) \end{aligned} \tag{K.28}$$

where expressions for the x– and y–components of $\vec{k}_1$, $\vec{k}'_1$, $\vec{k}_2$ and $\vec{k}'_2$ are given in Appendix I.

Substitution of Eq. (K.28) into Eqs. (K.18) to (K.25) yields

$$\begin{aligned}
s_i \cdot s_f &= -\cos(\theta_{\rm lab}) \\
s_i \cdot K_1 &= -\frac{1}{m_1^*}(k_1')_y \\
s_i \cdot K_2 &= -\frac{1}{m_2^*}(k_2')_y \\
s_i \cdot P_2 &= -\frac{1}{m_2^*}(k_2)_y \\
s_f \cdot K_2 &= \frac{1}{m_2^*}[(k_2')_x \sin(\theta_{\rm lab}) - (k_2')_y \cos(\theta_{\rm lab})] \\
s_f \cdot P_1 &= \frac{1}{m_1^*}(k_1)_x \sin(\theta_{\rm lab}) \\
s_f \cdot P_2 &= \frac{1}{m_2^*}[(k_2)_x \sin(\theta_{\rm lab}) - (k_2)_y \cos(\theta_{\rm lab})] \,. \qquad \text{(K.29)}
\end{aligned}$$

Finally, with Eqs. (K.12) and (K.13) in Eq. (K.11), and substitution of the latter into Eqs. (K.17) and (3.88) (see Chapter 3), the complete expression for $D_{s's}$ is obtained.

K.2 Polarization transfer observable: $D_{\ell'\ell}$

The polarization transfer observable $D_{\ell'\ell}$ corresponds to the following choice of initial and final spin orientations in the rest frame of the nucleon in Eqs. (K.18) to (K.25):

$$\begin{aligned}
\hat{t} &= \hat{\ell} \\
\hat{t}' &= \hat{\ell}' \,. \qquad \text{(K.30)}
\end{aligned}$$

Before, writing down explicit expressions for the spin–dependent terms in Eqs. (K.18) to (K.25), it is necessary to write derive explicit expressions for the following quantities:

$$\begin{aligned}
\vec{k}_1 \cdot \hat{t} &= |\vec{k}_1| \hat{\ell} \cdot \hat{\ell} = |\vec{k}_1| \\
\vec{k}_1 \cdot \hat{t}' &= |\vec{k}_1| \hat{\ell} \cdot \hat{\ell}' = |\vec{k}_1| \cos(\theta_{\rm lab}) \\
\vec{k}_1 \cdot \vec{k}_1' &= |\vec{k}_1| |\vec{k}_1'| \hat{\ell} \cdot \ell' = |\vec{k}_1| |\vec{k}_1'| \cos(\theta_{\rm lab}) \\
\vec{k}_1' \cdot \hat{t} &= |\vec{k}_1'| \hat{\ell}' \cdot \hat{\ell} = |\vec{k}_1'| \cos(\theta_{\rm lab}) \\
\vec{k}_1' \cdot \hat{t}' &= |\vec{k}_1'| \hat{\ell}' \cdot \hat{\ell}' = |\vec{k}_1'| \\
\vec{k}_1' \cdot \vec{k}_2 &= |\vec{k}_1'| |\vec{k}_2| \hat{k}_2 \cdot [\hat{\ell} \cos(\theta_{\rm lab}) + \hat{s} \sin(\theta_{\rm lab})] = [(k_1')_x (k_2)_x + (k_1')_y (k_2)_y] \\
\vec{k}_1' \cdot \vec{k}_2' &= |\vec{k}_1'| |\vec{k}_2'| \hat{k}_2' \cdot \hat{\ell}' = |\vec{k}_1'| |\vec{k}_2'| \hat{k}_2' \cdot [\hat{\ell} \cos(\theta_{\rm lab}) + \hat{s} \sin(\theta_{\rm lab})] = [(k_1')_x (k_2')_x + (k_1')_y (k_2')_y]
\end{aligned}$$

$$
\begin{aligned}
\vec{k}_2 \cdot \hat{t} &= |\vec{k}_2| \hat{k}_2 \cdot \hat{\ell} = |\vec{k}_2| \cos(\theta_{\rm lab}) \\
\vec{k}_2 \cdot \hat{t}' &= |\vec{k}_2| \hat{k}_2 \cdot \hat{\ell}' = |\vec{k}_2| \hat{k}_2 \cdot [\hat{\ell} \cos(\theta_{\rm lab}) + \hat{s} \sin(\theta_{\rm lab})] = (k_2)_x \cos(\theta_{\rm lab}) + (k_2)_y \sin(\theta_{\rm lab}) \\
\vec{k}_2' \cdot \hat{t} &= |\vec{k}_2'| \hat{k}_2' \cdot \hat{\ell} = (k_2')_x \\
\vec{k}_2' \cdot \hat{t}' &= |\vec{k}_2'| \hat{k}_2' \cdot \hat{\ell}' = |\vec{k}_2'| \hat{k}_2' \cdot [\hat{\ell} \cos(\theta_{\rm lab}) + \hat{s} \sin(\theta_{\rm lab})] = (k_2')_x \cos(\theta_{\rm lab}) + (k_2')_y \sin(\theta_{\rm lab}) \\
\hat{t} \cdot \hat{t}' &= \hat{\ell} \cdot \hat{\ell}' = \cos(\theta_{\rm lab})
\end{aligned}
\tag{K.31}
$$

where expressions for the x– and y–components of $\vec{k}_1$, $\vec{k}_1'$, $\vec{k}_2$ and $\vec{k}_2'$ are given in Appendix I. Substitution of Eq. (K.31) into Eqs. (K.18) to (K.25) yields

$$
\begin{aligned}
s_i \cdot s_f &= \frac{|\vec{k}_1||\vec{k}_1'| - E_1^* E_1'^* \cos(\theta_{\rm lab})}{(m_1^*)^2} \\
s_i \cdot K_1 &= \frac{E_1'^* |\vec{k}_1| - E_1^* |\vec{k}_1'| \cos(\theta_{\rm lab})}{(m_1^*)^2} \\
s_i \cdot K_2 &= \frac{E_2'^* |\vec{k}_1| - E_1^* (k_2')_x}{m_1^* m_2^*} \\
s_i \cdot P_2 &= \frac{E_2^* |\vec{k}_1| - E_1^* (k_2)_x}{m_1^* m_2^*} \\
s_f \cdot K_2 &= \frac{E_2^* |\vec{k}_1'|}{m_1^* m_2^*} - [(k_2')_x (k_1')_x + (k_2')_y (k_1')_y] \frac{E_1'^*}{m_1^* m_2^* |\vec{k}_1'|} \\
s_f \cdot P_1 &= \frac{E_1^* |\vec{k}_1'| - E_1'^* |\vec{k}_1| \cos(\theta_{\rm lab})}{(m_1^*)^2} \\
s_f \cdot P_2 &= \frac{E_2^* |\vec{k}_1'|}{m_1^* m_2^*} - [(k_2)_x (k_1')_x + (k_2)_y (k_1')_y] \frac{E_1'^*}{m_1^* m_2^* |\vec{k}_1'|} \, .
\end{aligned}
\tag{K.32}
$$

Finally, with Eqs. (K.12) and (K.13) in Eq. (K.11), and substitution of the latter into Eqs. (K.17) and (3.88) (see Chapter 3), the complete expression for $D_{\ell' \ell}$ is obtained.

K.3 Polarization transfer observable: D_{nn}

The polarization transfer observable D_{nn} corresponds to the following choice of initial and final spin orientations in the rest frame of the nucleon in Eqs. (K.18) to (K.25):

$$
\begin{aligned}
\hat{t} &= \hat{n} \\
\hat{t}' &= \hat{n}' = \hat{n} \, .
\end{aligned}
\tag{K.33}
$$

Before writing down explicit expressions for the spin–dependent terms in Eqs. (K.18) to (K.25), it is necessary to write derive explicit expressions for the following quantities:

$$\begin{aligned}
\vec{k}_1 \cdot \hat{t} &= |\vec{k}_1|\hat{\ell} \cdot \hat{n} = 0 \\
\vec{k}_1 \cdot \hat{t}' &= |\vec{k}_1|\hat{\ell} \cdot \hat{n} = 0 \\
\vec{k}'_1 \cdot \hat{t} &= |\vec{k}'_1|\hat{\ell}' \cdot \hat{n} = 0 \\
\vec{k}'_1 \cdot \hat{t}' &= |\vec{k}'_1|\hat{\ell}' \cdot \hat{n} = 0 \\
\vec{k}_2 \cdot \hat{t} &= |\vec{k}_2|\hat{k}_2 \cdot \hat{n} = (k_2)_z \\
\vec{k}_2 \cdot \hat{t}' &= |\vec{k}_2|\hat{k}_2 \cdot \hat{n} = (k_2)_z \\
\vec{k}'_2 \cdot \hat{t} &= |\vec{k}'_2|\hat{k}'_2 \cdot \hat{n} = (k'_2)_z \\
\vec{k}'_2 \cdot \hat{t}' &= |\vec{k}'_2|\hat{k}'_2 \cdot \hat{n} = (k'_2)_z \\
\hat{t} \cdot \hat{t}' &= \hat{n} \cdot \hat{n} = 1
\end{aligned} \tag{K.34}$$

where expressions for the x– and y–components of $\vec{k}_1$, $\vec{k}'_1$, $\vec{k}_2$ and $\vec{k}'_2$ are given in Appendix I. Substitution of Eq. (K.34) into Eqs. (K.18) to (K.25) yields

$$\begin{aligned}
s_i \cdot s_f &= -1 \\
s_i \cdot K_1 &= 0 \\
s_i \cdot K_2 &= -\frac{(k'_2)_z}{m_2^*} \\
s_i \cdot P_2 &= -\frac{(k_2)_z}{m_2^*} \\
s_f \cdot K_2 &= -\frac{(k'_2)_z}{m_2^*} \\
s_f \cdot P_1 &= 0 \\
s_f \cdot P_2 &= -\frac{(k'_2)_z}{m_2^*} .
\end{aligned} \tag{K.35}$$

Finally, with Eqs. (K.12) and (K.13) in Eq. (K.11), and substitution of the latter into Eqs. (K.17) and (3.88) (see Chapter 3), the complete expression for D_{nn} is obtained.

K.4 Polarization transfer observable: $D_{\ell' s}$

The polarization transfer observable $D_{\ell' s}$ corresponds to the following choice of initial and final spin orientations in the rest frame of the nucleon in Eqs. (K.18) to (K.25):

$$\begin{aligned} \hat{t} &= \hat{s} \\ \hat{t}' &= \hat{\ell}' . \end{aligned} \tag{K.36}$$

Before, writing down explicit expressions for the spin–dependent terms in Eqs. (K.18) to (K.25), it is necessary to write derive explicit expressions for the following quantities:

$$\begin{aligned}
\vec{k}_1 \cdot \hat{t} &= |\vec{k}_1| \hat{\ell} \cdot \hat{s} = 0 \\
\vec{k}_1 \cdot \hat{t}' &= |\vec{k}_1| \hat{\ell} \cdot \hat{\ell}' = |\vec{k}_1| \cos(\theta_{\rm lab}) \\
\vec{k}_1 \cdot \vec{k}_1' &= |\vec{k}_1| \, |\vec{k}_1'| \hat{\ell} \cdot \hat{\ell}' = |\vec{k}_1| \, |\vec{k}_1'| \cos(\theta_{\rm lab}) \\
\vec{k}_1' \cdot \hat{t} &= |\vec{k}_1'| \hat{\ell}' \cdot \hat{s} = |\vec{k}_1'| \hat{s} \cdot [\hat{\ell} \cos(\theta_{\rm lab}) + \hat{s} \sin(\theta_{\rm lab})] = |\vec{k}_1'| \sin(\theta_{\rm lab}) \\
\vec{k}_1' \cdot \hat{t}' &= |\vec{k}_1'| \hat{\ell}' \cdot \hat{\ell}' = |\vec{k}_1'| \\
\vec{k}_1' \cdot \vec{k}_2 &= |\vec{k}_1'| \, |\vec{k}_2| \hat{\ell}' \cdot \hat{k}_2 = |\vec{k}_1'| \, |\vec{k}_2| \hat{k}_2 \cdot [\hat{\ell} \cos(\theta_{\rm lab}) + \hat{s} \sin(\theta_{\rm lab})] = (k_1')_x (k_2)_x + (k_1')_y (k_2)_y \\
\vec{k}_1' \cdot \vec{k}_2' &= |\vec{k}_1'| \, |\vec{k}_2'| \hat{\ell}' \cdot \hat{k}_2' = |\vec{k}_1'| \, |\vec{k}_2'| \hat{k}_2' \cdot [\hat{\ell} \cos(\theta_{\rm lab}) + \hat{s} \sin(\theta_{\rm lab})] = (k_1')_x (k_2')_x + (k_1')_y (k_2')_y \\
\vec{k}_2 \cdot \hat{t} &= |\vec{k}_2| \hat{k}_2 \cdot \hat{s} = (k_2)_y \\
\vec{k}_2 \cdot \hat{t}' &= |\vec{k}_2| \hat{k}_2 \cdot \hat{\ell}' = |\vec{k}_2| \hat{k}_2 \cdot [\hat{\ell} \cos(\theta_{\rm lab}) + \hat{s} \sin(\theta_{\rm lab})] = (k_2)_x \cos(\theta_{\rm lab}) + (k_2)_y \sin(\theta_{\rm lab}) \\
\vec{k}_2' \cdot \hat{t} &= |\vec{k}_2'| \hat{k}_2' \cdot \hat{s} = (k_2')_y \\
\vec{k}_2' \cdot \hat{t}' &= |\vec{k}_2'| \hat{k}_2' \cdot \hat{\ell}' = |\vec{k}_2'| \hat{k}_2' \cdot [\hat{\ell} \cos(\theta_{\rm lab}) + \hat{s} \sin(\theta_{\rm lab})] = (k_2')_x \cos(\theta_{\rm lab}) + (k_2')_y \sin(\theta_{\rm lab}) \\
\hat{t} \cdot \hat{t}' &= \hat{s} \cdot \hat{\ell}' = \hat{s} \cdot [\hat{\ell} \cos(\theta_{\rm lab}) + \hat{s} \sin(\theta_{\rm lab})] = \sin(\theta_{\rm lab})
\end{aligned} \tag{K.37}$$

where expressions for the x– and y–components of $\vec{k}_1$, $\vec{k}_1'$, $\vec{k}_2$ and $\vec{k}_2'$ are given in Appendix I. Substitution of Eq. (K.37) into Eqs. (K.18) to (K.25) yields

$$\begin{aligned}
s_i \cdot s_f &= -\frac{{E_1}'^* \sin(\theta_{\rm lab})}{m_1^*} \\
s_i \cdot K_1 &= -\frac{(k_1')_y}{m_1^*} \\
s_i \cdot K_2 &= -\frac{(k_2')_y}{m_2^*} \\
s_i \cdot P_2 &= -\frac{(k_2)_y}{m_2^*}
\end{aligned}$$

$$
\begin{aligned}
s_f \cdot K_2 &= \frac{E_2'^* |\vec{k}_1'|}{m_1^* m_2^*} - [(k_1')_x (k_2')_x + (k_1')_y (k_2')_y] \frac{E_1'^*}{|\vec{k}_1'| m_1^* m_2^*} \\
s_f \cdot P_1 &= \frac{E_2^* |\vec{k}_1'| - E_1'^* |\vec{k}_1| \cos(\theta_{\rm lab})}{(m_1^*)^2} \\
s_f \cdot P_2 &= \frac{E_2^* |\vec{k}_1'|}{m_1^* m_2^*} - [(k_1')_x (k_2)_x + (k_1')_y (k_2)_y] \frac{E_1'^*}{|\vec{k}_1'| m_1^* m_2^*} \, .
\end{aligned} \tag{K.38}
$$

Finally, with Eqs. (K.12) and (K.13) in Eq. (K.11), and substitution of the latter into Eqs. (K.17) and (3.88) (see Chapter 3), the complete expression for $\mathrm{D}_{\ell' s}$ is obtained.

K.5 Polarization transfer observable: $\mathrm{D}_{s'\ell}$

The polarization transfer observable $\mathrm{D}_{s'\ell}$ corresponds to the following choice of initial and final spin orientations in the rest frame of the nucleon in Eqs. (K.18) to (K.25):

$$
\begin{aligned}
\hat{t} &= \hat{\ell} \\
\hat{t}' &= \hat{s}' \, .
\end{aligned} \tag{K.39}
$$

Before, writing down explicit expressions for the spin–dependent terms in Eqs. (K.18) to (K.25), it is necessary to write derive explicit expressions for the following quantities:

$$
\begin{aligned}
\vec{k}_1 \cdot \hat{t} &= |\vec{k}_1| \hat{\ell} \cdot \hat{\ell} = |\vec{k}_1| \\
\vec{k}_1 \cdot \hat{t}' &= |\vec{k}_1| \hat{\ell} \cdot \hat{s}' = |\vec{k}_1| \hat{\ell} \cdot [-\hat{\ell} \sin(\theta_{\rm lab}) + \hat{s} \cos(\theta_{\rm lab})] = -|\vec{k}_1| \sin(\theta_{\rm lab}) \\
\vec{k}_1 \cdot \vec{k}_1' &= |\vec{k}_1| |\vec{k}_1'| \hat{\ell} \cdot \hat{\ell}' = |\vec{k}_1| |\vec{k}_1'| \cos(\theta_{\rm lab}) \\
\vec{k}_1 \cdot \vec{k}_2 &= |\vec{k}_1| |\vec{k}_2| \hat{\ell} \cdot \hat{k}_2 = |\vec{k}_1| (k_2)_x \\
\vec{k}_1 \cdot \vec{k}_2' &= |\vec{k}_1| |\vec{k}_2'| \hat{\ell} \cdot \hat{k}_2' = |\vec{k}_1| (k_2')_x \\
\vec{k}_1' \cdot \hat{t} &= |\vec{k}_1'| \hat{\ell}' \cdot \hat{\ell} = |\vec{k}_1'| \cos(\theta_{\rm lab}) \\
\vec{k}_1' \cdot \hat{t}' &= |\vec{k}_1'| \hat{\ell}' \cdot \hat{s}' = 0 \\
\vec{k}_2 \cdot \hat{t} &= |\vec{k}_2| \hat{k}_2 \cdot \hat{\ell} = (k_2)_x \\
\vec{k}_2 \cdot \hat{t}' &= |\vec{k}_2| \hat{k}_2 \cdot \hat{s}' = |\vec{k}_2| \hat{k}_2 \cdot [-\hat{\ell} \sin(\theta_{\rm lab}) + \hat{s} \cos(\theta_{\rm lab})] = -(k_2)_x \sin(\theta_{\rm lab}) + (k_2)_y \cos(\theta_{\rm lab}) \\
\vec{k}_2' \cdot \hat{t} &= |\vec{k}_2'| \hat{k}_2' \cdot \hat{\ell} = (k_2')_x \\
\vec{k}_2' \cdot \hat{t}' &= |\vec{k}_2'| \hat{k}_2' \cdot \hat{s}' = |\vec{k}_2'| \hat{k}_2' \cdot [-\hat{\ell} \sin(\theta_{\rm lab}) + \hat{s} \cos(\theta_{\rm lab})] = -(k_2')_x \sin(\theta_{\rm lab}) + (k_2')_y \cos(\theta_{\rm lab}) \\
\hat{t} \cdot \hat{t}' &= \hat{\ell} \cdot \hat{s}' = \hat{\ell} \cdot [-\hat{\ell} \sin(\theta_{\rm lab}) + \hat{s} \cos(\theta_{\rm lab})] = -\sin(\theta_{\rm lab})
\end{aligned} \tag{K.40}
$$

where expressions for the x– and y–components of $\vec{k}_1$, $\vec{k}'_1$, $\vec{k}_2$ and $\vec{k}'_2$ are given in Appendix I. Substitution of Eq. (K.40) into Eqs. (K.18) to (K.25) yields

$$\begin{aligned}
s_i \cdot s_f &= \frac{E_1^* \sin(\theta_{\text{lab}})}{m_1^*} \\
s_i \cdot K_1 &= \frac{E_1{}'^* |\vec{k}_1| - E_1^* (k'_1)_x}{(m_1^*)^2} \\
s_i \cdot K_2 &= \frac{E_2{}'^* |\vec{k}_1| - E_1^* (k'_2)_x}{m_1^* m_2^*} \\
s_i \cdot P_2 &= \frac{E_2^* |\vec{k}_1| - E_1^* (k_2)_x}{m_1^* m_2^*} \\
s_f \cdot K_2 &= \frac{(k'_2)_x \sin(\theta_{\text{lab}}) - (k'_2)_y \cos(\theta_{\text{lab}})}{m_2^*} \\
s_f \cdot P_1 &= \frac{|\vec{k}_1| \sin(\theta_{\text{lab}})}{m_1^*} \\
s_f \cdot P_2 &= \frac{(k_2)_x \sin(\theta_{\text{lab}}) - (k_2)_y \cos(\theta_{\text{lab}})}{m_2^*} \,.
\end{aligned} \tag{K.41}$$

Finally, with Eqs. (K.12) and (K.13) in Eq. (K.11), and substitution of the latter into Eqs. (K.17) and (3.88) (see Chapter 3), the complete expression for $\mathrm{D}_{s'\ell}$ is obtained.

K.6 Induced polarization or analyzing power: A_y

For calculating the induced polarization or analyzing power, it is necessary to evaluate Eq. (K.7) where the three–spin vector $\hat{s}_f$ is given by

$$\hat{s}_f = \hat{n} = \hat{y} \,. \tag{K.42}$$

With (see Appendix I)

$$\begin{aligned}
\vec{k}_1 &= |\vec{k}_1| \hat{x} \\
\vec{k}'_1 &= |\vec{k}'_1| \cos(\theta_{\text{lab}}) \hat{x} + |\vec{k}'_1| \cos(\theta_{\text{lab}}) \hat{y} \\
\vec{k}_2 &= (k_2)_x \hat{x} + (k_2)_y \hat{y} + (k_2)_z \hat{z} \\
\vec{k}'_2 &= (k'_2)_x \hat{x} + (k'_2)_y \hat{y} + (k'_2)_z \hat{z}
\end{aligned} \tag{K.43}$$

and imposing energy and momentum conservation, one can write down the following explicit expression for Eq. (K.7):

$$\sum_{s_1, s_2, s'_2} \mathcal{M}^* \mathcal{M} = 2 \,\mathrm{Im} \left[t_S^* \, t_V + 2 t_T^* \, t_A - \frac{m_1^*}{m_2^*} (t_A^* \, t_V + 2 t_T^* \, t_S) \right] \frac{1}{m_1^{*2} \, m_2^*}$$

$$\{E_2'^{*}|\vec{k}_1|(k_1')_y - E_1'^{*}|\vec{k}_1|(k_2')_y + E_1^{*}[(k_2')_y(k_1')_x - (k_1')_y(k_2')_x]\}\,. \quad \text{(K.44)}$$

Bibliography

[Ab70] M. Abramowitz and I. A. Stegun, eds., *Handbook of Mathematical Functions with Formulas, Graphs and Mathematical Tables* (Dover Publications, New York, 1970).

[Ai83] Ian J. R. Aitchison and Anthony J.G. Hey, *Gauge Theories in Particle Physics* (Adam Hilger Ltd, Bristol, 1983).

[Al73] M. Alonso and H. Valk, *Quantum Mechanics: Principles and Applications* (Addison–Wesley Publishing Company, Reading, 1973).

[Al82] W. M. Alberico, M. Ericson, and A. Molinari, Nucl. Phys. **A379**, 429 (1982).

[Al84] W. M. Alberico, M. Ericson, and A. Molinari, Phys. Rev. **C30**, 1776 (1984).

[Al87] W. M. Alberico, A. De Pace, M. Ericson, Mikkel B. Johnson, and A. Molinari, Phys. Lett. **183B**, 135 (1987).

[Al88] W. M. Alberico, A. De Pace, M. Ericson, Mikkel B. Johnson, and A. Molinari, Phys. Rev. **C38**, 109 (1988)

[Al91] C. Alvarez, H. F. Arellano, F. A. Brieva, and W. G. Love, in *Proceedings of the International Conference on Spin and Isospin in Nuclear Reactions, Telluride, Colorado, 1991*, edited by S. W. Wissink, C. D. Goodman, and G. E. Walker (Plenum Press, New York, 1991), p. 219.

[Am63] K. A. Amos and I. E. McCarthy, Phys. Rev. **132**, 2261 (1963).

[Am66] K. A. Amos, Nucl. Phys. **77**, 225 (1966).

[Am83] R. D. Amado, J. Piekarewicz, D. A. Sparrow, and J. A. McNeil, Phys. Rev. C**28**, 1663 (1983).

[An81] B. D. Anderson, A. R. Baldwin, A. M. Kalenda, R. Madey, J. W. Watson, C. C. Chang, H. D. Holmgren, R. W. Koontz, and J. R. Wu, Phys. Rev. Lett. **46**, 226 (1981).

[Ar86] R. A. Arndt and D. Roper, VPI and SU Scattering Analysis Interactive Dialin Program and Data Base.

[Au61] N. Austern, Ann. Phys. **15**, 299 (1961).

[Au70] N. Austern, *Direct Nuclear Reactions* (Wiley, New York, 1970).

[Ba89] M. L. Barlett, G. W. Hoffmann, L. Ray, G. Pauletta, K. H. McNaughton, J. F. Amann, K. W. Jones, J. B. McClellend, M. W. McNaughton, R. Fergerson, D. Lopiano, Phys. Rev. C**40**, 2697 (1989)

[Be81] F. E. Bertrand, Nucl. Phys. **A354**, 440 (1981).

[Be82] G. F. Bertsch and O. Scholten, Phys. Rev. C **25**, 804 (1982).

[Be93] George F. Bertsch, Leonid Frankfurt, and Mark Strikman, Science, Vol. 259, 773 (1993).

[Bj64] J. D. Bjorken and S. Drell, *Relativistic Quantum Mechanics* (McGraw–Hill, New York, 1964).

[Bl82] E. Bleszynski, M. Bleszynski, and C. A. Whitten, Jr., Phys. Rev. C **26**, 727 (1982).

[Bo81] J. Boguta, Nucl. Phys. **A372**, 386 (1981).

[Bo82] A. Bouyssy, Nucl. Phys. **A381**, 445 (1982).

[Br62] D. M. Brink and G. R. Satchler, *Angular Momentum* (Oxford University Press, Oxford, 1962).

[Br76] G. E. Brown and A. D. Jackson, *The Nucleon–Nucleon Interaction* (North–Holland Publishing Company, Amsterdam, 1976).

[Br77] F. A. Brieva and J. R. Rook, Nucl. Phys. **A291**, 299 (1977).

[Br77a] F. A. Brieva and J. R. Rook, Nucl. Phys. **A291**, 317 (1977).

[Br78] F. A. Brieva and J. R. Rook, Nucl. Phys. **A297**, 206 (1978).

[Br78a] F. A. Brieva and J. R. Rook, Nucl. Phys. **A307**, 493 (1978).

[Br90] F. A. Brieva and W. G. Love, Phys. Rev. C **42**, 2573 (1990).

[Br92] F. A. Brieva, W. G. Love, and K. Nakayama, Phys. Rev. C **46**, 565 (1992).

[Br94] G. E. Brown and J. Wambach, Nucl. Phys. **A568**, 895 (1994).

[Br95] G. E. Brown, M. Buballa, Zi Bang Li, and J. Wambach, Nucl. Phys. **A593**, 295 (1995).

[By78] J. Bystricky, F. Lehar, and P Winternitz, Le Journal de Physique, Vol. **39**, 1 (1978).

[Ca84] T. A. Carey, K. W. Jones, J. B. McClelland, J. M. Moss, L. B. Rees, and N. Tanaka, Phys. Rev. Lett. **53**, 144 (1984).

[Ca95] D. S. Carman, *Inclusive and Exclusive Quasifree $(\vec{p},Np)$ Reaction Studies from ^2H and ^{12}C at 200 MeV*, Ph.D Thesis, Indiana University (1995), unpublished.

[Ca95a] D. S. Carman, *AIP Conference Proceedings of the Eighth International Symposium on Polarization Phenomena in Nuclear Physics*, edited by Edward J. Stephenson and Steven E. Vigdor, (American Institute of Physics, New York, 1995), p. 445.

[Ce82] L. S. Celenza, W. S. Pong, and C. M. Shakin, Phys. Rev. C **25**, 3115 (1982).

[Ce86] L. S Celenza and C. M. Shakin, *Relativistic Nuclear Physics*, (World Scientific, Singapore, 1976).

[Ch77] S. A. Chin, Ann. Phys. **108**, 301 (1977).

[Ch77a] N. S. Chant and P. G. Roos, Phys. Rev. C **15**, 57 (1977).

[Ch80] R. E. Chrien, T. J. Krieger, R. J. Sutter, M. May, H. Palevsky, R. L. Stearns, T. Kozlowski, and T. Bauer, Phys. Rev. C **21**, 1014 (1980).

[Ch81] T. Chen, R. E. Segel, P. T. Debevec, John Wiggins, P. P. Singh, and J. V. Maher, Phys. Lett. **103B**, 192 (1981).

[Ch83] N. S. Chant and P. G. Roos, Phys. Rev. C **27**, 1060 (1983).

[Ch88] X. Y. Chen, L. W. Swenson, F. Farzanpay, D. K. McDaniels, Z. Tang, Z. Xu, D. M. Drake, I. Bergqvist, A. Brockstedt, F.E. Bertrand, D.J. Horen, J. Lisantti, K. Hicks, M. Vetterli, and M. J. Iqbal, Phys. Lett. **205B**, 436, (1988).

[Ch89] C. Chan, T. E. Drake, R. Abegg, D. Frekers, O. Häusser, K. Hicks, D. A. Hutcheon, L. Lee, C A. Miller, R. Schubank, E. J. Stephenson, and S. Yen, J. Phys. G **15**, L55 (1989).

[Ch89a] X. Y. Chen, L. W. Swenson, F. Farzanpay, D. K. McDaniels, Z. Xu, Z. Tang, D. M. Drake, I. Bergqvist, A. Brockstedt, J. Lisantti, F. Bertrand, D. J. Horen, K. Hicks, M. Vertterli, and M. J. Iqbal, Nucl. Phys. **A505**, 670 (1989).

[Ch90] C. Chan, T. E. Drake, R. Abegg, D. Frekers, O. Häusser, K. Hicks, D. A. Hutcheon, L. Lee, C A. Miller, R. Schubank, and S. Yen, Nucl. Phys. **A510**, 713 (1990).

[Ch93] X. Y. Chen, T. N Taddeucci, J. B. McClellend, T. A. Carey, R. C. Byrd, L. J. Rybarcyk, W. Sailor, D. J. Mercer, D. L. Prout, S. DeLucia, B. Luther, D. G. Marchlenski, E. Sugarbaker, J. Rapaport, E. Gülmez, C. Whitten, Jr., C. D. Goodman, W. Huang, Y. Wang, W. P. Alfort, Phys. Rev. C **47**, 2159 (1993).

[Cl83] B. C. Clark, S. Hama, and R. L. Mercer in *The Interaction Between Medium Energy Nucleons in Nuclei - 1983*, Proceedings of the Workshop of the Interaction Between Medium Energy Nucleons in Nuclei, AIP Conf. Proc. No. 97, edited by H. O. Meyer (AIP, New York, 1983).

[Cl83a] B. C. Clark, S. Hama, R. L. Mercer, L. Ray, and B. D. Serot, Phys. Rev. Lett. **50**, 1644 (1983).

[Cl85] B. C. Clark in *Los Alamos Workshop on Relativistic Dynamics and Quark–Nuclear Physics*, (John Wiley & Sons Ltd, New York, 1986).

[Co72] D. M. Corley, N. S. Wall, H. Palevsky, J. L. Friedes, R. J. Sutter, G. W. Bennet, W. D. Simpson, G. C. Phillips, G. W. Igo, and R. L. Stearns, Nucl. Phys. **A184**, 437 (1972).

[Co80] A.A. Cowley, C. C. Chang, and H. D. Holmgren, Phys. Rev. C **22**, 2633(1980).

[Co89] E. D. Cooper and O. V. Maxwell, Nucl. Phys. **A493**, 468 (1989).

[Co92] E. D. Cooper, S. Hama, B. C. Clark, and R. L. Mercer, Phys. Rev. C **47**, 297 (1993).

[Co95] Full relativistic Coulomb wave functions are calculated in the code "Runt" kindly supplied by Tim Cooper.

[De91] A. De Pace and M. Viviani, Phys. Lett. **254**, 20 (1991).

[De93] A. De Pace and M. Viviani, Phys. Rev. C **48**, 2931 (1993).

[De94] De Pace, Nucl. Phys. **A577**, 143c (1994).

[El66] L. R. B. Elton, Nucl. Phys. **89**, 69 (1966).

[Ed94] C. M. Edwards, Ph.D Thesis, University of Minnesota (1994), unpublished.

[Ei59] R. M. Eisberg, Nucl. Phys. **10**, 571 (1959).

[Ei81] J. M. Eizenberg, Nucl. Phys. **A355**, 269 (1981).

[Er94] M. Ericson, Nucl. Phys. **A577**, 147c (1994).

[Es84] H. Esbensen and G. F. Bertsch, Ann. Phys. (N.Y.) bf 157, 255 (1984).

[Es85a] H. Esbensen, H. Toki and G. F. Bertsch, Phys. Rev. C **31**, 1816 (1985).

[Es85] H. Esbensen and G. F. Bertsch, Phys. Rev. C **32**, 553 (1985).

[Es86] H. Esbensen and G. F. Bertsch, Phys. Rev. C **34**, 1419 (1984).

[Fe71] A. L. Fetter and J. D. Walecka, *Quantum Theory of Many–Particle Systems* (McGraw–Hill Publishing Company, New York, 1971).

[Fe88] R. Fergerson, J. McGill, C. Glashausser, K. Jones, S. Nanda, Sun Zuxun, M. Barlett, G. Hoffmann, J. Marshall, J. McClelland, Phys. Rev. C **38**, 2193 (1988).

[Fe92] H. Feshbach, *Theoretical Nuclear Physics: Nuclear Reactions* (John Wiley & Sons, Inc., New York, 1992).

[Fo88] S. V. Förtsch, A. A. Cowley, J. V. Pilcher, D. M. Whittal, J. J. Lawrie, J. C. Van Staden, and E. Friedland, Nucl. Phys. **A485**, 258 (1988).

[Fr81] B. Friedman and V. R. Panharipande, Phys. Lett. **100B**, 205 (1981).

[Ga90] C. Gaarde, Nucl. Phys. **A507**, 79c (1990).

[Gl83] N. K. Glendenning, *Direct Nuclear Reactions* (Academic Press, New York, 1983).

[Go80] H. Goldstein, *Classical Mechanics*
(Addison–Wesley Publishing Company, Reading, 1980).

[Gr87] D. Griffiths, *Introduction to Elementary Particles*
(John Wiley & Sons, New York, 1987).

[Gr89] W. Greiner, *Quantum Mechanics* (Springer–Verlag, Berlin, 1989).

[Gr90] W. Greiner, *Relativistic Quantum Mechanics* (Springer–Verlag, Berlin, 1990).

[Gr91] E. K. U. Gross, E. Runge, and O. Heinonen, *Many–Particle Theory*
(Adam Hilger, Bristol, 1991).

[Gr92] W. Greiner, *Quantum Electrodynamics* (Springer–Verlag, Berlin, 1992).

[Gr94] W. Greiner, *Quantum Chromodynamics* (Springer–Verlag, Berlin, 1994).

[Gr96] W. Greiner, *Field Quantization* (Springer–Verlag, Berlin, 1996).

[Gu91] M. Guidry, *Gauge Field Theories: An Introduction with Applications*
(John Wiley & Sons, Inc., New York, 1991).

[Gu95] T. Gu, *Measurements of* $(\vec{p},p')$ *and* $(\vec{p},p'x)$ *Reaction on* ^2H *and* $^{3,4}He$ *at 200 MeV*,
University of Maryland (1995), unpublished.

[Ha88] O. Häusser, R. Abegg, R. G. Jeppesen, R. Sawafta, A. Celler, A. Green, R. L. Helmer, R. Henderson, K. Hicks, K. P. Jackson, J. Mildenberger, C. A. Miller, M. C. Vetterli, S. Yen, M. J. Iqbal, and R. D. Smith, Phys. Rev. Lett. **61**, 822 (1988).

[Ha90] S. Hama, B. C. Clark, E. D. Cooper, H. S. Sherif, and R. L. Mercer,
Phys. Rev. C **41**, 2737 (1990).

[Ha91] O. Häusser, M. C. Vetterli, R. W. Fergerson, C. Glashausser, R. G. Jeppesen, R. D. Smith, R. Abegg, F. T. Baker. A. Celler, R. L. Helmer, R. Henderson, K. Hicks, M. J. Iqbal, K. P. Jackson, K. W. Jones, J. Lisantti, J. Mildenberger, C. A. Miller, R. S. Sawafta, S. Yen. Phys. Rev. C **43**, 230 (1991).

[Ha98] C. L. Hautala, *Measurement of Polarization Observables in the Quasielastic Region on ^{nat}Ca and ^{nat}Pb using the $(\vec{p},\vec{n})$ Reaction at 200 MeV*, Ph.D Thesis, Ohio University (1998), unpublished.

[Hi89] K. H. Hicks, M. C. Vetterli, A. Cellar, R. L. Helmer, R. S. Henderson, K. P. Jackson, R. G. Jeppesen, A. Trudel, S. Yen, Phys. Rev. C **40**, R2445 (1989).

[Hi90] G C Hillhouse, *Nuclear reactions with Polarized Spin-$\frac{1}{2}$ Beams*, M.Sc Thesis (University of Stellenbosch, 1990), unpublished.

[Hi93] K. H. Hicks, W. P. Alford, A. Celler, R. S. Henderson, K. P. Jackson, C. A. Miller, M. C. Vetterli, S. Yen, F. Brieva, C. J. Horowitz, and J. Piekarewicz, Phys. Rev. C **47**, 260 (1993).

[Hi94] G. C. Hillhouse and P. R. De Kock, Phys. Rev. C **49**, 391 (1994).

[Hi95] G. C. Hillhouse and P. R. De Kock, Phys. Rev. C **52**, 2796 (1995).

[Hi97] G. C. Hillhouse, B. I. S van der Ventel, S. M. Wyngaardt, and P. R. De Kock, *Proceedings of the RCNP International Mini Workshop on Nuclear Medium Effect via Nucleon Induced Reactions*, Journal of the Physical Society of Japan, Vol. 42, No. 1 (August 1997), p 49.

[Hi98] G. C. Hillhouse, B. I. S van der Ventel, S. M. Wyngaardt, and P. R. De Kock, Phys. Rev. C **57**, 448 (1998).

[Ho81] C. J. Horowitz and J. D. Walecka, Nucl. Phys. **A364**, 429 (1981).

[Ho81a] C. J. Horowitz and B. D. Serot, Nucl. Phys. **A368**, 503 (1981).

[Ho84] C. J. Horowitz, Nucl. Phys. **A412**, 228 (1984).

[Ho85] C. J. Horowitz, Phys. Rev. C **31**, 1340 (1985).

[Ho86] C. J. Horowitz and M. J. Iqbal, Phys. Rev. C **33**, 2059 (1986); **34**, 2012(E) (1986).

[Ho88] C. J. Horowitz and D. P. Murdock, Phys. Rev. C **37**, 2032 (1988).

[Ho90] C. J. Horowitz and J. Piekarewicz, Nucl. Phys. **A511**, 461 (1990).

[Ho91a] C. J. Horowitz, D. P. Murdock, and B. D. Serot, in *Computational Nuclear Physics I*, edited by K. Langanke, J. A. Maruhn, and S. E. Koonin (Springer–Verlag, Berlin, 1991), p. 129.

[Ho91b] C. J. Horowitz, in *Proceedings of the International Conference on Spin and Isospin in Nuclear Reactions, Telluride, Colorado, 1991*, edited by S. W. Wissink, C. D. Goodman, and G. E. Walker (Plenum Press, New York, 1991), p. 415.

[Ho92] B. R. Holstein, *Topics in Advanced Quantum Mechanics* (Addison–Wesley Publishing Company, New York, 1992).

[Ho94] C. J. Horowitz and J. Piekarewicz, Phys. Rev. C **50**, 2540 (1994).

[Ho94a] C. J. Horowitz and J. Piekarewicz, Nucl. Phys. **A577**, 137c (1994).

[Ho97] C. J. Horowitz, *Proceedings of the RCNP International Mini Workshop on Nuclear Medium Effect via Nucleon Induced Reactions*, Journal of the Physical Society of Japan, Vol. 42, No. 1 (August 1997), p 7.

[Ic89] M. Ichimura and Ken Kawahigashi, T. S. Jørgensen, and C. Gaarde, Phys. Rev. C **39**, 1446 (1989); **46**, 2117(E) (1992).

[Ic92] Munetake Ichimura and K. Kawahigashi, Phys. Rev. C **45**, 1822 (1992).

[Ic92a] M. Ichimura, *Proceedings of the sixth Frenco–Japanese Colloquium on Nuclear Structure and Interdisciplinary Topics*, 1992, edited by N. Alamanos, S. Fortier, and F. Dykstra, p. 49, Saint–Malo (unpublished).

[Ic94] Munetake Ichimura, Kimiaki Nishida, and Ken Kawahigashi, Nucl. Phys. **A577**, 123c (1994).

[Ic97] Munetake Ichimura, *Proceedings of the RCNP International mini workshop on nuclear medium effect via nucleon induced reactions*, Journal of the Physical Society of Japan, Vol. 42, No. 1 (August 1997), p 21.

[Ik95] Y. Ikebata, Phys. Rev. C **52**, 890 (1995).

[Iq88] M. J. Iqbal, in *Proceedings of the International Conference on Spin Observables of Nuclear Probes, Telluride, Colorado, 1988*, edited by C. J. Horowitz, C. D. Goodman, and G. E. Walker (Plenum Press, New York, 1991), p. 53.

[Ja70] D. F. Jackson, *Nuclear Reactions* (Methuen & Co Ltd, London, 1970).

[Ja83] M. Jaminon in *The Interaction Between Medium Energy Nucleons in Nuclei – 1983*, Proceedings of the Workshop of the Interaction Between Medium Energy Nucleons in Nuclei, AIP Conf. Proc. No. 97, edited by H. O. Meyer (AIP, New York, 1983).

[Ja81] M. Jaminon and C. Mahaux, Phys. Rev. C **24**, 1353 (1981).

[Je77] J. P. Jeukenne, A. Lejeune, and C. Mahaux, Phys. Rev. C **16**, 80 (1977).

[Ka78] J. Källne, A. W. Stetz, R. M. Woloshyn, Phys. Lett. **74B**, 170 (1978).

[Ka90] C. Kalbach, Phys. Rev. C **41**, 1656 (1990).

[Ka93] M. Kaku, *Quantum Field Theory: A Modern Introduction* (Oxford University Press, Oxford, 1993).

[Ke80] J. Kelly, W. Bertozzi, T. N. Buti, F. W. Hersman, C. Hyde, M. V. Hynes, B. Norum, F. N. Rad, A. D. Bacher, G. C. Emery, C. C. Foster, W. P. Jones, D. W. Miller, B. L. Berman, W. G. Love, and F. Petrovich, Phys. Rev. Lett. **45**, 2012 (1980).

[Ki95] H. Kim, *Neutrino–Nucleus Scattering and Relativistic Nuclear Structure Effects*, Ph.D Thesis, Indiana University (1995), unpublished.

[Ko76] D. C. Kocher, F. E. Bertrand, E. E. Gross, and E. Newman, Phys. Rev. C **14**, 1392 (1976).

[Ko85] A. M. Kobos, E. D. Cooper, J I. Johansson, and H. S. Sherif, Nucl. Phys. **A445**, 605 (1985).

[Ko86] S. E. Koonin, *Computational Physics* (Benjamin, Reading MA, 1986).

[Kr70] F. R. Wall and N. S. Wall, Phys. Rev. C **1**, 138 (1970).

[Ku85] H. Kurasawa and T. Suzuki, Nucl. Phys. **A445**, 685 (1985).

[La90] R. H. Landau, *Quantum Mechanics II: A Second Course in Quantum Theory* (John Wiley & Sons, Inc., New York, 1991).

[Li84] J. Lisantti, J. R. Tinsley, D. M. Drake, I. Bergqvist, L. W. Swenson, D. K. McDaniels, F. E. Bertrand, E. E. Gross, D. J. Horen, and T. P. Sjoreen, Phys. Lett. **147B**, 23 (1984).

[Li89] K. Lim and C. J. Horowitz, Nucl. Phys. **A501**, 729 (1989).

[Li94] P. Li, *Measurement of Spin Observables in (p, 2p) Quasifree Scattering from very Light Nuclei.*, Ph.D Thesis, Indiana University (1994), unpublished.

[Li95] M. K. Liou, Y. Li, W. M. Schreiber, and R. W. Brown, Phys. Rev. C **52**, R2346 (1995).

[Lo81] I. Lovas, Nucl. Phys. **A367**, 509 (1981).

[Lo81a] W. G. Love and M. A. Franey, Phys. Rev. C **24**, 1073 (1981).

[Ma79] C. Mahaux in *Microscopic Optical Potentials*, edited by H. V. von Geramb (Springer, New York, 1979), p. 1.

[Ma84] H, Machner, D. Protić, G. Riepe, J. P. Didelez, N. Frascaria, E. Gerlic, E. Hourani, and M. Morlet, Phys. Lett. **138B**, 39 (1984).

[Ma82] T. Matsui, and B. D. Serot, Ann. Phys. (N.Y.) **83**, 107 (1982).

[Ma86] J. A. Marshall, M. L. Barlett, R. W. Fergerson, G. W.Hoffmann, E. C.Milner, L. Ray, J.F. Amann, B. E. Bonner, and J. B. McCelland, Phys. Rev. C **34**, 1433 (1986).

[Ma86a] P. Maritz and M. A. Muller, *Elementêre Analise*, (A. A. Balkema, Cape Town, 1986).

[Ma90] O. V. Maxwell and E. D. Cooper, Nucl. Phys. **A513**, 584 (1990).

[Ma93] O. V. Maxwell and E. D. Cooper, Nucl. Phys. **A565**, 740 (1993).

[Ma93a] B. C. Markham, private communication.

[Ma93b] B. C. Markham et. al., Bul. Am. Phys. Soc. **38** (1993).

[Ma94] O. V. Maxwell and E. D. Cooper, Nucl. Phys. **A574**, 819 (1994).

[Ma96] O. V. Maxwell, Nucl. Phys. **A600**, 509 (1996).

[Ma96a] O. V. Maxwell and E. D. Cooper, Nucl. Phys. **A603**, 441 (1996).

[Mc59] I. E. Eisberg, Nucl. Phys. **11**, 574 (1959).

[Mc62] I. E. McCarthy, Phys. Rev. **128**, 1237 (1962).

[Mc68] I. E. McCarthy, *Introduction to Nuclear Theory* (Wiley, New York, 1968).

[Mc83] J. A. McNeil, J. R. Shepard, and S. J. Wallace, Phys. Rev. C **50**, 1439 (1983).

[Mc83a] J. A. McNeil, L. Ray, and S. J. Wallace, Phys. Rev. C **27**, 2123 (1983).

[Mc84] J. A. McGill, C. Glashausser, K. Jones, S. K. Nanda, M. Barlett, R. Fergerson, J. A. Mashall, E. C. Milner, and G. W. Hoffmann, Phys. Lett. **134B**, 157 (1984).

[Mc84a] J. A. McGill, G. W. Hoffmann, M. L. Barlett, R. W. Fergerson, E. C. Milner, R. E. Chrien, R. J. Sutter, T. Kozlowski, R. L. Sterns, Phys. Rev. C **28**, 204 (1984).

[Mc86] D. K McDaniels, J. R. Tinsley, J. Lisantti, D. M. Drake, I. Bergqvist, L. W. Swenson, F. E. Bertrand, E. E. Gross, D. J. Horen, T. P. Sjoreen, R. Liljestrand, and H. Wilson, Phys. Rev. C **33**, 1943 (1986).

[Mc92] J. B. McClellend, T. N. Taddeucci, X. Y. Chen, W. P. Alfort, R. C. Byrd, T. A. Carey, S. DeLucia, C. D. Goodman, E. Gülmez, W. Huang, B. Luther, D. G. Marchlenski, D. J. Mercer, D. L. Prout, J. Rapaport, L. J. Rybaryck, W. Sailor, E. Sugarbaker, Y. Wang, and C. Whitten, Jr., Phys. Rev. Lett. **69**, 582 (1992).

[Me66] M. A. Melkanoff, T. Sawada and J Raynal, Methods Comp. Phys. **6** (Academic Press, New York, 1966).

[Me70] E. Merzbacher, *Quantum Mechanics* (Wiley, New York, 1970).

[Me81] H. O. Meyer, P. Schwandt, G. L. Moake, and P. P. Singh, Phys. Rev. C **23**, 616 (1981).

[Mi78] A B. Migdal, Rev. Mod. Phys. **50**, 107 (1978).

[Mi91] L D. Miller, Ann. Phys. **91**, 40 (1991).

[Mo53] P. M. Morse and H. Feshbach, *Methods of Theoretical Physics: Part I* (McGraw–Hill, New York,1953)

[Mo82] J. M. Moss, T. A. Carey, J. B. McClelland, N. J. DiGiacomo, S. J. Seestrom–Morris, G. F. Bertsch, O. Scholten, G. S. Adams, M. Gazzaly, N. Hintz, and S. Nanda Phys. Rev. Lett. **48**, 789 (1982).

[Mo82a] J. M. Moss, Phys. Rev. C **26**, 2063 (1982).

[Mu87a] D. P. Murdock, *Proton Scattering as a Probe of Relativity in Nuclei*, Ph.D Thesis, Massachusetts Institute of Technology (1987), unpublished.

[Mu87b] D. P. Murdock and C. J. Horowitz, Phys. Rev. C **35**, 1442 (1987).

[Na90] O. Nachtmann, *Elementary Particle Physics: Concepts and Phenomena* (Springer–Verlag, Berlin, 1990).

[Ne66] R. G. Newton, *Scattering Theory of Waves and Particles* (McGraw–Hill Book Company, New York, 1966).

[Ne88] J. W. Negele and H. Orland, *Quantum Many–Particle Systems* (Addison–Wesley Publishing Company, New York, 1988).

[Ni95] Kimiaki Nishida and Munetake Ichimura, Phys. Rev. C **51**, 269 (1995).

[No81] J. V. Noble, Nucl. Phys. **A368**, 447 (1981).

[Ok87] Y. Okuhara, B. Castel, I. P. Johnstone, and H. Toki, Phys. Lett. **186B**, 113 (1987).

[Os92] F. Osterfeld, Rev. Mod. Phys. **64**, 491 (1992).

[Ot97a] H. Otsu, *Study of Reaction Mechanisms for* (p,n) *and* (p,p') *quasi elastic scatterings*, Ph.D Thesis, University of Tokyo (1997), unpublished.

[Ot97b] H. Otsu, H. Sakai, H. Okamura, T. Wakasa, K. Hatanaka, S. Ishida, N. Sakamoto, T. Uesaka, Y. Satou, S. Fujita, A. Okihana, N. Koori, and M. B. Greenfield, *Proceedings of the RCNP International Mini Workshop on Nuclear Medium Effect via Nucleon Induced Reactions*, Journal of the Physical Society of Japan, Vol. 42, No. 1 (August 1997), p 13.

[Pa81] M. K. Pal, *Theory of Nuclear Structures* (Scientific and Academic Editions, New Delhi, 1981).

[Pa94] V. R. Pandharipande, J. Carlson, Steven C. Pieper, R. B. Wiringa, and R. Schiavilla, Phys. Rev. C **49**, 789 (1994).

[Pa98] M. Palarczyk, C. M. Riedel, D. Dehnhard, M. A. Espy, M. A. Franey, J. L. Langenbrunner, L. C. Bland, D. S. Carman, B. Brinkmöller, R. Madey, Y. Wang, J. W. Watson, and N. S. Chant, Phys. Rev. C **58**, 645 (1998).

[Pi84] *Physics Today*, Vol. **47**, 20 (1984).

[Pi95] J. Piekarewicz and J. R. Shepard, Phys. Rev. C **51**, 806 (1995).

[Pr95] D. L. Prout, C. Zafiratos, T. N. Taddeucci, J. Ullmann, R. C. Byrd, T. A. Carey, P. Lisowski,J. B. McChelland, L. J. Rybarcyk, W. Sailor, W. Amian, M. Braunstein, D. Lind, D. J. Mercer, D. Cooper, S. DeLucia, B. Luther, D. G. Marchlenski, E. Sugarbaker, J. Rapaport, B. K. Park, E. G"ulmez, C. A. Whitten, Jr., C. D. Goodman, W. Huang, D. Ciscowski, and W. P. Alford, Phys. Rev. C **52**, 228 (1995).

[Ra85] L. Ray and G. W. Hoffmann, Phys. Rev. C **31**, 538 (1985).

[Ra94] J. Rapaport and E. Sugarbaker, Ann. Rev. Nucl. Part. Sci. **44**, 109 (1994).

[Ra98] J. Rapaport, private communication.

[Re86] L. B. Rees, J. M. Moss, T. A. Carey, K. W. Jones, J. B. McClelland, N. Tanaka, A. D. Bacher, and H. Esbensen, Phys. Rev. C **34**, 627 (1986).

[Ra92] L. Ray, G. W. Hoffmann, and W. R. Coker, Phys. Rep. **212**, 223 (1989).

[Re89] P. G. Reinhardt, Rep. Prog. Phys. **52**, 439 (1989)

[Ro60] M. E. Rose, *Relativistic Electron Theory* (Wiley, New York).

[Ro81] G. Roy, L. G. Greeniaus, G. A. Moss, D. A. Hutcheon, R. Liljestrand, R. M. Woloshyn, D. H. Boal, A. W. Stetz, K. Aniol, A. Willis, N. Willis, and R. McCamis, Phys. Rev. C **23**, 1671 (1981).

[Ro84] E. Rost, J. R. Shepard, E. R. Siciliano , and J. A. McNeil, Phys. Rev. C **29**, 209 (1984).

[Ro87] E. Rost and J. R. Shepard, Phys. Rev. C **35**, 681 (1987).

[Sa67] J. J. Sakurai, *Advanced Quantum Mechanics* (Addison–Wesley Publishing Company, Reading, 1967).

[Sa80] H. Sakai, K. Hosono, N. Matsuoka, S. Nagamachi, A. Okada, K. Maeda, and H. Shimiz, Nucl. Phys. **A344**, 41 (1980).

[Sa83] G. R. Satchler, *Direct Nuclear Reactions* (Oxford University Press, New York, 1985).

[Sa83a] H. Sakai, N. Matsuoka, T. Saito, A. Shimizu, K. Hatanaka, and M. Ejiri, RCNP Annual Report (1983).

[Sa85] J. J. Sakurai, *Modern Quantum Mechanics* (Addison and Wesley Publishing Corporation Incorporated, New York, 1985).

[Sa90] S. L. Sala and Einar Hille *Calculus: One and Several Variables*, 6th Edition (John Wiley and Sons, New York, 1990).

[Sa94] H. Sakai, M. B. Greenfield, K. Hatanaka, S. Ishida, N. Koori, H. Okamura, A. Okihana, H. Otsu, N. Sakamoto, Y. Satou, T. Uesaka, and T. Wakasa, Nucl. Phys. **A577**, 111c (1994).

[Sa96] H. Sakai, private communication.

[Se85] R. E. Segel, S. M. Levenson, P. Zupranski, A. A. Hassan, and S. Mukhopadhyay, Phys. Rev. C **32**, 721 (1985).

[Se86] B. D. Serot and J. D. Walecka, in *Advances in Nuclear Physics*, edited by J. W. Negele and E. Vogt (Plenum Press, New York, 1986), Vol. 16, p. 116.

[Se97] B. D. Serot and J. D. Walecka, Int. J. Mod. Phys. **E6**, 515 (1997).

[Sh83] C. M. Shakin in *The Interaction Between Medium Energy Nucleons in Nuclei – 1983*, Proceedings of the Workshop of the Interaction Between Medium Energy Nucleons in Nuclei, AIP Conf. Proc. No. 97, edited by H. O. Meyer (AIP, New York, 1983).

[Sh83a] J. R. Shepard, J. A. McNeil, and S. J. Wallace, Phys. Rev. Lett. **50**, 1443 (1983).

[Sh84] J. R. Shepard, E. Rost, and J. Piekarewicz, Phys. Rev. C **30**, 1604 (1984).

[Sh86] E. Shiino, Y. Saito, M. Ichimura, H. Toki, Phys. Rev. C **34**, 1004 (1986).

[Sh88] T. Shigehara, K. Shimizu, and A. Arima, Nucl. Phys. **A477**, 583 (1988).

[Si90] A. G. Sitenko, *Theory of Nuclear Reactions* (World Scientific, Singapore, 1990).

[Sm85] R. D. Smith and S. J. Wallace, Phys. Rev. C **32**, 1654 (1985).

[Sm88] R. D. Smith, in *Proceedings of the International Conference on Spin Observables of Nuclear Probes, Telluride, Colorado, 1988*, edited by C. J. Horowitz, C. D. Goodman and G. E. Walker (Plenum Press, New York, 1991), p. 53.

[Sm88a] R. D. Smith and J. Wambach, Phys. Rev. C **38**, 100 (1988).

[Sp74] Murray R. Spiegel, *Schaum's Outline of Theory and Problems of Advanced Calculus*, SI (Metric) Edition (McGraw–Hill Book Company, New York, 1974).

[St97] S. W. Steyn, *Multistep Direct Reactions in Nuclei*, Ph.D Thesis, University of Stellenbosch (1997), unpublished.

[Sw89] L. W. Swenson, X. Y. Chen, J. Lisantti, D. K. McDaniels, I. Bergqvist, F. E. Bertrand, D. J. Horen, E. E. Gross, C. Glover, R. O. Sayer, B. L. Burks, O. Häusser, K. Hicks, and M. J. Iqbal, Phys. Rev. C **40**, 246 (1989).

[Sw92] R. de Swiniarski, D. L. Pham, and J. Raynal, Z. Phys. A **343**, 179 (1986).

[Ta72] J. R. Taylor, *Scattering Theory* (John Wiley & Sons, Inc., New York, 1972).

[Ta91] T. N. Taddeucci, in *Spin and Isospin in Nuclear Interactions*, edited by S. W. Wissink, C. D Goodman, and G. E. Walker (Plenum Press, New York, 1991).

[Ta91a] T. N. Taddeucci, R. C. Byrd, T. A. Carey, J. B. McCelland, L. J. Rybarcyk, W. C. Sailor, D. E. Ciskowski, C. D. Goodmann, W. Huang, E. Gülmez, D. Marchlenski, E. Sugarbaker, D. Prout, J. Rapaport, Nucl. Phys. **A527**, 393c (1991).

[Ta94] T. N. Taddeucci, B. A. Luther, L. J. Rybarcyk, R. C. Byrd, J. B. McClellend, D. L. Prout, S. DeLucia, D. A. Cooper, D. G. Marchlenski, E. Sugarbaker, B. K Park, Thomas Sams, C. D. Goodman, J. Rapaport, M. Ichimura, and K. Kawahigashi, Phys. Rev. Lett. **73**, 3516 (1994).

[To87] M. Tosaki, M. Fujiwara, K. Hosono, T. Noro, H. Ito, T. Yamazaki, and H. Ikegami, Nucl. Phys. **A463**, 429c (1987).

[Tj85] J. A. Tjon and S. J. Wallace, Phys. Rev. C **32**, 1667 (1985).

[Tj85a] J. A. Tjon and S. J. Wallace, Phys. Rev. Lett. **54**, 1357 (1985).

[Tj85b] J. A. Tjon and S. J. Wallace, Phys. Rev. C **32**, 267 (1985).

[Tj87] J. A. Tjon and S. J. Wallace, Phys. Rev. C **36**, 1085 (1987).

[Tj87a] J. A. Tjon and S. J. Wallace, Phys. Rev. C **36**, 280 (1987).

[Tz83] Y. Tzeng and T. Tamura Phys. Lett. **129B**, 379 (1983).

[Va88] D. A. Varshalovich, A. N. Moskalev and V. K. Khersonskii, *Quantum Theory of Angular Momentum* (World Scientific, Singapore, 1988).

[Wa66] N. S. Wall and P. R. Roos, Phys. Rev. **150**, 811 (1966).

[Wa72] J. W. Wachter, W. A. Gibson, and W. R. Burrust, Phys. Rev. C **6**, 1496 (1972).

[Wa74] J. D. Walecka, Ann. Phys. **83**, 491 (1974).

[Wa82] J. Wambach, Phys. Rev. C **46**, 807 (1992).

[Wa87] S. J. Wallace, Ann. Rev. Nucl. Part. Sci. **37**, 267 (1987).

[Wa93] L. Wang, *The* $^{10}B(\vec{p},\vec{n})^{10}C$ *Reaction and Quasifree Scattering on p–Shell Nuclei at 186 MeV*, Ph.D Thesis, Indiana University (1993), unpublished.

[Wa94] L. Wang, X. Yang, J. Rapaport, C. D. Goodman, C. C. Foster, Y. Wang, J. Piekarewicz, E. Sugarbaker, D. Marchlenski, S. de Lucia, B. Luther, L. Rybarcyk, T. N. Taddeucci, and B. K. Park, Phys. Rev. C **50**, 2438 (1994).

[Wa85] Stephen J. Wallace in *Los Alamos Workshop on Relativistic Dynamics and Quark–Nuclear Physics*, (John Wiley & Sons Ltd, New York, 1986).

[Wa96] T. Wakasa, *Study of Nuclear Isovector Spin Responses from Polarization Transfer in* (p, n) *Reactions at Intermediate Energies*, Ph.D Thesis,
University of Tokyo (1996), unpublished.

[Wa97] T. Wakasa, H. Sakai, H. Okamura, H. Otsu, T. Nonaka, S. Fujita, T. Uesaka, Y. Satou, T. Ohnishi, G. Yokoyama, M. B. Greenfield, S. Ishida, N. Sakamoti, K. Hatanaka, and M. Ichimura, *Proceedings of the RCNP International mini workshop on nuclear medium effect via nucleon induced reactions*, Journal of the Physical Society of Japan, Vol. 42, No. 1 (August 1997), p 35.

[We85] J. S. Wesick, P. G. Roos, N. S. Chant, C. C. Chang, A. Nadasen, L. Rees, N. R. Yoder, A. A. Cowley, S. J. Mills, and W. W. Jacobs, Phys. Rev. C **32**,1474 (1985).

[We87] K. Wehrberger and F. Beck, Phys. Rev. C **35**, 298 (1987).

[Wh90] D. M. Whittal, A.A. Cowley, J. V. Pilcher, S. V. Förtsch, F. D. Smit, and J. J. Lawrie, Phys. Rev. C **42**, 309 (1990).

[We93] K. Wehrberger, Phys. Rep. **225**, 275 (1993).

[Wo90] Samuel S. M. Wong, *Introductory Nuclear Physics*
(Prentice–Hall International, Inc., United States of America, 1990).

[Wu79] J. R. Wu, C. C. Chang, and H. D. Holmgren, Phys. Rev. C **19**, 698 (1979).